

*NASA Conference Publication 2368  
Part 1*

# **Large Space Antenna Systems Technology 1984**

*Compiled by  
William J. Boyer  
Langley Research Center*

Proceedings of a conference sponsored jointly by  
the NASA Office of Aeronautics and Space Technology  
and NASA Langley Research Center and held in  
Hampton, Virginia  
December 4-6, 1984

**NASA**  
National Aeronautics  
and Space Administration  
**Scientific and Technical  
Information Branch**

**1985**



**Page intentionally left blank**

## PREFACE

This publication is a compilation of the papers presented at the NASA Conference on Large Space Antenna Systems Technology, held at the Langley Research Center, Hampton, Virginia, December 4-6, 1984. The conference was sponsored jointly by the NASA Office of Aeronautics and Space Technology (OAST) and the NASA Langley Research Center. The conference was organized into seven sessions: Mission Applications for Large Space Antenna Systems, Large Space Antenna Structural Systems, Materials and Structures Technology, Structural Dynamics and Control Technology, Electromagnetics Technology, Large Space Antenna Systems and the Space Station, and Flight Test and Evaluation. All speakers and topics were selected by the session co-chairmen and included representation from industry, universities, and government. The program was organized to provide a comprehensive review of space missions requiring large antenna systems and of the status of key technologies required to enable these missions.

The general co-chairmen for the conference were Dr. Leonard A. Harris, Director for Space, NASA Office of Aeronautics and Space Technology, and Paul F. Holloway, Deputy Director, Langley Research Center. The program chairmen were Dr. Earle K. Huckins III, Head, Large Space Antenna Systems Technology, Langley Research Center, and William J. Boyer, Head, Office of Space Flight Experiment Definition and Integration, Langley Research Center. The conference committee wishes to express its appreciation to the session chairmen, authors, and conference administrative assistants for their outstanding contributions to the meeting.

This publication was expedited and enhanced through the efforts of the staff of the Research Information and Applications Division, Langley Research Center.

The use of trade names or names of manufacturers in this report does not constitute an official endorsement of such products or manufacturers, either expressed or implied, by the National Aeronautics and Space Administration.

**Page intentionally left blank**

## CONTENTS

PREFACE . . . . .	iii
ATTENDEES . . . . .	xi

### PART 1

#### SESSION 1: MISSION APPLICATIONS FOR LARGE SPACE ANTENNA SYSTEMS

NASA MOBILE SATELLITE PROGRAM . . . . .	1
George Knouse and William Weber	
ALTERNATIVES FOR SATELLITE SOUND BROADCAST SYSTEMS AT HF AND VHF . . . . .	27
Bruce E. LeRoy	
DEVELOPMENT CONCERNS FOR SATELLITE-BASED AIR TRAFFIC CONTROL SURVEILLANCE SYSTEMS . . . . .	39
Keith D. McDonald	
APPLICATION OF PUSHBROOM ALTIMETRY FROM SPACE USING LARGE SPACE ANTENNAS . . .	63
C. L. Parsons, J. T. McGoogan, and F. B. Beck	
ORBITING MULTI-BEAM MICROWAVE RADIOMETER FOR SOIL MOISTURE REMOTE SENSING . . .	73
J. C. Shiue and R. W. Lawrence	
LOW-FREQUENCY MICROWAVE RADIOMETER FOR N-ROSS . . . . .	87
J. P. Hollinger and R. C. Lo	
LARGE SPACE ANTENNA TECHNOLOGY APPLIED TO RADAR-IMAGING, RAIN-RATE MEASUREMENTS, AND OCEAN WIND SENSING . . . . .	97
R. K. Moore and S. P. Gogineni	
ADVANCED TWO-FREQUENCY OCEAN SENSING RADAR USING HIGH RESOLUTION ANTENNA BEAMS . . . . .	109
D. E. Weissman and J. W. Johnson	
QUASAT - AN ORBITING VERY LONG BASELINE INTERFEROMETER PROGRAM USING LARGE SPACE ANTENNA SYSTEMS . . . . .	117
J. F. Jordan, R. E. Freeland, G. S. Levy, and D. L. Potts	
LDR SYSTEM CONCEPTS AND TECHNOLOGY . . . . .	127
Bruce Pittman	

#### SESSION 2: LARGE SPACE ANTENNA STRUCTURAL SYSTEMS

WRAP-RIB ANTENNA TECHNOLOGY DEVELOPMENT . . . . .	139
R. E. Freeland, N. F. Garcia, and H. Iwamoto	

DEVELOPMENT OF THE 15-METER HOOP/COLUMN ANTENNA SYSTEM . . . . .	167
T. G. Campbell, D. H. Butler, K. Belvin, and B. B. Allen	
BOX TRUSS DEVELOPMENT AND ITS APPLICATIONS . . . . .	213
J. V. Coyner	
RECENT ADVANCEMENT IN GEO TRUSS REFLECTOR CONCEPT (Paper unavailable at time of publication)	
J. A. Fager	
SYNCHRONOUSLY DEPLOYABLE TETRAHEDRAL TRUSS REFLECTOR . . . . .	237
H. G. Bush, C. L. Herstrom, P. A. Stein, and R. R. Johnson	
ANTENNA TECHNOLOGY FOR QUASAT APPLICATION . . . . .	251
John S. Archer and William B. Palmer	
CABLE-CATENARY LARGE ANTENNA CONCEPT . . . . .	271
W. Akle	
EXTREME PRECISION ANTENNA REFLECTOR STUDY RESULTS . . . . .	279
G. R. Sharp, L. D. Gilger, and K. E. Ard	

### SESSION 3: MATERIALS AND STRUCTURES TECHNOLOGY

NASA SPACE MATERIALS RESEARCH . . . . .	301
Darrel R. Tenney, Stephen S. Tompkins, and George F. Sykes	
NEW CONCEPTS IN DEPLOYABLE BEAM STRUCTURES . . . . .	331
Marvin D. Rhodes	
PRECISION SPACE STRUCTURES . . . . .	349
Keto Soosaar	
PRECISION ANTENNA REFLECTOR STRUCTURES . . . . .	361
John M. Hedgepeth	
INTELSAT ACTIVITIES ON LARGE ANTENNA STRUCTURES (Paper unavailable at time of publication)	
J. Agrawal	
SPACE STATION STRUCTURES . . . . .	375
W. Schneider	
VERIFICATION FOR LARGE SPACE STRUCTURES . . . . .	393
J. Chen and J. Garba	
AN OPTIMIZATION STUDY TO MINIMIZE SURFACE DISTORTIONS OF A HOOP/COLUMN ANTENNA . . . . .	407
G. A. Wrenn	
STRUCTURAL DYNAMICS ANALYSIS . . . . .	423
J. Housner, M. Anderson, W. Belvin, and G. Horner	

AFWAL SPACE CONTROL TECHNOLOGY PROGRAM . . . . .	447
V. O. Hoehne	

## PART 2<sup>\*</sup>

### SESSION 4: STRUCTURAL DYNAMICS AND CONTROL TECHNOLOGY

ON-ORBIT SYSTEMS IDENTIFICATION OF FLEXIBLE SPACECRAFT . . . . .	465
Larry Taylor and Larry D. Pinson	
AN EIGENSYSTEM REALIZATION ALGORITHM FOR APPLICATION TO MODAL TESTING . . . .	483
Jer-Nan Juang	
SUMMARY OF GALILEO MODAL TESTS (Paper unavailable at time of publication)	
J. Chen	
MSFC DATA ANALYSIS OF THE SAFE/DAE EXPERIMENT . . . . .	505
R. W. Schock, T. E. Nesman, and D. K. Reed	
LANGLEY RESEARCH CENTER PHOTOGRAMMETRIC MEASUREMENTS OF SOLAR ARRAY	
DYNAMICS: PRELIMINARY RESULTS . . . . .	517
M. Larry Brumfield, Richard S. Pappa, James B. Miller, and Richard R. Adams	
LARGE ANTENNA CONTROL METHODS: CURRENT STATUS AND FUTURE TRENDS . . . . .	547
G. Rodriguez, Y. H. Lin, and M. H. Milman	
EXPERIMENTAL DEVELOPMENT OF A FAILURE DETECTION SCHEME FOR LARGE	
SPACE STRUCTURES . . . . .	569
Raymond C. Montgomery and Jeffrey P. Williams	
DYNAMIC VERIFICATION OF LARGE SPACE STRUCTURES . . . . .	591
D. K. Tollison and H. B. Waites	
PASSIVE AND ACTIVE CONTROL OF SPACE STRUCTURES ( PACOSS) . . . . .	603
G. Morosow, H. Harcrow, and L. Rogers	
APPLICATION OF THE MAXIMUM ENTROPY/OPTIMAL PROJECTION CONTROL DESIGN	
APPROACH FOR LARGE SPACE STRUCTURES . . . . .	617
D. C. Hyland	

### SESSION 5: ELECTROMAGNETICS TECHNOLOGY

ELECTROMAGNETIC ANALYSIS FOR SURFACE TOLERANCE EFFECTS ON LARGE SPACE	
ANTENNAS . . . . .	655
C. R. Cockrell and R. C. Rudduck	

---

<sup>\*</sup>Part 2 is presented under separate cover.

APPLICATION OF MODERN APERTURE INTEGRATION (AI) AND GEOMETRICAL THEORY OF DIFFRACTION (GTD) TECHNIQUES FOR ANALYSIS OF LARGE REFLECTOR ANTENNAS . . .	675
Roger C. Rudduck	
FEED SYSTEM DESIGN CONSIDERATIONS FOR LARGE SPACE ANTENNA SYSTEMS. PART I - MULTIPLE APERTURES WITH NON-OVERLAPPING FEEDS . . . . .	693
M. C. Bailey	
FEED SYSTEM DESIGN CONSIDERATIONS FOR LARGE SPACE ANTENNA SYSTEMS. PART II - SINGLE APERTURE WITH OVERLAPPING FEEDS . . . . .	703
V. Jamnejad	
DIFFRACTION ANALYSIS OF MESH DEPLOYABLE REFLECTOR ANTENNAS . . . . .	715
Y. Rahmat-Samii	
DETERMINATION OF ELECTROMAGNETIC PROPERTIES OF MESH MATERIAL USING ADVANCED RADIOMETER TECHNIQUES . . . . .	737
R. F. Harrington and H-J C. Blume	

#### SESSION 6: LARGE SPACE ANTENNA SYSTEMS AND THE SPACE STATION

THE SPACE STATION AS A CONSTRUCTION BASE FOR LARGE SPACE STRUCTURES . . . . .	757
R. M. Gates	
UTILIZATION OF SPACE STATION BY THE LARGE DEPLOYMENT REFLECTOR . . . . .	771
L. W. Bandermaun and W. H. Alff	
LARGE DEPLOYABLE REFLECTOR (LDR) REQUIREMENTS FOR SPACE STATION ACCOMMODATIONS . . . . .	775
David A. Crowe, Michael J. Clayton, and Fritz C. Runge	
THE ORBITAL ASSEMBLY OF A LARGE ANTENNA ( Paper unavailable at time of publication)	
D. Waltz	
A CONCEPT FOR A MOBILE REMOTE MANIPULATOR SYSTEM . . . . .	793
Martin M. Mikulas, Jr., Harold G. Bush, Richard E. Wallsom, and J. Kermit Jensen	
SPACE-BASED ANTENNA MEASUREMENT SYSTEM CONCEPTS FOR SPACE STATION OPERATION . . . . .	809
C. Louis Cuccia, Thomas G. Campbell, W. L. Pritchard, and Jud Lyon	

#### SESSION 7: FLIGHT TEST AND EVALUATION

IN-SPACE PERFORMANCE OF THE TDRSS ANTENNA SYSTEM (Paper unavailable at time of publication)	
B. C. Tankersley	
SOLAR ARRAY EXPERIMENT (SAE) FLIGHT EXPERIENCE . . . . .	845
Henry C. Hill, Leighton E. Young, and Gary F. Turner	

ASSEMBLY CONCEPT FOR CONSTRUCTION OF ERECTABLE SPACE STRUCTURE (ACCESS)	
NEUTRAL BUOYANCY TESTING RESULTS . . . . .	855
Walter L. Heard, Jr.	
EXPERIMENTAL ASSEMBLY OF STRUCTURES IN EVA (EASE) NEUTRAL BUOYANCY TESTING	
RESULTS (Paper unavailable at time of publication)	
D. L. Akin	
SPACE TECHNOLOGY EXPERIMENTS PLATFORM (STEP) STATUS - AN IN-SPACE TEST	
FACILITY . . . . .	877
Jack E. Harris	
CONTROL OF FLEXIBLE STRUCTURES (COFS) FLIGHT EXPERIMENT BACKGROUND AND	
DESCRIPTION . . . . .	893
Brantley R. Hanks	
SHUTTLE-ATTACHED ANTENNA FLIGHT EXPERIMENT DEFINITION STUDY (FEDS) . . . . .	909
G. J. Hannan	
ELECTRO-SCIENCE REQUIREMENTS FOR SHUTTLE-ATTACHED ANTENNA FLIGHT	
EXPERIMENTS . . . . .	929
William L. Grantham, Emedio M. Bracalente, and Lyle C. Schroeder	



**Page intentionally left blank**

LSAST-1984 CONFERENCE ATTENDEE LIST

ABOIM, DR. CARLOS A.  
ACHARD, ROBERT T.  
ADAMS, RICHARD R.  
ADELMAN, HOWARD M.  
AGNEW, DONALD L. (DON)  
AKIN, DR. D. L.  
AKLE, W.  
ALFF, WILLIAM  
ALLEN, BIBB B.  
ALLEN, JR., JOHN L.  
AMOS, DR. ANTHONY K.  
ANDERSON, DR. MELVIN S.  
ANDERSON, DR. WILLARD W.  
ANDREAS, ROBERT J.  
ARAYA, ROBERTO  
ARCHER, DR. JOHN S.  
ARMSTRONG, ERNEST  
ASHLEY, PROFESSOR HOLT  
ASWANI, MOHAN

BAILEY, DR. MARION C.  
BAINUM, PETER M.  
BALDWIN, C. A.  
BARNARD, MICHAEL J.  
BARRETT, MICHAEL F.  
BARTLETT, WAYNE M.  
BASU, J. P.  
BAYARD, DAVID S.  
BEASLEY, GARY P.  
BEATTY, MARVIN  
BECK, FRED B.  
BECOUVARAKIS, TIM G.  
BEHUN, VAUGHAN  
BELVIN, W. KEITH  
BENNETT, WILLIAM  
BENTON, MAX D.  
BERMAN, DR. FRED  
BLANKENSHIP, CHARLES P.  
BLUME, DR. H. J. C.  
BOENSCH, FRANK D.  
BOUNDY, ROBERT A.  
BOYER, WILLIAM J.  
BRACALENTE, EMEDIO M.  
BREAKWELL, JOHN  
BRITT, C. L.  
BROWN, LARRY J.  
BRUMFIELD, M. L. (LARRY)  
BURMEISTER, GEORGE J.  
BUTLER, DAVID H.

ANCO ENGINEERS  
U.S. AIR FORCE  
NASA LANGLEY RESEARCH CENTER  
NASA LANGLEY RESEARCH CENTER  
EASTMAN KODAK COMPANY  
MASSACHUSETTS INSTITUTE OF TECHNOLOGY  
TRW INCORPORATED  
LOCKHEED MISSILES & SPACE COMPANY  
HARRIS CORPORATION, GASD  
NASA LANGLEY RESEARCH CENTER  
AIR FORCE OFFICE OF SCIENTIFIC RES.  
NASA LANGLEY RESEARCH CENTER  
NASA LANGLEY RESEARCH CENTER  
HARRIS CORPORATION, GASD  
UCLA  
TRW INCORPORATED  
NASA LANGLEY RESEARCH CENTER  
STANFORD UNIVERSITY  
AEROSPACE CORPORATION

NASA LANGLEY RESEARCH CENTER  
HOWARD UNIVERSITY  
NASA LANGLEY RESEARCH CENTER  
TRW INCORPORATED  
HONEYWELL, SYSTEMS & RESEARCH CENTER  
NASA LEWIS RESEARCH CENTER  
PERKIN-ELMER  
JET PROPULSION LABORATORY  
NASA LANGLEY RESEARCH CENTER  
NASA LANGLEY RESEARCH CENTER  
NASA LANGLEY RESEARCH CENTER  
NASA LANGLEY RESEARCH CENTER  
KENTRON  
NASA LANGLEY RESEARCH CENTER  
SYSTEMS ENGINEERING FOR POWER, INC.  
AEC-ABLE ENGINEERING COMPANY, INC.  
GEORGIA INSTITUTE OF TECHNOLOGY  
NASA LANGLEY RESEARCH CENTER  
NASA LANGLEY RESEARCH CENTER  
U.S. AIR FORCE  
JET PROPULSION LABORATORY  
NASA LANGLEY RESEARCH CENTER  
NASA LANGLEY RESEARCH CENTER  
LOCKHEED MISSILES & SPACE COMPANY  
RESEARCH TRIANGLE INSTITUTE  
HONEYWELL, SSAVD  
NASA LANGLEY RESEARCH CENTER  
BOEING AEROSPACE CORPORATION  
NASA LANGLEY RESEARCH CENTER

LSAST-1984 CONFERENCE ATTENDEE LIST - CONTINUED

CAMARDA, CHARLIE  
CAMARET, TIM  
CAMPBELL, BRUCE  
CAMPBELL, THOMAS G.  
CARD, DR. MICHAEL F.  
CHEN, DR. JAY-CHUNG  
CLAYTON, MICHAEL J.  
COCKRELL, DR. CAPERS R.  
COFFEE, JR., CLAUDE W.  
COON, KENNETH C.  
COPPA, ANTHONY  
COUCH, LANA M.  
COUGHLIN, THOMAS B.  
COYNER, JR., J. V.  
CROOP, HAROLD C.  
CROWE, DAVID A.  
CRUMBLY, K. H. (KEN)  
CUCHANSKI, MICHAEL  
CUDNEY, JR., HARLEY H.

DARRAH, JOHN H.  
DAUKAS, ANTHONY (TONY)  
DAVIS, LARRY D.  
DE LAFONTAINE, JEAN  
DEAN, ED  
DEAVER, JOSEPH  
DI BATTISTA, JOHN D.  
DIARRA, C. MODIBO  
DIGLIO, JOHN  
DORSEY, JOHN T.  
DUSTIN, MILES O.

EDIGHOFFER, HAROLD  
EVANS, RON

FADDOUL, JAMES R.  
FARMER, JEFFERY T.  
FENG, G. C.  
FICHTER, W. B.  
FIGGE, I. E. (WARD)  
FOLDES, PETER  
FONTANA, ANTHONY  
FREELAND, ROBERT E.  
FREEMAN, JR., W. T.  
FULTON, DR. ROBERT E.

GANSSLE, EUGENE R.  
GARCIA, NICHOLAS F.  
GARIBOTTI, JOSEPH F.

NASA LANGLEY RESEARCH CENTER  
ROCKWELL INTERNATIONAL-ROCKETDYNE DIV.  
ASTRO RESEARCH CORPORATION  
NASA LANGLEY RESEARCH CENTER  
NASA LANGLEY RESEARCH CENTER  
JET PROPULSION LABORATORY  
EASTMAN KODAK COMPANY  
NASA LANGLEY RESEARCH CENTER  
NASA LANGLEY RESEARCH CENTER  
JET PROPULSION LABORATORY  
GENERAL ELECTRIC  
NATIONAL AERONAUTICS & SPACE ADMINISTRATION  
JOHNS HOPKINS UNIVERSITY  
MARTIN MARIETTA CORPORATION  
U.S. AIR FORCE  
EASTMAN KODAK COMPANY  
NASA LANGLEY RESEARCH CENTER  
RCA ASTRO ELECTRONICS  
STATE UNIVERSITY OF NEW YORK AT BUFFALO

HQ SPACE COMMAND/XPN  
ASTRO RESEARCH CORPORATION  
HARRIS CORPORATION, GASD  
DEFENCE RESEARCH ESTABLISHMENT OTTAWA  
NASA LANGLEY RESEARCH CENTER  
NRL, BENDIX AEROSPACE  
NATIONAL AERONAUTICS & SPACE ADMINISTRATION  
HOWARD UNIVERSITY  
GRUMMAN AEROSPACE CORPORATION  
NASA LANGLEY RESEARCH CENTER  
NASA LEWIS RESEARCH CENTER

EDIGHOFFER INCORPORATED  
SPERRY

NASA LEWIS RESEARCH CENTER  
NASA LANGLEY RESEARCH CENTER  
LOCKHEED-EMSCO  
NASA LANGLEY RESEARCH CENTER  
ATLANTIC RESEARCH CORPORATION  
FOLDES INCORPORATED  
NASA LANGLEY RESEARCH CENTER  
JET PROPULSION LABORATORY  
NASA LANGLEY RESEARCH CENTER  
GEORGE WASHINGTON UNIVERSITY

RCA ASTRO-ELECTRONICS  
LOCKHEED MISSILES & SPACE COMPANY  
HR TEXTRON INCORPORATED

LSAST-1984 CONFERENCE ATTENDEE LIST - CONTINUED

GARRETT, DR. L. BERNARD  
GATES, RICHARD M.  
GIESY, D. P.  
GOGINENI, DR. S. P.  
GOSLEE, JOHN W. (BILL)  
GRANTHAM, WILLIAM L.  
GYNTHER, DANIEL E.

NASA LANGLEY RESEARCH CENTER  
BOEING AEROSPACE COMPANY  
KENTRON INTERNATIONAL, INC.  
UNIVERSITY OF KANSAS  
NASA LANGLEY RESEARCH CENTER  
NASA LANGLEY RESEARCH CENTER  
MRJ, INCORPORATED

HADAEGH, FRED  
HAGAMAN, JANE A.  
HAGEN, HOWARD G.  
HAIGHT, R. W.  
HALE, DR. ARTHUR L.  
HALL, JR., JOHN B. (JACK)  
HAM, FRED M.  
HAMIDI, MASSIH  
HAMILTON, EDWARD C.  
HAMMELL, ALLAN K.  
HANKS, BRANTLEY R.  
HANNAN, GENE J.  
HARCROW, HARRY  
HARRINGTON, DR. RICHARD F.  
HARRIS, JACK E.  
HARRISON, DENNIS C.  
HEARD, JR., WALTER L. (DOUG)  
HEDGEPEETH, DR. J. M.  
HERSTROM, CATHERINE L.  
HILL, HENRY C.  
HILL, J. E.  
HILL, THOMAS E.  
HIRSCHBEIN, MURRAY  
HOEHNE, VERNON  
HOLCOMB, DR. LEE B.  
HOLLOWAY, PAUL F.  
HOLLOWAY, III, S. E. (CHIP)  
HOOK, W. RAY  
HORNER, DR. GARNETT C.  
HORTA, LUCAS G.  
HORTON, JOHN B.  
HOUSNER, DR. JERROLD M.  
HOWLAND, RAY  
HSING, JOHN C.  
HUANG, FELIX  
HUDSON, WAYNE R.  
HYLAND, DR. DAVID C.

JET PROPULSION LABORATORY  
NASA LANGLEY RESEARCH CENTER  
LOCKHEED MISSILES & SPACE COMPANY  
LOCKHEED MISSILES & SPACE COMPANY  
GENERAL DYNAMICS CONVAIR  
NASA LANGLEY RESEARCH CENTER  
HARRIS CORPORATION, GASD  
JET PROPULSION LABORATORY  
NASA MARSHALL SPACE FLIGHT CENTER  
HONEYWELL INCORPORATED  
NASA LANGLEY RESEARCH CENTER  
LOCKHEED MISSILES AND SPACE COMPANY  
MARTIN MARIETTA DENVER AEROSPACE  
NASA LANGLEY RESEARCH CENTER  
NASA LANGLEY RESEARCH CENTER  
HARRIS CORPORATION  
NASA LANGLEY RESEARCH CENTER  
ASTRO RESEARCH CORPORATION  
NASA LANGLEY RESEARCH CENTER  
MARSHALL SPACE FLIGHT CENTER  
LOCKHEED MISSILES & SPACE COMPANY  
GENERAL ELECTRIC-SPACE SYSTEMS DIV.  
NATIONAL AERONAUTICS & SPACE ADMINISTRATION  
AIR FORCE WRIGHT AERONAUTICAL LABS.  
NATIONAL AERONAUTICS & SPACE ADMINISTRATION  
NASA LANGLEY RESEARCH CENTER  
NASA LANGLEY RESEARCH CENTER  
NASA LANGLEY RESEARCH CENTER  
NASA LANGLEY RESEARCH CENTER  
NASA LANGLEY RESEARCH CENTER  
TRW INCORPORATED  
NASA LANGLEY RESEARCH CENTER  
THE HOWLAND CO., INC.  
COMSAT  
ITEK OPTICAL SYSTEMS  
NATIONAL AERONAUTICS & SPACE ADMINISTRATION  
HARRIS CORPORATION, GASD

IRVINE, THOMAS B.  
IWAMOTO, HENRY H.

NASA LEWIS RESEARCH CENTER  
LOCKHEED MISSILES & SPACE COMPANY

LSAST-1984 CONFERENCE ATTENDEE LIST - CONTINUED

JACOBS, ERNEST  
JACOCKS, JR., MILTON L.  
JAMNEJAD-DAILAMI, DR. VAHRAZ  
JEANS, J. R.  
JOHNSON, JAMES W.  
JONES, PETER A.  
JONES, WILLIAM R.  
JORDAN, DR. JAMES F.  
JOSHI, SURESH M.  
JUANG, DR. JER-NAN

KADER, JAC  
KAMINSKAS, RIM A.  
KECKLER, CLAUDE R.  
KELLERMEIER, HANS  
KENDALL, BRUCE  
KEY, RICHARD  
KIDD, ALAN  
KINGSBURY, MICHAEL G.  
KLICH, PHILLIP J.  
KOPRIVER, FRANK  
KROEN, MARIAN L.  
KULICK, SHEL  
KYSER, ALBERT C.

LAKE, MARK S.  
LAMBERTY, BERNARD J.  
LAWRENCE, ROLAND W.  
LE ROY, BRUCE E.  
LEVY, GERALD S.  
LIGHTNER, E. BURTON  
LIN, DR. YU-HWAN  
LIN, J. GENE  
LINDBERG, ROBERT  
LIPS, KENNETH W.  
LOPRIORE, MARIO  
LOVELACE, U. M. (WOODY)  
LYON, JUD  
LYONS, M.G.

MALLETTE, MICHAEL F.  
MALONE, JOHN E.  
MANSOUR, WAGDY A.  
MANTUS, MORTON  
MC DONALD, K. D.  
MC GOWAN, PAUL  
MECK, DR. ULRICH  
MIKULAS, JR., DR. MARTIN M.

AEROSPACE CORPORATION  
NASA LANGLEY RESEARCH CENTER  
JET PROPULSION LABORATORY  
U.S. GOVERNMENT  
NASA LANGLEY RESEARCH CENTER  
EASTMAN KODAK COMPANY  
NASA LANGLEY RESEARCH CENTER  
JET PROPULSION LABORATORY  
NASA LANGLEY RESEARCH CENTER  
NASA LANGLEY RESEARCH CENTER

KADER ROBOTICS CORPORATION  
TRW INCORPORATED  
NASA LANGLEY RESEARCH CENTER  
MBB COMPANY, SPACE DIVISION  
NASA LANGLEY RESEARCH CENTER  
JET PROPULSION LABORATORY  
SPAR AEROSPACE LIMITED  
BRUNSWICK CORPORATION-DEFENSE DIV.  
NASA LANGLEY RESEARCH CENTER  
JL ASSOCIATES  
NASA LANGLEY RESEARCH CENTER  
GENERAL DYNAMICS  
INSTRUMECH

NASA LANGLEY RESEARCH CENTER  
BOEING AEROSPACE COMPANY  
NASA LANGLEY RESEARCH CENTER  
NASA LEWIS RESEARCH CENTER  
JET PROPULSION LABORATORY  
NASA LANGLEY RESEARCH CENTER  
JET PROPULSION LABORATORY  
CONTROL RESEARCH CORPORATION  
NAVAL RESEARCH LABORATORY  
DEPT. OF COMMUNICATIONS  
ESA-ESTEC  
NASA LANGLEY RESEARCH CENTER  
HOWLAND COMPANY, INCORPORATED  
INTEGRATED SYSTEMS INC.

UNIVERSITY OF VIRGINIA  
NASA JOHN F. KENNEDY SPACE CENTER  
GEORGE WASHINGTON UNIVERSITY  
GRUMMAN AEROSPACE CORPORATION  
FEDERAL AVIATION ADMINISTRATION  
NASA LANGLEY RESEARCH CENTER  
MBB COMPANY  
NASA LANGLEY RESEARCH CENTER

LSAST-1984 CONFERENCE ATTENDEE LIST - CONTINUED

MILLER, CHRISTOPHER C.  
MILLER, JAMES B.  
MISERENTINO, ROBERT  
MOBLEY, TOM  
MONTEITH, JAMES H.  
MONTGOMERY, DR. RAYMOND C.  
MONTGOMERY, JOHN  
MOORMAN, JOSEPH C.  
MORRIS, DAVID P.  
MOULTON, RICH

NARKIS, YAHLI  
NEWTON, ROBERT B.  
NEWTON, RON  
NICHOLS, STEPHEN A.  
NIMMO, NANCY  
NOBLITT, B. G.  
NOOR, AHMED K.  
NYGREN, EVERT C.

OAKES, THOMAS J.  
OSBORNE, ERIC P.

PALUSZEK, MICHAEL  
PAPPA, RICHARD S.  
PATTERSON, L. ROY  
PINSON, DR. LARRY D.  
PITCAIRN, IAN  
PITTMAN, R. BRUCE  
POHLEN, L. J. (LARRY)  
POLLOCK, SAMUEL J.  
PORTER, AL

QUARTARARO, RICHARD

RAHMAT-SAMII, DR. YAHYA  
RANEY, J. P.  
RANSOM, JAMES  
RAO, S. K.  
REDDY, A. S. S. R.  
REICHHARDT, TONY  
RHODES, MARVIN D.  
RICE, ROBERT B.  
ROBERTSON, ANDREW  
ROBERTSON, BRENT  
RODGERS, FREDERICK C.  
ROGERS, DR. L. C.

MARTIN MARIETTA CORPORATION  
NASA LANGLEY RESEARCH CENTER  
NASA LANGLEY RESEARCH CENTER  
MARTIN MARIETTA CORPORATION  
NASA LANGLEY RESEARCH CENTER  
NASA LANGLEY RESEARCH CENTER  
MARTIN MARIETTA DENVER  
NASA LANGLEY RESEARCH CENTER  
HONEYWELL, SSAVD  
HEXCEL

UNIVERSITY OF VIRGINIA  
MARTIN MARIETTA AERO.-MICHOD DIV.  
AEROJET TECHSYSTEMS COMPANY  
NAVAL ELECTRONIC SYSTEMS COMMAND  
NASA LANGLEY RESEARCH CENTER  
TELEDYNE BROWN ENGINEERING  
GEORGE WASHINGTON UNIVERSITY  
FORD AEROSPACE & COMMUNICATIONS CORP.

GOODYEAR AEROSPACE CORPORATION  
NASA GODDARD SPACE FLIGHT CENTER

C.S. DRAPER LABORATORY  
NASA LANGLEY RESEARCH CENTER  
ORI, INCORPORATED  
NASA LANGLEY RESEARCH CENTER  
UNITED TECHNOLOGIES RES. CENTER-OATL  
NASA AMES RESEARCH CENTER  
HQ USAF SPACE DIVISION, SD/YOM  
AFWAL/FIBAC  
HEATH TECHNIA

HR TEXTRON INCORPORATED

JET PROPULSION LABORATORY  
NASA LANGLEY RESEARCH CENTER  
AEROSPACE CORPORATION  
SPAR AEROSPACE LIMITED  
HOWARD UNIVERSITY  
SPACE WORLD MAGAZINE  
NASA LANGLEY RESEARCH CENTER  
MARTIN MARIETTA CORPORATION  
GENERAL DYNAMICS-CONVAIR  
UNIVERSITY OF VIRGINIA  
ATLANTIC RESEARCH CORPORATION  
AF WRIGHT AERONAUTICAL LABS./FIBA

LSAST-1984 CONFERENCE ATTENDEE LIST - CONTINUED

ROMERO, JAMES M.  
ROWELL, L. F. (LARRY)  
RUDDUCK, DR. R. C.  
RUNGE, FRITZ C.

NATIONAL AERONAUTICS & SPACE ADMINISTRATION  
NASA LANGLEY RESEARCH CENTER  
OHIO STATE UNIVERSITY  
MCDONNELL DOUGLAS ASTRONAUTICS COMPANY

SANTOS-MASON, BEATRICE  
SATTER, CELESTE M.  
SAUNDERS, CHARLES G.  
SCHILLING, DR. RALPH F.  
SCHMID, PAUL E.  
SCHNEIDER, DR. WILLIAM C.  
SCHOCK, RICHARD W.  
SCHOEN, NEIL C.  
SCHRADER, JAMES H.  
SCHROEDER, LYLE C.  
SCHY, ALBERT A.  
SHARP, G. RICHARD  
SHIEH, RONG C.  
SHIELDS, DAVID  
SHIUE, DR. JAMES C.  
SHORE, CHARLES P.  
SIGNORELLI, JOEL  
SINGH, SAHJENDRA N.  
SMITH, DAVEY L.  
SNYDER, E. GLENN  
SOKOL, SAMUEL  
SOOSAAR, DR. KETO  
SOROCKY, STEPHEN J.  
STEIN, BLAND A.  
STEIN, PETER A.  
STEVENSON, DONALD L.  
STIEBER, MICHAEL E.  
SUNDARARAJAN, NARASIMHAN  
SUSSMAN, JERRY  
SYKES, GEORGE F.

NASA LANGLEY RESEARCH CENTER  
CAMBRIDGE RESEARCH ASSOCIATES  
NASA LANGLEY RESEARCH CENTER  
TRW FEDERAL SYSTEMS DIVISION  
U.S. GOVERNMENT  
NASA JOHNSON SPACE CENTER  
NASA MARSHALL SPACE FLIGHT CENTER  
TRW INCORPORATED  
RESEARCH TRIANGLE INSTITUTE  
NASA LANGLEY RESEARCH CENTER  
NASA LANGLEY RESEARCH CENTER  
NASA LEWIS RESEARCH CENTER  
MRJ, INCORPORATED  
U.S. GOVERNMENT  
NASA GODDARD SPACE FLIGHT CENTER  
NASA LANGLEY RESEARCH CENTER  
AFRPL/DYSS  
VIGYAN RESEARCH ASSOCIATES, INC.  
AFWAL/FIBG  
ROCKWELL SPACE  
NASA LANGLEY RESEARCH CENTER  
CAMBRIDGE RESEARCH ASSOCIATES  
SPAR AEROSPACE LIMITED  
NASA LANGLEY RESEARCH CENTER  
NASA LANGLEY RESEARCH CENTER  
E.I. DU PONT DE NEMOURS & CO., INC.  
COMMUNICATIONS RESEARCH CENTRE  
OLD DOMINION UNIV. RES. FOUNDATION  
U.S. GOVERNMENT  
NASA LANGLEY RESEARCH CENTER

TALBOT, JOE  
TANKERSLEY, DR. B. C.  
TAYLOR, JR., L. W. (LARRY)  
TENNEY, DR. DARREL R.  
THOMAS, MITCHELL  
THOMPSON, CHARLES CLARK  
TILSON, JR., PAUL E.  
TOLIVAR, FERNANDO  
TOLLISON, DANNY K.  
TOLSON, ROBERT  
TOMPKINS, STEPHEN S.

NASA LANGLEY RESEARCH CENTER  
HARRIS CORPORATION, GASD  
NASA LANGLEY RESEARCH CENTER  
NASA LANGLEY RESEARCH CENTER  
L'GARDE, INC.  
UNITED TECHNOLOGIES RESEARCH CENTER  
U.S. AIR FORCE  
JET PROPULSION LABORATORY  
CONTROL DYNAMICS COMPANY  
NASA LANGLEY RESEARCH CENTER  
NASA LANGLEY RESEARCH CENTER

LSAST-1984 CONFERENCE ATTENDEE LIST - CONCLUDED

TRACY, DANIEL J.	BOEING AEROSPACE COMPANY
TSENG, G. T.	AEROSPACE CORPORATION
TUMULTY, WILLIAM T.	NATIONAL AERONAUTICS & SPACE ADMINISTRATION
VAN VOOREN, ROBERT H.	TRW INCORPORATED
VANDER VELDE, WALLACE E.	MASSACHUSETTS INSTITUTE OF TECHNOLOGY
VENKAYYA, VIPPERLA B.	AIR FORCE WRIGHT AERONAUTICAL LABS.
VICTER, IRA	ROCKWELL INTERNATIONAL
WADA, BEN K.	JET PROPULSION LABORATORY
WALL, JOE	HONEYWELL SYSTEMS AND RESEARCH CENTER
WALLSOM, RICHARD E.	KENTRON
WALZ, JOSEPH E.	NASA LANGLEY RESEARCH CENTER
WANG, HARRY S. C.	AEROSPACE CORPORATION
WARD, JR., JAMES C.	NASA LANGLEY RESEARCH CENTER
WATSON, JUDITH J.	NASA LANGLEY RESEARCH CENTER
WEBER, III, DR. WILLIAM J.	JET PROPULSION LABORATORY
WEGROWICZ, L. A.	SPAR AEROSPACE LIMITED
WEIDLER, DARRYL	MIT LINCOLN LABORATORY
WEIDMAN, DR. DEENE J.	NASA LANGLEY RESEARCH CENTER
WEISS, MICHAEL A.	FAIRCHILD SPACE COMPANY
WEISSMAN, DR. DAVID E.	HOFSTRA UNIVERSITY
WELIK, GEORGE	LOCKHEED MISSILES & SPACE COMPANY
WELLING, REBECCA L.	LOCKHEED RESEARCH & DEVELOPMENT DIV.
WENDEL, W. R.	SPACE STRUCTURES INTERNATIONAL
WILLIAMS, JAMES L.	NASA LANGLEY RESEARCH CENTER
WILLIAMS, JEFFREY P.	NASA LANGLEY RESEARCH CENTER
WISSINGER, ALAN B.	PERKIN-ELMER
WITT, WILLIAM P.	AIR FORCE WEAPONS LABORATORY
WOO, KENNETH	JET PROPULSION LABORATORY
WOODS, JR., ARTHUR A.	LOCKHEED MISSILES & SPACE COMPANY
WRENN, G. A.	KENTRON INTERNATIONAL
WRIGHT, HOWARD T.	NASA LANGLEY RESEARCH CENTER
WRIGHT, ROBERT L.	NASA LANGLEY RESEARCH CENTER
YOUNG, JOHN W.	NASA LANGLEY RESEARCH CENTER
ZAGHLOUL, AMIR	COMSAT LABORATORIES
ZIMCIK, DR. D. G.	COMMUNICATIONS RESEARCH CENTRE



NASA MOBILE SATELLITE PROGRAM

George Knouse  
NASA Headquarters  
Washington, DC

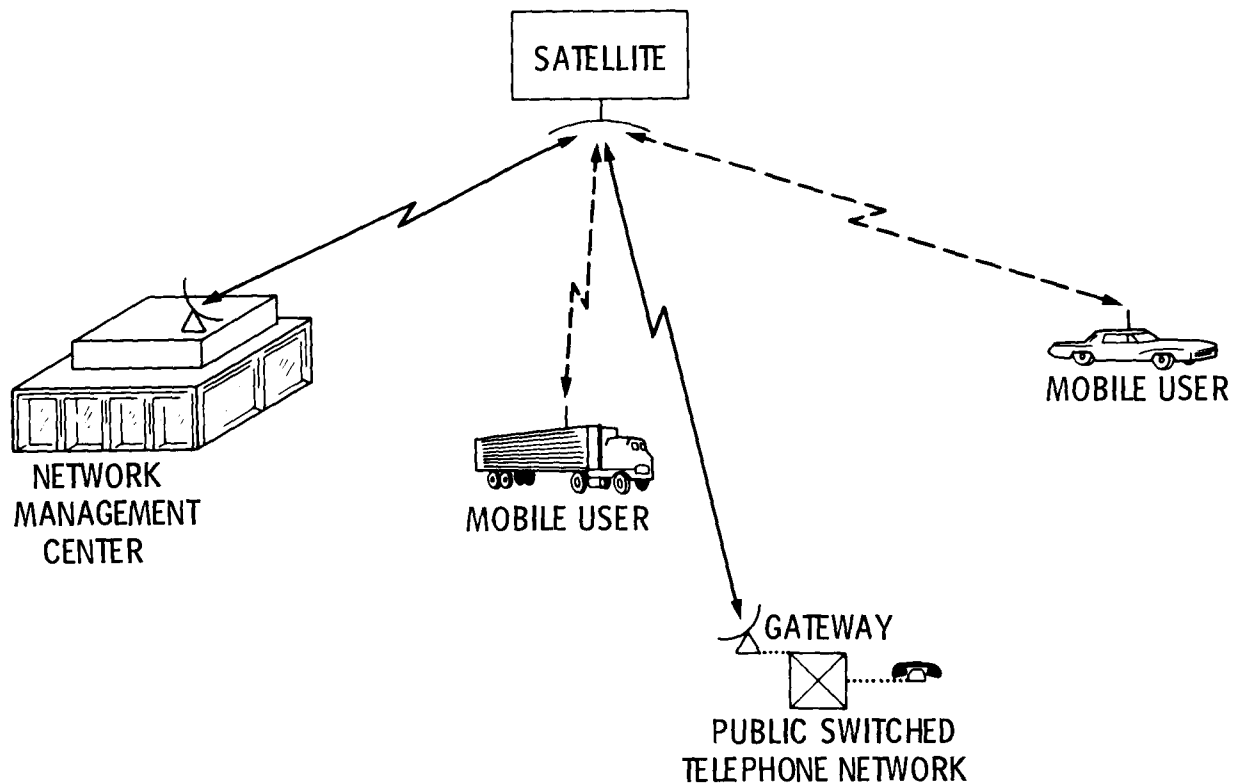
William Weber  
Jet Propulsion Laboratory  
Pasadena, CA

Large Space Antenna Systems Technology - 1984

December 4-6, 1984

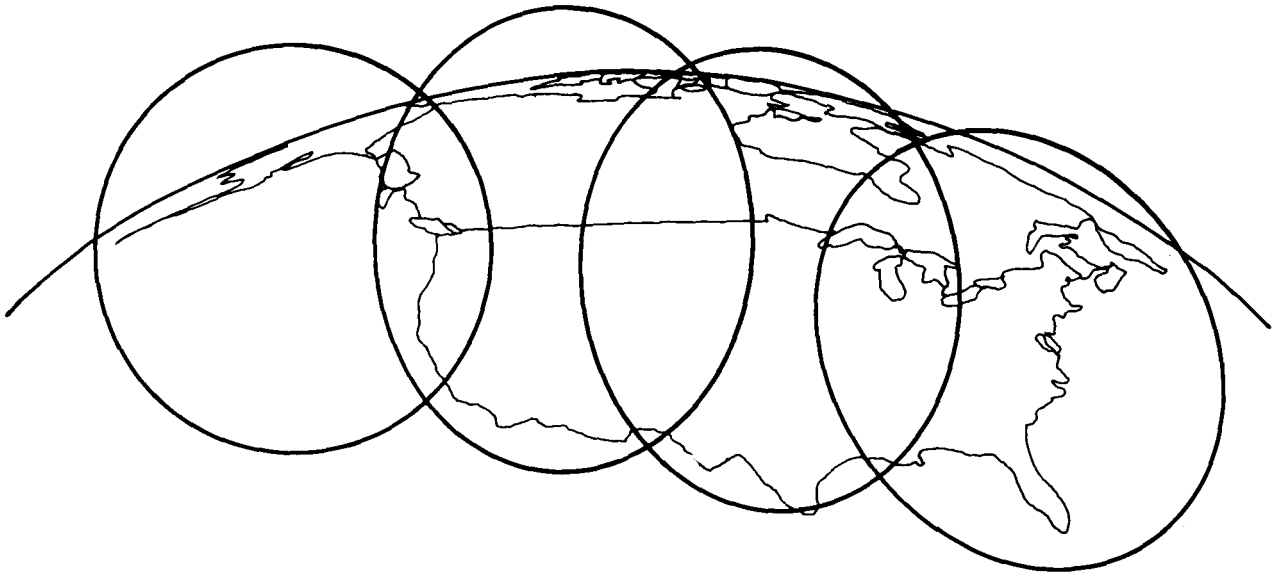
**MOBILE SATELLITE CONCEPT  
FUNCTIONAL DESCRIPTION**

A Mobile Satellite System (MSS) provides communications over large geographic areas between mobile terminals (whether on land, sea, or in the air) and their associated base stations. Communications between the mobiles and the base stations or telephone gateway stations are relayed by a geostationary satellite. A network management center provides call setup and channel allocation and controls the operation of the network. A typical coverage area would include the 48 states, Alaska, and surrounding coastal waters, thus augmenting existing and planned terrestrial systems that are concentrated primarily in higher population areas. Representative services include telephony, two-way radio, dispatch, message and low-speed data, paging, and position location. Potential markets include both commercial and government applications such as interstate trucking, remote oil/gas drilling, business, and emergency response communications such as required for emergency medical service and wide-area law enforcement.



## A POSSIBLE FIRST-GENERATION MSS BEAM COVERAGE PATTERN

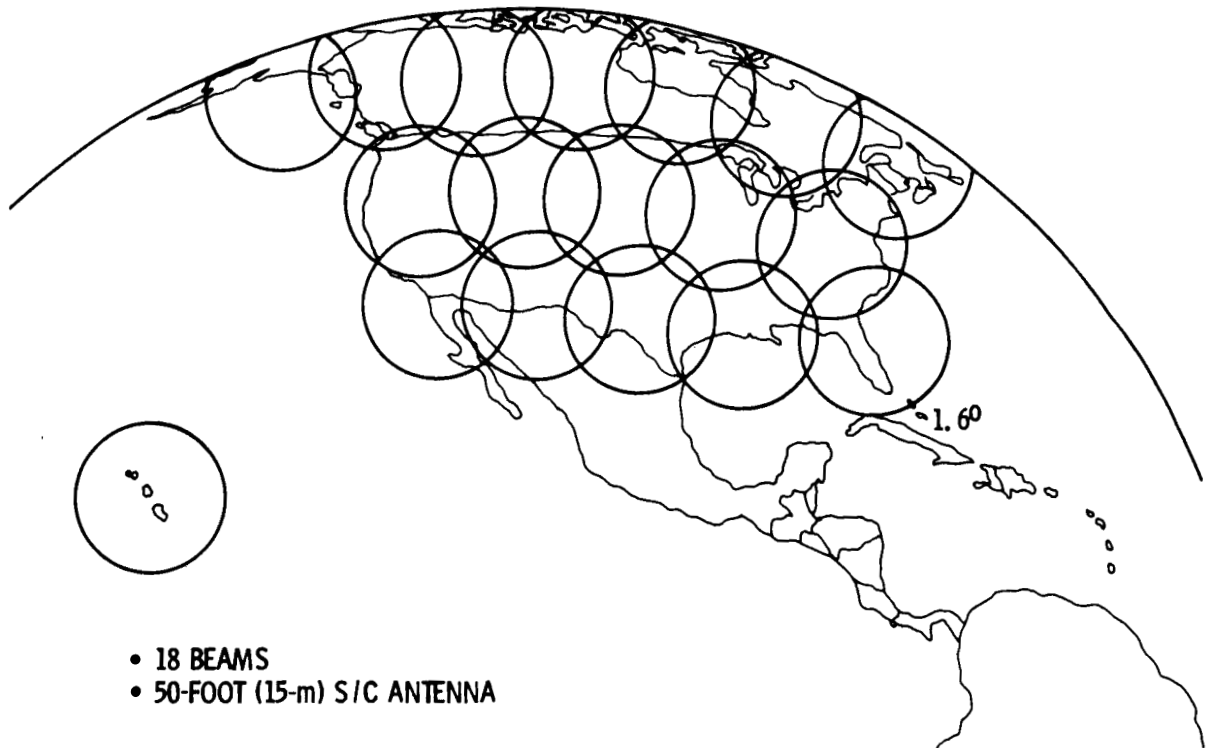
The MSS satellite will most likely be a conventional communications satellite bus with a relatively large deployable antenna, in the range of 10 to 30 feet in diameter. One possible design might include a 25 ft UHF antenna with a four beam pattern covering both the US and Canada. The first-generation system may be a joint venture between the US and Canada; however, it will be built and operated by the private sector. NASA and the Canadian Department of Communications (DOC) have worked cooperatively for the past five years toward accelerating the introduction of this new satellite service. Three companies in the US and one in Canada have expressed their intent to operate such systems. The FCC will soon issue a Notice of Proposed Rulemaking for frequencies in the 806-890 MHz band and will request applications for licenses for MSS. NASA is working with the FCC, US industry, DOC, and other government agencies to assure the launch of this new system by the end of the decade.



25-FOOT (7.6-m) SPACECRAFT ANTENNA

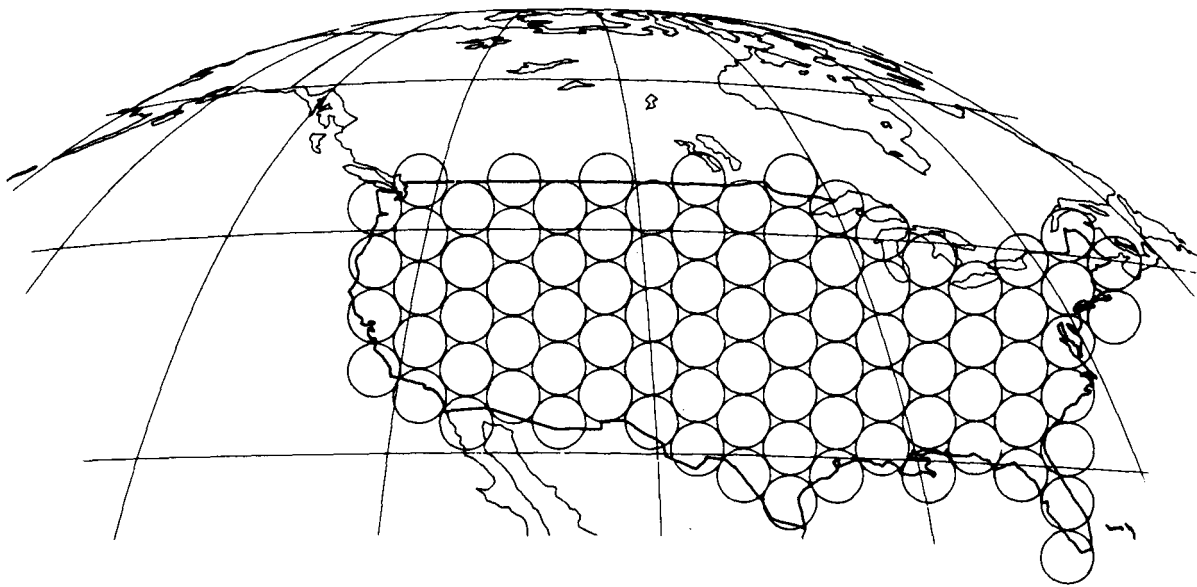
## A POSSIBLE SECOND-GENERATION MSS BEAM PATTERN

The figure shows a possible second-generation MSS beam pattern resulting from a UHF 50-ft antenna. System studies by NASA, JPL, and their contractors have indicated that the second generation will be launched in the mid-1990s, have an antenna in the range of 15 to 25 meters, and use large communications satellite buses which are already in the planning stages. Frequency reuse among the antenna beams will provide greatly expanded channel capacity for the expected limited-frequency allocation.



### A POSSIBLE THIRD-GENERATION MSS BEAM PATTERN

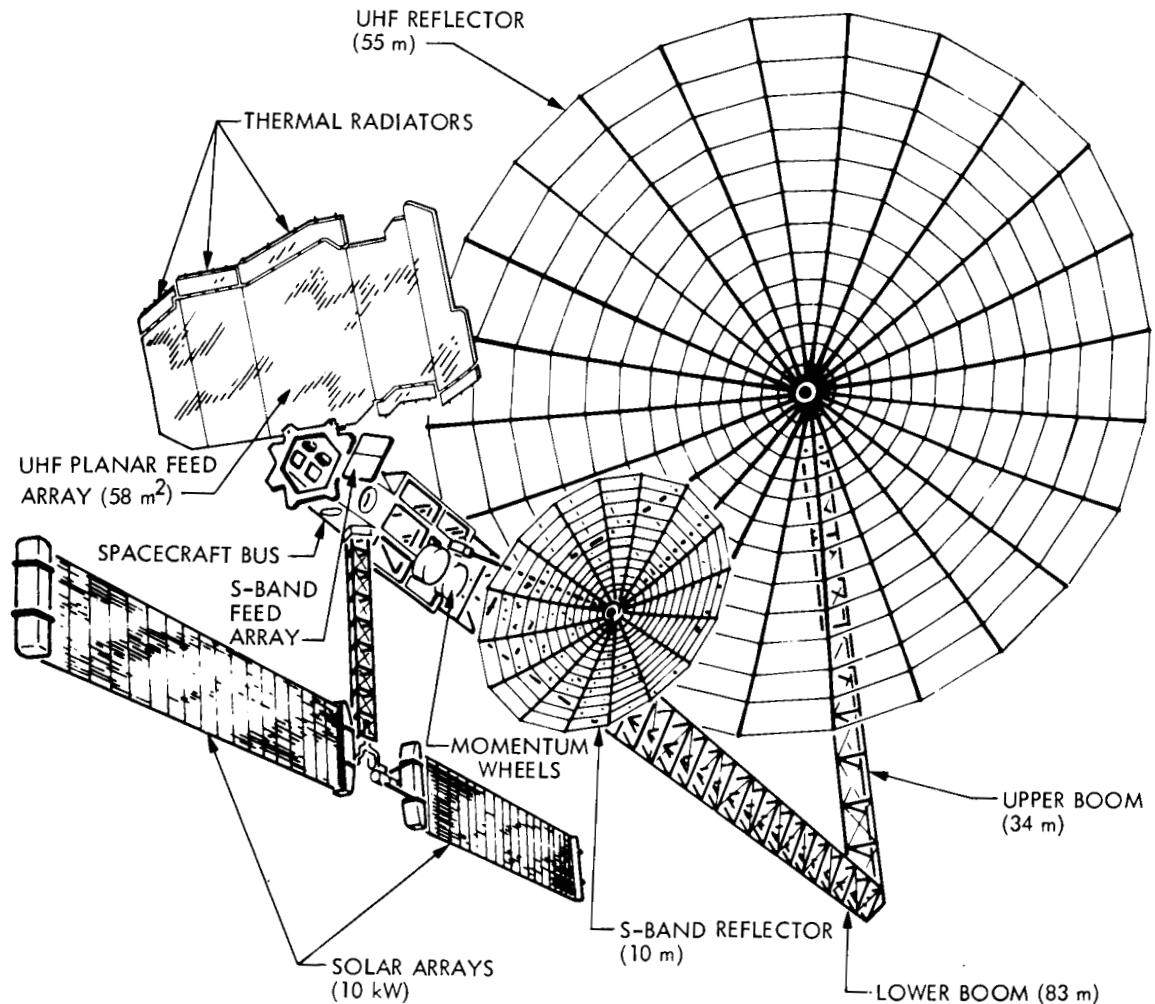
The figure shows a possible third-generation MSS beam pattern resulting from a UHF 180-ft antenna. System studies have indicated that the third generation will be launched near the turn of the century, have an antenna in the 40 to 55 meter range, and require totally new satellite design concepts. Such a system could provide affordable mobile services to hundreds of thousands, if not millions, of users.



- APPROXIMATELY 90 BEAMS
- 180-FOOT (55-m) S/C ANTENNA

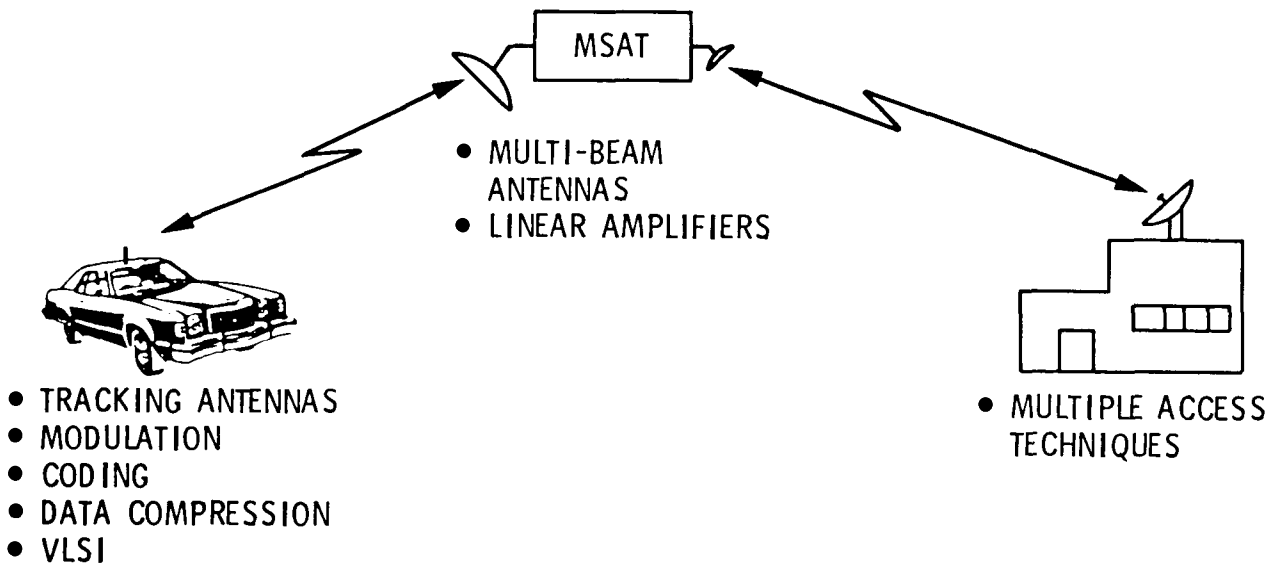
### CONCEPTUAL DESIGN OF THIRD-GENERATION MSS

The figure shows the conceptual design of a third-generation system with a 55 meter, UHF, Lockheed wrap-rib deployable antenna. The 90 beams are generated by a planar feed array and beam-forming network. In this design, UHF frequencies are used for the satellite-to-mobile communications links while S-band is used for the satellite-to-base station links.



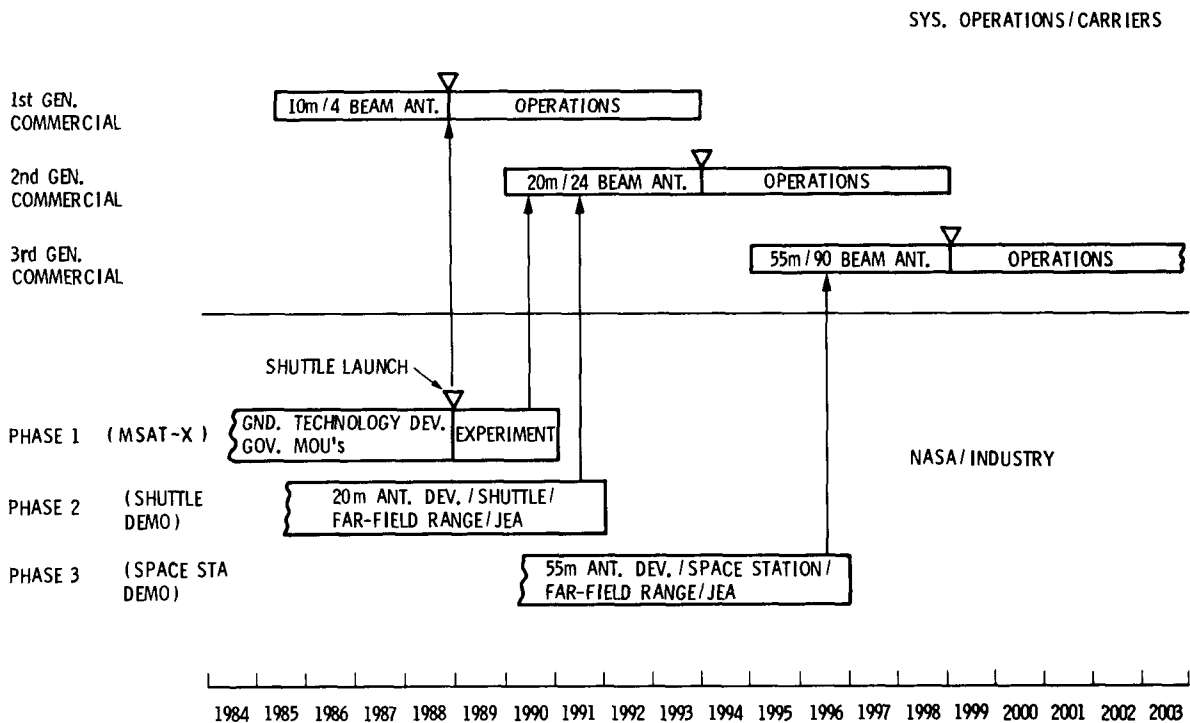
## CONSTRAINTS THAT DRIVE TECHNOLOGY

Three key resources in the development, growth, and financial viability of a mobile satellite service are satellite power, RF spectrum, and orbital slots. The high-risk technologies in the NASA development program are directed toward conserving these critical resources. Space segment technologies to alleviate these constraints are multiple-beam antennas with frequency reuse, linear power amplifiers to reduce the intermodulation problems inherent in single-channel-per-carrier MSS operation, and possibly satellite switching and on-board signal processing. Ground segment technologies include: high gain, satellite tracking mobile vehicle antennas; narrow-bandwidth and power efficient modulation techniques; coding and error correction for the fading and noisy mobile channels; speech processing and data compression; VLSI to reduce size and cost; and multiple access and networking techniques for efficient utilization of the channels. The NASA Mobile Satellite Program includes the development of all of these technologies.



## A PHASED MOBILE SATELLITE PROGRAM PLAN

The NASA program is structured in three phases to support the planned commercial launch schedule. All phases employ the Joint Endeavor Agreement (JEA) mechanism for program implementation. This approach directly supports the President's Space Policy to make NASA incentives available to commercial entities that are willing to take significant investment risks to establish and market new space services and products. Phase 1, called the Mobile Satellite Experiment (MSAT-X), is directed toward the development of ground segment technology needed for future MSS generations. Technology validation and pre-operational experiments with other government agencies will be carried out during the two-year period following launch. The satellite channel capacity needed to carry out these experiments will be obtained from industry under a barter-type agreement in exchange for NASA-provided launch services. Phase 2 will develop and flight test the multibeam spacecraft antenna technology needed to obtain substantial frequency reuse for second-generation commercial systems. Industry will provide the antenna, and NASA will fly it on the Shuttle and test it on-orbit. Phase 3 is similar to Phase 2 but will develop an even larger multibeam antenna and test it on the Space Station.

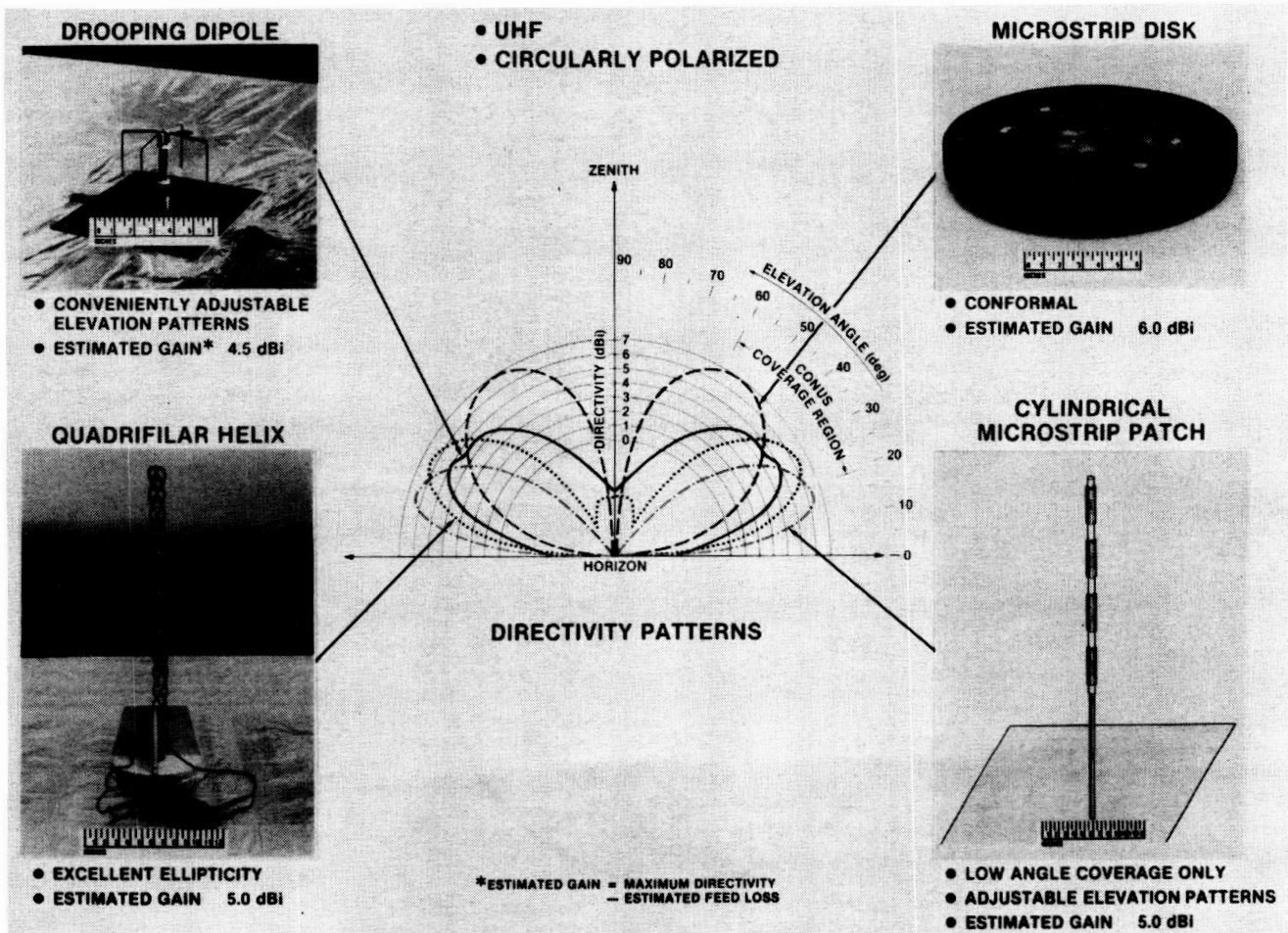




## PHASE 1/MSAT-X TECHNOLOGY DEVELOPMENT

### LOW-GAIN VEHICLE ANTENNA TECHNOLOGY DEVELOPMENT

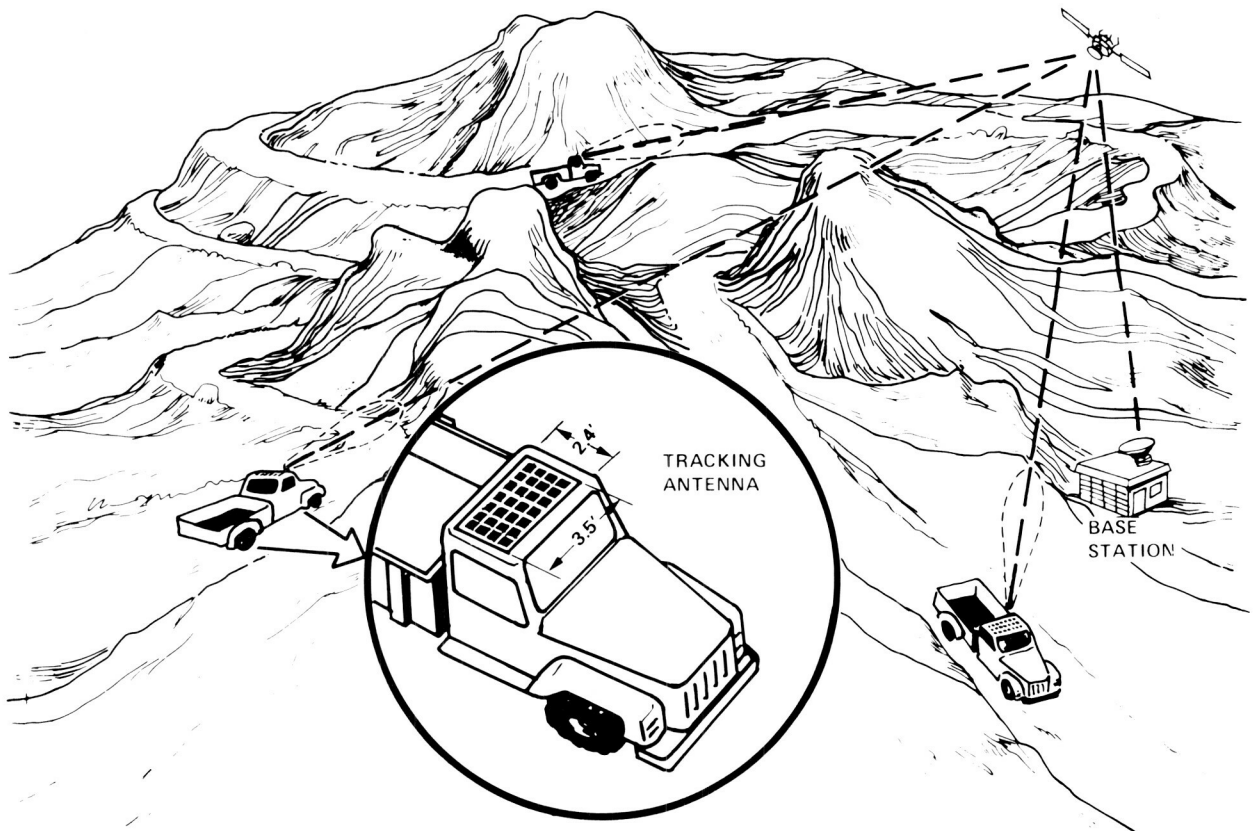
These are four low-gain vehicle antennas that have been developed in-house at JPL for MSS use. Each antenna type provides at least 4 dBi of peak gain and is omni-directional in azimuth. The individual designs differ in cost, gain, elevation angle coverage, size, and aesthetics. The first-generation MSS will employ antennas similar in design.



## PHASE 1/MSAT-X TECHNOLOGY DEVELOPMENT

### MEDIUM-GAIN TRACKING ANTENNA

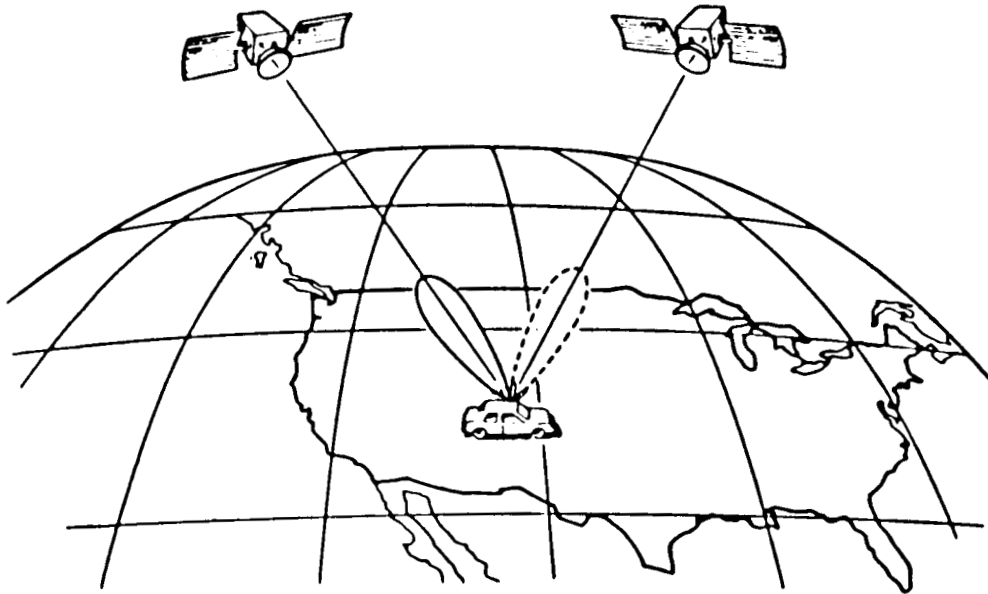
The medium-gain, satellite tracking vehicle antenna is a key technology development in the NASA program. Not only can it provide more gain, but it can also reduce the effects of multipath fading, thereby significantly reducing the power burden on the satellite. The goal of this development is an antenna with 10 dBi of gain, automatic satellite tracking in azimuth and elevation, and a low physical profile. As shown on the next page, another goal is to enable two satellite operation. Accomplishing all this at low cost will be a significant challenge.



## PHASE 1/MSAT-X TECHNOLOGY DEVELOPMENT

### MEDIUM-GAIN ANTENNA IN TWO-SATELLITE OPERATION

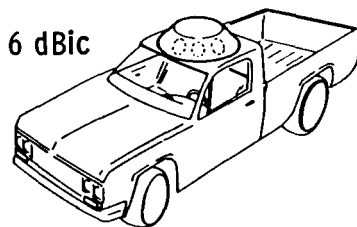
An additional goal of the medium-gain, tracking antenna is the ability to reject signals to/from a second satellite through the control of its sidelobes. Such antennas would enable a doubling of the MSS capacity through the use of two satellites operating at the same frequencies.



## PHASE 1/MSAT-X TECHNOLOGY DEVELOPMENT

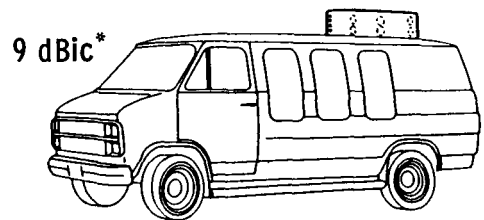
### MEDIUM-GAIN ANTENNA CONCEPTS

JPL currently has contracts with Ball Aerospace and Cubic Corporation to study concepts suitable for the medium-gain, tracking antenna. These studies seek to quantify the expected cost of these antennas as a function of antenna gain and profile. All designs have used microstrip patches. The tracking mechanisms have included mechanical steering, electronic switching, or electronic phase shifting in decreasing order of profile height, but in increasing order of cost. Future contracts will develop promising concepts to the prototype stage. These antennas will eventually be tested with the first-generation mobile satellite system as a part of the MSAT-X experiment phase.



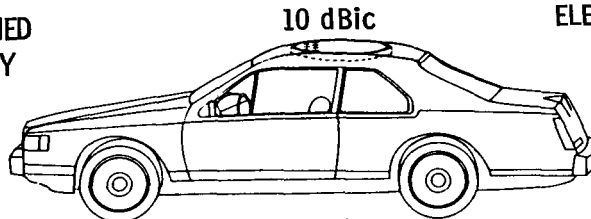
6 dBic

ELECTRONICALLY SWITCHED  
TRUNCATED CORE ARRAY



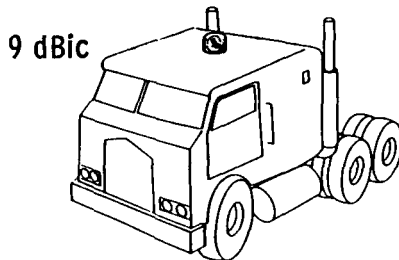
9 dBic\*

ELECTRONICALLY SWITCHED  
CYLINDRICAL ARRAY



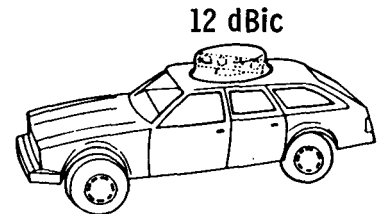
10 dBic

CONFORMAL ELECTRICALLY STEERED  
PHASED ARRAY



9 dBic

MECHANICALLY STEERED  
HELIX



12 dBic

MECHANICALLY STEERED  
TILTED ARRAY

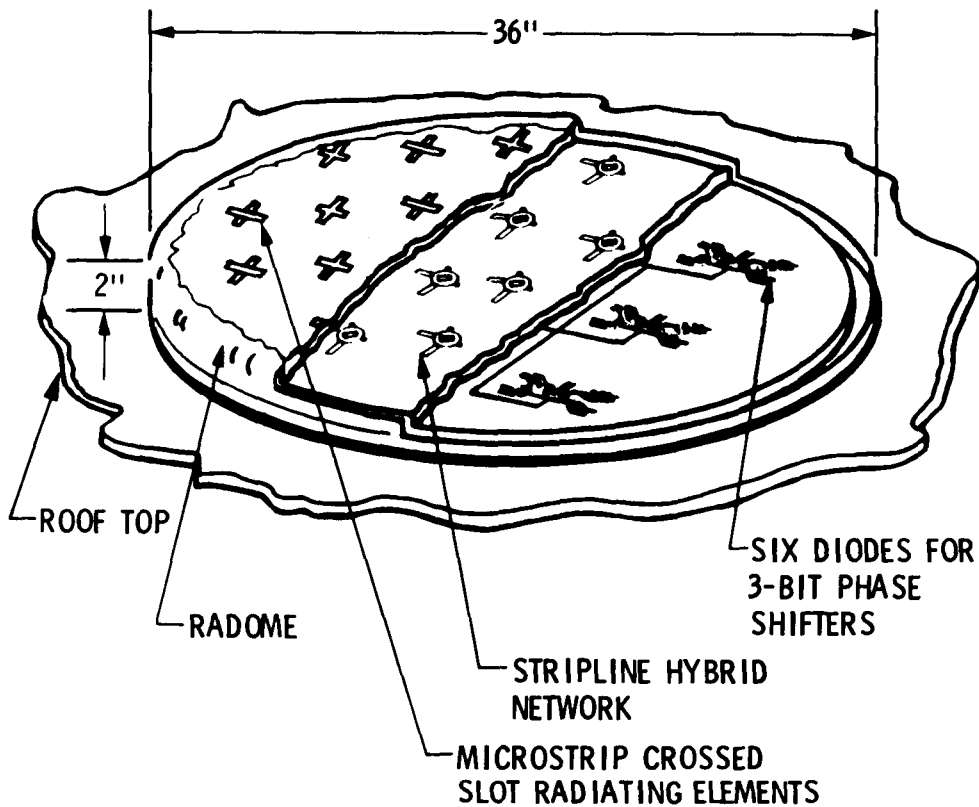
PRODUCED BY BALL AEROSPACE

\*DECIBEL ISOTROPIC CIRCULAR (dBic)

## PHASE 1/MSAT-X TECHNOLOGY DEVELOPMENT

### PHASED-ARRAY VEHICLE ANTENNA

The center concept from the previous page is further depicted in this drawing. This concept has the promise of very low profile and fully electronic operation. The expected cost at this time is, however, prohibitive. The technology challenges will be to reduce the component costs in this concept or to develop other concepts more suited to low-cost implementation.



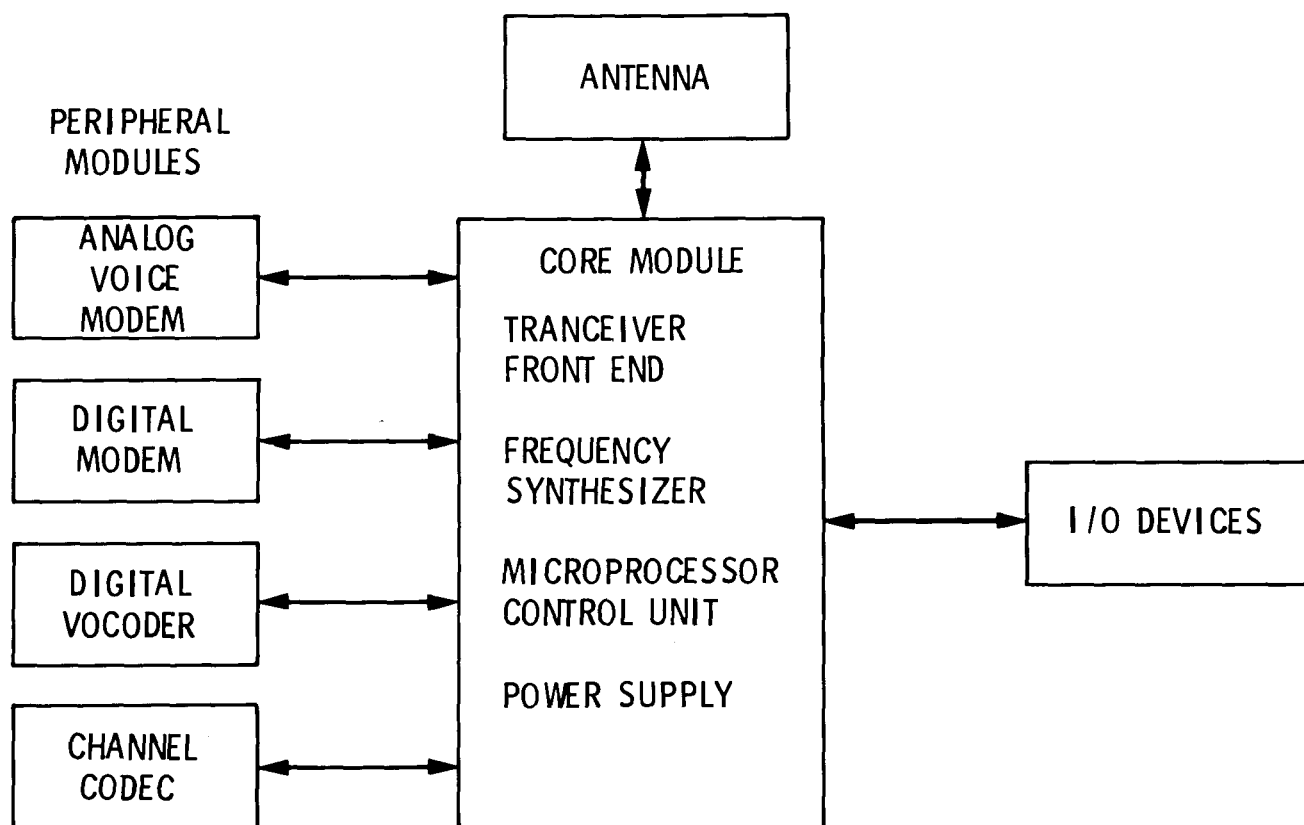
PROPOSED BY BALL AEROSPACE

## PHASE 1/MSAT-X TECHNOLOGY DEVELOPMENT

### MODULAR MOBILE RADIO TERMINALS

The MSAT-X program also includes the development of mobile radio components and technologies which will alleviate the bandwidth and power constraints for future MSS generations. Key developments will include a modular mobile radio for testing new modulation and transmission techniques with the first-generation system; narrow bandwidth analog and digital modulation techniques for voice and data transmission; coding and error correction techniques to overcome the effects of noise and fading; and digital speech processing and data compression techniques for narrow bandwidth digital voice transmission. The goal is to reduce the required channel bandwidth from the current mobile standard of 30 kHz (analog FM) to 5 kHz for both digital voice and data, while at the same time reducing the required transmitted power. In addition to the mobile terminal technologies, MSAT-X will develop networking techniques for the efficient control and management of the MSS network. Techniques addressed will include multiple-access techniques and adaptive channel assignment techniques for combined voice and variable bandwidth data. The goal is to maximize the utilization of the available channels. The experiment phase of MSAT-X will include tests with the first commercial MSS of all the MSAT-X technology developments in mobile terminals, mobile antennas, base stations, and network management techniques.

### MODULE DIAGRAM



## PHASE 1 NASA/INDUSTRY JOINT ENDEAVOR

In order to validate the advanced ground segment technology, NASA, contingent on FCC's rulemaking and regulatory process, intends to enter into a Joint Endeavor Agreement with private industry. The joint endeavor between NASA and the owner/operator of the first commercial mobile satellite system will be based on a barter-type agreement under which the US entity or system operator would supply a percentage of the satellite channel capacity to NASA for the advanced technology validation and other government agency pre-operational experiments in exchange for NASA-provided launch services. (NASA has already signed Memoranda of Understanding with six other government agencies in anticipation of their participating with NASA in these technology validation and pre-operational experiments.) The US system operator, possibly in conjunction with its Canadian counterpart, i.e. Telesat, would specify, procure, own, and operate the space segment. This approach has precedent and is supported by US industry.

- NASA PROVIDES STANDARD LAUNCH SERVICES
- U. S. SYSTEM OPERATOR SUPPLIES CHANNEL CAPACITY
- NASA USES CHANNELS FOR
  - GROUND TERMINAL TECHNOLOGY VALIDATION FOR 2nd-GENERATION SYSTEMS
  - SUPPORT OTHER GOVERNMENT EXPERIMENTERS

## PHASE 2/3 PROGRAM GOAL

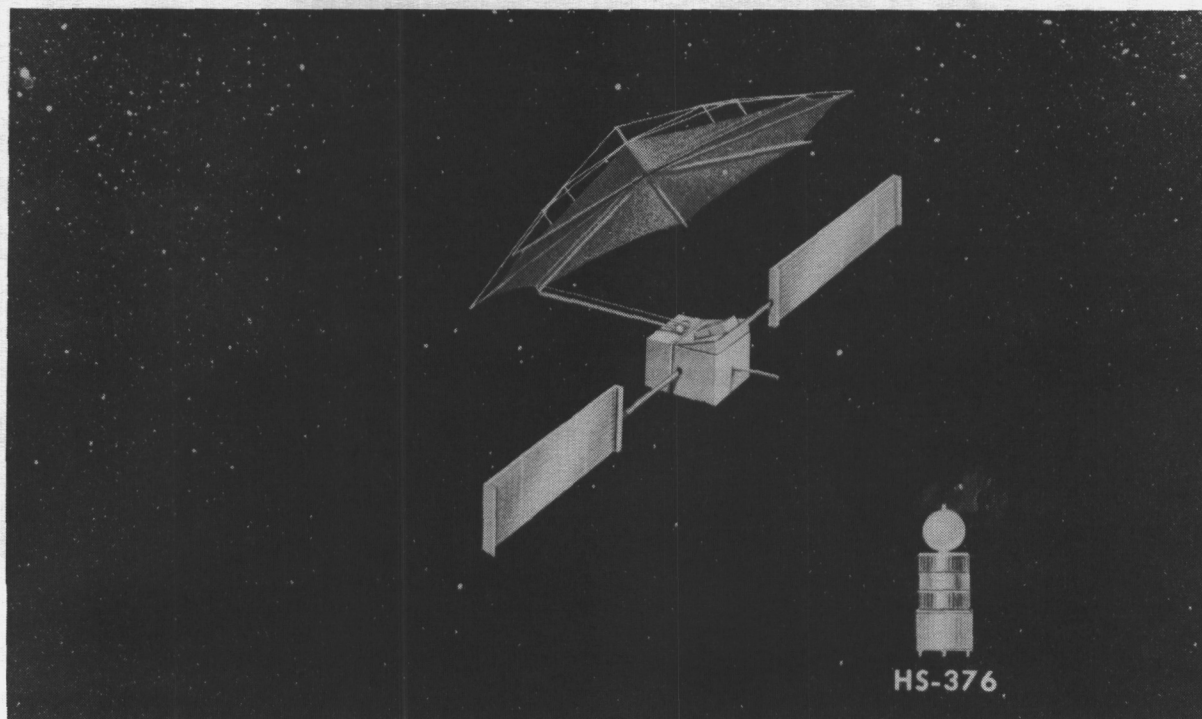
The second and third phases of NASA's program are to provide the critical enabling technology of spacecraft multibeam antennas required for second- and third-generation MSS. Antennas of this type are able to reuse the limited frequency resource four to twenty times and reduce RF power per channel requirements by factors of 10 to 100 or more over that of a first-generation system. This magnitude of increased performance will allow satellite capacity to grow in accordance with expected market demands and will decrease user costs. Further, it will make possible adding a higher proportion of high resource services such as mobile telephones. Phase 2 will emphasize the development and flight test on the Shuttle of the antenna system for the second-generation MSS, while Phase 3 will emphasize the development of the third-generation antenna with a flight test on the Space Station.

PROVIDE THE CRITICAL ENABLING  
SPACECRAFT MULTI-BEAM ANTENNA  
TECHNOLOGY REQUIRED FOR THE SECOND- AND  
THIRD-GENERATION MOBILE SATELLITE  
SYSTEMS



## A SECOND-GENERATION MOBILE SATELLITE

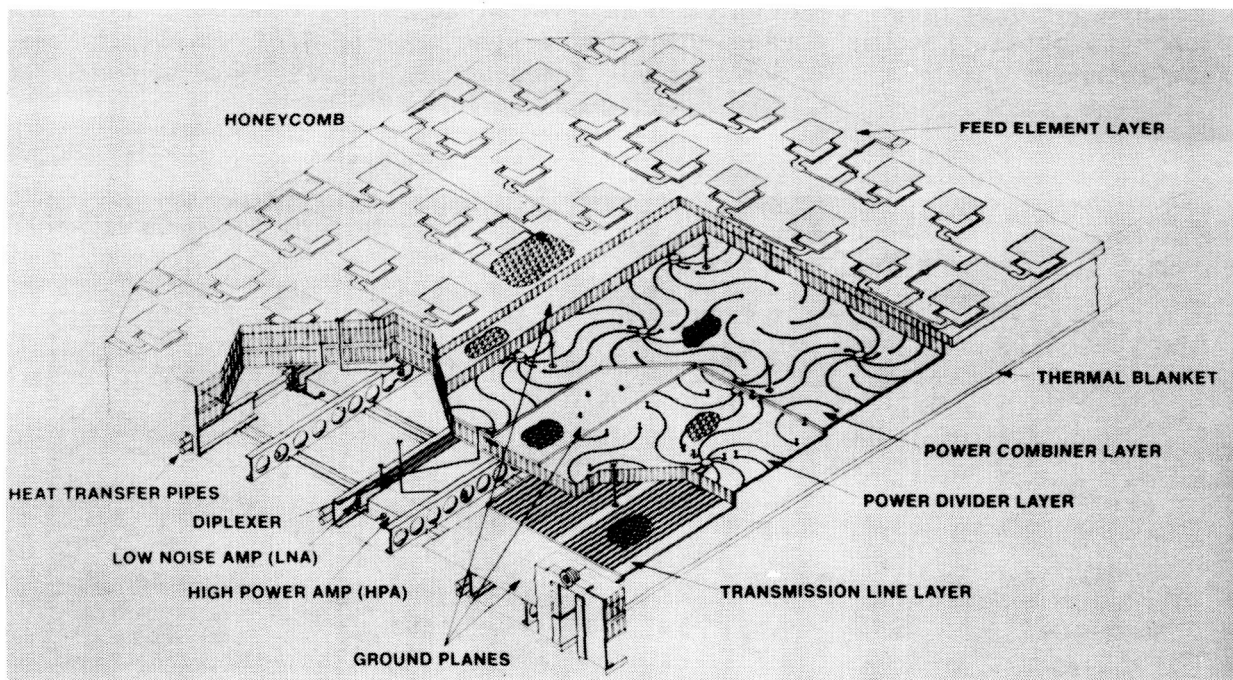
A candidate second-generation antenna system might include a 20-meter reflector and a multiple-beam feed array producing 24 beams for the US and Canada. This beam pattern allows the available band of frequencies to be reused about six times. A spacecraft with this type of antenna might weigh 2500 pounds on-orbit with a prime power capability of about 3.5 to 4.5 kW. The Hughes HS-376 spacecraft is shown for size comparison. Clearly the antenna system dominates the satellite and is the key technology to enable the second-generation satellite. In the RF area, the key aspect of the antenna development is the multiple-beam feed array and the beam-forming network (BFN) which distributes the signals to the feed array elements. The feed array and BFN must: be lightweight; transmit and receive simultaneously with a 5% frequency separation; provide multiple beams with sufficiently low sidelobes to enable frequency reuse; and maintain its performance through the thermal and dynamic distortions in the space environment. The challenges in the mechanical and structural areas of the antenna include the reflector, the booms and masts between the spacecraft bus and the reflector and feeds, and the feed array assembly itself. Each of these components must deploy properly, achieve reflector/feed alignment and surface accuracy, be lightweight yet be rigid during control system maneuvers, and maintain tolerances through thermal variations. The demand for low sidelobes to obtain frequency reuse dictates a precision of 1/60 wavelength rms surface accuracy which implies 6 mm at UHF frequencies.



## PHASE 2 TECHNOLOGY DEVELOPMENT

### MSS INTEGRATED PLANAR FEED ARRAY

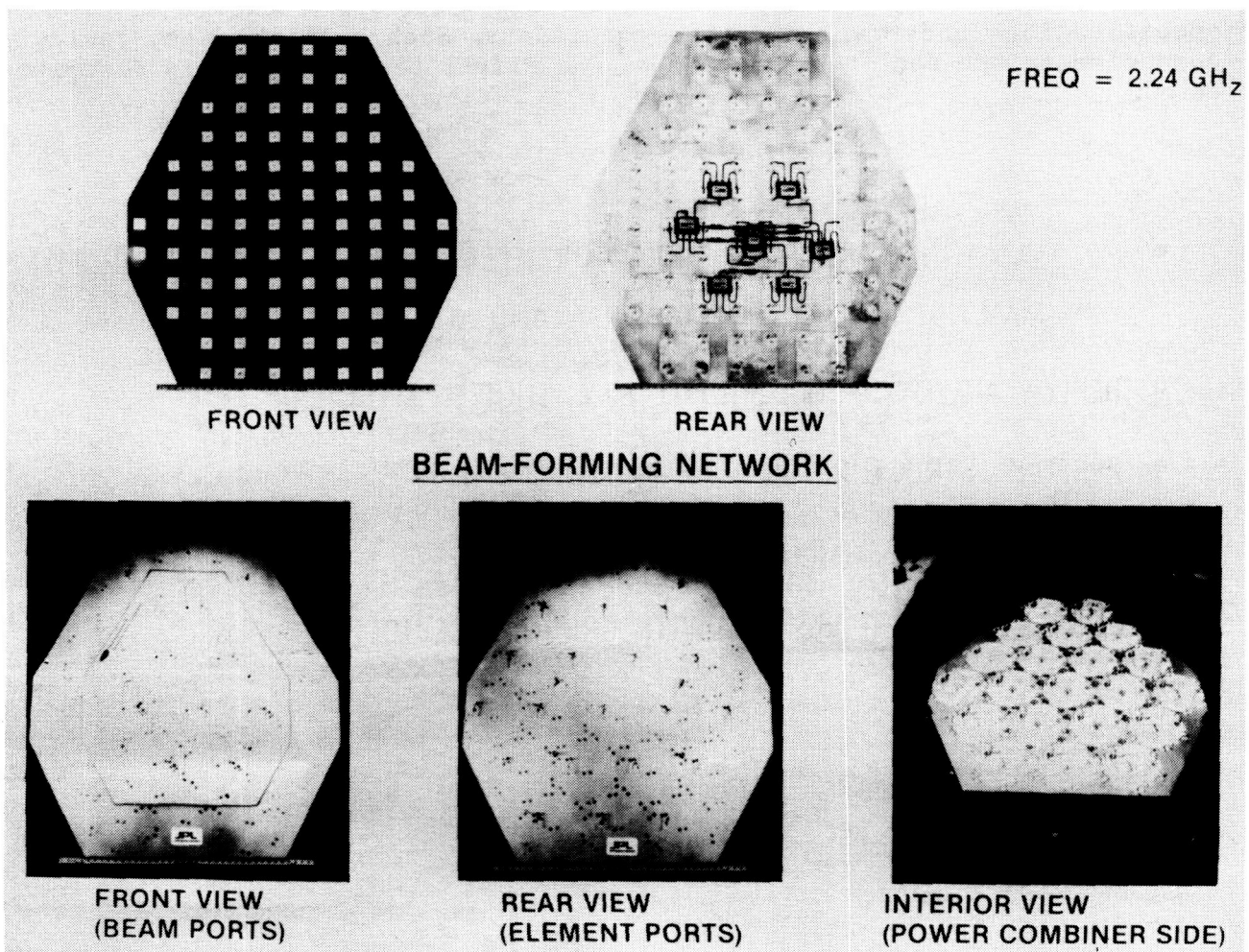
A key element in the antenna system is the multibeam feed array. The accompanying chart shows a cutaway drawing of the assembly. The top layer contains the microstrip feed elements. Four patches form a sub-element and seven sub-elements form a cluster which produces a single beam. The design uses over-lapping cluster feeds where adjacent beams may share 4 sub-elements. Using this concept, one can synthesize feeds with large, effective apertures, resulting in low sidelobes, yet solving the feed packing problem in the tight space available in the focal plane. The beam-forming network is formed from an intricate network of microstrip layers. The electronics, i.e., HPA's, LNA's, and diplexers, are also housed in the feed-array assembly as can be seen in the chart.



## PHASE 2 TECHNOLOGY DEVELOPMENT

### EIGHT-BEAM OVERLAPPING CLUSTER FEED

Currently, JPL is implementing an eight-beam breadboard based on the conceptual design on the previous page. The breadboard will consist of the microstrip feed array and the matching beam-forming network. The beam-forming network has been fabricated by Ford Aerospace. To reduce the physical size of the breadboard the feed was designed to operate at S-band. When completed and tested, this breadboard feed will be further tested with the 15-meter deployable reflector developed by NASA/Langley and the Harris Corporation.



## PHASE 2 TECHNOLOGY DEVELOPMENT

### ANTENNA FLIGHT TEST

Ground testing of an entire 20-meter, second-generation MSS antenna system to predict system performance on-orbit is possible but would be extremely difficult and expensive, and the results may be of dubious value. A flight test of the entire antenna system would greatly reduce the risk and uncertainty of launching such an antenna and would at the same time validate ground test procedures for future antenna systems. The NASA Shuttle is ideally suited for performing the majority of 0-g, dynamic, and thermal tests required to space qualify this antenna system. The broad objectives of this second-generation MSS antenna flight test are: demonstrate the reliable deployment of the antenna system structure; measure the aperture precision and feed alignment; measure the thermal and dynamic structural characteristics of the entire antenna system; and verify through RF measurements that the antenna meets all predicted performance specifications under all expected conditions. Such a flight test could be conducted by the end of the decade. One flight test scenario is described below.

- FLY FULL ANTENNA SYSTEM (REFLECTOR, FEEDS, BOOMS, ETC.) ON SHUTTLE
  - MAY NOT NEED FULL FEED ARRAY AND ALL BOOMS
- DEPLOY ANTENNA FROM SHUTTLE BAY (SHUTTLE ATTACHED)
- PERFORM STRUCTURAL AND RF MEASUREMENTS
- REFURL ANTENNA - RETURN WITH SHUTTLE
- CORRELATE FLIGHT RESULTS WITH GROUND PREDICTIONS

## PHASE 2 TECHNOLOGY DEVELOPMENT

### FLIGHT TEST ANTENNA SPECIFICATIONS

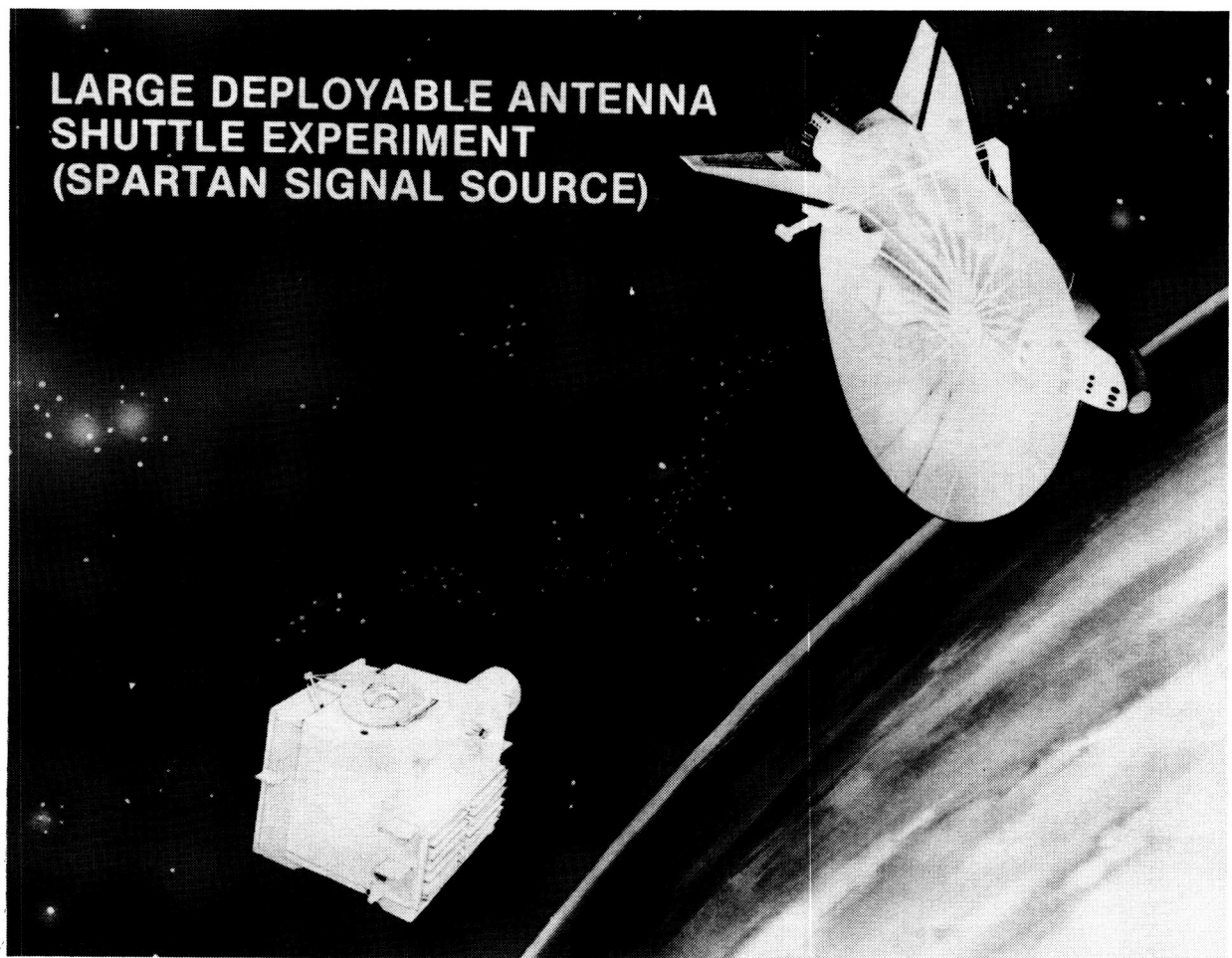
The flight test antenna, to be of value for the second-generation MSS, must have the minimal specifications listed below. L-band is included as a candidate growth frequency for MSS. Ideally the test feed should have at least two beams at both UHF and L-band, one boresight feed and one off-axis feed at each frequency.

- 20-m OFFSET-FED DEPLOYABLE ANTENNA
- $F/D = 1.0 - 1.5$
- RMS SURFACE ERROR
  - 3 mm FOR L-BAND
  - 6 mm FOR UHF
- BEAM ARRANGEMENTS
  - MULTIPLE BEAMS
    - AT LEAST 2 BEAMS

## PHASE 2 TECHNOLOGY DEVELOPMENT

### FLIGHT TEST WITH SPARTAN SPACECRAFT

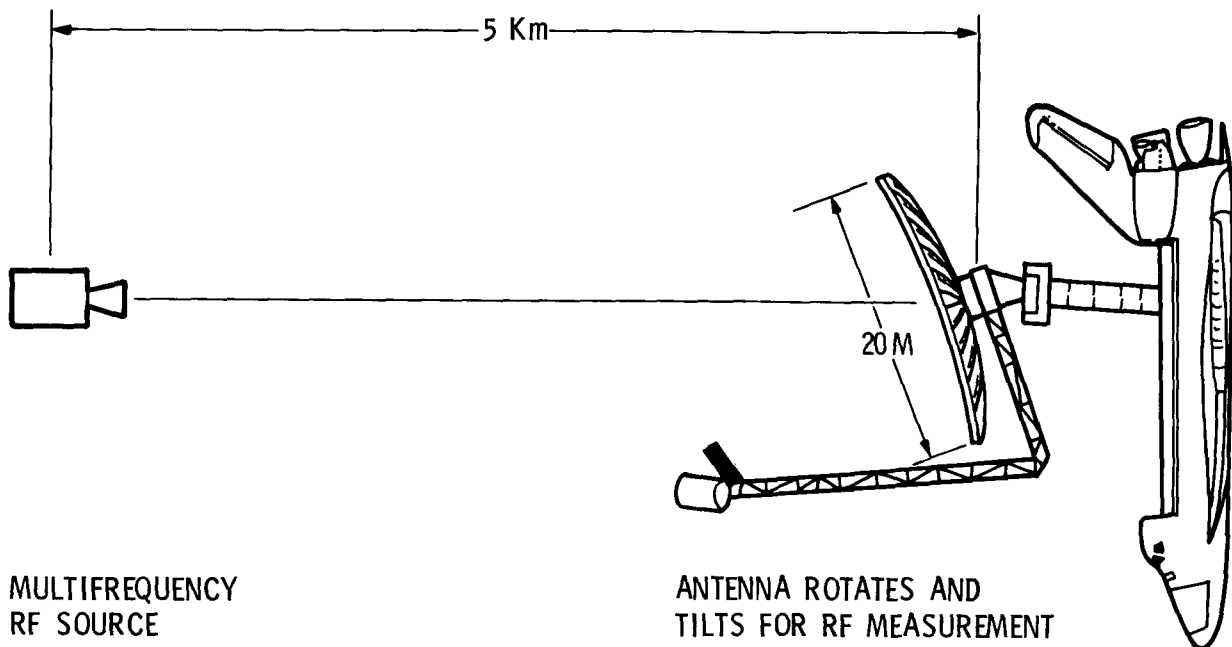
One possible configuration for the flight RF far-field performance tests is depicted below. The Spartan is a reusable and retrievable spacecraft under development at NASA Goddard. For the antenna flight tests the Spartan payload could include an RF beacon and be positioned at 5 km from the Shuttle. Following RF tests the Shuttle would retrieve the Spartan and return it and the refurled antenna.



## PHASE 2 TECHNOLOGY DEVELOPMENT

### RF FAR-FIELD MEASUREMENTS

The Spartan could be positioned at 5 km from the Shuttle for the far-field measurements at both UHF and L-band. The antenna would require articulation in azimuth and elevation about its attachment point, or some other movement mechanism, to obtain the beam patterns.





## PHASE 2 TECHNOLOGY DEVELOPMENT

### NASA/INDUSTRY JOINT ENDEAVOR ON FLIGHT TEST

The second-generation antenna is technology intended for use by the private sector. NASA's new space commercialization program was formed to assist industry develop this type of technology through cooperative development programs when such development is of benefit to both NASA and industry. A suggested split of responsibilities in this endeavor is as follows. Industry would be responsible for the design, development, and implementation of the flight test antenna. NASA would be responsible for: the design, development, and implementation of an on-orbit test facility including the possible use of the Spartan spacecraft; Shuttle integration and launch of the test article; on-orbit tests of the test antenna including all instrumentation and data reduction; and, as appropriate, other technology tests and experiments, including alternative feeds. If possible, the antenna will be refurled on-orbit and returned to the manufacturer.

- INDUSTRY (ANTENNA MANUFACTURER)
  - DESIGN, DEVELOP AND FABRICATE ANTENNA SYSTEM FLIGHT PROTOTYPE
- NASA
  - DESIGN, DEVELOP AND FABRICATE ON-ORBIT TEST FACILITY
  - LAUNCH ANTENNA ON SHUTTLE
  - PERFORM ON-ORBIT TESTS, REDUCE DATA AND TRANSFER TO INDUSTRY



## SUMMARY

NASA, industry, the FCC, and Canada have increased their efforts to enable the commercialization of the mobile satellite service by the end of the decade. NASA has served as the focal point in the many areas of this development process. NASA has defined a three-phase program of development of ground and space segment technologies which will enhance and enable the second and third generation mobile satellite systems. NASA is prepared to enter into a joint endeavor with industry to acquire channel capacity on the first commercial system for the purpose of conducting advanced technology experiments and for the use of other government agencies. NASA is also prepared to enter into a joint endeavor with industry to build and flight test on the Shuttle a second generation MSS antenna system.

**Page intentionally left blank**

ALTERNATIVES FOR SATELLITE SOUND BROADCAST SYSTEMS  
AT  
HF AND VHF

Bruce E. LeRoy  
NASA Lewis Research Center  
Cleveland, Ohio

Large Space Antenna Systems Technology - 1984

December 4-6, 1984

NASA and the United States Information Agency (USIA) are currently engaged in a joint program to assess the technical and economic feasibility of direct sound broadcast satellite systems to meet USIA mission needs. A Memorandum of Agreement (MOA) initiating the activity was signed by the Agency administrators in March of 1983. The MOA calls for a series of interrelated studies to provide the respective Agency managements with information on the potential role of direct broadcast satellites. As shown in figure 1, initial studies focused on HF propagation phenomena and broadcast coverage requirements. These studies, completed in early 1984, served as the basis for parallel systems studies currently in progress. The systems studies are to provide a data base on various satellite configurations and systems concepts capable of supporting potential broadcast requirements ranging from a small fraction to a substantial addition to USIA requirements. NASA LeRC is managing the systems study contracts (TRW and Martin Marietta), which will be completed in mid 1985. NASA LeRC is supporting USIA/Voice of America in the assessment of future receiver populations and the cost effectiveness study.

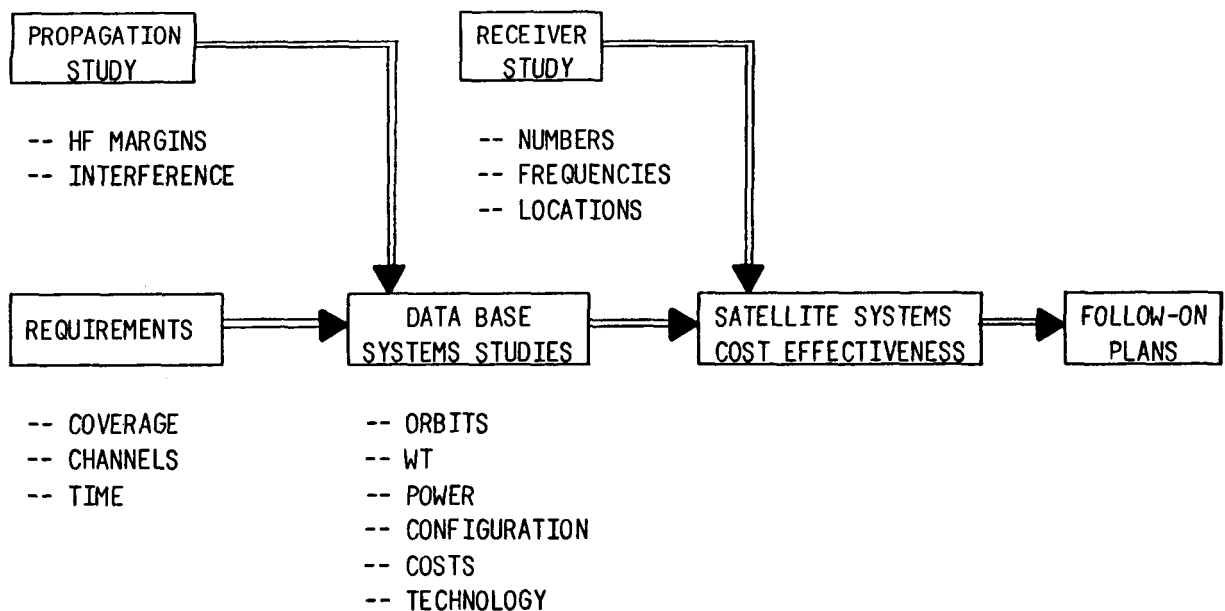


Figure 1. Phased program approach.

The scope of the data base systems studies is quite large, covering systems operating at HF (15 - 26 MHz), VHF (60 MHz), L-band (1.5 GHz), and Ku-band (12 GHz). Geographical coverage ranges from single small countries to nearly worldwide. Except for Ku-band, power requirements vary over two orders of magnitude, and consequently, low Earth orbits (LEO) are considered for the lower frequency systems where launch constraints prohibit geostationary satellites.

Figures 2 and 3 indicate typical link parameters for HF and VHF geostationary satellites. Under the assumptions indicated, a net transmit power of 10 kW into a 270 m apperture is required to produce a single audio channel in a 3° beam at 26 MHz. Under normal conditions, such a signal is of "reasonable" quality when received by a commercial grade receiver in suburban areas. If ionospheric scintillation is present, however, deep fades may occur which render the signal useless. At VHF, power and antenna requirements are halved and scintillation is much less a problem.

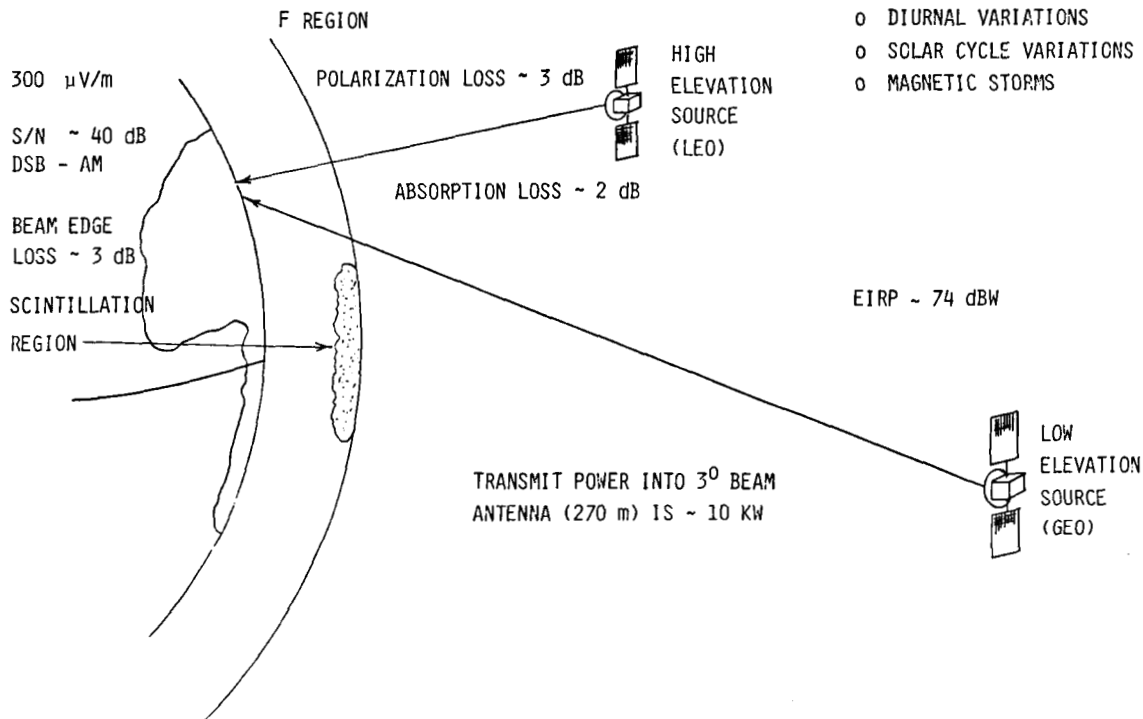


Figure 2. HF link analysis (26 MHz).

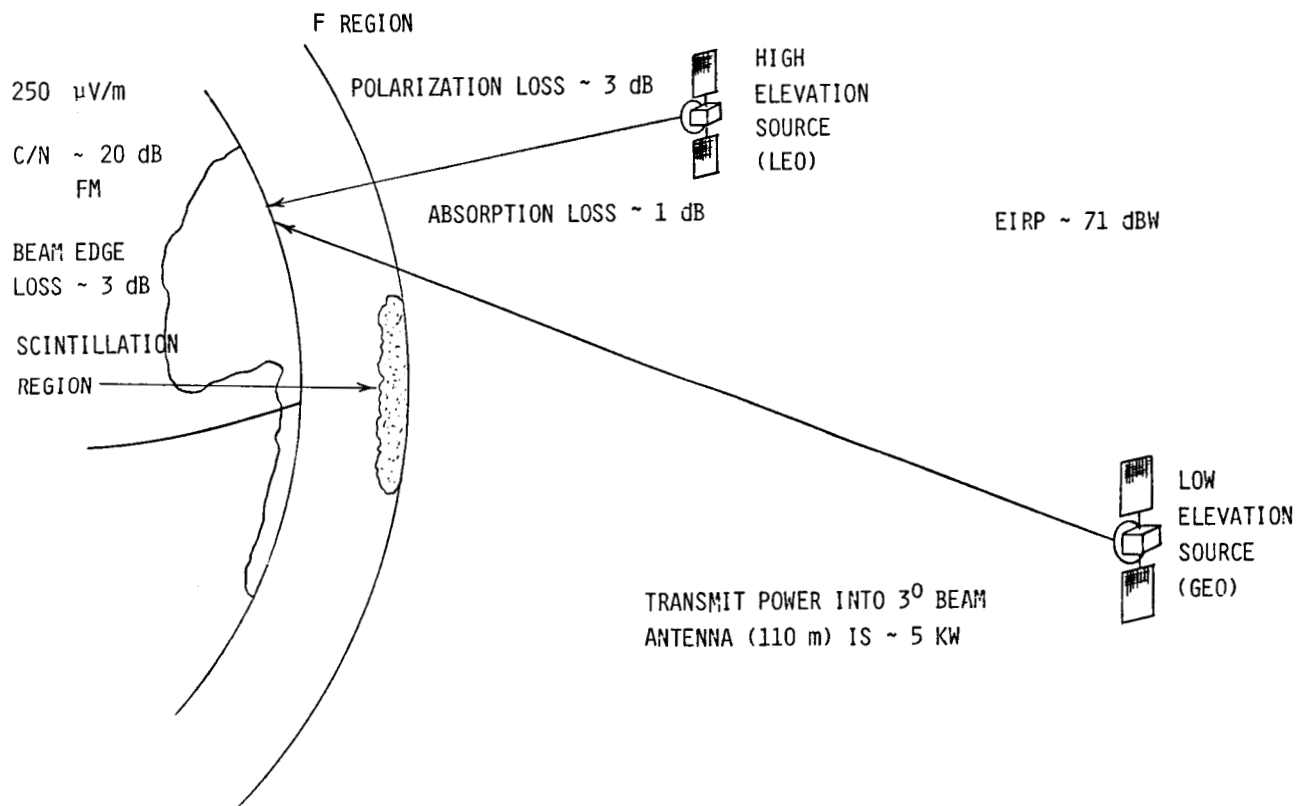


Figure 3. VHF link analysis (60 MHz).

For both HF and VHF systems, LEO and GEO orbits present distinct advantages and disadvantages. While GEO orbits permit continuous contact with the target broadcast area, ease of program uplink, and manageable solar array degradation, such orbits also require extremely large antennas, may not be capable of providing a signal to latitudes beyond  $+50^\circ$ , and due to launch constraints, have very little capacity. Alternatively, inclined low Earth orbits permit smaller antennas, increased channel capacity per satellite, and can cover all latitudes. However, the use of such orbits presents operational problems in uplinking program material, steering broadcast beams and solar arrays to the desired orientations, allows only limited contact time, and presents a more severe radiation environment. These general trends are depicted in figures 4 and 5. Note that for constant area coverage, broadcast power is a constant. Note also that while LEO orbits require a smaller antenna, they require more prime power than GEO orbits due to radiation damage effects.

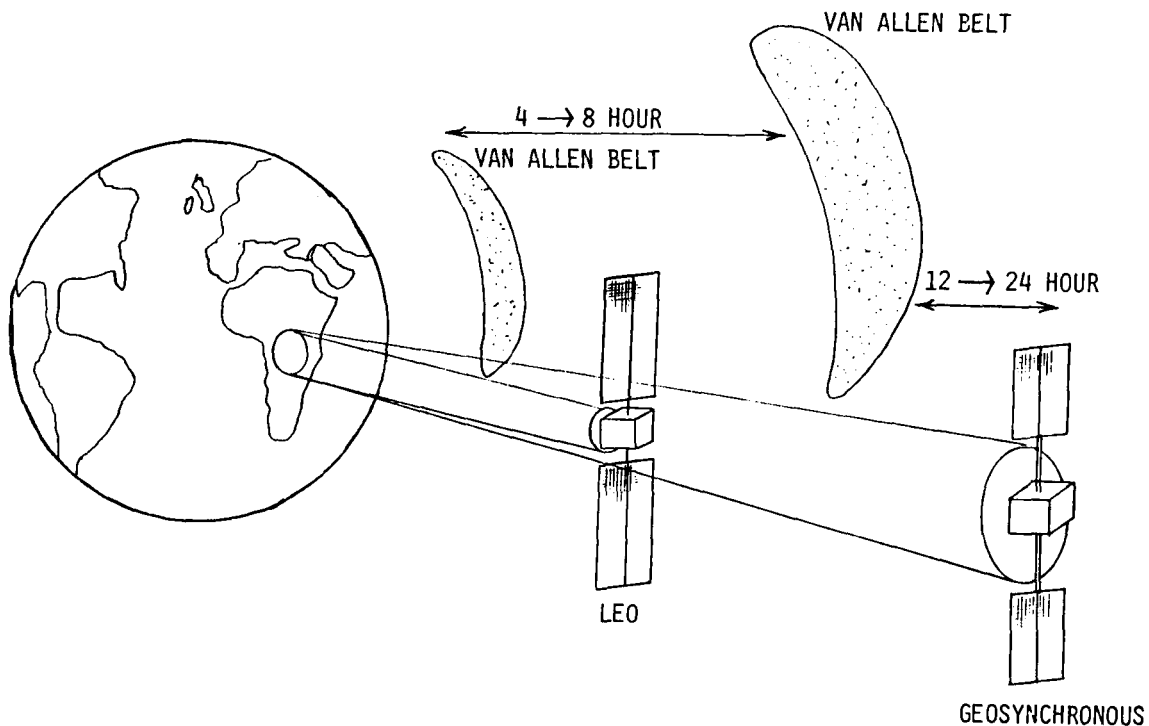
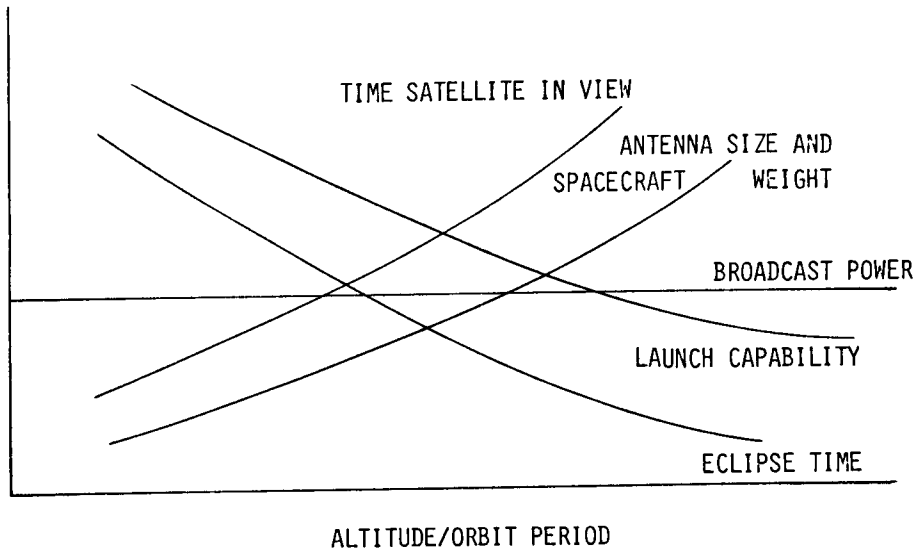


Figure 4. Impact of orbit period.

(FOR CONSTANT AREA COVERAGE)



(FOR CONSTANT SATELLITE ANTENNA SIZE)

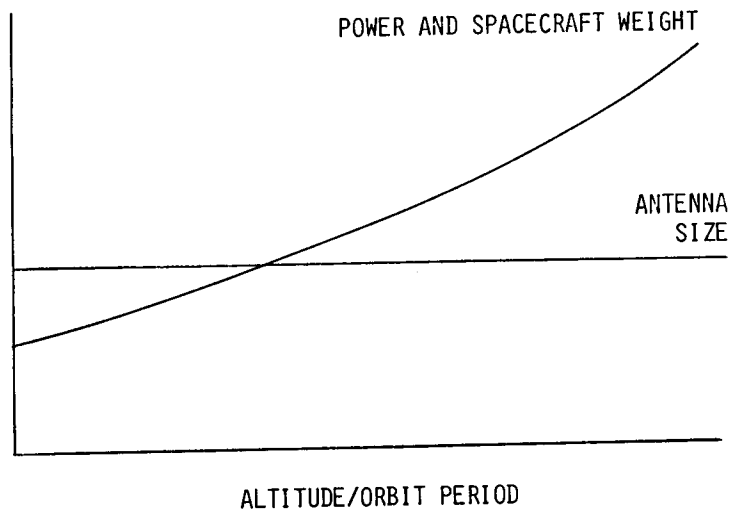


Figure 5. General trade-off trends.



Figure 6 below depicts the required antenna aperture sizes for constant area coverage as a function of orbit altitude. In practice, apertures used by LEO satellites are larger than those indicated to compensate for beam spreading as the beams are steered away from the sub-satellite point.

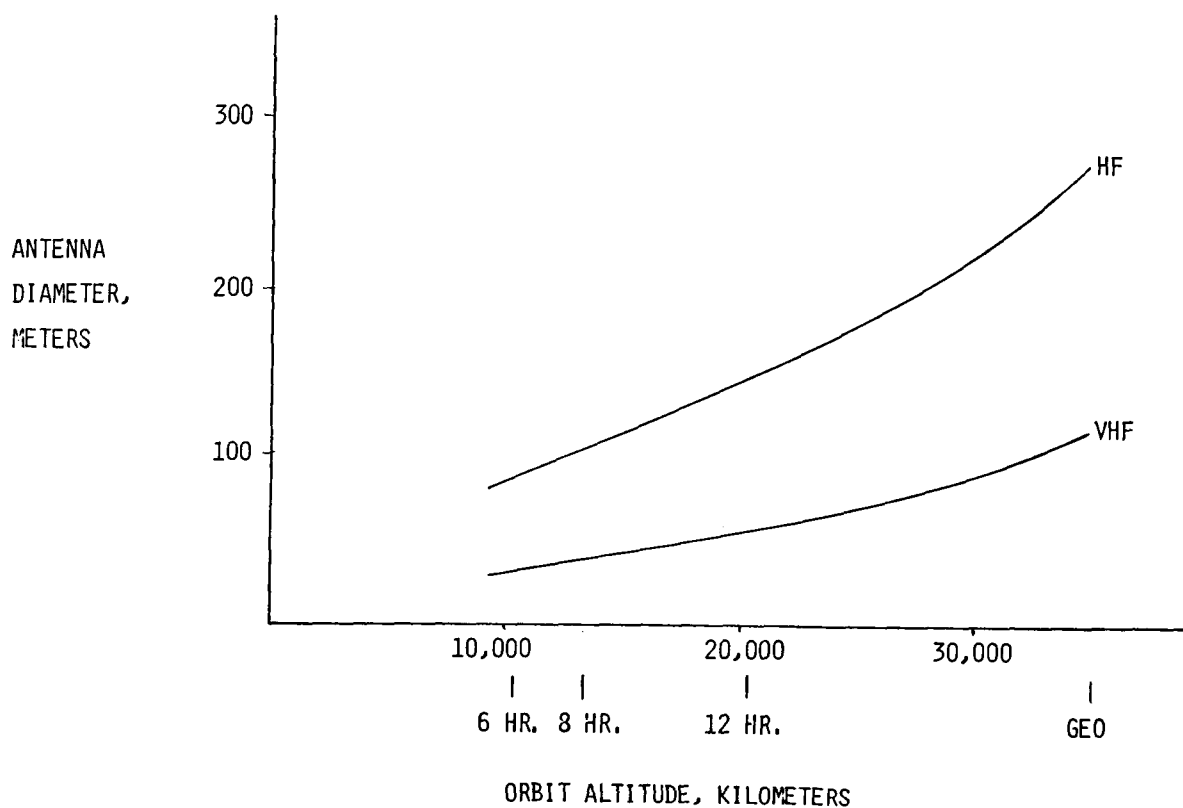


Figure 6. Antenna diameter versus altitude equivalent  $3^\circ$  beamwidth.

Figures 7 through 11 depict antenna concepts developed by our contractors, TRW and Martin Marietta. The TRW LEO concept (figs. 7 and 8) uses high gain (10 - 11 dB) elements in a square phased array to reduce overall aperture size. The TRW GEO concept (fig. 9) uses their cable-catenary antenna. The Martin Marietta LEO concept (figs. 10 and 11) is based on the box truss ring structure. A variable aperture approach is used to illuminate various target broadcast zones differing in apparent size at the satellite. This approach requires transmitters to operate at various power levels as the effective aperture is changed.

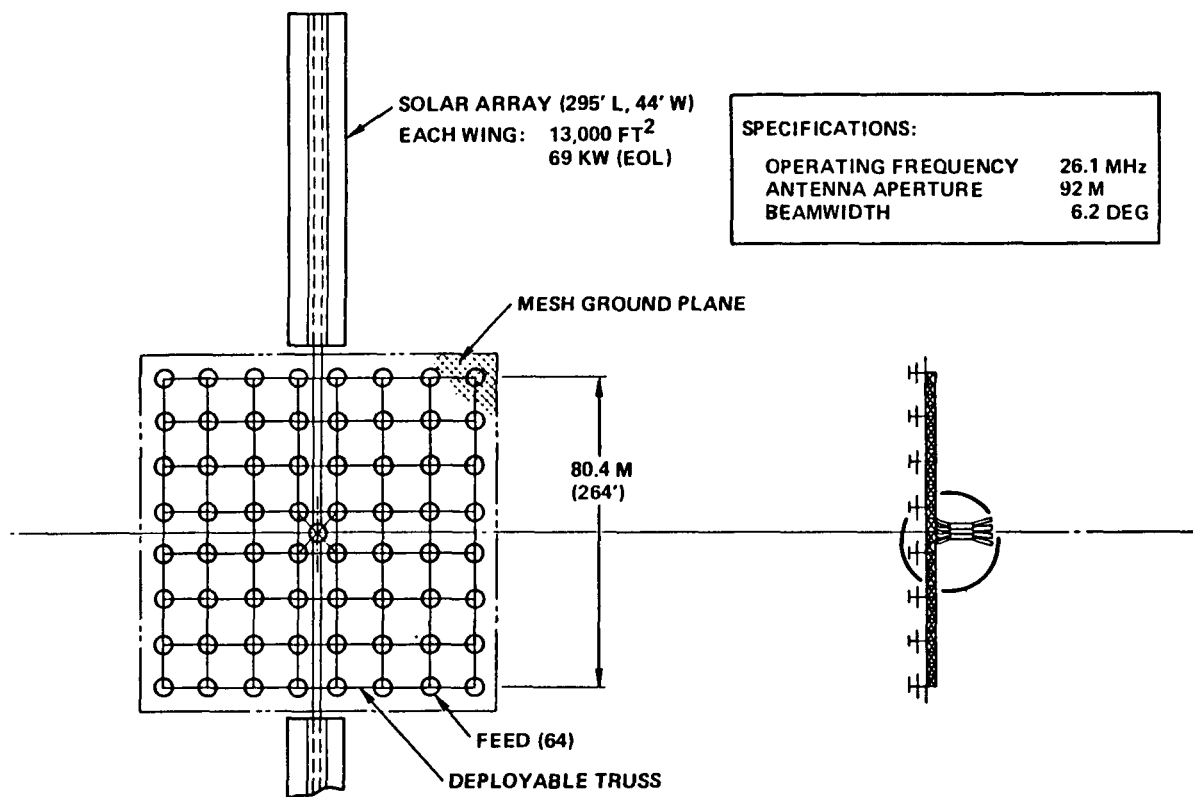


Figure 7. Satellite concept for 8-hr orbit.

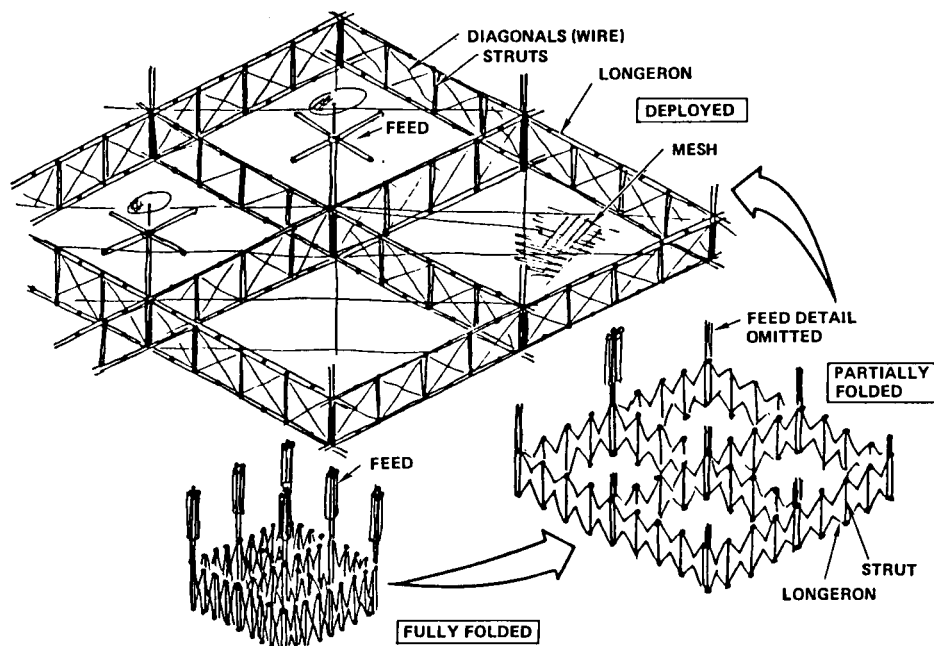


Figure 8. Cross-beam structure stowage and deployment.

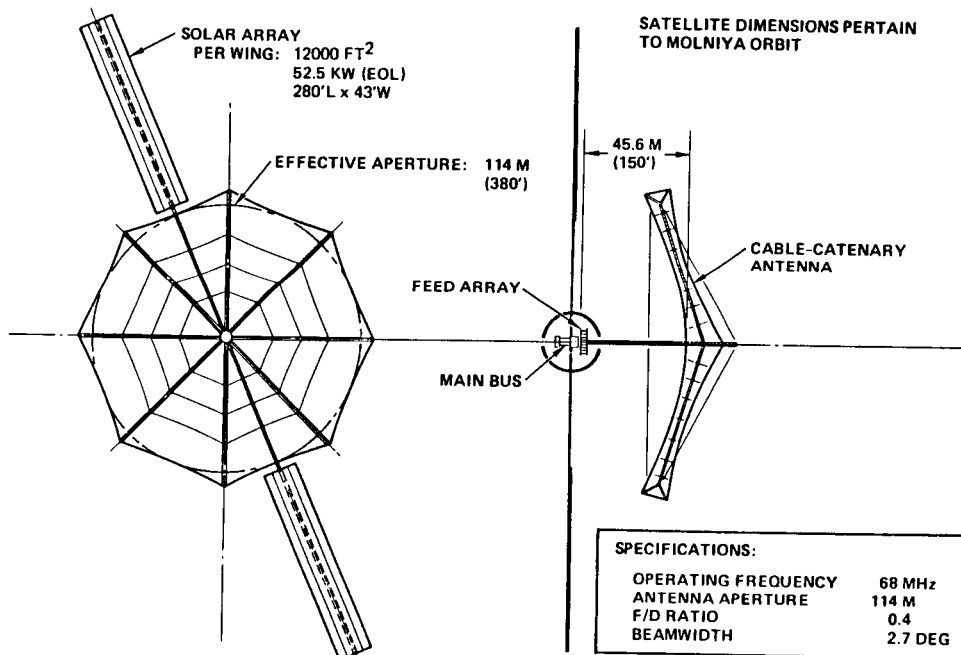


Figure 9. Satellite concept for Molniya and geostationary orbits.

- PHASE ARRAY USING INDIVIDUAL TRANSMITTER FOR DIPOLE RADIATING ELEMENT
- BOX TRUSS RING SUPPORTS ARRAY SURFACE
- TYPICAL 26 MHZ DESIGN (SECTION VIEW)

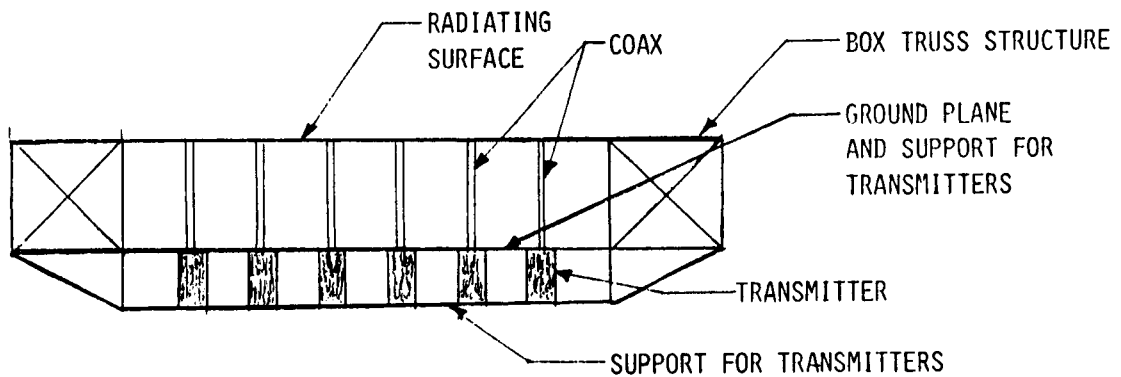


Figure 10. LEO antenna concept.

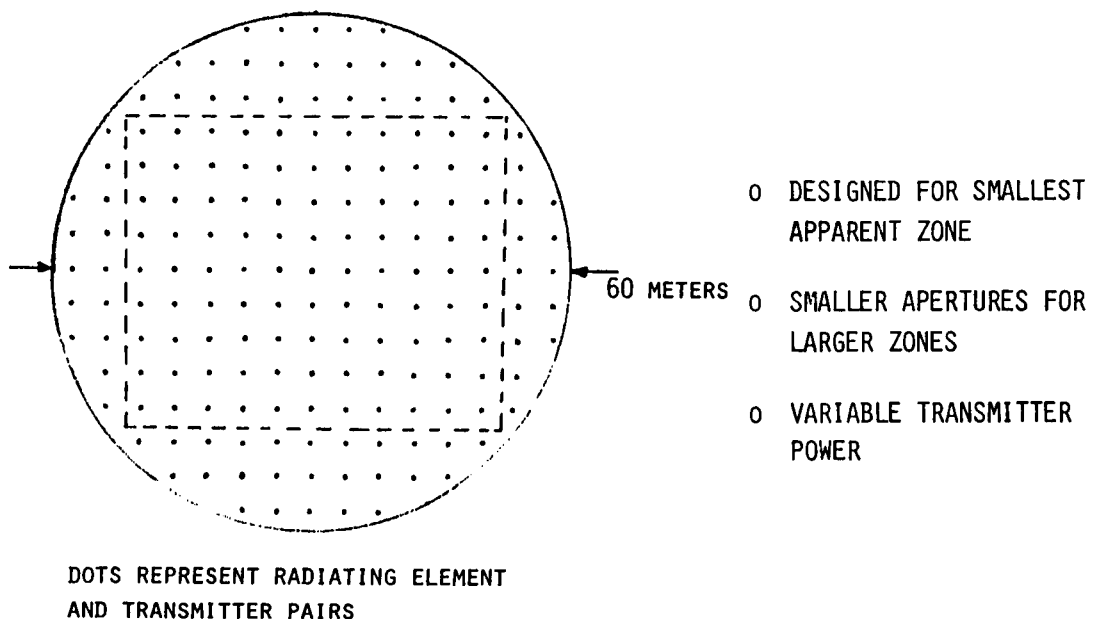


Figure 11. Variable aperture approach.

Obviously, the satellite concepts present technology challenges, particularly in the areas of power generation, handling and distribution, antenna system size, RF power handling, and electric and physical control. At LEO, a particular concern is high-power-plasma interaction.

Most HF and VHF configurations studied to date have been quite large and expensive, consuming full Shuttle-Centaur capability. An HF concept closer to current state of the art is depicted in figure 12. Such a satellite would provide limited service at very low signal strength--but may be an appropriate first-generation concept.

Finally, note that the concepts--as technically intriguing as they are--are only part of a data base. That data base will be used along with other technical, economic, political, and regulatory information to address the broader issue of whether, in fact, satellites offer the USIA a cost-effective means of meeting their mission needs.

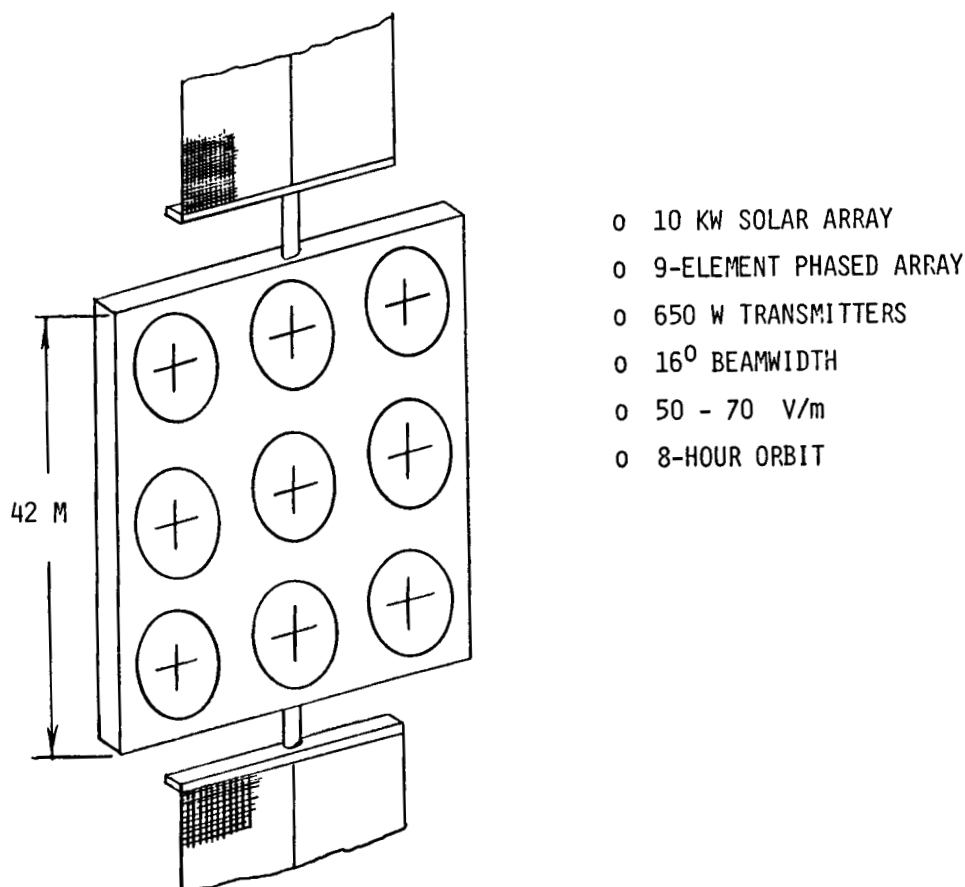


Figure 12. Low-capability first-generation system.

**Page intentionally left blank**

DEVELOPMENT CONCERNS FOR  
SATELLITE-BASED AIR TRAFFIC CONTROL SURVEILLANCE SYSTEMS

Keith D. McDonald  
Federal Aviation Administration  
Washington, DC

Large Space Antenna Systems Technology - 1984

December 4, 1984

### Abstract

This paper describes some preliminary results of an investigation directed toward the configuration of a practical system design which can form the baseline for assessing the applications and value of a satellite-based air traffic surveillance system for future use in the National Airspace System (NAS). This work has initially studied the characteristics and capabilities of a satellite configuration which would operate compatibly with the signal structure and avionics of the next generation air traffic control secondary surveillance radar system, the Mode S system. A compatible satellite surveillance system concept is described and an analysis is presented of the link budgets for the various transmission paths. From this, the satellite characteristics are established involving a large multiple feed L-band antenna of approximately 50 meter aperture dimension. Trade-offs involved in several of the alternative large aperture antennas considered are presented as well as the influence of various antenna configurations on the performance capabilities of the surveillance system. The features and limitations of the use of large aperture antenna systems for air traffic surveillance are discussed. Tentative results of this continuing effort are summarized with a brief description of follow-on investigations involving other space-based antenna systems concepts.



## INTRODUCTION

With the increasingly widespread use of satellites for communications, navigation, and surveillance, it has appeared appropriate from time to time to investigate their application to various air traffic control functions in the National Airspace System. The Federal Aviation Administration (FAA) has participated in investigations of this area since about 1965 and a number of successful and useful applications have been identified. However, the use of satellites in the National Airspace System has been minimal to date primarily because of economic considerations.

The principal technique currently used for the surveillance of air traffic is radar which was introduced into the ATC system shortly after World War II. To improve coverage reliability and to provide a means for aircraft to transmit encoded altitude information to the air traffic control (ATC) system, transponders which receive interrogations from the ground-based ATC radars at 1030 MHz and reply at 1090 MHz have been implemented on board aircraft. This cooperative radar system is called a secondary surveillance system; the secondary surveillance system for ATC in the United States is the air traffic control radar beacon system (ATCRBS). An upgrading of the radar beacon system is planned which provides for the selective addressing of all aircraft in the airspace. This selective address capability, by agreement of the International Civil Aviation Organization (ICAO), is referred to as the Mode Select, or the Mode S system. A national standard for the Mode S system has been published recently specifying its performance, capabilities, and data transmission formats (Ref. 1).

With the introduction of the Mode S concept, the possible compatibility of this technology with satellite systems has been considered. Basically, the question is if a space-based surveillance system can be configured that would be compatible with the Mode S signal structure and the Mode S transponder avionics that are planned for implementation, and would such a system have capabilities and benefits of sufficient merit to consider it further. The initial results of an investigation of these questions are addressed in this paper. The investigation is essentially a feasibility study, and in no way is meant to indicate FAA plans for implementation or current considerations for incorporation of a satellite-based surveillance system into the National Airspace System. However, there appear to be a number of advantages and benefits which are inherent in the use of a space-based surveillance system. It is to investigate the technical feasibility, identify an exemplary system configuration and determine preliminary operating parameters that this investigation was conducted.

## OBJECTIVES OF THE STUDY

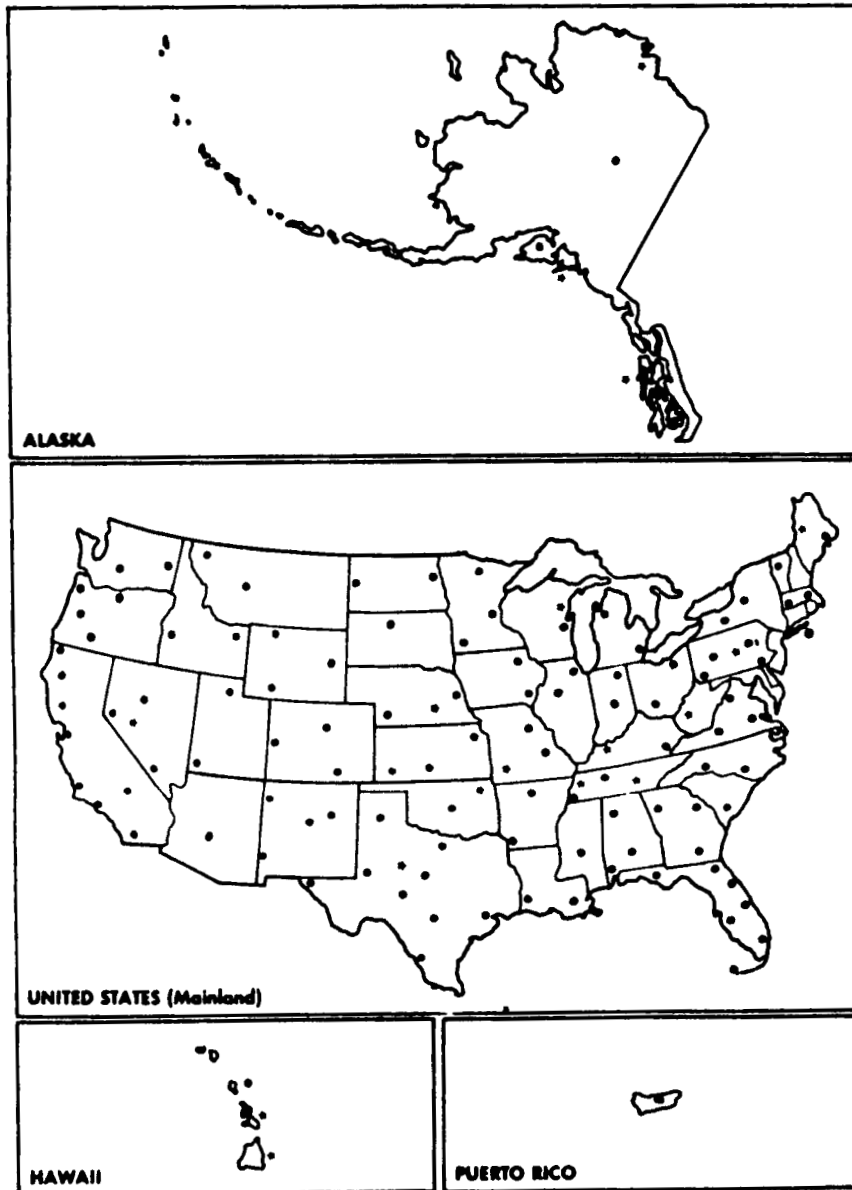
Figure 1 lists the objectives of the study, which were to assess technical feasibility and obtain an indication of the cost involved in developing and implementing a compatible satellite surveillance system (CSSS). It was desired to configure a representative system design or designs, and to analyze the performance capabilities for the system in its various modes of operation. It was also desired to identify the critical concerns which require additional development in technology, or other activities to be accomplished, to provide a viable candidate system for consideration. It was recognized at the outset that certain limitations of the Mode S ground-based system design and the transponder characteristics in particular placed serious constraints on the compatible use of space-based systems and that these factors might preclude the development of any satellite configuration that was practical and economically viable.

1. DETERMINE TECHNICAL FEASIBILITY AND COST
  - o SATELLITE-BASED ATC SURVEILLANCE AND DATA LINK SYSTEM
  - o COVERAGE OF CONUS, ALASKA, HAWAII, ADJACENT AREAS
  - o USE OF MODE S SIGNAL STRUCTURE AND AVIONICS
2. CONFIGURE REPRESENTATIVE SYSTEM DESIGNS
  - o ESTABLISH PERFORMANCE
  - o ESTIMATE COST
3. DETERMINE SYSTEM PERFORMANCE CAPABILITIES
  - o EN ROUTE AND TERMINAL AREA
  - o SURVEILLANCE AND DATA LINK
  - o ALTITUDE ACCURACY
  - o COMPARISON WITH ALTERNATIVES
4. IDENTIFY CRITICAL AREAS OF CONCERN
  - o ISSUES
  - o ACTIVITIES
  - o RESOURCES
  - o SCHEDULE
  - o COORDINATION

Figure 1

## EN ROUTE RADAR SURVEILLANCE SYSTEM SENSOR DISTRIBUTION

Figure 2 illustrates the approximate distribution of en route surveillance resources throughout the United States, Canada, and Alaska, including Hawaii and Puerto Rico. As of 1984, there were 130 en route and 197 terminal area sensors for a total of 327 sensors. By the turn of the century, acquisition plans for Mode S call for about 151 en route and 239 terminal sensors for a total of 390. The current Mode S buy is for 137 sensors which are to be in service by about 1990.

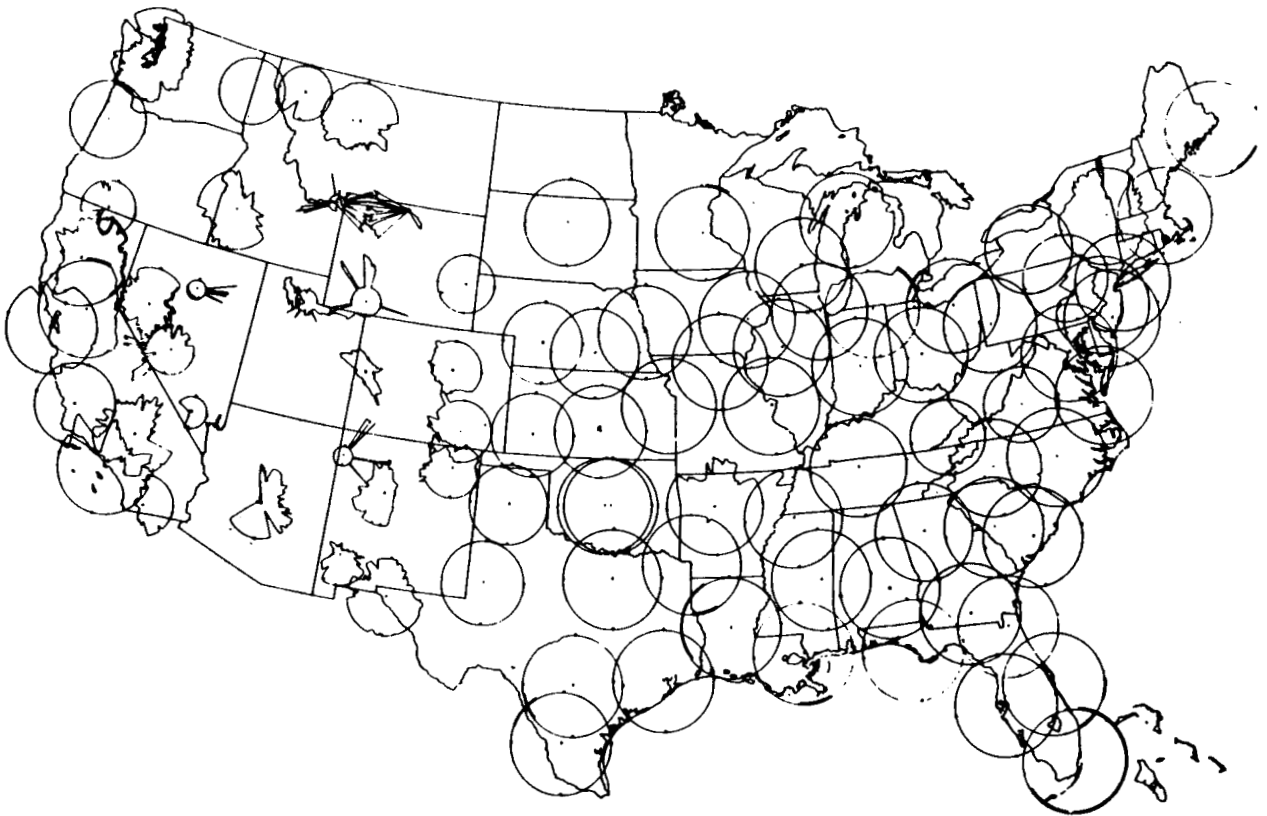


1981-1985 SYSTEM  
EN ROUTE SURVEILLANCE

Figure 2

### ARSR COMPOSITE COVERAGE MAP

Figure 3 shows the air route surveillance radar coverage. This map is based on a 10,000-foot mean sea level (MSL) contour. As is apparent from the map, visibility in the western part of the country is severely restricted by the terrain. It is also apparent that the eastern part of the country is very well covered with secondary surveillance radar facilities.



10,000 FT. MSL, MAXIMUM RANGE  $R_{\max}$  = 100 n.mi.

Figure 3

## ASSUMPTIONS AND CONSTRAINTS

The assumptions and constraints for the compatible satellite surveillance system study are shown in Figure 4. The coverage would be basically the United States, including Alaska and Hawaii, as well as adjacent areas, such as the nearer coastal regions of the Atlantic, Pacific, and the Gulf of Mexico, and the adjoining borders with Mexico and Canada. The capacity of the system is sized to handle an instantaneous airborne count (IAC) of 50,000 aircraft which is believed to correspond to that which may be realistic sometime beyond the turn of the century. The current maximum IAC is approximately one-third of this number. The system is to provide three-dimensional position determination and data link (DL) capabilities consistent with those provided by the Mode S system. The user update rate is to correspond with the current system with the exception that more frequent updates are to be provided on an adaptable basis so that update intervals of one to ten seconds are obtainable. The system is to be continuously available and will require top-mounted antennas on the aircraft to provide the reliable link with the satellite constellation. One of the principal features of the system is that it is to provide access to low-altitude aircraft, many substantially below the current 6-10,000 foot minimums generally associated with the current ground-based radar systems operating in the continental United States (CONUS). Access to near-ground level is to be provided over the entire CONUS if possible. It was recognized that the interference and garble effects associated with the operation of the current radar beacon system may be a significant constraining factor and therefore these interference effects are considered in the study. The potential implementation time frame is for the late 1990's.

### COMPATIBLE SATELLITE SURVEILLANCE SYSTEM STUDY

#### ASSUMPTIONS AND CONSTRAINTS

1. COVERAGE OF UNITED STATES AND ADJACENT AREAS
2. INSTANTANEOUS AIRBORNE COUNT (IAC) OF 50,000 AIRCRAFT
3. 3D POSITION DETERMINATION AND DATA LINK
4. MODE S SIGNAL AND AVIONICS COMPATIBLE
5. USER UPDATE RATE OF ONCE EVERY 1-10 SECONDS
6. CONTINUOUS SYSTEM AVAILABILITY
7. TOP MOUNTED ANTENNAS ON AIRCRAFT
8. ACCESS TO LOW ALTITUDE AIRCRAFT
9. INTERFERENCE AND GARBLE EFFECTS TO BE CONSIDERED
10. POTENTIAL IMPLEMENTATION TIME FRAME OF LATE 1990's

Figure 4

## POTENTIAL BENEFITS AND CONCERNS

The potential benefits and concerns of the system are indicated on Figure 5. These items occur in three general areas: first, the operational improvements which may be feasible using the satellite-based system; second, the cost considerations involved, primarily directed toward the eventual replacement or elimination of some of the ground-based facilities by the satellite system; and third, the operational limitations that may be associated with the system, in particular those which may arise due to the interference and garbling problems associated with the signal environment of the ATCRBS and the Mode S systems.

1. OPERATIONAL IMPROVEMENTS
  - o IMPROVED COVERAGE; 3D; LOW ALTITUDE
  - o OFF-SHORE COVERAGE
  - o SURVEILLANCE ALTITUDE INDEPENDENT OF AIRCRAFT ALTIMETER
  - o ATMOSPHERIC AND ALTIMETRY CALIBRATION FEASIBLE
  - o ACCURACY IMPROVEMENT POTENTIAL
2. COST CONSIDERATIONS
  - o POSSIBLY LESS EXTENSIVE NETWORK OF TERRESTRIAL FACILITIES
  - o ELIMINATION OF RADARS DEPENDENT ON PRIMARY RADAR REQUIREMENTS
3. OPERATIONAL LIMITATIONS
  - o INTERFERENCE ENVIRONMENT DURING ATCRBS TO MODE S TRANSITION MAY LIMIT SYSTEM PERFORMANCE

Figure 5

## COMPATIBLE SURVEILLANCE SATELLITE SYSTEM CONCEPT

Figure 6 indicates the system concept in pictorial form for the compatible surveillance satellite system. A constellation of five satellites is indicated in the figure, four of which are "receive only" satellites and one of which provides transmissions to the Mode S transponder equipped aircraft. As indicated in the figure, the central ground station (CGS) is provided with a backlink from all of the receive satellites and provides the surveillance and datalink information to the various area control facilities. There may be any number of CGS's; however the computing capability and the antenna systems necessary for these stations will probably restrict their number to possibly three or four throughout the country.

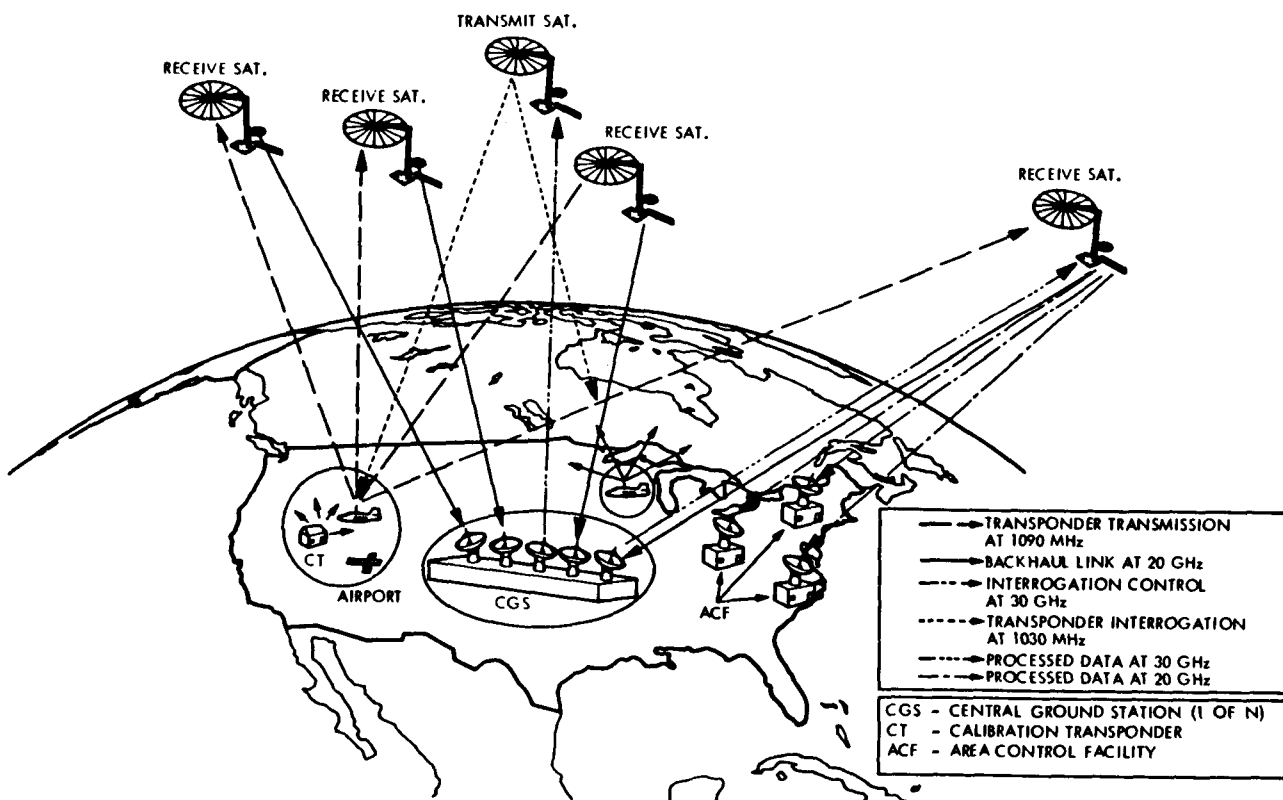


Figure 6

## CSSS SYSTEM CONCEPT

Figure 7 provides some of the basic information relating to the system concept. The satellite receive system constellation receives the signals from each transponder and by means of a translating repeater (transponder) retransmits that information at another convenient downlink frequency to the CGS, where the various signals are separated by the identification (ID) codes placed on the transmissions by the aircraft originally. The ranges from the satellites to the aircraft are then determined by the computer system which enables the determination of aircraft positions. The transmissions from the aircraft transponder can be either as replies to a transmit satellite interrogation or as "squitter" replies similar to those associated with the ATCRBS and Mode S transponders. The squitter transmission occurs approximately every second spontaneously from each aircraft transponder.

1. AIRCRAFT MODE S TRANSPONDER TRANSMISSIONS ARE PICKED UP BY CONSTELLATION OF GEOSYNCHRONOUS RECEIVE SATELLITES WITH FAVORABLE GEOMETRY
2. TRANSPONDER TRANSMISSIONS CAN BE SPONTANEOUS (SQUITTER) OR IN RESPONSE TO AN INTERROGATION FROM A SATELLITE
3. SATELLITE SENDS RECEIVED SIGNALS DOWN OVER A BACKHAUL LINK TO TWO OR MORE GEOGRAPHICALLY SEPARATED CENTRAL GROUND STATIONS (CGS)
4. CENTRAL GROUND STATIONS NORMALLY COMPUTE TRANSPONDER LOCATION FROM AIRCRAFT -SATELLITE-CGS SIGNAL TIME OF ARRIVAL DIFFERENCES
5. SYSTEM CAN ALSO MEASURE CGS-AIRCRAFT TWO WAY RANGE BY INTERROGATING
6. CENTRAL GROUND STATIONS ALSO MANAGE THE DATA LINK WHICH INCLUDES THE SCHEDULING OF DATA MESSAGE TRAFFIC TO AND FROM AIRCRAFT
7. PROCESSED AIRCRAFT POSITION INFORMATION, AS WELL AS DATA LINK INFORMATION, IS DISTRIBUTED BY THE GROUND STATIONS VIA SATELLITE (AND OTHER MEANS) TO THE APPROPRIATE FACILITIES (I.E. ACF'S)

Figure 7



## AIRCRAFT REPLY PATHS TO SATELLITES

The reply paths from the aircraft to the satellite constellation are shown in Figure 8. This illustrates the requirement for three or four satellites to receive each aircraft's reply. Four satellites are required for operation of the system in the squitter mode. The advantage of utilizing the squitter transmission is that the transmit satellite is only required to provide interrogations for datalink messages from the aircraft. This would require a "message waiting" bit in the squitter reply format, which is a change from the current Mode S signal structure. In the squitter mode of operation, it is necessary to measure the times of arrival from the four satellites; however, it avoids the transponder delay associated with the aircraft transponder and provides an accurate means for determining aircraft position.

If the interrogation/reply technique is used with a transmit satellite interrogating for a reply message, then only three receive satellites are required to obtain a position determination. However, the transponder "jitter" and the cable length delays associated with the aircraft transponder must be incorporated in the position accuracy error budget, and some additional degradation in the position determination accuracy occurs. The central ground stations manage the datalink transmissions to the aircraft and the distribution of the datalink messages from the aircraft. Reliability of the datalink messages should be excellent since they normally are received over three or four independent links.

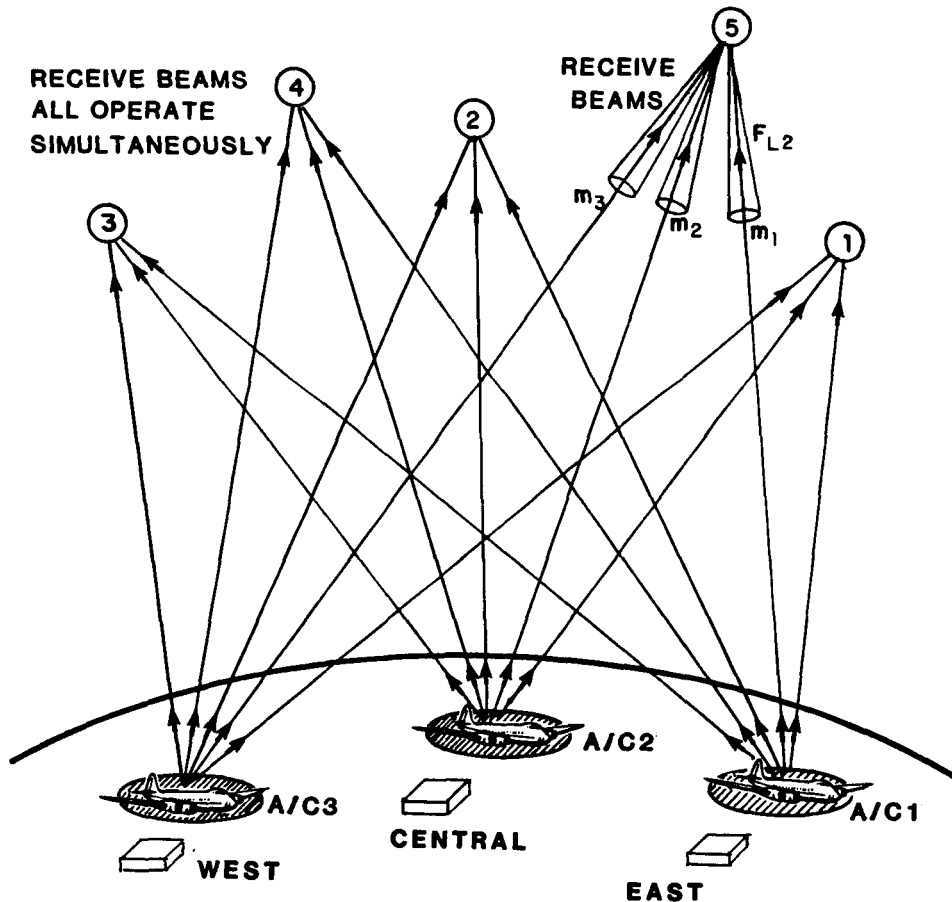


Figure 8

## CSSS AIRCRAFT-TO-SATELLITE LINK BUDGET

Figures 9 and 10 provide preliminary link budgets for the aircraft-to-satellite and the satellite-to-aircraft links of the compatible satellite surveillance system. The aircraft-to-satellite link is based upon an aircraft transponder transmitter power of 70 watts peak, corresponding to the minimum power required for operation in the ATC system. An antenna gain of unity is assumed for the circularly polarized top-mounted aircraft antenna. The spacecraft receiver system noise temperature is estimated at about 360 Kelvin, somewhat higher than the noise temperature of the radiation from the earth contained in the antenna beam width. A spacecraft receiver system bandwidth of about 10 MHz is assumed, which is somewhat liberal, and a signal-to-noise ratio of about 14 dB is obtained. The corresponding signal energy to noise density value is about 21.0 dB, which is approximately 5 dB above that required for a bit error rate (BER) of 1 part in  $10^5$ . The time of arrival measurement error for these values considering a demodulation loss of about 6 dB is approximately 30 nanoseconds, corresponding to a 30-foot ranging error. Since the satellite constellation provides a position dilution of precision (PDOP) factor of about 3, the position determination accuracy is about 100 ft. in three dimensions.

It should be recognized that the link budget closure requires a spacecraft antenna gain of approximately 52 dB which translates to a 50-meter diameter antenna at the 1030-1090 MHz operating frequencies. The principal driver leading to this large aperture antenna is the 70 watt aircraft transmitter power available from the minimal Mode S transponder.

A/C TRANSMITTER POWER; MINIMUM OF 70 WATTS PEAK	18.5 dBw	
A/C ANTENNA GAIN	0.0 dB	
EIRP	18.5 dBw	on-axis
FREQUENCY: 1090 MHz		
RANGE LOSS: 40,000 Km	185.2 dB	
S/C ANTENNA GAIN (D = 50 METERS)	52.0 dB	
S/C RECEIVER CIRCUIT LOSS	0.3 dB	
S/C ANTENNA POINTING LOSS (TRIPLE CROSSOVER)	4.0 dB	
POLARIZATION LOSS	0.0	
S/C RECEIVED SIGNAL POWER	-119.0 dBw	
S/C RECEIVER SYSTEM NOISE TEMP: 360 K	-203.0 dBw	$N_o$
S/C RECEIVER SYSTEM BW: 10 MHz	70.0 dBHz	
S/C RECEIVER SYSTEM NOISE POWER	-133.0 dBw	
SIGNAL TO NOISE RATIO, SNR	14.0 dB	RF SNR
DATA DETECTION, BIT RATE: 1Mbps	60.0 dB	
DEMODULATION LOSS	3.0 dB	
$E_b/N_o$	21.0 dB	AVAILABLE
$E_b/N_o$ REQUIRED FOR BER OF $10^{-5}$	16.0 dB	BER: $1E-5$
AVAILABLE MARGIN	5.0 dB	
TIME OF ARRIVAL, PREAMBLE RATE: 2 Mbps	63.0 dB	
DEMODULATION LOSS	6.0 dB	
CARRIER ENERGY TO NOISE DENSITY, $E_b/N_o$	15.0	AVAILABLE
$E_b/N_o$ REQUIRED FOR TOA < 30 n. SEC.	15.0	
AVAILABLE MARGIN	0.0	

Figure 9

## CSSS SATELLITE-TO-AIRCRAFT LINK BUDGET

The satellite-to-aircraft link shown in Figure 10 also requires the 50-meter aperture antenna, primarily due to the poor sensitivity of the transponder receiver. The specified receiver sensitivity is -74 dBm, which corresponds to a noise temperature for the receiver of approximately 9,000 Kelvin. Assuming a spacecraft transmitter power of 5 kilowatts peak and the 50-meter antenna aperture, a carrier energy to noise density of 21.4 dB is obtained at the user transponder. This is about 9 dB above that required for a BER of 1 part in  $10^5$ . The available margin is essentially zero for the minimum triggering level required for the Mode S transponder.

S/C TRANSMITTER POWER (5 K WATTS PEAK)	37.0 dBw	
S/C TRANSMITTER CIRCUIT LOSSES	1.0 dB	
S/C ANTENNA GAIN (D = 50 m.)	<u>52.0 dB</u>	
EIRP	88.0 dBw	on-axis
FREQUENCY: 1030 MHz		
RANGE LOSS; 40,000 km	184.7 dB	
S/C TRANSMIT ANTENNA POINTING LOSS	<u>4.0 dB</u>	TRIPLE CROSSOVER
RECEIVED SIGNAL POWER	-100.7 dBw	
RECEIVER SYSTEM NOISE TEMPERATURE; 9000 K	-189.1 dBw	$N_o$
BIT RATE; 4 Mbps	66.0 dB	
DEMODULATION LOSS	1.0 dB	
CARRIER ENERGY TO NOISE DENSITY, $E_b/N_o$	21.4 dB	AVAILABLE
$E_b/N_o$ REQUIRED FOR BER OF $1E-5$	<u>12.0 dB</u>	REQUIRED
AVAILABLE MARGIN	9.4 dB	
MINIMUM TRIGGERING LEVEL	<u>-101.0 dBw</u>	WORST CASE
AVAILABLE MARGIN	0.3 dB	ABOVE MTL

Figure 10

## SATELLITE SYSTEM LINK DESIGN REQUIREMENTS

Satellite system link design requirements are tabulated in Figure 11. The 50-meter antenna aperture requires approximately 100 beams to cover the United States and the other areas under consideration. Therefore, a reasonably complex feed structure is required in addition to the large aperture antenna system. The normal operation of the CSSS is to use the "squitter" mode from the aircraft transponders. In this mode of operation, spontaneous reply transmissions containing the aircraft ID occur approximately once a second. These replies provide the basis for obtaining position determination from the system. The replies are received by each satellite in the constellation and relayed to the central ground station for position determination. A message waiting pulse is incorporated in the squitter transmission which informs the CGS if a data link message is waiting to be transmitted by an aircraft. An interrogation through the transmitter satellite to the aircraft transponder allows the datalink message to be sent. This mode of operation minimizes the prime power and size of the transmit satellites in the system. Transmissions may occur simultaneously on a number of beams depending on the traffic requirements for the aircraft in the ATC system. The duty cycle for the transmissions from satellite to aircraft is estimated to be in the order of 1 to 10 percent.

### RECEIVE

- o RECEIVE ON  $\sim 100$  BEAMS SIMULTANEOUSLY
- o MAXIMIZE RECEIVER LISTENING TIME IF SQUITTERS ARE OF PRIME INTEREST
- o RECEIVE NOISE TEMPERATURE 360 K

### TRANSMIT

- o TRANSMIT ON FROM 1 TO (TBD) BEAMS SIMULTANEOUSLY
- o 5 KW PEAK RF POWER FOR THE  $\frac{\text{CONUS}}{100}$  BEAM SIZE
- o 18  $\mu$ SEC PULSES (OCCASIONAL 32  $\mu$ SEC PULSES) TRANSMITTED
- o DUTY CYCLE OF ABOUT LESS THAN 1% TO 10% (TBD)

Figure 11

## PHASED ARRAY TRANSMIT ANTENNA TRADE-OFFS

The advantages and disadvantages of a phased array transmit antenna are summarized in Figure 12. If a phased array transmit antenna is used, a smaller antenna is feasible because the beam agility of the phased array technique allows directing the antenna boresight toward the aircraft under surveillance. This avoids the triple crossover beam pointing loss of 4 dB in the previous power budgets. This factor combined with the greater ease with which high power levels can be generated with the phased array allows the substantial decrease in antenna dimension. It appears that a 14.5 meter array would be adequate; however, substantially increased prime power would be required for its operation.

### 14.5M ARRAY VS 50M REFLECTOR

#### ADVANTAGES

- GRACEFUL DEGRADATION
- POINT BEAM ANYWHERE  
MINIMIZE POINTING LOSS
- AVOID FAILURE OF SPECIFIC  
BEAMS DUE TO SEVERAL LOCALIZED  
FAILURES
- RECEIVE SATELLITES LISTEN ON  
ALL BEAMS ALL THE TIME
- NO LNA PROTECTION CIRCUITRY  
OR DIPLEXERS IN RECEIVE SATELLITES
- MINIMAL DESIGN WORK TO AVOID  
BREAKDOWN (PA's ARE LESS THAN  
A FEW HUNDRED WATTS)

#### DISADVANTAGES

- SEPARATE S/C DESIGN
- SEPARATE SAT-GROUND STATION  
2-WAY KU BAND LINK
- LARGER SOLAR-POWER SYSTEM
- LARGER SPOT BEAM
- TRANSMIT ON ONLY ONE BEAM  
AT A TIME
- ARRAY DISTORTION CORRECTION  
SYSTEM REQUIRED

Figure 12

## STRAWMAN SYSTEM DESIGN

The strawman system design characteristics are shown in Figure 13. The satellite constellation is to include both geostationary and synchronous inclined orbit satellites. A constellation of five inclined and two geostationary satellites would provide a system with redundancy in both the inclined and equatorial orbital planes. This arrangement would normally provide four satellites in view of the United States with five in view half of the time. The spacecraft commonality concerns relating to the use of independent transmit satellites or combined transmit-receive spacecraft are yet to be determined. In any case, the satellite RF systems basically consist of translating transponders which form a "bent pipe" return link to the ground for transponder replies. The system would require top-mounted circularly polarized aircraft antennas.

- o SATELLITES CONSTELLATION TO INCLUDE BOTH GEOSTATIONARY AND NON-GEOSTATIONARY SATELLITES
- o TOP-MOUNTED CIRCULARLY POLARIZED AIRCRAFT ANTENNA
- o SATELLITES (OPERATING UNDER A MIXED ATCRBS/MODE S ENVIRONMENT) BASED ON 50 M WRAP RIB OFFSET FED ANTENNA
- o APPROXIMATELY 100 RECEIVE BEAMS
- o TRANSMIT-RECEIVE S/C COMMONALITY TO BE DETERMINED
- o COMBINATION OF ACTIVE AND PASSIVE SURVEILLANCE MODES
- o RECEIVE SATELLITE BENT PIPE FOR TRANSPONDER REPLIES

Figure 13

## OFFSET-FED WRAPPED RIB LARGE APERTURE ANTENNA

Figure 14 illustrates a typical offset-fed wrapped-rib large aperture antenna similar to the type developed for the land mobile satellite system.

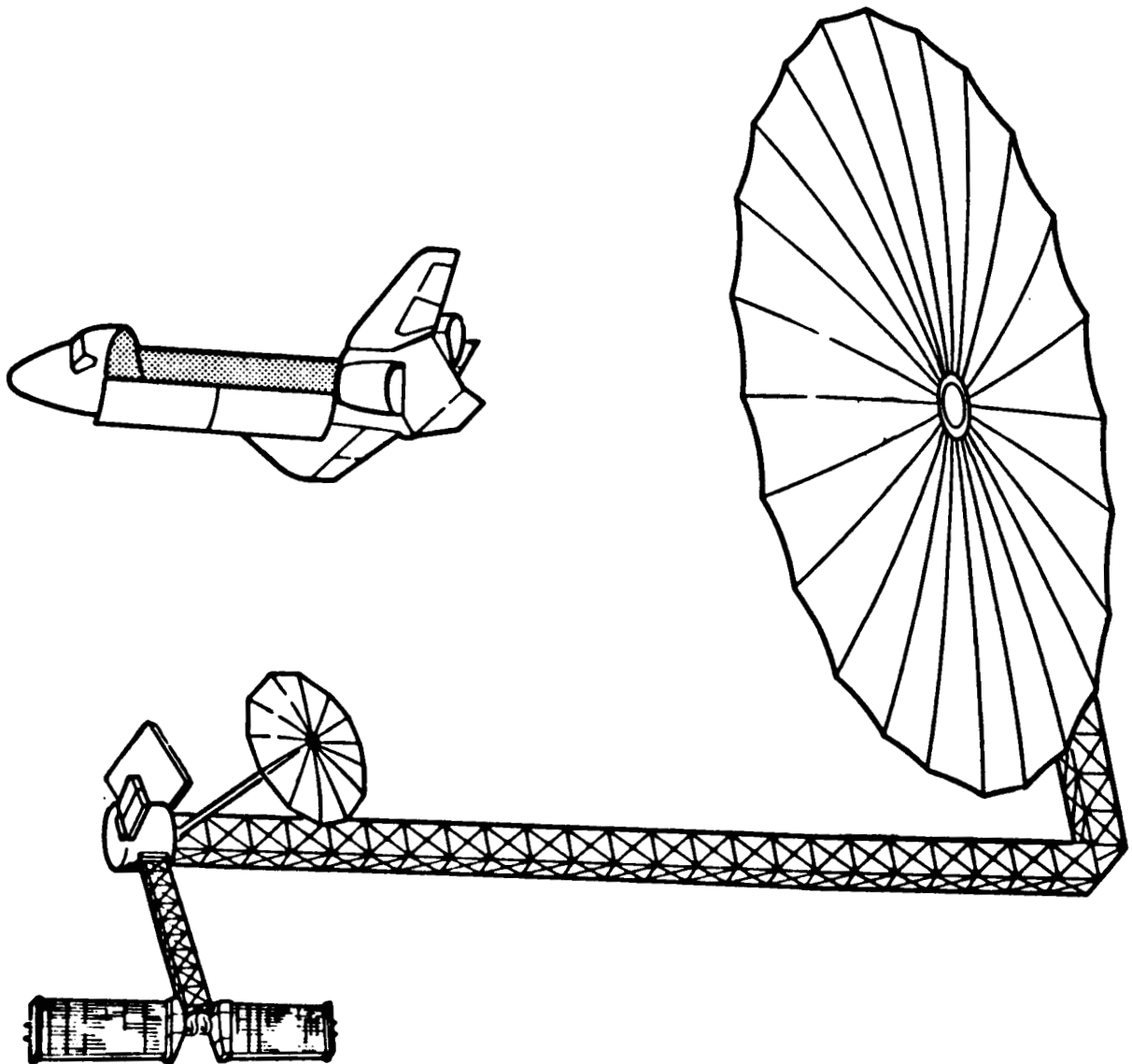


Figure 14

## PRINCIPAL ANTENNA CONFIGURATIONS CONSIDERED

Other approaches which appear feasible for obtaining the aperture dimensions required are shown in Figure 15 and include the offset and axisymmetric wrapped-rib designs, the offset-fed quadruple aperture hoop column antenna, and the phased array transmit antenna which has been described.

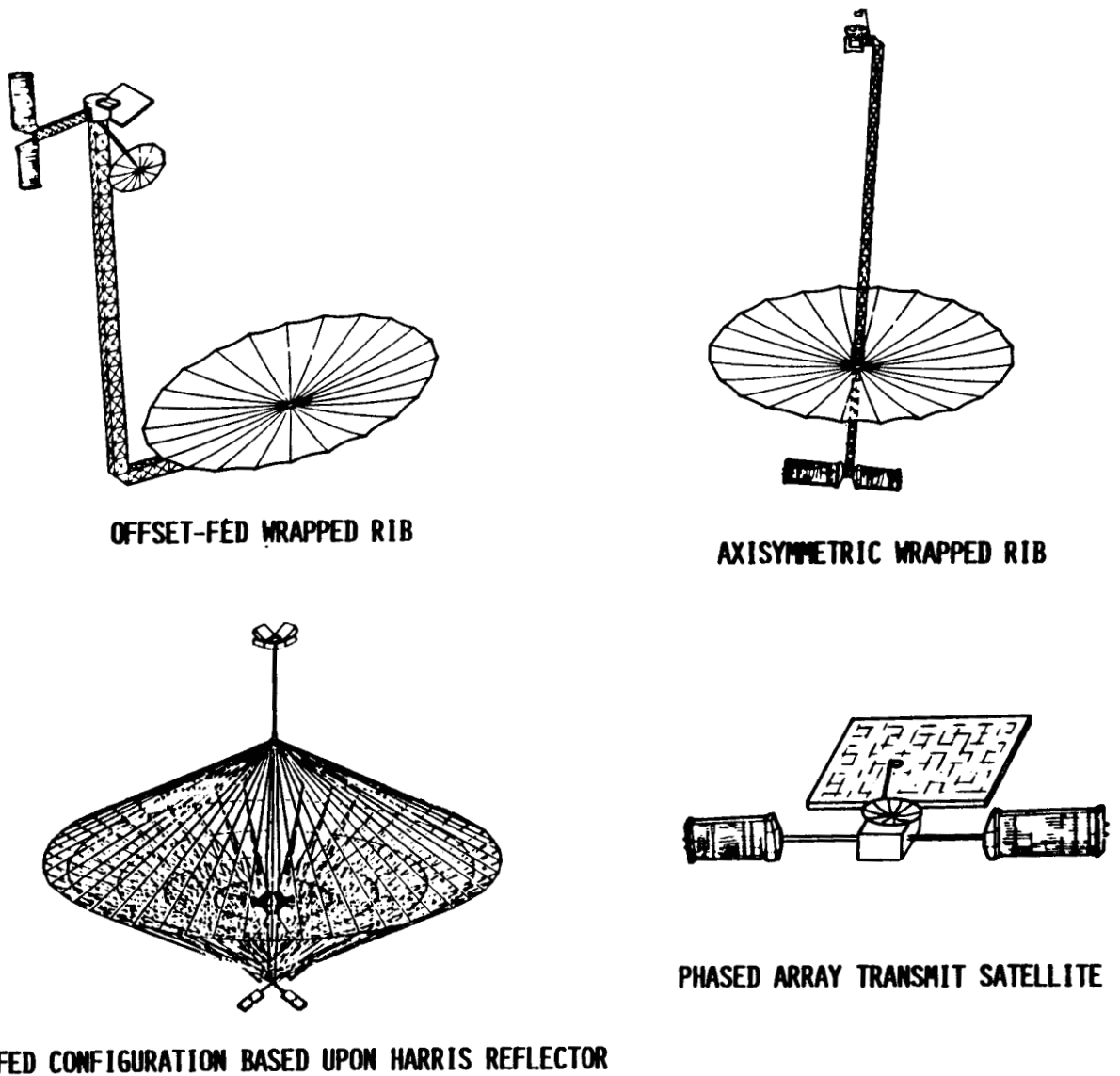


Figure 15



## REPRESENTATIVE MULTI-BEAM SURVEILLANCE SATELLITE CONFIGURATION

Figure 16 shows a representative multi-beam antenna surveillance satellite system which could be configured for the receive mode or for the combined transmit-receive modes of operation with the CSSS.

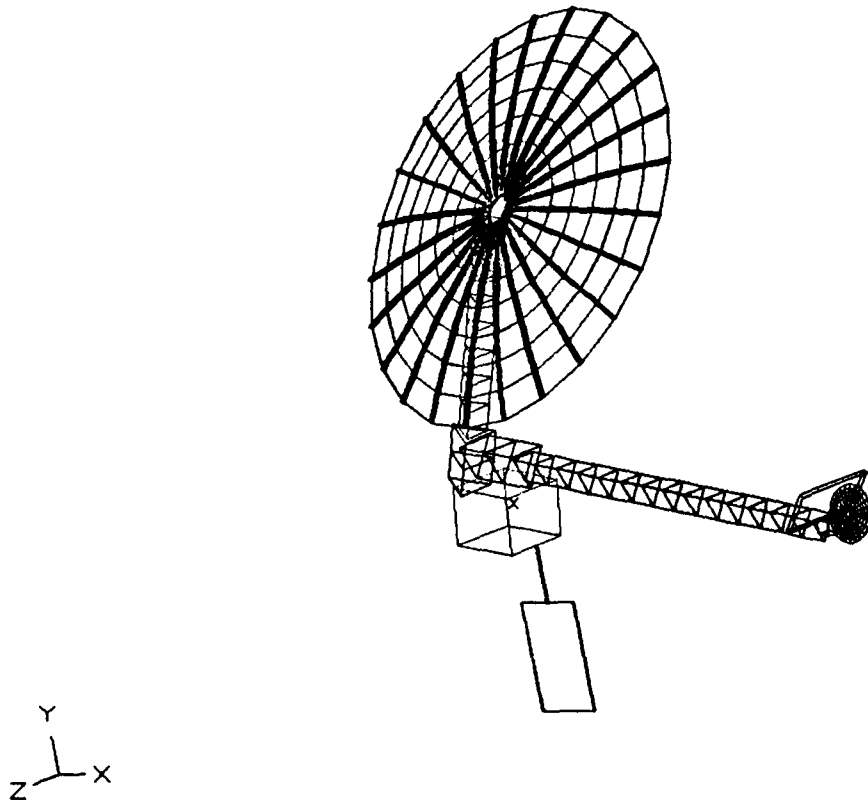
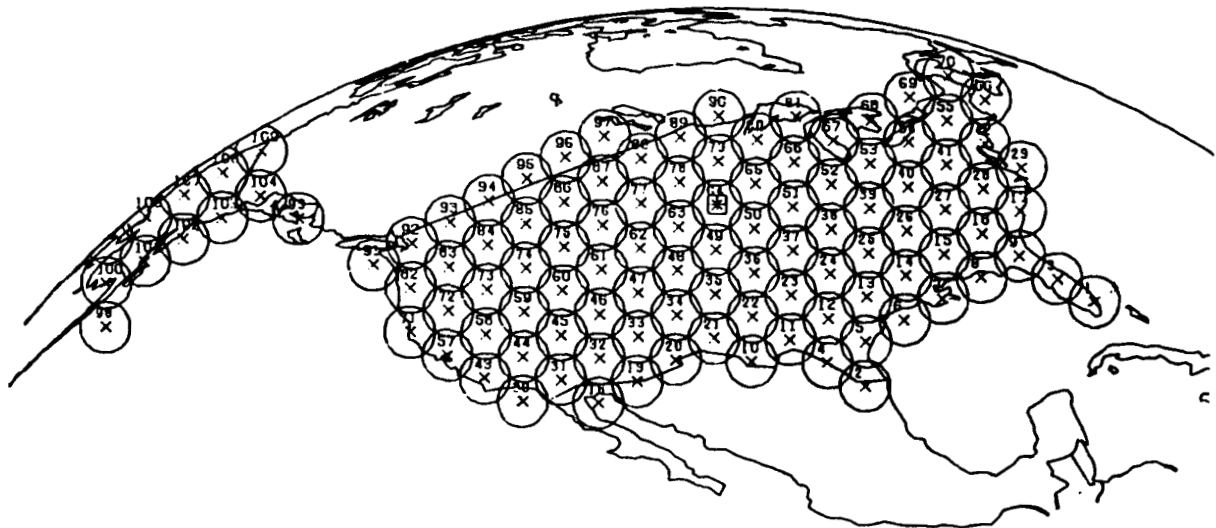


Figure 16

## SURVEILLANCE SATELLITE ANTENNA BEAM LAYOUT - SATELLITE PERSPECTIVE

The surveillance satellite antenna beam layout is shown in Figure 17 for a satellite in geostationary orbit at a location of 120 degrees West Longitude. This figure provides a satellite perspective of both the earth and the coverage beams.



SURVEILLANCE SATELLITE ANTENNA BEAM LAYOUT

SATELLITE POSITION: 120°W LONGITUDE GEOSTATIONARY ORBIT

Figure 17

## SURVEILLANCE SATELLITE ANTENNA BEAM LAYOUT - MERCATOR PROJECTION

The CSSS antenna patterns shown in Figure 18 illustrate the coverage of the beams on a mercator projection of the earth. The lengthening of the beams near the limb of the earth is clearly indicated.

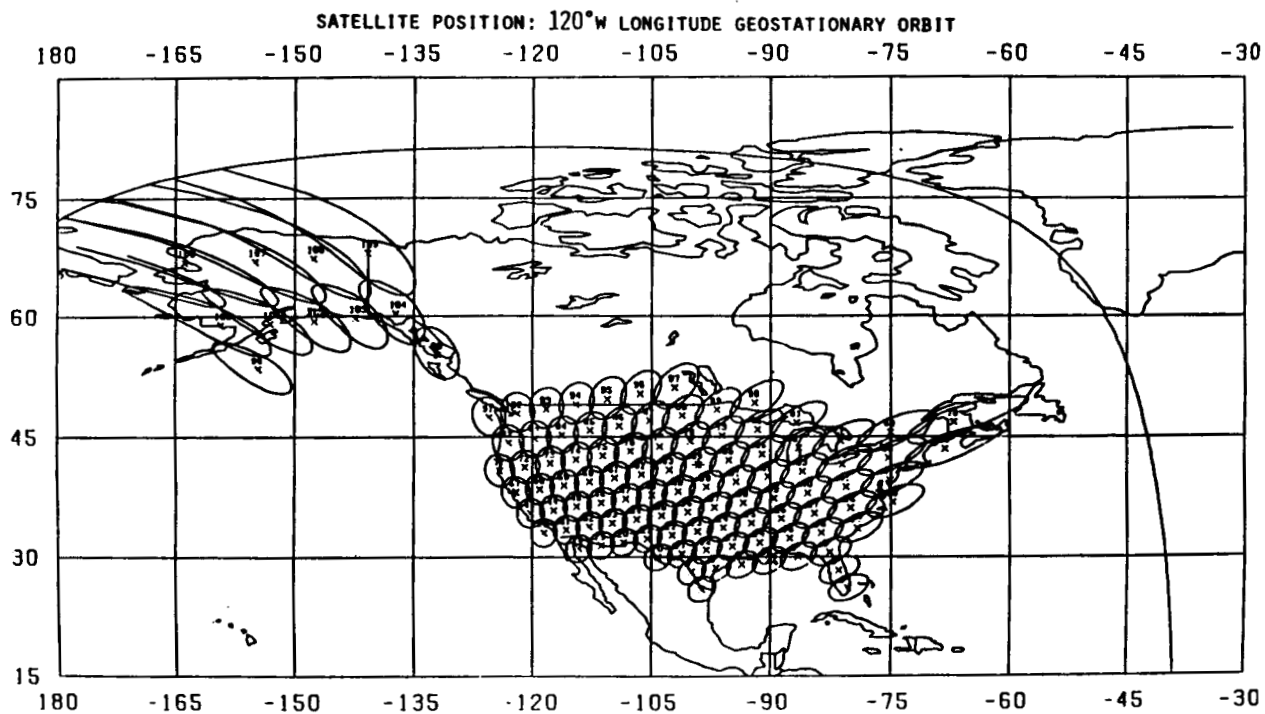


Figure 18

## DEPLOYABLE ANTENNA TECHNOLOGY READINESS DATES

Figure 19 is a chart (Ref. 2) illustrating the projected technology readiness dates for antenna reflector sizes which are deployed by satellite. This chart addresses precision deployables, advanced concepts, and existing concepts. As indicated, the existing concepts should be mature and available in the 1993-1995 time frame. The surface tolerance estimates for 50-meter antenna apertures indicated on the chart are considerably beyond those required for the 50-meter aperture antenna employed in the CSSS.

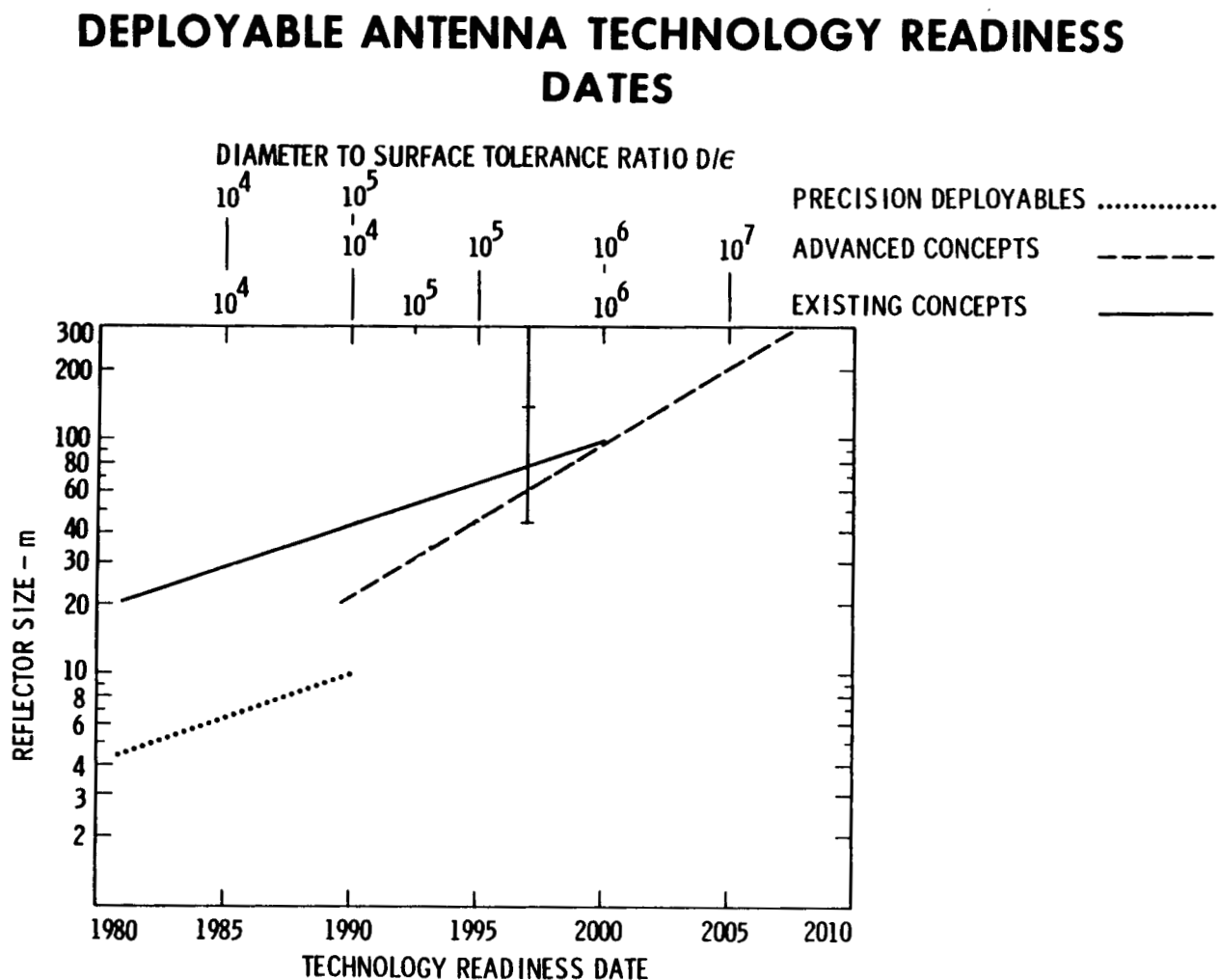


Figure 19

## CONCLUSIONS

The basic conclusions relating to the technical feasibility, practicality, and viability of the Mode S compatible surveillance satellite system are presented in Figure 20. Unless a number of applications for large aperture antenna and feed systems occur in the next few years, it does not appear likely that antennas in the 50-meter class will be economically viable even though several types appear technically feasible.

Investigation of this technology is continuing with the analysis of concepts and techniques which combine a) the use of smaller and more economically viable antenna apertures in space, b) the operation of the system in the aeronautical L-band where authorized allocations for satellite-based systems for aeronautical applications exist, and c) the modification of the Mode S transponder to operate at L-band frequencies, including the incorporation of a more sensitive receiver and a more capable transmitter system.

The investigation reported in this paper demonstrated many of the features and concerns in using satellites for ATC applications in the national airspace system. It appears clear that their potential is substantial and that further effort is needed for an attractive, useful, viable system to be developed.

- o COMPLETE COMPATIBILITY WITH ALL MODE S TRANSPONDER PARAMETERS RESULTS IN AN EXPENSIVE SPACECRAFT DESIGN.
- o MODE S TRANSPONDER LOW OUTPUT POWER (70 W GENERAL AVIATION) AND THE INTERFERENCE ENVIRONMENT AT 1090 MHz DRIVE THE RECEIVE SATELLITE ANTENNA SIZE TO THE 50 METER DIAMETER RANGE.
- o MODE S TRANSPONDER HIGH MINIMUM TRIGGERING LEVEL (OF -74 DBM) RESULTS IN A VERY HIGH POWER SATELLITE TRANSMITTER. INTERROGATION RATES ABOVE A FEW THOUSAND PER SECOND CAN DRIVE TRANSMIT SATELLITE PRIME POWER REQUIREMENTS ABOVE PRACTICAL LEVELS.
- o THE STRAWMAN SYSTEM DESIGN CAN PROVIDE ACCURATE AIRCRAFT POSITION DETERMINATION AND DATA LINK OPERATION OVER AREAS OF CONUS WHERE THE ATCRBS SENSOR COUNT IS IN THE RANGE OF 10 TO 20 OR LESS WITHIN A RECEIVE BEAM (ALSO IAC DEPENDENT).
- o THE MODE S COMPATIBLE SURVEILLANCE SATELLITE SYSTEM APPEARS TECHNICALLY FEASIBLE BUT CURRENT COST CONSIDERATIONS MAKE ITS IMPLEMENTATION QUESTIONABLE.
- o A COST EFFECTIVE SATELLITE SURVEILLANCE SYSTEM WHICH USES THE MODE S FORMAT WILL REQUIRE MODIFICATION TO THE MODE S TRANSPONDERS.

Figure 20

## ACKNOWLEDGMENTS

Several of the figures included in this paper are based on the contributions of Mr. A. Vaisnys and Mr. R. Freeland of the Jet Propulsion Laboratory of the California Institute of Technology. Their assistance and support are appreciated in the continuing investigations of the technical and economic feasibility of satellite systems for surveillance and related applications.

## REFERENCES

1. U.S. National Aviation Standard for The Discrete Address Beacon System (now the Mode S system), Department of Transportation, Federal Aviation Administration, Order 6365.1, December 9, 1980, with changes dated February 23, 1982.
2. Freeland, Robert E., "A Deployable Antenna Concept Development," in the AIAA Space System Technology Workshop No. 3, Kirtland Air Force Base, March 28, 1984.

APPLICATION OF PUSHBROOM ALTIMETRY  
FROM SPACE USING LARGE SPACE ANTENNAS

C. L. Parsons and J. T. McGoogan  
NASA Goddard Space Flight Center  
Wallops Island, VA 23337

and

F. B. Beck  
NASA Langley Research Center  
Hampton, VA 23665

Large Space Antenna Systems Technology - 1984  
December 4-6, 1984

## OCEAN DYNAMICS FEATURES

The Earth's oceans are now known to contain dynamical features, such as currents and eddies, which have a direct correspondence to atmospheric features. Eddies and the meanderings of the major currents are mesoscale fluctuations which have analogues in the cyclones, anticyclones and fronts of our weather. Hence, it is important to develop the means to monitor their development, movement, and dissipation if we are to understand the dynamics of the oceans. One technique is to use passive infrared radiometry to map the sea surface temperature variations resulting from ocean dynamics. Figure 1 shows such an image produced by the Advanced Very High Resolution Radiometer (AVHRR); it contains the Gulf Stream flowing across the bottom of the scene and a prominent warm core ring above it.

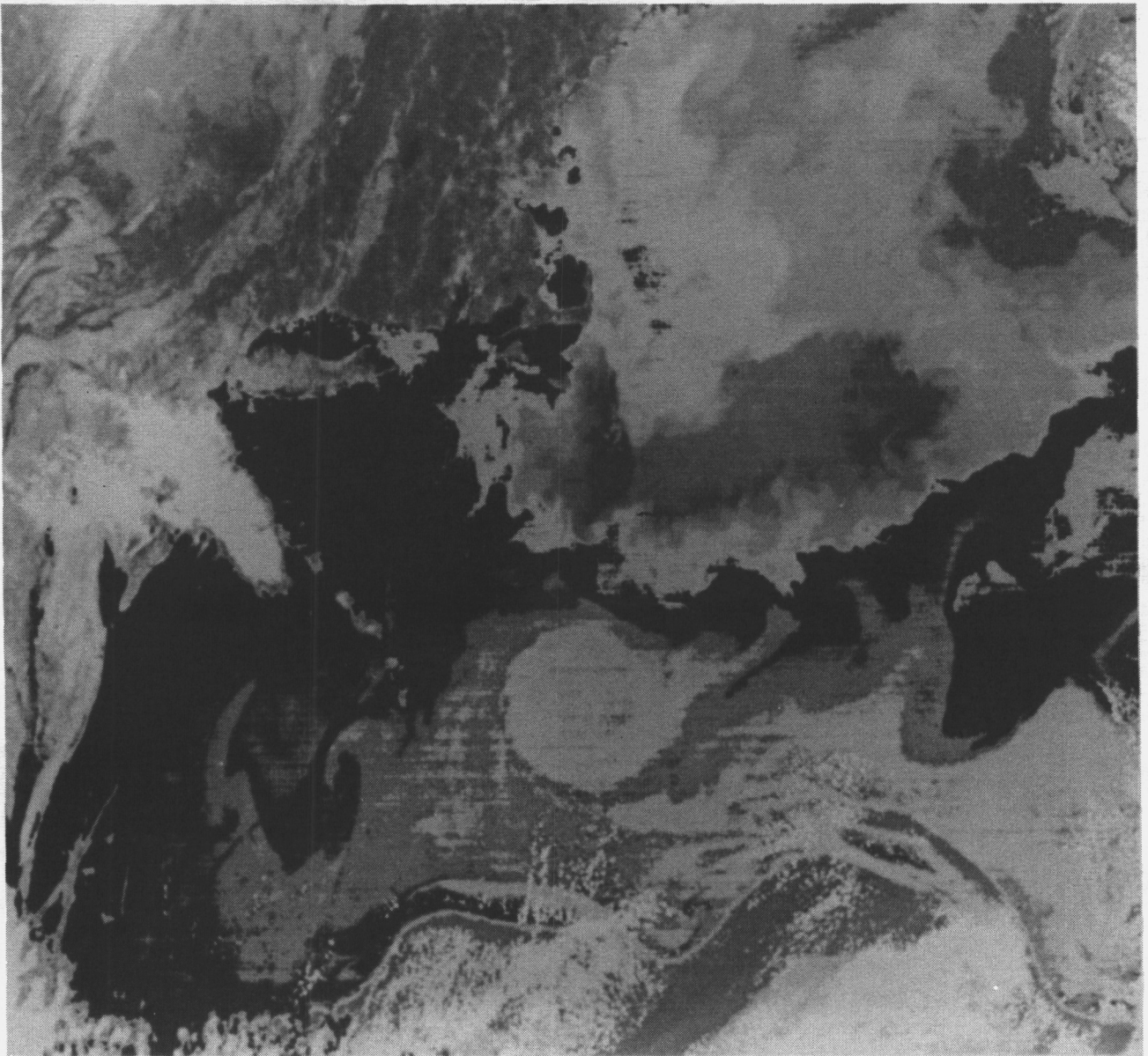


Figure 1



## CONVENTIONAL ALTIMETRIC SIGNATURE OF THE GULF STREAM

In addition to sea surface temperature, the ocean can be monitored using the visible wavelengths (as in the case of the Coastal Zone Color Scanner) or microwaves. Active microwave instruments offer the potential of all-weather monitoring because they are unaffected by the atmosphere. The GEOS-3 radar altimeter produced the topographic record shown in Figure 2 as it traversed the Gulf Stream. Because this current is nearly geostrophic, the one-meter dynamic height differential between its eastern and western walls could be related directly to current velocity if the orientation of the satellite's groundtrack with respect to the current's flow axis was known. With conventional nadir-tracking altimeters such as SKYLAB, GEOS-3, and SEASAT this information is not available.

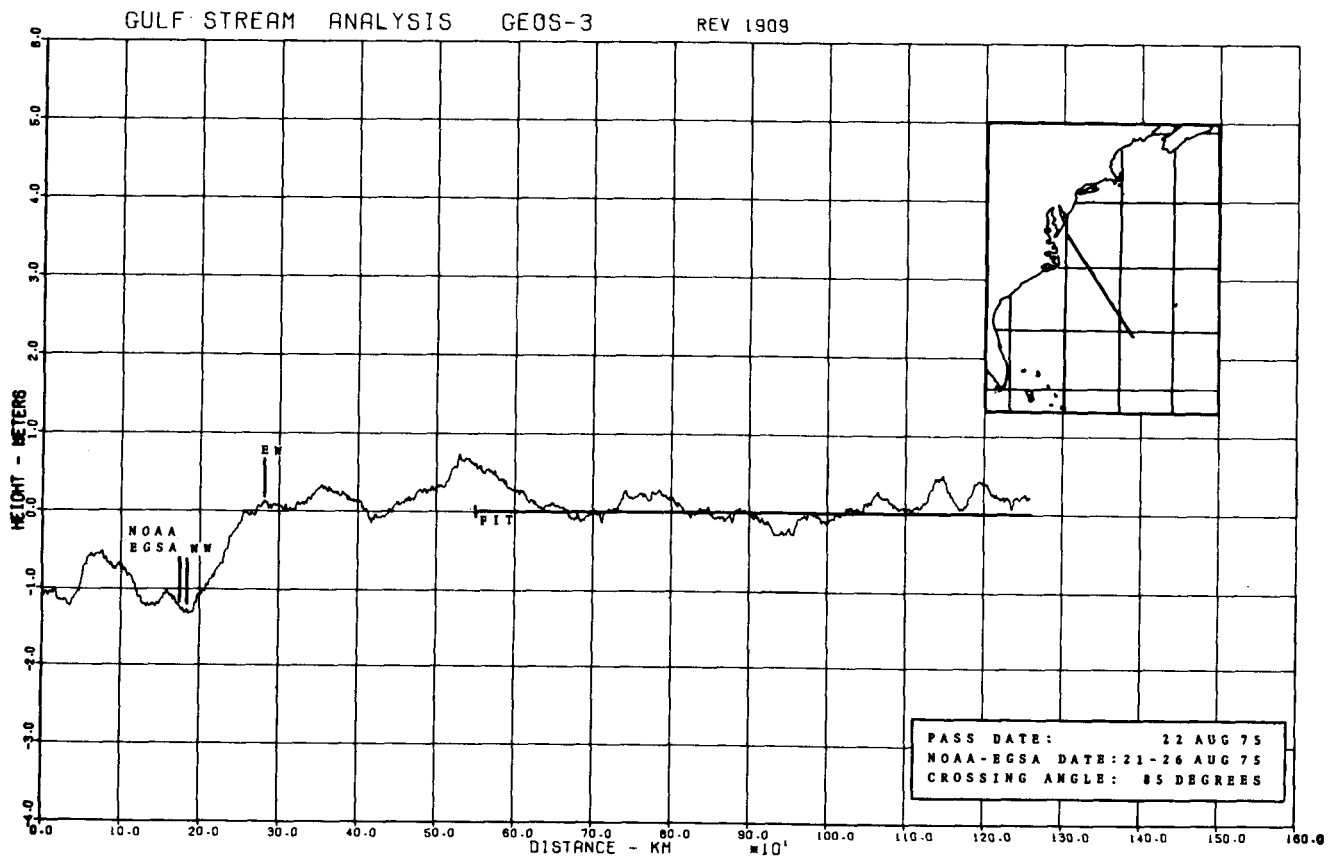


Figure 2

# CAPABILITIES OF MULTIBEAM ALTIMETRY

The top of Figure 3 shows the results of a simple simulation of a five-beam altimeter raking across an eddy which has a radius of 30 km and a maximum height signature of 45 cm. The interbeam spacing at the ground is 10 km. The altimeter is assumed to have a height resolution of only 10 cm; still, the shape of the eddy is clearly detected. Using a numerical differentiation formula, these measured topographic heights can easily be used to compute velocity.

The bottom of Figure 3 shows the computed velocity pattern. A clear maximum velocity is seen at a distance of 10 km from the eddy center. This is exactly the pattern that should be observed based on the eddy model used in the simulation. By using a numerical computation of the Laplacian of the height field, the circulation of the eddy can be calculated. This "curvature" measurement is independent of the attitude of the sensor. These results are not dependent on highly sophisticated advancements in technology but only on the addition of off-nadir beams, which seems to be within reach based upon NASA Langley's 15-m antenna progress.

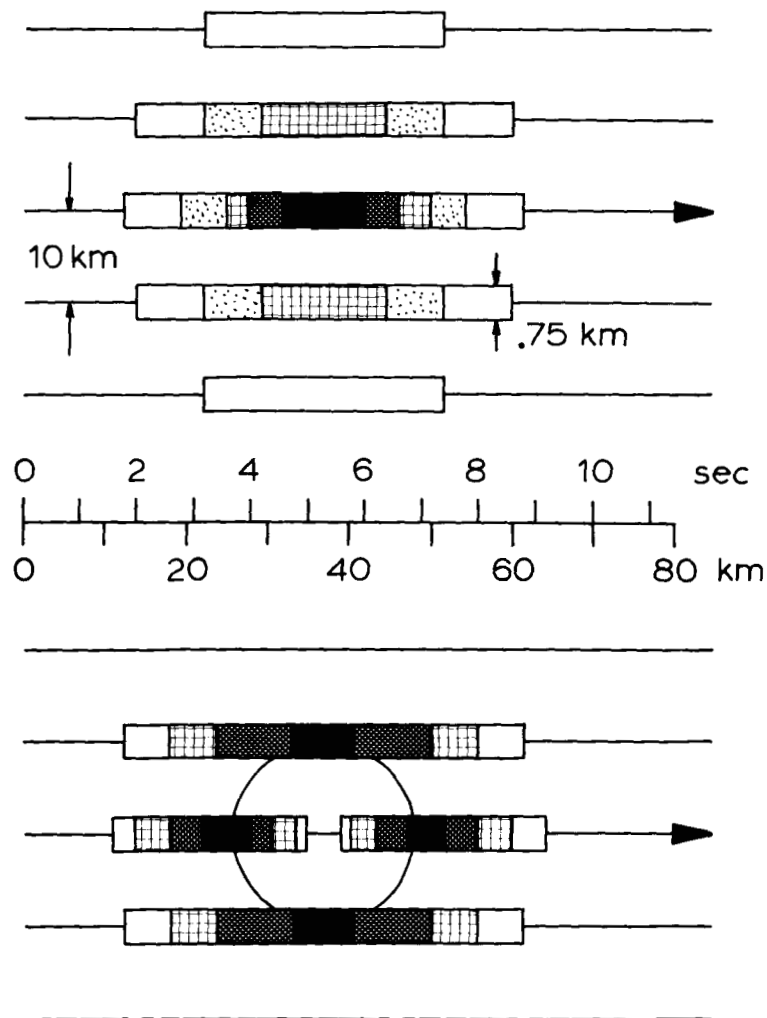


Figure 3

## INTERFEROMETRIC MULTIBEAM TECHNIQUE

To do precision altimetry, a range tracker needs a sharp waveform returned from the ocean surface. Off-nadir, the waveform tends to smear and stretch. Therefore, either a large real aperture system is needed to narrow the beamwidth and hence the duration of the returned waveform, or an interferometric technique schematically shown in Figure 4 can be used. Two antenna dishes of diameter  $d$  and separated by distance  $D$  are fed from the same rf source to produce multi-lobed beams where the lobe width is set by  $D$  and the overall envelope is a function of  $d$ . In this example, each antenna has two offset feeds so that two off-nadir beams are simultaneously generated. The signal returned will show a multi-peaked response as a result of the interferometer lobe intersections on the surface.

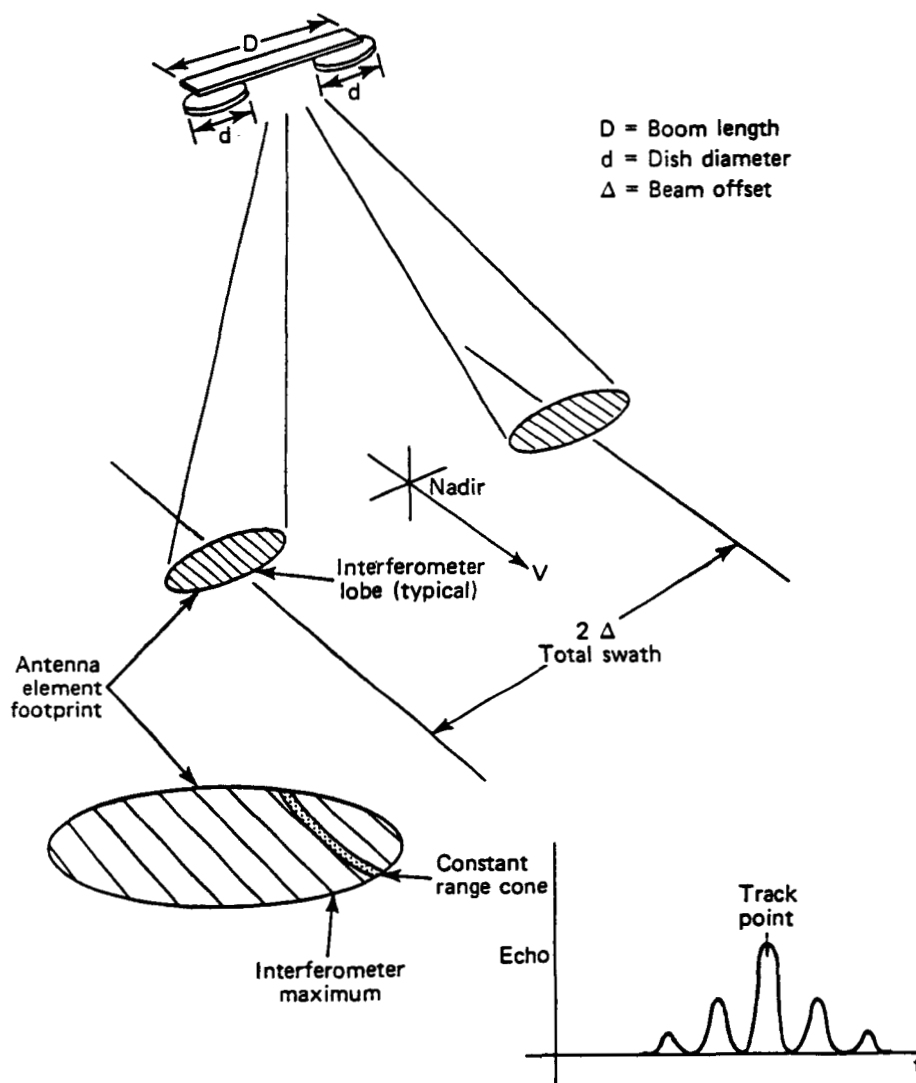


Figure 4

## USE OF THE 15-METER HOOP/COLUMN ANTENNA

A cooperative study with Langley Research Center personnel has been conducted to determine the suitability of the 15-m hoop/column antenna for multi-beam altimetry. Figure 5 shows an artist's view of its deployment on Shuttle. The antenna has the feature that its surface can be used in quadrants with each quadrant separately illuminated by microwave feed horns located on plates mounted to the center post. This is ideally suited for interferometry. By placing five feed horns on each of the two plates associated with opposite quadrants of the 15-m antenna, orienting them properly, and illuminating approximately 3-m-diameter spots within the two quadrants, it is possible to produce beam footprints centered at nadir  $\pm 1.5^\circ$ , and  $\pm 3.0^\circ$  off-nadir.

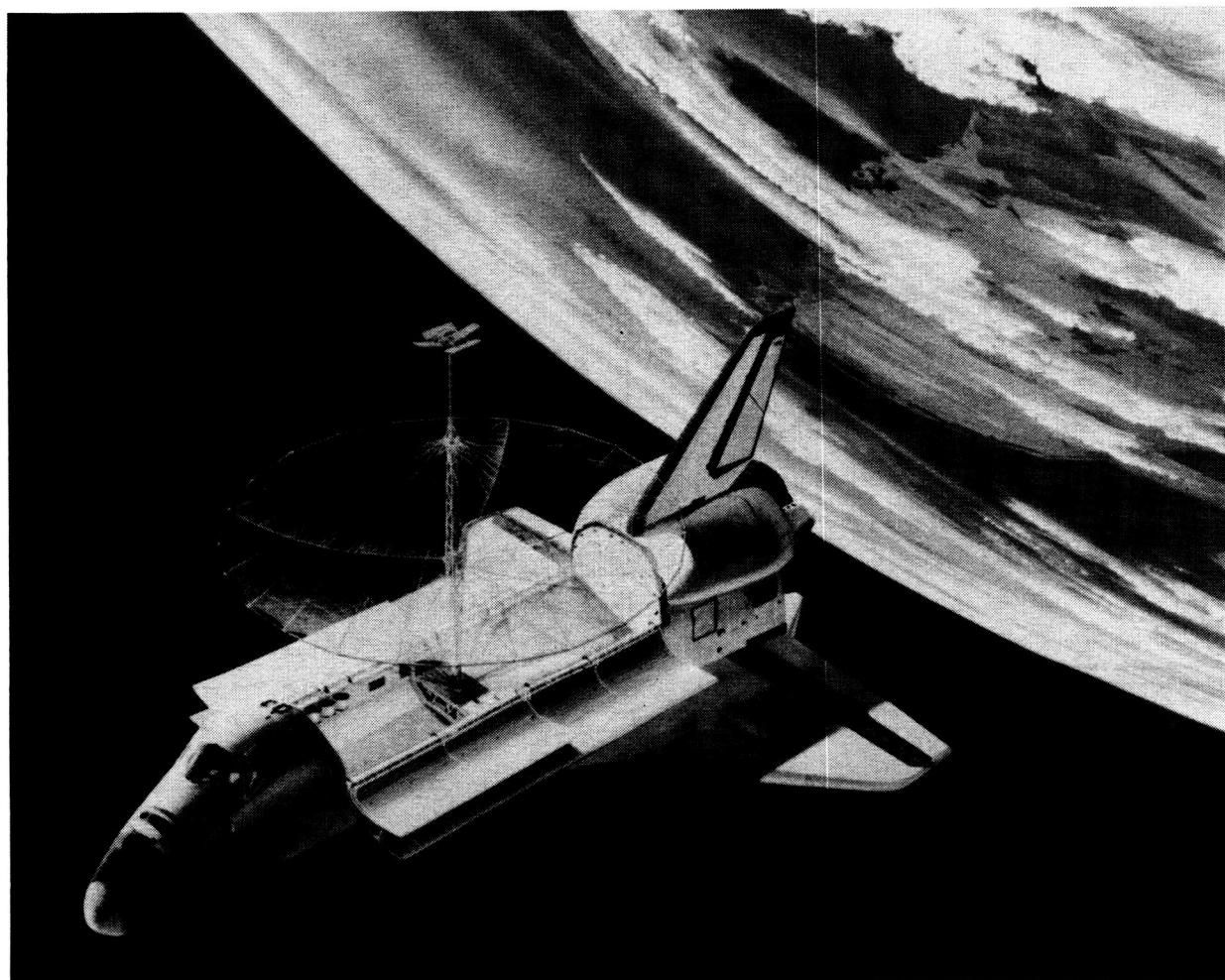
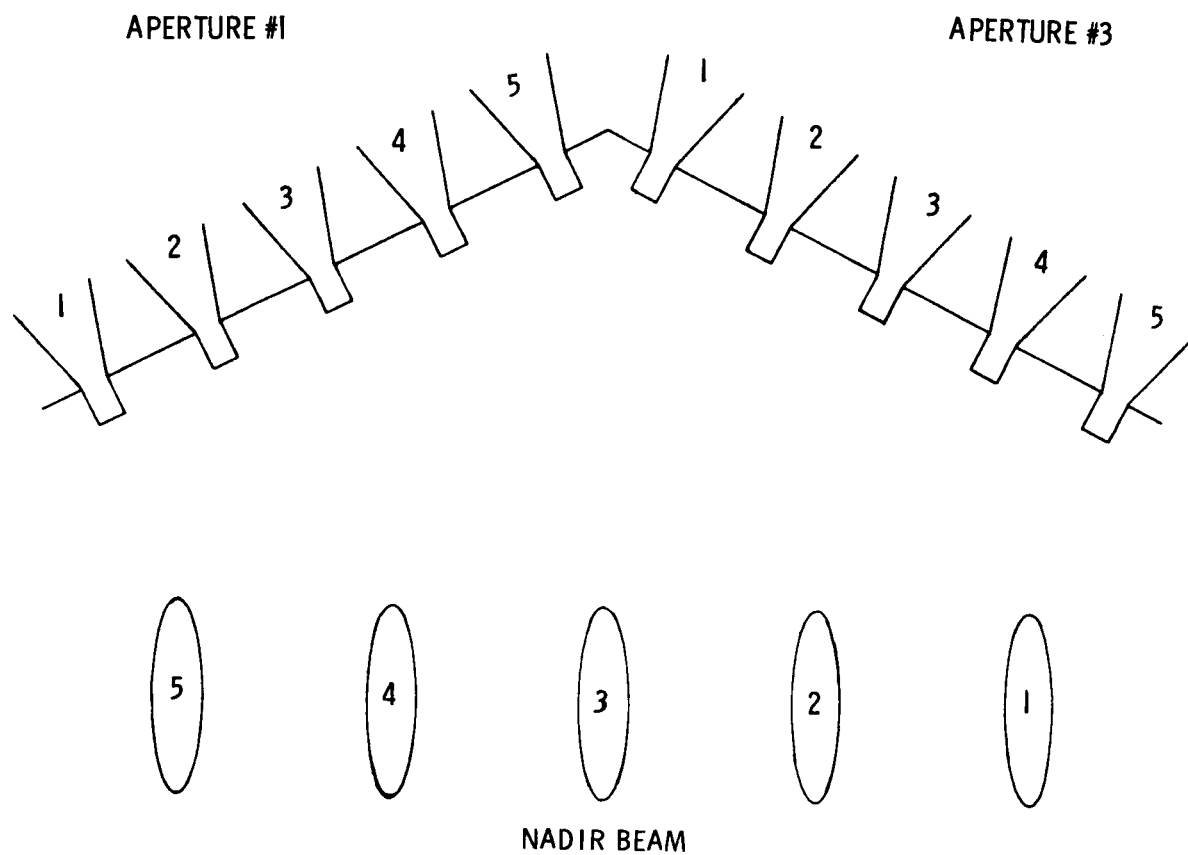


Figure 5

### FEED HORN ARRANGEMENT

The arrangement of the five pairs of feed horns on the mounting plates is shown in Figure 6. This produces five footprints each of which contains 20 interference lobes.



### FEED PANELS WITH ACROSS-TRACK BEAM FOOTPRINTS

Figure 6

# MULTIBEAM ALTIMETER FOOTPRINT LOBE PATTERN

The envelope of the antenna pattern resulting for the  $-1.5^\circ$  angle footprint is shown in Figure 7. The lobe structure resulting from the interference between the appropriate pair of feed horns trained on this footprint is contained within the envelope. For this antenna configuration, the lobe angular spacing is  $.146^\circ$ , which is equivalent to a real-aperture dish diameter of 8.65 m. The gain at the center lobe of each envelope is on the order of 52 dB, which is ample for real-aperture altimetry at Shuttle altitudes.

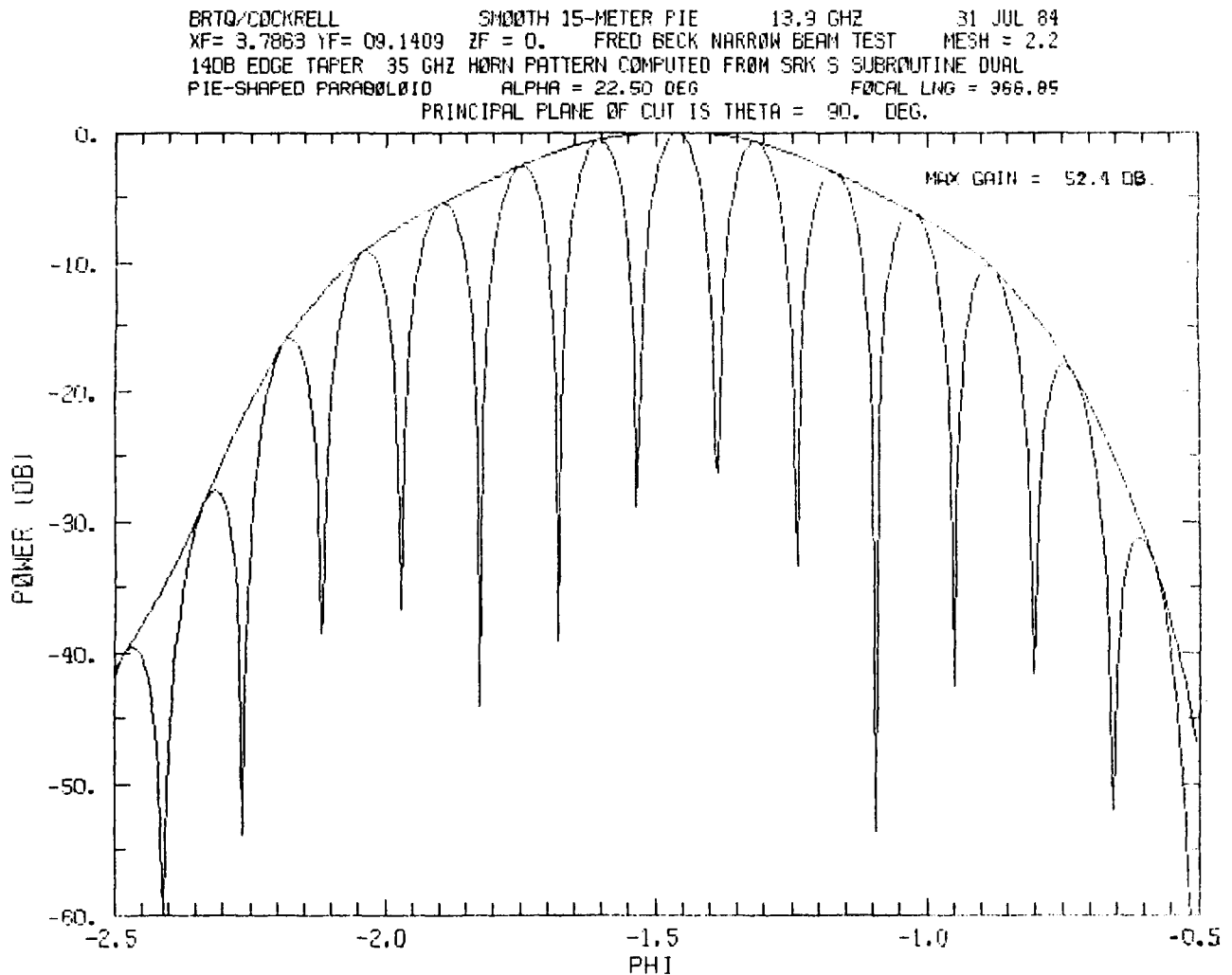


Figure 7

## DATA PROCESSING TECHNIQUES

Because satellite attitude uncertainties directly translate into height measurement errors, it is crucial that pointing be known as precisely as possible. However, for a Shuttle multibeam altimetry mission that is concerned mainly with the monitoring of eddies and currents, advantage can be made of crossing arc analyses. Over a particular area of interest, an ascending orbit and a descending orbit produce 25 intersections for a 5-beam multibeam system (fig. 8). If the measured height differences at the 25 points are minimized, then the tilt will be effectively removed. For a Shuttle mission experiment incorporating a multibeam altimeter with the 15-m antenna there are no known impediments in the way of successfully measuring mesoscale ocean dynamic features for the first time.

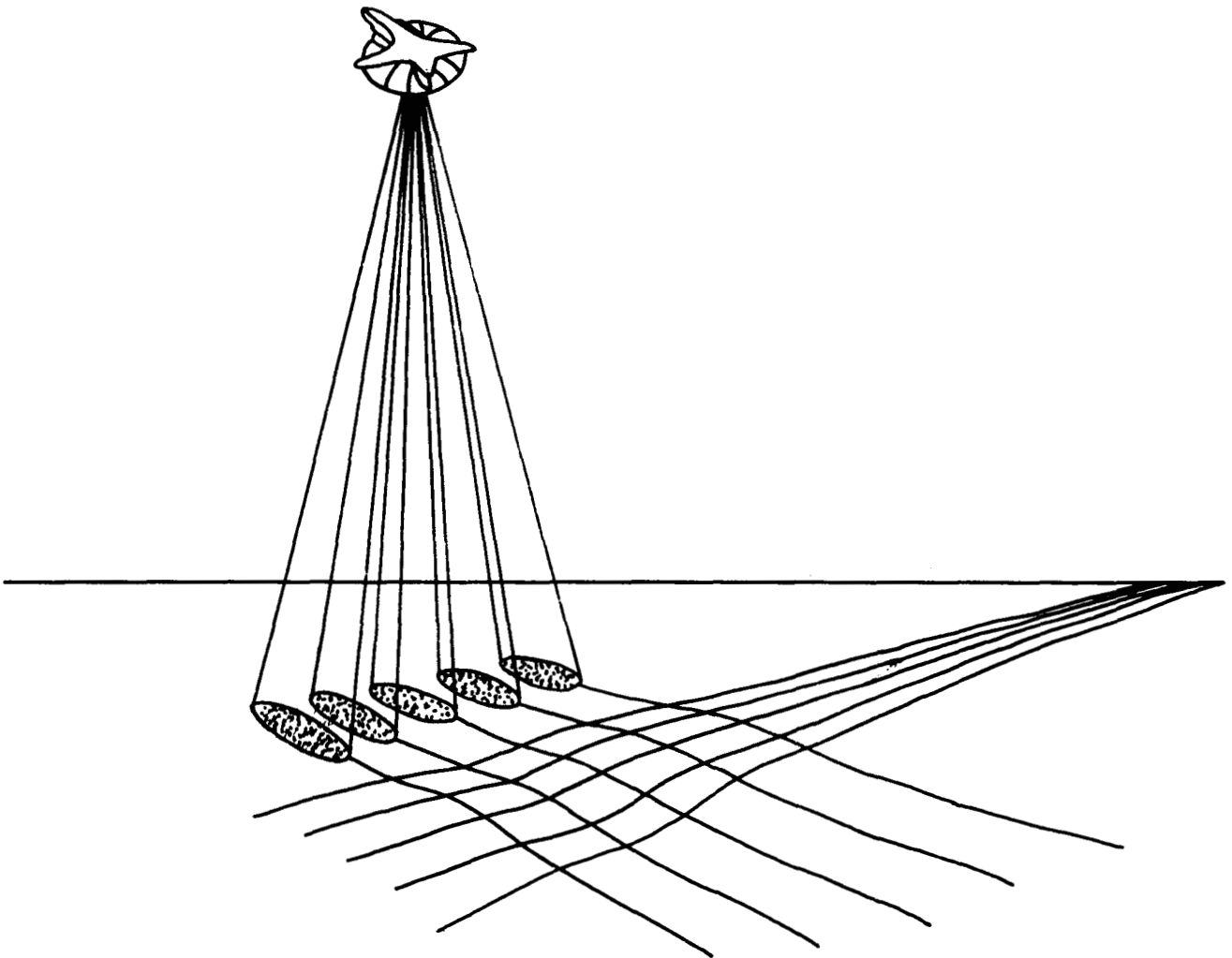


Figure 8

**Page intentionally left blank**



ORBITING MULTI-BEAM MICROWAVE RADIOMETER FOR SOIL MOISTURE  
REMOTE SENSING

J. C. Shiue  
NASA Goddard Space Flight Center  
Greenbelt, Maryland

R. W. Lawrence  
NASA Langley Research Center  
Hampton, Virginia

Large Space Antenna Systems Technology - 1984  
December 4-6, 1984

## INTRODUCTION

Knowledge of soil moisture is useful to many scientific disciplines. For example, in atmospheric circulation modeling for meteorology and climatology, soil moisture is an important boundary condition which affects the evapotranspiration process, which in turn influences humidity, cloud formation and precipitation. In hydrology, knowledge of soil moisture is needed for reservoir management, drought survey, and flood prediction. In agriculture applications, timely moisture information can be used to aid preplanting and irrigation scheduling, and routine soil moisture survey can help determine crop stress and increase the crop yield forecast accuracy.

The presence of water molecules, which are highly polar, increases the dielectric constant of the soil, which, in turn, causes a reduction in soil surface emissivity. Microwave emissivity can be ascertained by measuring the microwave brightness temperature and physical (thermal) temperature of the soil surface. Microwave radiometers are used to measure the brightness temperature whereas physical temperature is frequently obtained from an infrared radiometer such as the Multi-Spectral Scanner (MSS) or Thematic Mapper aboard the Landsats.

The "sensing depth" of passive microwave (defined here as the depth below the surface such that 63 percent of the power received by the radiometer emanated from the volume between this depth and the top surface) decreases with increasing sensing frequency. Consequently, in order to penetrate deep into the soil, low frequencies are preferred. However, because the resolution of passive microwave is determined by the real aperture antenna, low frequency implies large antenna aperture, especially from satellites. Moreover, at frequencies below L-band, there are radio frequency interferences (RFIs), both man-made and extra-terrestrial in nature. As a good compromise, the 21 cm hydrogen band (1.413 HGz), protected for radio astronomy purposes, is the prime frequency for radiometric remote sensing of soil moisture from space.

## THE EFFECT OF SOIL MOISTURE ON EMISSIVITY

Figure 1 shows, for the uppermost 25 cm of soil, some experimental data of measured soil surface emissivity at 1.4 GHz vs soil moisture together with two linear regression lines. The bare surface (solid line) has more "sensitivity" to soil moisture change. For one percent change in soil moisture (by dry weight), the corresponding change in emissivity is about 1.3 percent. The dashed line is from the combination of several types of vegetation covered surface and its sensitivity is greatly reduced.

In terms of microwave brightness temperature, the dynamic range of bare surface is about 90 K, and that of the mixed vegetation as shown in Fig. 1 is about 20 K. As we shall see later, a large spaceborne microwave radiometer has a typical measurement accuracy of about 3 K; hence, one can ascertain several levels of soil moisture from passive microwave, even in the vegetation covered areas.

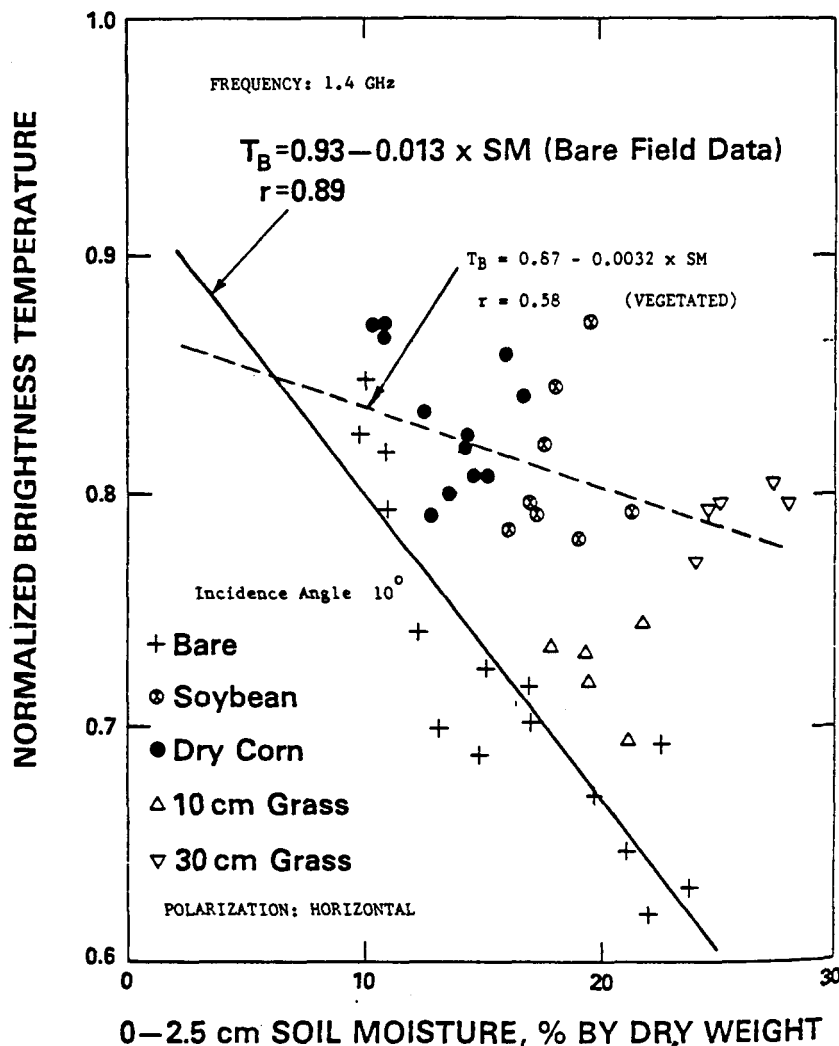


Figure 1 (Adapted from ref. 1)

## OTHER FACTORS INFLUENCING EMISSIVITY

However, microwave emissivity alone is not enough for soil moisture determination, because there are other factors that tend to complicate the interpretation of the soil moisture. Therefore, other ancillary data are also needed to help improve soil moisture retrieval. Surface geometric characteristics, such as vegetation canopy and surface roughness, will reduce the sensitivity of emissivity to soil moisture change. Of the two factors, vegetation canopy is the more serious one. This effect must be removed before meaningful interpretation from vegetated areas can be made, because vegetation can reduce the sensitivity by up to 50 percent. By using measurements from visible and near IR wavelengths, one can differentiate bare from vegetated areas, and also ascertain the biomass of the vegetation. The roughness effect can be estimated with either dual polarization or multiple frequency techniques. In general, this effect is not as severe as that of vegetation canopy.

The microwave emissivity is also different for different soil texture, due to the different binding force of host soil particles. However, since the primary interest from most scientific or application points of view is the available water from the soil, this effect becomes unimportant. It turns out that the emissivity as a function of "available water" (field capacity) is nearly independent of soil texture.

Figure 2 depicts the theoretical sensing depth vs frequency for several soil moisture contents and vertical profiles.

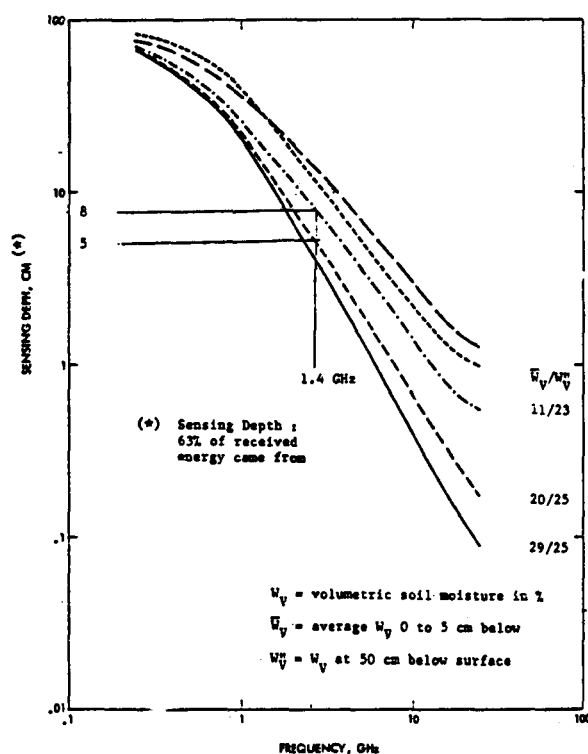


Figure 2 (From ref. 2)

## A MULTI-BEAM MICROWAVE RADIOMETER WITH 15-M ANTENNA

For soil moisture sensing, both high spatial resolution and large swath width are desirable system parameters. It is also important that the radiometer map a given area continuously. However, at times not all three conditions can be fully achieved and trade-offs must be made. Since mechanical scanning is impractical for such a large antenna, a multiple-feed design is used to achieve the large swath width.

Figure 3 shows the side and front views of the current quad aperture design 15-meter hoop/column antenna, as currently designed. The front view shows the four 6.09-meter sub-apertures.

The current design is a multiple beam/multiple quadrant offset reflector system. Four separate areas of illumination (sub-apertures) on the parent reflector are shown. The surface is shaped as if it were four offsets; thus, the parent reflector is cusped.

As a result of the large physical size of the feed arrays needed, only two six-meter sub-apertures of the 15-meter parent aperture are planned. Feed arrays then are able to produce a total of 29 beams across the ground track of the sensor platform. The reflector shape will include two sub-apertures rather than the four currently under construction. The resulting arrangement is called a "pushbroom" configuration.

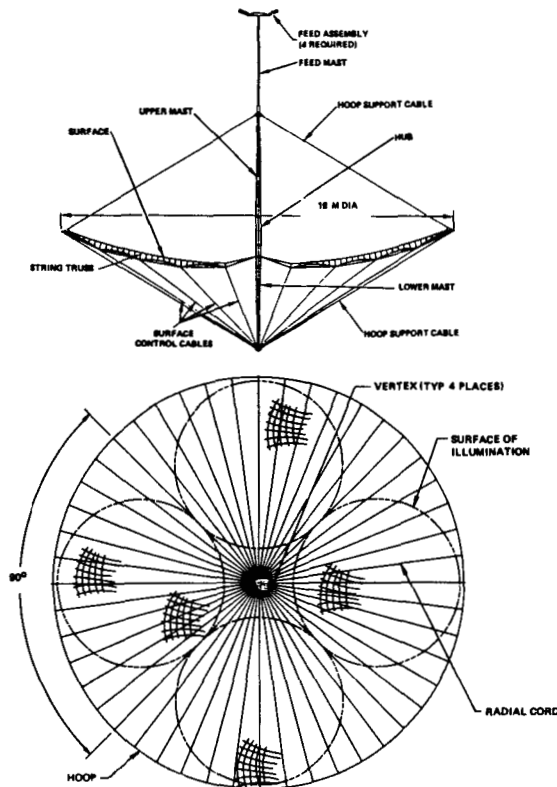


Figure 3

## BEAM FORMATION

Only two sub-apertures are used for the radiometer mission, as shown in Figure 4. The feed arrays are located between the two sub-apertures so as to minimize the blockage. The top array contains 14 separate feeds and illuminates sub-aperture #1. Similarly, the bottom feed array contains 15 separate feeds and illuminates sub-aperture #3.

The center of the bottom feed array generates beam #15 which is pointed at nadir. The two feeds at the end of this feed array yield the two edge beams, #1 and #29. The remaining 12 feeds of this array produce the other odd numbered beams. The top feed array produces 14 even numbered beams, #2 through #28, whose positions are interspersed among the 15 beams produced by the bottom feed array.

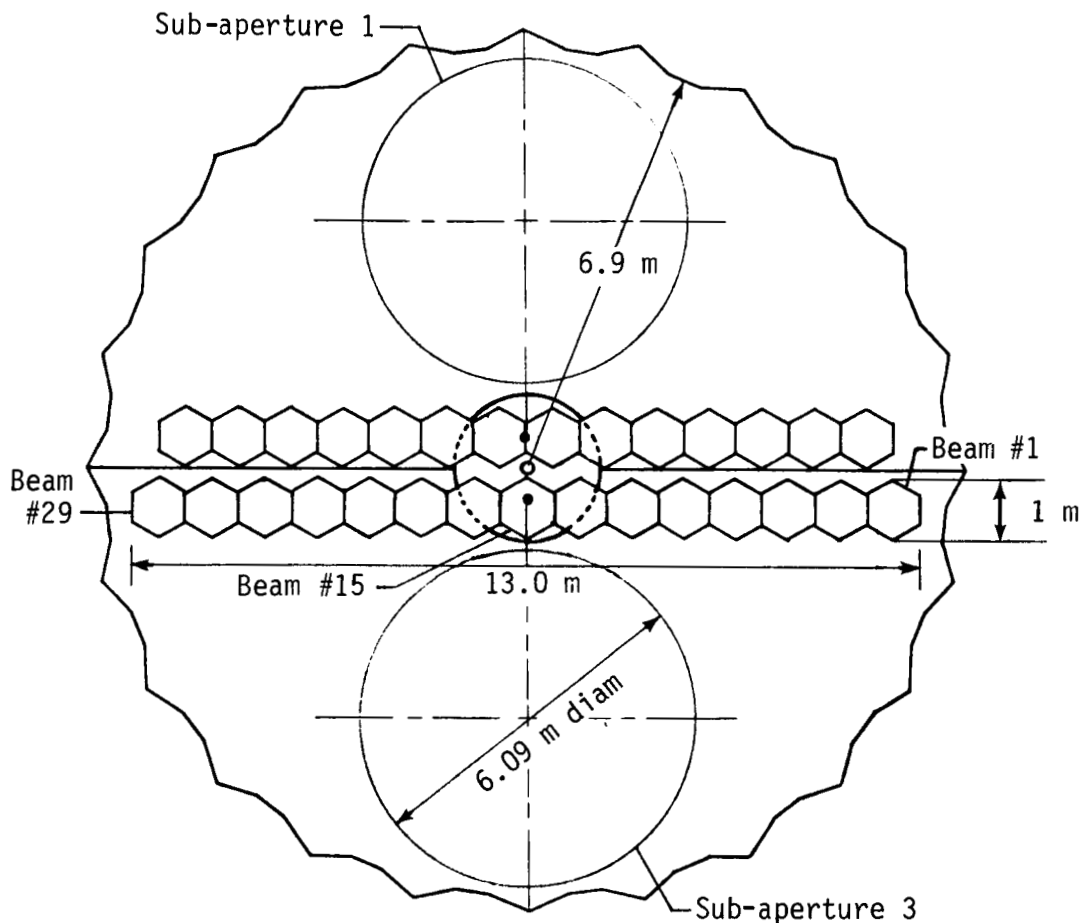


Figure 4

# FOOTPRINT LOCATION FOR THE 15-M HOOP-COLUMN PUSHROOM RADIOMETER

Figure 5 shows one-half of the interspersed beams, from #15 (nadir) to #29. The remaining beams #1 to #14 are the mirror image of Figure 5, symmetrical about the vertical 90 degree line.

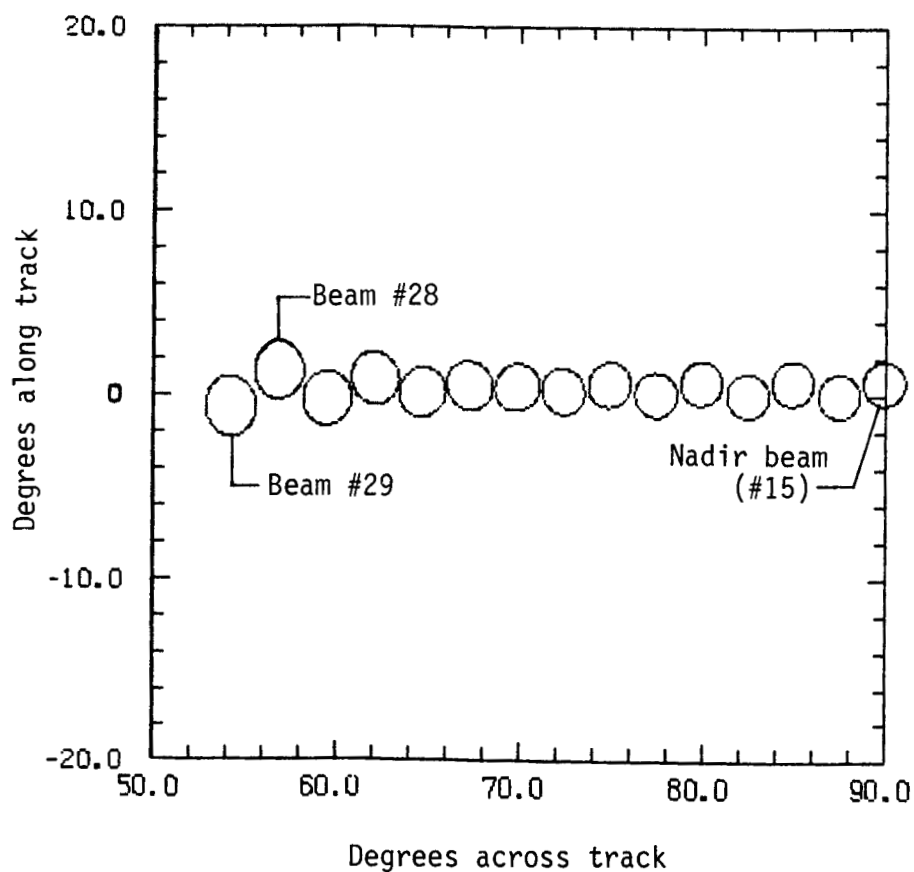
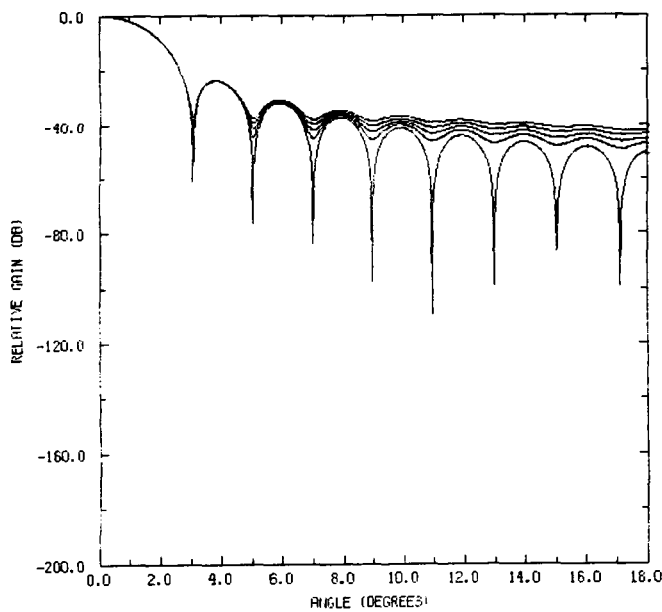


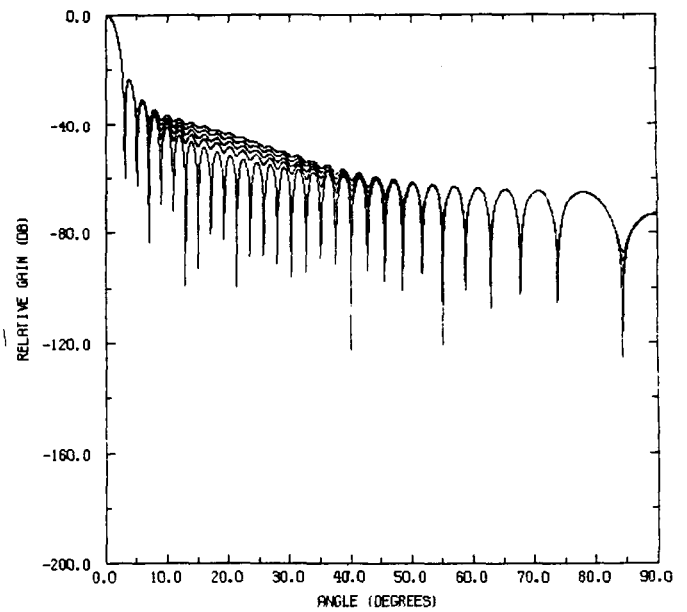
Figure 5

## ANTENNA GAIN PATTERN OF THE CENTER BEAM

The secondary radiation (antenna gain) pattern of the nadir beam (#15) is shown in Figure 6a. The primary radiation pattern of the feed is assumed to have a shape of "cosine  $\theta$ " raised to 1.5, where  $\theta$  is the angle from the center of the 6.09 m sub-aperture. The five separate patterns correspond to the different reflector surface roughness sizes of 0, 50, 69, 90, and 110 mils (RMS). The correlation length  $C$  is assumed to be 10 inches. It is seen that the phase errors due to random surface roughness tend to fill the space between the far outside lobes; the main lobe pattern is hardly changed. Figure 6b is also the secondary radiation pattern of the nadir beam, with the angle extended to 90 degrees.



(a)



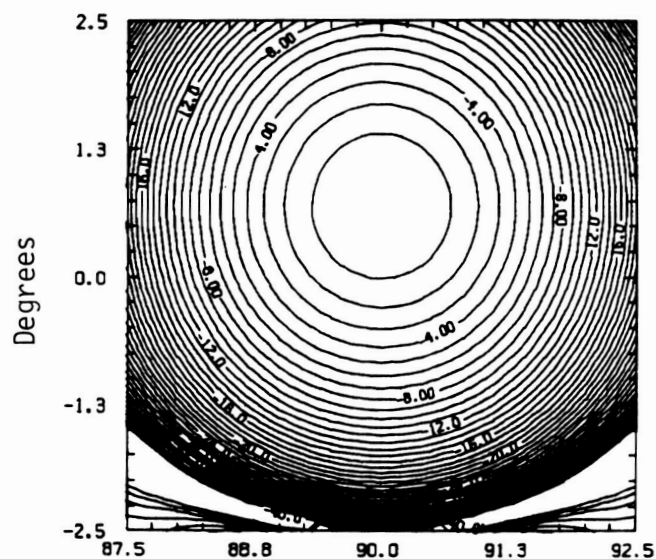
(b)

Figure 6

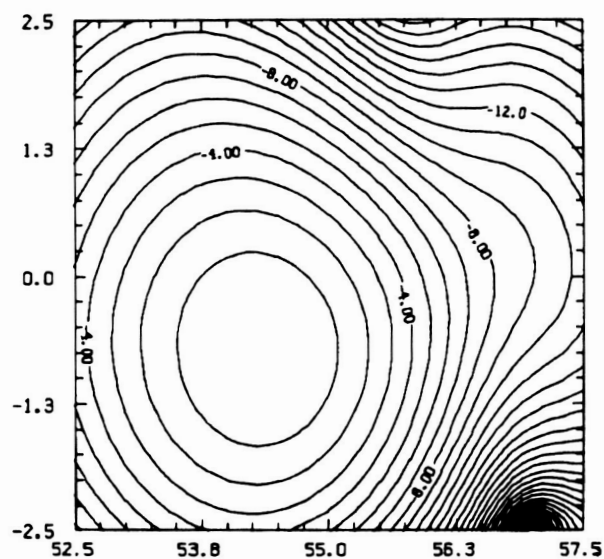


# ANTENNA RADIATION PATTERN

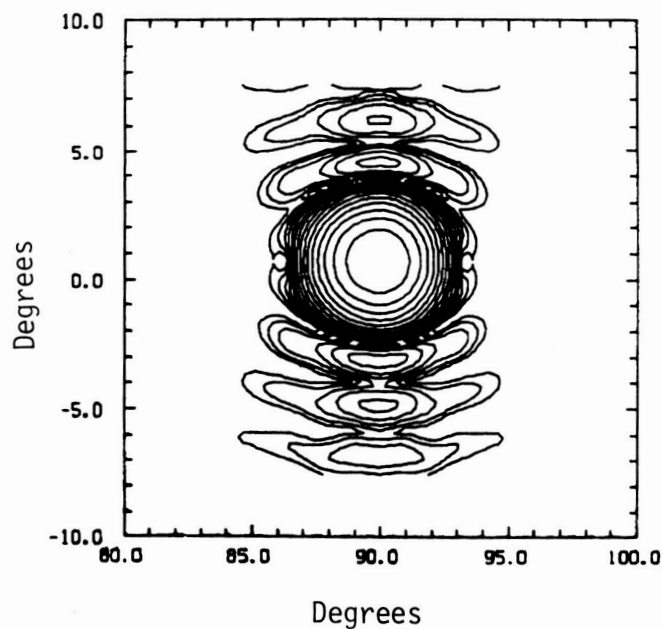
Figure 7a is a plot of the contour of the secondary radiation pattern of the nadir beam (#15) within 2.5 degrees of nadir. Figure 7b is a similar plot for the main lobe of Beam #29. Figure 7c is a plot of Beam #15's radiation pattern out to 10 degrees. The contour interval is 1 dB.



(a)



(b)



(c)

Figure 7

## LOSS DUE TO REFLECTOR ROUGHNESS

Figure 8 shows the effect of reflector surface roughness on beam efficiency. For a 100 mil RMS, the resulting reduction in beam efficiency due to surface roughness will be about 2 percent, if one starts with an ideally smooth reflector surface with a beam efficiency of 90 percent.

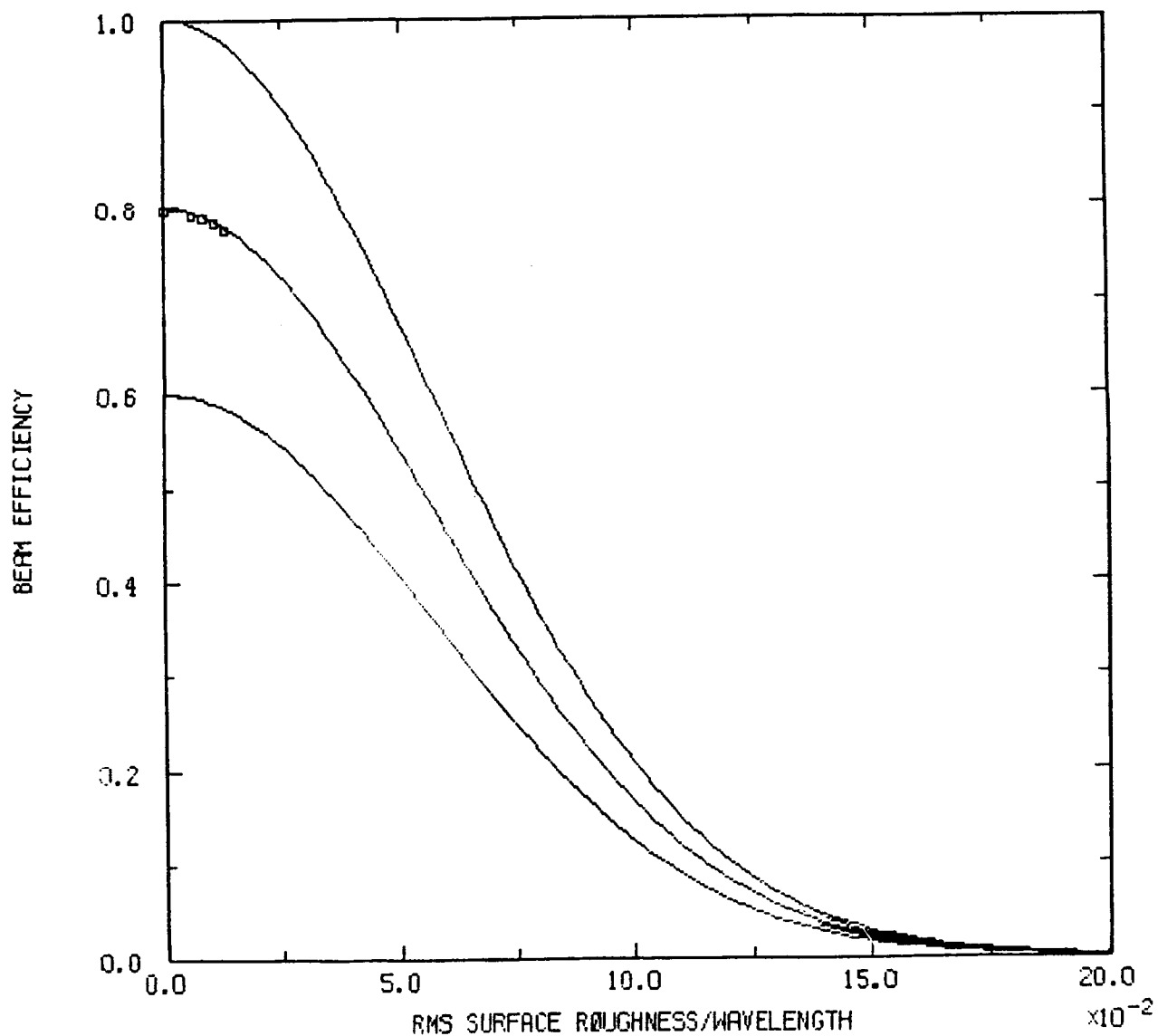


Figure 8

## SUMMARY OF SYSTEM PARAMETERS OF THE RADIOMETER

From a 300 km orbit, the 2.25 degree beam width would yield a nadir spatial resolution of 13.1 km at nadir. For the swath edge beams (#1 and #29), the footprint size is degraded to 18.7 km x 14.7 km. The radiometer will yield a swath of 458.4 km. The nadir angle at the edge of the swath is about 37 degrees, and the corresponding incidence angle is 39 degrees. The time it takes for the sub-satellite point to move a footprint diameter is 1.77 sec. From a 300 km orbit, the equatorial drift is about 2500 km per orbit. With the 458 km swath width, the radiometer can produce a global soil moisture map in 6 days.

The system parameters and accuracy budget of the microwave radiometer are as given in Table 1.

Frequency:	1.413 GHz
Bandwidth	27 MHz
Effective Antenna	
Aperture Diameter:	6.09 m
Number of Beams:	29
Polarization:	Horizontal
Beam Efficiency:	85 to 90%
Temperature Sensitivity:	0.36 K <sup>*</sup>
Integration Time:	1 sec. (assumed)
I.F. Bandwidth:	13.5 MHz
System Noise Figure:	2 dB (dsb)
Antenna Temperature:	280 K
Feed Loss:	1.5 dB
Mesh Loss:	0.17 dB
Calibration Accuracy Estimate:	
Antenna Mesh (emissivity/transmissivity)	2.3 to 2.8 K
Feed Loss	0.3 to 0.6 K
Receiver Calibration Error	2.0 K
	RSS
	3.1 to 3.5 K

\* Does not include spatial antenna effects such as the inversion from antenna brightness temperature or the defined resolution cell.

Table 1

## SUMMARY OF RADIOMETER SYSTEM REQUIREMENTS

The power, weight, and communications requirements of the 29 channel microwave radiometer are given in Table 2.

### POWER REQUIREMENTS

Assembly	Power Per Radiometer
Front-end	1.8 W
Video	2.7 W
Signal Processing	3.5 W
Total Power Per Channel	<u>8.0 W</u>
DC/DC Converter Efficiency	80%
Total Power for 29 Channels	290 W
Misc. Power	10 W
Total Power	<u>300 W*</u>

### WEIGHT REQUIREMENTS

Feed Panel:	150 oz
Radiometer	
Front-end	16 oz
Thermal	16 oz
Video	10 oz
Signal Proc.	18 oz
Enclosure	80 oz
Total wt Per Channel:	290 oz
Total wt for 29 Channels	525 lb
Interconnecting Structure	75 lb
Total Weight	<u>600 lb*</u>

### DATA RATE REQUIREMENT

Radiometer Duty Cycle	64 BPS
Reference Temperature	16 BPS
Multiplexed Physical Temperature	16 BPS
Total Per Channel	<u>96 BPS</u>
Coding Overhead:	28 Coded 8 Bit Word/Sec
Total Bit Rate: (29 Beams)	6496 BPS

\* Does not include requirements for thermal control system.

Table 2

## REFERENCES

1. Wang, J. R., J. C. Shiue, and J. E. McMurtrey III, Microwave remote sensing of soil moisture content over bare and vegetated fields, Geophys. Res. Lett., 7, 801-804, 1980.
2. Njoku, E. G., J. P. Scheilde, and A. B. Kahle, Joint microwave and infrared studies for soil moisture determination, Rept. SM-Y0-00495, Jet Propulsion Laboratory, Sept. 1980.

**Page intentionally left blank**

LOW-FREQUENCY MICROWAVE RADIOMETER FOR N-ROSS

J. P. Hollinger and R. C. Lo  
Space Sensing Applications Branch  
Aerospace Systems Division  
Naval Research Laboratory  
Washington, D. C.

Large Space Antenna Systems Technology - 1984  
December 4-6, 1984

## Abstract

The all-weather, global determination of sea surface temperature (SST) has been identified as a requirement needed to support naval operations. The target SST accuracy is  $\pm 1.0$  K with a surface resolution of 10 km. Investigations of the phenomenology and technology of remote passive microwave sensing of the ocean environment over the past decade have demonstrated that this objective is presently attainable. Preliminary specification and trade-off studies have been conducted to define the frequency, polarization, scan geometry, antenna size, and other essential parameters of the Low-Frequency Microwave Radiometer (LFMR). It will be a dual-polarized, dual-frequency system at 5.2 and 10.4 GHz using a 5.9-meter deployable mesh surface antenna. It is to be flown on the Navy-Remote Ocean Sensing System (N-ROSS) satellite scheduled to be launched in late 1988.

### 1. Introduction

The all-weather, global determination of sea surface temperature (SST) has been identified as a requirement needed to support naval operations. The target SST accuracy is specified as  $\pm 0.5$  K at a surface resolution of 10 km with an accuracy of  $\pm 1.0$  K and surface resolution of 25 km acceptable. Passive microwave radiometry has the potential of meeting this requirement.

During the period 1972-78 the Naval Air Systems Command (NAVAIR) supported investigations of the microwave radiometric properties of the ocean and atmosphere which led to the specification of the Remote Ocean-surface Measurement System (ROMS). Although ROMS was not built, the understanding of the phenomenology and technology developed for it directly contributed to subsequent systems. In 1978 NASA launched an experimental sensor, the Scanning Multichannel Microwave Radiometer (SMMR), on both the SEASAT and NIMBUS-7 satellites to explore the all-weather measurement of sea surface temperature, as well as other oceanographic and atmospheric parameters, with microwave radiometry. The SMMR employs a 79-cm diameter antenna and dual-polarized radiometers at 6.6, 10.7, 18.0, 21.0, and 37.0 GHz with the 6.6-GHz frequency primarily chosen for its sensitivity to SST. Results from SMMR indicate that the SST can be measured to an RMS sensitivity  $\pm 1.2$  K or better with it (1). However, the surface

resolution of SMMR at 6.6 GHz is only 150 km.

The next generation of passive microwave sensors planned by NASA was the Large Antenna Multichannel Microwave Radiometer (LAMMR) as part of the sensor complement of the National Oceanic Satellite System (NOSS). LAMMR was planned as a seven-frequency, dual-polarized radiometric system with a four-meter antenna and a performance goal for SST of  $\pm 0.5$ -K precision,  $\pm 1.0$ -K absolute accuracy, and 24-to 36-km spatial resolution. Although NOSS and LAMMR were not built due to funding limitations, the design studies performed and the continuing development of the necessary technology have demonstrated that the SMOP OR is presently attainable.

The Navy-Remote Ocean Sensing System (N-ROSS) is a planned oceanographic satellite in the Navy core program for POM-84 with funding beginning in FY'85 to meet the SMOP OR. The sensor complement of N-ROSS is to include a scatterometer to measure the marine wind field; an altimeter to measure wave spectra, the Earth's geoid, and to locate fronts and eddies; and a Mission Sensor Microwave/Imager (SSM/I) to measure sea ice, precipitation, atmospheric moisture, and surface winds. All-weather measurement of sea surface temperature will require the development of a second passive microwave system. Critical to the development of this system is the selection of the operating frequency and other instrument characteristics compatible with Earth sources of RFI and optimized to functionally integrate with the SSM/I and N-ROSS.

### 2. Sensitivity and Retrieval Accuracy

A primary criterion for the selection of frequency for the low-frequency microwave radiometer (LFMR) is sensitivity to, and thus the retrieval of, sea surface temperature (SST). The present sensitivity study is limited to the frequency range of 2 to 14 GHz since frequencies below 2 GHz and above 14 GHz are relatively insensitive to SST (2). Three different approaches are used to examine the sensitivity question. They are: (a) theoretical studies, (b) interpretation of satellite data, and (c) the use of aircraft data. The theoretical studies are the most versatile in that wide ranges of environmental conditions can be simulated, and many frequencies and frequency combinations can be examined. Functional relationships are built into the theoretical models providing the freedom to examine various trade-off relationships. Satellite and aircraft



data have, of course, the advantage of being actual measurements. They are, however, restricted in frequency and range of environmental conditions. The combination of all three studies provides a more complete basis for the determination of the microwave radiometric sensitivity to SST.

The rate of change of brightness temperature with respect to sea surface temperature, calculated using the geophysical model (3) developed by NRL, is given in Figure 1 as a function of frequency for several mean sea surface temperatures. The climatology (4) of the ocean-atmosphere system used with the model was compiled for mid-latitude summer conditions. The calculations are for vertical polarization of an incidence angle of 53.1°. All the parameters of the ocean-atmosphere system are kept constant except the SST for the calculation of the derivative.

The sensitivity is much greater over the frequency range of 6 to 10 GHz for very warm water, i.e., a SST of 30°C. However, the sensitivity decreases drastically, especially at the higher end of the frequency range, as the water temperature becomes colder. At 10 GHz and beyond, little sensitivity remains for the colder SST values. The sensitivity trend is reversed at the lower end of the frequency range, e.g., between 2 and 3 GHz. These frequencies are more sensitive to colder than to warmer water. Judging from Figure 1 the optimal frequency range for overall sensitivity appears to be in the 4-to 6-GHz range.

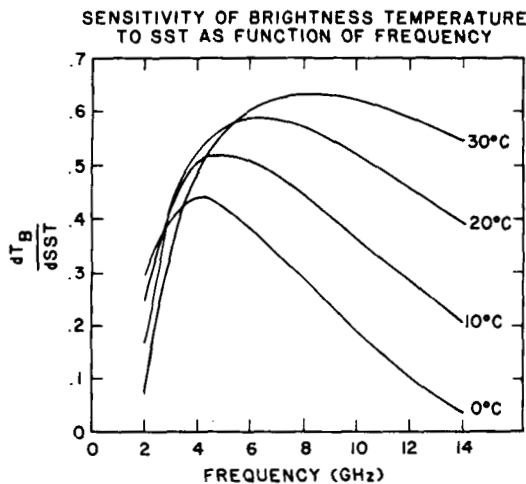


Figure 1. Sensitivity of Brightness Temperature to SST as a Function of Frequency.

The choice of an optimum frequency not only depends on the sensitivity to SST but also on the sensitivity to other environmental parameters. If a given frequency is more sensitive to another parameter, such as wind speed, it will primarily provide information concerning that parameter rather than SST, even though the sensitivity to SST may also be significant. Some of the most significant geophysical parameters for the micro-

wave frequency range of interest are salinity, SST, wind speed, integrated atmospheric liquid water (clouds), and integrated atmospheric water vapor. The changes in the vertically polarized brightness temperature as a function of frequency are depicted in Figure 2 for those geophysical parameters. The incidence angle used in the calculations is again chosen to be the same as that of the SSM/I instrument, 53.1°, since there are advantages to choosing the same scan geometry for the LFM/R because of possible mutual support and applications between the two instruments. The sensitivity to SST is dominant between about 2 and 10 GHz. Above about 10 GHz the effects due to water, both liquid and vapor, exceed that of SST while below about 2 GHz salinity effects are greater.

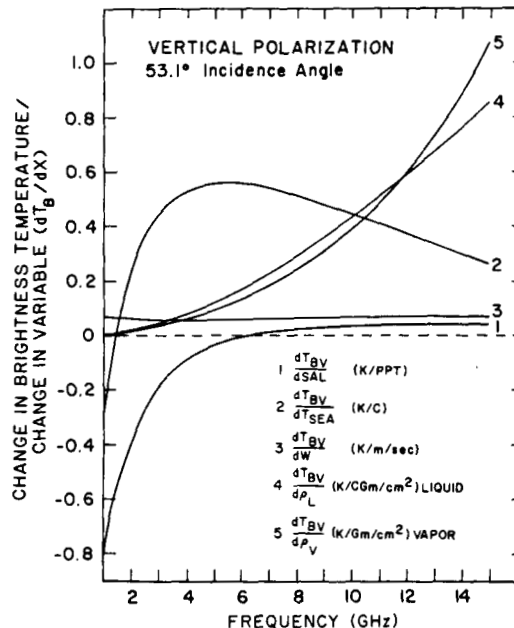


Figure 2. The Sensitivity of Vertical Brightness Temperature to Geophysical Parameters as a Function of Frequency.

However in order to examine the true relative sensitivity to various environmental parameters, the brightness temperature change caused by representative changes in the other relevant parameters must be examined. Assuming that the Navy's operational requirements for the other parameters are met, i.e., residual errors of 1 part per thousand for salinity, 2 m/sec for surface wind speed, 0.01 gm/cm² for columnar density of liquid water, and 0.2 gm/cm² for columnar density of water vapor along with the minimum requirement of 1°C for SST, the corresponding resultant changes in brightness temperature were calculated. These changes in brightness temperature are given in Figure 3. As to be expected from Figure 2 the salinity effect ceases to be significant for frequencies higher than about 3 GHz, and the vertically polarized brightness temperature is relatively insensitive to wind speed and water vapor. Liquid water is the only serious contender with SST and then only at the higher frequencies, above about 10 GHz.

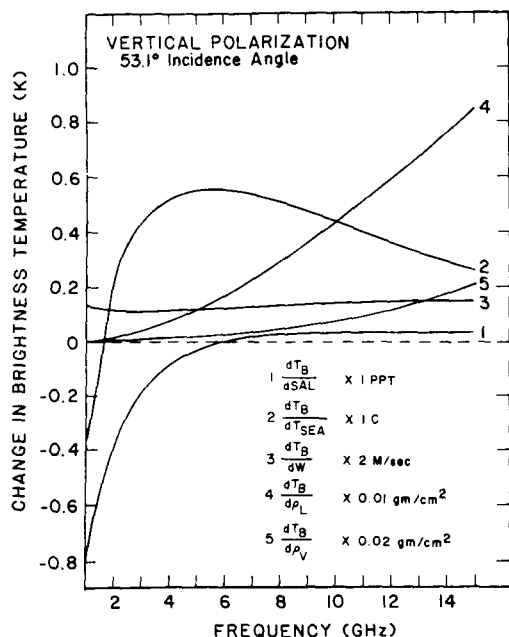


Figure 3. Changes in Vertical Brightness Temperature Caused by Changes in Geophysical Parameters.

Similar calculations are presented for the horizontally polarized brightness temperature in Figure 4. Wind speed and liquid water are the

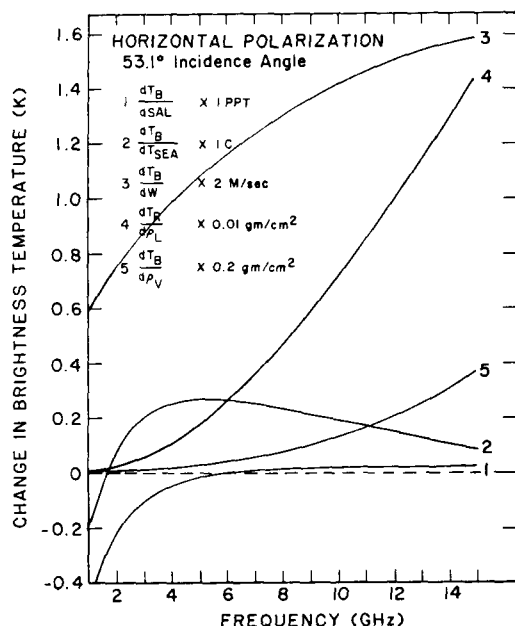


Figure 4. Changes in Horizontal Brightness Temperature Caused by Changes in Geophysical Parameters.

dominating environmental parameters. The sensitivity to water vapor is also higher than that of SST beyond 11 GHz. Thus, horizontal polarization

primarily contains information concerning wind speed and liquid water. It therefore provides a means to remove the effect of these parameters from the vertically polarized brightness temperature and enhances the accuracy of the SST estimation. The horizontally polarized brightness temperature of the LFMF could also be used in conjunction with the SSM/I to enhance the retrieval of surface wind speed and liquid-water content.

The theoretical sensitivity studies indicate that a frequency in the 4-to 6-GHz region is optimal for the overall retrieval of SST, and a frequency in the 8-to 10-GHz region is optimal for the retrieval of the SST of warm ocean water. The studies also indicate that both vertical and horizontal linear polarization are required for the retrieval of SST.

### 3. Satellite Data

Two types of real data are available for the LFMF frequency selection. The first of these is satellite data. Among the satellite instruments that have been flown during the past decade, the only instrument which contains a multiple frequency passive microwave radiometer containing frequencies in the required range of from 4 to about 10 GHz is the Scanning Multichannel Microwave Radiometer (SMMR). Both the SEASAT and the NIMBUS-7 satellites, launched in 1978, carried a SMMR. A number of serious problems complicate the proper interpretation of the SMMR data. However, careful selection of data and definition of retrieval algorithms have led to reasonable retrievals of the SST (1,5).

A study of the sensitivity of the two lowest frequencies (6.6, 10.7 GHz) of the SEASAT SMMR to SST and an analysis of the SST retrieval using these two frequencies were conducted by Frank Wentz of Remote Sensing Systems (RSS) (6). The total mission of SEASAT lasted 104 days, from June 28 to October 10, 1978. Wentz filtered the total SEASAT SMMR data set according to the following criteria: (1) only the middle two of the four 150-km SMMR brightness temperature cells for each scan are used in order to eliminate severe cross-track polarization error, (2) all data within 800 km of land are discarded to avoid side-lobe contamination problems, (3) only night-time data are used to avoid the Faraday rotation effect, sun glitter effect, Sun entering the cold reference horn, and thermal gradients caused by heating effects which make the interpretation of day-time data unreliable, (4) only data from the second half of SEASAT's 3-month period were selected because the 18-GHz channel, which is used in the SST retrieval algorithm, showed a significant time dependent drift during the first half of the period. The climatological data used for comparison with the SEASAT SMMR SST retrievals (7,8) were compiled by NOAA. Table 1 contains the most relevant results from the RSS study. The complete results of the RSS SMMR study are available in a NRL report in preparation (J. P. Hollinger and R. C. Lo, NRL Report 5375, 1984). The slope between the brightness temperature and the climatological SST value is directly proportional to the cross correlation

TABLE 1  
STATISTICS FROM THE N-ROSS SST STUDY USING  
SEASAT SMMR AND CLIMATOLOGY

		SST RETRIEVAL* vs CLIMATOLOGY				BRIGHTNESS TEMPERATURE*** vs CLIMATOLOGY			
		SLOPE****		STD. DEV.**		SLOPE		STD. DEV.**	
		6.6 GHz	10.7 GHz	6.6 GHz	10.7 GHz	6.6 GHz	10.7 GHz	6.6 GHz	10.7 GHz
< 15°C	COLD WATER	1.0152	1.0432	1.85	2.37	0.3491	0.1996	2.95	3.59
15-25°C	TEPID WATER	0.8239	0.7352	1.40	1.63	0.4853	0.4065	1.96	2.41
> 25°C	WARM WATER	1.1269	1.1618	1.24	1.17	0.6379	0.9061	1.05	1.44
< 10 gm/cm <sup>2</sup>	CLEAR	0.9270	0.8874	1.51	1.89	0.4504	0.3668	4.15	4.82
10-25 gm/cm <sup>2</sup>	CLOUDY	0.8697	0.8065	1.78	2.14	0.3513	0.2461	4.65	5.50
25-200 gm/cm <sup>2</sup>	RAIN	0.8686	0.8201	1.77	2.24	0.3090	0.1984	5.06	5.94
< 7 m/s	LIGHT WIND	0.9330	0.8503	1.38	1.68	0.5641	0.5280	2.67	3.05
7-14 m/s	MEDIUM WIND	0.8980	0.8422	1.70	2.10	0.4946	0.4143	3.61	4.55
> 14 m/s	HIGH WIND	0.9487	0.9951	2.05	2.60	0.4633	0.3727	3.19	3.78

\* SST RETRIEVALS ARE MADE USING 6.6 H, 6.6 V, (OR 10.7 H, 10.7 V), 18 V and 21 V SMMR CHANNELS.

\*\* STANDARD DEVIATION OF THE DIFFERENCE BETWEEN EITHER THE SST RETRIEVALS OR THE  $T_b$ 's, AND THE SST CLIMATOLOGY.

\*\*\* THE VERTICAL POLARIZED BRIGHTNESS TEMPERATURES ARE USED.

\*\*\*\* SLOPE OF THE REGRESSION LINE BETWEEN THE SST CLIMATOLOGY AND THE PARTICULAR VARIABLE.

## 5. Retrieval Accuracy Simulations

The confirmation of the theoretical sensitivity studies by the satellite and aircraft measurement results provides the practical basis for detailed theoretical retrieval and trade-off studies. The range of environmental conditions chosen is given in Table 2 and covers all but the most extreme conditions likely to be encountered. The frequency pairs were chosen to contain a lower frequency from the optimal region of 4 to 6 GHz and a higher frequency which will have greater sensitivity in warmer ocean waters and provide greater spatial resolution. The effects of instrumental noise,  $\Delta T$ , and of using SSM/I environmental products in the SST retrieval are of particular interest. The SSM/I is expected to provide estimates of wind speed, water vapor, and liquid water at accuracies of 2 m/sec, 0.2 gm/cm<sup>2</sup>, and 0.01 gm/cm<sup>2</sup>, respectively.

TABLE 2

### ENVIRONMENTAL CONDITIONS

SST (C)	-2 to 30
Wind Speed (m/sec)	2 to 17
Salinity (PPT)	33 to 37
Columnar Density of Water Vapor (gm/cm <sup>2</sup> )	0.6 to 6.0
Columnar Density of Liquid Water (gm/cm <sup>2</sup> )	0.0 to 0.08
Air Temperature (C)	0 to 32

Retrievals based on either 8.6 or 10.7 GHz alone are not adequate to meet the operational requirements using SSM/I products. Retrievals at 4.3 and for the 4.3; 8.6-GHz combination are shown in Figure 5 and for 5.1 and the 5.1; 10.7-GHz pair in Figure 6. The additional frequency improves the retrieval results much more significantly than including the SSM/I products implying that the SSM/I products are not necessary for a dual-frequency LFM/R. This would relieve constraints on the spacecraft interface design imposed by requiring common lines of sight for both the LFM/R and the SSM/I. Another benefit of using a dual-frequency system is redundancy in case of partial failure, such as the loss of one channel. The dual-frequency system also provides higher accuracy and the higher frequency channels provide better surface resolution in warm ocean water regions. The 4.3; 8.6-GHz combination appears to be slightly better than the 5.2; 10.7-GHz system in retrieval accuracy. But both of these combinations are adequate to meet the operational requirements if a system noise of about 0.5 K or less can be achieved.

## 6. RFI, Faraday Rotation, and Sun Glint

A survey of potential RFI sources germane to satellite-borne microwave radiometers was performed at NRL (10) in connection with design studies for LAMMR. The results show that there is a band at least 200-MHz wide around 4.3 GHz which is relatively emitter free. Similarly, the 400-MHz wide

coefficient between the two variables. The brightness temperatures are sorted according to the corresponding climatological SST values into cold water, tepid water, and warm water categories. The slope at 10.7 GHz is higher than that at 6.6 GHz for warm water indicating higher sensitivity. The reverse is true for cold and tepid water. This result is in agreement with the theoretical results. The SMMR brightness temperatures were also used to retrieve SST. The retrieval accuracies based upon the 6.6-GHz channels are superior to the retrievals based on the 10.7-GHz channels for all cases of liquid-water content and surface wind speed. The 10.7-GHz retrievals are most accurate for tepid and warm water. This confirms the previous conclusions based on theoretical calculations that the frequency region of 4 to 6 GHz provides the most sensitive overall estimator of the SST except for warm water.

## 4. Aircraft Measurements

During November-December 1982, NRL conducted a series of airborne radiometric measurements of SST. The instrument complement included the NASA Langley Stepped Frequency Microwave Radiometer (SFMR) (9) and the NRL SSM/I simulator with channels at 19 H and V, 22 V, and 37 H and V mounted on a pallet aboard the NRL RP3A aircraft. The pallet can be tilted to provide incidence angles from nadir to 53 degrees. The SFMR is vertically polarized and is electronically stepped over the range of 4 to 7.5 GHz. The frequencies chosen for data collection are 4.530, 4.994, 6.594, and 7.394 GHz centered on a bandpass of 50 MHz. A precision radiometric thermometer (PRT-5) provides the surface truth measurements of SST. Flights were conducted across the Gulf Stream, the continental shelf off the Norfolk, VA coast, Gulf of St. Lawrence, the Labrador Sea, and Frobisher Bay covering a SST range from 20 to 25°C. Due to various instrumental difficulties and failures, very little of the SFMR data is actually usable for this study. In general the brightness temperature dependence on SST determined from these data is somewhat greater than that from the SEASAT SMMR statistics or the theoretical studies. Even though the extent of the aircraft data is very limited, the results are in general agreement with the theoretical calculations and substantiate the theoretical approach.

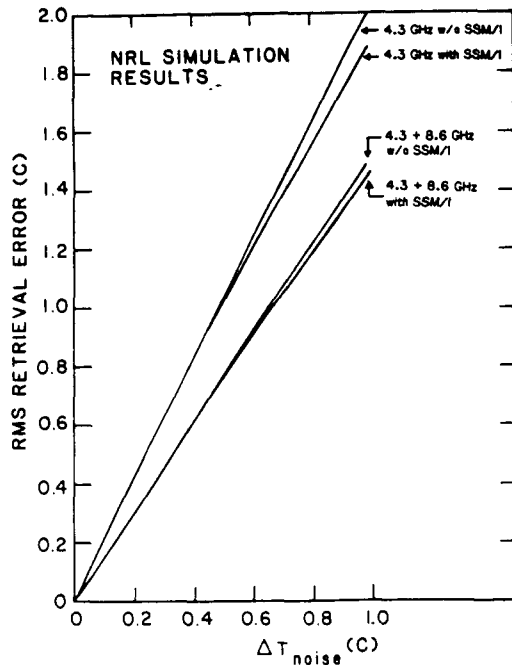


Figure 5. Retrieval Simulations Using 4.3 GHz Alone and 4.3, 8.6 GHz Combination.

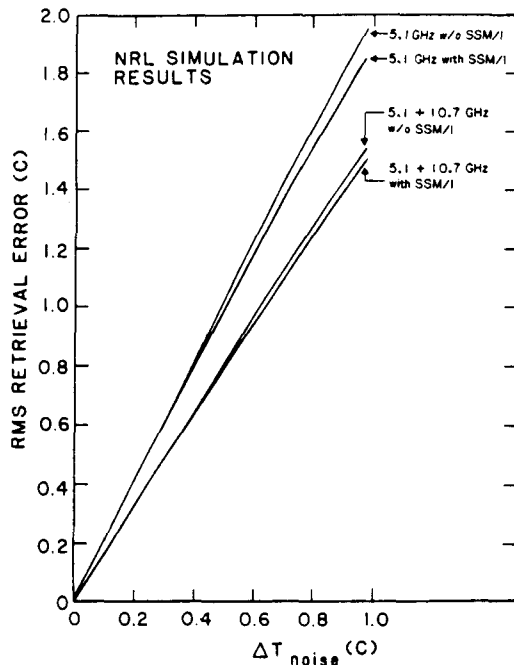


Figure 6. Retrieval Simulations Using 5.1 GHz Alone and 4.3, 8.6 GHz Combination.

band centered around 5.2 GHz has relatively few emitters. Based on this information, tentative frequency combinations for consideration are 4.3, 8.6 GHz and 5.2, 10.4 GHz, with the higher frequency in each pair arbitrarily chosen an octave above the lower frequency. The 5.2; 10.4-GHz combination is to be preferred on the basis of providing

higher surface resolution if other considerations allow it. A more significant RFI parameter is the total power of the radio emitters rather than their number. The study did not address the power emitted and did not survey the whole frequency range of present interest. Further RFI investigations are clearly necessary before a final frequency selection for the LFM is made.

## 7. Faraday Rotation

The plane of polarization of microwave radiation propagating upward through the Earth's ionosphere is rotated by an angle,  $\Delta\theta$ , by Faraday rotation (11). The amount of rotation depends upon the magnitude and orientation with respect to the direction of propagation of the Earth's magnetic field and the density of electrons along the propagation path. It is given by

$$\Delta\theta = \frac{2.36 \times 10^4}{f^2} \int N H \cos\phi \, dr \quad (1)$$

where  $f$  is the observational frequency in Hertz,  $H$  is the Earth's magnetic field in Gauss,  $N$  is the electron number density in  $\text{cm}^{-3}$ , and  $dr$  is an element of length along the path of integration through the ionosphere in cm (12). Ionospheric Faraday rotation determined from equation (1) using the mean values of 0.47 Gauss for  $H$ ,  $45^\circ$  for  $\phi$ , and  $3.8 \times 10^{13} \text{ cm}^{-2}$  for the integral of  $N$  along the propagation path is given in Figure 7 as a function of frequency. Rotation can be as much as three or more times the values given in Figure 7 during the solar sunspot maximum and for extreme values of  $H \cos\phi$ . It should be noted that N-ROSS is scheduled for launch near sunspot maximum. Thus Faraday rotations of several degrees may be expected at the lower frequencies of interest.

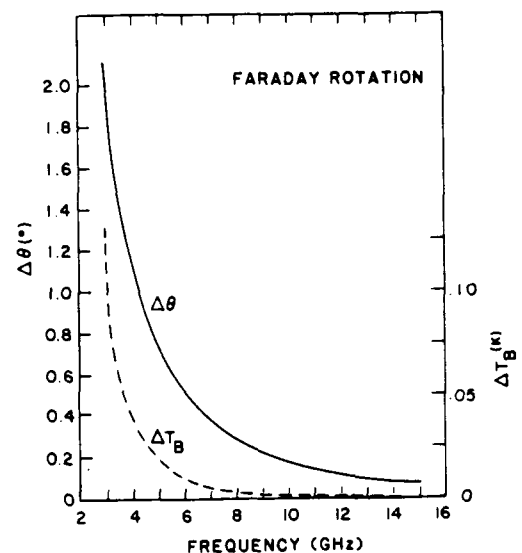


Figure 7. Rotation of the Plane of Polarization and Subsequent Brightness Temperature Error Caused by Ionospheric Faraday Rotation.

The rotation of the plane of polarization by ionospheric Faraday rotation, if uncorrected, will result in an error in the measured vertical and horizontal linearly polarized brightness temperature of  $\Delta T_B$  given by

$$\Delta T_B = (T_{BV} - T_{BH}) \sin(2\theta + \Delta\theta) \sin \Delta\theta \quad (2)$$

Here  $T_{BV}$  and  $T_{BH}$  are the true vertical and horizontal brightness temperatures of the radiation at the Earth's surface,  $\theta$  is the angular orientation that the plane of reception of the receiving antenna at the satellite makes with respect to the surface vertical, and  $\Delta\theta$  is the Faraday rotation. If  $\theta$  is large compared to  $\Delta\theta$ ,

$$\Delta T_B \approx (T_{BV} - T_{BH}) \sin 2\theta \sin \Delta\theta \quad \theta \gg \Delta\theta \quad (3)$$

then  $\Delta T_B$  is proportional to  $\sin \Delta\theta$ . This is the case with SMMR where the plane of polarization rotates with scan angle. If  $\theta$  can be held constant at 0°, independent of scan angle, then

$$\Delta T_B = (T_{BV} - T_{BH}) \sin^2 \Delta\theta \quad \theta = 0 \quad (4)$$

and  $\Delta T_B$  is proportional to  $\sin^2 \Delta\theta$ . This can be a very large difference. For example for  $T_{BV} - T_{BH} = 100$  K,  $\theta = 25^\circ$  and  $\Delta\theta = 3^\circ$ , equation (3) gives a brightness temperature of 4 K whereas an error of only 1/4 K results from equation (4) when  $\theta = 0$ . Therefore, an important design consideration is to maintain the reception plane of polarization aligned with vertical at the Earth's surface independent of scan angle. The expected error, under the mean conditions assumed above, calculated using equation (4) is also plotted in Figure 7 using a value of 100 K for  $T_{BV} - T_{BH}$  which is an upper limit over the frequency range being considered. For example, at 4.3 GHz, the error is approximately 0.03 K and may be as large as 0.1 K under severe ionospheric conditions. The error decreases quickly with increasing frequency, and normally will not be important and can be ignored. If necessary, a relatively simple correction can be made to remove the bulk of the effect since Faraday rotation is systematic and well understood. Only if the plane of polarization rotates with scan angle will Faraday rotation be a problem.

Sun glint is caused by the specular reflection of solar radiation from the sea surface. The Sun is very intense at microwave frequencies, especially during periods of high sunspot activity when it can have brightness temperatures as high as 40,000 K at 10 GHz and more than 200,000 K at 5 GHz. Therefore, it can cause a large contribution to the observed brightness temperature when the specular point falls within the footprint of the observing radiometer. The brightness temperature error caused by sun glint is a function of angle relative to the specular angle and the surface roughness of the sea which is primarily a function of wind speed. Studies have been performed (13) for the purpose of defining a cone angle about the direction where sun glint presents a problem in environmental parameter retrievals. Consideration has also been given to the possibility of generating a correction algorithm. These studies indicate sun glint effects can cause brightness

temperature increases in excess of 1 K for angles within  $\pm 20^\circ$  of bistatic for the SMMR 6.6-GHz channel. Unfortunately, the sun glint problems cannot be avoided nor be obviated by system design or frequency selection. Fortunately, sun glint problems are minimized by the Sun synchronous early morning orbit planned for N-ROSS. The 98.1° retrograde N-ROSS orbit is shown in Figure 8 with solar positions at summer and winter solstice and the equinoxes indicated for both a 7:15 a.m. and an 8:15 a.m. equatorial crossing. The limit of the LFMR scan is shown by the small circle labeled "swath edge." There will be no specular solar reflection for any Sun position within this circle. However, under rough surface conditions, scattered solar radiation will be received from directions considerably away from the specular direction (13). Thus, sun glint will be a problem at some scan angles over some portions of the orbit, primarily near the swath edge in the summer. Criteria for its detection and elimination must be determined in a way similar to that done for the SMMR (13) experiment. This problem will have to be addressed in the processing software rather than instrument design.

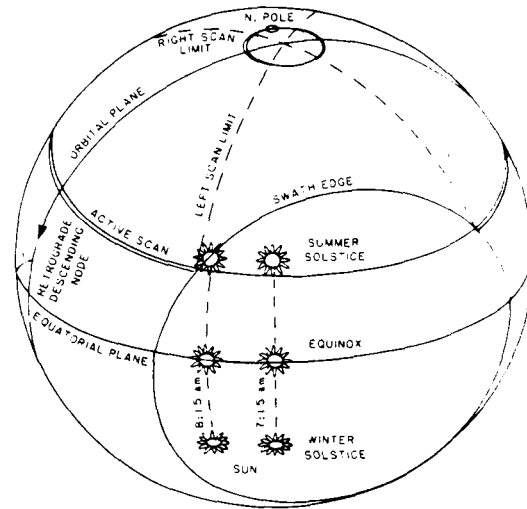


Figure 8. The Relationship Between the Seasonal Sun and the N-ROSS LFMR Scan Geometry.

#### 8. Baseline Model of the LFMR

The sensitivity and retrieval accuracy studies indicate that the 4.3, 8.6-GHz-frequency combination may be marginally better for SST retrieval than the 5.2, 10.4-GHz pair. However, any possible slight improvement in SST retrieval accuracy obtainable with the lower frequency combination is negligible compared to the 21-percent increase in surface resolution provided by the higher frequency combination. Since both accuracy and resolution are important considerations, the 5.2, 10.4-GHz combination will better meet the operational requirement than will the 4.3, 8.6-GHz pair. Further, uncertainties in the

measured brightness temperature caused by Faraday rotation will be about half as large for the higher frequency combination and, since solar intensity decreases with increasing frequency, sun glint problems will also be somewhat smaller. For these reasons the frequencies of 5.2 and 10.4 GHz are selected over 4.3 and 10.6 GHz for the baseline instrument.

An incidence angle near  $50^\circ$  is required to enable corrections for marine wind speed and a conical scan geometry, similar to that of the SSM/I (14), is indicated for the same reasons that led to its use for SMMR, SSM/I, and LAMMR. The adoption of a scan geometry identical to the SSM/I will facilitate data comparisons between the two instruments and will ease the development of algorithms using different combinations of channels from both systems. Further it will enable a common format and use much of the same software for data display, handling, and distribution. The SSM/I is conically scanned at a  $53.1^\circ$  incidence angle. Measurements of the scene are obtained over a  $102.4^\circ$  scan angle centered on the satellite ground track. A scan period of 1.9 seconds leads to a 12.5-km spacing between successive scans for a satellite altitude of 833 km.

In order to obtain 25-km resolution in the along-track direction at 5.2 GHz, a 5.9-m diameter antenna is required. This would provide  $15 \times 25$  km resolution at 5.2 GHz and  $8 \times 13$  km resolution at 10.4 GHz. The resolution at 10.4 GHz with a 5.9-m antenna is about 10 percent better than the SSM/I at 85.5 GHz. Samples at 7.5-km cross track are required for Nyquist sampling at 5.2 GHz. Nyquist sampling is very important to prevent aliasing and allow the full use of the antenna resolution for locating and mapping thermal fronts and eddies, ice edges, and other surface features. In order to obtain Nyquist sampling at 10.4 GHz as well as at 5.2 GHz, a second dual-polarized 10.4-GHz system must be added. This would be a second feed, offset in both the along-and cross-track directions, so as to provide two series of 10.4-GHz samples spaced by 3.8 km in the along-track direction each scan. Sampling each 3.8 km along the scan direction produces a  $3.8 \times 3.8$ -km grid. System temperatures of 250 K are obtainable with FET amplifiers at 5 and 10 GHz. If a calibration scheme similar to that used for the SSM/I can be designed for the LFMR, a total power radiometer can be used. Bandwidths of 300 MHz and 500 MHz are achievable at 5 and 10 GHz and should be compatible with RFI considerations. Ocean scene temperatures would be about 130 K and 150 K leading to RMS noise of 0.44 K and 0.50 K per sample at 5.2 and 10.4 GHz. Sampling both polarizations, with 12-bit precision, will result in 2.7 Kb/s and 10.8 Kb/s data rates at the two instrument conditions, and performance data require a total data rate of 14.0 Kb/s. All of these considerations of sampling, resolution, noise, and data rate for a 5.9-m antenna are summarized in Figure 9.

The 5.9-m antenna, six-channel, Nyquist-sampled system meets the operational requirement in both accuracy and resolution. Since the major

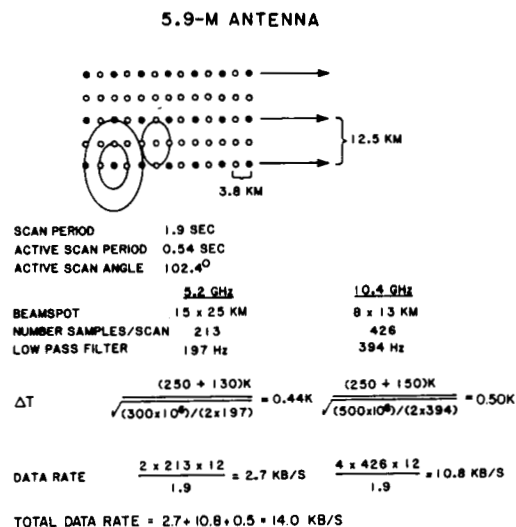


Figure 9. Summary of the Baseline System with a 5.9-Meter Antenna.

expense and weight of the system are required by the antenna, the addition of two dual-polarized radiometers and feeds at 10.4 GHz to a minimum 5.2-GHz system will only marginally increase the weight and power requirements, and the data rate of 14 Kb/s is modest. The dual-frequency, dual-polarized six-channel system provides greater accuracy over a larger range of SST, better surface resolution in warm ocean water regions, a stand-alone system independent of the SSM/I and redundancy in the event of partial system failure.

Nyquist sampling in both along-and cross-track directions will allow maximum use of the antenna resolution in mapping surface features. It should be noted the data can always be smoothed in post processing to decrease the RMS sample noise and increase retrieval accuracy to the same reduced surface resolution as would have been obtained originally if the data had not been Nyquist sampled. The reverse is not possible. If the scene is not Nyquist sampled, no postprocessing will restore the surface features to the maximum resolution allowed by the antenna.

The baseline system is given in Table 3. The weight, volume, and power requirements given for the antenna and radiometer were obtained from discussions with Harris Corporation and extrapolations from SMMR, SSM/I, and LAMMR.

TABLE 3  
BASELINE SYSTEM

Dual Frequency - 5.2 and 10.4 GHz  
Dual Polarization - Horizontal and vertical linear polarization  
45° Conical Scan (53.1° incidence angle at Earth's surface)  
1.9-second period; 102.4° scan width

Antenna - 5.9-m diameter  
- 70-lb maximum weight  
- 22-ft<sup>3</sup> stowed volume  
- 20 watts power  
- point accuracy  $\pm 0.1^\circ$ ; precision  $\pm 0.02^\circ$

Resolution - 15 x 25 km - 5.2 GHz  
8 x 13 km - 10.4 GHz

Radiometer - Total Power  
- Externally Calibrated  
- Bandwidth 300 MHz - 5.2 GHz  
500 MHz - 10.4 GHz  
-  $\Delta T$  Noise 0.44 K - 5.2 GHz  
0.50 K - 10.4 GHz  
- 24 lb weight; 24 watts power  
- Six Channels (H, V - 5.2 GHz;  
2H, 2V - 10.4 GHz)  
- Nyquist Sampled; 14.0 Kb/s data rate

Orbit - 833-km Altitude; 98.7 Inclination  
(Polar Orbit)  
- DMSP Constellation  
- Three-Year Mission Life

#### 9. References

1. Hofer, R., Njoku, E. G., and Waters, I. W., "Microwave Radiometric Measurements of Sea Surface Temperature from the SEASAT Satellite First Results," Science, Vol. 212, June 1981.
2. Hollinger, J. P., Lerner, R. M., and Wisler, M. M., An Investigation of the Remote Determination of Sea Surface Temperature Using Microwave Radiometry, Naval Research Laboratory Memorandum Report 3159, November 1975.
3. Wisler, M. M. and Hollinger, J. P., Estimation of Marine Environmental Parameters Using Microwave Radiometric Remote Sensing Systems, Naval Research Laboratory Memorandum Report 3661, November 1977.
4. Hollinger, J. P., Lerner, R. M., Troy, B. E., and Wisler, M. M., Joint Services 5D-2 Microwave Scanner Definition Study, Naval Research Laboratory Memorandum Report 3807, August 1978.
5. Bernstein, R. L., "Sea Surface Temperature Mapping with the SEASAT Microwave Radiometer," Journal of Geophysical Research, Vol. 87, No. C10, pp. 7865-7872, September 1982.
6. Wentz, F. J., Comparison of Sea Surface Temperature Retrievals Using 6.6 and 10.7 GHz, Remote Sensing Systems Technical Report 092183, San Francisco, Ca, September 1983.

7. Reynolds, R. W., A Monthly Climatology of Sea Surface Temperature, NOAA Technical Report NW S31, June 1982.

8. Reynolds, R. W., "A Comparison of Sea Surface Temperature Climatologies," Journal of Climate and Applied Meteorology, Vol. 22, No. 3, March 1983.

9. Harrington, R. F., The Development of a Stepped Frequency Microwave Radiometer and its Application to Remote Sensing of the Earth, NASA Technical Memorandum 81837, Langley Research Center, June 1980.

10. Crandall, D., Survey of Potential Radio Frequency Interference Sources, Naval Research Laboratory Memorandum Report 4200, May 1980.

11. Lawrence, R. S., Little, C. G., and Chivers, H. J. A., "A Survey of Ionospheric Effect Upon Earth-Space Radio Propagation," Proc. IEEE, Vol. 52, pp 4-27, 1964.

12. Allen, C. W., Astrophysical Quantities, 2nd Edition, The Athlone Press, University of London, 1963.

13. Wentz, F. J., The Effect of Sea-Surface Sun Glitter on Microwave Radiometer Measurements, Remote Sensing Systems Report No. 110481, November 1981.

14. Hollinger, J. P. and Lo, R. C., SSM/I Project Summary Report, Naval Research Laboratory Memorandum Report 5055, April 1983.

**Page intentionally left blank**



LARGE SPACE ANTENNA TECHNOLOGY APPLIED TO  
RADAR-IMAGING, RAIN-RATE MEASUREMENTS,  
AND OCEAN WIND SENSING

R. K. Moore and S. P. Gogineni  
Remote Sensing Laboratory  
University of Kansas Center for Research, Inc.  
Lawrence, Kansas

Large Space Antenna Systems Technology - 1984  
December 4-6, 1984

## ABSTRACT

During the last decade, the utility of spaceborne microwave remote-sensing systems for ocean windspeed measurement, ocean wave-imaging and sea-ice studies has been demonstrated. Development of large space antennas offers some interesting possibilities for rain-rate measurements, ocean and ice studies, and radar imaging.

The joint use of active and passive sensors using the 15-m antenna for ocean, ice, and soil moisture studies; rain-rate measurements; and radar imaging is considered. Verification of the frequency-agile rain radar concept with Shuttle offers the possibility of much needed rain-rate statistics over the ocean.

### 1.0 INTRODUCTION

Significant progress has been made in recent years in the application of microwave sensors to oceanographic, sea-ice, soil-moisture and snow studies. Most of these were aimed at understanding the interaction of electromagnetic waves with ocean and terrain, and determining the optimum radar parameters. These studies have proven the utility of microwave sensors for surveying the Earth's resources.

The inherent limitation in spaceborne passive microwave systems is poor resolution; large antenna technology will allow the development of systems with smaller footprints. The only spaceborne microwave system currently offering high resolution is synthetic aperture radar (SAR). However, spaceborne SARs have some major disadvantages including high data rates and the large amount of processing required to produce images. Some of the operations associated with the survey and exploitation of natural resources require near-real-time information. The availability of large space antennas makes it possible to develop systems with modest usable resolutions and near-real-time processing capability.

In addition, a large space antenna offers an opportunity to measure precipitation using microwave systems from space. The attenuation experienced by the signal as it propagates through the rain can be estimated by a radiometer. The main problem with measurement of precipitation from space is separating the rain echo from that of the background. Backscatter from rain varies rapidly with frequency as opposed to a slower variation from terrain or ocean. Scattering from the atmosphere can be distinguished from that of the background by using two closely spaced frequencies and taking advantage of the rapid variation of atmospheric phenomena.

In this paper, the joint use of a radar/radiometer for monitoring sea-ice, ocean windspeed, soil moisture and rain-rate is considered.

### 2.0 LOW-POWER RADAR/RADIOMETER

During the last decade Moore and Fung [1] and Gray et al. [2] have demonstrated the usefulness of complementary active and passive microwave systems for measuring windspeed over the ocean, sea-ice concentration and type, and geological mapping. Most of these studies were conducted with a coarse-resolution radiometer and scatterometer or fine-resolution SAR. The footprint size of the radiometers used in these early studies was generally 2-4 times larger than that of the

scatterometers. This made it difficult to examine the relationship between active and passive sensors and also introduced errors in the estimation of windspeed.

Development of a truly complementary sensor with similar resolution and coincident coverage will be useful in studying the application of such a sensor to the scientific and operational problems associated with sea ice, soil moisture and ocean studies.

During the last few years, the University of Kansas made several broadband radar backscatter measurements from sea ice [3] to define optimum radar parameters. The experimental results indicate that there was a significant contrast between first-year (FYI) and multiyear (MYI) ice at all frequencies in C, X and Ku bands, but negligible contrast at L-band, as shown in Figures 1a and 1b. The contrast between thin ice and multiyear ice also increased with incidence angle, as shown in Figure 2a.

The Canada Centre for Remote Sensing collected simultaneous active and passive signatures of sea ice with an airborne system during the last few years. The results of their investigations indicated that the ambiguity associated with an active sensor can be eliminated by using a passive sensor or vice-versa, as shown in Figure 2b.

Some of the ice parameters such as boundary positions, percentage of area covered, etc. can be determined with a modest resolution (about a 1-km) system. Although contrast between FYI and MYI for cross-polarization is greater than that for like-polarization, cross-polarized measurements from space are not given serious consideration because, since the cross-polarized scattering coefficient is significantly lower than that for like polarization, additional power is required. The power required to measure the cross-polarized scattering coefficient with large antennas is not as great. Therefore, large antenna technology will have significant impact on system design considerations for sea-ice monitoring.

Moore et al. [4] reported that large errors in the estimation of windspeed can occur because of variability of rain rates within a beam. Simulations were performed, assuming that only part of the radiometer footprint that overlaps the scatterometer footprint was filled with rain, as shown in Figure 3a. The results of these simulations are shown in Figure 3b. Therefore, errors associated with in-beam rain variability can be eliminated by using a scatterometer and radiometer with similar resolution. The 15-m diameter of the large antenna will allow the development of an active/passive system with similar resolutions for both sensors.

The low-power radar-radiometer combination can also be used in soil moisture studies. It was reported by Ulaby et al. [5] that radar backscatter is strongly correlated with moisture content at 4.5 GHz and incidence angles between 10° and 20°. Surface roughness has less effect at 4.5 GHz than at 1.5 GHz, as shown in Figure 4.

Shuttle-based modest resolution radar/radiometer systems will be useful for several remote-sensing experiments on a variety of targets. These experiments can verify the potential for higher orbit (up to synchronous) operational sensors.

No detailed study to define the optimum parameters for these systems has been conducted, but we believe the systems with parameters given in Table 1 can meet the needs for sea-ice, soil moisture and ocean studies.

**TABLE 1**  
**CW RADAR**

Height	500 km
Wavelength	2 cm
Aperture Efficiency	60%
Noise Figure	3 dB
Required Signal-to-Noise Ratio	10 dB or more
Scattering Coefficient	-40 dB
Incidence Angle	40°
Filter Bandwidth	7 kHz
Along-track cell width	1.11 km
Across-track cell width	1.4 km
Transmitter Power	< 1.5 W
Sensor Package:	
Frequency	Radar 5 GHz
Radiometer	15 GHz
Polarization	Radar VV, VH
Radiometer	VV, HH
Incidence Angle	40° or greater
Aperture	15 m for ice

---

The use of radar and radiometer with coincident beams based on the same antenna will permit easy development of modest resolution radar images within the radiometer beam, but images with considerably better resolution than those of the radiometer. For mapping applications of the radiometer this will allow better delineation of edges and regions of inhomogeneity within the radiometer beam. At the same time, it will permit use of the synergistic effects of combined radar and radiometer measurements of such parameters as sea-ice type and concentration, soil moisture, and oceanic patterns associated with internal waves and submarine topography.

This application is possible because the radar may use either range resolution or Doppler beam sharpening in the azimuth direction (or both) to produce small pixels within the footprint of the antenna, and therefore within the beam of the radiometer. With the high gain of the large pencil-beam antenna, the radar power requirement is extremely low; for a radar with the footprint determined solely by the beam (a beam-limited scatterometer) the required power is less than that of the local oscillator of the radiometer/radar receiver in low Earth orbit, and less than a watt at synchronous orbit. Doppler beam sharpening allows footprint widths within the beam down to about  $\sqrt{\lambda R}$ , where  $\lambda$  is the wavelength and R is the slant range. This improved resolution can be achieved with no increase in transmitter power and with a relatively simple processor. Range resolution can be improved at the expense of additional transmitter power, but improvements up to about a factor of 10 fail to raise the power much above that of the local oscillator in LEO and still result in power levels easily attained with solid-state transmitters in GEO with the 50-m or larger antenna.

### 3.0 RAIN RADAR

The need for global precipitation statistics in the study of weather and climate is well established [6]. Remote-sensing devices operating in the visible, infrared and microwave spectrum can be used for global precipitation measurements. Although visible and infrared systems are very useful in delineating areas of precipitation, these systems usually do not give satisfactory estimates of precipitation statistics [6]. Radar systems operating in the microwave spectrum have proven very useful for measuring rain rate over large areas, but the accuracy of radar rain gauges is not as good as that of conventional point rain gauges. It is, however, possible to measure the rain-rate statistics over a region of several thousand square kilometers, an almost impossible feat with point rain gauges. Microwave radiometers are also useful for measuring the rain rate, but the relationship between rain rate and the measured brightness temperature is difficult to interpret in areas of variable background emission. Also, the non-beam-filling effects introduced by the poor resolution of spaceborne passive systems introduces large errors.

The spaceborne microwave system with the greatest potential for globally measuring rain rate over both the ocean and land is a radar in combination with a radiometer. Two promising radar methods for measuring rain rate from space are: (1) surface target attenuation radar (STAR) [7] and (2) frequency agile rain radar (FARR) [8]. The STAR system is based on the assumption that the path-averaged rain rate can be determined by measuring the attenuation experienced by the signal as it propagates through rain. The calibration target for estimating attenuation is the surface. This requires measurement of backscatter from the surface through rain and under clear weather conditions. The major disadvantage of this method is that the scattering properties of the surface change in the presence of rain. Backscatter from the ocean is changed when the rain strikes the surface of the water. The scattering coefficient of terrain is also strongly influenced by the moisture content and presence of free water on the surface.

The frequency-agile rain radar uses two closely spaced frequencies to distinguish rain echo from that of the background. The backscatter from raindrops generally increases very rapidly, as shown in Figure 5, but backscatter from ocean or terrain increases slowly with frequency, as shown in Figure 6. The differential scattering coefficient can be considered proportional to the rain.

CW or pulse radars operating at 14 and 17 GHz can be used to measure the rain rate. Although the power requirement for CW radars is lower than that for pulse radars, their rain-rate retrieval algorithm is more complex. Since the concept of measuring rain rate from space is new and untested, further research is required to define optimum system parameters.

The pixel size to eliminate the non-beam filling effect in intense rain should not be more than 5 km. Therefore one of the main problems, the non-beam filling effect, can be eliminated by using a sufficiently large antenna. The availability of the 15-m antenna makes it possible to measure rain rate with spaceborne radar at lower orbits and the future availability of 50-m or larger antennas extends this possibility to synchronous orbits.

#### 4.0 CONCLUSIONS

Use of a large antenna on a spacecraft will permit combined radar and radiometer measurements from both low Earth orbits and geosynchronous orbits that can significantly enhance our ability to measure parameters of the Earth's surface and atmosphere. The Shuttle is useful for testing these concepts, even though it is not a good vehicle for operational measurements of these parameters because of the short mission durations.

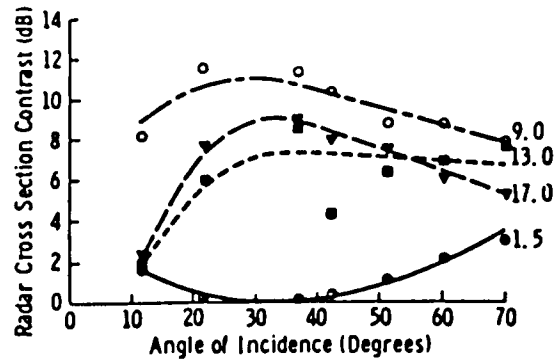
Radars and radiometers have both been shown useful for monitoring sea ice and soil moisture. Use of systems with coincident beams for the active and passive systems will permit synergistic use of these sensors to attain better results than possible with either alone. The large antenna will permit much finer resolutions for the radiometers than previously available, thereby making them more useful. It will also permit simultaneous use of radars with very low transmitted powers. The pixel size for the radar within the radiometer beam can be improved without increasing the power by Doppler beam sharpening and can be improved significantly with only a small increase in power by use of range resolution.

Measurements of the rainfall rate can be achieved by combined radar-radiometer methods using the fine resolutions attainable with the large antenna. With smaller antennas, rainfall measurements are difficult because cell sizes are typically under 10 km and often under 5 km; the large antenna permits narrow enough beams to overcome this problem. Synergistic radiometric and radar measurements using multiple frequencies for both will improve the accuracy compared with that attainable with either sensor alone and at a single frequency.

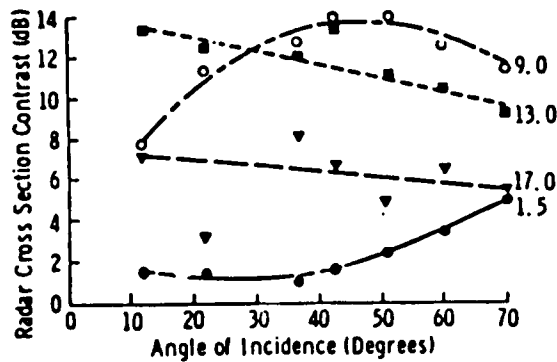
Many of the techniques for Earth and atmosphere observation presented here can be tested using the 15-m antenna on the Shuttle, although operation will require longer missions at higher altitudes. Since many of these concepts have been studied only in minimal detail, more extensive studies, simulations and, in some cases, aircraft tests are called for so that the tests using the Shuttle may achieve optimal results.

## REFERENCES

1. Moore, R.K. and Fung, A.K.: Radar Determination of Winds at Sea. Proc. IEEE, vol. 67, no. 11, Nov. 1979, pp. 1504-1521.
2. Gray, A.L.; Hawkins, R.K.; Livingstone, C.E.; Arsenault, L.D.; and Johnstone, W.M.: Simultaneous Scatterometer and Radiometer Measurements of Sea-Ice Signatures. IEEE J. Oceanic Engineering, vol. OE-7, no. 1, Jan. 1982, pp. 20-32.
3. Onstott, R.G.; Moore, R.K.; Gogineni, S.; and Delker, C.: Four Years of Low-Altitude Sea Ice Broad-Band Backscatter Measurements. IEEE J. Oceanic Engineering, vol. OE-7, Jan. 1982, pp. 44-50.
4. Moore, R.K.; Chaudhry, A.H.; and Birrer, I.J.: Errors in Scatterometer-Radiometer Wind Measurement Due to Rain. IEEE J. Oceanic Engineering, vol. OE-8, no. 1, Jan. 1983, pp. 37-49.
5. Ulaby, F.T.; Batlivala, P.P.; and Dobson, M.C.: Microwave Backscatter Dependence on Surface Roughness, Soil Moisture and Soil Texture: Part I--Bare Soil. IEEE Trans. on Geoscience Elec., vol. GE-16, no. 4, Oct. 1978, pp. 286-295.
6. Atlas, D. and Thiele, O.W., eds.: Executive Summary. Precipitation Measurements from Space: Workshop Report. NASA Goddard Space Flight Center, Oct. 1981, pp. vi-xi.
7. Atlas, D.; Eckerman, J.; Meneghini, R.; and Moore, R.K.: The Outlook for Precipitation Measurements from Space. Atmosphere-Ocean, vol. 20, no. 1, 1982, pp. 50-61.
8. Moore, R.K.: Use of Combined Radar and Radiometer Systems in Space for Precipitation Measurement -- Some Ideas. Precipitation Measurements from Space: Workshop Report [D. Atlas and O.W. Thiele, eds.]. NASA Goddard Space Flight Center, Oct. 1981, pp. D-301 - D-325.
9. Onstott, R.G. and Gogineni, S.P.: Active Measurements of Arctic Sea Ice Under Summer Conditions. Accepted for publication in J. Geophys. Res., 1984.
10. Lhermite, R.: Satellite-Borne Dual Millimeter Wave Length Radar. Precipitation Measurements From Space: Workshop Report [D. Atlas and O.W. Thiele, eds.]. NASA Goddard Space Flight Center, Oct. 1981, pp. D-277 - D-282.



(a)

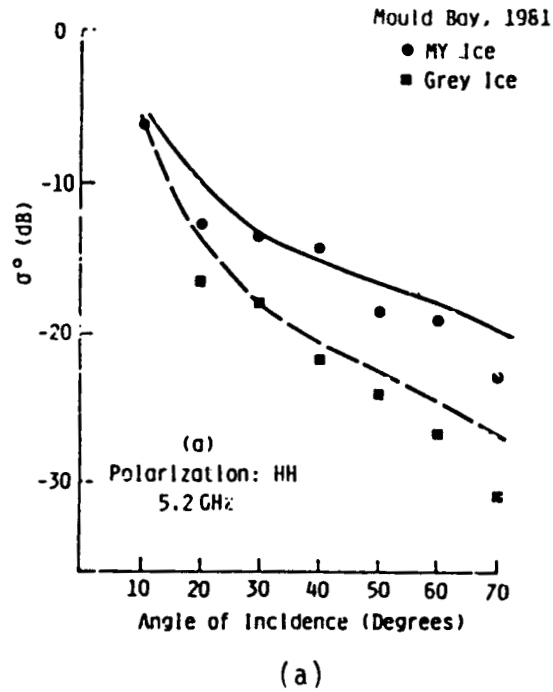


(b)

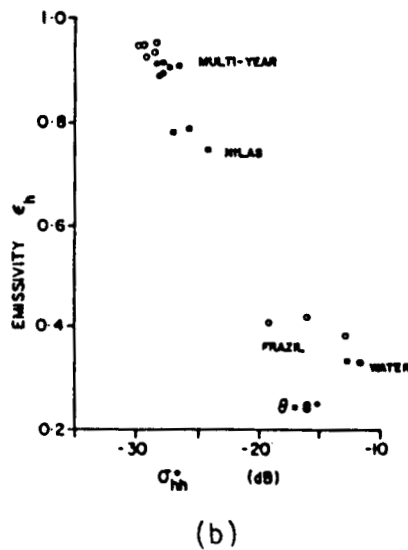
(© 1982 IEEE)

Figure 1. Difference between radar cross section of thick first-year and multiyear ice at 1.5, 9.0, 13.0, and 17.0 GHz with (a) vertical polarization and (b) cross polarization (ref. 3).





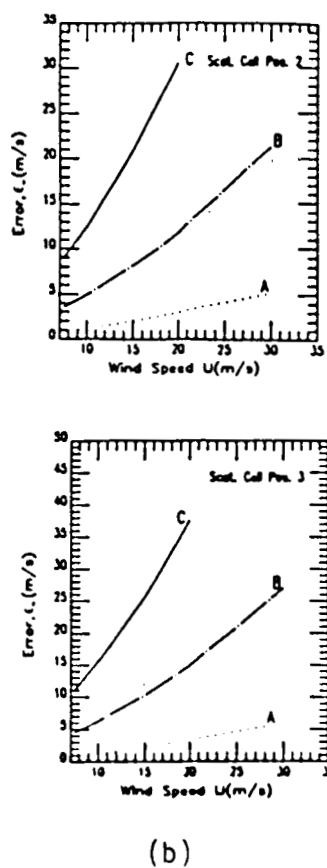
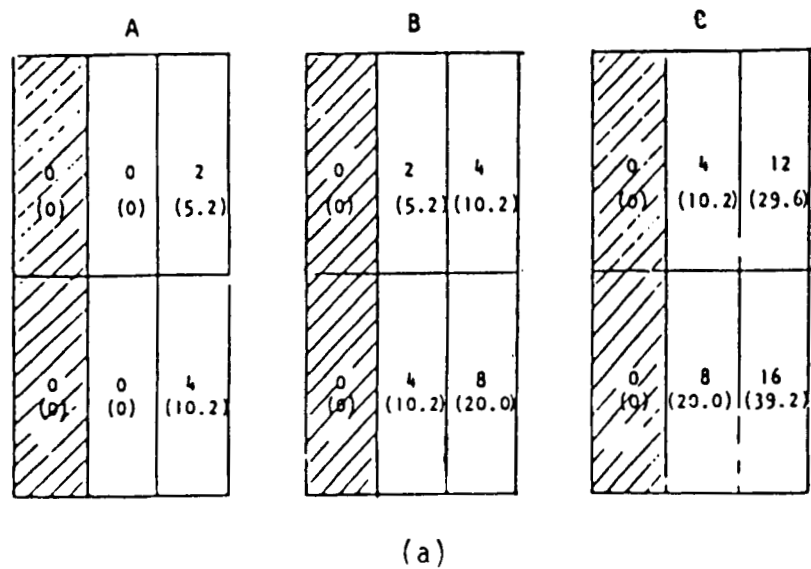
Scattering coefficient of thin ice and multiyear ice at 5.2 GHz (ref. 9).



Comparison of passive and active signatures of sea ice (ref. 2).

(© 1982 IEEE)

Figure 2. Scattering coefficient of thin ice and multiyear ice and comparison of passive and active signatures of sea ice.

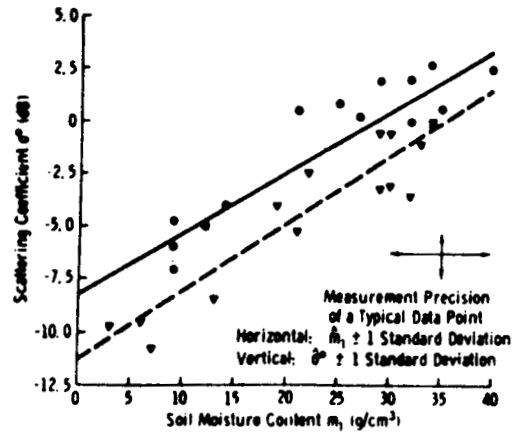


(© 1983 IEEE)

Figure 3. Errors in scatterometer-radiometer wind measurement (ref. 4).

Polarization: HH  
 Angle of Incidence (Degrees): 10  
 Frequency (GHz): 4.25

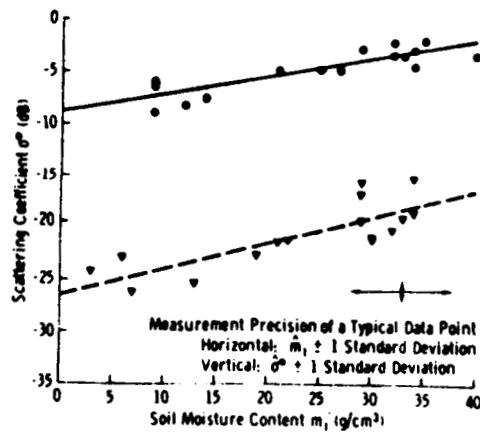
	RMS Height (cm)	Correlation Coefficient $\rho$	Sensitivity S (dB/.01 g/cm <sup>3</sup> )
—●—	4.1	0.90	0.28
—▼—	1.1	0.80	0.32



(a)

Polarization: HH  
 Angle of Incidence (Degrees): 20  
 Frequency (GHz): 1.5

	RMS Height (cm)	Correlation Coefficient $\rho$	Sensitivity S (dB/.01 g/cm <sup>3</sup> )
—●—	4.1	0.87	0.17
—▼—	1.1	0.82	0.24



(b)

(© 1978 IEEE)

Figure 4. Comparison of the backscatter response to  $m_1$  of a smooth surface and a rough surface of (a)  $\theta = 10^\circ$ ,  $f = 4.25$  GHz and (b)  $\theta = 20^\circ$ ,  $f = 1.5$  GHz (ref. 5).

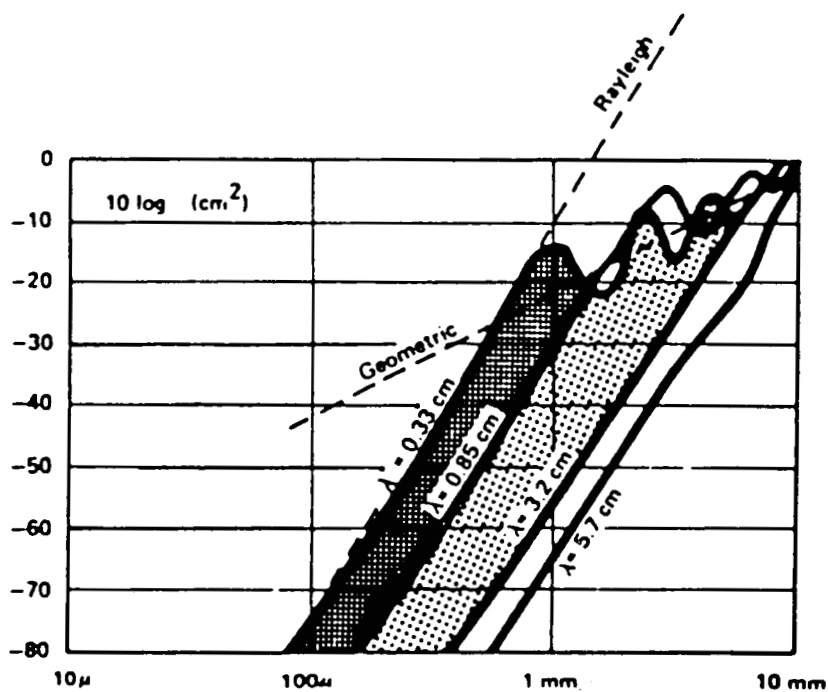


Figure 5. Backscattering cross section of water spheres as a function of diameter for the radar wavelengths (ref. 10).

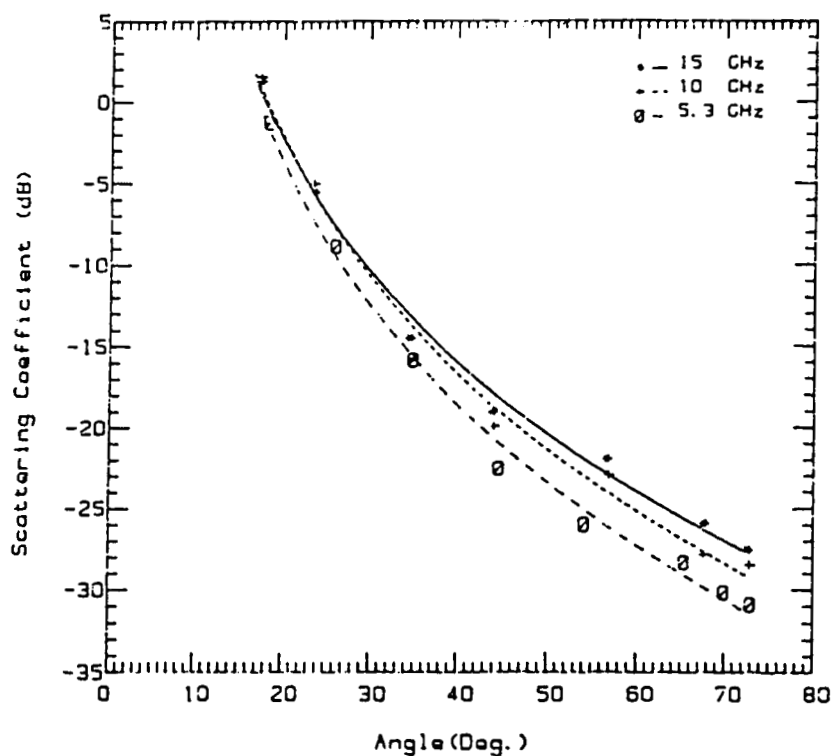


Figure 6. Angular response of scattering coefficient at  $U = 6.5 - 8.3 \text{ m/sec}$  crosswind, VV-Pol., January 28, 1984.

ADVANCED TWO-FREQUENCY OCEAN SENSING RADAR USING  
HIGH RESOLUTION ANTENNA BEAMS

D.E. Weissman  
Hofstra University  
Hempstead, New York

J.W. Johnson  
NASA Langley Research Center  
Hampton, Virginia

Large Space Antenna Systems Technology - 1984  
December 4 - 6, 1984

## INTRODUCTION

The opportunity to use a large space antenna system for remote sensing applications permits the creation of an advanced ocean sensing radar that combines the abilities of previously developed techniques. The 15 meter antenna will permit much higher angular and spatial resolution at the surface that will lead to techniques of observing ocean wave heights and the directional spectrum that had not previously been feasible from space. At the same time, sensors to measure ocean surface winds can be in operation and the data from both can be combined to increase the accuracy of each individual sensor. This paper outlines the existing capabilities and sensor techniques with typical data characteristics for the individual measurement of sea surface quantities.

## APPLICATION NEEDS

After the SEASAT Scatterometer demonstrated the potential of measuring global winds from space on a real-time basis, plans for more advanced ocean sensing satellites moved rapidly ahead. While instrumentation, antenna systems, and algorithms are being refined for future scatterometers, a fundamental limitation will be that the radar cross section of the surface will not depend on wind speed alone. This limitation appears as a scatter in the calibration data (fig.1) which limits the precision of inverting operational data into wind speed. Recent studies (ref. 1) have shown that the radar cross section of surface will depend on sea state (RMS wave slope or height) and air-sea temperature difference in addition to wind speed. Sensors that can measure the surface wave spectrum also depend on wind speed (refs.2,3). One solution is to use a multi-sensor that can measure both quantities from space, since each sensor output depends on two variables. Then the two unknowns can be inferred from the two independent equations (or algorithms). This idea is not part of existing plans for future satellites, so the possibility of developing a new approach with a shuttle-based radar and antenna system is very attractive. A large space antenna would be a significant benefit to an ocean observing system because of its ability to provide spatial resolution in a beam-limited mode. The entire radar system could be based on processing narrow bandwidth signals, which is usually simpler than other approaches for achieving spatial resolution.

# SCATTEROMETER MEASUREMENTS

SEASAT Scatterometer measurements have been processed and analyzed with the best available information on sea surface conditions, with atmospheric correction to neutral stability (see ref. 1). Inherent in these and other data sets is a random fluctuation or data scatter about a "best fit" approximation function between the radar cross section and the wind speed (fig. 1). This indicates that other sea surface variables are influencing the backscattered power, in addition to the wind. Tower-based measurements yielded backscatter data (ref. 1) along with surface wave measurements that show a strong effect of the RMS wave slope on the cross section. Work is in progress to further analyze and interpret this data set with application to future spaceborne Scatterometer measurements.

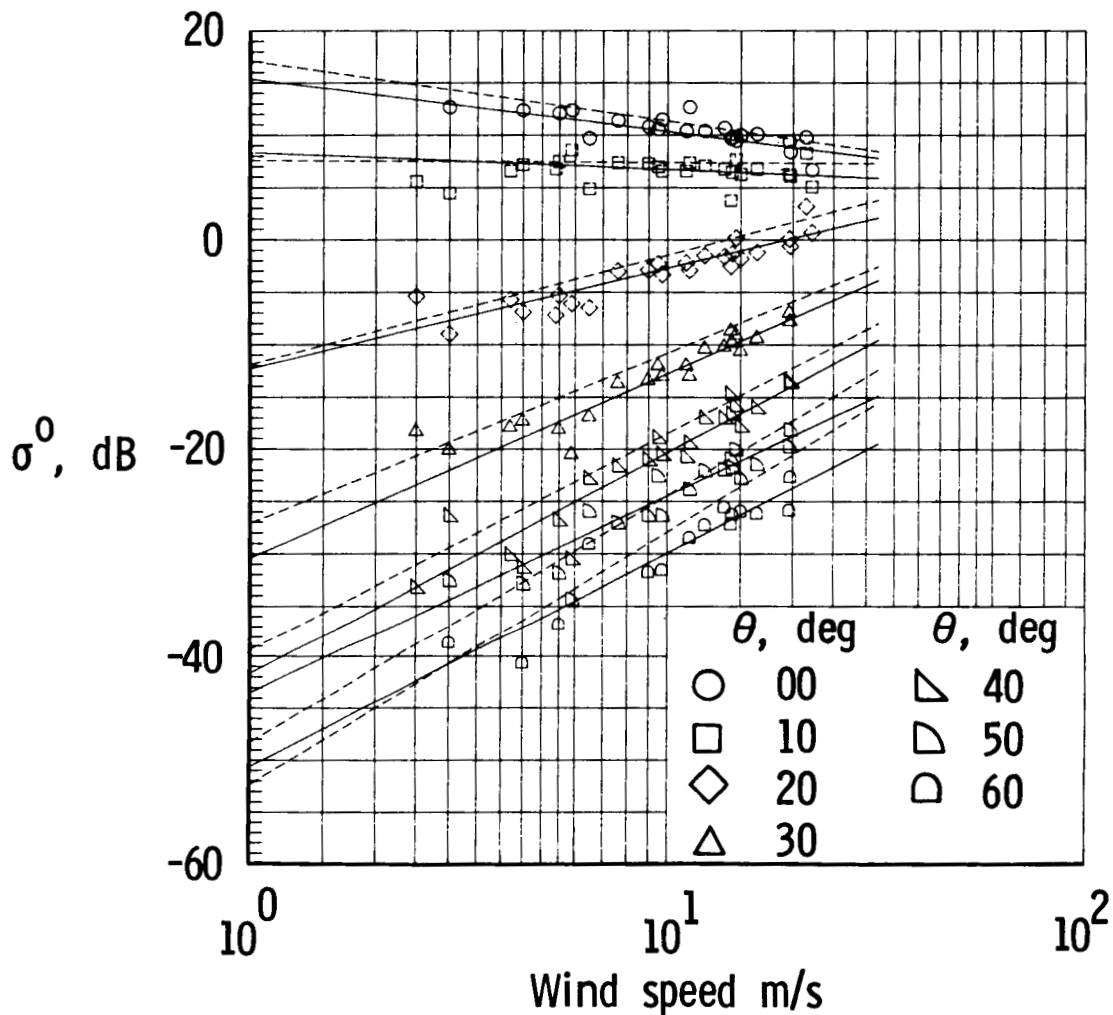


Figure 1

## WAVE HEIGHT MEASUREMENTS

An excellent example of sea state measurements using a narrowband beam-limited radar is the nadir looking Dual Frequency Correlation Radar that requires a narrowbeam antenna to measure RMS waveheight (ref. 4). These previous measurement programs using this radar from an aircraft platform showed the capability of measuring wave height over a variety of sea conditions. The known limitations for higher altitudes were more narrow beamwidths with altitude and near nadir pointing control. The normalized correlation function between two closely spaced frequencies decreases as the RMS wave height increases (see fig. 2 -theoretical function for aircraft conditions with different sea state values). In the past, space applications were considered but the required antenna technology was not available. The current new Large Space Antenna technology creates an opportunity to achieve the required beamwidth and near nadir pointing control that can make the system feasible. There is also the prospect that with a sufficiently narrow beamwidth, a wider swath than the "near nadir" region will be accessible, making coincident measurements with the Scatterometer possible.

## RADAR DECORRELATION WITH SURFACE ROUGHNESS

Beamwidth = 1.5 deg.

Altitude = 10 000 ft.

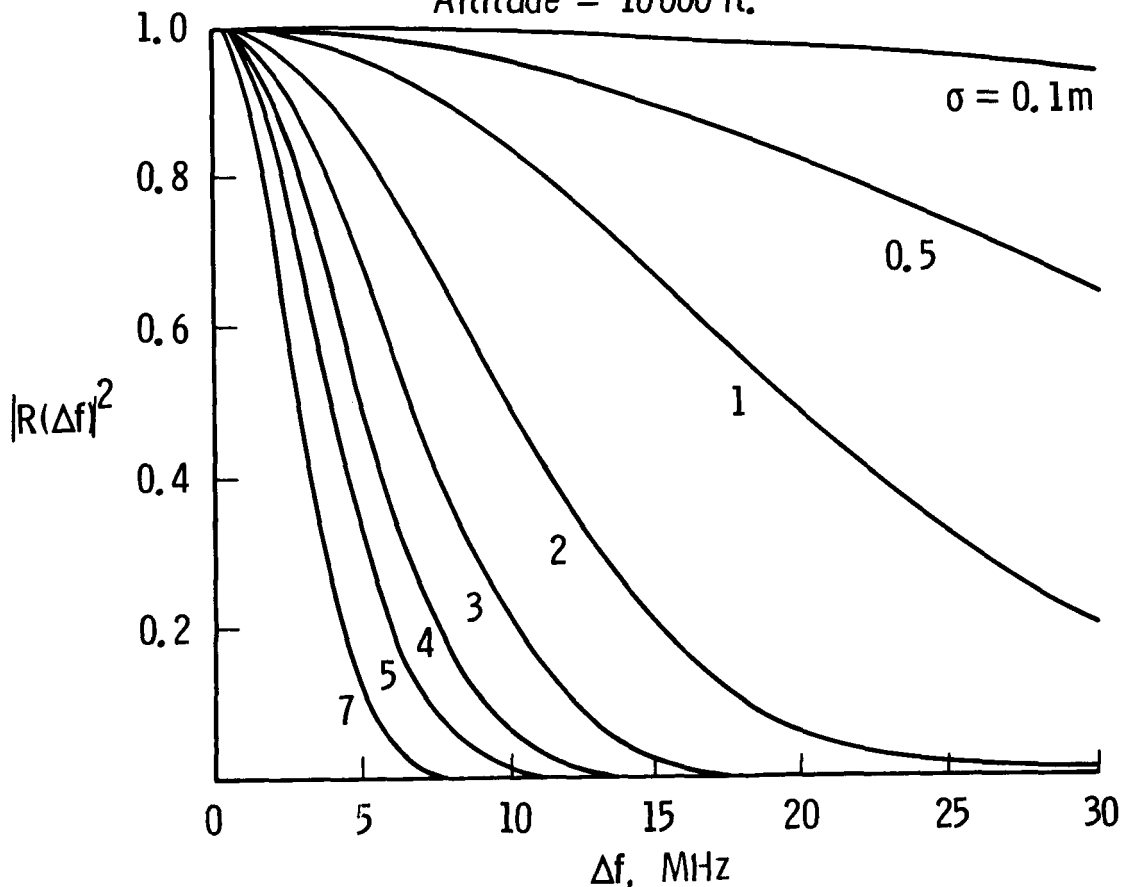


Figure 2



## WAVE SPECTRUM MEASUREMENTS

Ocean wave spectrum measurement with microwave sensors is becoming a more accurate art, with a sounder physical basis, as several sensor techniques (synthetic aperture radar, short pulse spectrometer, and Delta-K) continue to improve. The measurement of ocean wave spectra from space is considered feasible. Consistent and compatible with the present narrowband radar mode under discussion here is the Delta-K radar (ref. 2,3). This instrument responds to one ocean wavelength at a time, within a sweep of measurements that spans the ocean spectrum. One set of results is shown in fig. 3, where the radar inferred spectrum compares well with that obtained by a highly accurate radar system (surface contour radar). However accurate results with the Delta-K instrument (and other oblique incidence sensors) require wind speed information in order to provide a reliable estimate for the modulation transfer function. The significant conclusion from these facts is that a wave sensor and Scatterometer (radar cross section) measurement can be combined "synergistically".

## TWO-FREQUENCY RADAR SURFACE SPECTRUM MEASUREMENTS

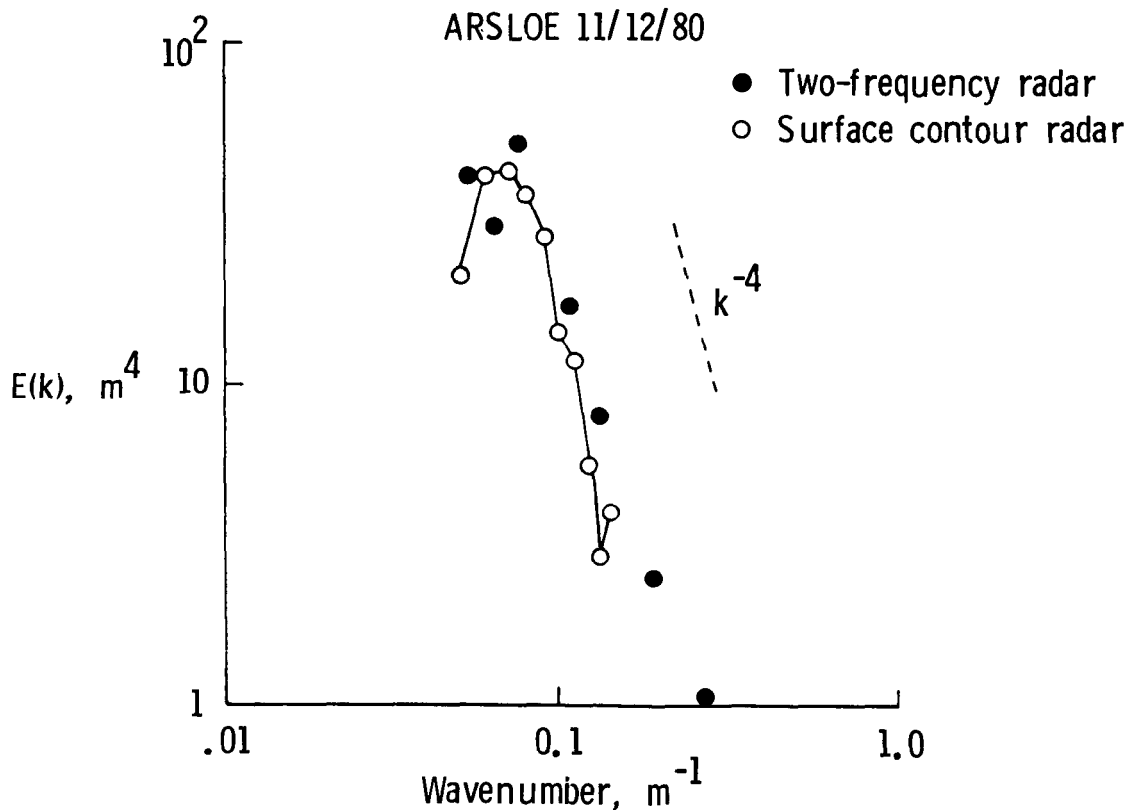


Figure 3

## SUMMARY

This paper seeks to call attention to a coherent set of facts that are interesting and important to existing and planned oceanographic remote sensing programs and which may open up a new sensor approach in this field. To demonstrate the feasibility of using a large space antenna (up to 15 meters in diameter) from a shuttle platform, a set of calculations were conducted using existing theoretical models of the nadir dual frequency scatterometer (ref. 4). These are basically design calculations to determine the necessary size (diameter) of a single aperture antenna as a function of altitude which would be needed to achieve an acceptable accuracy (an error correlation factor of 0.5 can be removed from the data with acceptable losses). The results of these calculations are shown in fig. 4 for a given set of radar and sea parameters (frequency = 14 GHz, RMS wave height = 0.25 meter and 1.0 meter). These show that for shuttle altitudes (200 to 400 km) antenna diameters less than 15 meters are capable of providing the desired performance.

This survey advocates that interesting and rewarding possibilities exist if we consider combining individual sensors into multi-sensors with the new large scale antenna technology that is on the horizon. We are in a fortunate position because much data is available from previous studies that could be used in a more focussed and integrated study of this approach. And many of the earlier individual system studies can serve as the basis for a new combined system study.

### ANTENNA SIZE REQUIREMENTS FOR 50% ERROR AT $R(\Delta f)^2 = 0.5$

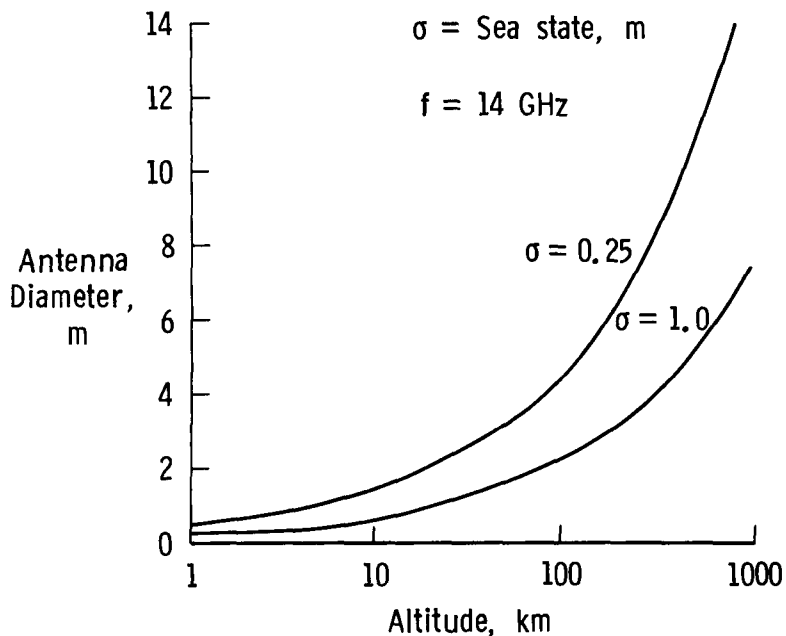


Figure 4

#### REFERENCES

1. Keller, W.C., Plant, W.J., Weissman, D.F., The Dependence of X-Band Microwave Sea Return on Atmospheric Stability and Sea State; J. Geophys. Res., Vol. 90, pp 1019-1029, Jan. 20, 1985
2. Johnson, J.W. and Weissman, D.F., Two-Frequency Microwave Resonance Measurements from an Aircraft: A Quantitative Estimate of the Directional Ocean Surface Spectrum; Radio Sci., Vol. 19, pp 841-854, May-June 1984
3. Weissman, D.E. and Johnson, J.W., Measurements of Ocean Wave Spectra and Modulation Transfer Function with the Airborne Two Frequency Scatterometer., Frontiers of Remote Sensing of the Oceans and Troposphere from Air and Space Platforms, URSI Comm. F Symposium, May 1984 - NASA CP-2303
4. Weissman, D.E. and Johnson, D.E., Dual Frequency Correlation Radar Measurements of the Height Statistics of Ocean Waves., IEEE Trans. Antennas and Propagat., Vol AP-25, No. 1, January 1977

**Page intentionally left blank**

QUASAT -  
AN ORBITING VERY LONG BASELINE INTERFEROMETER  
PROGRAM USING LARGE SPACE ANTENNA SYSTEMS

J. F. Jordan  
R. E. Freeland  
G. S. Levy  
D. L. Potts  
Jet Propulsion Laboratory  
California Institute of Technology  
Pasadena, California

Large Space Antenna Systems Technology - 1984  
December 4-6, 1984

## THE QUASAT MISSION CONCEPT

QUASAT, which stands for QUASAR SATELLITE, is the name given to a new mission being studied by NASA. The QUASAT mission concept involves a free-flying earth-orbiting large radio telescope, which will observe astronomical radio sources simultaneously with ground radio telescopes. The mission concept is illustrated in Figure 1.

The primary goal of QUASAT is to provide a system capable of collecting radio frequency data which will lead to a better understanding of extremely high energy events taking place in a variety of celestial objects including quasars, galactic nuclei, interstellar masers, radio stars and pulsars.

QUASAT's unique scientific contribution will be the increased resolution in the emission brightness profile maps of the celestial objects.

In 1980 the National Academy of Sciences' Astronomy Survey Committee listed an orbiting VLBI antenna as a high priority for a national astronomical endeavor.

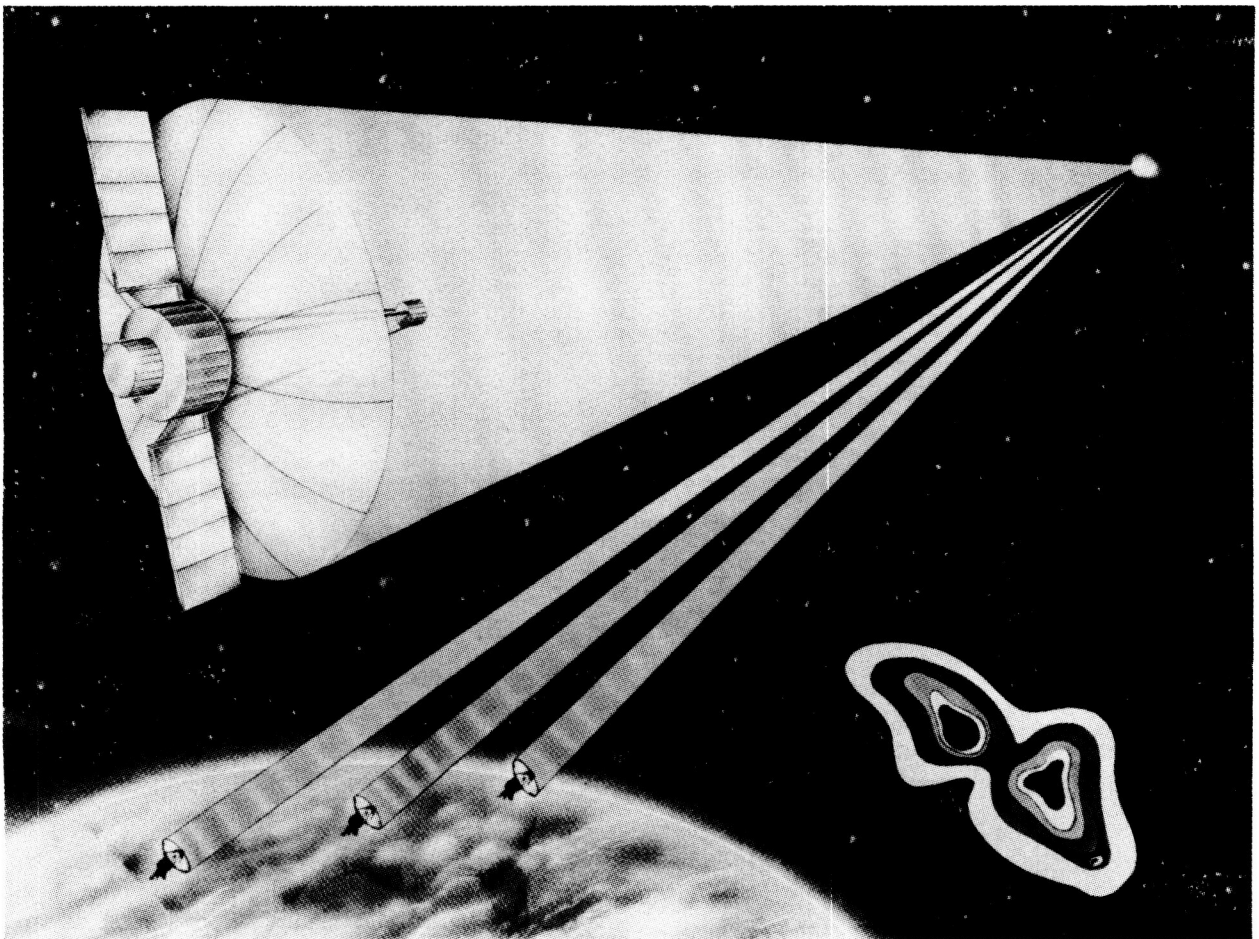


Figure 1  
High Resolution Interferometry From Space

## APERTURE SYNTHESIS

Increased resolution in the maps of celestial objects is made possible by the larger baselines, created by spaceborne antenna, compared to the maps created by networks of ground antennas alone. For the past 15 years, radio astronomers have employed Very Long Baseline Interferometry (VLBI) techniques to synthesize apertures whose size is determined by the distance between antennas rather than the diameters of the antennas themselves. The radio signals from two observing antennas are recorded on high density recording tapes simultaneously, and the tapes are, at a later time, correlated to produce information equivalent to the Fourier transform of the brightest profile of the observed celestial object at a frequency of  $\lambda/D$ ,  $\lambda$  being the observed wavelength and  $D$  being the projection of the antenna-to-antenna baseline onto the plane perpendicular to the direction to the observed object. As more antennas are added to the observing network and the network geometry evolves as the earth rotates, an effective large aperture is synthesized. An antenna in space creates the ability to synthesize an aperture larger than the earth as illustrated in Figure 2.

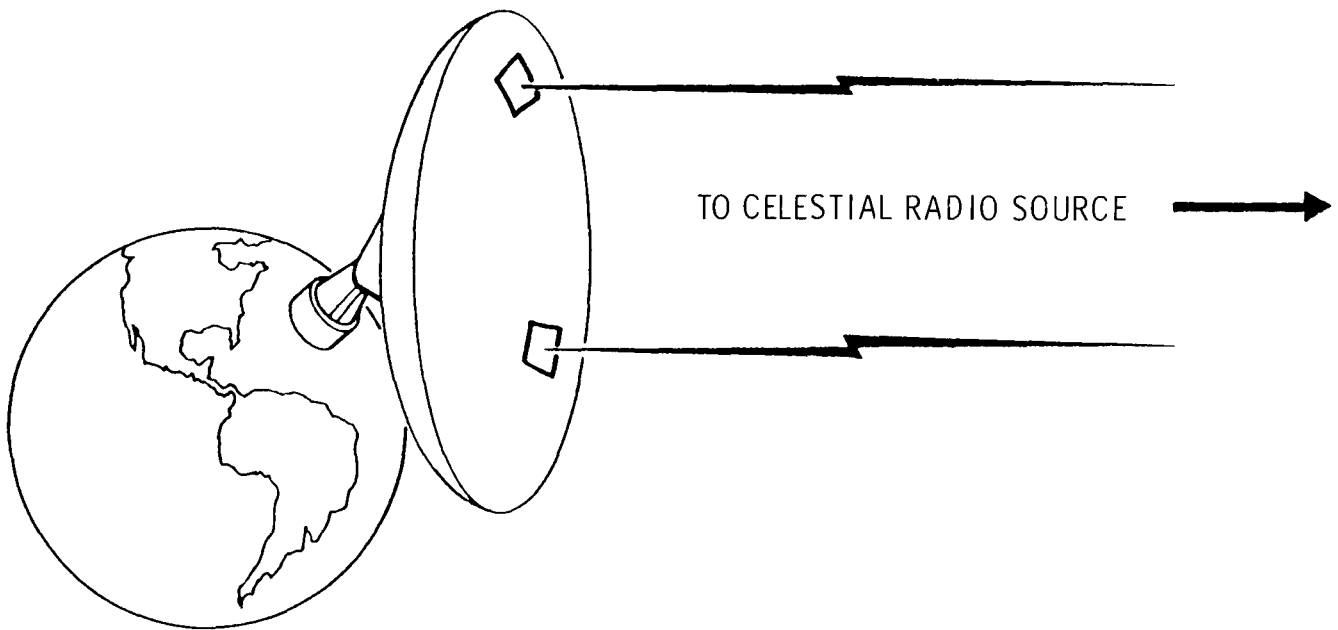


Figure 2  
Synthesizing an Antenna Aperture Larger Than the Earth

## MISSION ASSESSMENT STUDY

QUASAT has been studied jointly by NASA and the European Space Agency during the past two years. In 1982 a joint American-European science working team was established which produced the preliminary mission requirements.

Radio reception at three distinct frequencies is desired; K-band (1.35 cm), C-band (6 cm) and L-band (18 cm), the primary interest being K-band. In addition, simultaneous right and left hand circular polarization reception with 30 dB separation between senses is desired.

High sensitivity is required. A signal-to-noise ratio of at least 6 to 1, which will allow detection of radio sources with source strength down to 140 mJy with an integration time of 300 seconds, is desired. The satisfaction of the requirement for high sensitivity and the short K-band wavelength forces a number of demands on the flight system: (1) a large deployable antenna of diameter 15-20 meters with sub-mm RMS surface accuracy, (2) a precision pointing system capable of control accuracy to within one minute of arc, (3) cooled receivers with system temperatures below 150K, (4) feeds and feed structures designed to accommodate optimal RF efficiency and (5) high bit rate (144 mbits/s) receiving capability along with the downlink to earth to enable real-time transmission of the signal to ground tracking antennas.

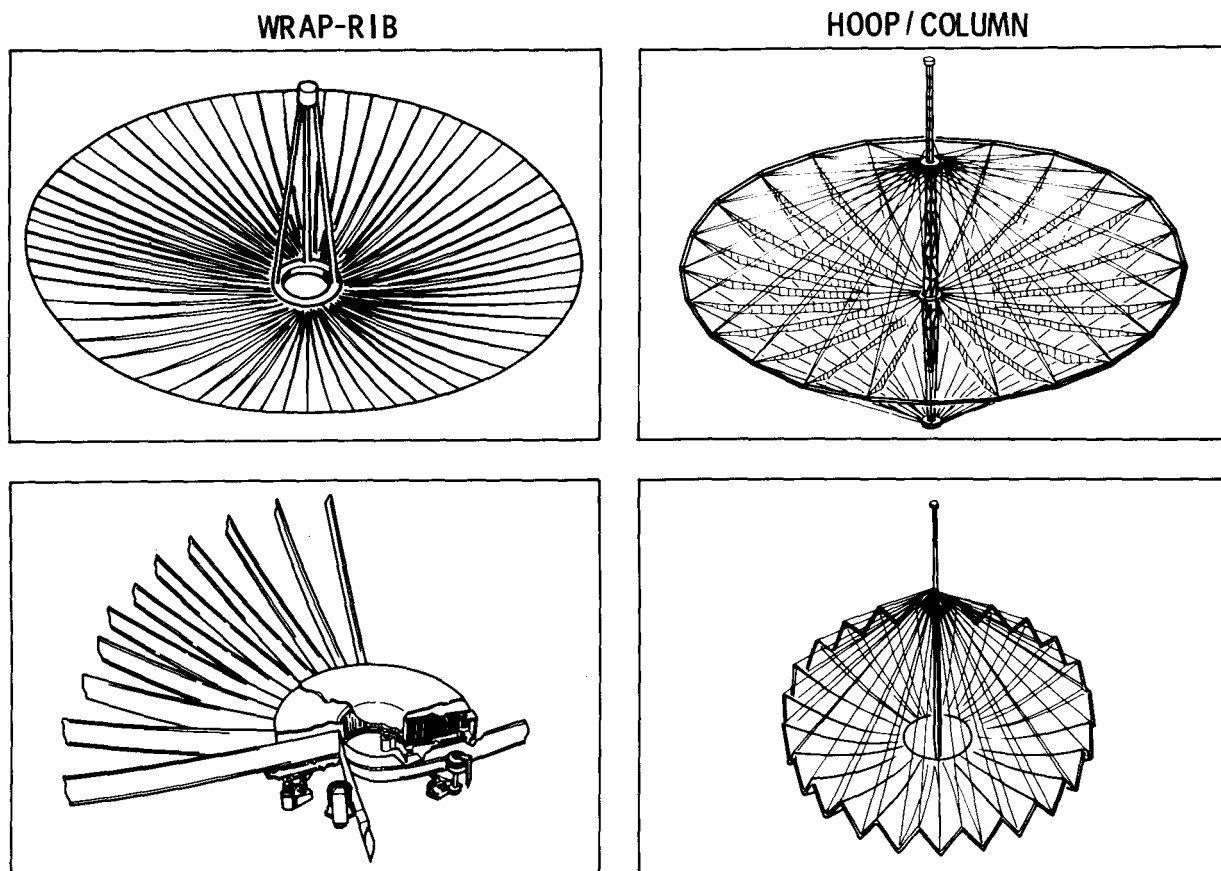


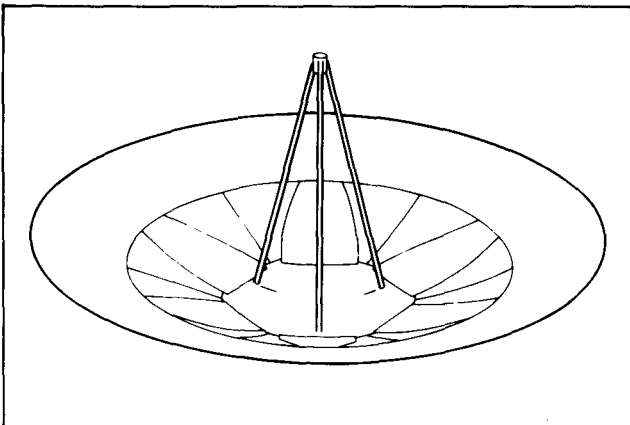
Figure 3  
Surveyed Antenna Concepts



## MISSION ASSESSMENT STUDY (Cont'd)

Since high resolution is achieved by the long baselines between the spaceborne antenna and the ground antennas, a high apoapsis altitude for the orbit, greater than 20,000 km, is desired. However, a low periapsis, less than 7000 km, is required to create the orbital precession necessary to evolve the optimal viewing directions throughout the celestial sphere. A high inclination, around  $60^\circ$ , is needed to provide the geometry for good aperture synthesis for viewing directions at a variety of celestial latitudes. Mission lifetime should be at least five years.

ADVANCED SUNFLOWER



TRUSS SUPPORTED PANEL

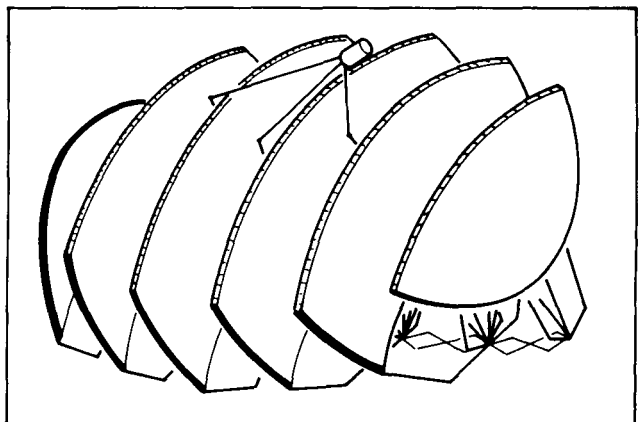
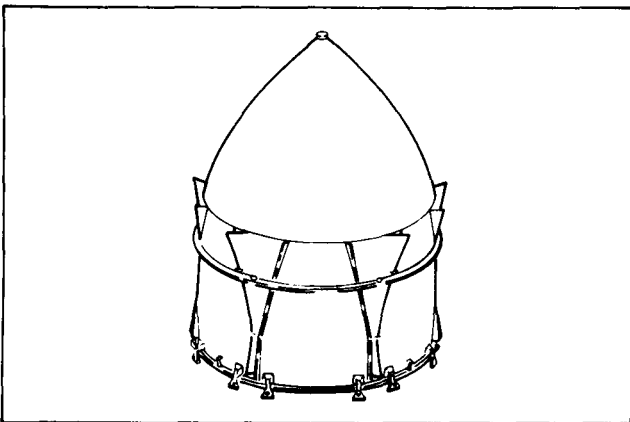
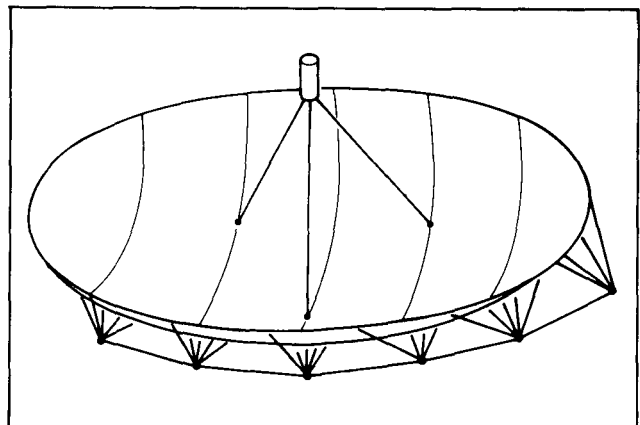


Figure 4  
Surveyed Antenna Concepts (Cont'd)

## MISSION ASSESSMENT STUDY (Cont'd)

In 1984, both NASA and ESA conducted mission feasibility assessment studies. On the American side, these studies were conducted by the Jet Propulsion Laboratory and consisted of an antenna feasibility study and a mission analysis/spacecraft and ground system preliminary design activity. Four small technology assessment contracts were awarded to American firms in order to obtain characteristics of the antenna concepts applicable to QUASAT. The four proposed concepts are illustrated in both a stowed or partially deployed state and a fully deployed state in Figures 3 and 4. The concepts include the Wrap-Rib antenna being developed at Lockheed Missiles and Space Company, the Hoop-Column antenna being developed at Harris Corporation, an advanced Sunflower concept proposed by TRW and a truss-supported panel-deployable concept proposed by Astro-Research Corporation. All four antenna concepts appear applicable to QUASAT.

In Europe, the ESA studies have concentrated on an inflatable antenna being developed by Contraves Corporation in Switzerland. See Figure 5.

Both American and European mission study results were presented at a workshop on Space VLBI and astrophysics, sponsored by the U.S. National Academy of Sciences and the European Science Foundation and held in June 1984 in Vienna, Austria.

### INFLATABLE

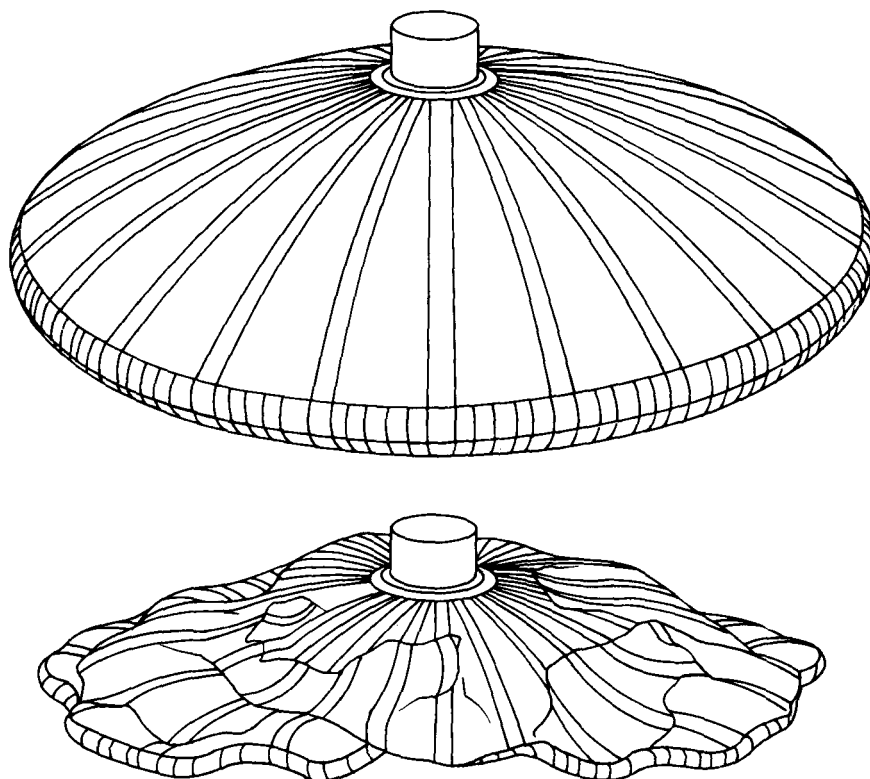


Figure 5  
Surveyed Antenna Concepts (Cont'd)

## THE FLIGHT SYSTEM

A preliminary flight system has been designed based on the Wrap-Rib antenna concept. It should be considered as an example flight system since at this time the antenna has not been selected. The flight system is illustrated in Figure 6. The spacecraft is solar powered with nine square meters of panel, which generate about 1000 watts. The feed tower is constructed of tubular truss links, which deploy from a tightly folded launch configuration, F/D is .4. The feeds and receivers for all three reception frequencies are located at prime focus, and cooling is provided passively from a two-square-foot radiating plate. Attitude is controlled by momentum wheels driven from star sensor readouts, and the rotational effects of gravity gradients are compensated by torquer bars.

The flight system is compatible with a launch using the Space Transportation System or the French Ariane launcher. If launched from the Shuttle, this flight system can fit on the Pam-D spintable, with a Star-48 solid fuel rocket providing the boost from Shuttle orbit to the proper apoapsis. The Star-27 solid-fuel rocket provides for raising the periapsis altitude.

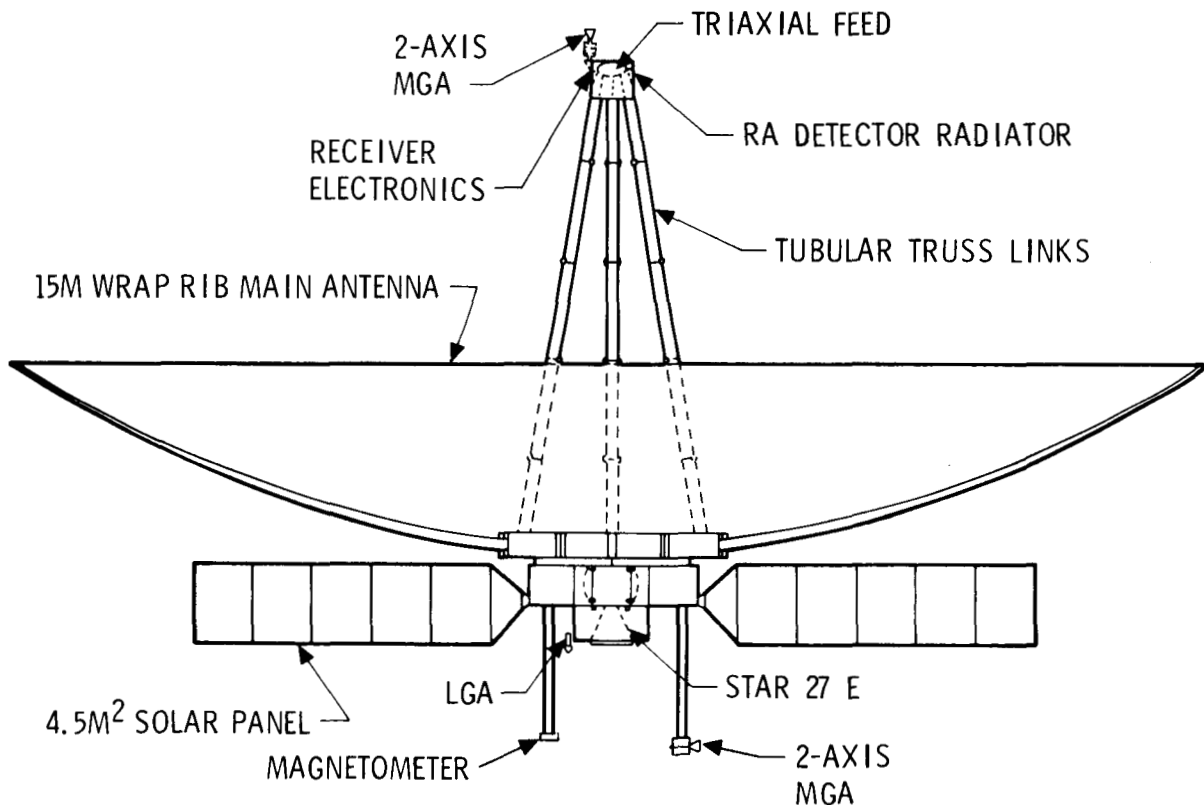


Figure 6  
Assessment Study Flight Configuration

## THE GROUND SYSTEM

Figure 7 provides a schematic diagram of the ground system which would support QUASAT. The spacecraft will be tracked by the NASA Deep Space Net. Radio telescopes around the world will co-observe with QUASAT. The network will include those in the Very Large Baseline Array (VLBA), a new VLBI-dedicated ground array being developed by the National Science Foundation.

The up and downlinks have been designed to utilize either the 26-meter or 34-meter antennas, the Deep Space Network communications, and the navigation capabilities of the DSN to optimize the science output. The DSN 70-meter DSN antennas may also be used, as required, to enhance the observational sensitivity.

Both the flight system and the radio astronomy ground antennas will produce similar data recordings at rates up to 144 MEGABITS per second, which will be correlated and analyzed at a central facility.

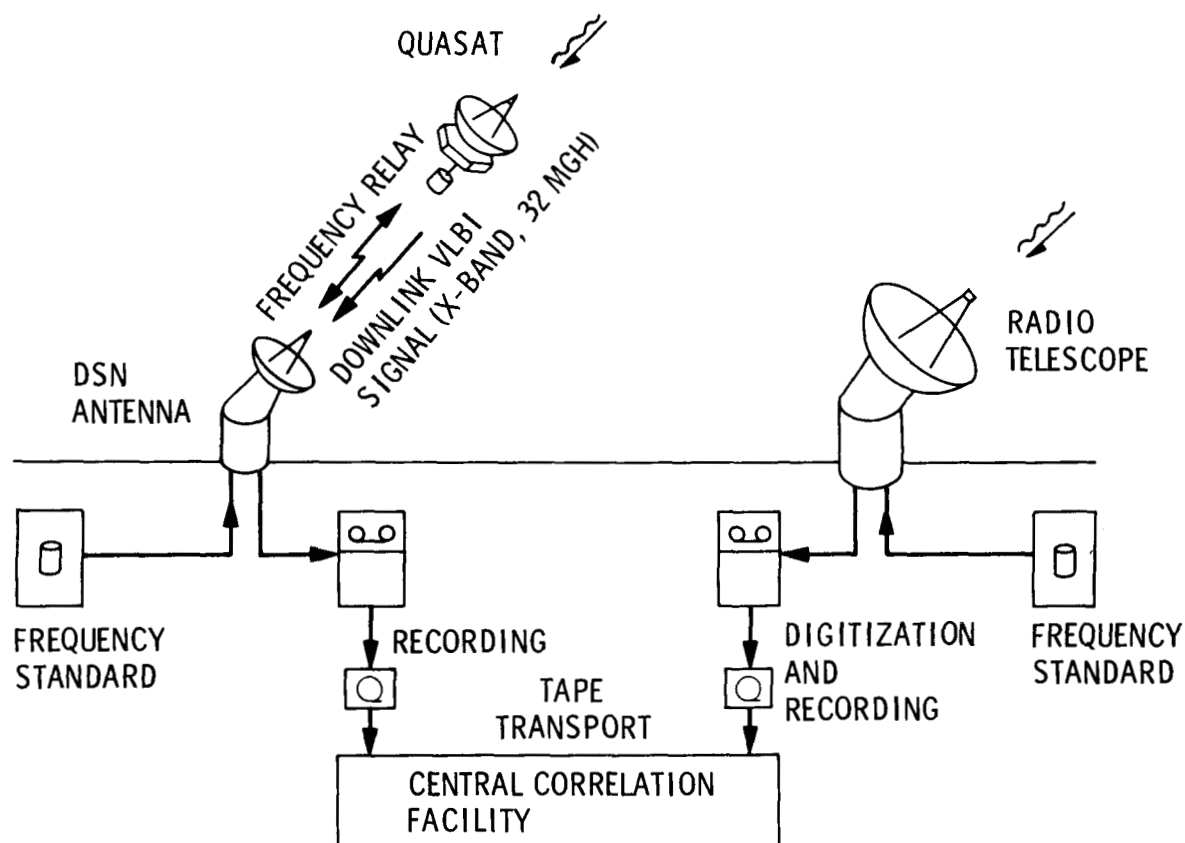


Figure 7  
Baseline Ground Configuration

## PROGRAM SCHEDULE

QUASAT is currently envisioned as a jointly supported NASA-ESA mission, with the mission costs lower to each agency. Of course, the mission may eventually be undertaken by a single agency. It is hoped that JPL and the Langley Research Center may develop joint advocacy for the mission, with LaRC taking the lead in flight antenna experiments using the QUASAT antenna as a long-term spaceborne laboratory for structural and RF testing.

The earliest new-start year is FY88, but a more realistic new-start year is 1990. Figure 8 provides a project schedule associated with the earliest possible new-start. The schedule calls for a 3½-year antenna procurement cycle and a possible launch by 1993.

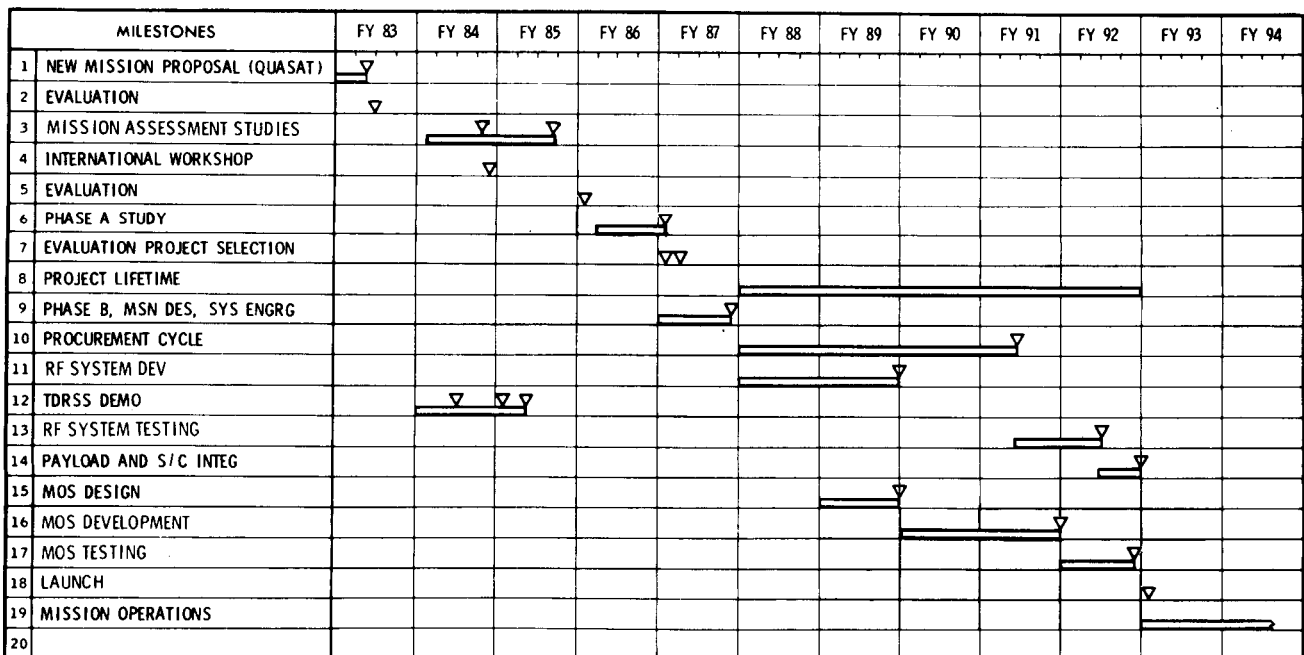


Figure 8  
Program Schedule

**Page intentionally left blank**

LDR SYSTEM CONCEPTS AND TECHNOLOGY

Bruce Pittman  
NASA Ames Research Center  
Moffett Field, California

Large Space Antenna Systems Technology - 1984  
December 4-6, 1984

The Large Deployable Reflector is a 20-meter-diameter infrared/submillimeter telescope planned for the late 1990's. The Astronomy Survey Committee of the National Academy of Sciences (Field Committee) recommended LDR as one of the two space-based observatories that should start development in the 80's. LDR's large aperture will give it unequaled resolution in the wavelength range from 30 - 1000 microns.

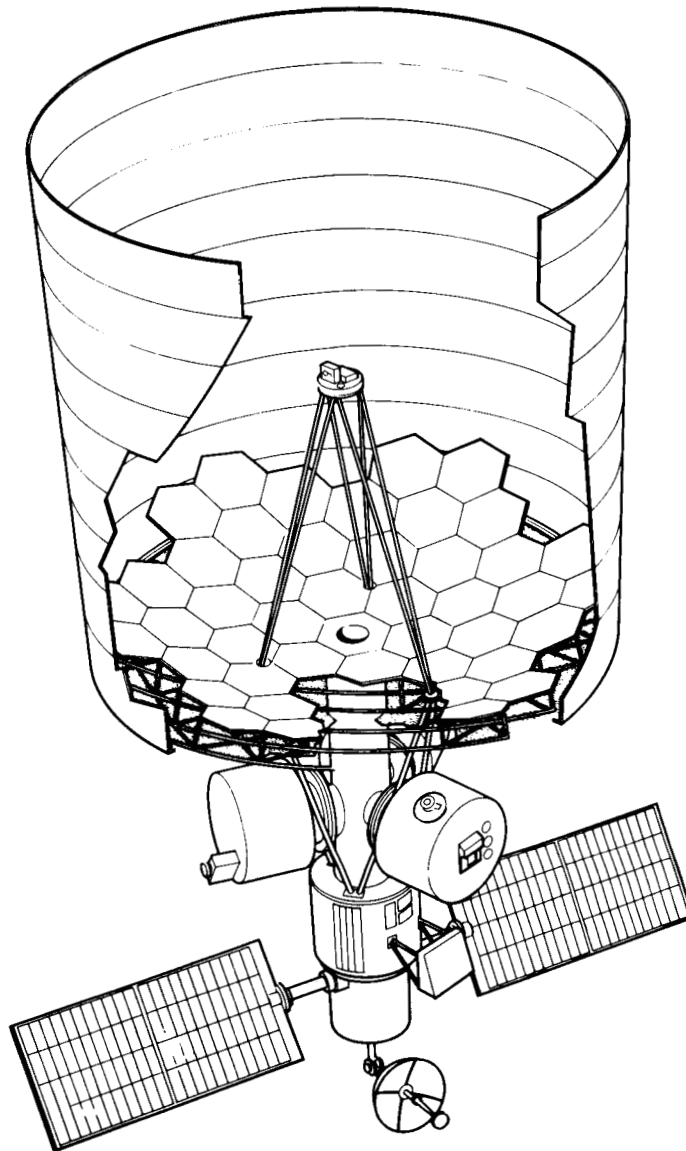
To meet LDR performance goals will call for advances in several technology disciplines including: optics, controls, thermal control, detectors, cryogenic cooling, and large space structures.

### **KEY LDR TECHNOLOGY DRIVERS**

- \* 20-METER-DIAMETER PRIMARY MIRROR**
- \* 2-4 MICRON RMS WAVEFRONT ERROR BUDGET**
- \* 0.06 ARC SEC POINTING ACCURACY**
- \* 1K THERMAL GRADIENT ACROSS THE PRIMARY**
- \* LARGE, COMPLEX INSTRUMENTS**
- \* 1-2 WATTS OF COOLING AT 4K**
- \* 10-YEAR LIFETIME**



**This is a view of LDR showing the thermal shade, primary and secondary mirrors, backup structures, instrument modules, spacecraft, and solar panels.**



One of the key challenges in the development of LDR is to understand the interdependence of all of the various systems. A major change in one system will almost certainly have a pronounced impact on several other systems. For example, a change in the thermal expansion of the support structure for the primary mirror will not only affect the primary optics, but will also affect the actuator system that positions the optics. The impact and interaction of the LDR systems must be clearly understood prior to Phase B.

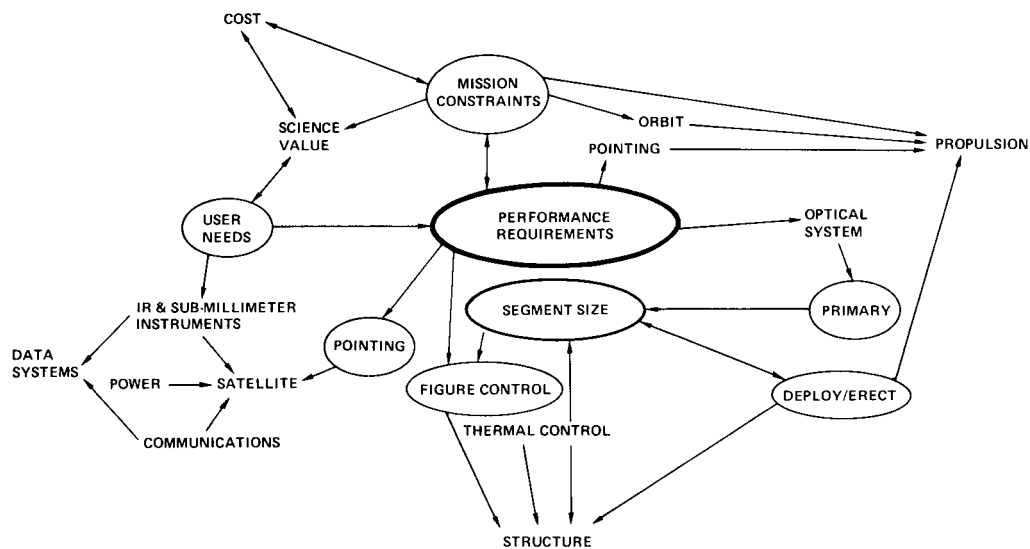
There are several key "system issues" or questions that have an impact on several LDR systems. The impact of these issues on the various LDR systems must be well understood before the proper decision can be made on how to implement LDR. Single or multiple Shuttle launches, polar or equatorial orbits, deployed or assembled construction, these are only a few of the systems issues that must be addressed prior to developing a comprehensive technology development plan.

## **LDR SYSTEM ISSUES**

**\* SEVERAL KEY "SYSTEM ISSUES" HAVE BEEN DEVELOPED; THE INTERRELATION MUST BE STUDIED**

- \* TRANSPORTATION TO ORBIT**
- \* ORBIT PARAMETERS**
- \* ORBITAL ENVIRONMENT**
- \* DEPLOYED OR ASSEMBLED CONSTRUCTION**
- \* OPTICAL CONFIGURATION**
- \* APERTURE SIZE**
- \* MIRROR SURFACE ACCURACY**
- \* CONTAMINATION CONTROL**

The principal LDR system relationships must be well understood before a technology development plan can be developed. This task was added at the beginning of the Technology Definition Plan Studies.



To produce a technology development plan for LDR, it was decided to undertake the System Concept and Technology Definition Studies. The purpose of the studies is to understand the interaction of the various systems of LDR and to understand the impact of the systems issues on the total system.

Two contractor teams were selected, each undertaking parallel \$450,000 studies; one team was headed by Eastman Kodak and the other by Lockheed.

The output of these studies will be two concepts for LDR, each of which could meet the LDR system requirements. A technology development plan will also be produced that will identify the augmentations that must be made in the OAST technology program if LDR is to be undertaken in the early 1990's without undue technological uncertainty.

## **SYSTEM CONCEPT AND TECHNOLOGY DEFINITION STUDIES**

- \* TWO INDEPENDENT STUDIES OF LDR SYSTEM  
CONSIDERATIONS AND TECHNOLOGY REQUIREMENTS**
- \* EACH CONTRACTOR WILL DEVELOP TWO CONCEPTS  
FOR LDR AND A TECHNOLOGY DEVELOPMENT PLAN**
- \* THE PLAN WILL:**
  - BE TIME PHASED**
  - BE RANKED BY PRIORITY**
  - HAVE INTERMEDIATE MILESTONES**
  - HAVE REQUIRED TECHNOLOGY LEVELS**
  - HAVE PRELIMINARY COST DATA**

**The LDR technology development plan will include several key technologies that have already been identified as key candidates.**

## **KEY LDR TECHNOLOGIES**

- \* OPTICS**
- \* STRUCTURES AND MATERIALS**
- \* POINTING AND CONTROLS**
- \* INSTRUMENTS AND CRYOGENICS**
- \* SYSTEMS ANALYSIS**

**LDR represents one of the most challenging astronomy projects ever undertaken by NASA. Due to this challenging nature there are several key decisions that must be made concerning how the program will be implemented. These decisions will have a substantial impact on the resulting technology development program. Until sufficient study has been made to allow these key questions to be answered, parallel technologies may have to be pursued in some areas.**

## **TECHNOLOGY DEVELOPMENT PLANNING**

- \* THE LDR TECHNOLOGY PROGRAM IS " PATH DEPENDENT"**
- \* THE TECHNOLOGY PATH TAKEN DEPENDS ON THE SYSTEMS APPROACH TAKEN:**
  - \* SINGLE OR MULTIPLE SHUTTLE LAUNCHES**
  - \* POLAR OR EQUATORIAL ORBITS**
  - \* DEPLOYED OR ASSEMBLED CONSTRUCTION**
  - \* SPACE STATION UTILIZATION**

The early LDR feasibility studies made the assumption that LDR will be automatically deployed from a single Shuttle launch. This caused severe weight and packaging constraints. Ultra-lightweight optics and structures were required to meet severe Shuttle weight constraints. In addition, deployment schemes with both high packaging efficiency and extreme deployed accuracy were needed.

One possible concept for reducing the volume constraint is the use of an Aft Cargo Carrier. This proposed device would fit on the end of the Shuttle External Tank and provide an additional 10,000 cubic feet of storage space with a diameter of 25 feet.

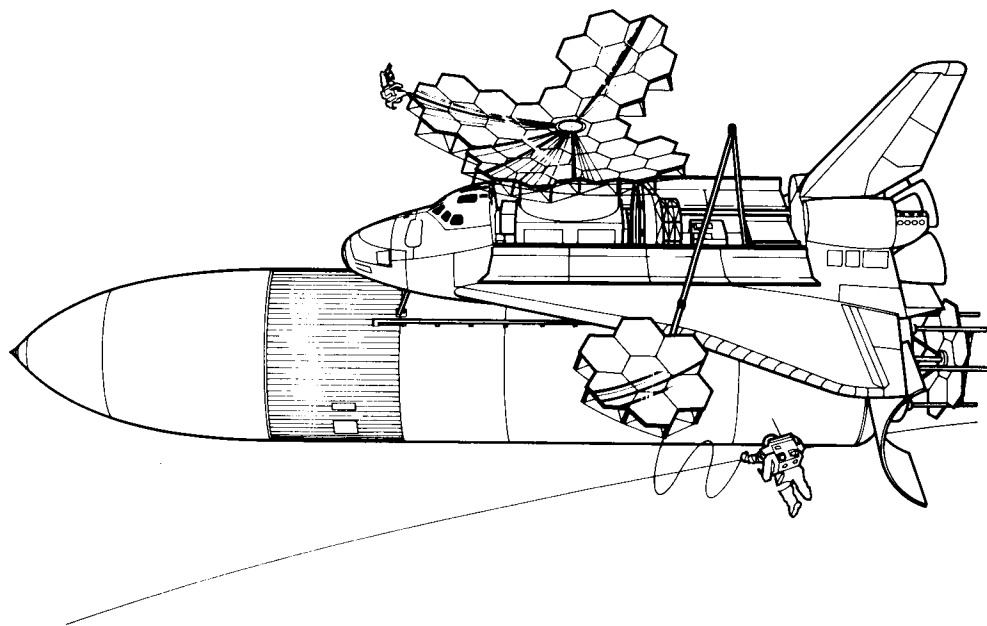
### **LDR CONCEPT #1**

- \* SINGLE SHUTTLE LAUNCH OPTION**
- \* SEMI-AUTOMATIC DEPLOYMENT**
- \* SHUTTLE AFT CARGO CARRIER**

### **KEY TECHNOLOGIES**

- \* LIGHTWEIGHT OPTICS & STRUCTURES**
- \* DEPLOYABLE STRUCTURES**
- \* SOPHISTICATED DEPLOYMENT MECHANISMS**

**The picture shows LDR being assembled in orbit using the Aft Cargo Carrier to store the segments of the primary mirror. The other portions of the LDR system are carried in the Cargo Bay.**





With the decision to deploy a manned space station within a decade, the possibility of assembling LDR in space using this facility became a serious consideration. Assembly in space has several advantages including using multiple Shuttle launches to eliminate both weight and volume constraints. If this path is pursued, then the technology program will focus on assembly of percision structures in space. It is important that this possibility be studied in the near term prior to the start of the detailed design of the station.

## **LDR CONCEPT #2**

### **\* MULTIPLE SHUTTLE LAUNCHES**

### **\* SPACE STATION ASSEMBLY**

### **KEY TECHNOLOGIES**

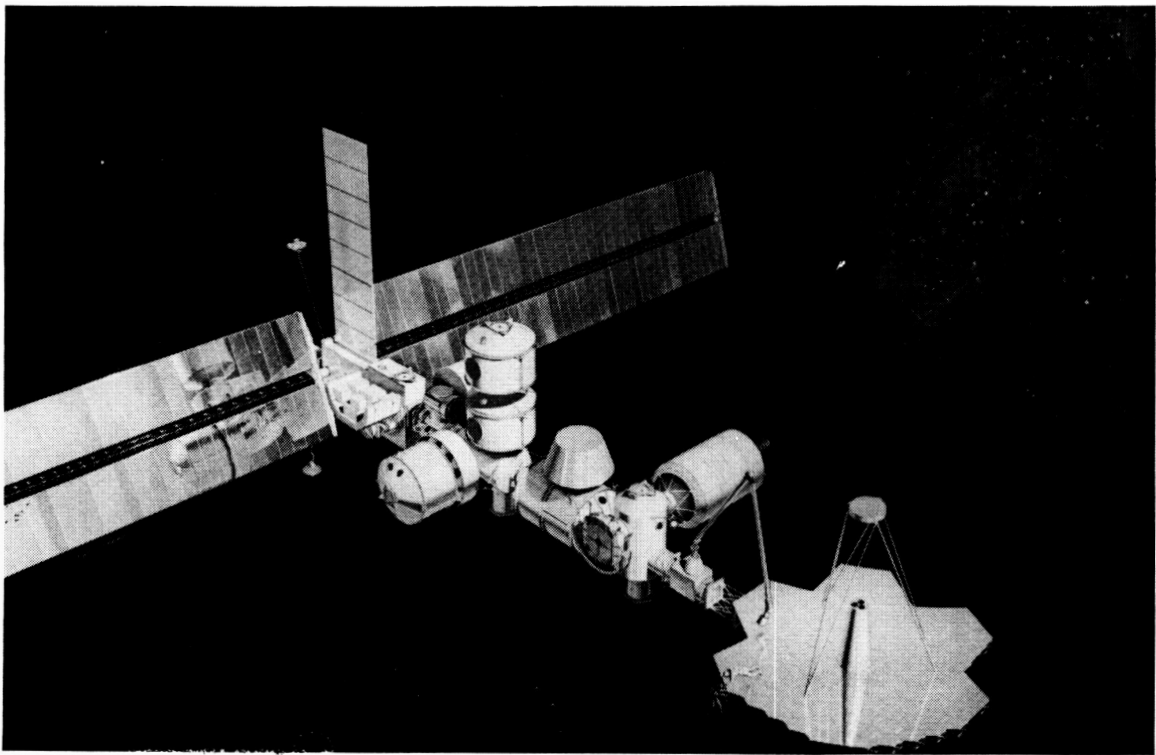
#### **\* ASSEMBLY OF LARGE SPACE STRUCTURES**

#### **\* ADVANCED REMOTE MANIPULATOR TECHNOLOGY**

#### **\* ROBOTICS**

#### **\* ADVANCED EVA**

**The picture shows LDR attached to the Space Station. The Station could be useful not only for initial assembly of LDR but also for initial alignment, refurbishment, and resupply.**



WRAP-RIB ANTENNA TECHNOLOGY DEVELOPMENT

R. E. Freeland  
Jet Propulsion Laboratory  
Pasadena, California

N. F. Garcia and H. Iwamoto  
Lockheed Missiles and Space Co.  
Sunnyvale, California

Large Space Antenna Systems Technology - 1984  
December 4-6, 1984

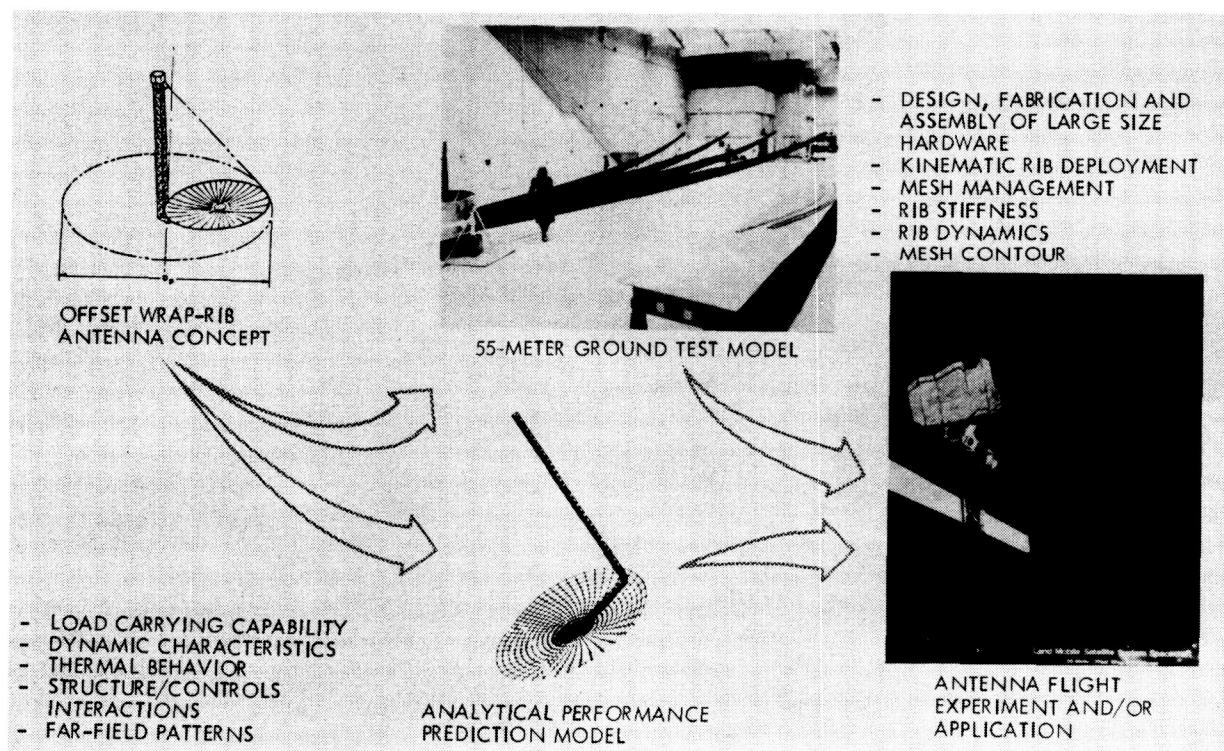
## LARGE DEPLOYABLE ANTENNA TECHNOLOGY DEVELOPMENT

The wrap-rib deployable antenna concept development is based on a combination of hardware development and testing along with extensive supporting analysis.

The proof-of-concept hardware models are large in size so they will address the same basic problems associated with the design fabrication, assembly and test as the full-scale systems which were selected to be 100 meters at the beginning of the program.

The hardware evaluation program consists of functional performance tests, design verification tests and analytical model verification tests. Functional testing consists of kinematic deployment, mesh management and verification of mechanical packaging efficiencies. Design verification consists of rib contour precision measurement, rib cross-section variation evaluation, rib materials characterizations and manufacturing imperfections assessment. Analytical model verification and refinement include mesh stiffness measurement, rib static and dynamic testing, mass measurement, and rib cross-section characterization.

This concept has been considered for a number of potential applications that include mobile communications, VLBI, and aircraft surveillance. In fact, baseline system configurations were developed by JPL, using the appropriate wrap-rib antenna, for all three classes of applications.

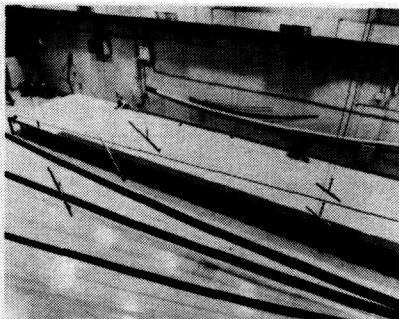


## PROOF-OF-CONCEPT WRAP-RIB ANTENNA MODELS

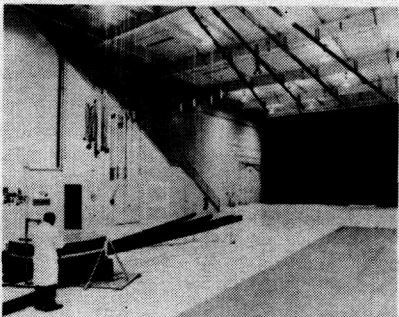
The proof-of-concept hardware model for the offset wrap-rib reflector is a sector of a 55-meter diameter structure. It consists of four graphite/epoxy lenticular ribs and three gold molybdenum wire mesh gore panels. The spacing of the ribs and density of the wire in the mesh are commensurate with surface accuracies accommodating 3 GHz RF operation.

Deployment of single ribs, four ribs, and the partial reflector is accommodated by a 0-G suspension system. This system is composed of a number of cables that utilize counter balances to vary the magnitude of support provided at five points along each rib. These cables are attached to bearings that ride along ceiling-mounted rails that follow the exact path of the ribs as they deploy from the hub structure. The cables are attached to the ribs at a distance of 5 meters from the hub and do not interfere with the mesh as it deploys from its stowed position between the ribs.

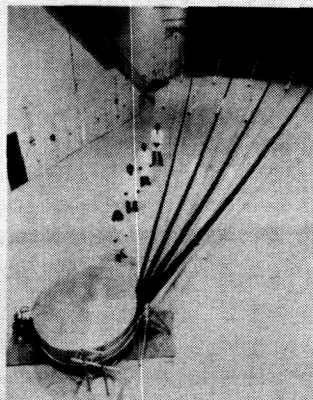
The mesh panels are laid out on bulk material that is loaded around its perimeter by a series of strings that go over pulleys for attachment to weights. The panels are then cut to the geometry required by the deployed ribs while maintaining the correct tension field.



MESH GORE PANEL FABRICATION



RIB DEPLOYMENT USING 0-G  
SUSPENSION SYSTEM



DEPLOYED SECTOR OF 55-METER  
REFLECTOR

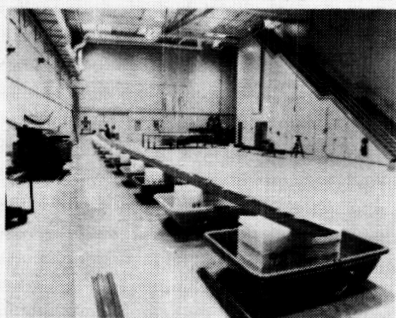
## WRAP-RIB ANTENNA TEST PROGRAM

The precision of curvature of the ribs was determined by establishing the geometry of a number of points along the unloaded structure with a theodolite. The rib structure was supported during the test by a number of soft foam blocks that were floating in individual tanks that were interconnected to maintain a common fluid level.

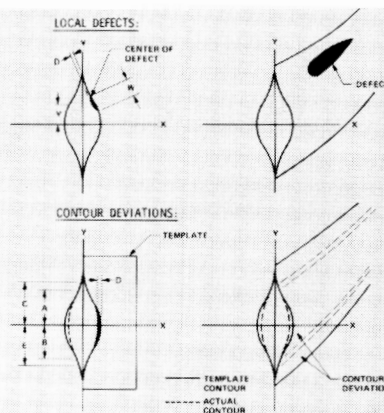
The measurement of the rib cross section was made by comparing the actual rib section with a number of templates that represent the desired lenticular shape as it varies along the rib. The rib deviations from the templates represent manufacturing error.

Static and dynamic characteristics of the ribs were determined by a series of simple static deflection and modal vibration tests. Each of the four ribs was tested for several deployed lengths for two different root boundary conditions. One rib root boundary was provided by the baseline deployment mechanism, the other by a rib root restraint.

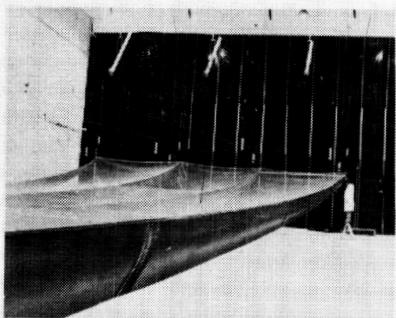
Mesh management was evaluated by repeated deployments of several schemes for stowing the mesh panels. These included folding the mesh on top of the ribs, partially between the ribs and entirely between the ribs. The most successful approach turned out to be folding the mesh between the ribs.



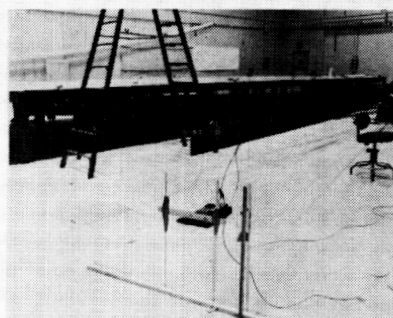
RIB CONTOUR MEASUREMENT



RIB CROSS SECTION



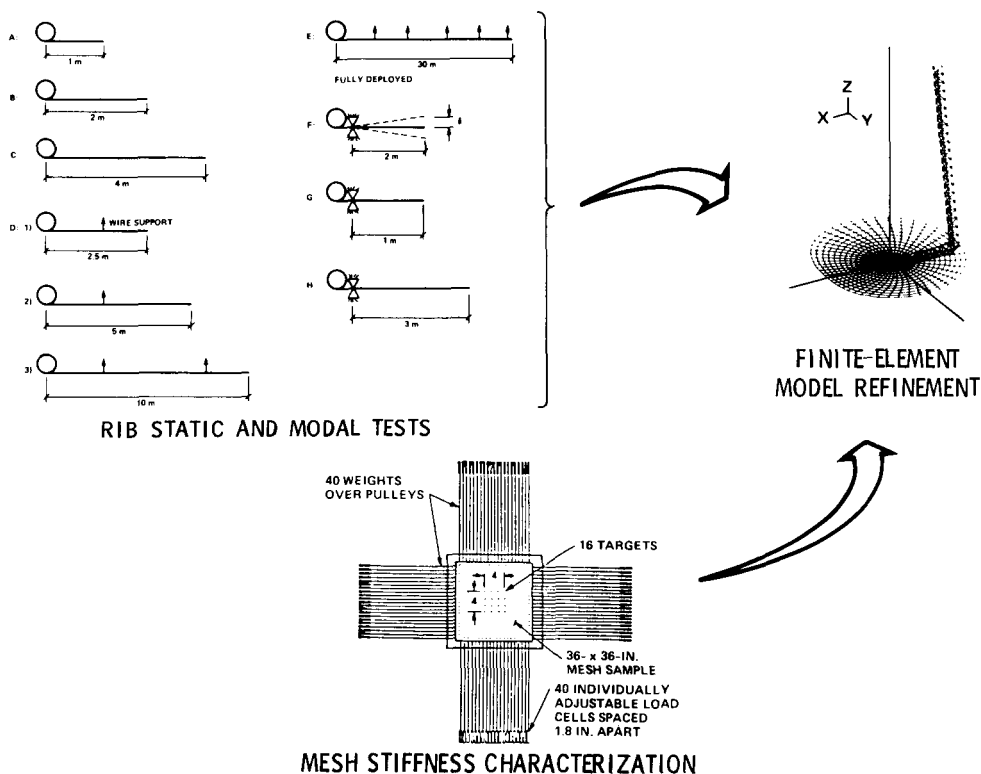
MESH MANAGEMENT



RIB STATIC AND MODAL TEST

## GROUND-BASED STRUCTURAL TEST TECHNIQUES

Ground-based test limitations of large, very flexible space structures preclude the meaningful preflight verification and demonstration of predicted space performance. The experimental determination of the practical limits of ground-based testing and the effects of manufacturing variations on structural performance can best be established by evaluation of full-size flight-type hardware. The 55-meter diameter hardware model has all the characteristics of large space structures, i.e., low frequency, high modal density, and nonlinear stiffness. The existing data base for this full-size hardware accounts for the design, fabrication, assembly, and testing of a number of different rib structures and rib structures attached to nonlinear mesh. The results of current and planned static and dynamic testing for a number of different boundary conditions for the same basic structure will be correlated with analytical predictions to determine the extent of testing required to adequately characterize this class of large space structures. Additionally, the manufacturing variations on full-sized, lightweight space hardware which have been experimentally determined will be used analytically to establish their sensitivity on structural system performance.

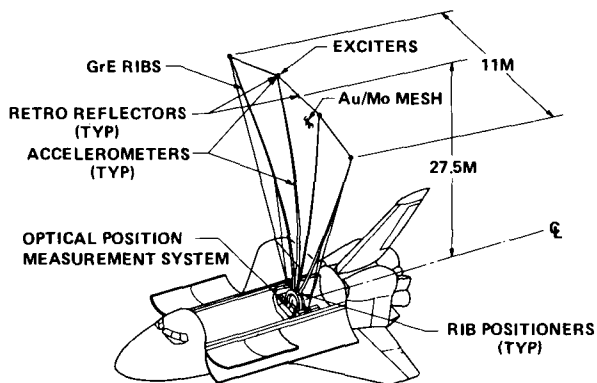


## WRAP-RIB ANTENNA FLIGHT EXPERIMENTS

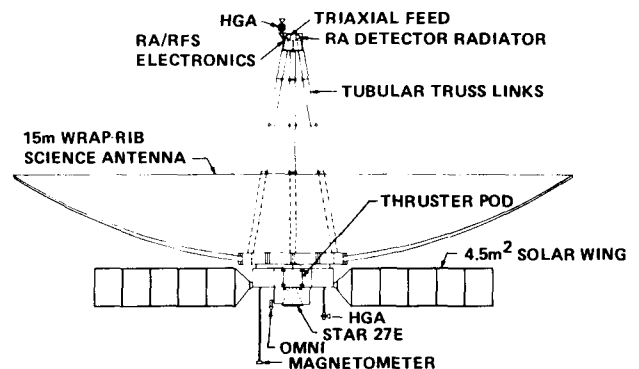
A number of flight experiments focused on extending and verifying technology for large deployable antenna systems have been defined over the past 12 or so years. The cost for either Shuttle-based or free-flying antenna experiments in the 30- to 50-meter size range has been prohibitive regardless of the potential technical value. This suggests the need for lower cost and less ambitious flight experiments. Such experiments might be based on using upgraded existing development hardware or by combining a basic science mission with a low-risk antenna technology experiment.

A Shuttle-based experiment using an upgraded version of the wrap-rib proof-of-concept model, which is a sector of a 55-meter diameter offset reflector, and the STEP has the benefits of using a generic large space structure. Namely, it has the structural characteristics of low frequencies, high modal density and coupling and nonlinear dynamic response. Such an experiment would address initial position variations, mesh management, surface precision and structural and thermal characteristics.

The QUASAT baseline science mission uses a 15-meter deployable K-band antenna for VLBI. This science antenna could be upgraded by adding the capability for surface measurement, surface adjustment and dynamic control. This would accommodate an experiment addressing initial position, surface precision, feed structure alignment and adjustment, thermal distortion and active surface control at a small fraction of the total mission cost.



STS ATTACHED EXPERIMENT WITH  
PROOF-OF-CONCEPT 55-METER MODEL  
USING STEP



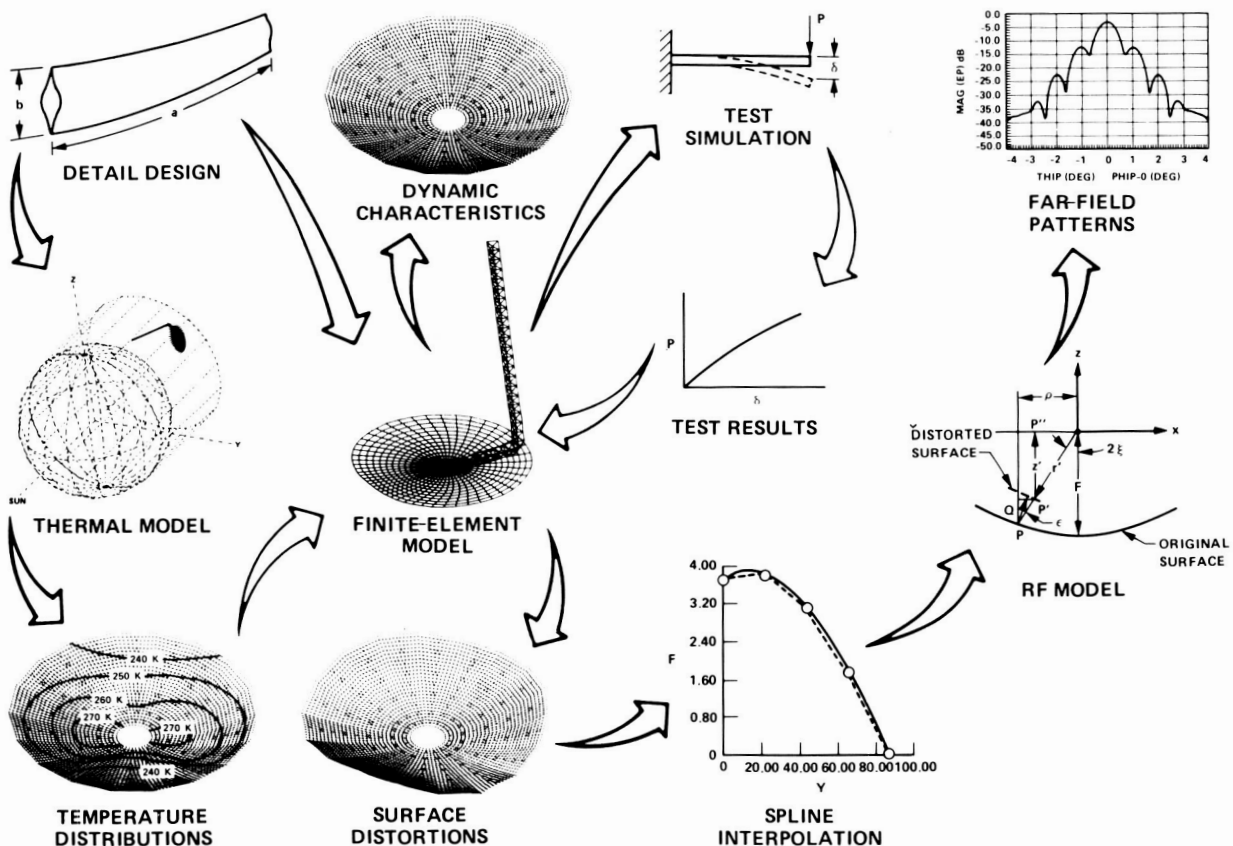
QUASAT FREE FLYER SCIENCE  
AND TECHNOLOGY MISSION



## ANTENNA SYSTEM INTEGRATED ANALYSIS

The deployable antenna system integrated analysis capability was developed to evaluate the potential value of antennas for classes of applications, to optimize specific structures for specific applications and to predict on-orbit system performance.

The finite-element model and thermal model were initially developed with results of the structural preliminary design. Results of component and assembly structural tests were used to refine the antenna system finite-element model. The thermal model was used to determine the antenna system temperature distributions for different Sun angles and orbital points. These temperature distributions are used with the finite-element model, which accounts for the concept surface approximation error to determine the overall aperture distortion. Additionally, this model generates the system dynamic characteristics which are needed for structural and control system evaluation and development. The surface errors, which are defined in terms of the coordinates and displacements of the grid points, are transformed into continuous functions by means of a spline interpolation routine. This result is the input to the RF analysis which utilizes a ray-tracing technique to generate the antenna for field patterns.

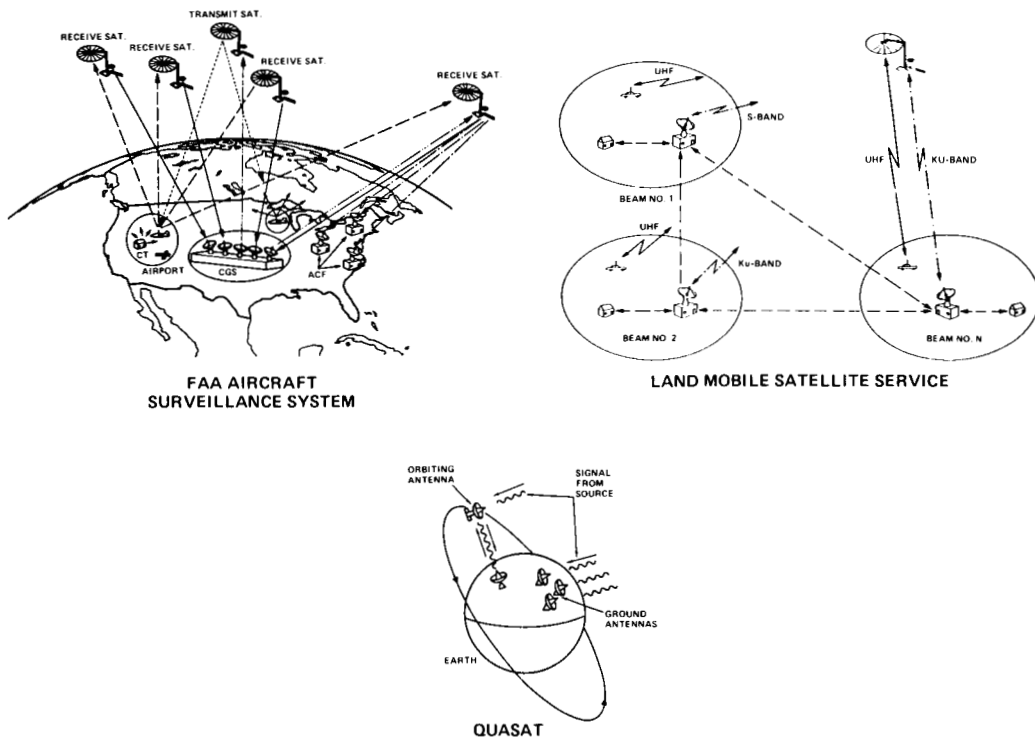


## POTENTIAL ANTENNA APPLICATIONS

Air Traffic Control (ATC) is currently accomplished by means of a network of terrestrial surveillance radars, airborne transponders, and an extensive communications network. The FAA is investigating the applicability of satellites to various aspects of ATC. A current air traffic surveillance study has shown the feasibility of using 5-8 geosynchronous satellite networks for supplementing the terrestrial system and increasing coverage. The satellites utilize an unblocked aperture antenna from 15 to 150 beams at L-band.

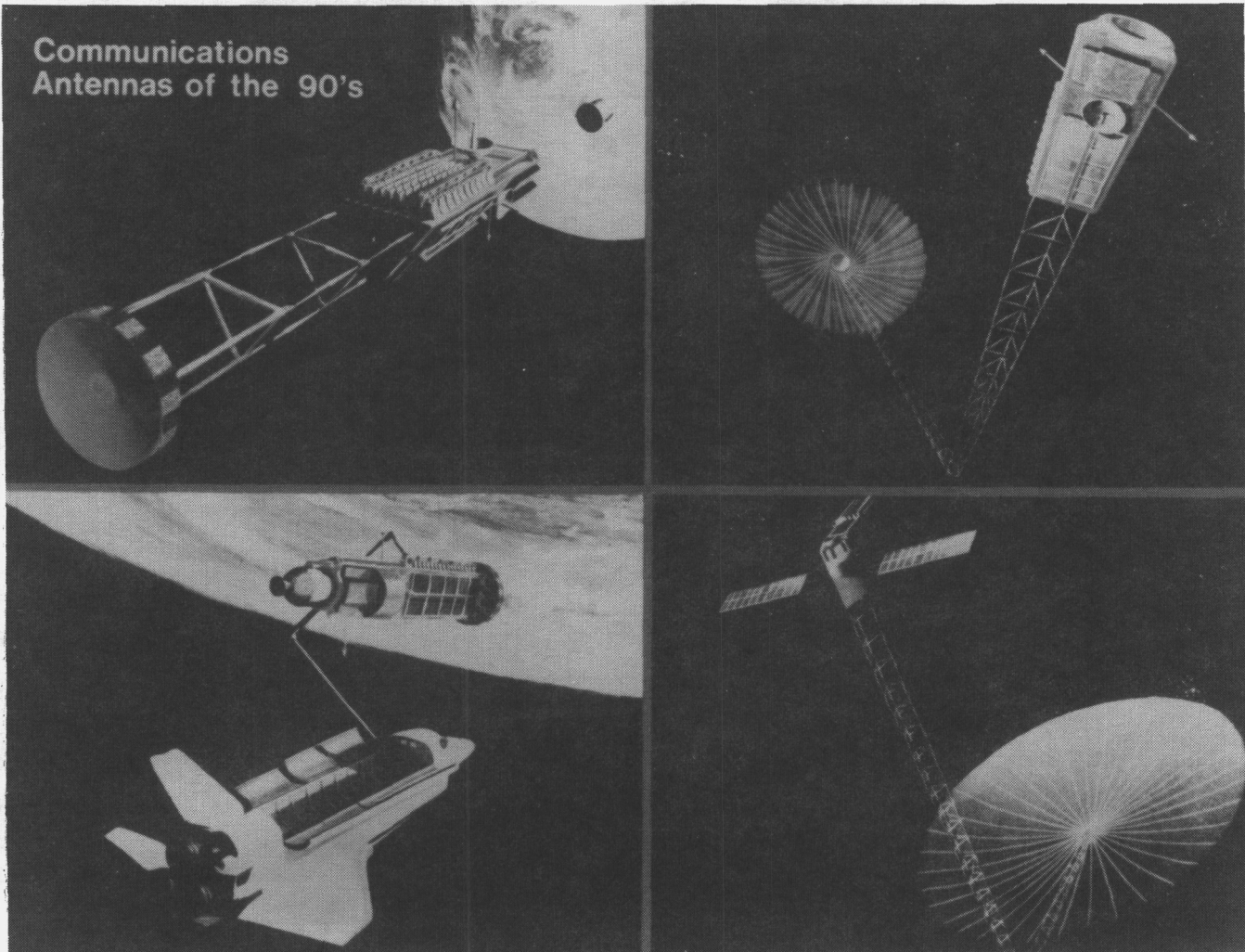
The QUASAT mission concept involves a free-flying, Earth orbital, large radio telescope, designed to observe astronomical radio sources simultaneously with ground telescopes. By using VLBI (Very Long Baseline Interferometry) data processing, a synthesized aperture larger than the diameter of the Earth can be achieved by the concept. This mission is based on a large deployable antenna, 15-20 meters in diameter, for operation at L-band, C-band, and K-band, the latter being of primary interest.

A mobile satellite system is a satellite-based communications network that provides voice and data communications to mobile users throughout a vast geographical area. Such a system is composed of a large number of users with small-size, low-gain UHF transmitters and a few large aperture, high-gain, multiple-beam antenna systems in parking orbit. The space antenna size is a function of the service desired and could range from 10 to 50 meters in diameter.



## OFFSET WRAP-RIB ANTENNA DEVELOPMENT PROGRAM

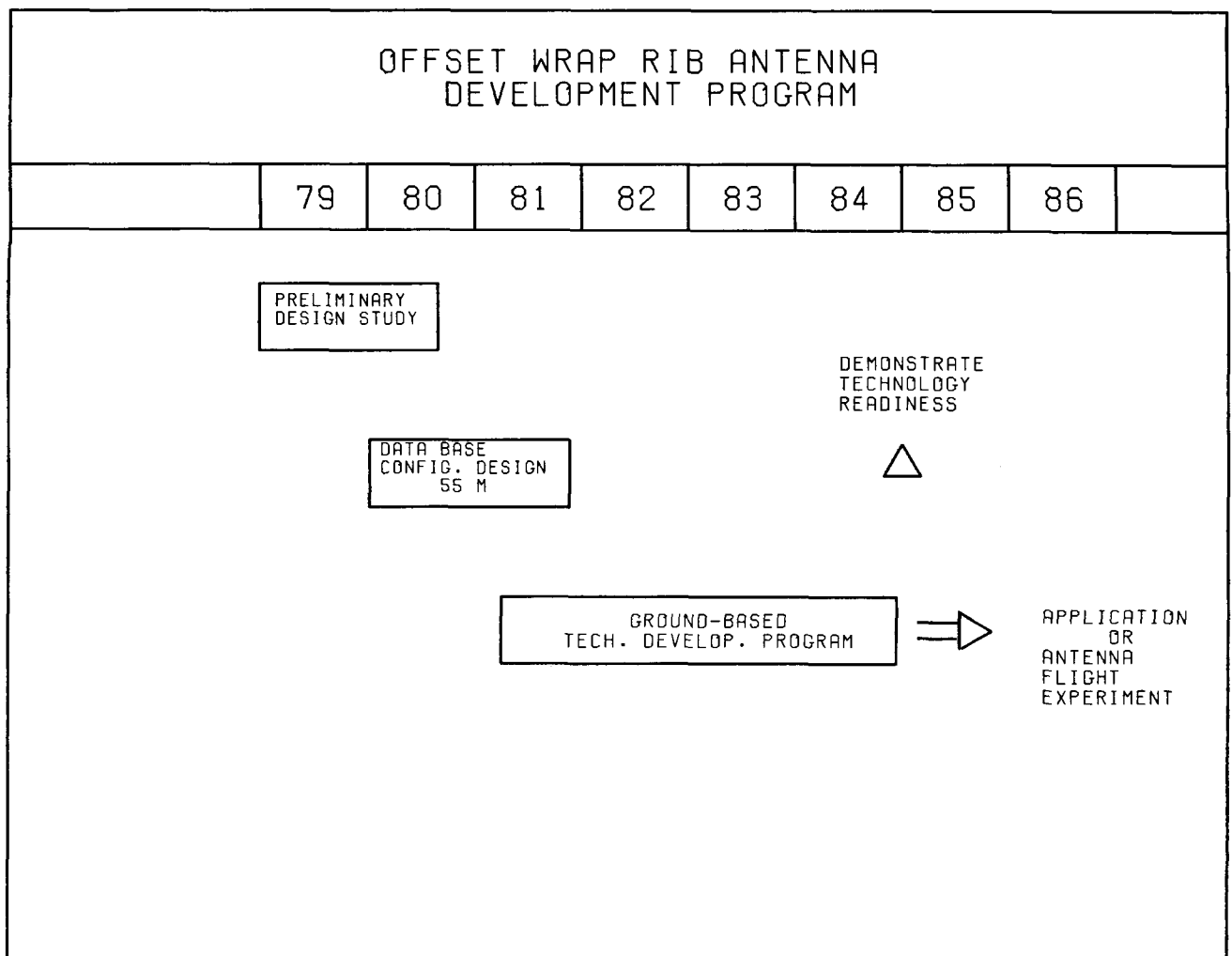
The antenna development program of the offset wrap-rib antenna concept, developed by Lockheed Missiles and Space Company and sponsored by NASA, is based on a ground test program of "proof-of-concept" hardware with analytical estimates of potential on-orbit performance conducted by Lockheed and Jet Propulsion Laboratories. The system concept is presented below and depicts a 100-m-diameter communications antenna.



## DEVELOPMENT PROGRAM

The elements of the development program (shown below) are the preliminary design study, data base configuration design, and ground-based technology development.

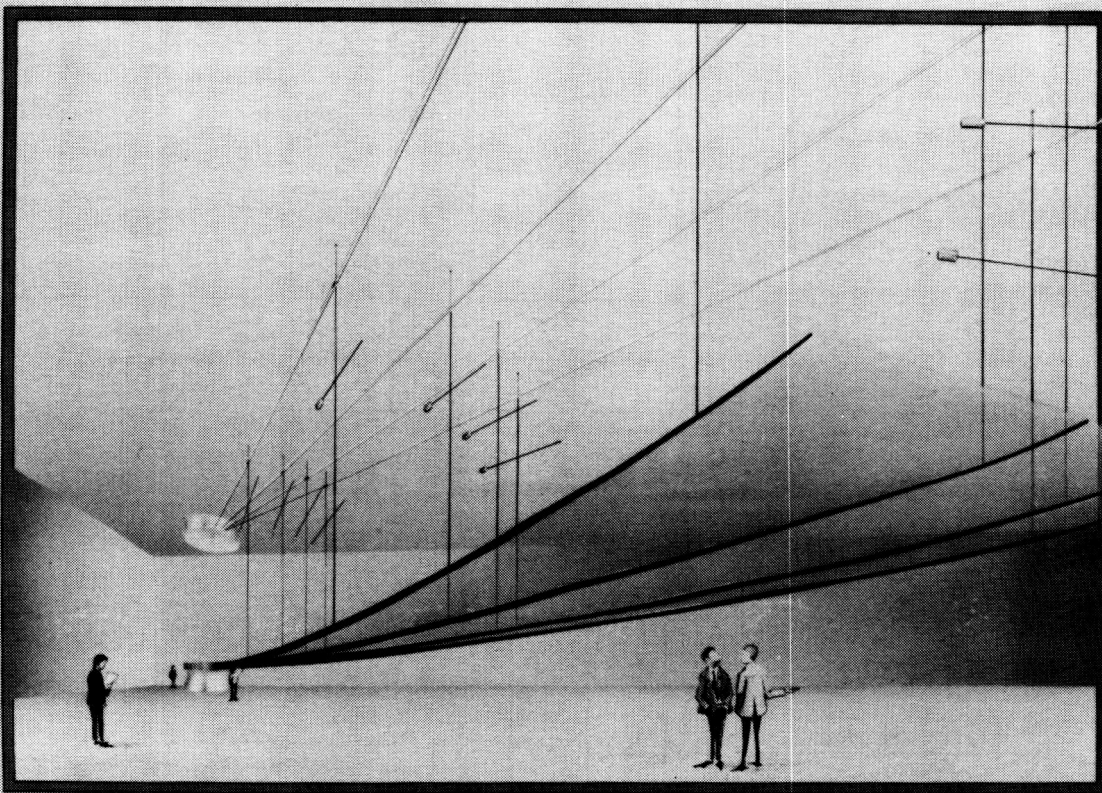
The preliminary design study characterized offset and symmetric reflectors for missions in the 100-m to 150-m-diameter range, identified critical technologies, ROM cost and schedules for development, and developed a technology plan for a low-cost, low-risk "proof-of-concept" demonstration.



## GROUND-BASED TEST PROGRAM

The data base configuration established a 55-m-diameter offset wrap-rib reflector design that could be used to design and demonstrate component manufacturing and assembly processes that are scalable to a 100-m to 150-m size and testable in a 1-G environment.

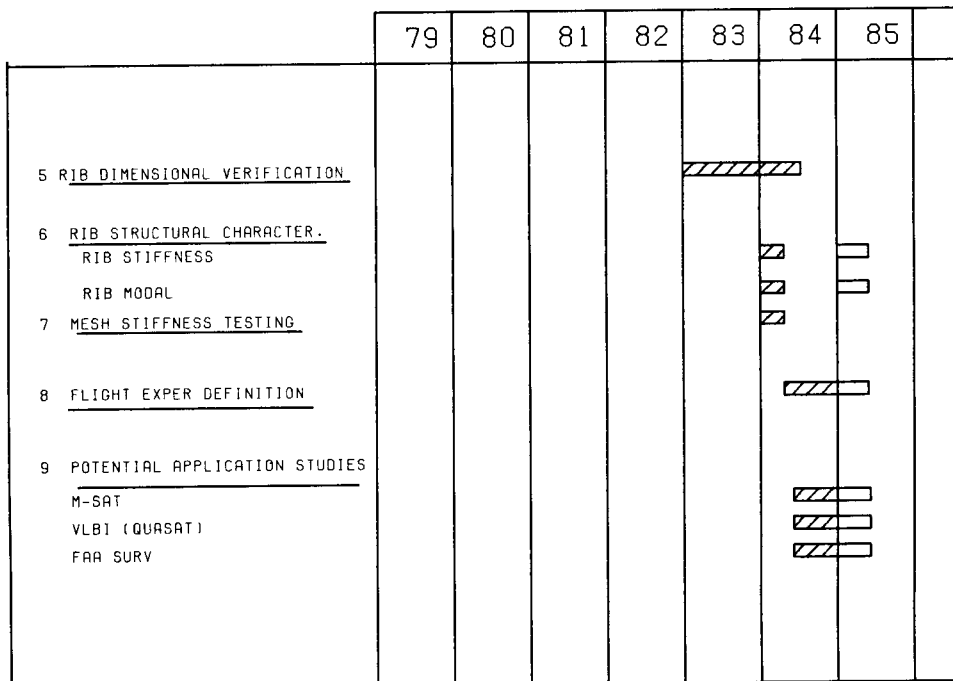
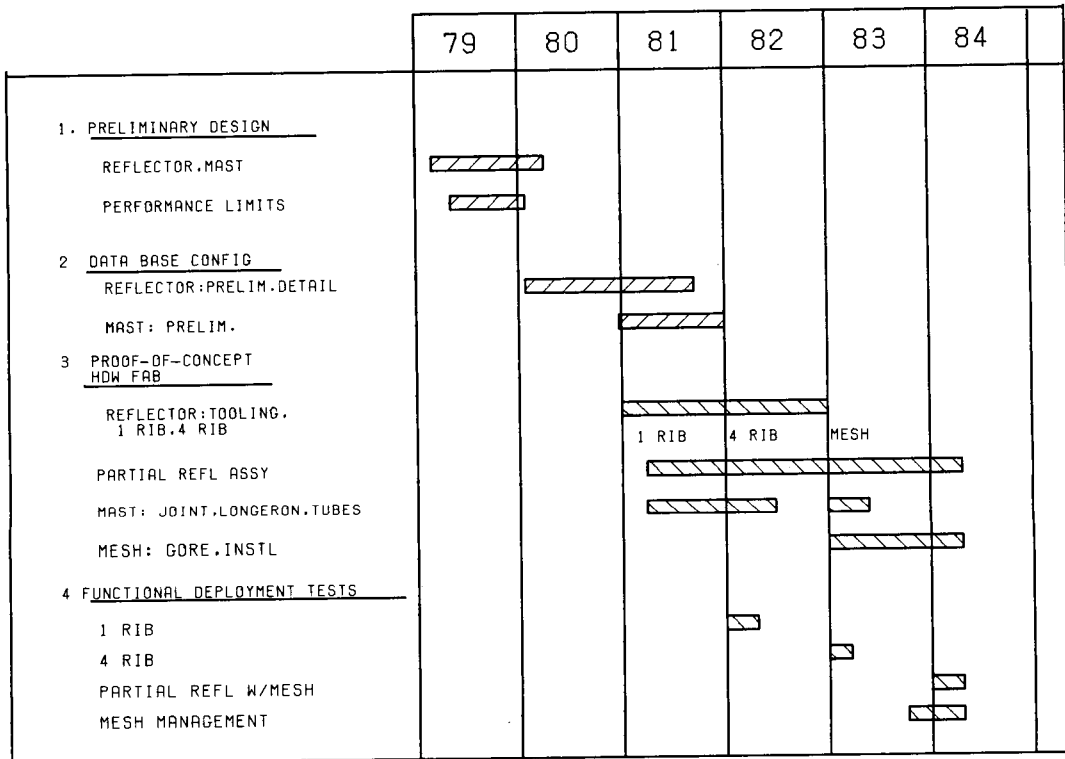
The ground-based technology program addressed the technology development required in design, manufacture, assembly and testing of the full-sized "proof-of-concept" hardware. Component ground testing provided design algorithm and analytical performance model updating. The partial reflector "proof-of-concept" hardware provided the test bed for 1-G deployment testing (shown below) and the final technology readiness demonstration for this concept.



Ground Test of 55-Meter Reflector

## PROGRAM TASKS

The specific program tasks are described in these two figures and present the full program activity to date.



## PROGRESS AGAINST OBJECTIVES

Significant progress was made in 1983 and 1984 in the area of component ground testing for analytical model updating. Paramount was the completion and deployment testing of the 55-meter partial reflector "proof-of-concept" hardware to demonstrate technology readiness. This figure presents an overview of completed tasks.

### 1983 - 1984 PROGRESS

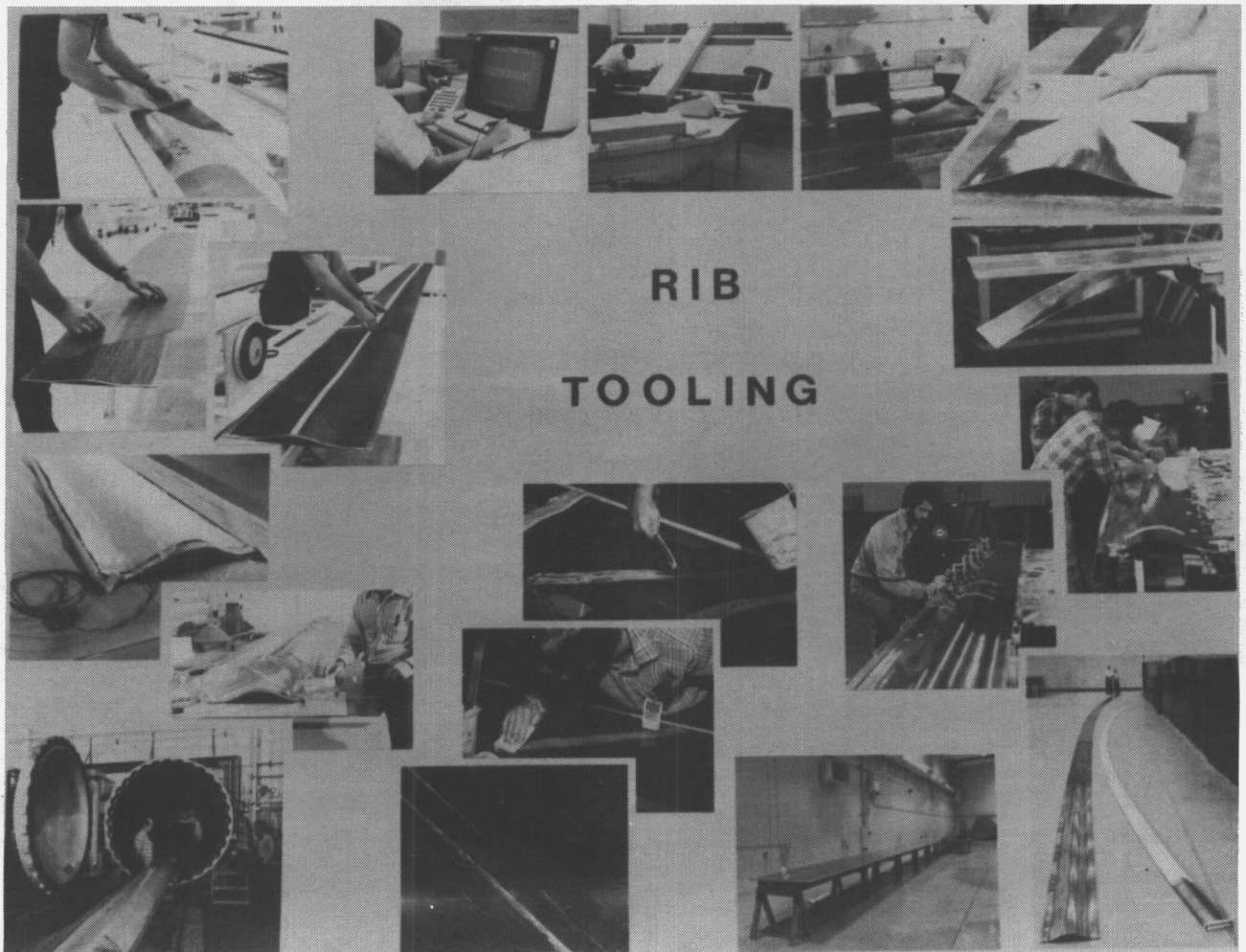
#### (TASKS COMPLETED)

- RIB DIMENSIONAL VERIFICATION
- RIB STRUCTURAL CHARACTERIZATION
- MESH STIFFNESS TESTING
- MESH GORE FABRICATION AND INSTALLATION
- MESH MANAGEMENT STUDIES
- PARTIAL REFLECTOR DEPLOYMENT TESTING
- FLIGHT EXPERIMENT DEFINITION STUDY
- POTENTIAL APPLICATION STUDIES



## RIB TOOLING

The engineering tool definition was accomplished using CADAM (Computer Graphics Augmented Design and Manufacturing System). The computer-generated numerical control tape drove the gerber flatbed plotter to scribe the flat pattern part for the tool contour templates to be used in bump forming and bump forming guidelines. The scribed Invar flat pattern sheets were bump formed in a hydraulic brake using steel dies against a hard rubber reactor. The three-dimensional variation of tool layup surface was maintained using the bump-forming guidelines for reflector curvature and the cross-sectional rib contour templates at intervals along the length of the tool. The finished formed Invar layup surface was placed in position over an Invar tool base and welded. To manufacture the rib segments, epoxy-impregnated graphite was placed on the layup tool in three layers (45/0/45). The completed graphite/epoxy layups were vacuum bagged and cured under temperature and pressured in an autoclave. The cured rib segments were in twenty-foot sections. The root end rib segment included a titanium rib hinge stiffener which was co-cured with the graphite/epoxy rib. The five rib segments were then placed end to end, aligned, marked, trimmed, butt jointed, spliced with strap and adhesive, vacuum bagged, and the adhesive allowed to cure. This completes a semi-lenticular rib half shown below.





## DEPLOYMENT MECHANISM AND RIB DEVELOPMENT

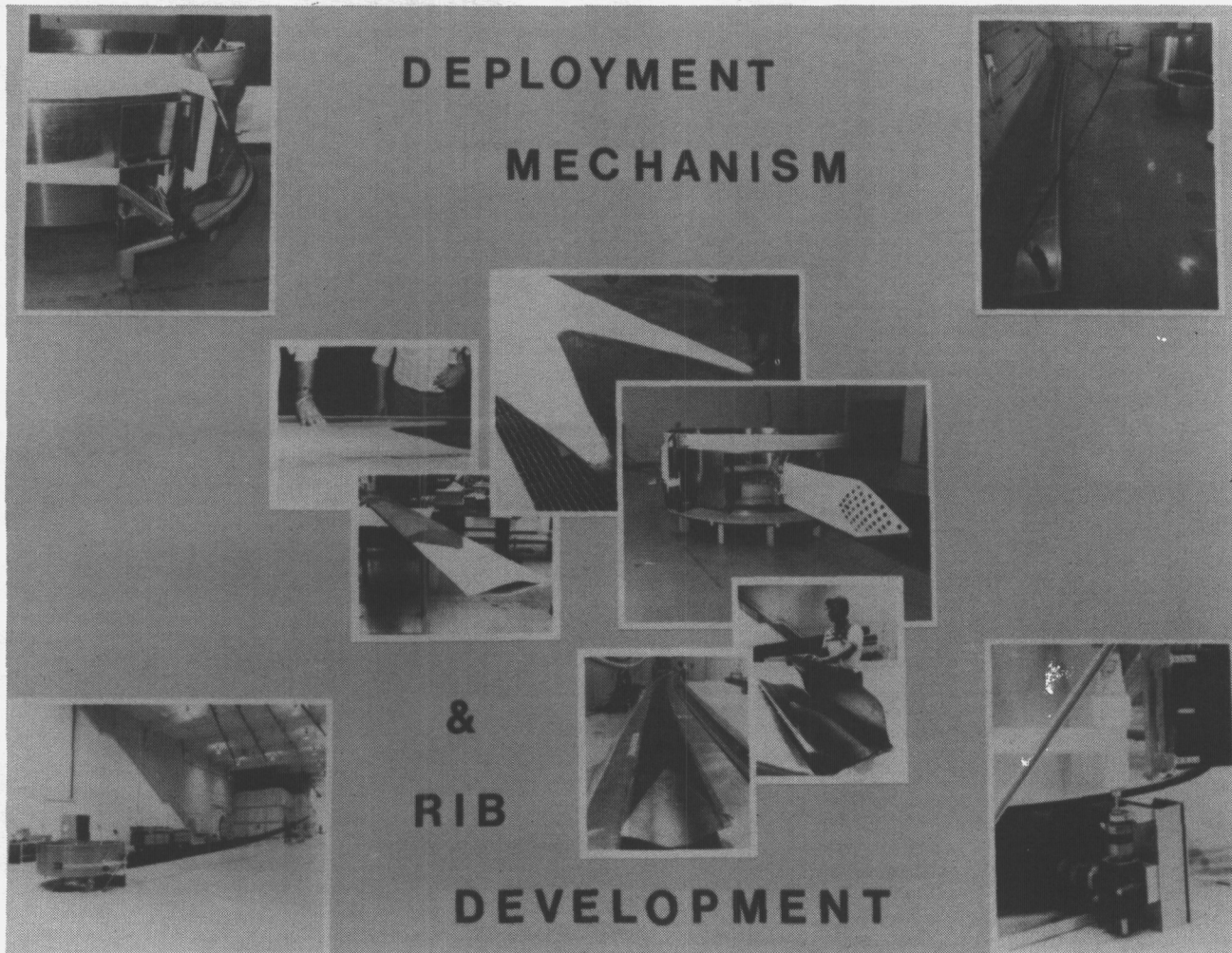
Several concepts for the rib root segment/hub interface were evaluated. The design requirements for the interface were to:

- Provide for flattening of rib for stowage
- Provide for 90° rotation of rib for stowage and deployment
- Provide for maximum deployed stiffness transfer from the rib to the hub

The design developed was a titanium root stiffener, co-cured with the graphite/epoxy rib and the rib hinge bonded and riveted to the stiffener.

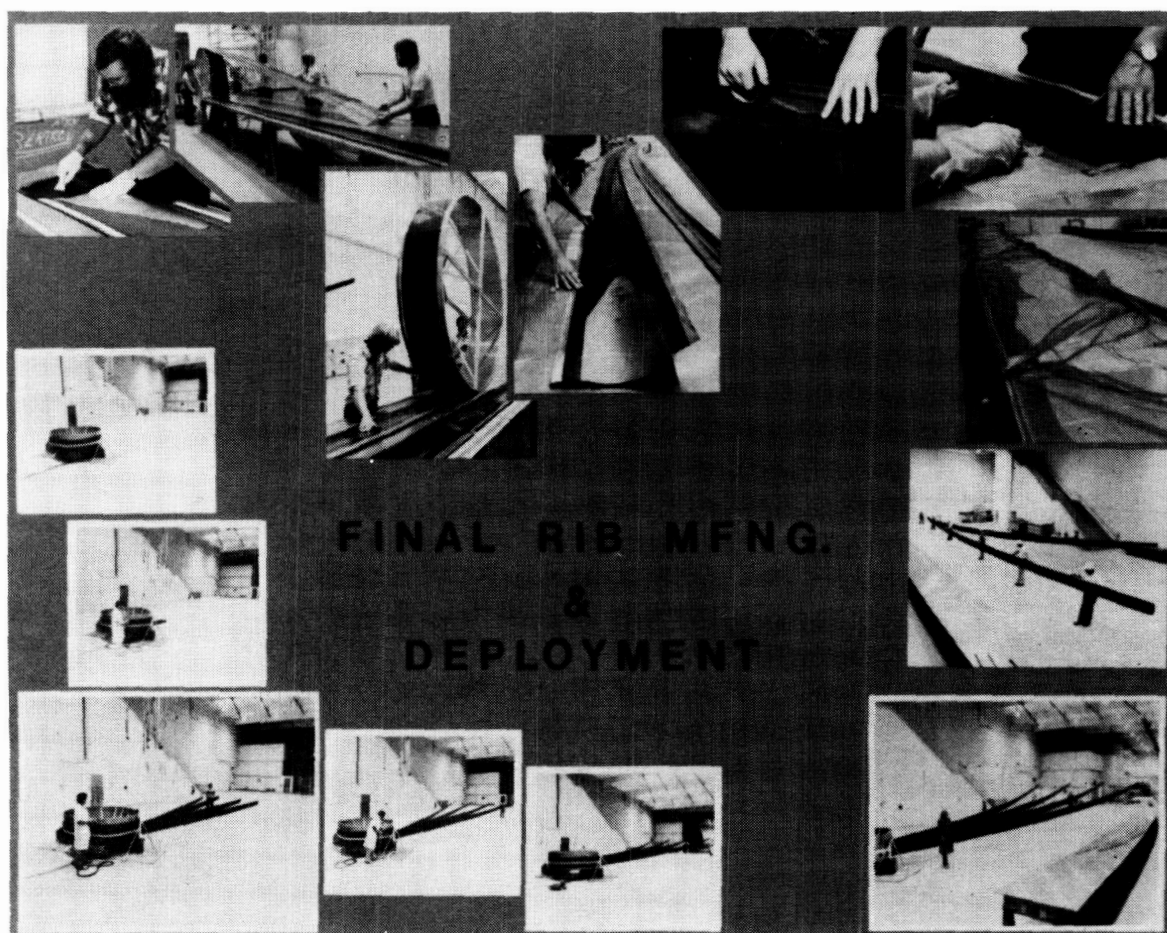
The initial deployment control mechanism was a tape "re-wrap" concept operated successfully except the tape tension could not be controlled adequately. The developed design concept employed a tape spool deployment mechanism utilizing an electromagnetic clutch/brake with a variable speed motor.

A single-rib system was then integrated with a simulated reflector hub and special test equipment (STE) and on November 6, 1981 the system was successfully cycled through the deployment and stowing operations shown below.



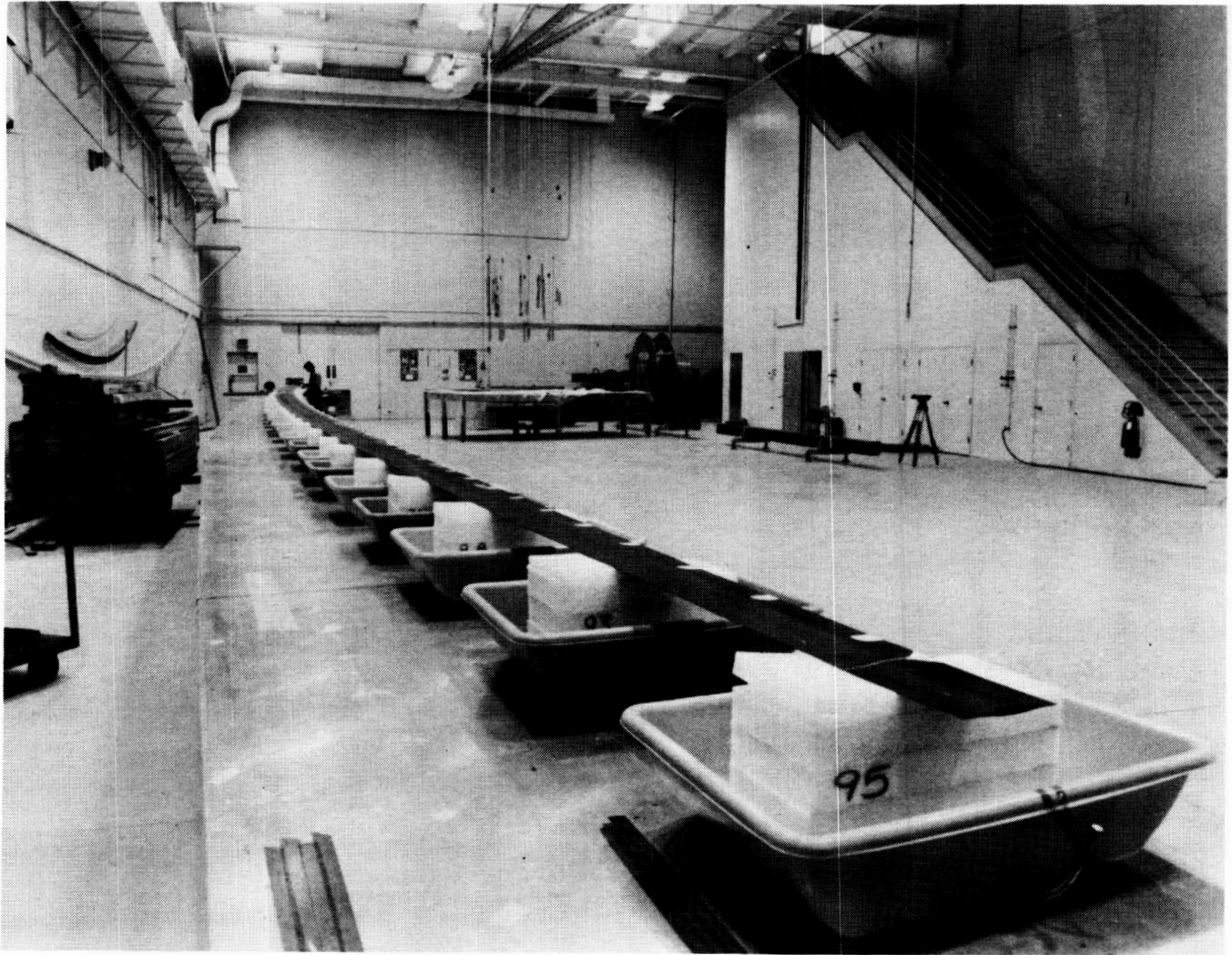
## FINAL RIB MANUFACTURING AND DEPLOYMENT

Semi-lenticular rib halves are bonded together along the upper and lower longitudinal edges to generate a full lenticular cross section. Since each rib half was spliced with the inside face down on the work table, one rib half was coiled onto a large diameter spool and unrolled in the required orientation adjacent to the other rib for lenticular bonding. The two rib half sections were aligned, bonded along the longitudinal edges, vacuum bagged and allowed to cure at room temperature. The rib was trimmed to the final configuration. On November 4, 1982, a four-rib partial reflector was successfully cycled through deployment and stowing cycles shown in this figure.



## RIB MEASUREMENT

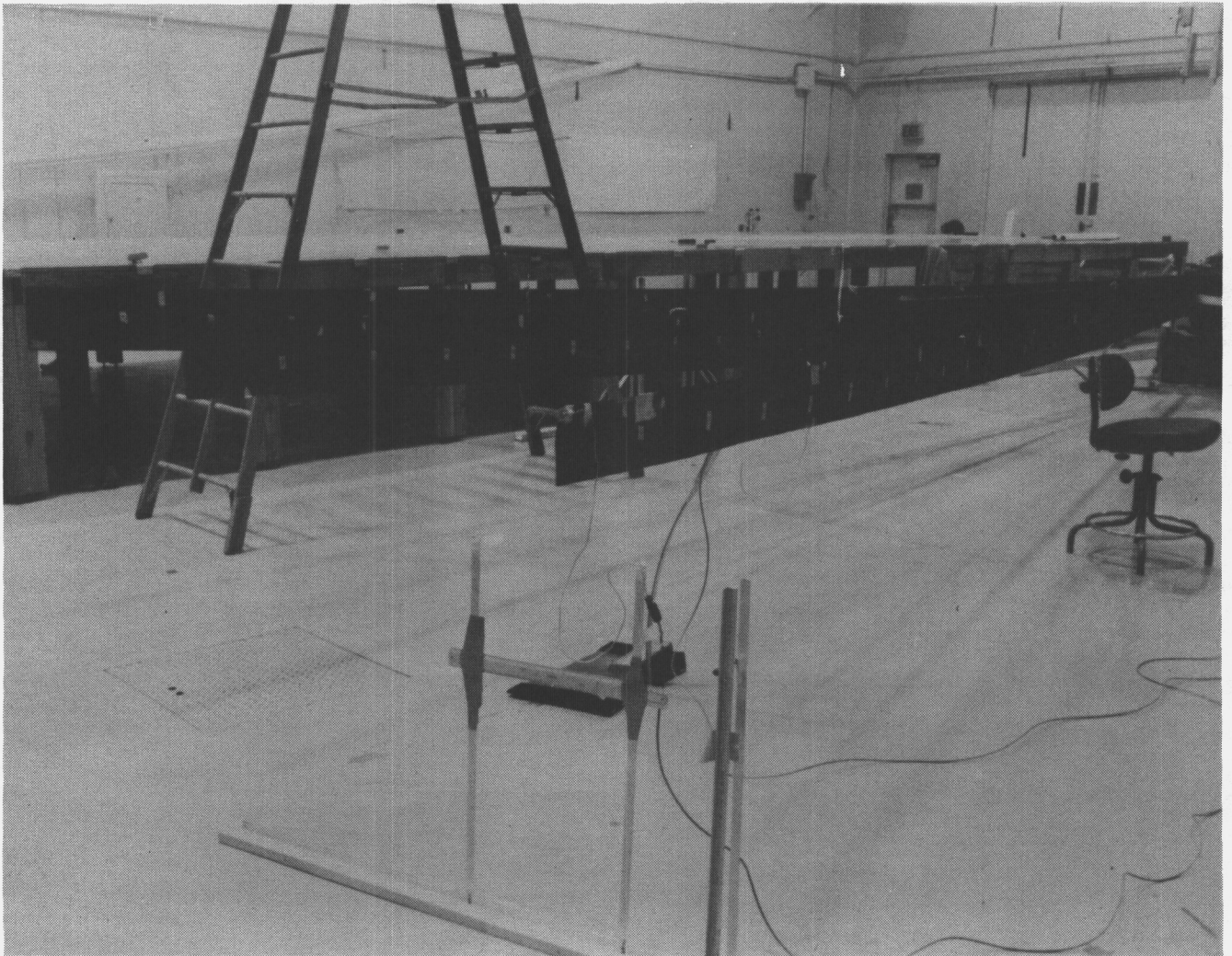
The concave contour edge of the rib assembly was measured in a simulated free state by a flotation system to verify the rib contour manufacturing to design requirement tolerances. The contour was measured by a triangulation method using two theodolites and targeted on a series of hairline marks scribed on the concave rib edge, as shown below.





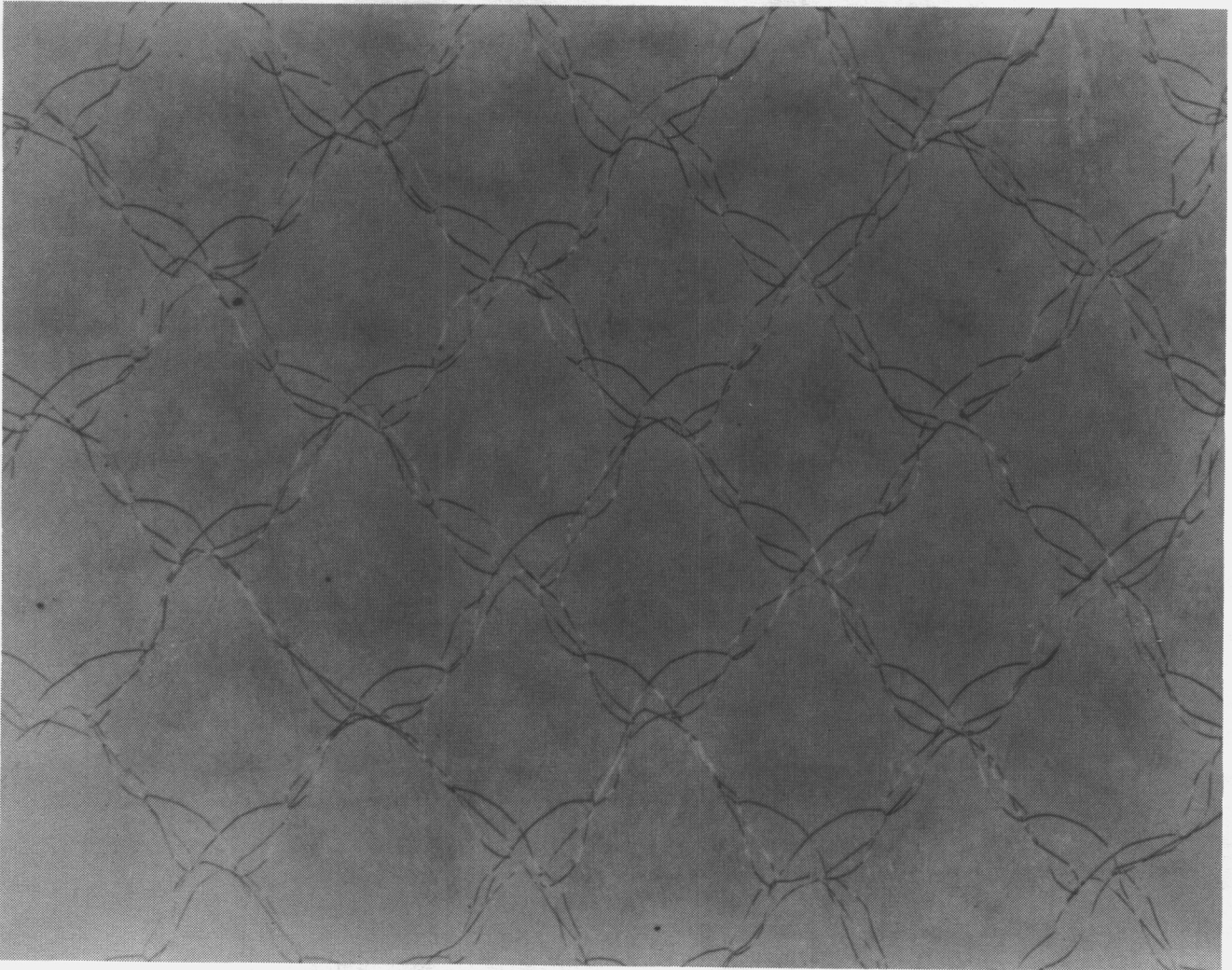
## RIB STRUCTURAL CHARACTERIZATION

Static deflection and modal tests were performed to obtain structural and dynamic data of the ribs at various stages of deployment. The test series was comprised of twelve test configurations, eight modal and four static deflection. The data will be used to upgrade structural analytical models for rib characterization (shown in this figure).



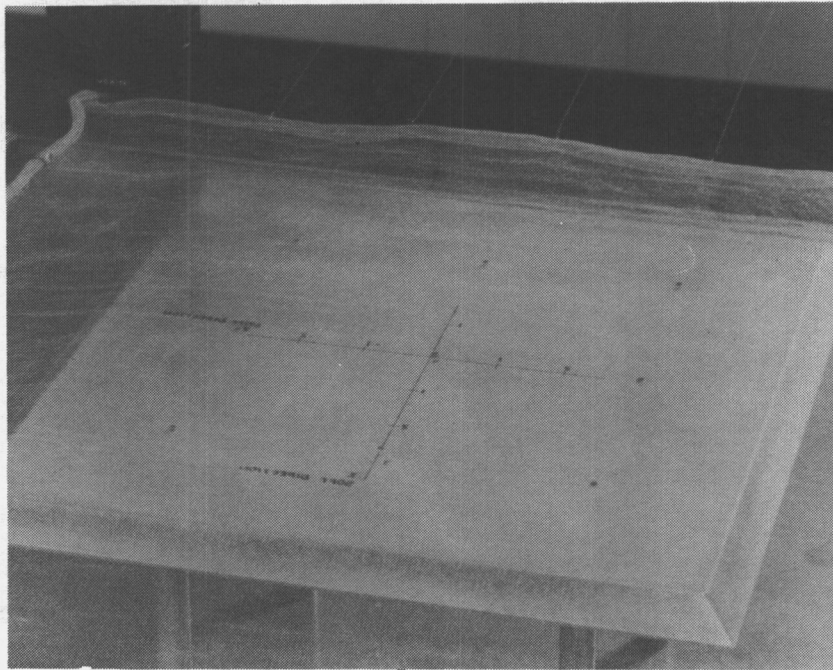
### MESH PANEL

The material, type, and cell size for the mesh panel are: (1) material: molybdenum wire (0.0012 dia), gold plated, (2) type: knit, diamond tricot, and (3) cell size: 4 cells/inch (3 GHz), see figure below.



## MESH STRUCTURAL CHARACTERIZATION

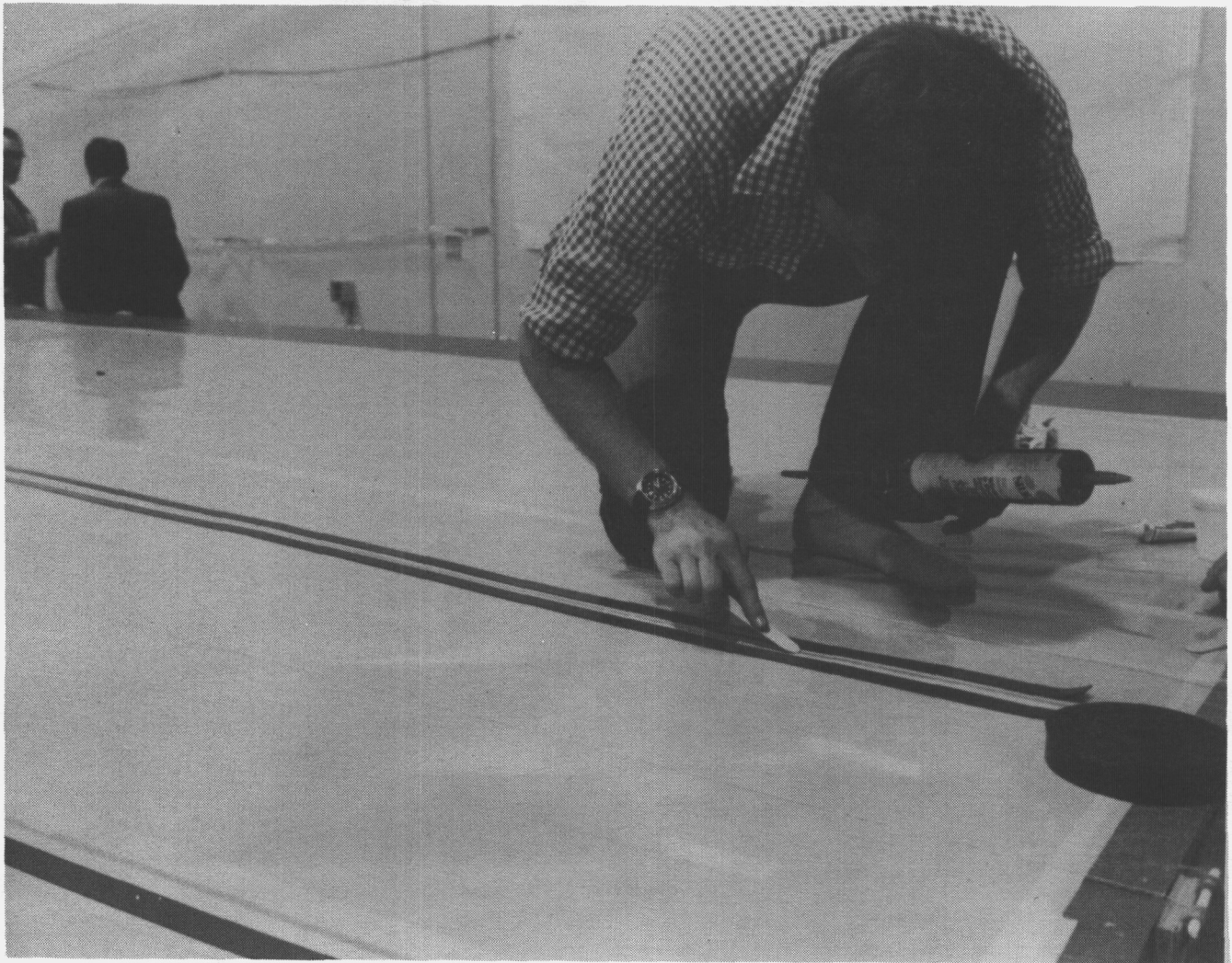
The mesh is tested to determine structural characteristics and effects due to various preloads. The biaxial stiffness test is accomplished on a special test fixture. The preloads are applied to the mesh and the strain response is measured via a camera located directly above the mesh. Through an accurate digital encoder the results are entered via keyboard to a computer for processing and storage (as shown in these figures).



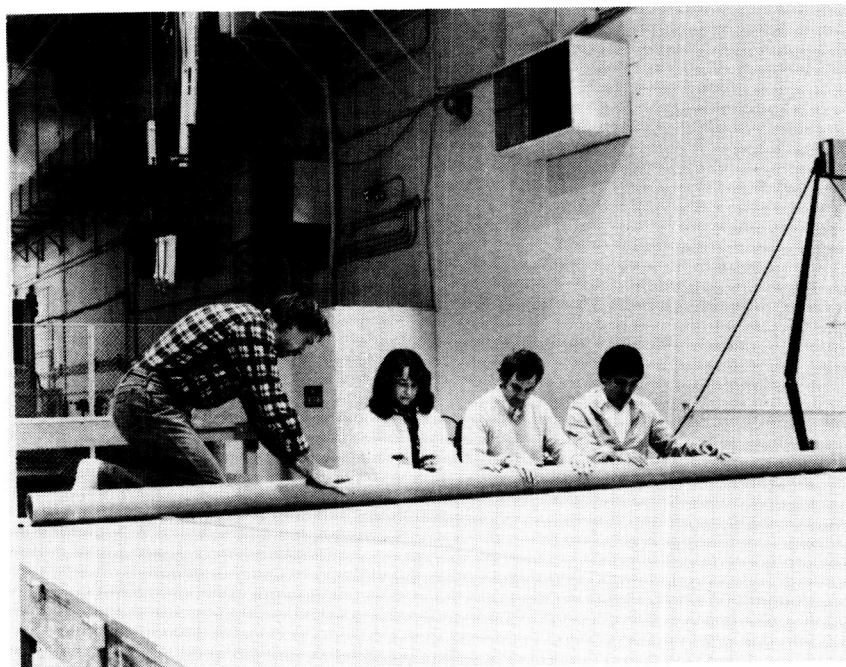
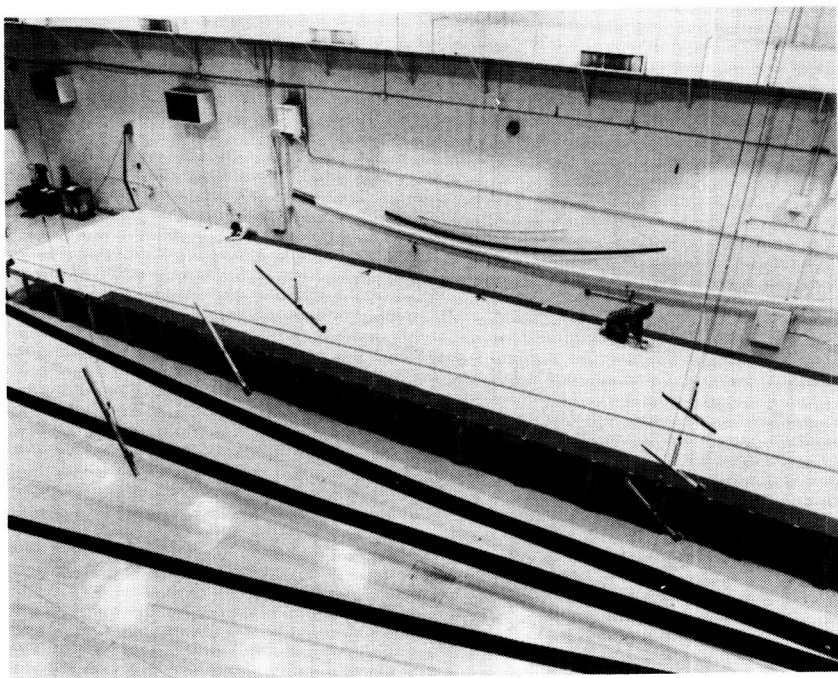


### MESH GORE FABRICATION

The mesh was unrolled onto a mylar flat pattern on a 16- x 92-ft table. The mesh was preloaded at the ends with weights and secured with magnetic tape. The Kevlar end condition was attached to the mesh with adhesive and cured at room temperature. The mesh gore was trimmed to the final size and rolled onto a tube ready for final installation (see the figure below and the next two figures).



## MESH GORE FABRICATION (CONTINUED)





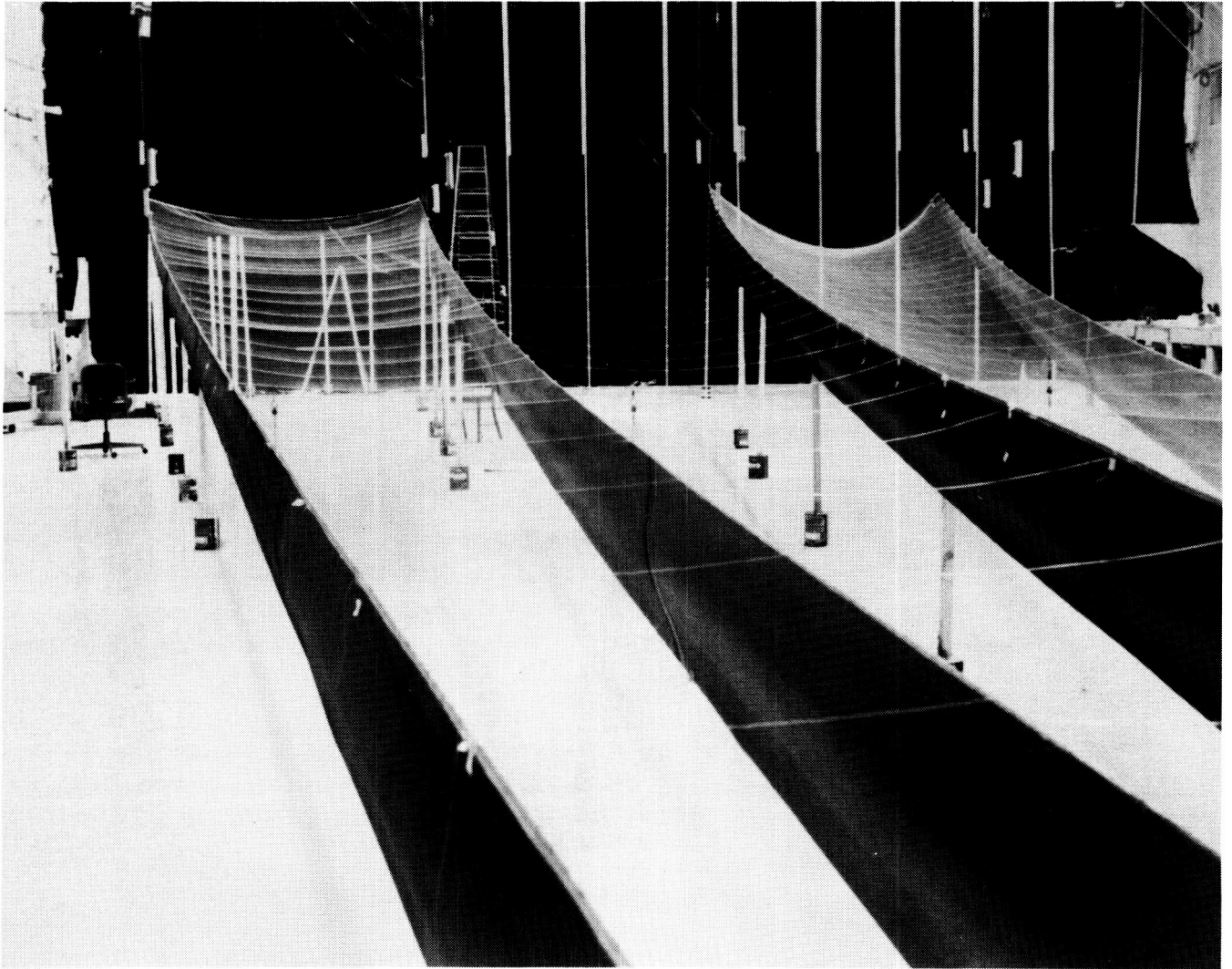
## INITIAL GORE POSITIONING

The mesh gore assembly was positioned for a preliminary check onto the rib assemblies. The rib assemblies were supported using a vertical support stand.



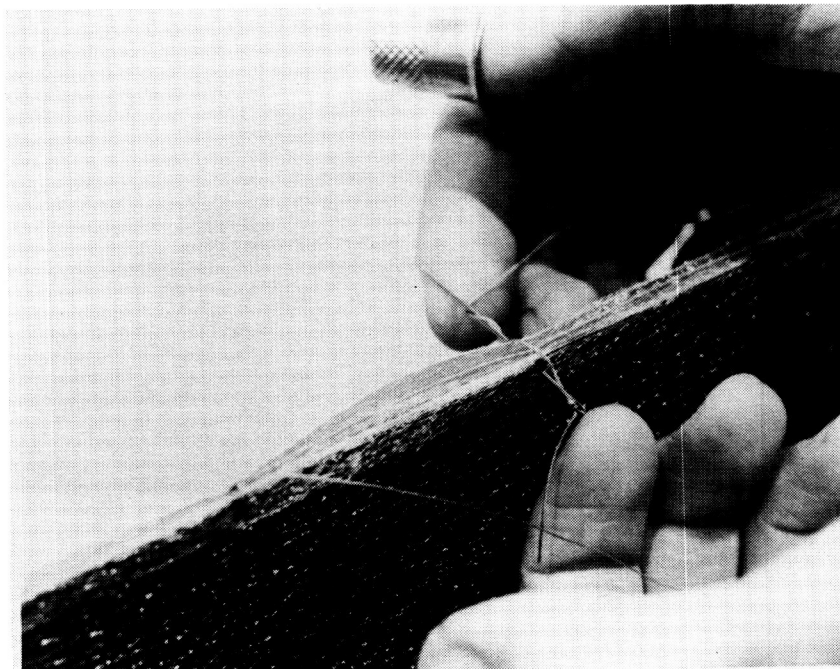
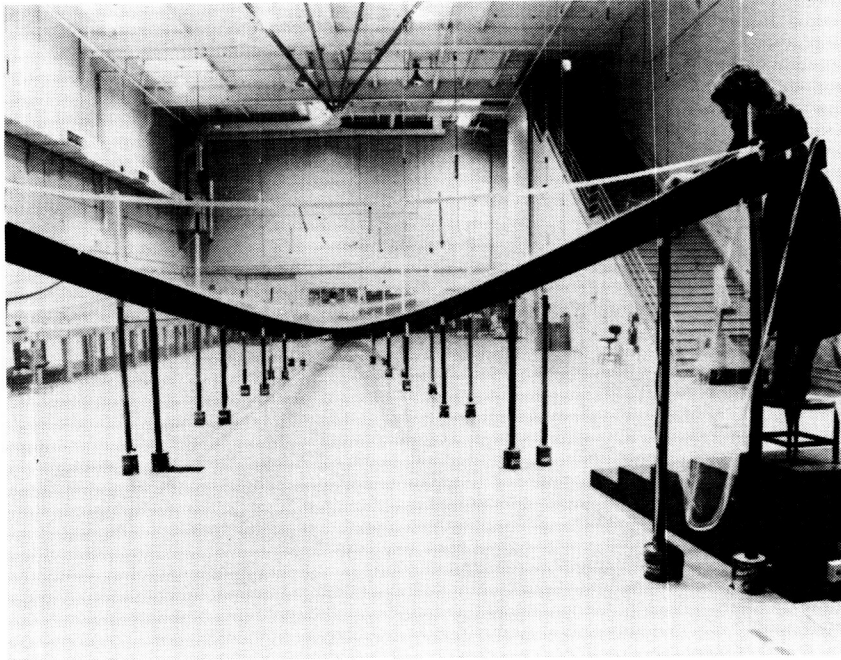
## MANUFACTURING SUPPORT LINES

Manufacturing aids were installed between the rib assemblies to support the mesh gore during final installation.



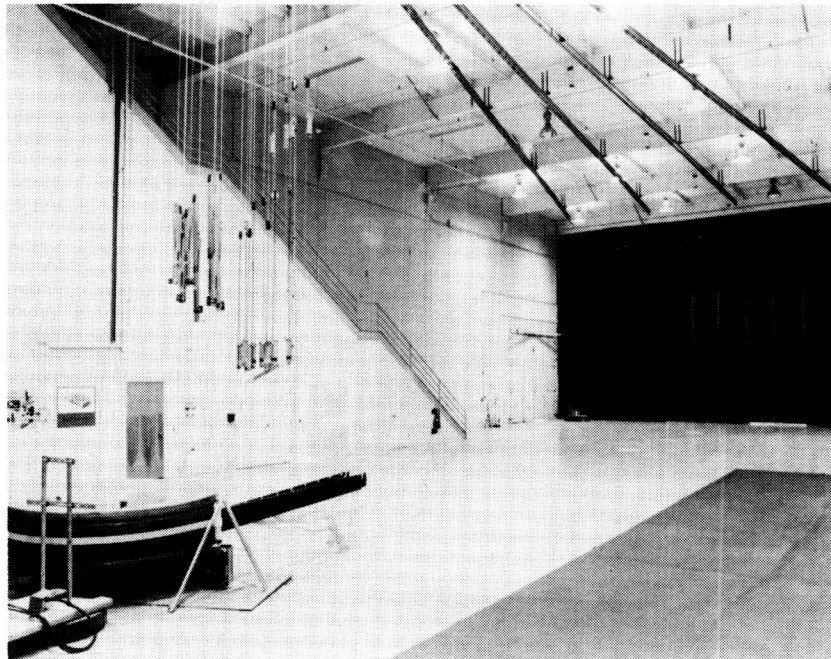
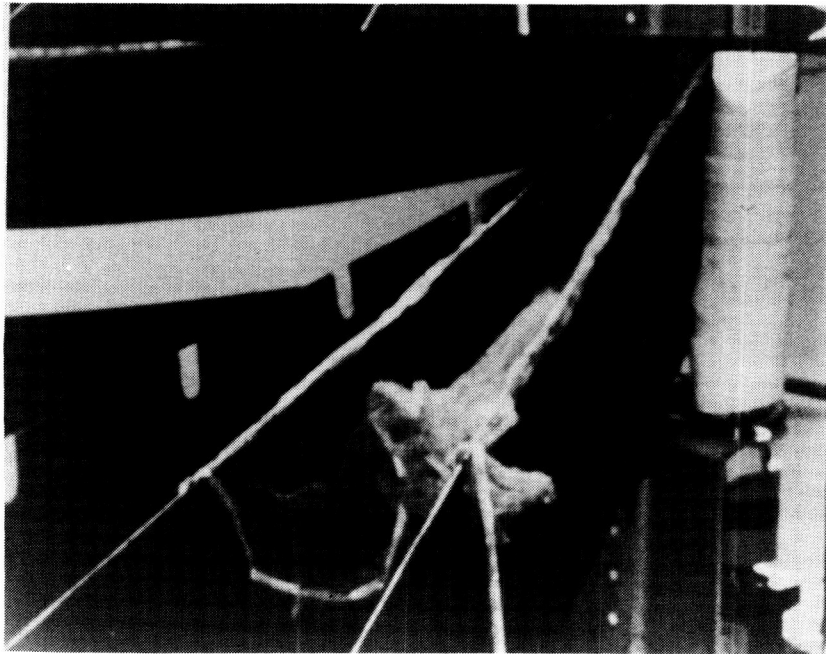
## MESH GORE ATTACHMENT

The ribs were aligned and positioned in the final configuration. The mesh gore was attached to the ribs with stitches through holes previously drilled along the top edges of the ribs. Each stitch was locked in place with a modified clinch knot.



## PRELIMINARY MESH MANAGEMENT STUDIES

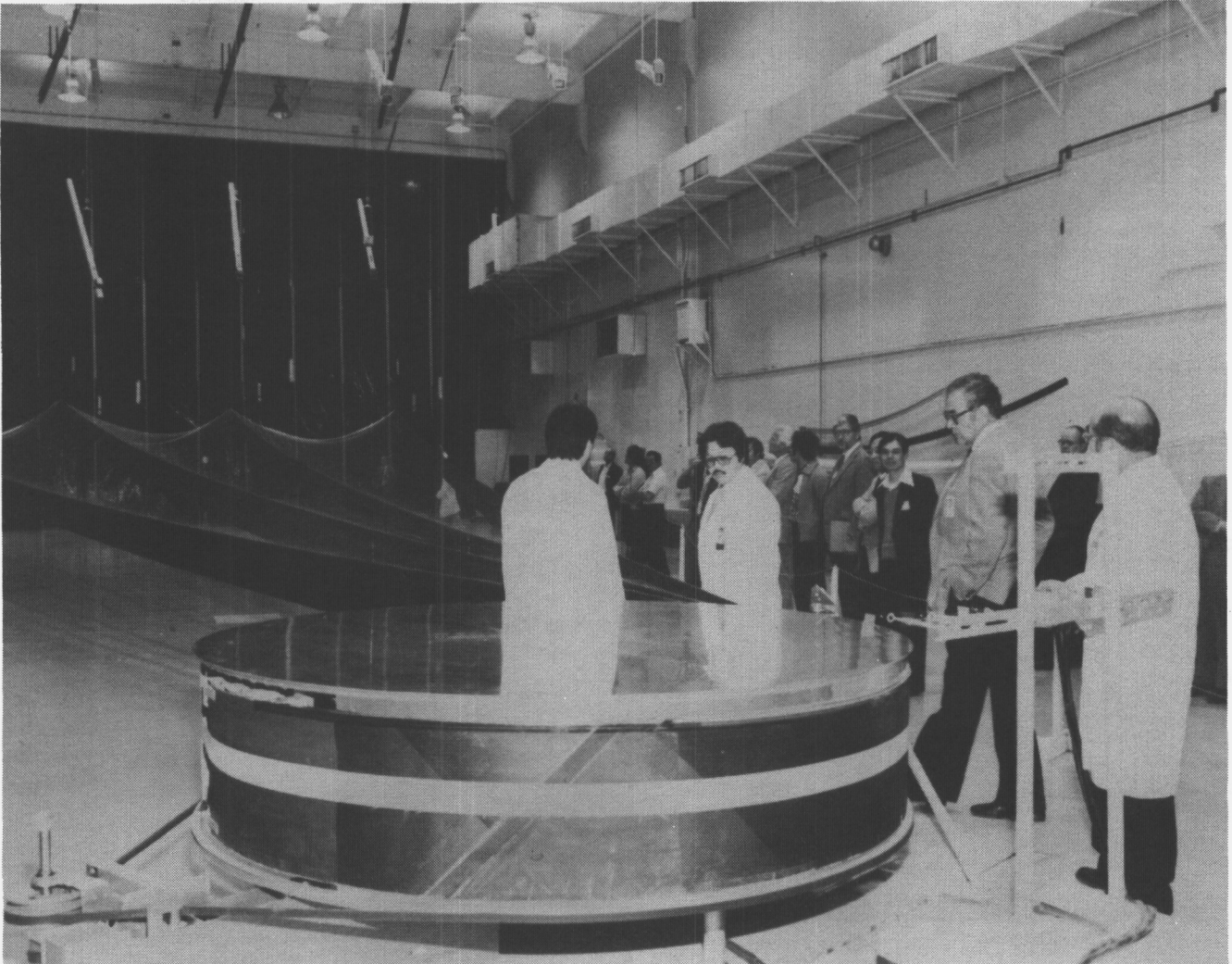
Initial studies were conducted with two "used" mesh gores installed on the partial reflector. The mesh gores were stowed in several different ways, including some worst-on-worst configurations. All deployments were successful with no mesh tearing or impairment of rib deployment. For the final deployment with "new" mesh gores, the pleat-type fold (accordian) configuration was selected and was stowed between the rib section during the stowage onto the hub assembly. Again all tests were successful with no mesh damage or impairment to deployment.



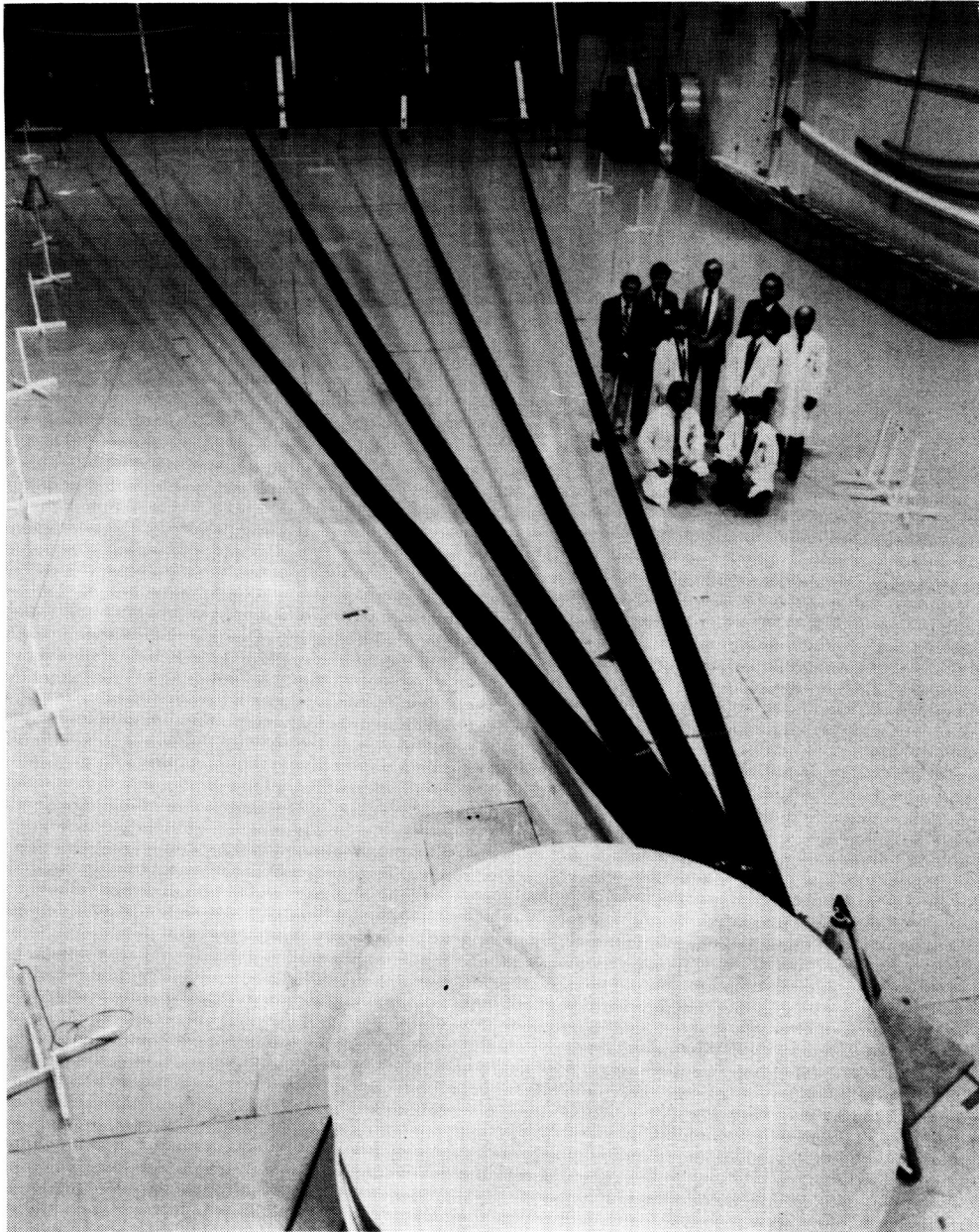


## COMPLETION OF DEPLOYMENT TESTS

The four-rib partial reflector proof-of-concept deployment was successfully demonstrated to JPL/NASA/Lockheed and the media on 30 March and 26 April 1984 (see figure below and on the next page).



COMPLETION OF DEPLOYMENT TASKS (CONTINUED)



DEVELOPMENT OF THE 15-METER HOOP/COLUMN ANTENNA SYSTEM

T. G. Campbell,  
D. H. Butler, and  
K. Belvin  
NASA Langley Research Center  
Hampton, Virginia

and

B. B. Allen  
Harris Corporation  
Melbourne, Florida

Large Space Antenna Systems Technology - 1984  
December 4-6, 1984

## INTRODUCTION

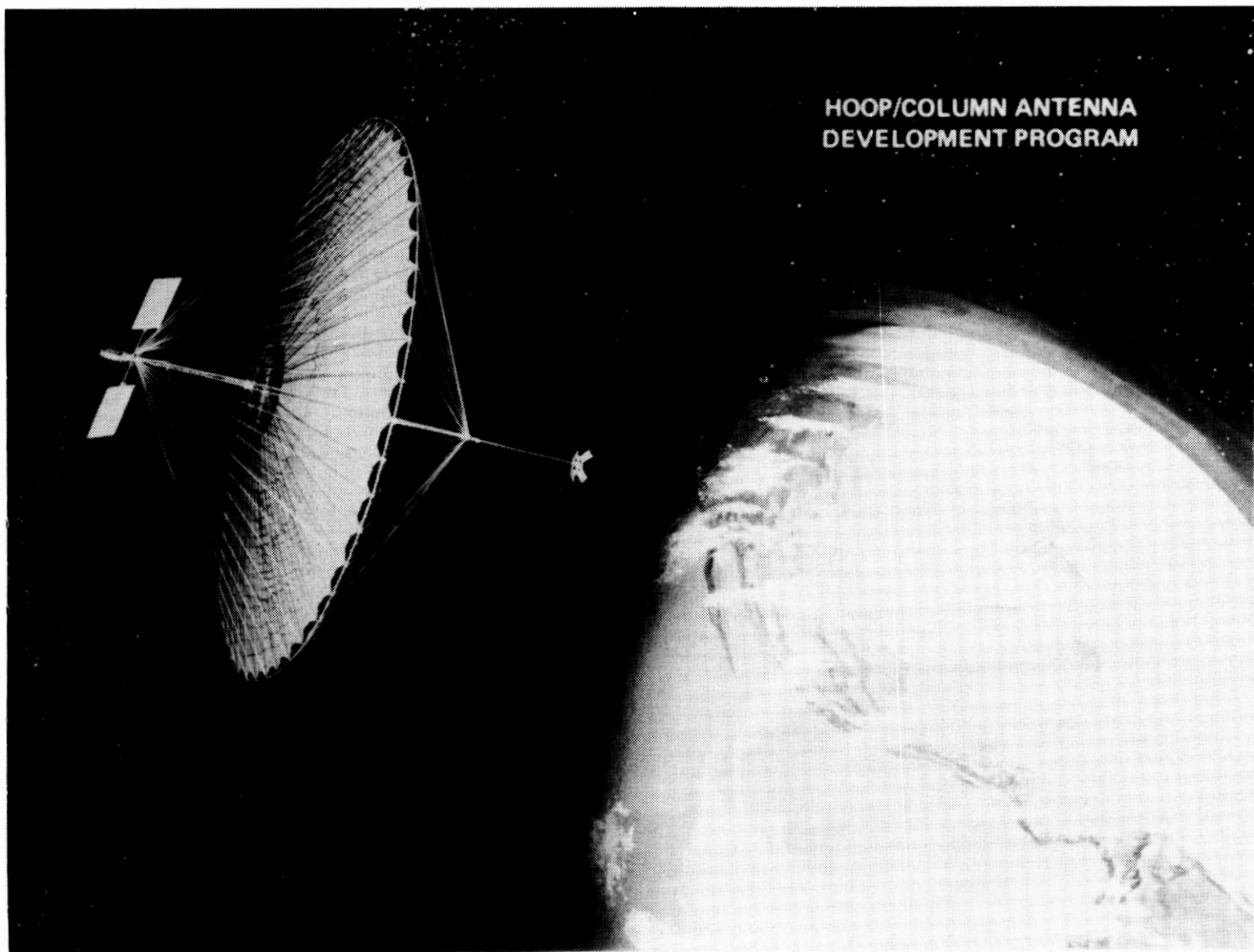
The development of the 15-meter hoop/column antenna system is presented. The 15-meter deployable structure is discussed along with the multiple-beam feed system development and the structures and RF testing planned in 1985. These topics are presented in accordance with the presentation agenda listed below.

- **OVERVIEW OF ANTENNA DEVELOPMENT ACTIVITIES**
- **DEVELOPMENT OF 15-METER REFLECTOR AND KINEMATIC DEPLOYMENT TESTS**
- **PRELIMINARY MODAL SURVEY TEST RESULTS AND FUTURE STRUCTURAL-DYNAMICS TESTS**
- **RADIO FREQUENCY SUBSYSTEMS AND NEAR-FIELD TESTING**
- **CONCLUDING REMARKS**



## HOOP/COLUMN ANTENNA CONFIGURATION

The hoop/column deployable antenna concept is shown here in an artist's rendering in a space application. This antenna concept is a symmetrical, cable-stiffened structure which is amenable to different reflector configurations: parabolic, spherical, and planar.



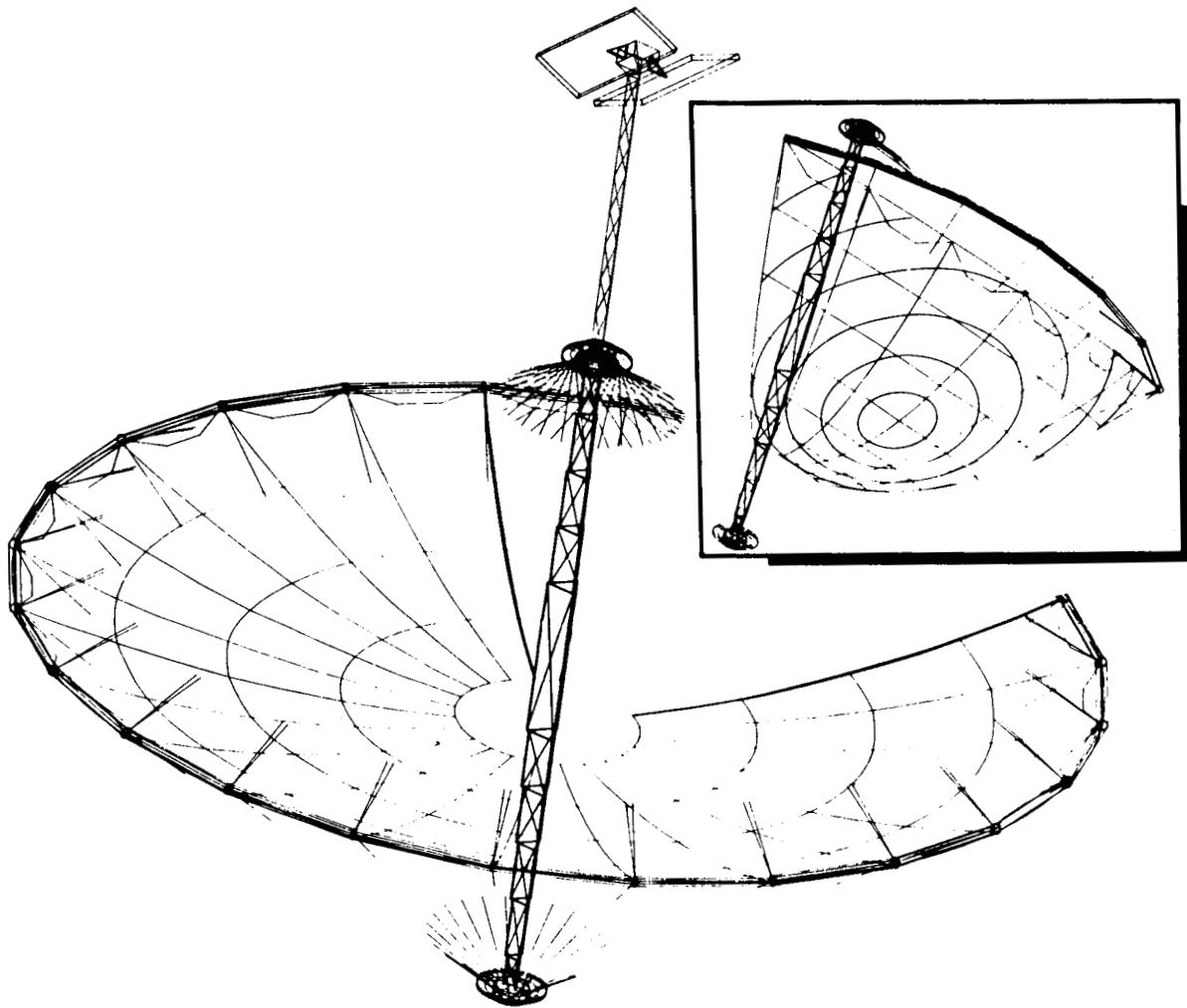
## TECHNOLOGY DEVELOPMENT OBJECTIVES

Since the beginning of the hoop/column technology development program in 1979, there have been numerous accomplishments ranging from structure development, mechanisms, and materials. A listing of the technology thrusts for the hoop/column large space antenna program is presented below.

- HOOP/COLUMN WILL BE THE FIRST TO DESIGN, ANALYSE, FABRICATE, AND VERIFY A 3 DIMENSIONAL, NON-LINEAR MESH REFLECTOR SURFACE.
- DEVELOPMENT OF A TRIANGULAR TRUSS, TELESCOPING COLUMN THAT IS SELF DEPLOYING (I.E., NO ROBOTICS REQUIRED)
- DEVELOPMENT OF COLUMN LATCHES THAT WILL SUBSTANTIALLY REDUCE (IF NOT ELIMINATE) NON-LINEAR JOINT BEHAVIOR RESULTING FROM CLEARANCES.
- THE 15 METER MODULE WILL VERIFY INTEGRATION OF 100M POINT DESIGN KINEMATIC CONCEPTS WITH THE DEMONSTRATED 50 METER SURFACE CONTOUR TECHNOLOGY.
- THE 15 METER MODULE CAN BE USED AS A LOW LEVEL VIBRATION TEST ARTICLE TO VERIFY STRUCTURAL/DYNAMIC CALCULATIONS ON A RELATIVELY LARGE PRETENSIONED STRUCTURE.
- MATERIALS DRIVEN IN CABLES AND CORD TAPE TECHNOLOGY.
- FINITE ELEMENT MODLE DEVELOPMENT AND UTILIZATION FOR STUDY OF LARGE TENSION/STABILIZED STRUCTURES.
- A TECHNOLOGY DRIVER FOR THE MULTIPLE BEAM FEED PROGRAM OF OAST.

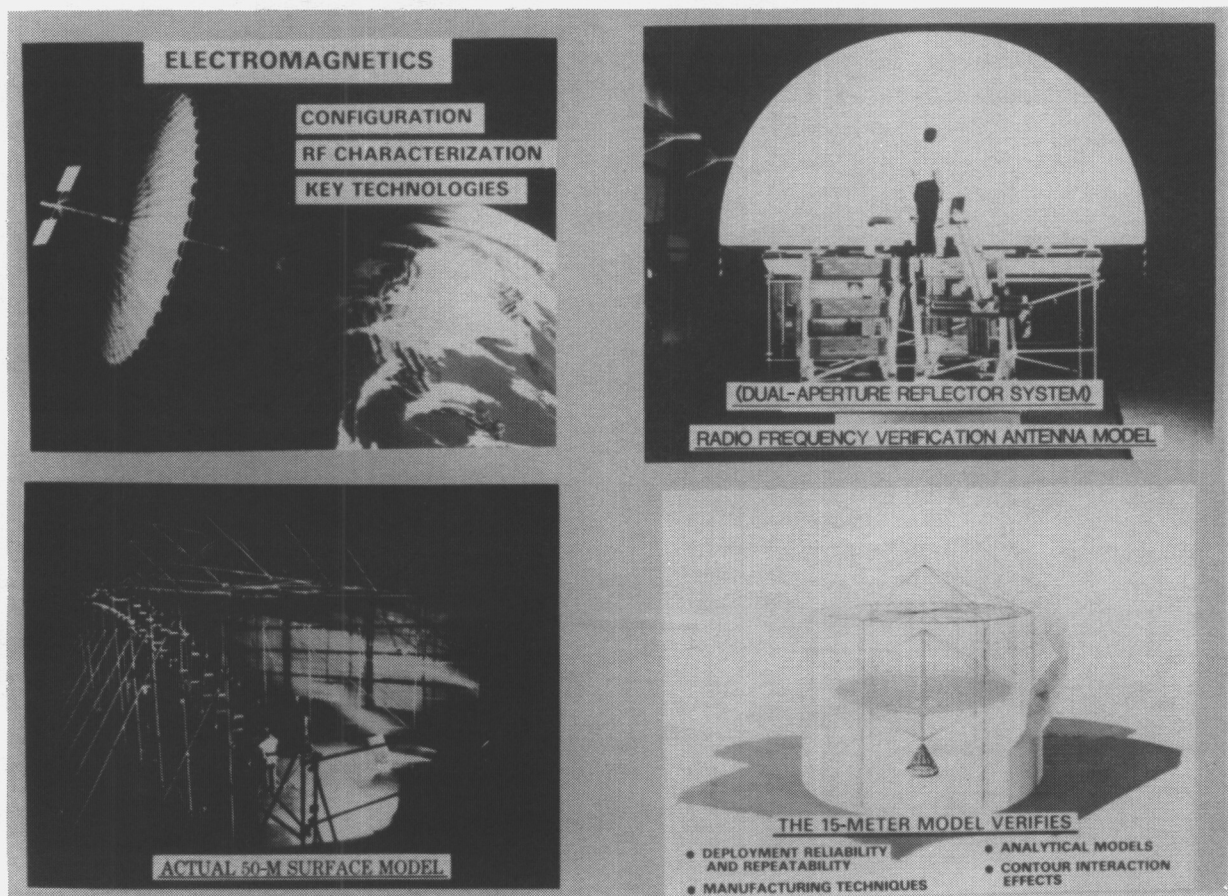
## MULTIPLE-APERTURE CONFIGURATION FOR MULTIPLE-BEAM ANTENNA SYSTEMS

A very important objective in the development of large space antenna technology is the capability for multiple-beam antenna systems. Since the hoop/column structure is symmetrical, the capability for providing an offset-fed reflector geometry is manifested through a multiple-aperture configuration contained by the hoop space frame. Shown in the figure below is the quad-aperture surface configuration for the 15-meter antenna. Each quad-aperture is an offset-fed parabolic reflector with each vertex offset from the centerline of the structure. The overall intent with this approach is to demonstrate the performance of offset mesh reflector systems for single-aperture and multiple-aperture applications.



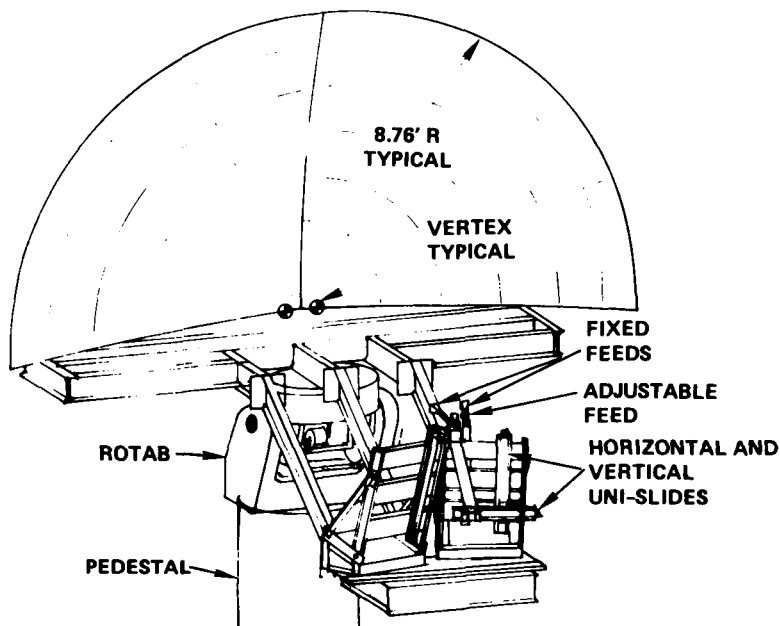
## ENGINEERING MODELS OF THE HOOP/COLUMN ANTENNA

Before the development of the 15-meter deployable antenna structure was initiated, large-scale engineering models were fabricated, tested, and evaluated. These models included hoop hinge models, telescoping mast models, and mesh management test models. The larger scale models are shown in the figure below: the radio frequency verification mode (RFV) and the static surface model of the 50-meter-diameter antenna. These models indicate stages of development leading to the final stage, the fabrication and test of a complete 15-meter deployable antenna.



## RADIO FREQUENCY VERIFICATION (RFV) MODEL

Shown below is a drawing of the RFV model that was used to demonstrate the feasibility of using the 15-meter antenna in a quad-aperture antenna configuration. The RFV model was designed to simulate two separate and adjacent parabolic offset-fed reflectors. Separate feed systems are used to illuminate each reflector and the capability for feed adjustment (to scan the beam) is provided. The test results using the RFV model demonstrated the need for feed aperture synthesis in an attempt to reduce the parasitic sidelobe radiation. Aperture synthesis analysis has been conducted and applied to the RFV test results, and the parasitic side lobe level has been reduced from 19 dB to 30 dB.



### OBJECTIVES:

- EVALUATE RF PARAMETERS CRITICAL TO THE MULTIBEAM QUAD-APERTURE ANTENNA PERFORMANCE
- PROVIDE VERIFICATION OF CRITICAL PARAMETERS THROUGH TEST AND ANALYSIS
- VERIFY ANALYTICAL METHODS

## TEST RESULTS USING THE STATIC SURFACE

Another significant milestone in the development of the hoop/column antenna was the construction and test of a four-gore segment of a 50-meter-diameter antenna. The boundary condition around the reflector test sections was provided by the aluminum scaffolding structure. The fabrication methods for the reflector surface and rear cord trusses were identical to the "build-to-dimension" techniques which would be implemented for a 50-meter class structure. The surface accuracy and defocus test results are listed in the table below.

**(INCHES)**

	PRETEST GOAL	MEASURED	TRANSLATED TO 100-METER	REQUIRED ON 100-METER
SURFACE ACCURACY RMS	0.083*	0.102	0.256	0.300**
DEFOCUS	1.554	0.556	4.622	10.000

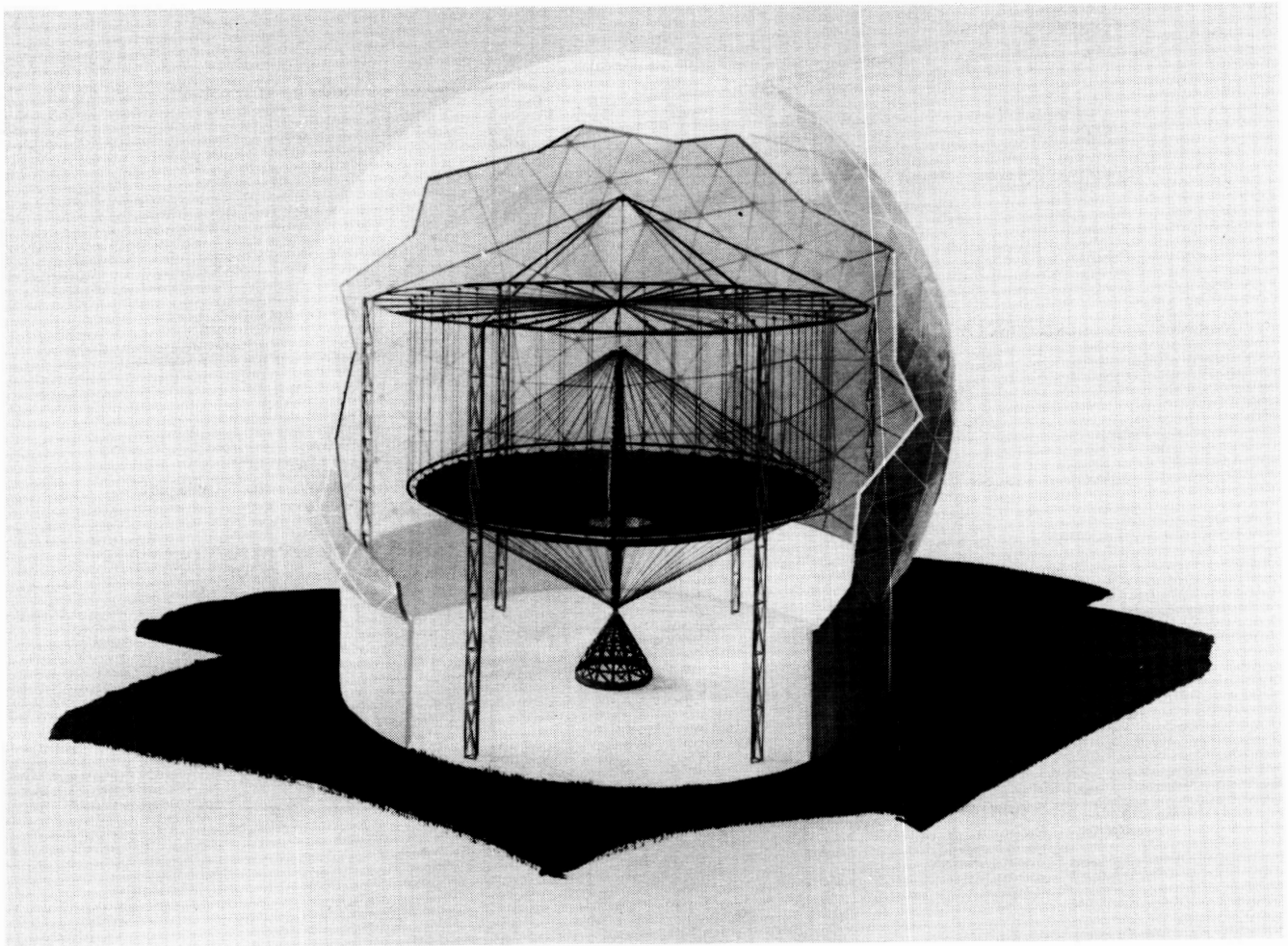
\* THE PRETEST SURFACE ACCURACY GOAL WAS NOT REALIZED  
BECAUSE IT DID NOT REFLECT UNCERTAINTIES DUE TO:

- WEIGHT
- THERMAL GRADIENTS
- BOUNDARY VARIATIONS

\*\* SURFACE ACCURACY REQUIREMENT OF 100-METER IS BASE  
ON A  $\lambda/80$  QUALITY.

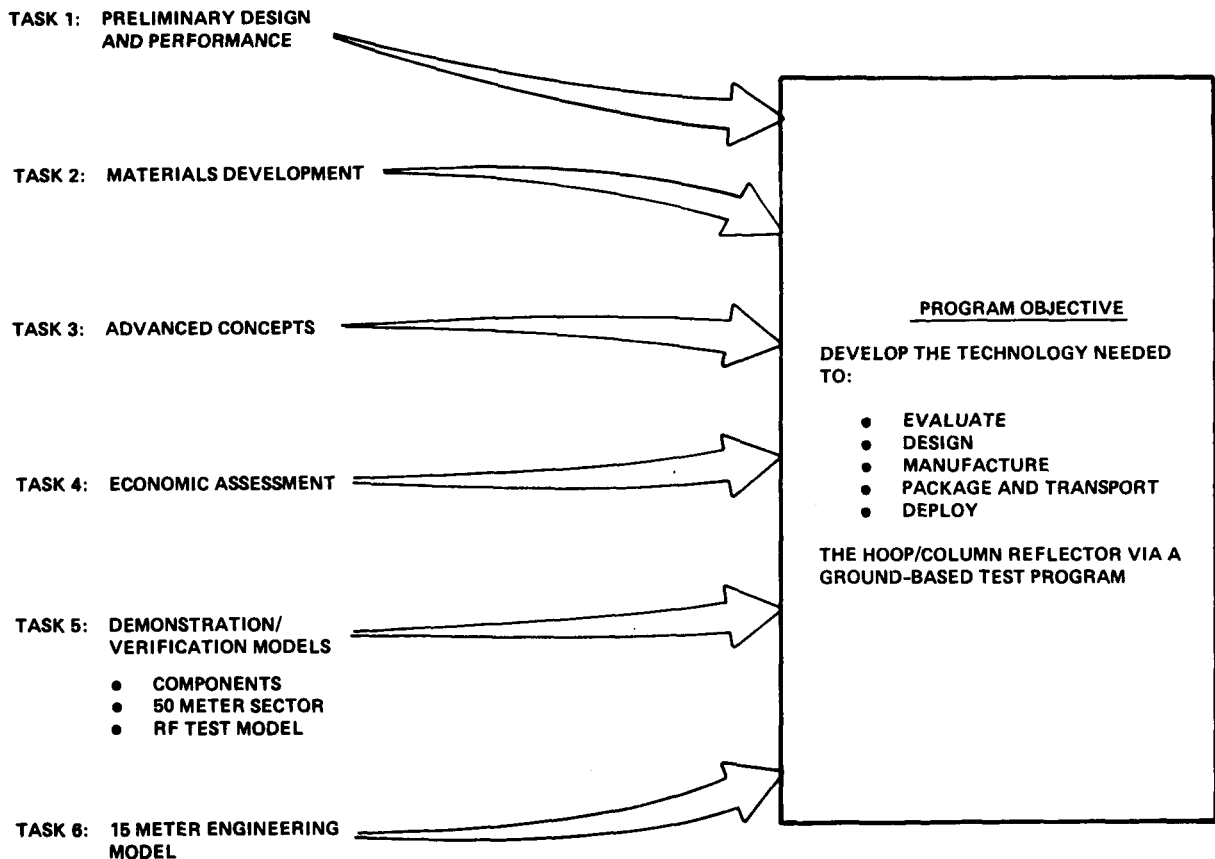
## CONFIGURATION OF THE 15-METER ANTENNA STRUCTURE

The final development activities are the development and test of the 15-meter deployable antenna shown in the figure below. The antenna is positioned and deployed under the counterbalance system in the radome facility at the Harris Corporation. The structure will be deployed and surface tested prior to the installation of the feed system for the RF tests. The 15-meter model will be capable of deployment and stow cycles, repeatability, and surface characterization measurements.



## TASK DESCRIPTIONS AND PROGRAM OBJECTIVE

The program consists of six tasks, each of which supports the primary objective which is to develop the technology necessary to evaluate, design, manufacture, package, transport and deploy the hoop/column reflector.

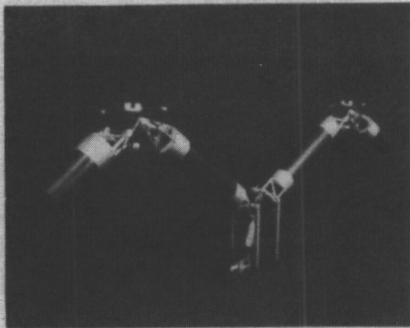




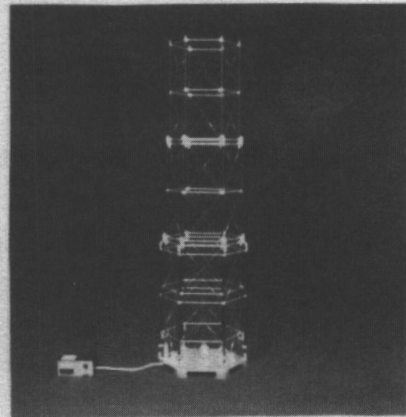
## DEMONSTRATION MODELS

Engineering models have been successfully completed and tested. The hoop model and mast model verified the kinematics of these major components. A mesh stowage model demonstrated a method of folding and managing the mesh. The 50-meter surface model confirmed our analytical and manufacturing techniques.

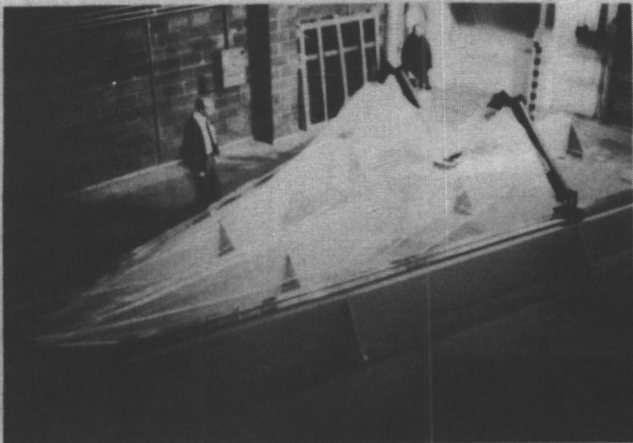
### DEMONSTRATION MODELS



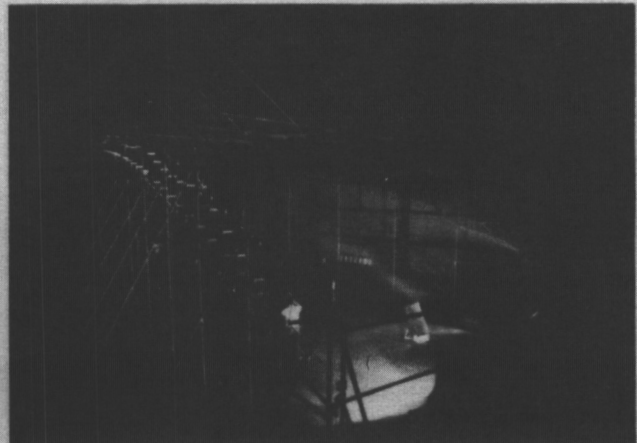
HOOP



MAST



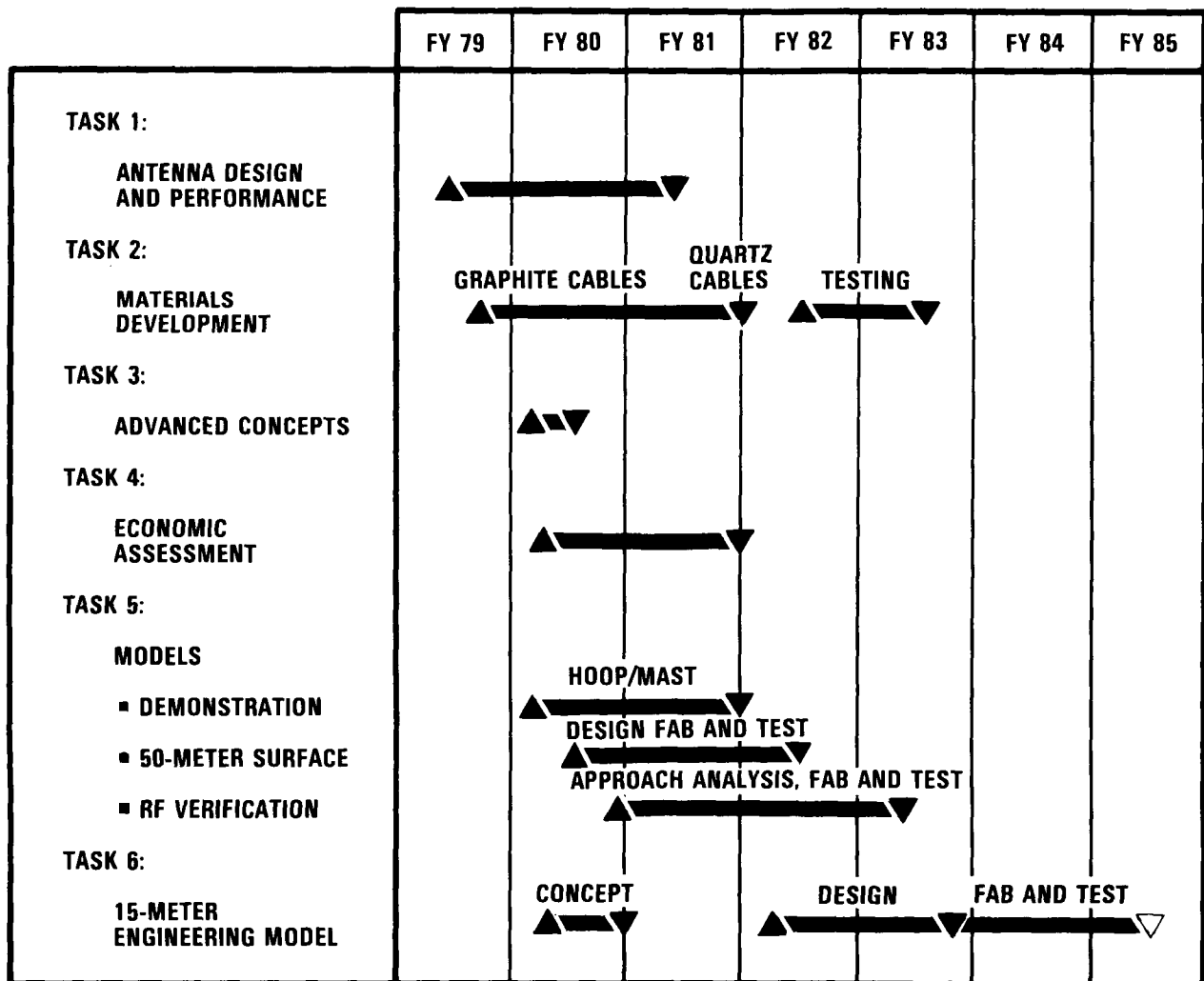
STOWAGE



SURFACE

## SCHEDULE SUMMARY

All tasks have been successfully completed with the exception of task 6 which is ongoing. Each of the 6 tasks is discussed in the following pages.



## 15-METER MODEL REQUIREMENTS

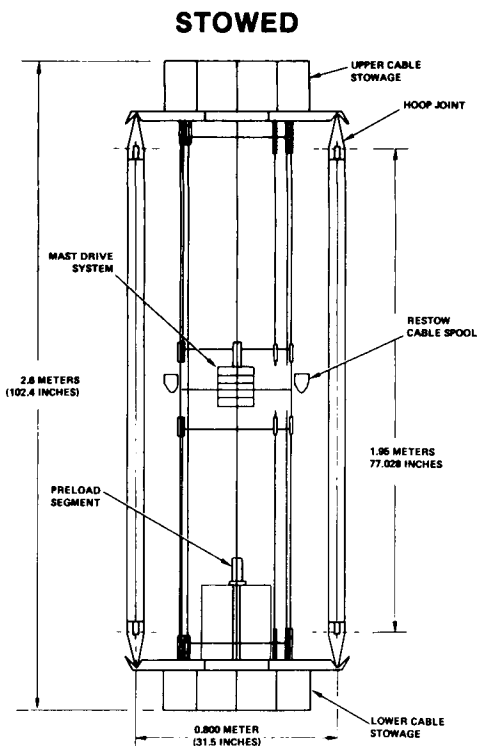
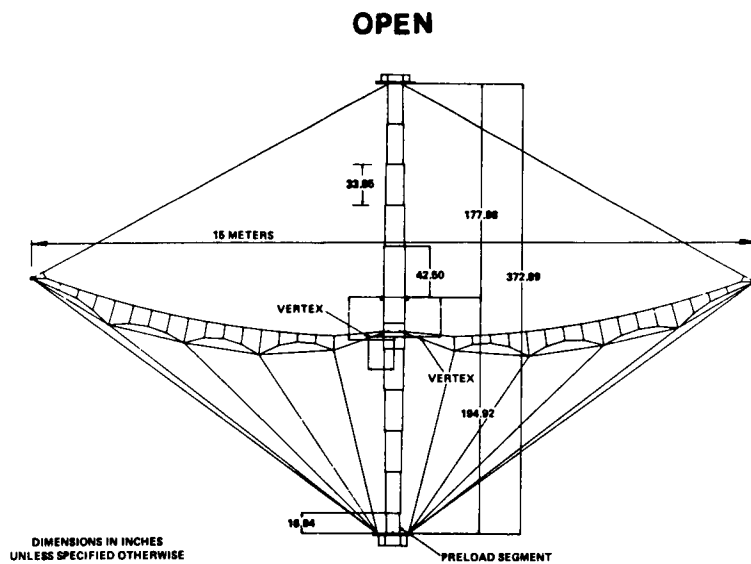
Specific requirements of the model are described below. The model is designed and fabricated in the same manner as a much larger antenna.

- **15-meter hoop diameter**
- **Direct scale-down of 100-meter hoop/column point design where practicable**
  - **Cost constraints**
  - **IG constraints**
  - **Load constraints**
- **Cup-up deployment/restow capability**
- **All deployment/restow operations hands-off WRT structure**
- **Without counterbalance—IG cup-up surface rms = 0.069 inch**
- **Frequency = 2 to 12 GHz**
- **Provide interfaces for ground handling fixtures and 250-pound feed mast**

**RF near-field  
test requirements**

## 15-METER MODEL - SIDE VIEWS

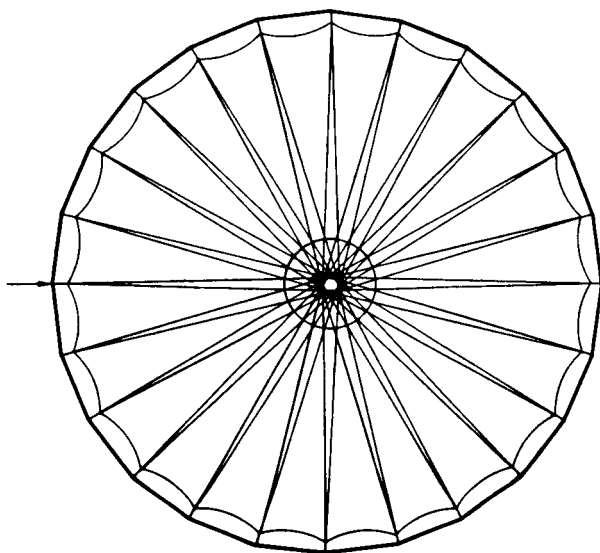
Key geometry features are shown in the figures below. The model, which is less than a meter in diameter when stowed, deploys to a diameter of 15 meters.



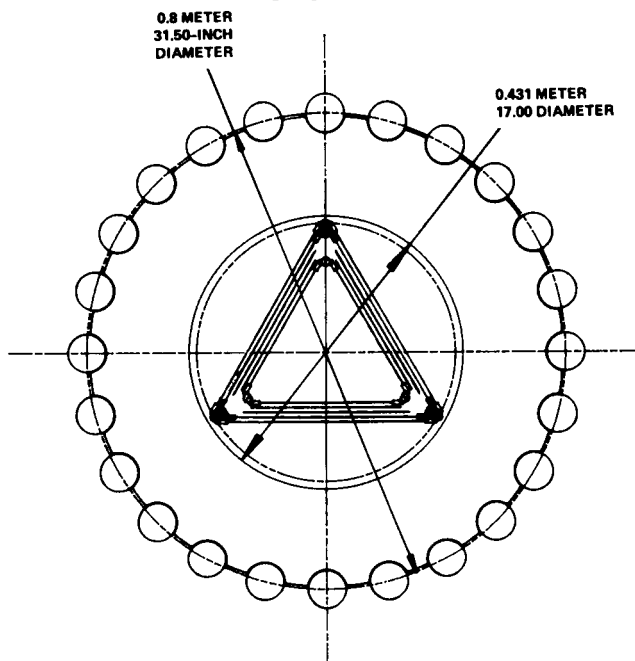
## 15-METER MODEL - TOP VIEWS

To enhance torsional stiffness the upper hoop support cables are crossed. The surface of the model is quad-aperture. Feeds, which will be retrofitted by NASA prior to RF testing, utilize the total quad-aperture area.

**OPEN**

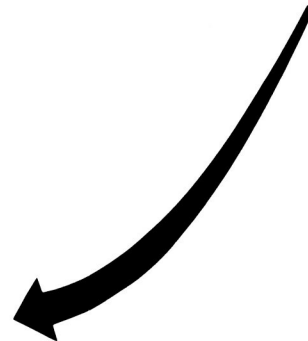
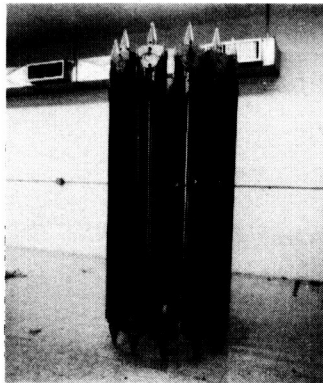
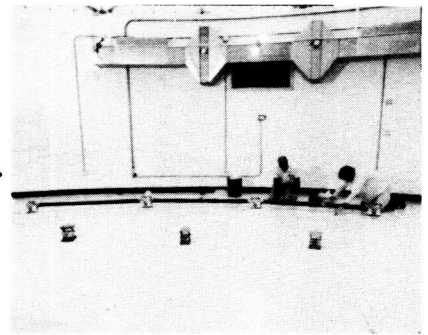
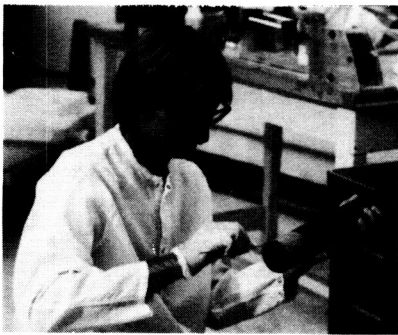


**STOWED**



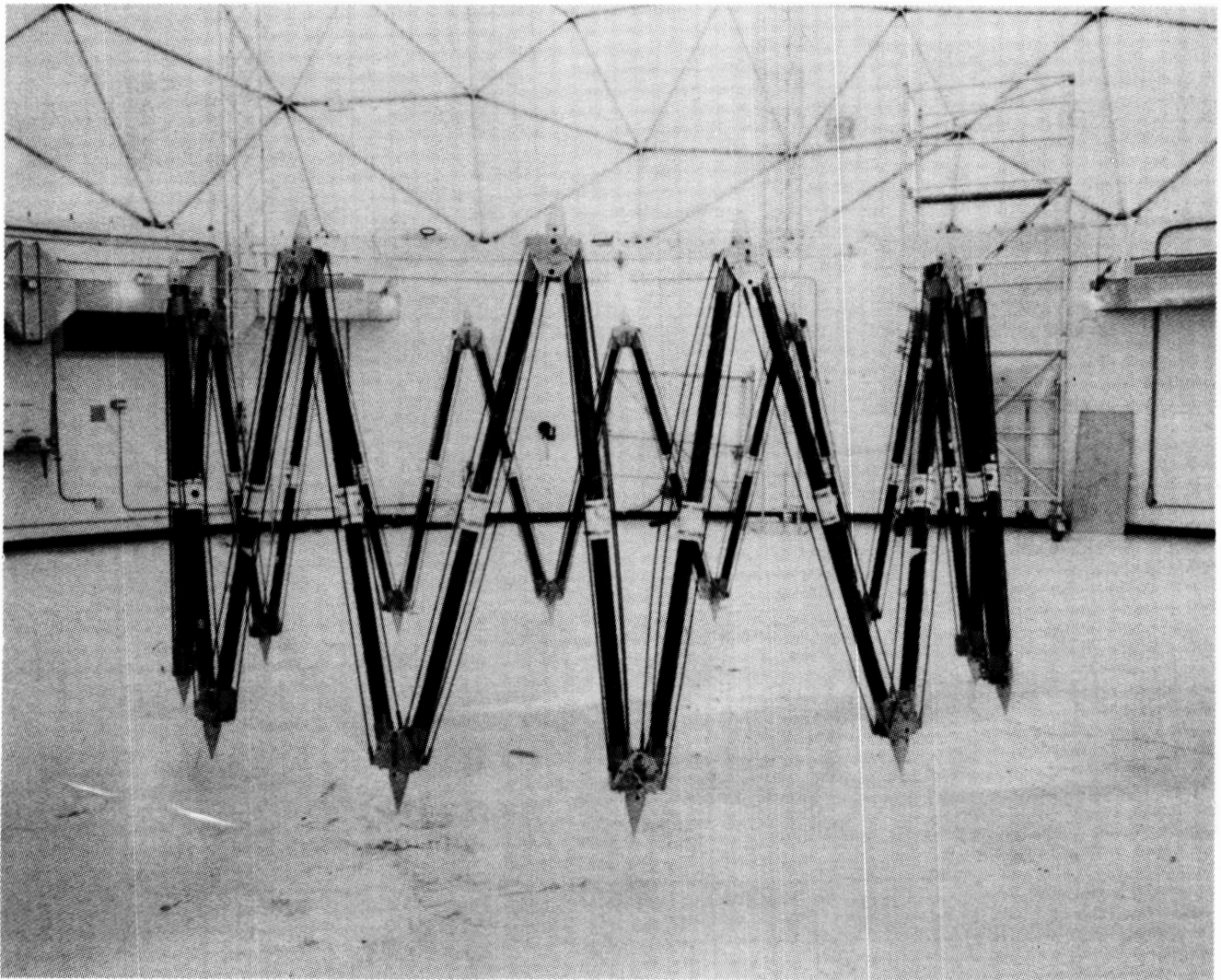
## FABRICATION - HOOP

The hoop is assembled and bonded in a fixture three segments at a time. This fixture, which is aligned by means of theodolites, controls the length of each of the segments to within .020 inch. After each of the eight three-segmented assemblies is completed, it is final assembled to the others and the hoop is completed.



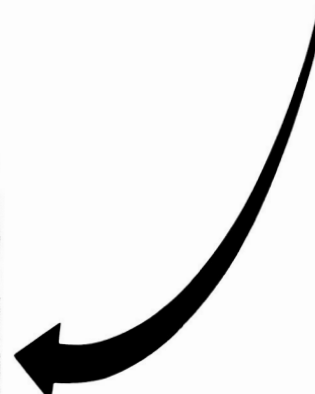
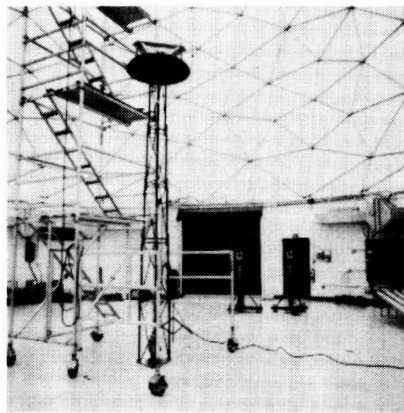
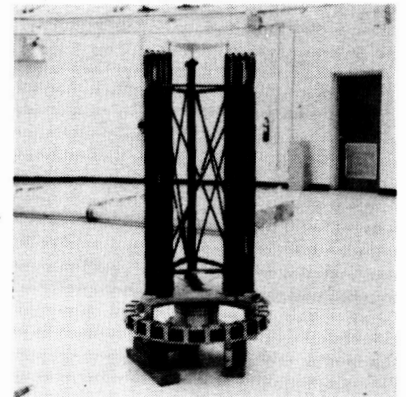
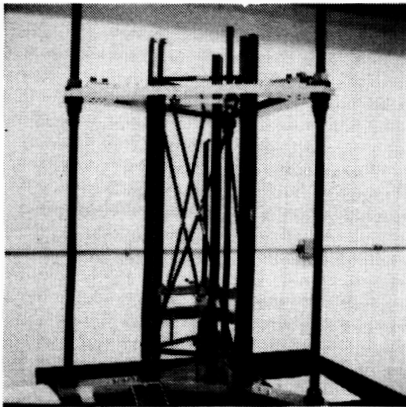
## DEPLOYMENT TESTS - HOOP

The hoop is attached to its counterbalance system and deployment tested to verify proper alignment of the mechanisms.



## FABRICATION - COLUMN SEGMENT

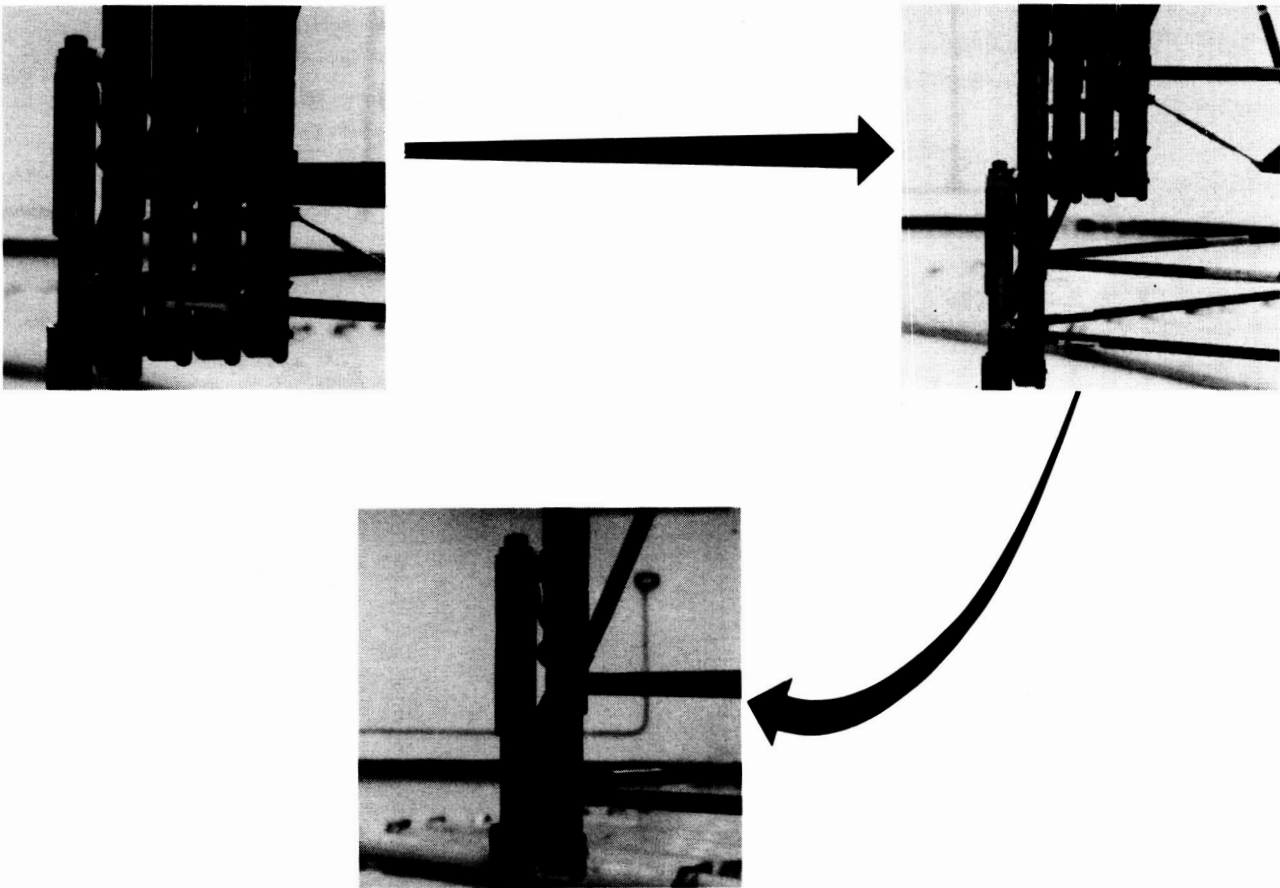
Each of the column segments is fabricated in the same fixture to ensure geometry requirements are met. The column is proofloaded after it is final assembled and adjusted.





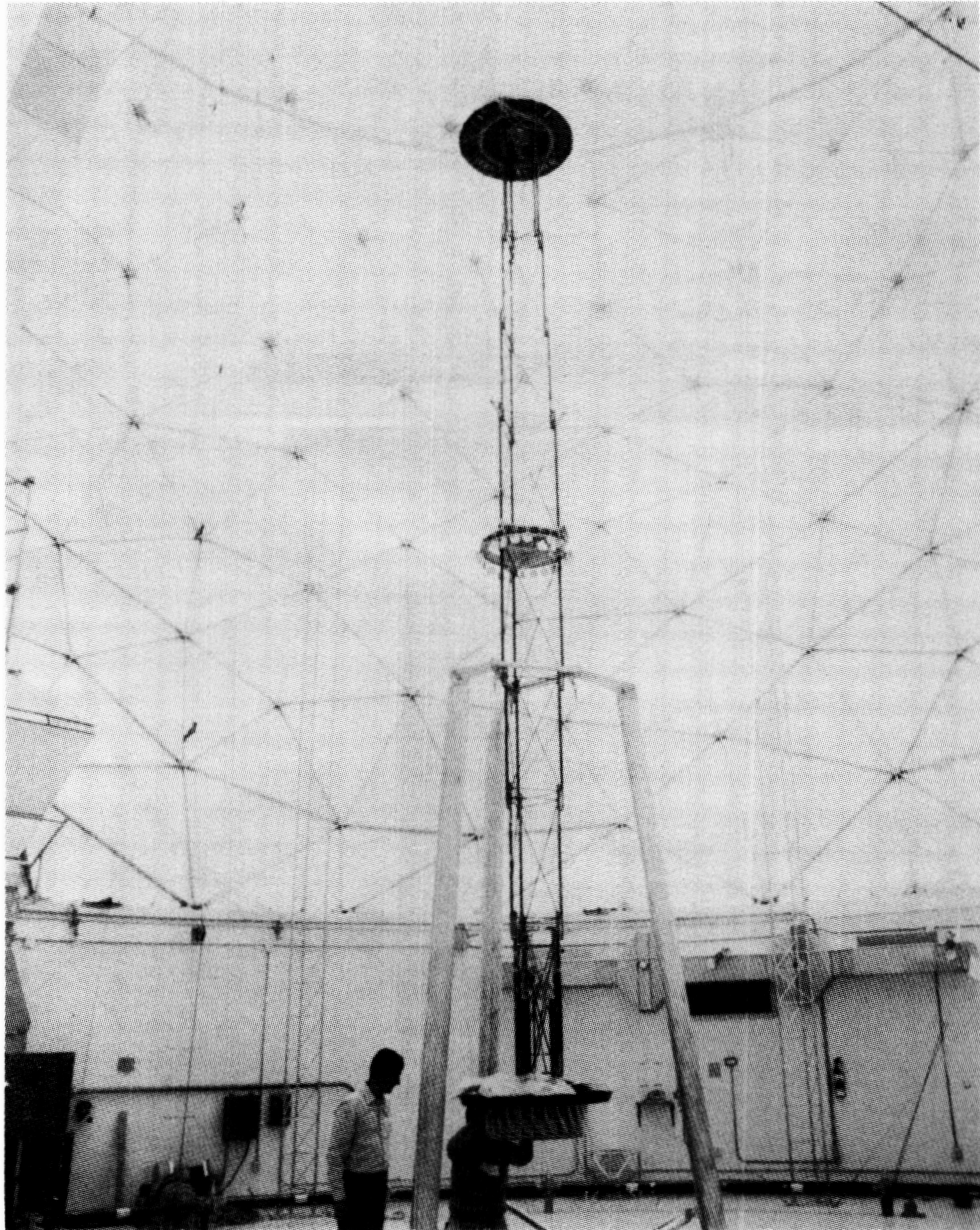
## LATCH SEQUENCE

The sequential lockup of the column is necessary to provide it with structural stiffness throughout its deployment. Latches are designed to lock up with their outboard counterparts and at the same time release themselves from their inboard counterparts. This event is shown in stages below. The resulting interface is one which provides compressive and tensile load-carrying capability.



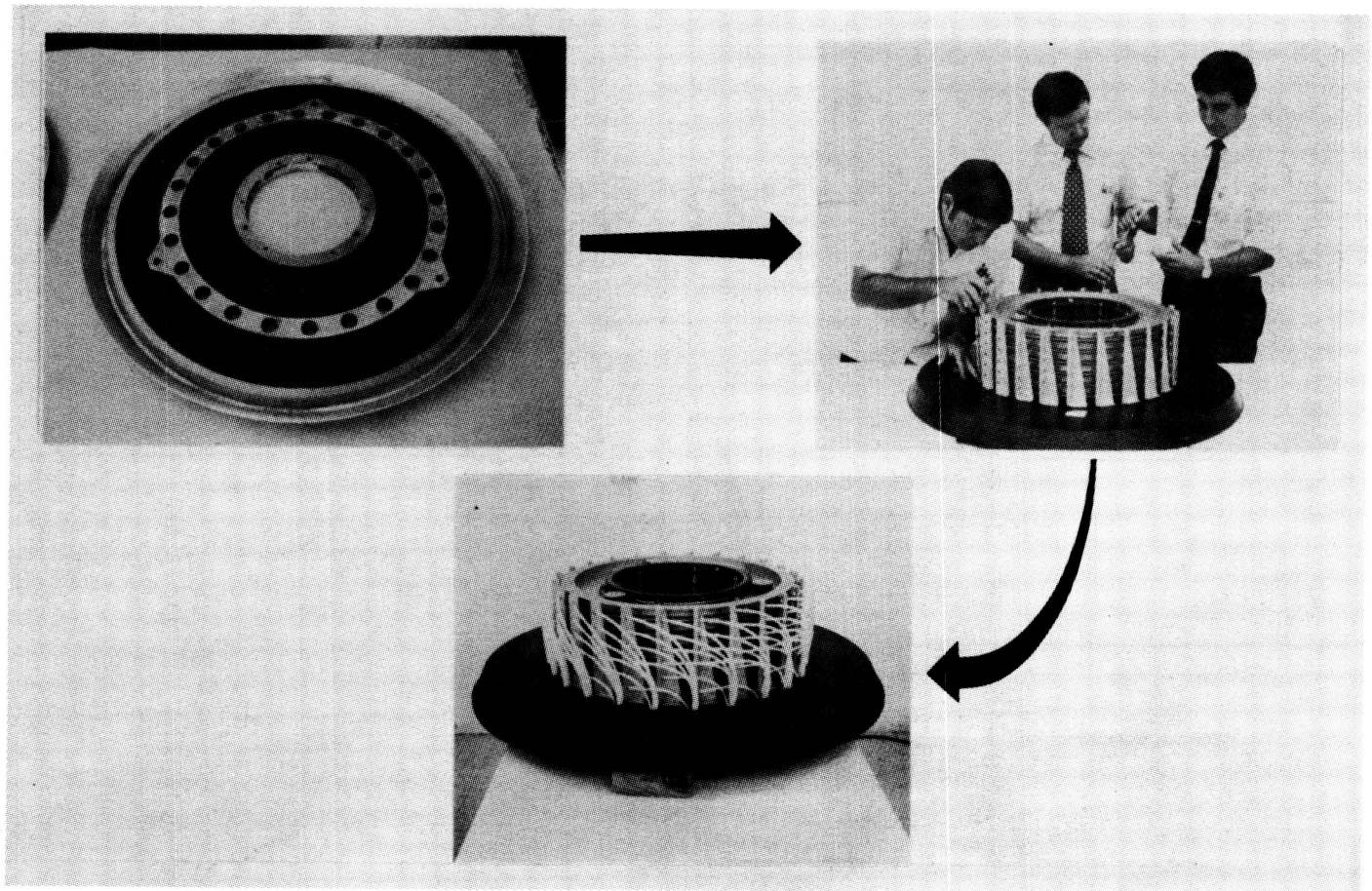
## DEPLOYMENT TESTS - COLUMN

The column is attached to the pedestal and run through a series of deployment cycle tests prior to interfacing with the hoop.



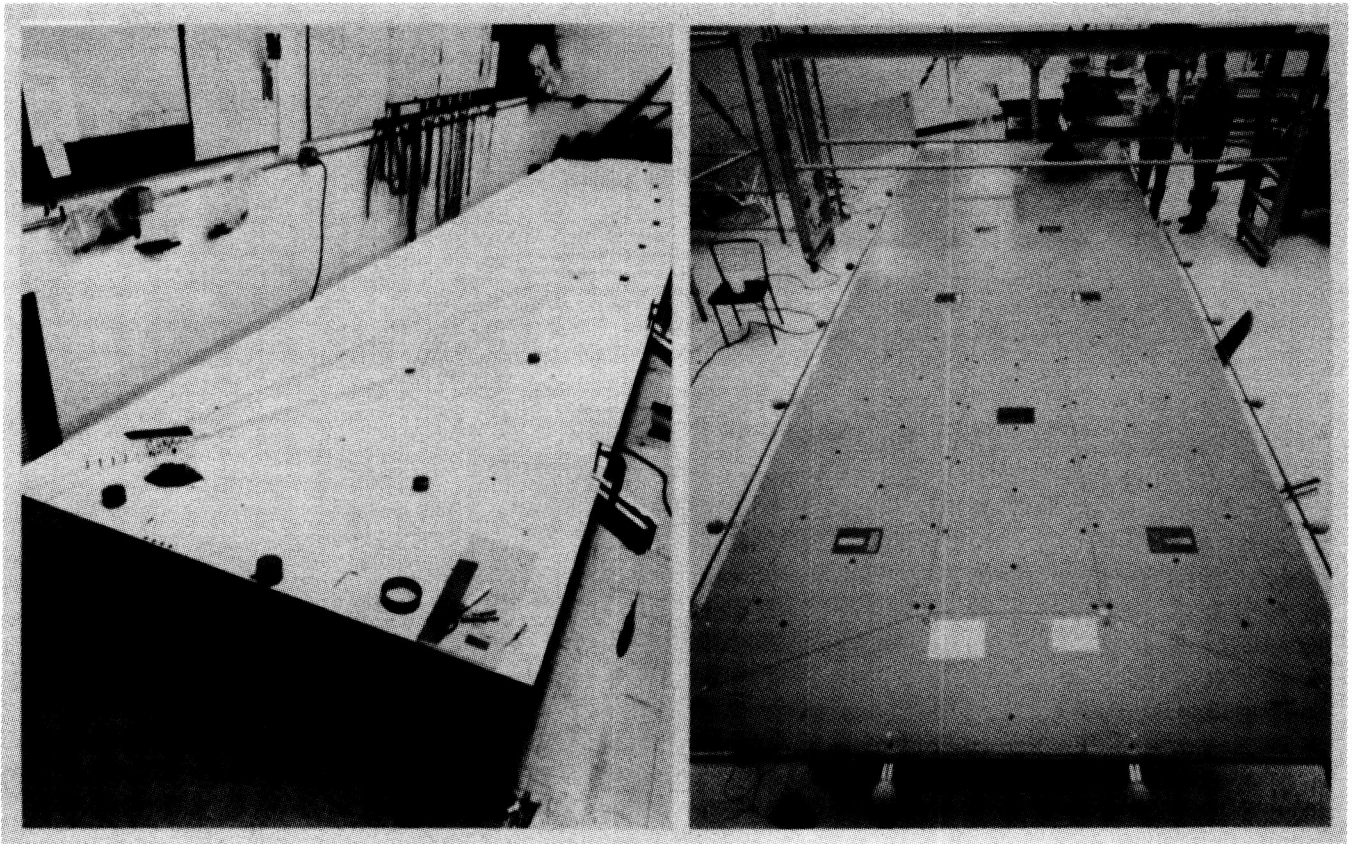
## FABRICATION - CABLE STOWAGE

The 15-meter model is manufactured in modular form. For example shown below is a cable stowage assembly under way. This assembly must efficiently pay out, retrieve, and manage 48 cords.



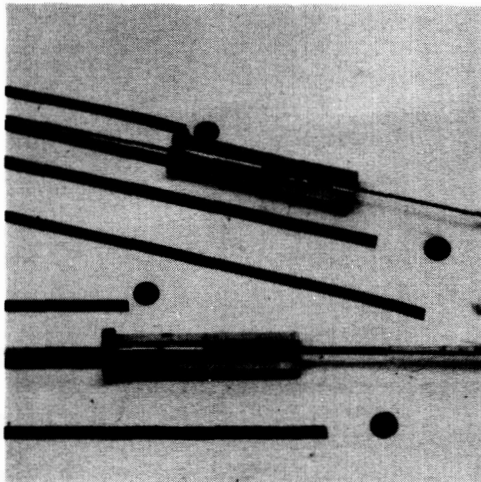
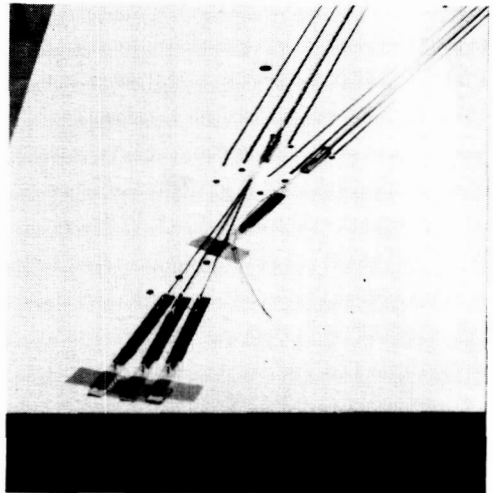
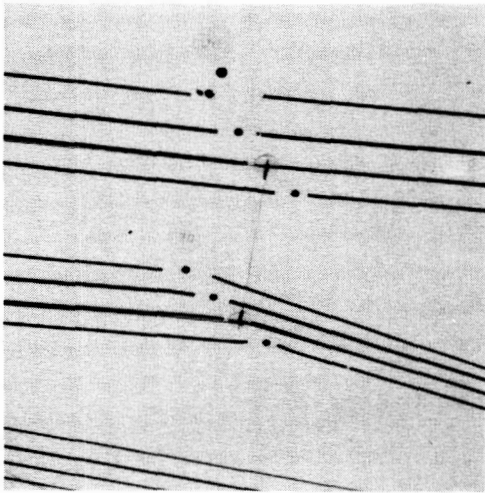
## FABRICATION - SURFACE

Fabrication of the RF reflective surface is under way. The surface is comprised of two major subassemblies. The rear truss assembly is shown on the left and the front cord assembly is shown on the right. The assemblies are stretched to their operational load and are bonded in place on 25-foot-long templates which maintain an overcome accuracy of .005 inch.



## SURFACE FABRICATION

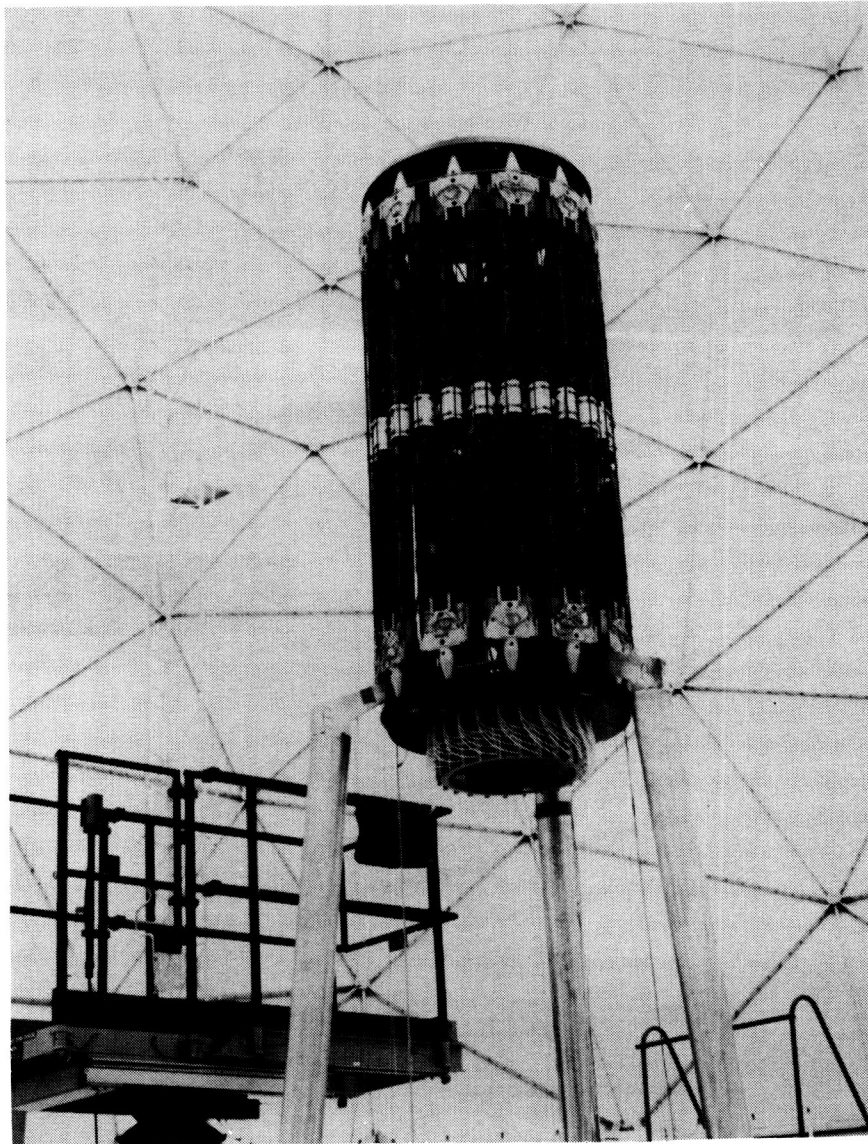
All cords and ties are pretensioned to their operational load prior to bonding by spring tensiometers which are precalibrated. The primary shapers (top left) of the gore edge cords are the vertical ties, the lengths of which are determined by the template interfaces. Ties and cords are manufactured from a unidirection multi-strand graphite yarn which is Teflon impregnated. The edge cords (top right) are bonded into sleeves which are also located by template fixturing. The cords are prepared for bonding by burning the Teflon from the cords. Epoxy is injected into the sleeve by means of a hypodermic needle.





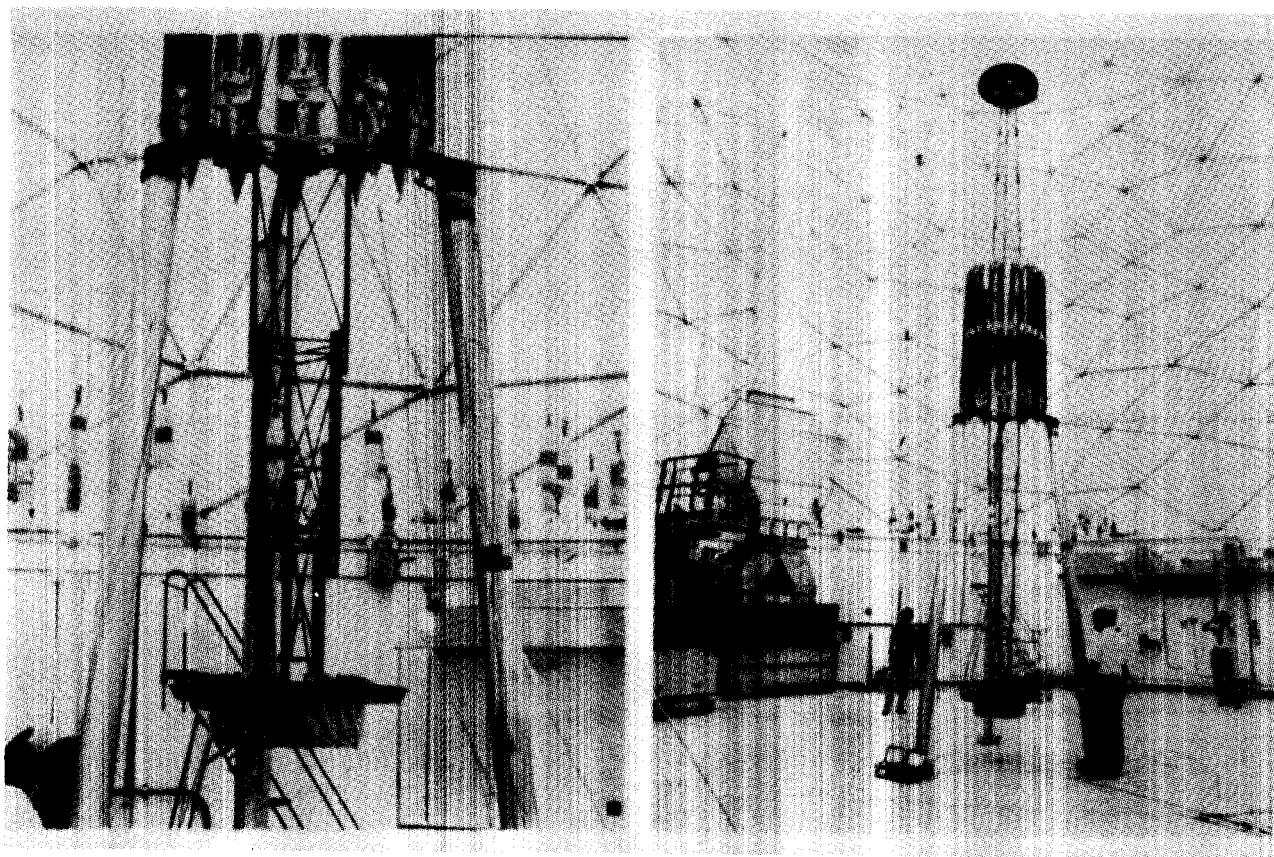
## 15-METER MODEL - STOWED

Deployment tests of the hoop/column structure have been successfully completed. The photograph was taken during the deployment sequences described previously. The model is shown sitting atop its three-legged pedestal. Both the hoop and the column are comprised of graphite (GFRP) tubular members.



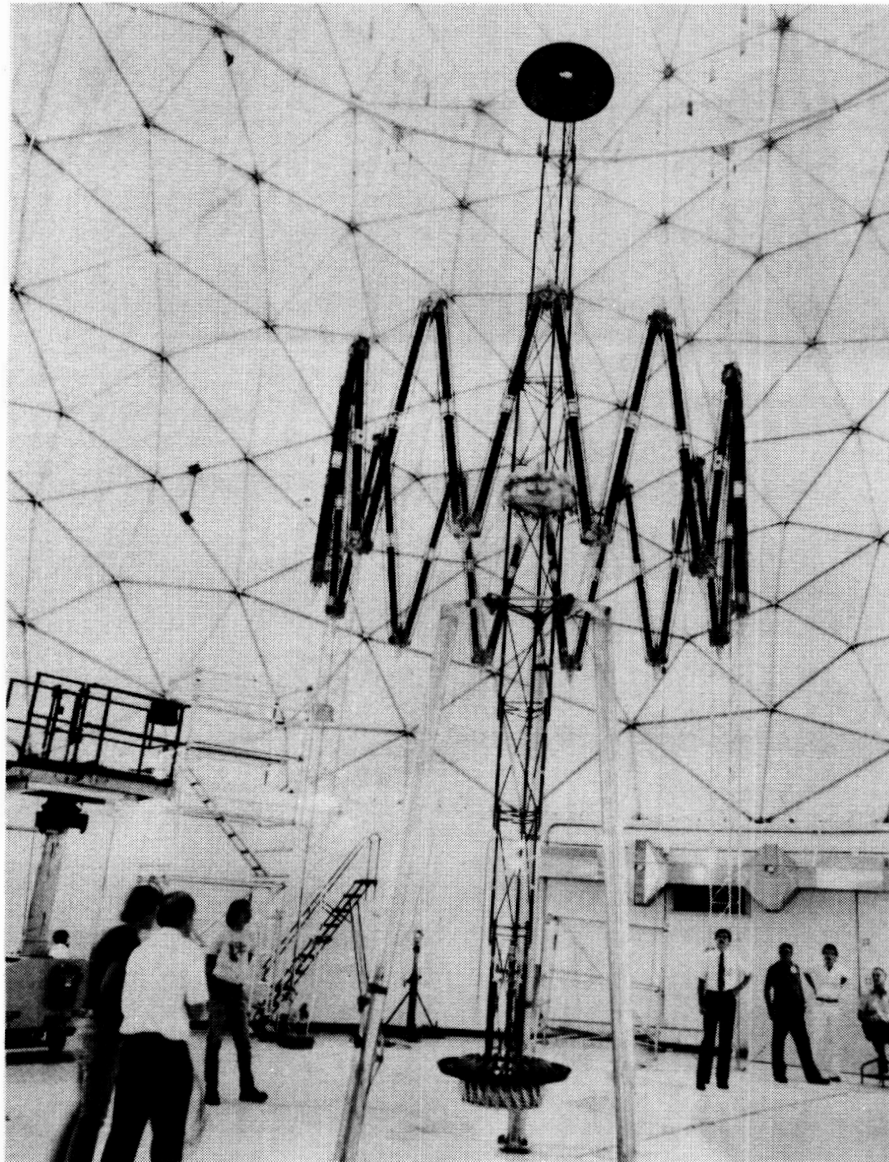
## COLUMN DEPLOYMENT

The model begins its deployment by the extension of the telescoping mast. It is driven by means of cables which are retrieved on a spool located in the center of the column.



## HOOP DEPLOYMENT - INTERMEDIATE STAGE

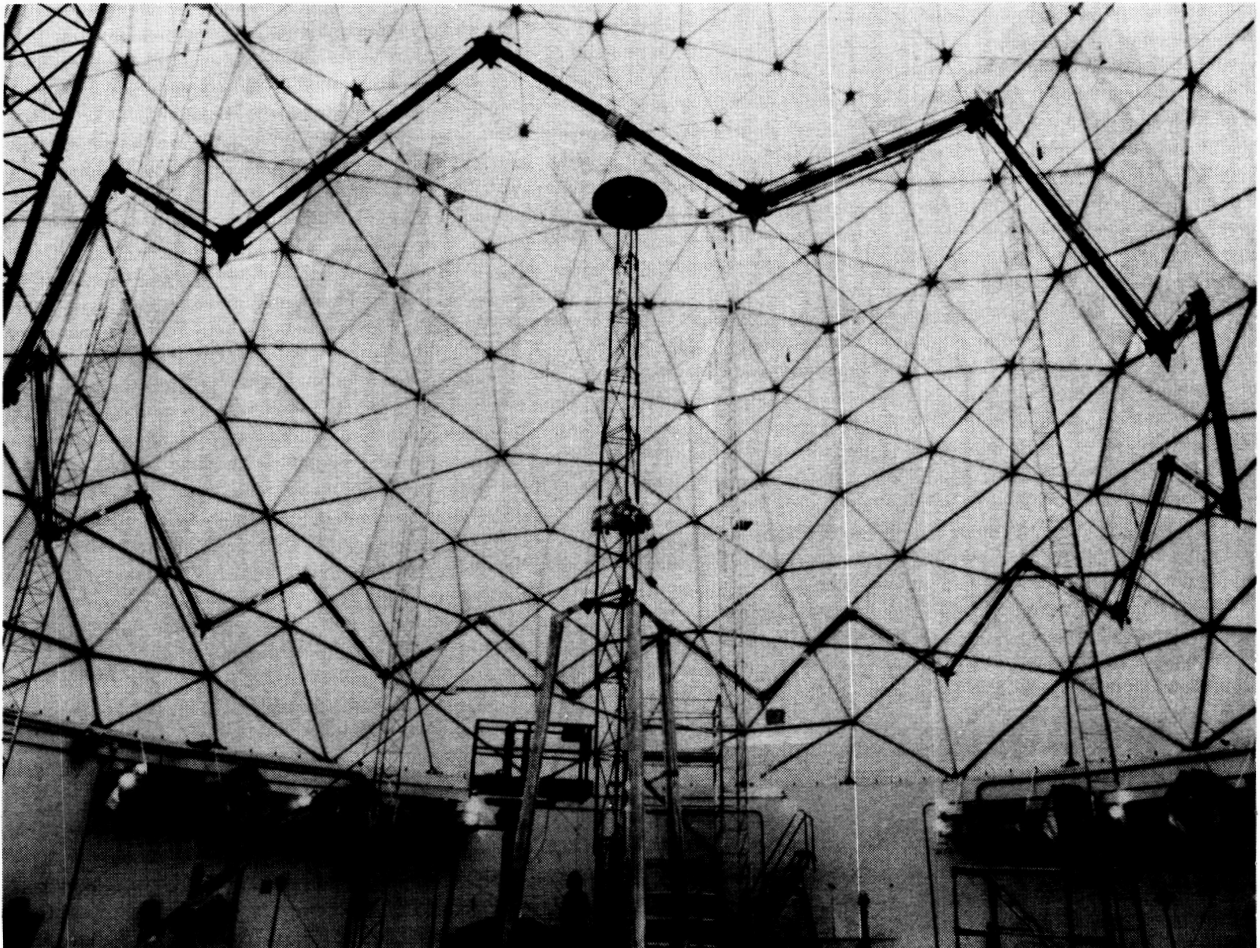
The hoop is shown in an intermediate stage of deployment. It is positioned during deployment by the upper and lower hoop support cables which emanate from the extremities of the column. The cables, which pay out from common spools, maintain tension throughout the deployment of the hoop.





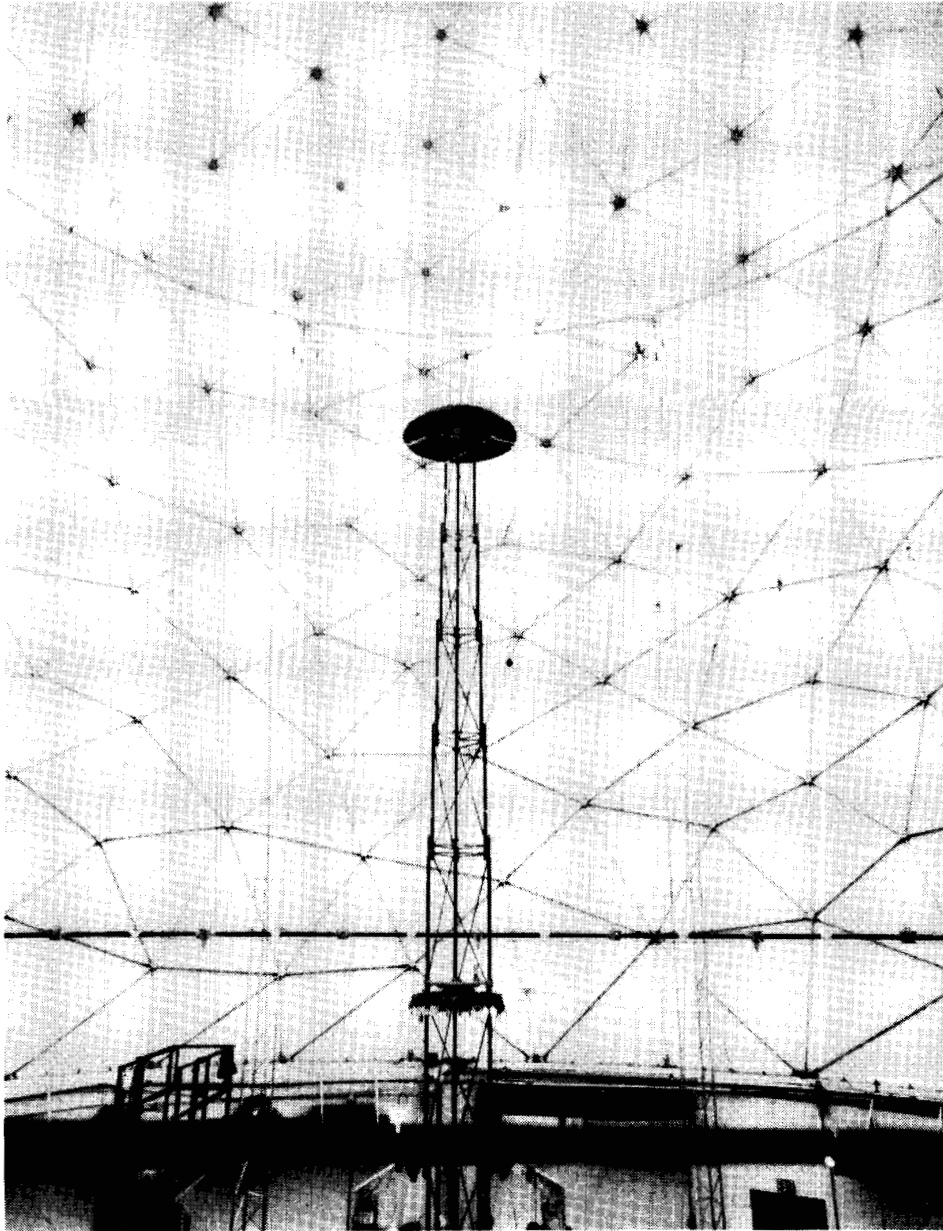
## HOOP DEPLOYMENT

The hoop maintains its symmetrical attitude throughout its deployment. Total time of the hoop deployment cycle is approximately 10 minutes. The energy to deploy the hoop is provided by 4 D.C. gear motors.



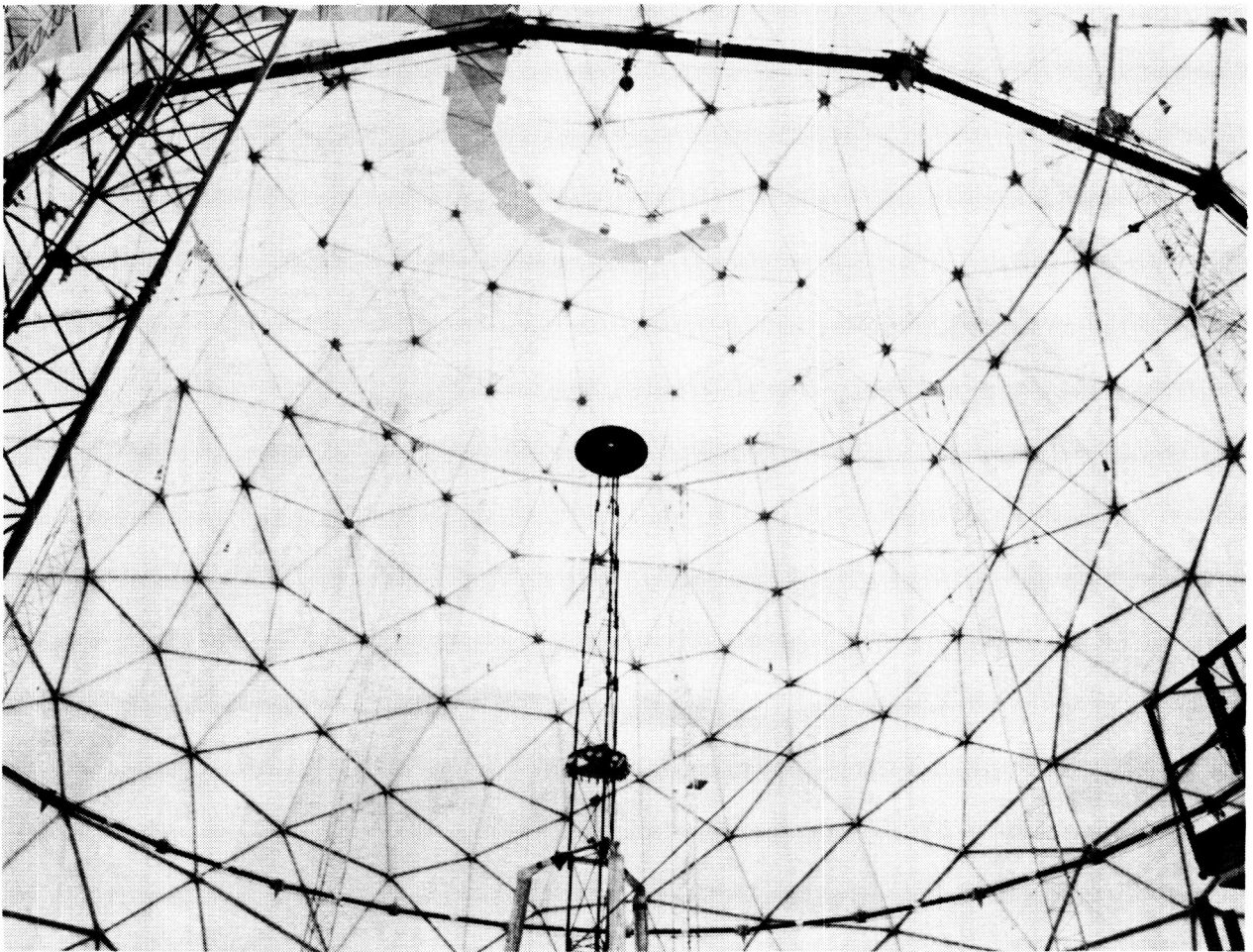
## FULLY DEPLOYED - PRELOAD SEGMENT EXTENSION

The model's final stage of deployment is the extension of the preload segment. Subsequent to this all members of the structure are preloaded and the model is self supporting.



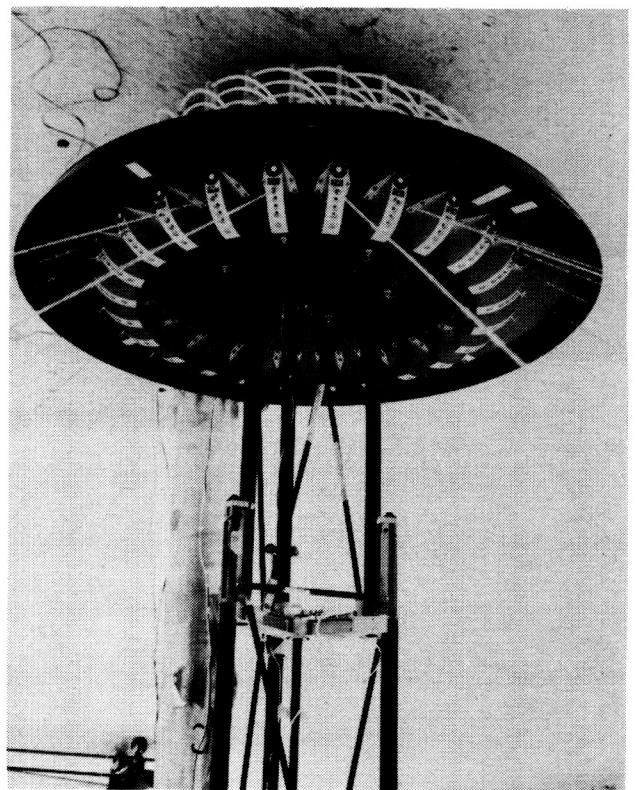
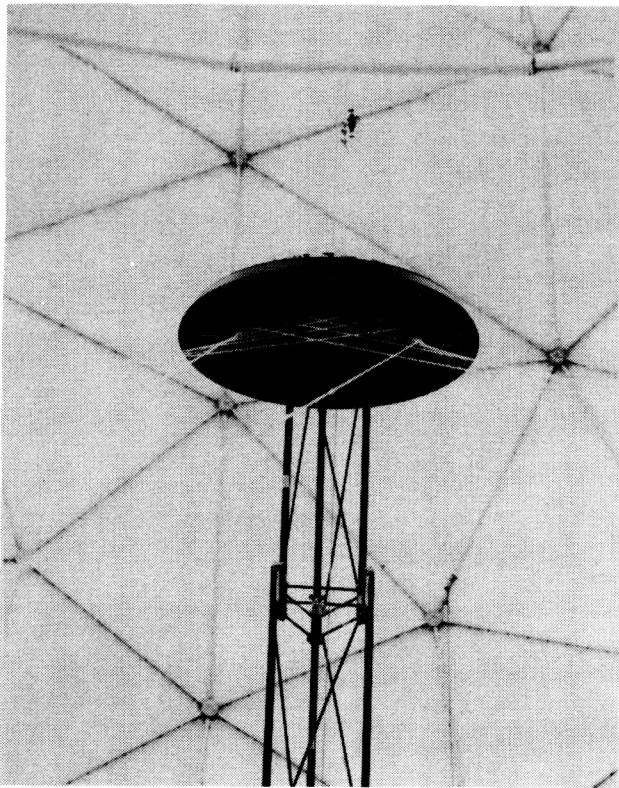
## FULLY DEPLOYED

After removal of all counterbalance interfaces the model was measured at the end of each of the three deployments to determine repeatability characteristics. Results show the structure to be within the accuracy required to achieve the eventual surface RMS.



## UPPER AND LOWER CABLE CONFIGURATION

The upper hoop support cords (left side) are crossed to enhance torsional stiffness. These cords, which are quartz to minimize RF interference, emanate from the upper cable stowage assembly. The lower hoop support cords (right side) are graphite to provide high stiffness as well as a low coefficient of thermal expansion.



## 15-M HOOP/COLUMN ANTENNA MODAL SURVEY WITHOUT SURFACE

A modal survey of the 15-meter hoop/column antenna was performed to identify the dominant vibration modes below 15 Hz. As described below, a roving impact hammer and one reference accelerometer were used to excite and measure all modes except the fundamental torsion mode. The torsion mode was excited by inducing an initial rotation of the hoop. The impact hammer technique was used because a limited time period was available. This method does not separate closely spaced modes; however, the objectives were achieved with the approach indicated below. Test and analytical results are presented with both the test boundary conditions and free-free boundary conditions. The analysis methods used to model the 15-meter antenna with the surface are described. Complete dynamic characterization tests of the antenna are planned after the surface is installed.

### ● OBJECTIVE:

- Experimental identification of modes with dominant hoop and column motion below 15 hertz

### ● APPROACH:

- Survey column with roving impact hammer and reference accelerometer to obtain frequency response functions using a two-channel FFT analyzer

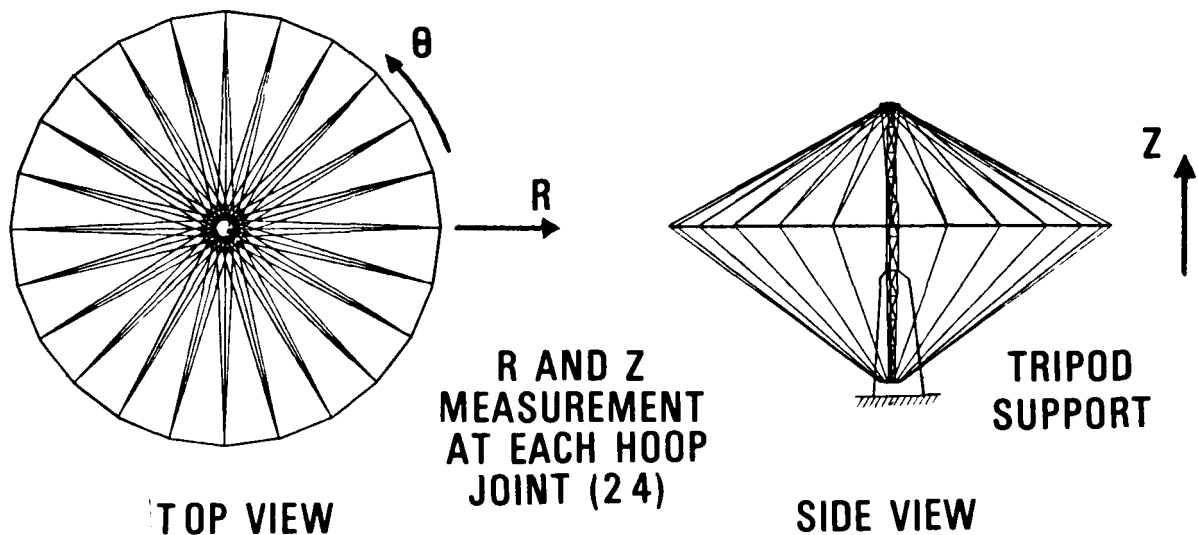
### ● PURPOSE:

- To determine frequency, mode shapes and damping for math model verification before surface installation

## 15-M ANTENNA MEASUREMENT LOCATIONS AND TEST CONFIGURATION

The antenna was tested by impacting the hoop at each of the 24 hoop joints. Both radial (R) and vertical (Z) measurements were made. Four additional measurements were made by impacting the column in the radial and circumferential ( $\theta$ ) directions at the upper and lower ends of the column. The low acceleration of the fundamental torsion mode required use of a proximity probe for accurate measurement of frequency and damping. The proximity probe was located on a fixed support with a target located on the hoop. An initial rotation of the hoop was induced by hand such that a free decay of this mode could be measured. An important influence on the test results is the type of boundary conditions imposed by the support structure which consisted of a tripod of six-in. aluminum tubes as shown below. The tripod was attached to the column somewhat below the column center. The tripod flexibility was included in the analysis.

- FREQUENCY RESPONSE FUNCTIONS MEASURED AT 52 LOCATIONS
- FIRST HOOP TORSION MODE EXCITED BY INITIAL DISPLACEMENT

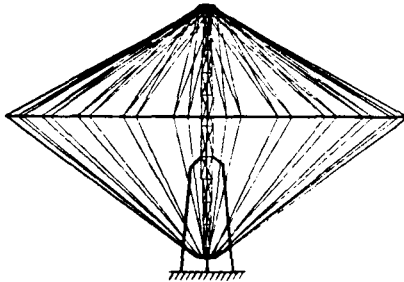




## FIRST FOUR MODES OF THE 15-M ANTENNA

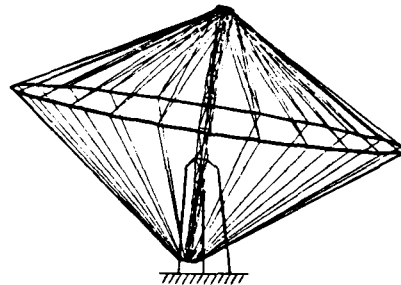
The mode shapes and frequencies of the first four modes are shown below. The fundamental mode involves torsion of the hoop about the vertical axis of the antenna and occurs at a frequency of 0.068 Hz. The second mode occurs at 0.785 Hz and involves rocking of the hoop and bending of the column. Since this mode shape has a harmonic number of  $N=1$ , two modes exist at this same frequency if the structure is exactly rotationally symmetric. The mode shapes are identical except for being rotated 90 degrees about the vertical axis. This double mode occurrence is true for harmonics from  $N=1$  to  $N=10$ . The third mode involves inplane translation of the hoop and bending of the column. This mode occurs at 1.36 Hz and is also a harmonic of  $N=1$ . The final mode shown is torsion of the lower half of the column and occurs at 3.13 Hz. Both the fundamental hoop torsion mode and the lower column torsion mode are referred to as harmonic number  $N=0$ .

**HOOP TORSION**



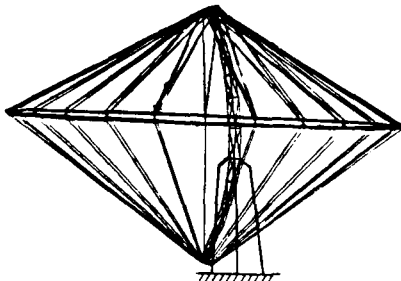
**f=0.068**

**HOOP ROCKING/COLUMN BENDING**



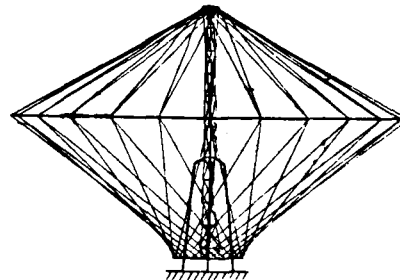
**f=0.785**

**HOOP INPLANE MOTION/COLUMN BENDING**



**f=1.36**

**LOWER COLUMN TORSION**

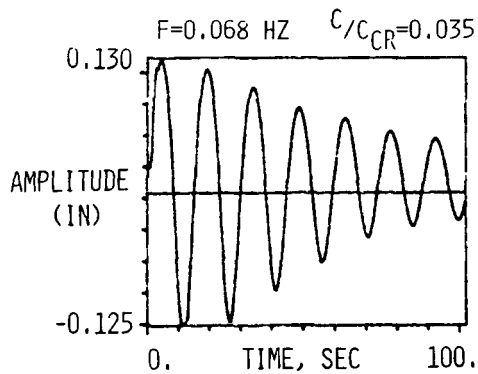


**f=3.13**

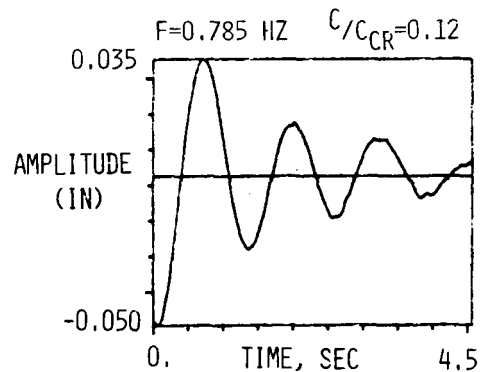
## DAMPING IDENTIFICATION FROM FREE DECAY TIME HISTORIES

To obtain data for damping estimation of the first four modes, free decay time histories were recorded for each mode. The time histories shown below are typical of the measurements. None of the curves exhibit pure exponential decay which is representative of viscous damping. Indeed, a structure such as the 15-meter hoop/column antenna probably obtains most of the damping from friction in the joints. Because the friction is nonlinear with the amplitude of vibration, the resulting free decay exhibits an exponential type of decay rather than a classical linear coulomb friction decay. A best fit calculation assuming linear viscous damping results in a critical damping ratio of 0.035, 0.12, 0.041 and 0.026, respectively, for the four modes. These values are considerably higher than estimates of large space antenna damping usually used in analytical simulations. The telescoping column joints are believed to contribute this high damping to the structure.

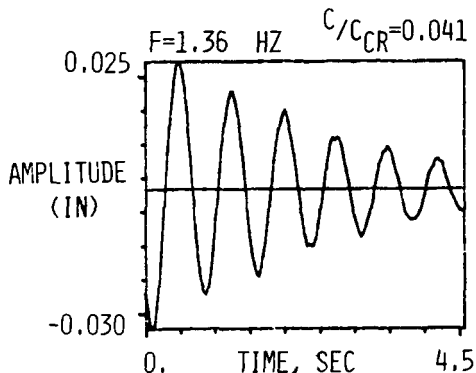
### HOOP TORSION



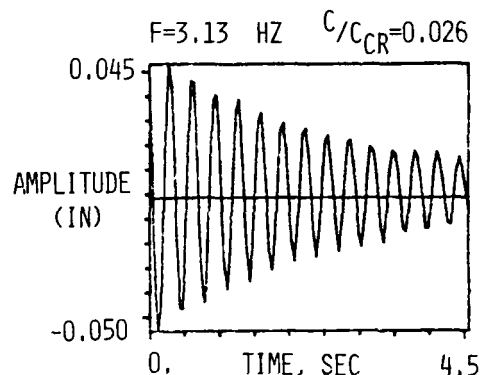
### HOOP ROCKING/COLUMN BENDING



### HOOP INPLANE MOTION/COLUMN BENDING



### LOWER COLUMN TORSION





## COMPARISON OF TEST AND ANALYSIS FREQUENCIES

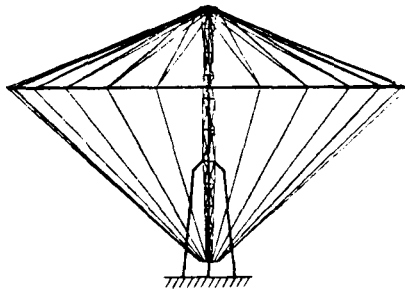
The table below shows a comparison of test natural frequencies to analysis frequencies predicted using the NASTRAN finite-element program. The first four analysis frequencies differ from the test results by 15%, 23%, 18% and -5.4%, respectively. The first three natural frequencies are lower in the test probably due to the flexibility of the column joints. The fourth mode is highly dependent on the rotational inertia of the lower column. It is felt the analysis model overestimates this rotational inertia. Between 7.5 and 10.0 Hz eight test frequencies were identified. These mode shapes involve hoop out-of-plane bending. Analysis predicts 22 modes occur in this frequency range with harmonic numbers from N=0 to N=11. The impact hammer test technique did not provide enough frequency resolution in the test results to identify more than the eight frequencies shown. From 12.05 to 14.55 Hz eight additional modes that involve in-plane hoop bending were obtained from test data. The table also shows cable frequencies that were measured by exciting each of the 72 cables. These frequencies range from 9.25 to 11.45 Hz. The analysis results used a nominal 21-lb load in each of the upper hoop support cables and 15.7 pounds in the lower hoop support cables.

MODE SHAPE DESCRIPTION	FREQUENCIES (Hz)	
	ANALYSIS	TEST
Hoop torsion	0.078	0.068
Hoop rocking/column bending	0.969	0.785
Hoop inplane motion/column bending	1.61	1.36
Lower column torsion	2.96	3.13
Hoop out-of-plane motion		7.50
		7.95
	22 Modes	8.15
	from 6.93 to 7.30	8.40
		8.60
		8.95
		9.20
		10.00
		12.05
		12.55
Hoop inplane bending		13.00
	10 Modes	13.25
	from 10.16 to 14.22	13.50
		13.75
		14.30
		14.55
Higher hoop rocking and column bending	11.85	11.65
	12.72	13.25
Lower cable modes	10.62	from 9.25 to 11.65
Upper cable modes	9.80	from 9.66 to 11.45

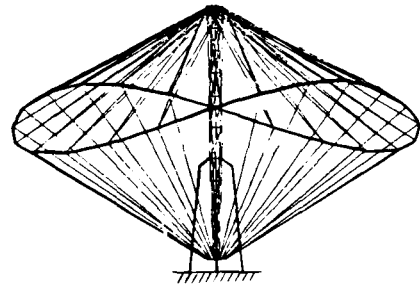
## OUT-OF-PLANE HOOP MODES (F=7.5 TO 10.0 HZ)

Shown below are four of the mode shapes typical of the modes in the frequency range from 7.5 to 10.0 Hz. These mode shapes were generated by analysis. The experimental data show these modes to be highly coupled and as such they were not identified completely from the test data. An important consideration in modeling these modes is the existence of a pin in each of the 24 hoop joints. These pins are oriented to allow free rotation of the hoop segments in the out-of-plane direction to facilitate deployment. The analysis results were generated with a perfect pin in each hoop joint. This results in the out-of-plane hoop modes to be spaced very close in frequency (i.e., 22 modes from 6.93 to 7.30). In reality, some degree of rotational stiffness exists in the hoop joints. This stiffness probably accounts for the experimental modes being spaced further apart in frequency (7.50 to 10.0 Hz).

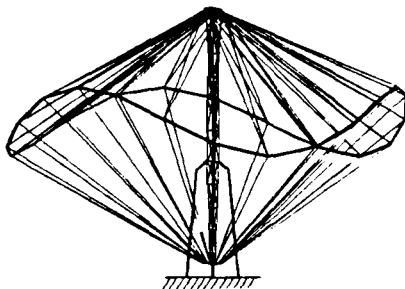
**OUT-OF-PLANE HOOP TRANSLATION**



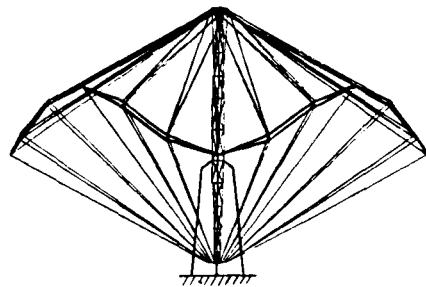
**OUT-OF-PLANE HOOP BENDING (N=2)**



**OUT-OF-PLANE HOOP BENDING (N=3)**



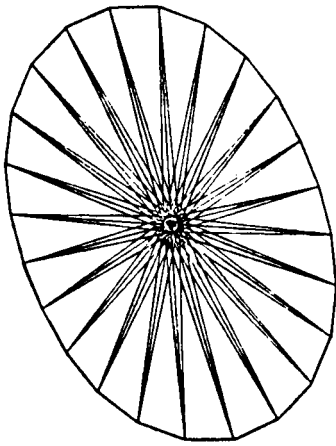
**OUT-OF-PLANE HOOP BENDING (N=4)**



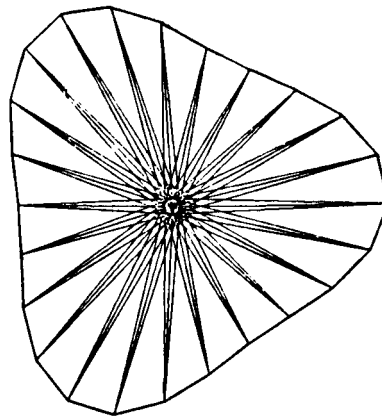
# IN-PLANE HOOP BENDING MODES (F=12.0 TO 14.5 HZ)

From 12.0 to 14.5 Hz, a number of modes were measured which exhibit in-plane hoop bending as shown. Again these modes were highly coupled, and the experimental technique did not provide the frequency resolution needed to completely characterize these modes. Nevertheless, the frequencies obtained from the test data correlate to the analysis frequencies reasonably well. The high degree of coupling will require a very extensive test program to uniquely identify these modes.

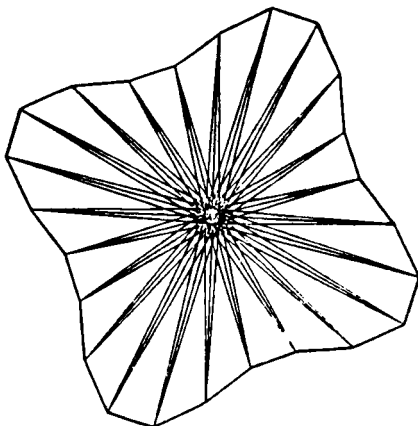
INPLANE HOOP BENDING (N=2)



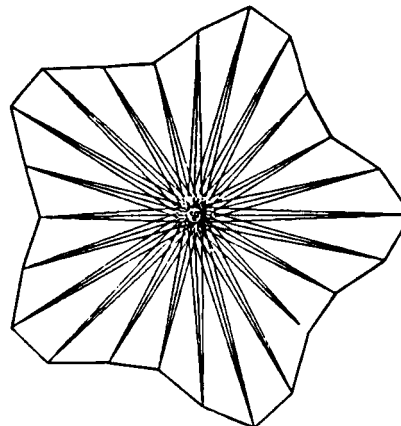
INPLANE HOOP BENDING (N=3)



INPLANE HOOP BENDING (N=4)



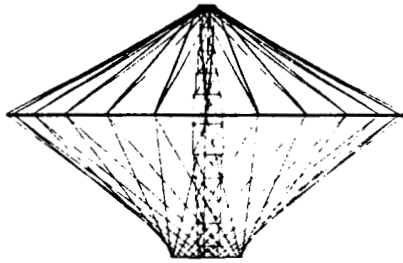
INPLANE HOOP BENDING (N=5)



## FIRST FLEXIBLE FREE-FREE MODES OF 15-M ANTENNA

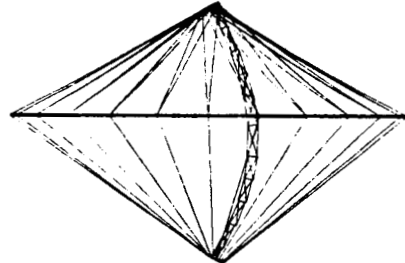
The results presented thus far are highly influenced by the boundary conditions of the test configuration. In space, the antenna would be a free flyer and as such would have free-free boundary conditions. The mode shapes below were generated analytically with free-free conditions. The fundamental flexible mode occurs at 2.47 Hz. This represents an increase by a factor of 36 from the fundamental hoop torsion mode with the test boundary conditions. The next two modes occur at 3.79 and 5.38 Hz. The last figure shows the beginning of a group of hoop out-of-plane bending modes. These modes were not considerably affected by the test boundary conditions.

LOWER COLUMN TORSION



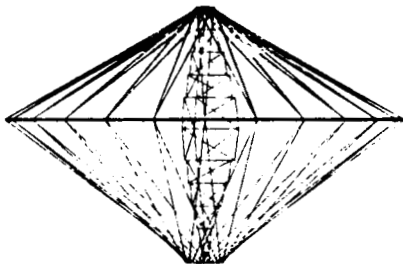
f=2.47

HOOP INPLANE MOTION/COLUMN BENDING



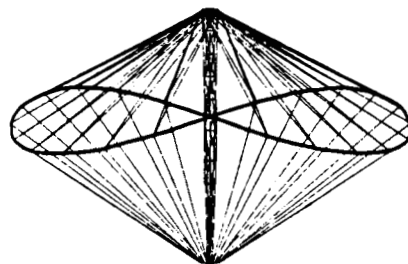
f=3.79

HOOP/COLUMN TORSION



f=5.28

HOOP OUT-OF-PLANE BENDING (N=2)



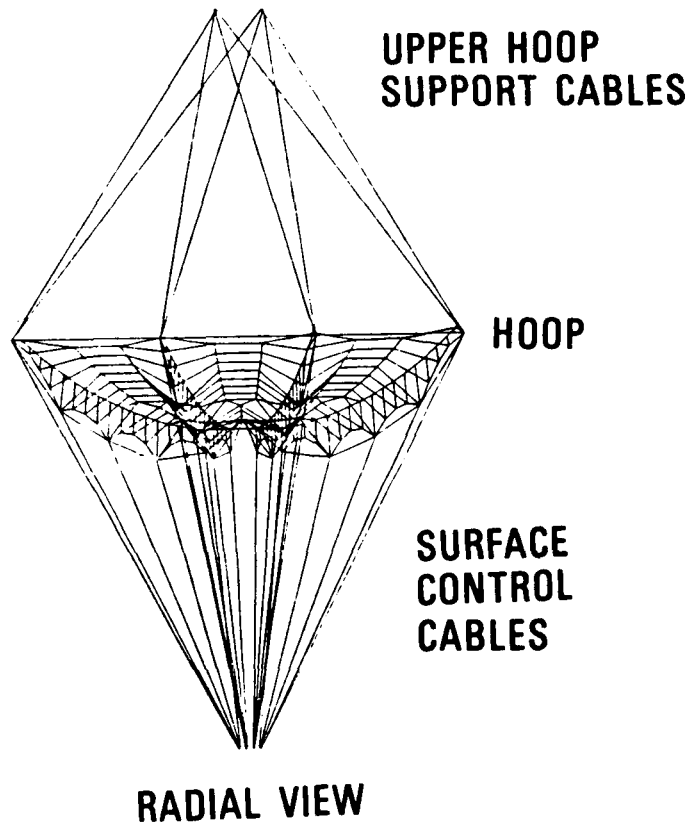
f=6.82

### THREE-GORE SURFACE MODEL

In addition to the test and analysis program to determine the 15-meter antenna dynamic properties without mesh, an extensive test and analysis program is under way to completely characterize the 15-meter model after the surface mesh is installed. The figure below shows the model being used to predict the static response of the 15-meter antenna with surface mesh. This three-gore or 45-degree model is the smallest repeating element of a quad-aperture antenna. The model contains appropriate boundary conditions for rotational symmetry. The model size, as indicated below, is large considering no intermediate grid points are used from joint to joint. The model has been extended to 24 gores as described in the next figure.

- **SMALLEST REPETITIVE ELEMENT FOR QUAD-APERTURE ANTENNA**
- **MODEL SIZE**

317 coordinates  
1097 degrees of freedom  
583 cable elements  
360 membrane elements  
11 beam elements



## TWENTY-FOUR GORE DYNAMIC MODEL WITH SURFACE MESH

The three-gore model has been extended to 24 gores to enable accurate modeling of mass and stiffness asymmetries resulting from fabrication tolerances or other sources. As outlined below, the model will be used to predict the vibration modes with surface mesh. Because of the model detail, the 24-gore model can be used as a benchmark with which one can compare various simplified models. For example, modeling of the antenna with repetitive symmetry will be performed.

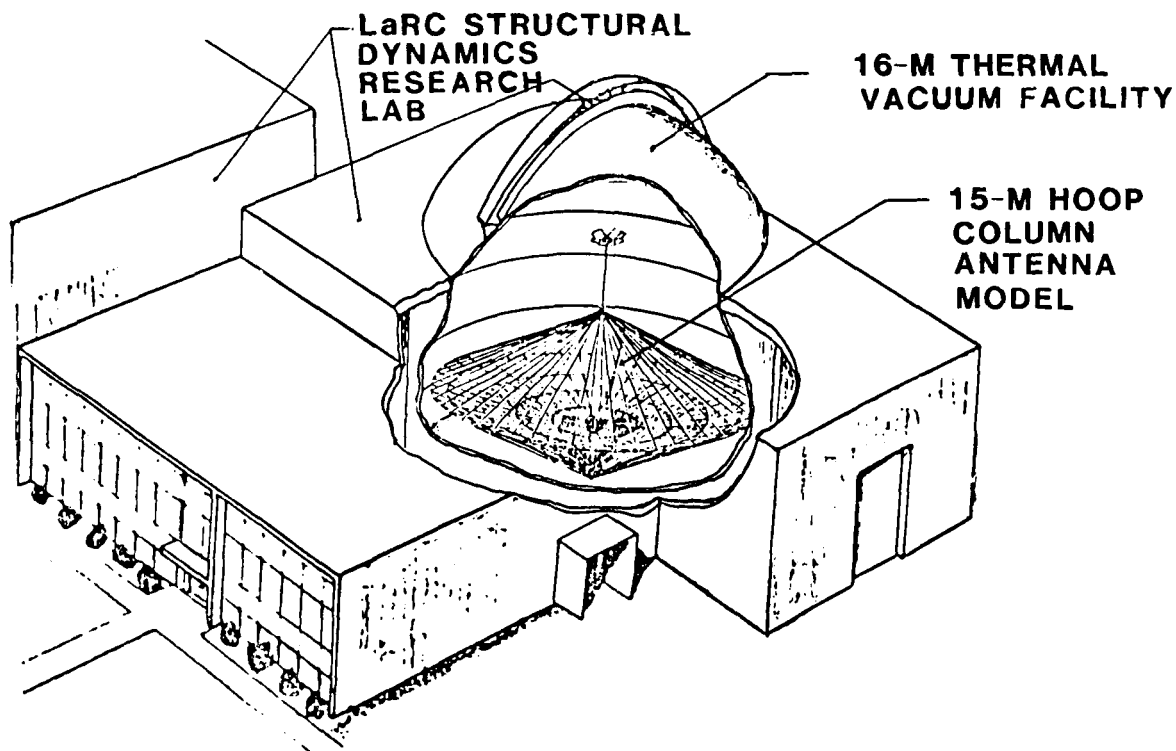
- **ROTATIONAL SYMMETRY NOT ASSUMED TO PERMIT ASYMMETRIC FABRICATION ERROR STUDIES**
- **MODELED WITH FINITE ELEMENTS USING THE EAL ANALYSIS PROGRAM**
  - **2096 Nodes**
  - **8816 Degrees of freedom**
  - **4664 Cable elements**
  - **2880 Two-dimensional membrane elements**
  - **286 Beam elements**
- **MODEL CAPABILITIES INCLUDE:**
  - **Dynamics**
    - **System identification of modes and frequencies**
    - **Transient response analysis**
  - **Statics**
    - **Member length error studies**
    - **Gravity load effects**
    - **Prediction of buckling**
- **PRIMARY PURPOSE OF MODEL IS EXPERIMENT CORRELATION AND TO PROVIDE BENCHMARK FOR COMPARISON WITH SIMPLIFIED MODELS**

## PLANNED DYNAMIC CHARACTERIZATION OF 15-M HOOP/COLUMN MODEL WITH MESH SURFACE

Extensive dynamic testing of the 15-meter model is planned to begin in August, 1985, and to last for about 1 year. These tests will be performed in the 16-meter thermal vacuum chamber at Langley as shown below. Various boundary conditions will be used to study the effects of 1-G support systems. Tests will also be performed in both atmospheric and near-vacuum pressures to study ambient air damping and apparent mass effects on the vibration modes. A parallel analysis program will be conducted to ascertain the degree of model sophistication required to accurately predict the model properties. Transient response tests will be used to verify reduced-order simulation models often proposed in control system designs.

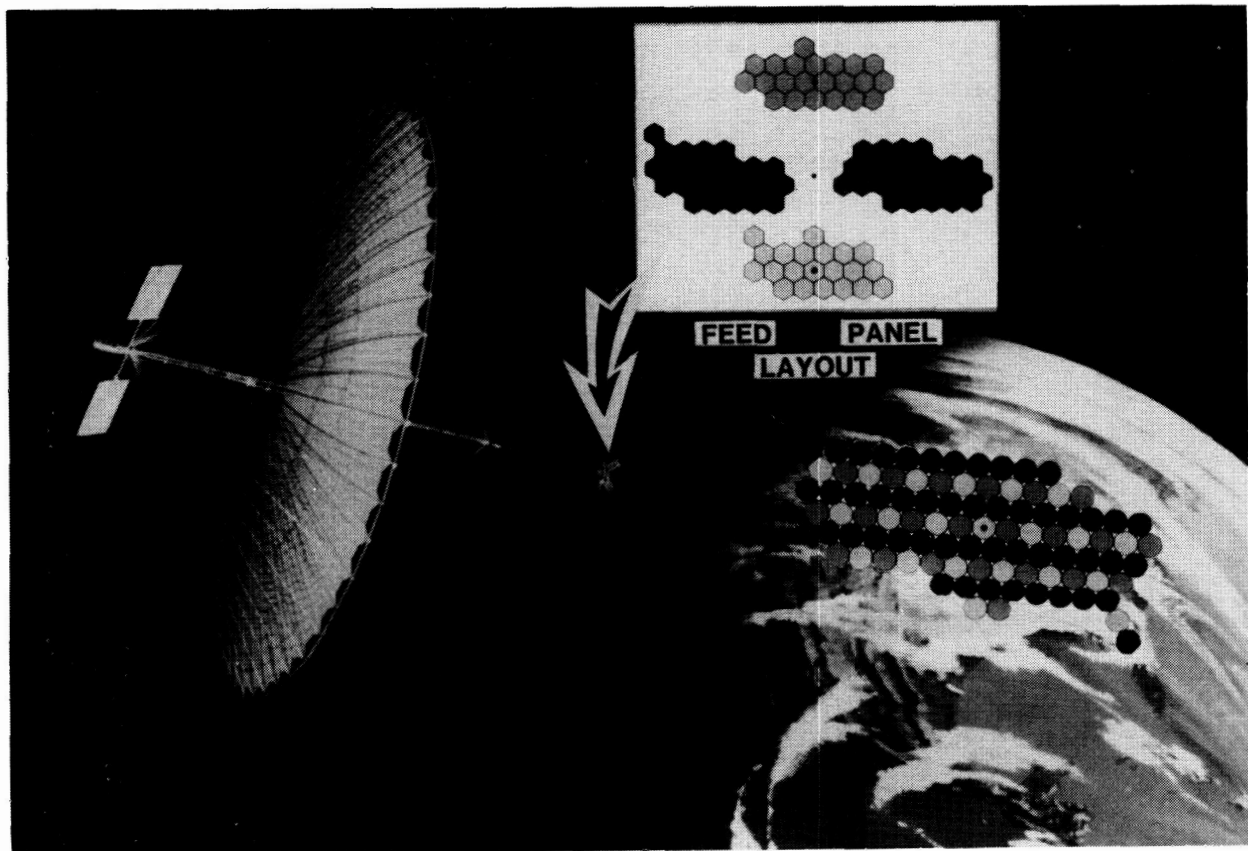
**Modal surveys and free response measurements for system identification**

• **Transient response tests to verify analytical simulation models**



## RADIO FREQUENCY SYSTEMS

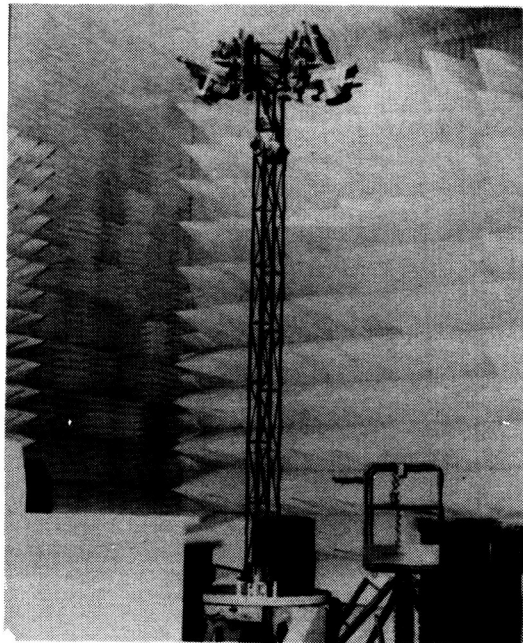
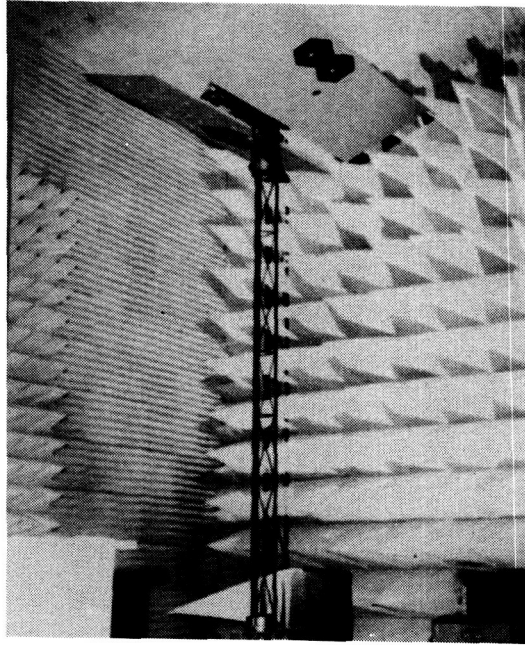
The radio frequency subsystems and plans for near-field testing the 15-meter antenna will now be presented. As indicated earlier, the 15-meter structure will consist of four offset reflectors, and feed systems are being developed by Langley and the Jet Propulsion Laboratory (JPL) to test the performance of multiple apertures (interleaved beams) and single apertures (overlapped beams), respectively, for future multiple-beam missions.





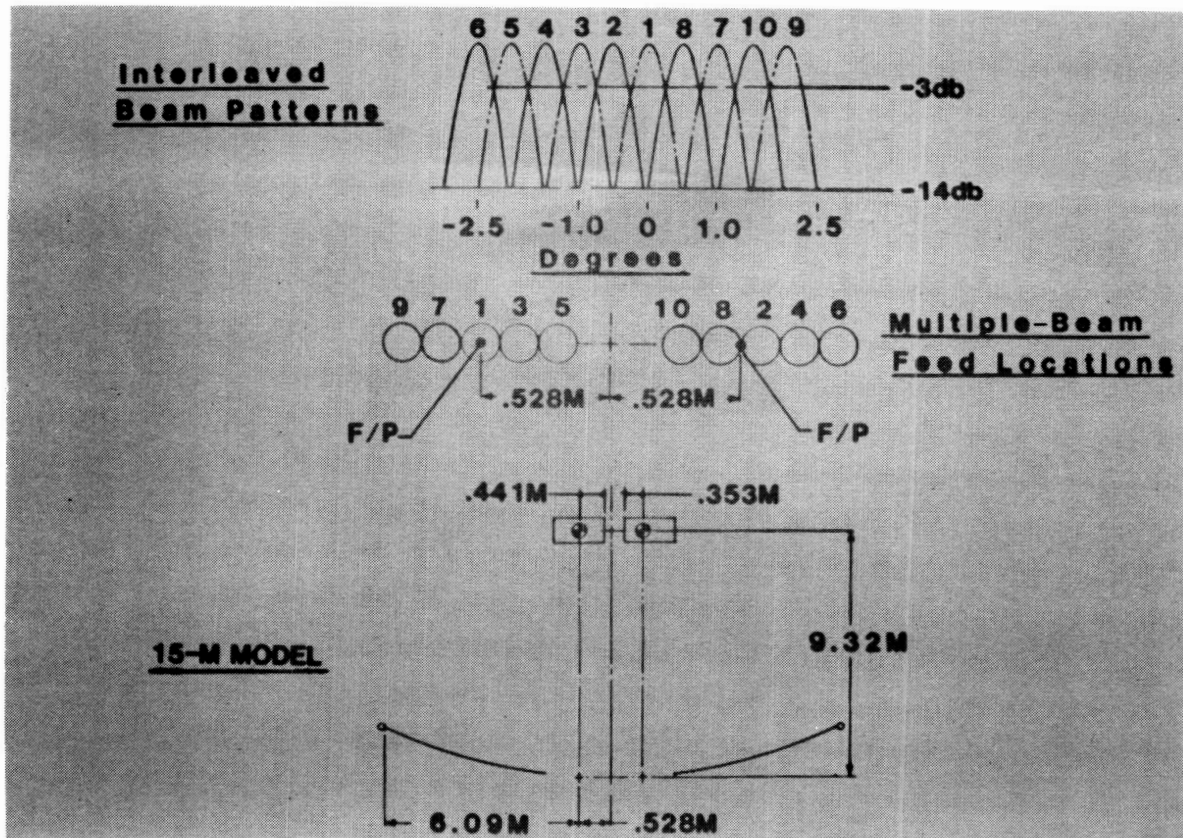
## FEED SYSTEM PANELS FOR THE 15-METER ANTENNA

The feed system panels developed by Langley are shown in the photographs below attached to the rigid-feed support mast. This mast will be attached to the end of the telescoping mast of the 15-meter structure for the antenna tests. Two feed panels will be used to demonstrate beam interleaving using two of the four apertures. The feed panels can be positioned in x, y, and z directions using the remote-controlled positioning system located beneath the feed panels.



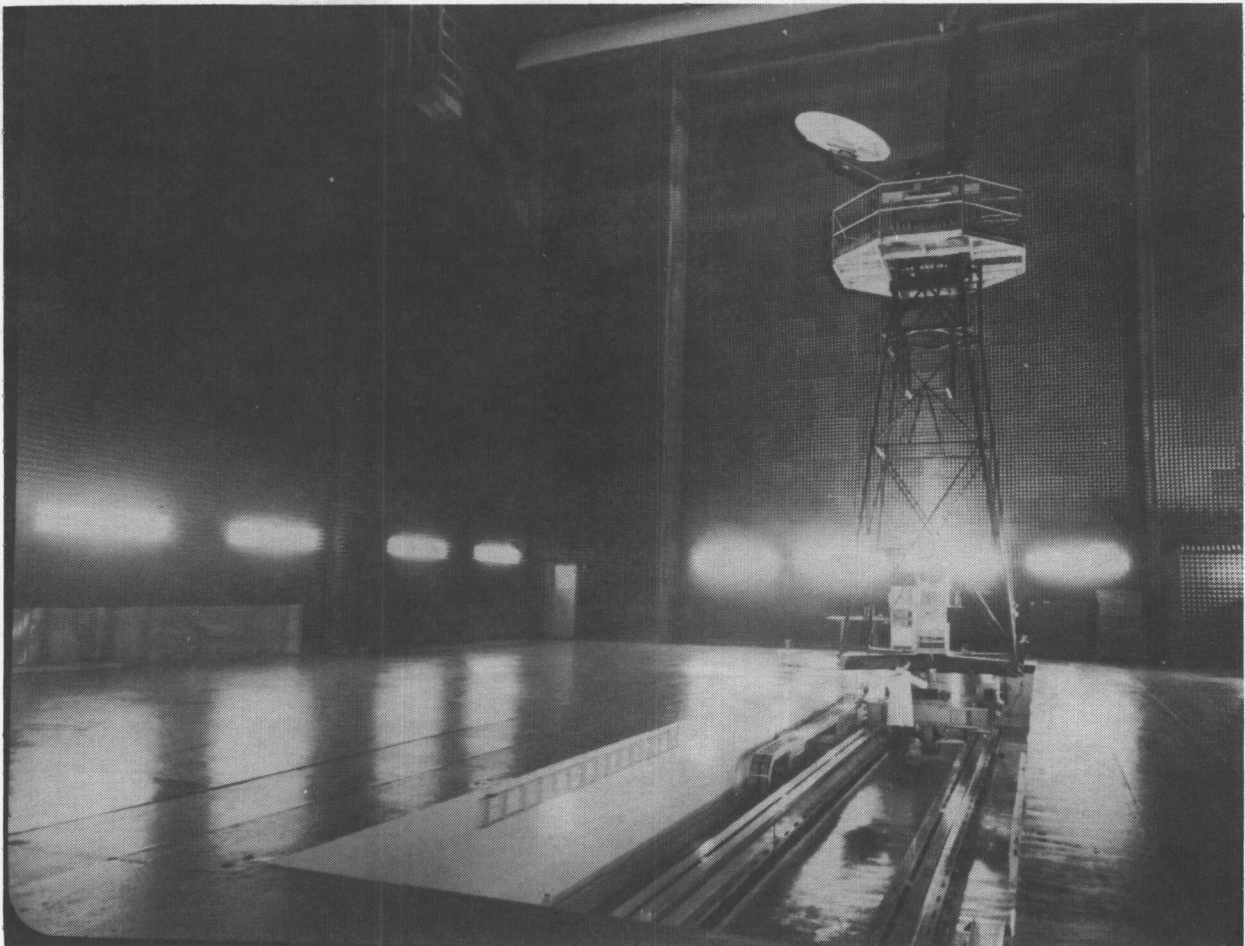
## CONCEPT OF INTERLEAVING BEAMS USING THE 15-METER QUAD-APERTURE ANTENNA

The concept of interleaving beams from the individual apertures is shown in the figure below. A method for interleaving ten beams using two diametrically opposed apertures is depicted. This approach will be tested using the 15-meter antenna during the RF test program.



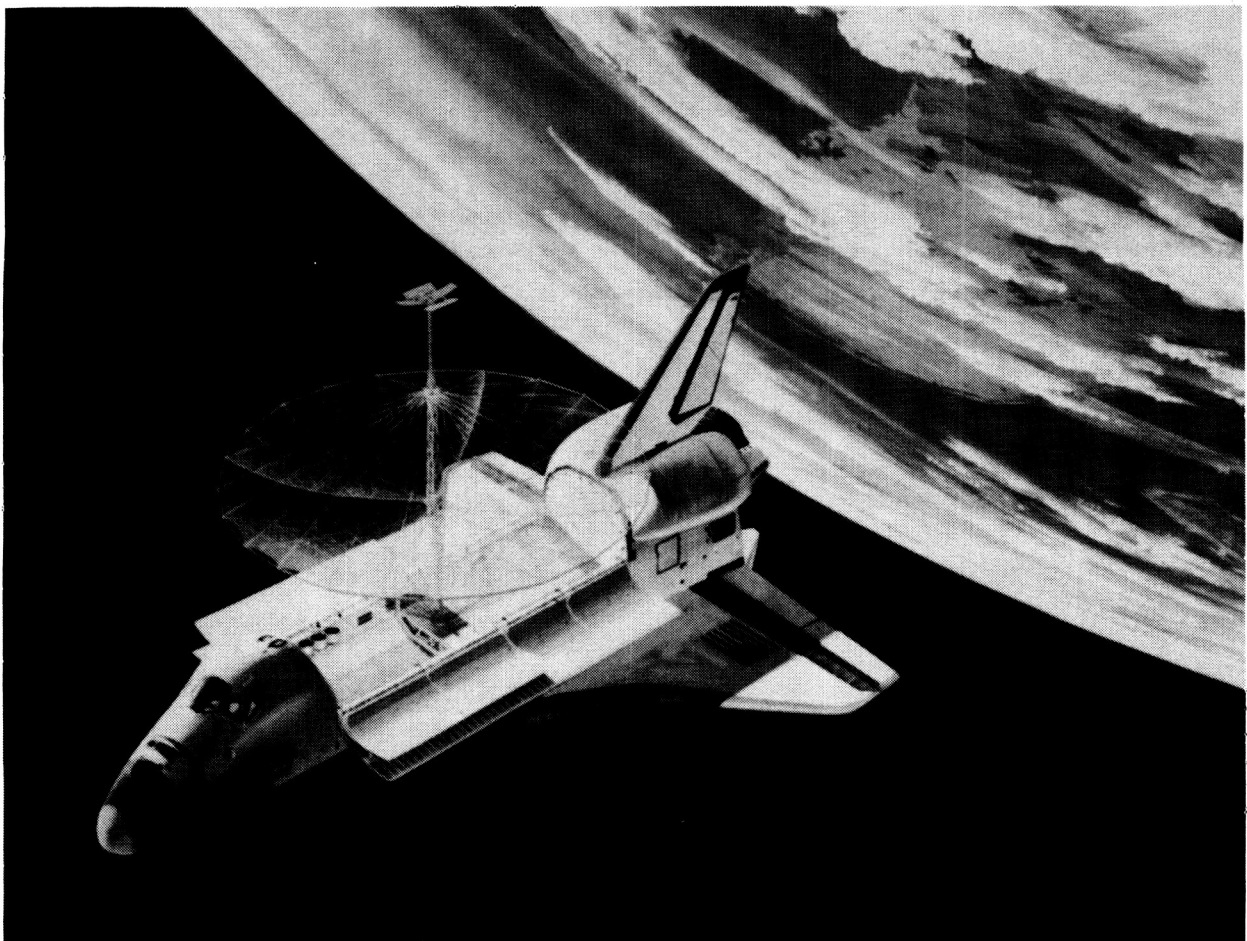
## NEAR-FIELD ANTENNA TEST FACILITY

Plans have been formulated for testing the 15-meter antenna in the Martin Marietta Near-Field Facility if schedules permit. A photograph of the facility is shown below during tests of the Langley/TRW offset-fed Ku-band antenna system. This test proved to be very effective in comparing near-field and far-field measured patterns for precision reflector antennas.



## SHUTTLE-ATTACHED CONFIGURATION FOR PROPOSED FLIGHT TESTS OF THE 15-METER ANTENNA

In conclusion, a photograph of the multiple-aperture 15-meter antenna is shown attached to Shuttle in a proposed flight experiment configuration. This antenna can be deployed in space and then restowed and brought back to Earth for future flight opportunities.



BOX TRUSS DEVELOPMENT

AND

ITS APPLICATIONS

J. V. Coyner

Martin Marietta Denver Aerospace  
Denver, Colorado

Large Space Antenna Systems Technology - 1984  
December 4-6, 1984

## TOPICS FOR DISCUSSION

Since 1977, Martin Marietta Denver Aerospace has aggressively pursued development of deployable structural systems applicable to a wide variety of Shuttle-transportable large space system requirements. This effort has focused on the deployable box truss, mechanisms and materials development, mesh reflector design and fabrication, gate frame truss design and fabrication, and offset-fed antenna design and analysis.

Figure 1 lists the activities that will be discussed in this paper.

- o BOX TRUSS DESIGN
- o MECHANISM AND MATERIALS DEVELOPMENT
  - METAL MATRIX COMPOSITE COMPONENTS
  - PRECISION JOINTS
  - ENHANCED PASSIVE DAMPING DESIGNS
- o MESH REFLECTOR DEVELOPMENT
- o GATE FRAME TRUSS FOR SOLAR ARRAYS
- o INTEGRATED OFFSET-FED ANTENNA SYSTEM
  - 15-METER SPINNING RADIOMETER
  - 60-X 120-METER PUSH BROOM RADIOMETER

Figure 1

## SUMMARY OF LSS ACTIVITY

Each year significant steps were taken in the maturity of the box truss design and the understanding of the supporting analysis. Figure 2 summarizes the evolution of the deployable box truss and related technology activities. During 1977 and 1978, the emphasis was placed on design and analytical verification of the box truss structure performance. During 1979, 1980, and 1981, design refinements and hardware fabrication were directed towards GFRP integration with primary emphasis on low cost. This activity culminated in the fabrication and demonstration of the 4.6-meter cube. During 1982, a full-scale prototype of a gate frame truss was fabricated and tested. Also, a mesh test model was fabricated to validate the mesh reflector analytical tools and to demonstrate fabrication techniques. During 1983 and 1984, mesh analytical work continued, metal matrix composite development made significant progress, precision joint designs were fabricated and demonstrated, and passive damping augmentation concepts were developed. During 1985, a mesh reflector will be integrated to the 4.6-meter cube, and dynamic testing of a 20-meter truss will be performed.

- 1977
  - O BOX TRUSS DESIGN CONCEIVED ON IR&D
  - O DESIGN DEVELOPED AND ANALYZED ON "ON-ORBIT ASSEMBLY" PROGRAM
  - O SINGLE-FRAME DEMONSTRATION MODEL FABRICATED
- 1978
  - O DESIGN AND FABRICATION OF SINGLE-FRAME PROTOTYPE STRUCTURE (GFRP TUBES AND METALLIC FITTINGS)
- 1979
  - O DESIGN REFINEMENT INTEGRATING LOW-COST GFRP FITTINGS AND MEMBERS
- 1980
  - O DESIGN OF GFRP 4.6-METER BOX TRUSS CUBE
  - O FABRICATION OF ALL COMPONENTS
- 1981
  - O ASSEMBLY AND TEST OF 4.6-METER CUBE
- 1982
  - O MESH MODEL FABRICATION AND TEST
  - O ASSEMBLY AND TEST OF GATE FRAME TRUSS
- 1983
  - O METAL MATRIX COMPONENT DESIGN, FABRICATION, TEST
  - O PRECISION JOINT DESIGN, FABRICATION, TEST
- 1984
  - O METAL MATRIX COMPONENT DESIGN, FABRICATION, TEST
  - O MESH TIE SYSTEM ANALYTICAL DEVELOPMENT
  - O PASSIVE DAMPING COMPONENT DEVELOPMENT
- 1985
  - O MESH INTEGRATION TO 4.6-METER CUBE
  - O DYNAMIC TEST OF STATICALLY DETERMINATE AND INDETERMINATE TRUSSES

Figure 2



## FULL-SCALE PROTOTYPE CUBE

During 1980, the design of each of the box truss components was reviewed and redesigned to achieve maximum weight, cost, and thermal stability while meeting the stowed, deploying, and deployed structure requirements. A prototype was made for each component and tested to verify manufacturing methods (feasibility and tolerance manageability) and stiffness, strength, and weight. By the end of 1980, all components for a full-scale prototype 15-ft, deployable box truss cube were completed and assembly had started. Final assembly was completed in 1981. Figure 3 shows the resulting prototype cube in a deployed and stowed configuration, respectively. Summarized below are the design features of the full-scale prototype cube:

### 4.6m deployable cube

Stows in 0.3m square by 4.6m long (0.15m per module)

- 36 modules (28m x 28m deployed) stow in 1m by 1m by 4.6m

All GFRP except for hinge pins and springs

High performance (high stiffness, low CTE)

Low weight - 27 kg

High accuracy - better than 0.1mm on all axes

50 N diagonal pretension

Exhibits ideal truss characteristics found in all box truss systems

- Purity of load paths, i.e., no bending moments in deployed structure

All components and members fully constrained when stowed

Every corner fitting stabilized by bonded interface to vertical tube

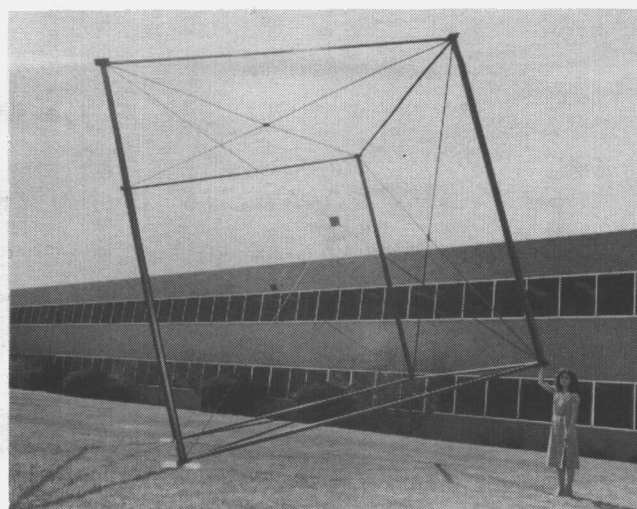
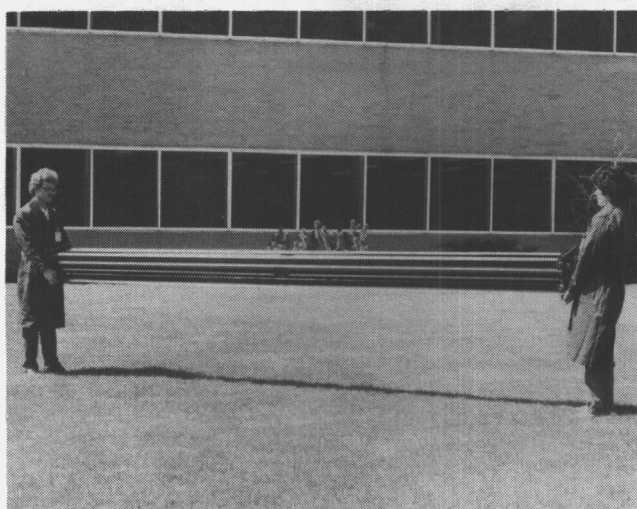


Figure 3



## METAL-MATRIX COMPOSITE COMPONENT DEVELOPMENT

Metal-matrix composites combine some of the best attributes of the resin matrix composites and the conventional metallic materials. Some of their major advantages over Gr/E are high resistance to laser and radiation damage, good thermal and electrical conductivity, no outgassing in the space thermal-vacuum environments and potential for automated fabrication. These composites offer higher specific modulus and a lower coefficient of thermal expansion than conventional metallic alloys. Our applications development in the use of metal-matrix composites is broadening and is reflected in the generation of basic material and design data.

Figure 4 summarizes the materials being developed and the parts being fabricated and tested.

### 0 WHY METAL MATRIX COMPOSITES

- HIGH RESISTANCE TO THERMAL DISTORTION ( ZERO CTE )
- HIGH SPECIFIC STIFFNESS
- HIGH CONDUCTIVITY

### 0 MATERIALS BEING DEVELOPED

- GRAPHITE MAGNESIUM
- GRAPHITE ALUMINUM
- SiC ALUMINUM

### 0 PARTS BEING FABRICATED AND TESTED

- MEMBER END FITTINGS
- TRUSS NODE FITTINGS
- MEMBERS WITH VARIOUS CROSS SECTIONS ( TUBE, SQUARE, CHANNEL, L, ROD)

Figure 4

## Gr/Al and Gr/Mg TRUSS MEMBERS

Continuous reinforced metal-matrix composites are reinforced by long continuous fibers unidirectionally or in crossplied configurations. Among the present systems boron/aluminum composites have been used for the Space Shuttle orbiter and a few other aerospace applications. However, their use has been extremely limited because of poor fabricability. To alleviate this problem, graphite-reinforced aluminum and magnesium alloys were developed and are ready to be used in space structures. Both Gr/Al and Gr/Mg composites offer excellent material properties for space applications; however, only Gr/Mg composites have the potential to achieve zero CTE.

Continuous Gr/Mg and Gr/Al are commonly produced by hot-pressing and diffusion-bonding the precursor wires to the face sheets. Although the process has produced some excellent products, forming complex shapes from flat products could present some material integrity problems. As a result, other processes such as pultrusion have been developed. Unidirectionally reinforced round or other symmetrical cross sections in Gr/Mg and Gr/Al have been successfully produced by pultrusion.

Gr/Mg components can also be produced by casting technology because of the recent development of wettable air-stable coatings. This definitely adds a greater dimension to the fabrication of Gr/Mg structures. Unfortunately, casting technology cannot now be applied to Gr/Al composites because of the lack of a suitable fiber coating.

Figure 5 is an example of Gr/AL pultrusion tube that was fabricated.

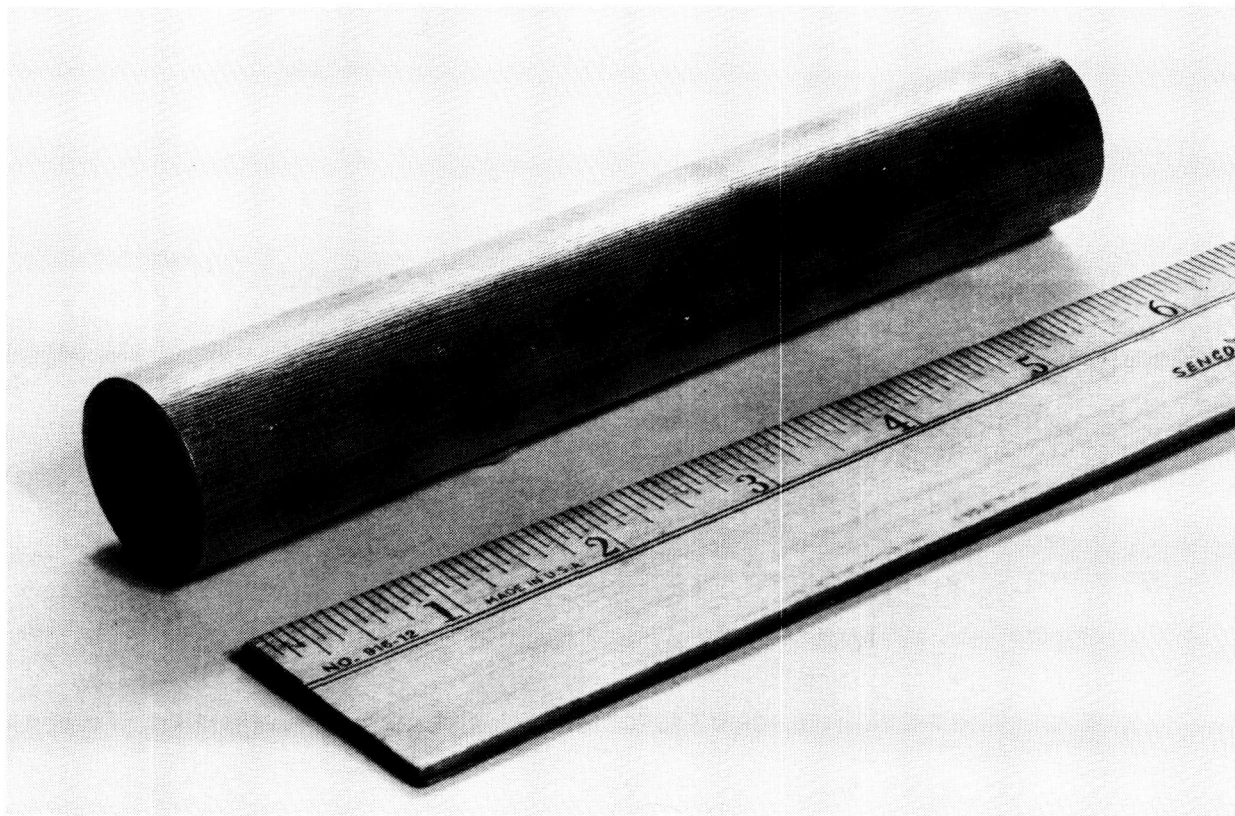


Figure 5

## SiC/Al FITTING DEVELOPMENT

Metal-matrix composites are generally classified by two categories -- discontinuous reinforced, and continuous reinforced. Discontinuous reinforced metal-matrix composites are reinforced by chopped fibers, whiskers or particulates. Most advanced systems in this category are SiC whisker- or particulate-reinforced aluminum and magnesium alloys; of these SiC/Mg offers higher specific stiffness and a slightly lower CTE than SiC/Al. However, SiC/Mg is still regarded as a developmental material and many fabrication questions must be answered before its application. On the other hand, SiC/Al composites are well developed in almost every phase of materials technology, including material properties and primary and secondary fabrication processes.

SiC whisker- or particulate-reinforced aluminum alloys are commonly produced by powder metallurgy techniques. The manufacturing processes have been developed to the point that high-quality products are produced with good interfacial bonds and low hydrogen pickup. Material properties close to the analytically predicted values are being realized.

SiC/Al composites can be fabricated in various shapes using such conventional processes for aluminum alloys as forging, extrusion sheet metal-forming machine, and mechanical joining. The only area of some concern could be the welding technology because porosity is sometimes observed in the fusion zone. Extensive Martin Marietta Aerospace experience in welding SiC/Al has produced welded products of the highest quality.

Figure 6 shows examples of 2 different types of SiC/Al fittings fabricated by Martin Marietta.

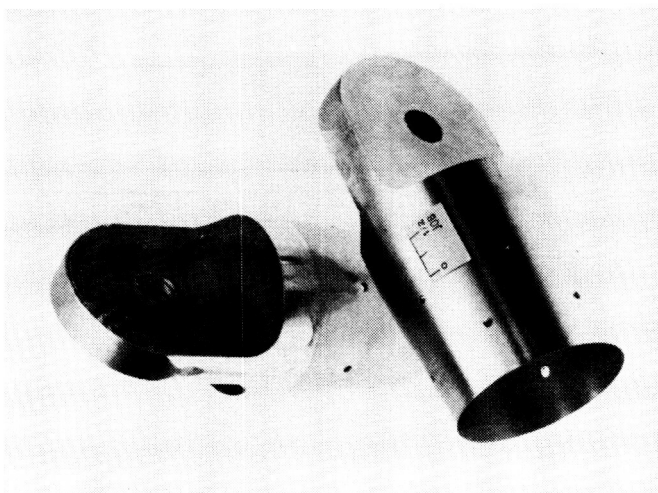
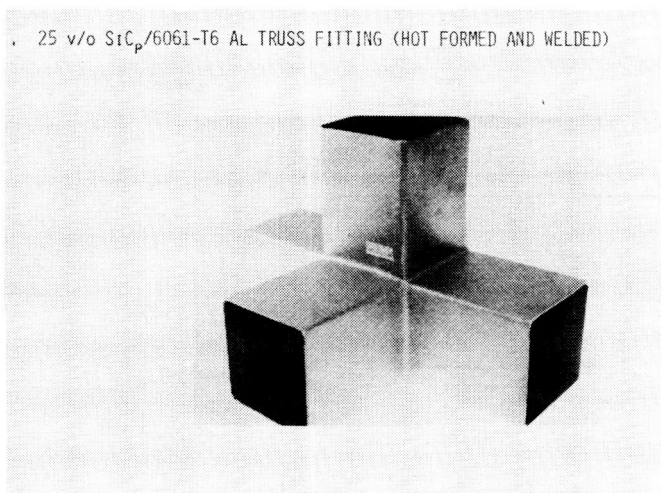


Figure 6

## PRECISION JOINT DESIGN AND FABRICATION

Three types of precision joints were designed, fabricated and tested to demonstrate their function and performance (precision tightening pin joints, precision 180-degree hinged joint and precision sliding joint).

The primary design requirements were:

1. Zero freeplay when in the fully deployed condition
2. Zero, or near-zero, coefficient of thermal expansion (CTE) through the joint
3. Continuity of stiffness through the joint
4. Manufacturing processes amenable to low-cost, low-volume production

Other design considerations included:

1. Long-term material stability in the space environment
2. Damping of deployment and other induced vibration
3. Thermal and electrical conductivity through the joints

Shown in Figure 7 are the design concepts fabricated and tested.

### PRECISION SLIDING JOINT DESIGN

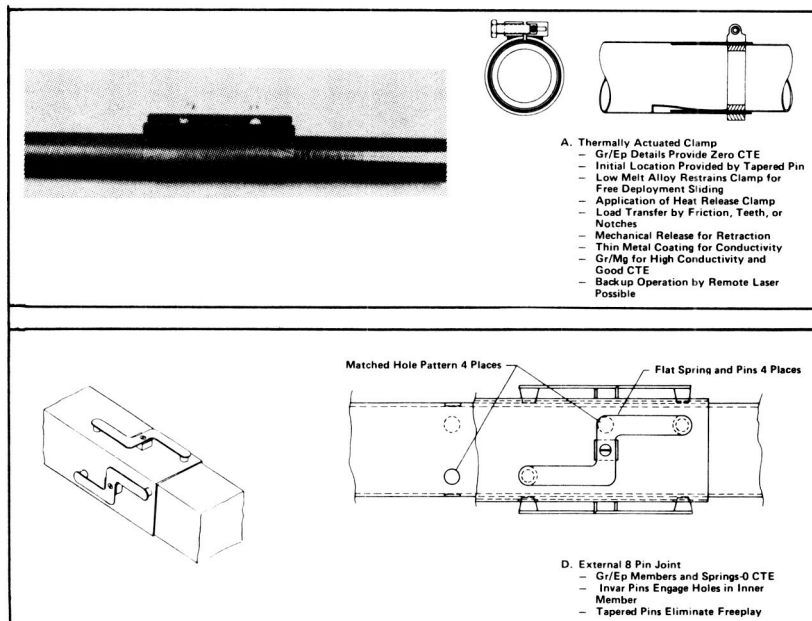
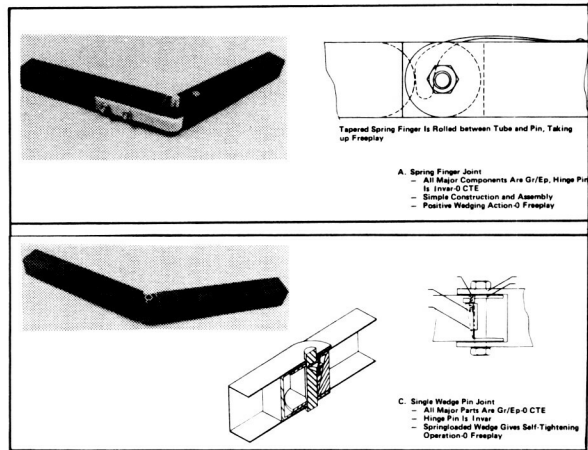


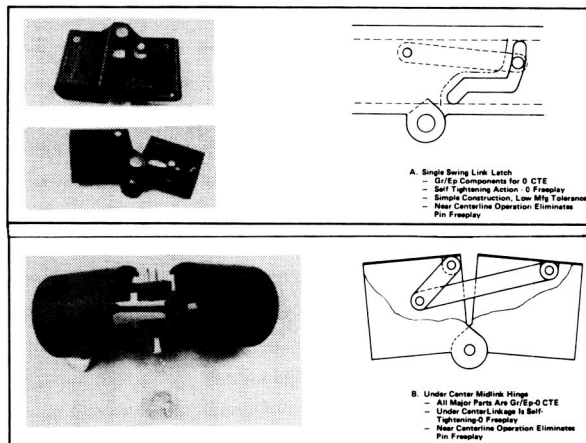
Figure 7

## PRECISION JOINT DESIGN AND FABRICATION (CONTINUED)

### PRECISION TIGHTENING PIN JOINT DESIGN



### PRECISION 180-DEGREE HINGED-JOINT DESIGN



### PRECISION 180-DEGREE HINGED-JOINT DESIGN

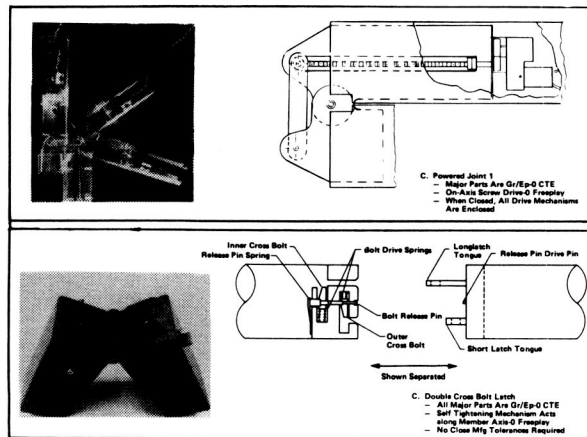


Figure 7 (Concluded)

## ENHANCED PASSIVE DAMPING DESIGNS

Future large space systems will be required to slew rapidly, point accurately, and focus electromagnetic radiation with great dimensional precision while subjected to a variety of environmental and on-board excitations. The success with which these requirements can be met depends largely on system damping (traditionally assumed to be 1% or less). Consequently, elaborate and expensive active control systems may be required to provide additional damping. An alternate means of increasing system damping is to add passive mechanical damping.

The ultimate objective of the Passive and Active Control of Space Structures (PACOSS) program is to develop new and possibly unconventional design procedures to apply viscoelastic damping treatments that, in concert with state-of-the-art active attitude, figure control, active vibration suppression, and other passive damping schemes, can be extended to the development of military large space systems (LSS) with a high level of confidence.

Martin Marietta has constructed two ground test articles being submitted to vibration testing (shown in the left side of Figure 8). The size of the articles relates to a generic large space structure. A damper mechanism is shown in the right side of Figure 8.

The truss articles being tested are called space age tuning forks, and vibrations are created to determine their ability to dampen. The vibration is 1 Hz, and damping is being increased to 3.8% headed toward 6% damping. Eventually, an advanced damping system is expected to function at 10%.

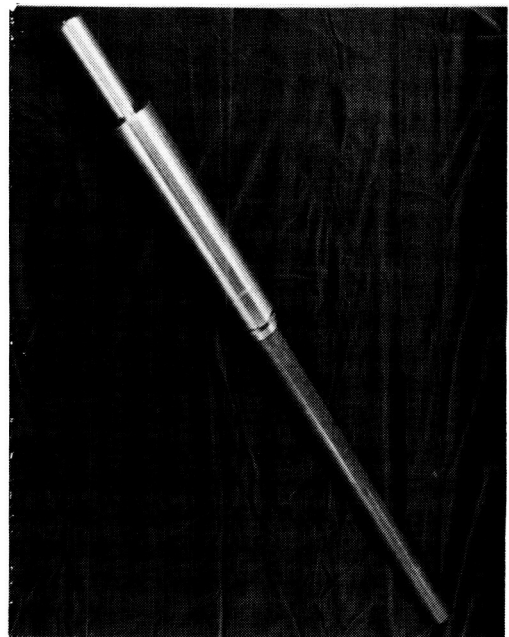
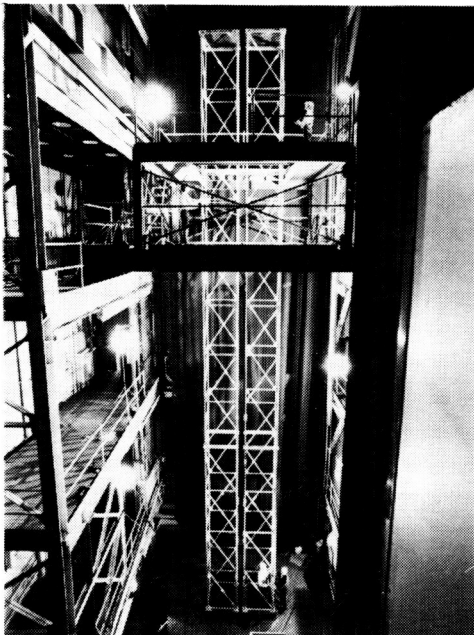


Figure 8

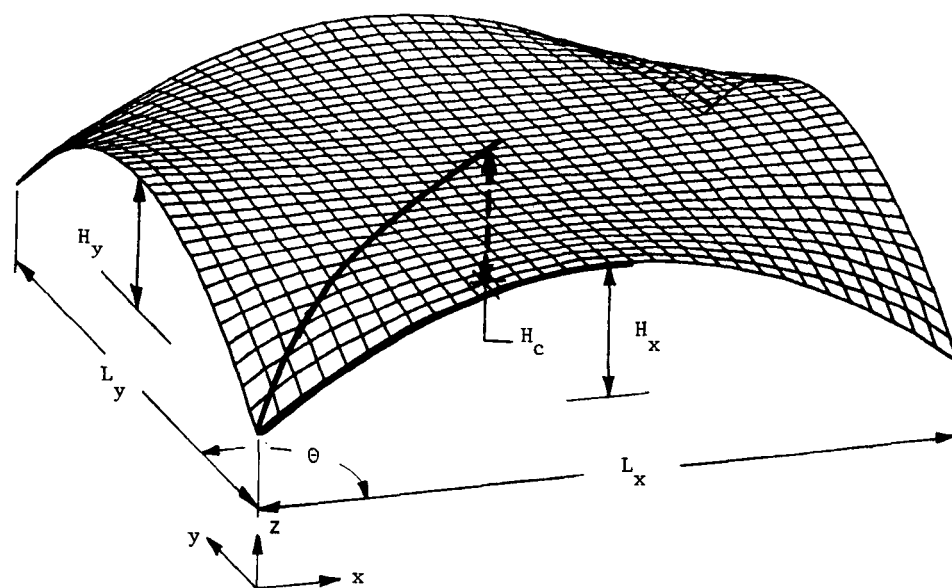
## REFLECTOR MESH ANALYSES

The capability to analyze the response of mesh reflectors supported and shaped by a tie-cord system has been developed. A very accurate reflective surface is vital to the performance of LSS antennas. The present design of the reflective surface uses a gold reflective mesh supported and shaped by a tie-cord system made up of either graphite or quartz.

A user-friendly and cost-effective mesh analysis method was developed that was directed specifically at the LSS reflector design problems. Pre- and post-processors were tailored for LSS configuration to reduce the cost of the analysis. Analysis technique included rapid methods for optimizing a particular design (e.g., permitting the analyst or designer to change material properties such as coefficient of thermal expansion (CTE) to represent on-orbit adjustment techniques. Accurate determination of these various disturbances to the reflective surface geometry required the use of non-linear stress-stiffened finite-element (FE) techniques. Stress stiffening, also known as tension stiffening, is the increase in lateral stiffness of a structural element due to the increase in positive axial strain (tension) in the element. Cost-effective algorithms were developed because existing FE programs, such as ANSYS, which have stress stiffening capabilities, are in such generalized form that the analysis is both time consuming and costly.

Figure 9 shows a typical computer-generated mesh pillow.

### RESULTS MESH SURFACE DESIGN



- MESH PILLOW SHAPE MEASURED FROM MESH PILLOW MODELS FABRICATED UNDER IRAD D-54D
- INPUT TO EMPIRICAL EQUATION
  - TIE CORD SPACING  $L_x$  AND  $L_y$
  - HEIGHT OF PILLOW IN CENTER  $H_c$
  - HEIGHT OF PILLOW AT CENTER OF EACH EDGE  $H_x$  AND  $H_y$
- EMPIRICAL EQUATION FORM

$$(0 \leq \theta \leq 45) Z = F(H_c, H_x, L_x, x, \theta)$$

$$(45 \leq \theta \leq 90) Z = F(H_c, H_y, L_y, y, \theta)$$

Figure 9



## MESH PILLOW TEST MODEL

An IR&D activity was initiated to design and understand a parabolic mesh reflector. This activity included fabrication of mesh models and surface distortion measurements. The shape of the reflective surface using the double-catenary cord system is defined by several factors: mesh tension and compliance, upper surface cord pattern (spacing), tension and stiffness, drop-cord stiffness and length, rear-cord stiffness and length, and local radius of curvature. Further, geometric saddling effects (pillowing) due to biaxial tensioned mesh and the upper surface cord pattern cause local deformations. Figure 10 (upper) shows a scale test model of a reflector surface. Measurements were made to determine pillow shape versus mesh tension and cord tension. When the panel's shape is duplicated and scaled to a mesh surface on a 15-meter reflector with an 11.94-meter focal length and average drop-cord spacing of 42.8 cm, the rms surface errors (best-fit mesh saddles relative to the ideal parabola) are 0.020 cm, and the worst-case deflections (drop-cord attachment points) are 0.067 cm behind the ideal parabola. Assuming  $1/40$  of a wavelength can be assigned to rms mesh distortions, the mesh surface design proposed would be appropriate for frequencies of 11 GHz. A smaller mesh test model (Figure 10, lower) was used to determine the optimum surface-cord tension for a mesh tie system.

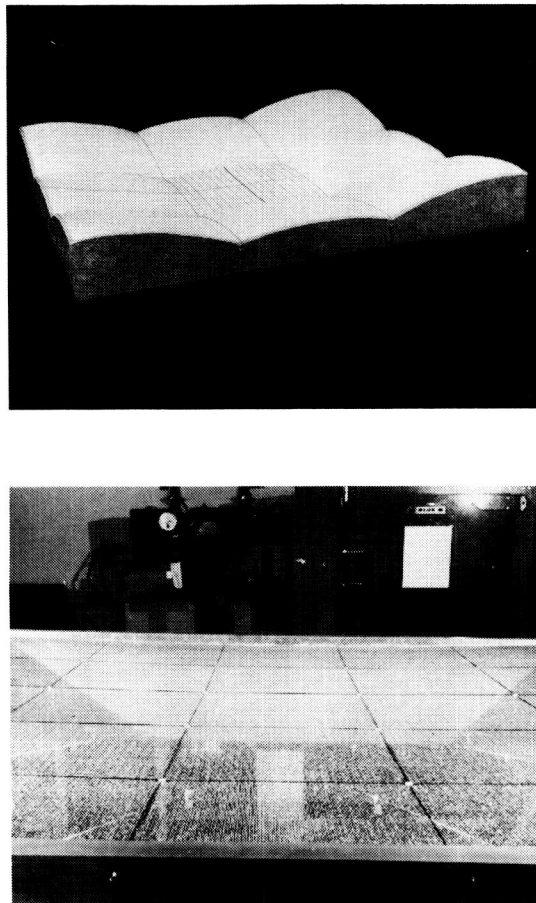


Figure 10



## GATE FRAME TRUSS FOR SOLAR ARRAYS

The gate frame truss (shown in Figure 11) that was developed to provide deployment and support for antenna array panels also has excellent potential for supporting solar array panels and blankets. The gate frame truss design was applied to improving the dynamic characteristics of the 25-kw NASA solar array and to provide a large solar array that can be packaged in one orbiter. The results of the study showed that for the 25-kw solar array, by replacing the lattice mast with a gate frame truss, a factor of 8 improvement in dynamics is realized. For the large solar array design, a 600-ft x 50-ft solar array was achieved in a single orbiter. This provides a 300-kw solar array assuming 10 watts/ft<sup>2</sup> power output. The 300-kw solar array also had the necessary volume and mass available in the orbiter for all subsystems to provide a complete free-flyer spacecraft.

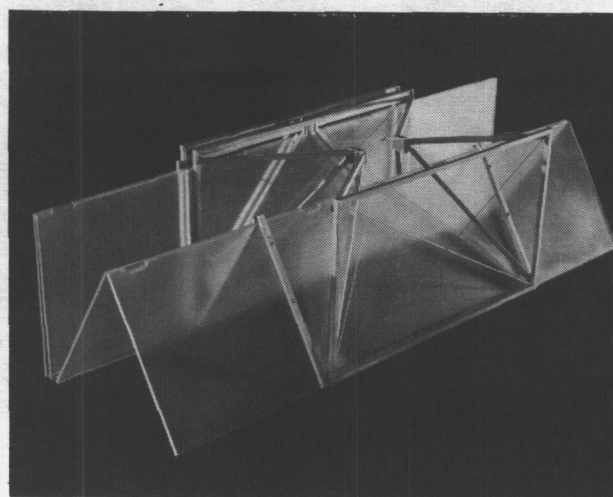
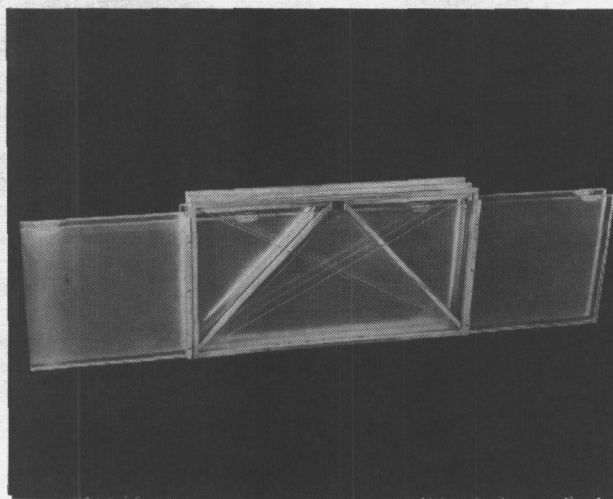


Figure 11

## FULL-SCALE GATE FRAME TRUSS MODEL

Figure 12 shows the full-scale single-box prototype of a gate frame truss that was fabricated and tested.

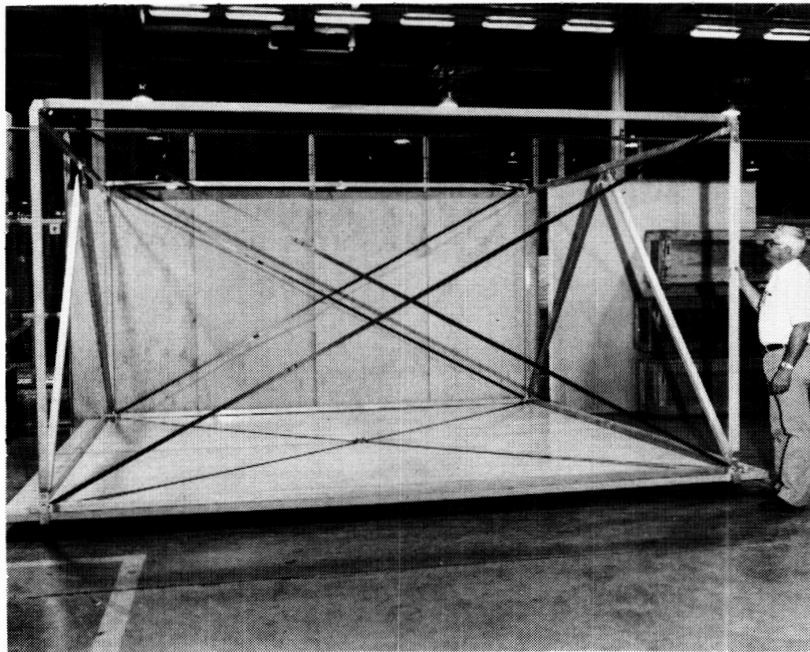
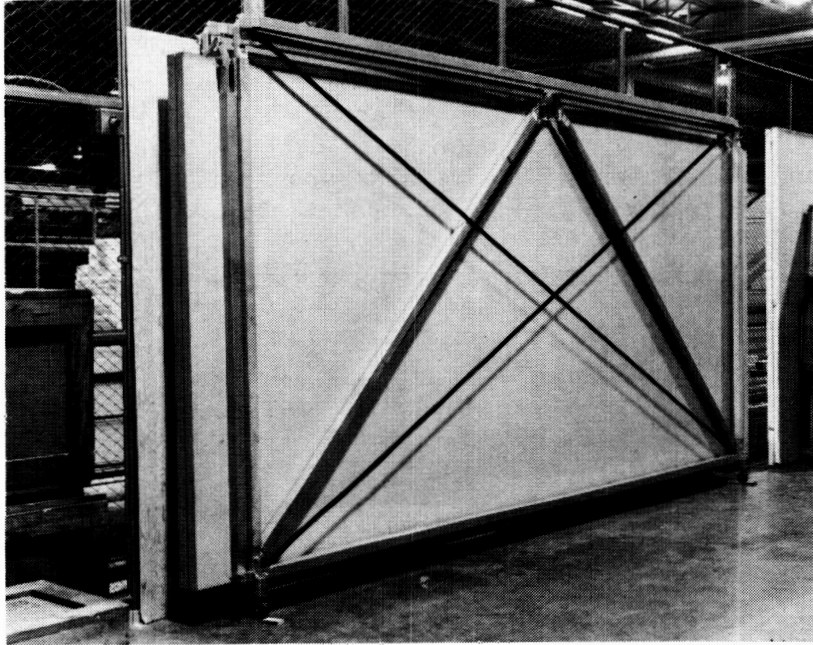


Figure 12

## 15-METER BOX TRUSS REFLECTOR WITH INTEGRATED FEED MAST\*

A unique deployable feed mast has been developed for the offset feed space deployable antenna. The novel feature of this design is that it uses an extension of the reflector truss structure rather than adding appendages. The design features efficient stowage, simple integration to the reflector structure, excellent thermal stability, light weight, and very high stiffness and dynamic stability. These features are achieved by using the efficiency and features of a deep truss structure. Previous offset feed masts were appendages added to the reflector structure and had less efficient packaging, more difficult integration, and substantially lower dynamic stability. Because of the high strength and stiffness, this mast can easily accommodate the more complicated and massive advanced feeds (e.g., line feeds, array feeds, and multi-frequency multi-beam feeds). A study was performed which required a 15-meter antenna with a deployed structural frequency of 12 Hz. This was easily achieved with the integrated offset feed mast. The results are summarized in Figure 13.

---

\* Work performed under Contract NAS5-26496.

### ANTENNA PERFORMANCE SUMMARY

O REFLECTOR DIAMETER, M	15.0
O FOCAL LENGTH, M	11.94
O REFLECTOR AND FEED SUPPORT MAST, KG	400.0
O FEED MASS ALLOCATION, KG	27.1
O BALLAST MASS, KG	22.7
O DEPLOYED FREQUENCY, Hz	
MODE 1	12.35
MODE 2	12.75
MODE 3	13.19
O STOWED ENVELOPE, M	3.84 DIA X 4.47
O STOWED FREQUENCY, Hz	17.2
O SURFACE ACCURACY (RMS) WORST-CASE, CM	0.097
O FEED LOCATION ACCURACY (AXIAL), CM	0.024
(CENTRIFUGAL CORRECTED)(LATERAL), CM	0.051

Figure 13

## DEPLOYMENT SEQUENCE

The structure is deployed in a controlled sequence of steps. Feed beams are deployed one cube at a time, and trusses are deployed one row of cubes at a time. In the latter case, the steps are accomplished in a preselected sequence with flat, cylindrical, and parabolic trusses, and virtually any beam shape.

As shown in Figures 14 and 15, the feed mast flips up first, after which the boxes on either side of the super box deploy outward. The bays on either side of the middle-deployed three are then deployed. Following this sequence, an entire row of five bays is deployed outward away from the feed mast. This is followed by each row deploying outward until the antenna support structure is fully self-deployed. The feed mast will then deploy its three boxes upward for the completion of the entire sequence. The deployment is controlled by latches between the cube-corner fittings. These latches release by remote control in proper sequence, initiating deployment of each section of the antenna support structure. The sequential nature of the deployment energy is an incremental manner, thereby reducing the possibility of producing structural failure in the deploying truss.

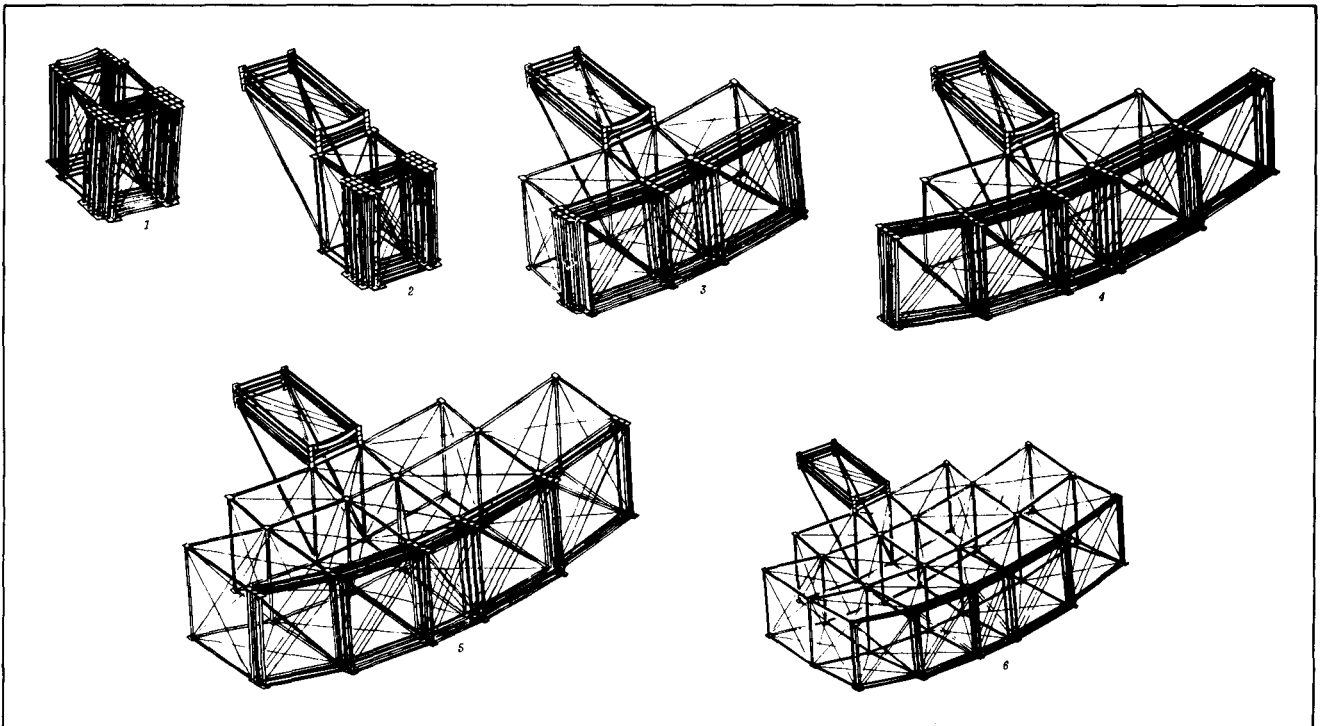


Figure 14

## DEPLOYMENT SEQUENCE - COMPLETION

Figure 15 shows the completion of the reflector deployment and the full feed mast deployment. Total deployment of the reflector and feed mast (10 steps) takes approximately 5 minutes.

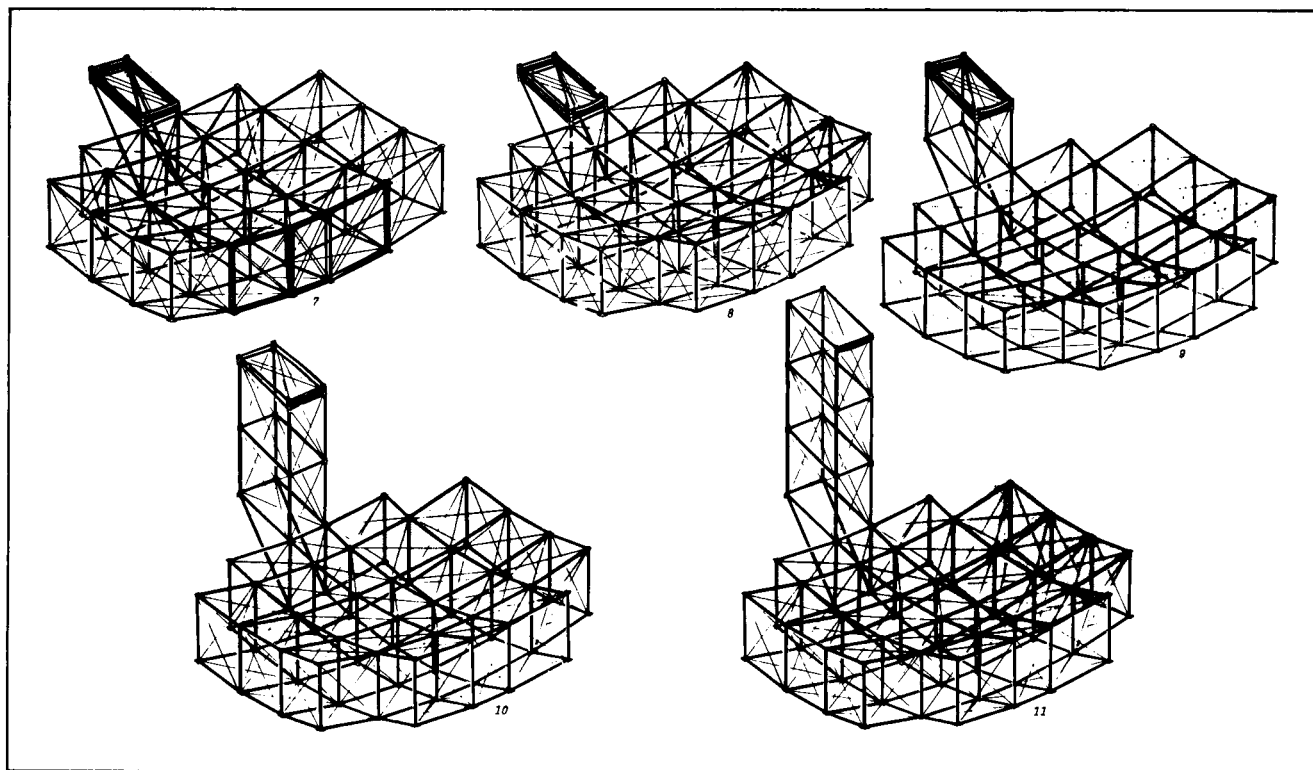


Figure 15

## 60- BY 120-METER RADIOMETER SPACECRAFT\*

The 60- by 120-m Earth observation spacecraft (EOS) shown in Figure 16 is designed using the deployable box truss structure to form both the parabolic dish and feed mast. The structure easily stows within the orbiter bay. The 4-bay by 8-bay antenna support structure has an extremely high stiffness-to-weight ratio. The structure is made thermally stable by using low coefficient of thermal expansion (CTE) graphite/epoxy composite layups. The dynamic stability created by integration of the feed mast and antenna support structure is the basis for the high 1.08-Hz fundamental frequency of this structure. The key feature of this unique design is that the feed support mast is an extension of the reflector truss structure rather than an added appendage. This design features efficient stowage, simple integration with the reflector structure, excellent thermal stability, light weight, and very high stiffness and dynamic stability. These features are directly attributable to the efficiency and features of a deep truss structure.

---

\* Work performed under Contract NAS1-16756.

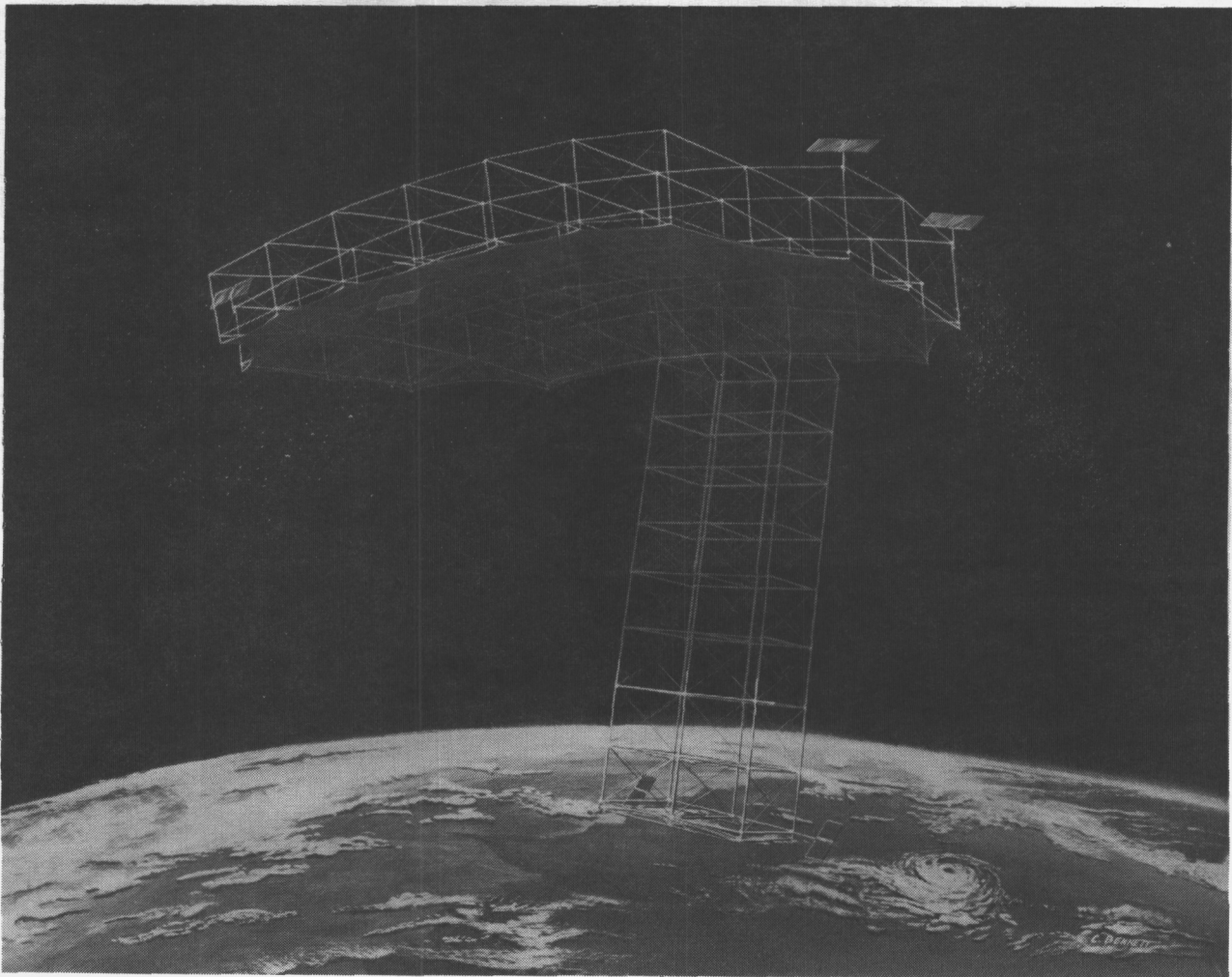


Figure 16

## RADIOMETER SATELLITE SUBSYSTEM SUMMARY

Figure 17 summarizes the system and subsystem performance for the EOS radiometer satellite. The results indicate that the integrated offset mast box truss design produces a rigid and stable base for the large microwave radiometer and its ancillary sensors and subsystems. Higher structural frequencies reduce the potential for control instabilities and ensure that the dynamic response to the environmental forcing functions will be relatively small.

### STRUCTURE

- 120M X 60M OFFSET LINE FED RADIOMETER
- 30M FEED ARC BOOM LOCATED 116.1M ABOVE SURFACE ON THE FOCAL AXIS
- BOX TRUSS, 15M BOXES SKEWED TO MEET PARABOLIC SHAPE (VERTICALS ALWAYS PARALLEL)
- STRUCTURE IS PARABOLIC IN BOTH DIRECTIONS - PARABOLIC CIRCULAR SHAPE ACHIEVED WITH STANDOFFS
- GRAPHITE MEMBERS AND CORDS
- STOWED VOLUME 4.25M X 17.8M
- SPHERICAL RADIUS 234.8
- TOTAL SYSTEM MASS 7635 KG
- FUNDAMENTAL DYNAMIC MODE 1.09 HZ

Frequency, GHz	Ground Resolution, km		Maximum No. Horns	Swathwidth, km
	Optimistic	Conservative		
1.4	2.95	14.75	58	173
5.5	0.88	4.5	90	350
10.68	0.41	2.06	88	18

- GOLD-PLATED MOLYBDENUM TRICOT KNIT MESH, 5.5 ENDS PER CM - ON 2M STANDOFFS
- F/D = 2, 58M EFFECTIVE APERTURE

Figure 17

## MASS PROPERTIES FOR EOS SPACECRAFT

Figure 18 summarizes the mass properties of the EOS spacecraft. Notice that the total structural weight (60-120m reflector and 116m feed mast) was only 2769 kg. The structure supported 4866 kg of payload and still had excellent dynamic characteristics.

### DYNAMIC ANALYSIS

Subsystem	Unit	Mass, kg/Unit	Total, kg
Feed Boom System	1	717	717
Electronics (GN&C, Communications & Data Processing)	1	110	110
Atmospheric Sounding Radar	1	70	70
Mesh and Tie System	6750 m <sup>2</sup>	0.044	297
Science Pallet (SAR & Structure)	1	189	189
Twin PPTs	4	84	336
Single PPT	4	44	176
Power			
- Solar Panels	6	50	300
- Battery Packs	6	90	540
Orbit Transfer System			
- Inboard Propulsion System	2	325	650
- Outboard Propulsion System	2	118	236
Slewing Propulsion System	4	316	1265
<b>Total Subsystem Mass</b>			<b>4866</b>
<b>Structural System</b>			
Cube Corner Fitting			
- Full	67	0.479	32
- 3/4	52	0.332	17
- 1/2	20	0.222	4
Midlink Hinge	231	0.452	104
Mesh Standoff	42	0.8976	38
Structural Members			2574
<b>Total Structure Mass</b>			<b>2769</b>
<b>Total Spacecraft Mass*</b>			<b>7635</b>

\*With slewing and orbit transfer.

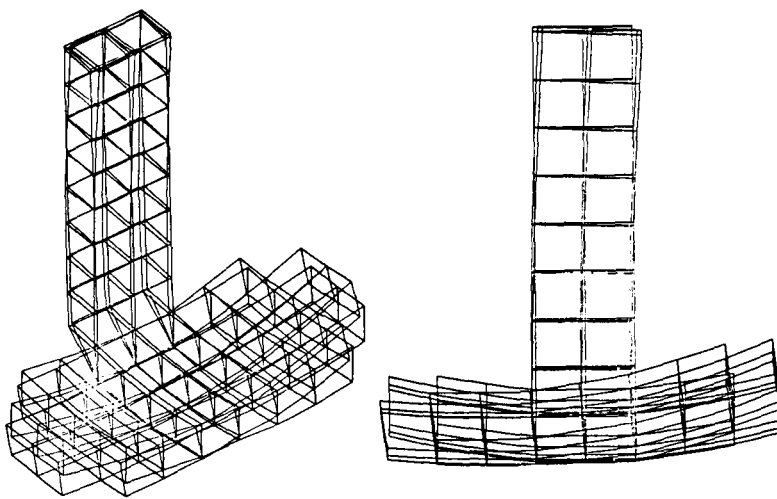
- MASSES OF VARIOUS SUBSYSTEMS AND STRUCTURAL COMPONENTS WERE LUMPED AT THE NODES
- MIDLINK HINGES, FEED BEAM, PROPELLANT MASSES WERE DISTRIBUTED ALONG THEIR RESPECTIVE MEMBERS
- THREE MASS CASES WERE ANALYZED FOR EOS

Figure 18



## DYNAMIC ANALYSIS OF EOS SPACECRAFT

Figure 19 summarizes the dynamic performance of the EOS spacecraft. The fundamental frequency was 1 Hz which is 10 to 1000 times higher than other types of offset-fed parabolic antenna systems of similar size.



- FIRST MODE SHAPE (1.09 HZ) OF EOS W/O SLEWING OR ORBIT TRANSFER PROPELLANT
- BY MAXIMIZING STIFFNESS, THE CONTROL SYSTEM CAN BE SIMPLIFIED

Mode	Mass, kg		
	Without Slewing/ Orbit Transfer, Hz	With Slewing/ Orbit Transfer, Hz	With Slewing/ Orbit Transfer, Hz
1	1.09	0.911	0.711
2	1.13	0.963	0.736
3	1.14	0.969	0.766
4	1.32	0.972	0.782
5	1.38	0.990	0.844
6	1.39	0.998	0.900
MASS	5547	6812	7635

Figure 19

**Page intentionally left blank**

RECENT ADVANCEMENT IN GEO TRUSS REFLECTOR CONCEPT<sup>\*</sup>

J. A. Fager  
General Dynamics Convair  
San Diego, California

Large Space Antenna Systems Technology - 1984  
December 4-6, 1984

<sup>\*</sup>Paper unavailable at time of publication.

**Page intentionally left blank**

SYNCHRONOUSLY DEPLOYABLE TETRAHEDRAL TRUSS REFLECTOR

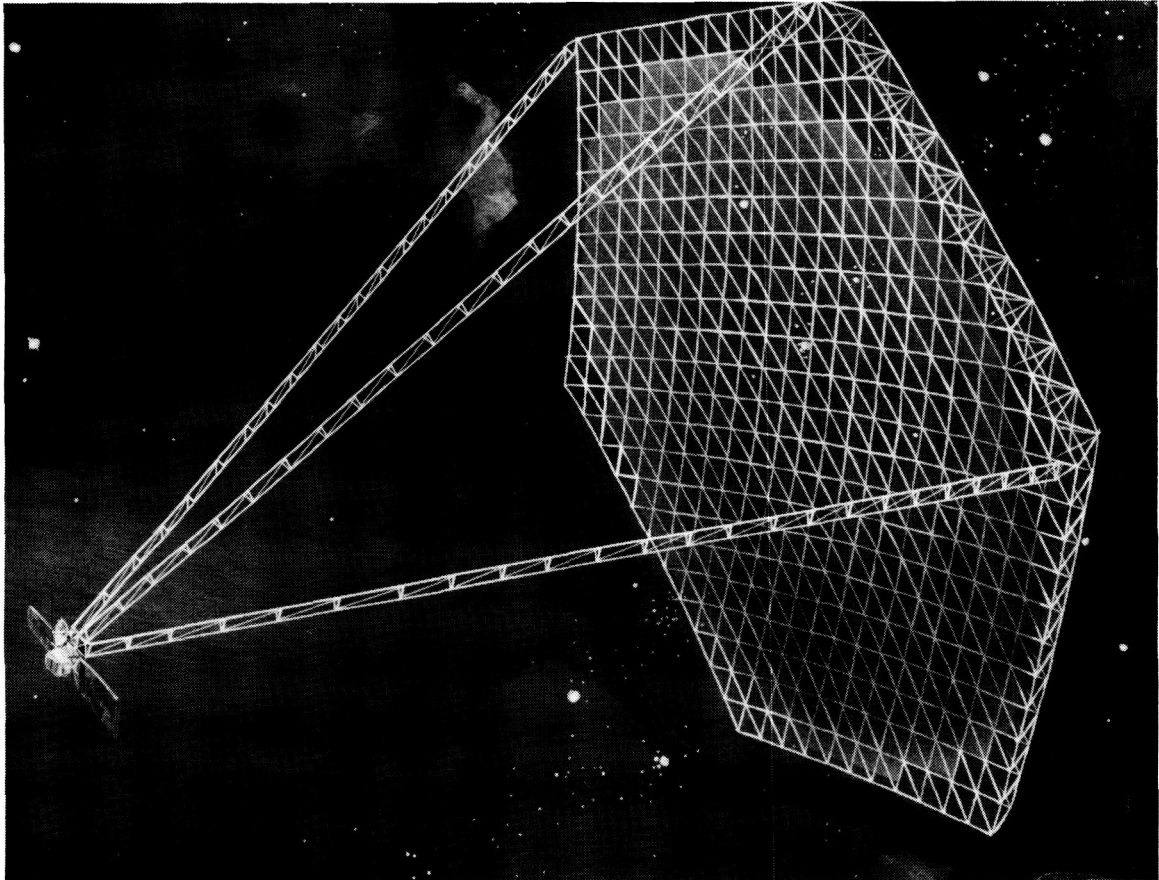
H. G. Bush  
C. L. Herstrom, and  
P. A. Stein  
NASA Langley Research Center  
Hampton, Virginia

R. R. Johnson  
Lockheed Missiles and Space Company  
Sunnyvale, California

Large Space Antenna Systems Technology - 1984  
December 4-6, 1984

## SYNCHRONOUSLY DEPLOYABLE TRUSS REFLECTOR

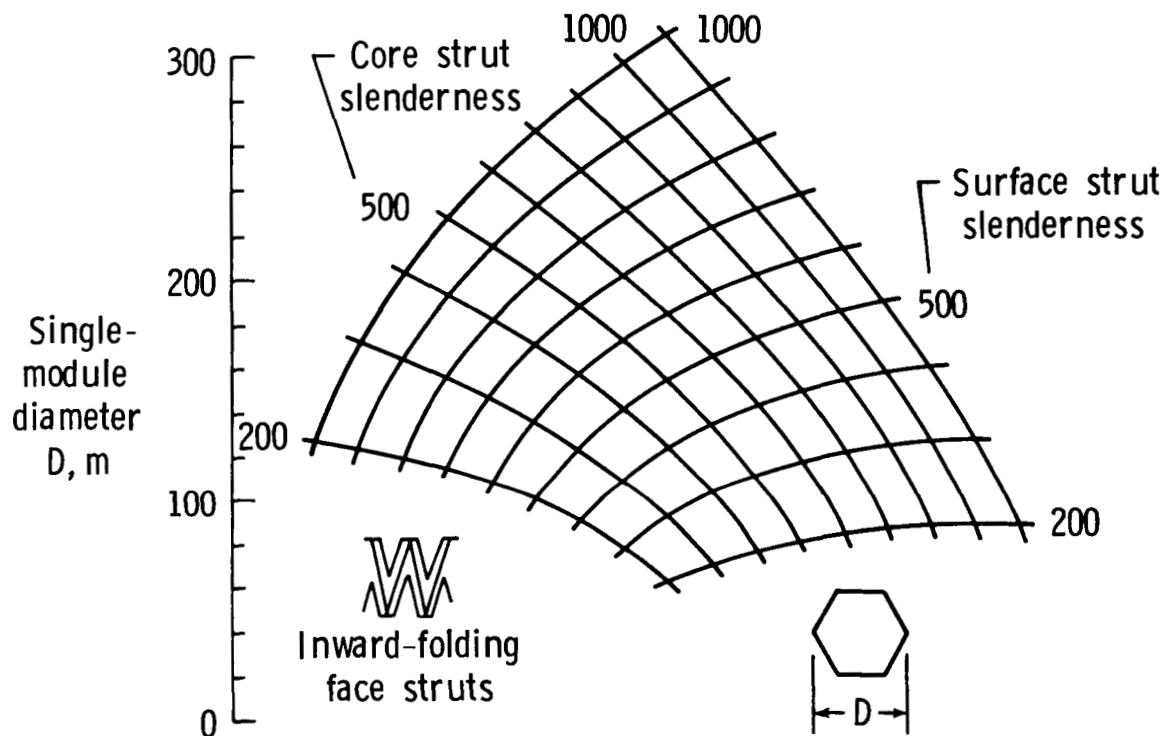
Various concepts have been examined for large antennas. Two examples of such concepts which have been extensively investigated are described in detail in references 1 and 2. Practical considerations limit these concepts to apertures of approximately 50 meters. For apertures above 50 meters, the high structural stiffness and compact packaging of the tetrahedral truss make this concept an attractive candidate for the reflector support structure. This paper will illustrate various features of a deployable, or foldable, doubly curved tetrahedral truss structure and the methods used to design the truss geometry and to synchronize deployment of the folding elements. An antenna with such a reflector structure is depicted in the figure which shows a side-mounted feed supported by a three-boom tripod. Particular application requirements will determine if a one- or three-boom feed support is required.



## TETRAHEDRAL TRUSS PACKAGING

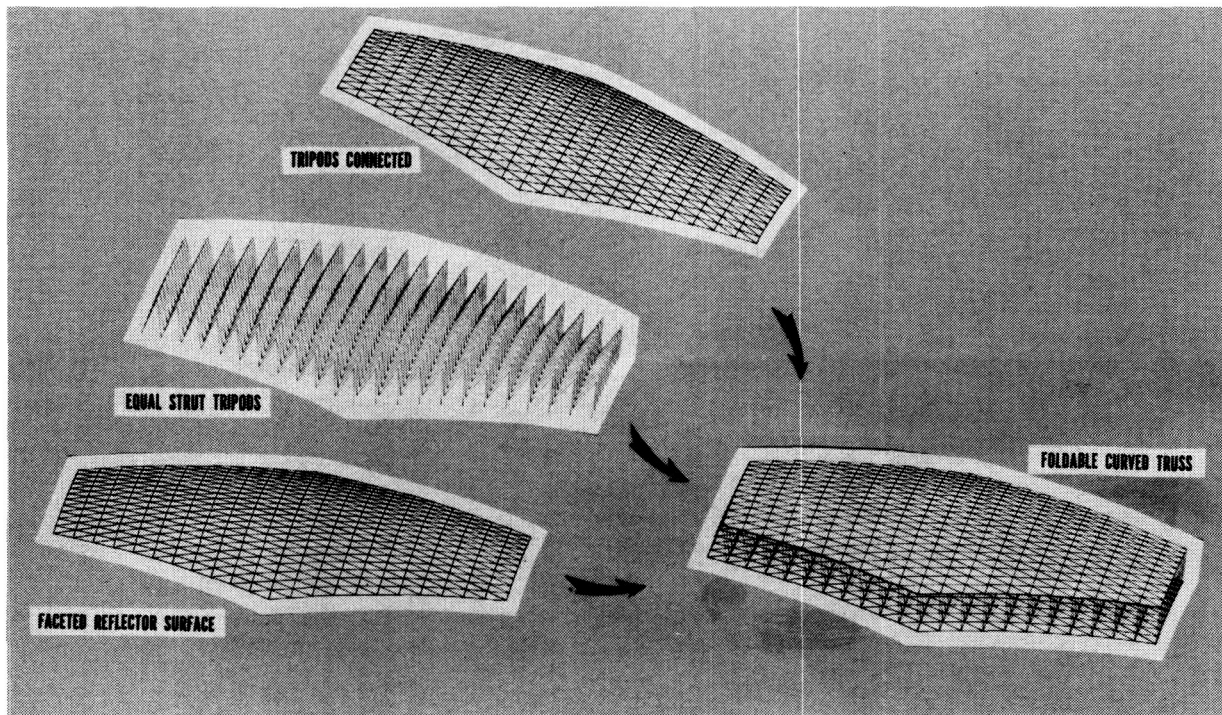
The tetrahedral truss considered herein uses inward-folding surface struts. The packaged geometry is illustrated in reference 3 and basic packaging equations are presented. The figure below presents the maximum diameter hexagonal planform tetrahedral truss that may be packaged within the diameter constraint of the Shuttle cargo bay. The deployed truss sizes are shown in the figure as a function of the surface and core strut slenderness ratios (i.e., length/radius of gyration). The figure shows that larger diameter deployed trusses require higher values of strut slenderness to package within the diameter of the cargo bay. Using struts with a slenderness of 1000 permits a 300-m-diameter truss to be packaged whereas a strut slenderness of 200 limits the maximum diameter truss module which can be transported via Shuttle to 60 m.

### REFLECTOR DIAMETER VERSUS STRUT SLENDERNESS



## ANTENNA REFLECTOR TRUSS CONSTRUCTION

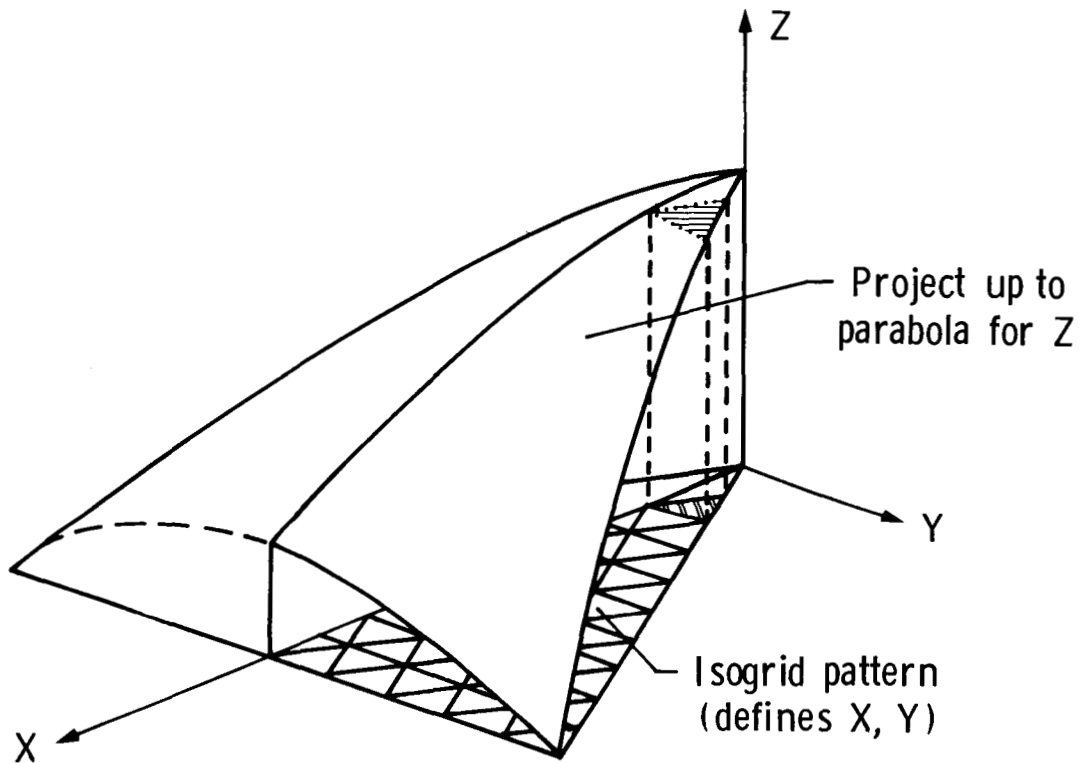
The geometric technique for defining a foldable truss concept is illustrated in the figure below. The desired doubly curved reflector surface is divided appropriately into a triangular pattern of points which are connected by struts. Equal length strut tripods are erected from the strut nodes on the convex side of the reflector surface. The tripod apices are connected with a triangular strut arrangement. The resulting configuration can be designed to fold into a compact package in which all the nodes within a surface lie in a plane. This feature permits "banding" the nodes solidly together to survive the vibrating environment resulting from the Shuttle being boosted into orbit. Use of inward-folding face struts (instead of outward folding) results in a package which is minimum length. This feature is important because a premium is placed on the cargo bay length occupied by a payload. In addition, inward-folding face struts are considered to pose fewer interference problems with any mesh reflector surface which is attached to the truss.





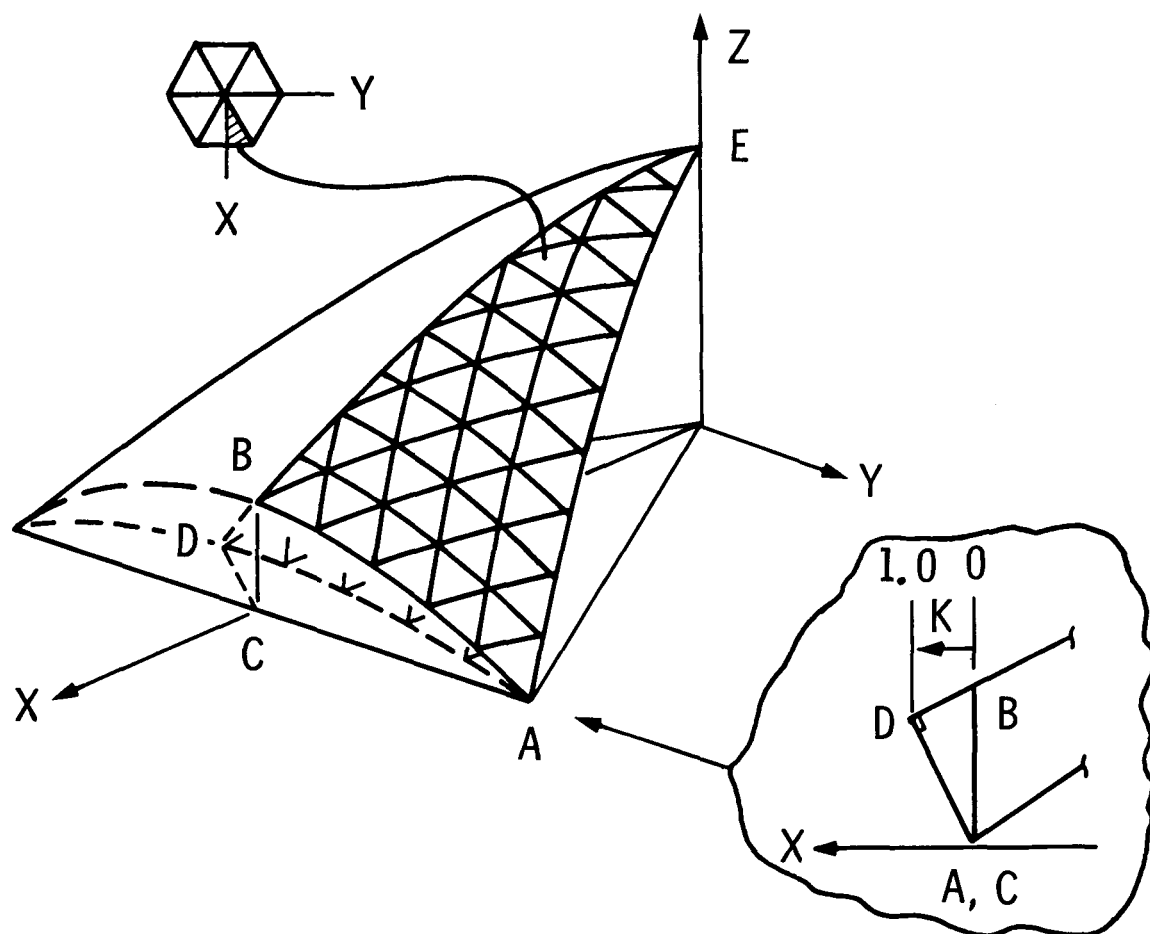
## NODAL DISTRIBUTION BY NORMAL PROJECTION

The method most commonly used to define the triangular nodal point pattern of a tetrahedral truss face on a parabolic reflector is known as normal projection. The method consists of forming an equilateral triangle pattern in a plane (i.e., the x-y plane) to determine the x and y coordinates to be used to fix node locations. The z coordinate is then calculated from the parabolic surface equation using the known x and y coordinates. This method corresponds to projecting each point of the planar equilateral triangle arrangement parallel to the z axis onto the parabolic surface, as shown in the figure, hence the term normal projection. Due to curvature of the parabolic surface, the triangular pattern thus formed exhibits a wide variation in strut length and in the local geometry of each node. These features have an adverse effect on design, fabrication, and, ultimately, cost of the reflector truss structure.



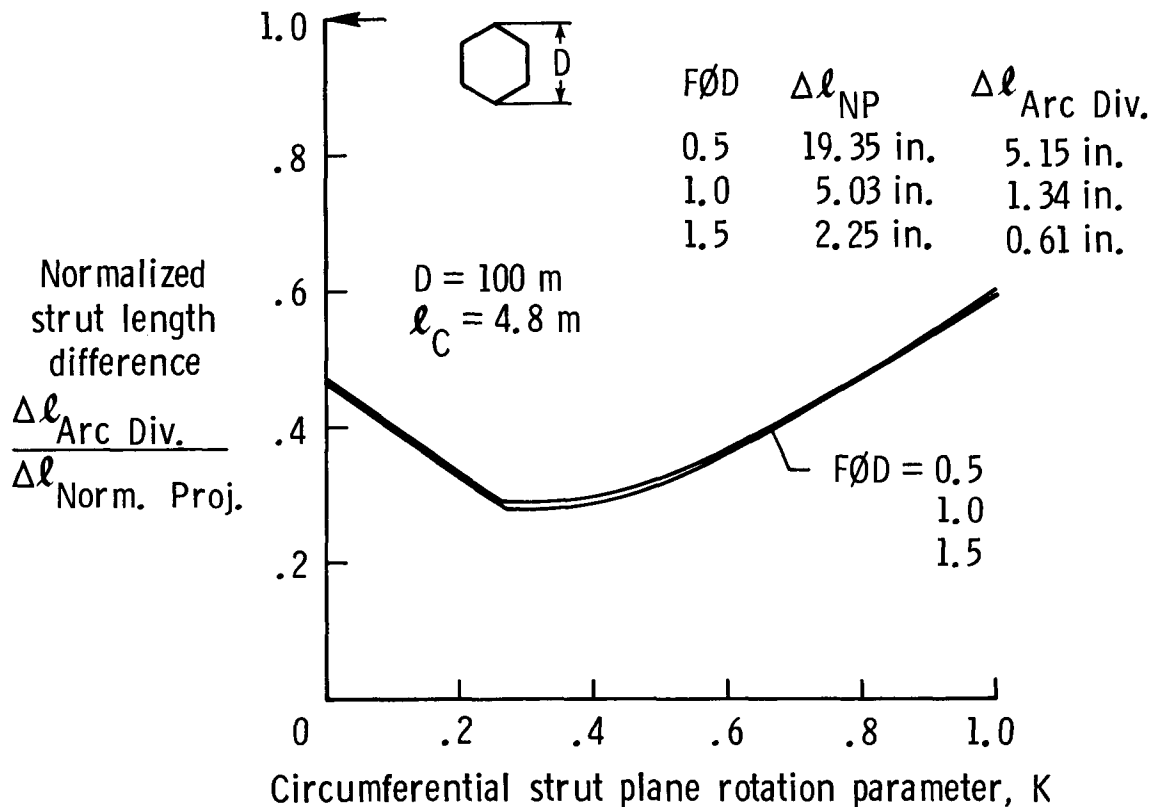
## NODAL DISTRIBUTION BY ARC DIVISION

Theoretically, it is possible to have an equilateral triangle (isogrid) strut arrangement only in a flat surface. It is not possible to achieve this in a doubly curved surface, such as a parabolic antenna reflector. However, the variation of geometric properties between nodes can be reduced if a nearly equilateral surface distribution of nodal points can be found. The figure below illustrates one such method. Considering first the shaded sector of a parabolic surface, bounded on the outside edge by arc AB, the meridional and circumferential boundaries of the sector are divided into the appropriate number of equal length arcs. Interior points are located by dividing each interior circumferential arc parallel to AB into the appropriate number of equal length arcs. A triangular truss thus formed exhibits a more nearly equal variation of strut lengths than does the normal projection technique. Further improvement is possible if the edge plane ABC (which was originally vertical as shown in the inset) is rotated outward about the line AC as shown in the figure (see ADC). Interior circumferential arcs are rotated in a similar manner and divided into equal length arcs. The rotation parameter  $k$ , shown in the inset, has a zero value when the plane containing each circumferential arc (similar to AB) is vertical, and has the value 1.0 when each plane is perpendicular to the meridian DE.



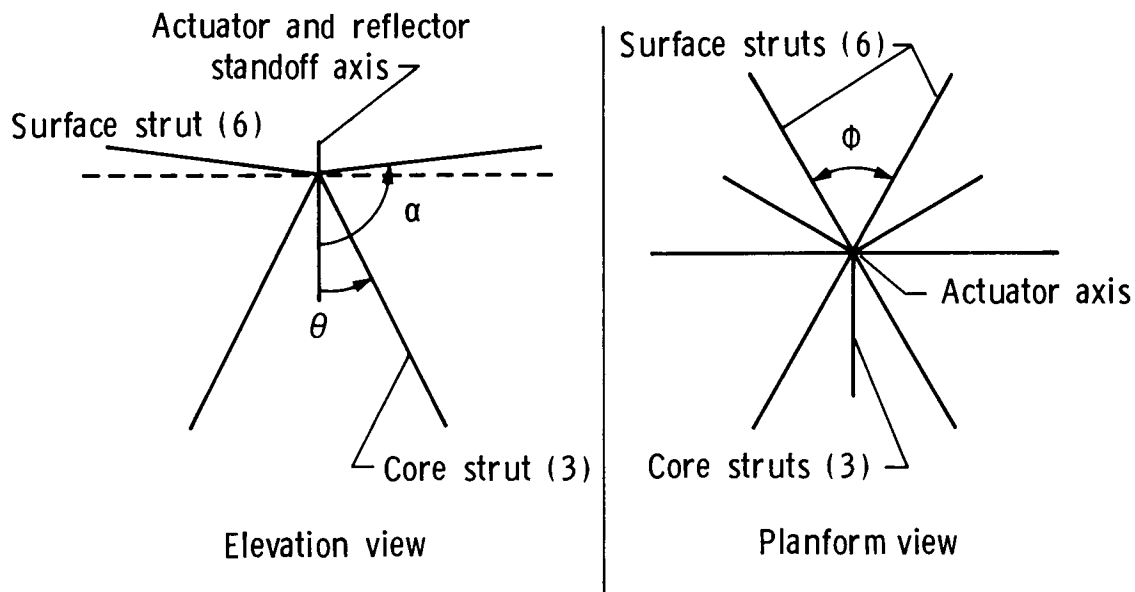
## STRUT LENGTH DIFFERENCE MINIMIZATION

The objective of redistributing nodal points by the arc division technique was to minimize differences in the strut lengths to aid in arriving at a common node design for each of the two truss surfaces. The figure shows the strut length error occurring for a 100-m-diameter parabolic truss with nodal point location determined by arc division (normalized with respect to similar values from normal projection). The strut length difference is shown for three values of truss curvature ( $F\phi D = .5, 1.0$  and  $1.5$ ). The normalized variation of strut length difference is shown to be essentially equal for all three values of  $F\phi D$ , and exhibits a "minimum" at a value of the geometric parameter  $k$  equal to  $0.27$ . Similar reductions in differences of the geometric angles  $\alpha$ ,  $\theta$ , and  $\phi$  also occur. While it is not possible to have geometrically identical nodes (within each truss surface), it appears that differences can be reduced to acceptable values such that a common node design for each surface appears feasible.



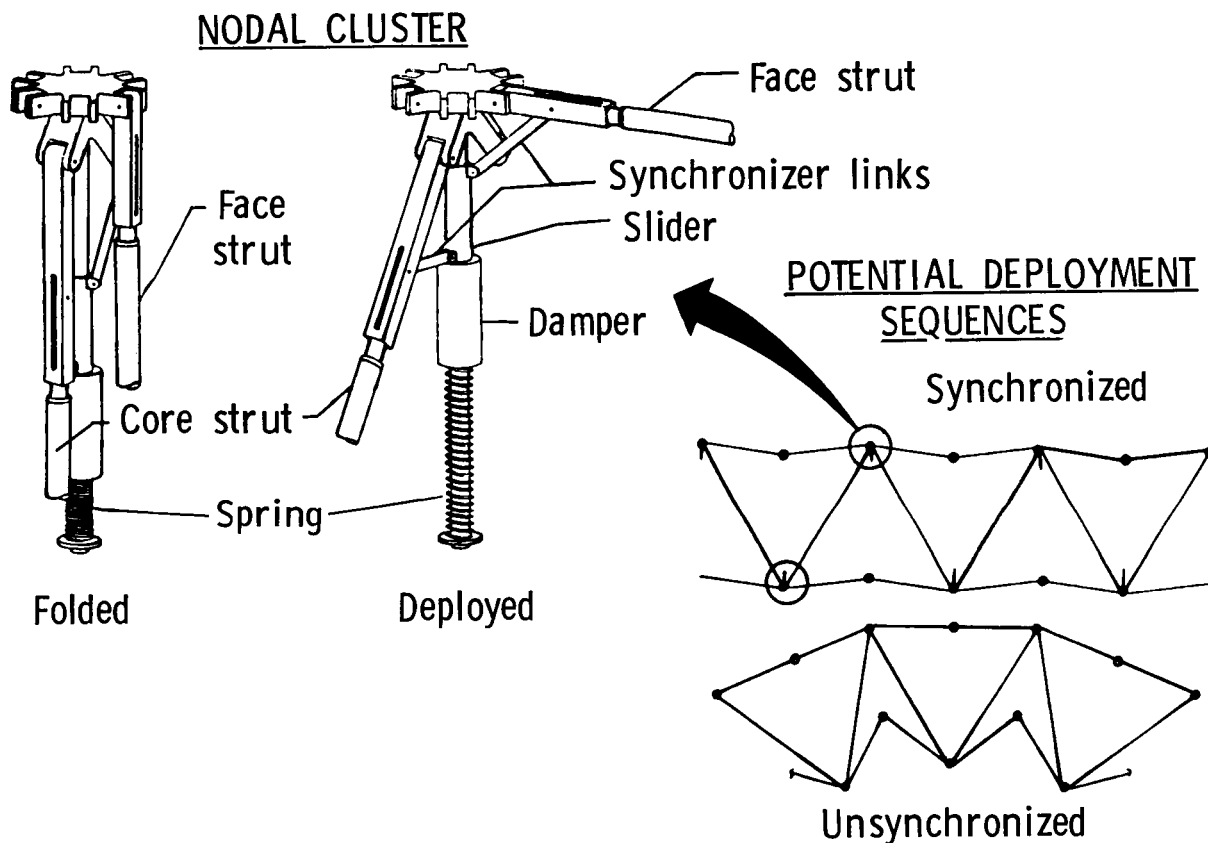
## NODAL GEOMETRY DEFINITION

The geometric layout of a tetrahedral node including the location of a local actuator axis is shown in the figure. The actuator axis is constructed perpendicular to the core strut tripod base and passes through the tripod apex. At each node, the three equal length core struts, by definition, each form an angle  $\theta$  with respect to the actuator axis. The angle  $\theta$  varies from node to node. Each face strut is shown to form an angle  $\alpha$  with respect to the actuator axis. The angle  $\alpha$  varies from strut to strut as well as node to node. The surface struts are shown in the planform view to form a projected angle  $\phi$  with respect to adjacent surface struts. The angle  $\phi$  varies from strut to strut as well as node to node. The objective of the arc division method of nodal distribution is to minimize the difference between surface strut lengths and additionally to minimize variations in the angles  $\alpha$ ,  $\theta$ , and  $\phi$ . Reduction of variations in the local geometric features of each node to a small enough magnitude will permit the use of a single-node design each for the convex and concave surfaces of the truss structure. This feature is a practical necessity for large deployable trusses.



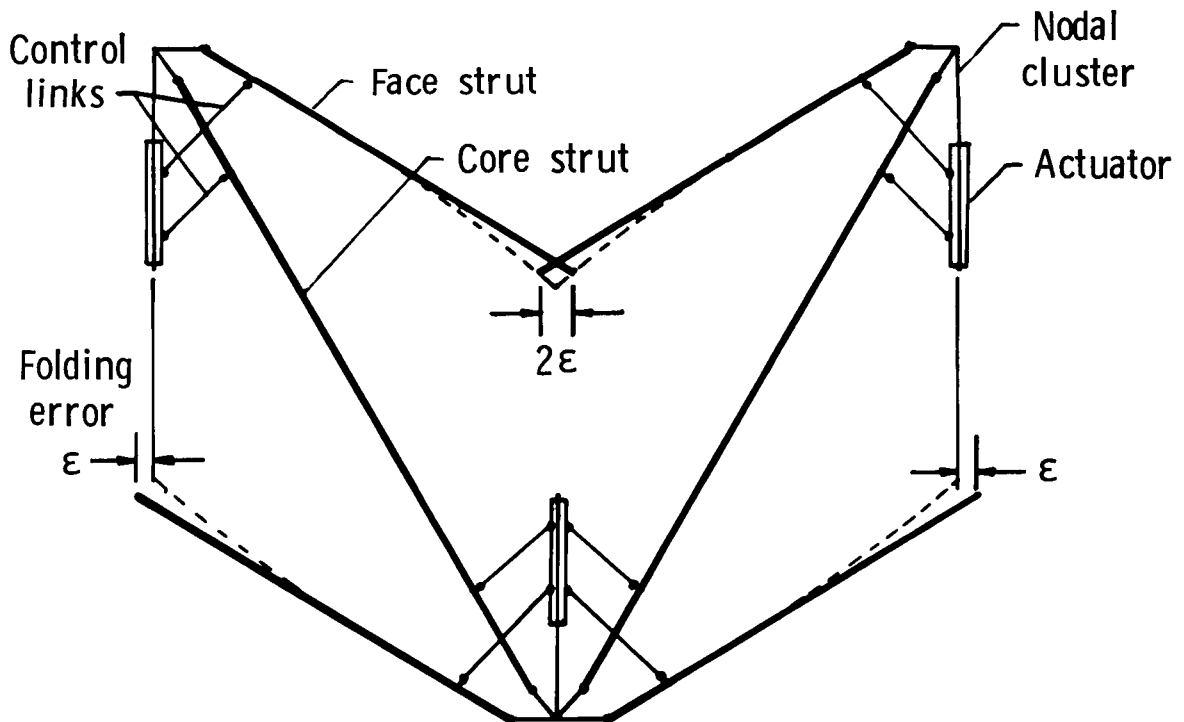
## STRUT SYNCHRONIZER DESIGN FEATURES

The method chosen to affect and regulate the deployment of the tetrahedral truss reflector is illustrated in the figure. The nodal cluster shown has a single-face and single-core strut attached for clarity. In actuality, up to six face struts and three core struts will be connected at a single node. Face and core struts are actuated and synchronized by mechanical links which are attached to a common slider. This slider is powered by a passive spring which is released at a rate determined by either (1) distributed local passive dampers as shown in the figure or (2) a global restraint (tether) system. The slider-crank synchronizer geometry is designed to preclude interference between deploying face and core members. Each node deploys independently in a manner that is compatible (free of interference) with adjacent nodes. Kinematic loops are formed between the truss surfaces which are connected by the core struts. These kinematic loops synchronize deployment of the truss surfaces.



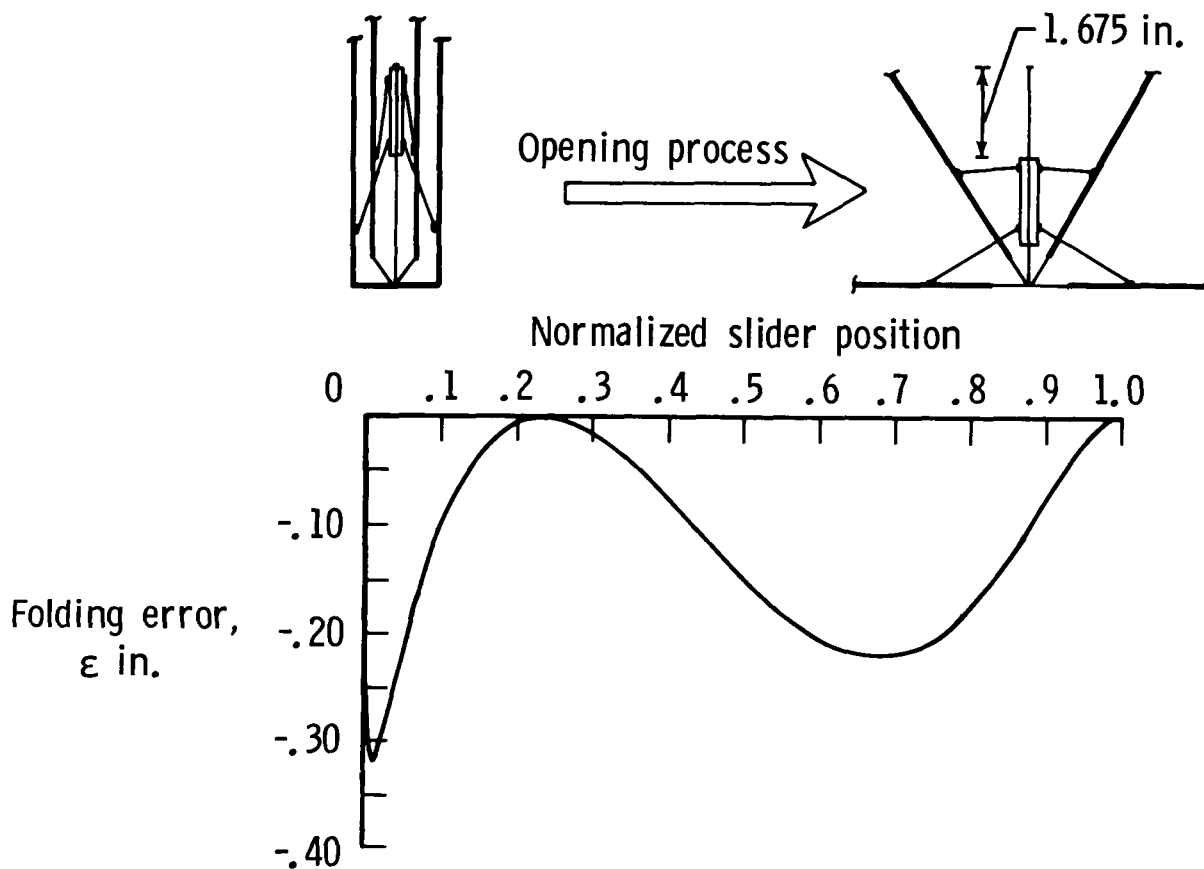
## STRUT SYNCHRONIZATION ANALYTICAL MODEL

The figure illustrates the geometry of the analytical model used to determine the synchronizer design which resulted in minimizing the folding error parameter,  $\epsilon$ , as shown. Pivot locations were iterated until the maximum value of  $\epsilon$  was minimized over the entire actuator and strut movement range--from fully folded to complete deployment. In the design approach illustrated by the figure, both the face and core struts are attached to a common actuator (slider). While  $\epsilon$  cannot be reduced to zero, it can be reduced to a small value which has negligible consequences on the kinematic deployment of a folded truss. Since the error  $\epsilon$  cannot be completely eliminated, it must be accommodated by bending of the struts using the design approach illustrated. An alternative approach, not illustrated or discussed, is to provide a two-piece actuator slide--spring connected--which will accommodate the kinematic error without strut bending.



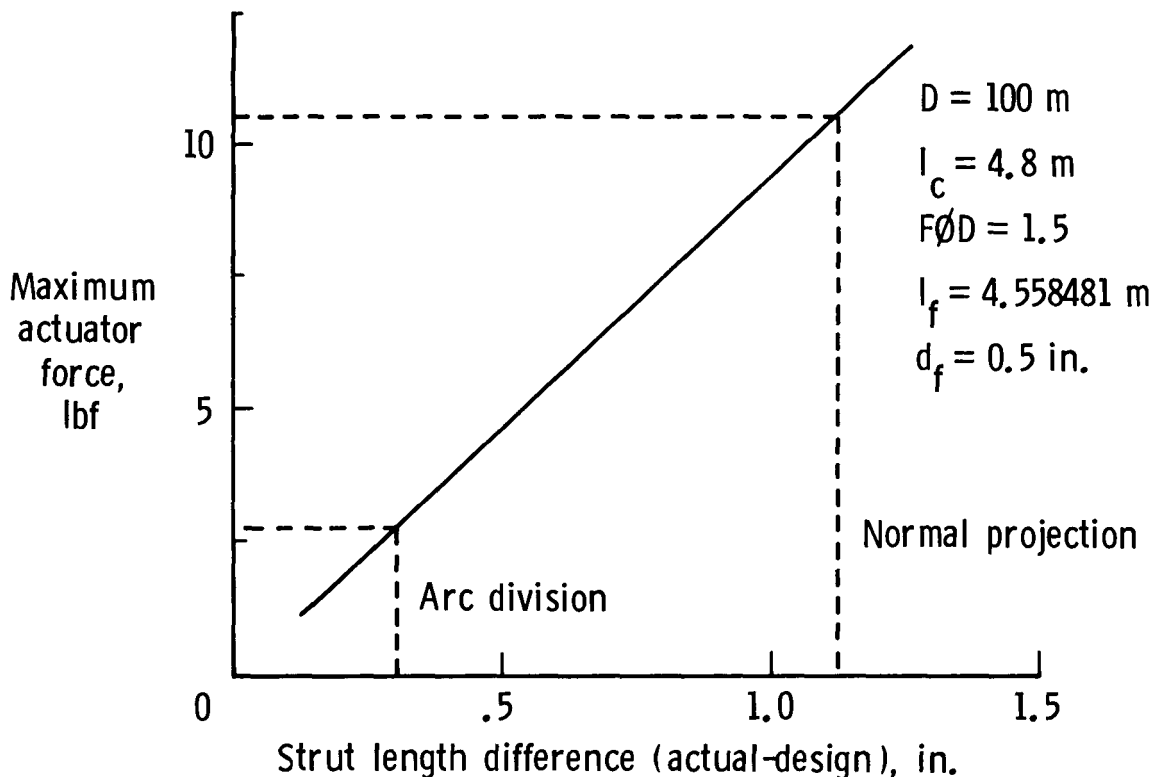
## FOLDING ERROR

The folding error  $\epsilon$ , defined previously, was calculated for a 100-m-diameter parabolic reflector structure ( $F/D = 1.5$ ). The analytical results are shown in the figure as a function of slider position. The kinematic linkage was designed for mean values of the design parameters, computed by the arc division method. The folding error  $\epsilon$  for this case is shown in the figure. The maximum magnitude of error is shown to be approximately .32 inches and occurs near the start of the deployment process. A second peak in folding error ( $\sim .22$  inches) occurs approximately 70% through the deployment operation. These values of error represent "hard" spots in the deployment process which must be overcome by the local actuator spring force.



## ACTUATOR FORCE REQUIREMENTS

A combined kinematics and force analysis was performed using the analytical model configuration discussed previously. A rigid-body kinematics code, ADAMS, was modified to permit strut bending during deployment. Using this approximate analysis, and neglecting friction, parametric studies were performed to determine the actuator force required to insure deployment of the truss configurations under investigation. The figure shows that the force required to overcome strut-bending deformations was found to be essentially linear with respect to surface strut length difference. The kinematic linkage was designed (i.e.,  $\epsilon$  was minimized) for median values of the nodal geometric parameters--including surface strut length. The force requirements were examined using this linkage design and different values of strut length. Plotted on the figure are the maximum strut length differences resulting from the arc division and normal projection techniques. Neglecting friction, the arc division method is shown to require an actuator force of approximately 3 lbf whereas the normal projection method requires approximately 11 lbf.





## CONCLUDING REMARKS

An arc division method for distributing truss nodal locations over a doubly curved reflector surface has been presented. This method has been shown to decrease differences in surface strut lengths and to increase the geometric similarity of all node configurations in each truss surface. These features enhance the design of a single node and strut synchronizer mechanism for each surface of the deployable tetrahedral truss examined. The folding error resulting from using this design approach was found to be minimal. Nodal actuator spring forces were calculated from an approximate analysis and found to be on the order of three pounds (neglecting friction) for the 100-m-diameter baseline reflector being considered.

Investigative efforts to date indicate the feasibility of using an arc division technique in conjunction with a strut synchronization approach for constructing and regulating operation of a deployable tetrahedral truss reflector.

- Slender struts required to achieve large-diameter single-module reflector surfaces
- Arc division method decreases strut length differences
- Use of single-node/synchronizer design appears feasible for each surface

## REFERENCES

1. Woods, A. A., Jr.; and Garcia, N. F.: Offset Wrap Rib Antenna Concept Development. NASA CP-2215, November 1981, pp. 439-469.
2. Sullivan, M. R.: Maypole (Hoop/Column) Concept Development Program. NASA CP-2215, November 1981, pp. 503-550.
3. Heard, W. L., Jr.; Bush, H. G.; Walz, J. E.; and Rehder, J. J.: Structural Sizing Considerations for Large Space Platforms. Journal of Spacecraft and Rockets, Vol. 18, No. 6, November-December 1981, p. 556.

ANTENNA TECHNOLOGY FOR  
QUASAT APPLICATION

John S. Archer and William B. Palmer  
TRW Electronics & Defense Sector  
Redondo Beach, California

Large Space Antenna Systems Technology - 1984  
December 4-6, 1984

## INTRODUCTION

This paper summarizes the results of a TRW study performed to provide JPL with antenna cost and design data for use in assessing the technical feasibility of QUASAT, a very long baseline interferometry (VLBI) mission in space. Science requirements for this mission have been defined by the NASA OVLBI Technical Working Group and the European Space Agency QUASAT Working Group (Paris, Oct. 1983). The mission concept involves a free-flying high-earth-orbiting spacecraft which carries a space-deployable radio antenna of about 15 meters in diameter with a receiving capability at K, C, and L bands.

TRW's approach to the requirements of the QUASAT antenna configuration adapted a hybrid growth version of the advanced Sunflower, or precision deployable, antenna concept. The basic precision deployable antenna concept uses a furlable rigid-panel reflector design as illustrated in figure 1, where it is shown mounted in the Shuttle bay.

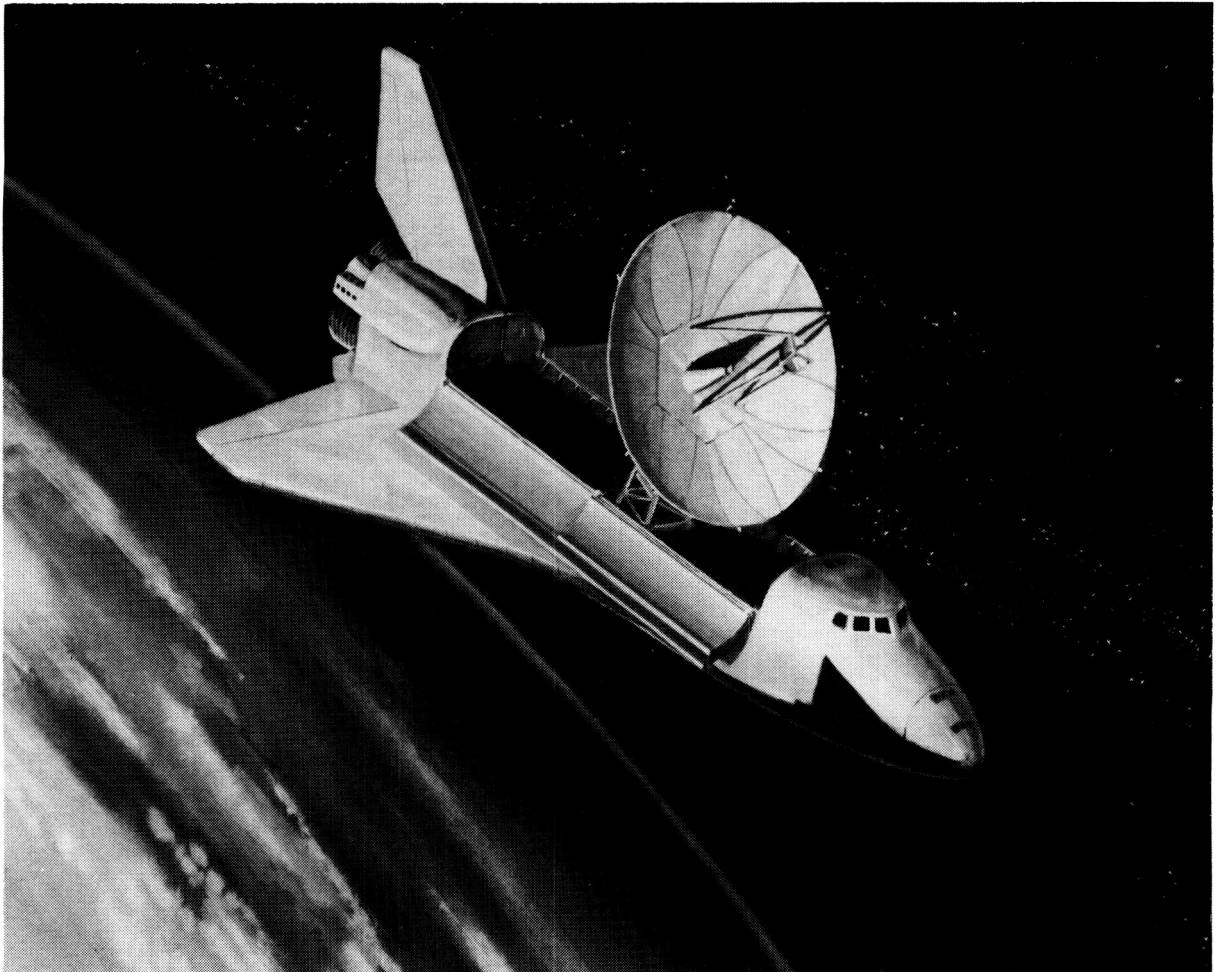


Figure 1. Precision deployable antenna in the Shuttle's bay.

## PRECISION DEPLOYABLE CONCEPT

TRW has been actively investigating the design of precision deployable antennas for several years. Figure 2 is an illustration of a 12-inch-diameter working model. Developed for a precision-contour reflector application, the concept can accommodate Cassegrain or focal-fed antenna applications requiring high-efficiency high-frequency apertures.

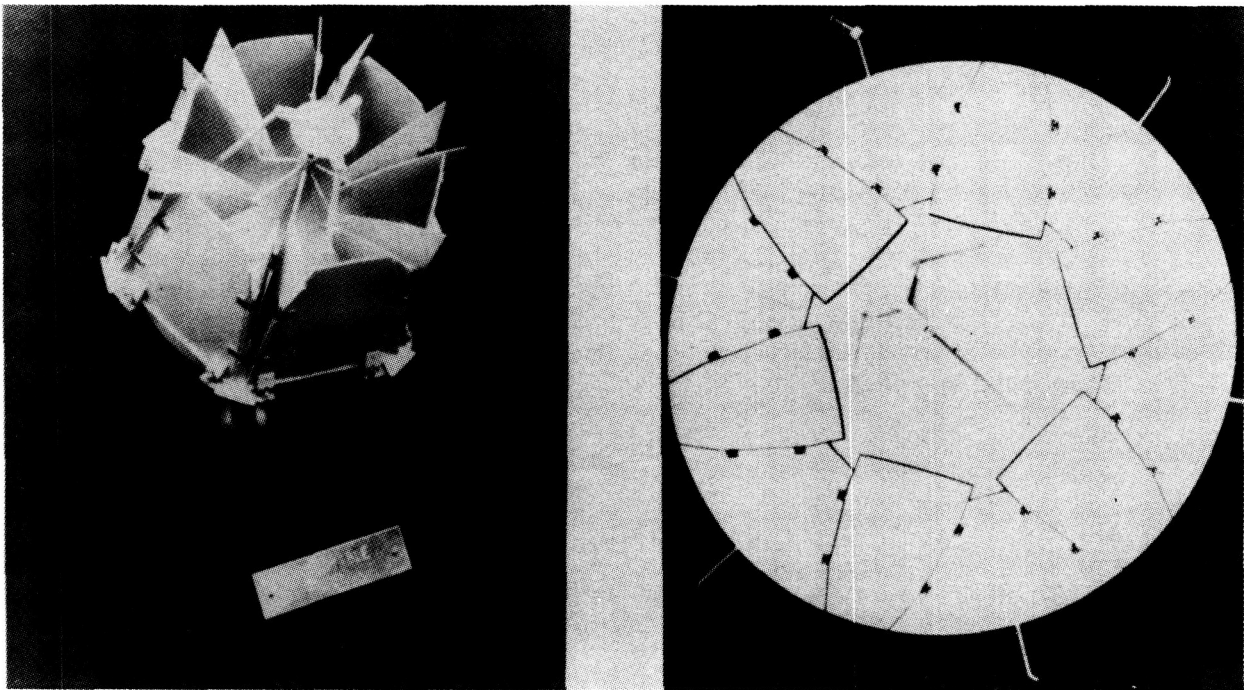


Figure 2. Deployable symmetrical aperture.

### 27.5-FOOT RESEARCH MODEL

Figures 3 and 4 show a design and the tooling which have been developed in TRW's ongoing research and development program for the precision deployable antenna. Information from this ongoing effort was used to prepare the technology and costing data provided in the figures which follow.

To provide a stiff, near-continuous surface, the antenna sections consist of rigid panels of graphite-epoxy facesheets covering aluminum honeycomb core sandwich. The center section, the one-piece honeycomb sandwich structure, is centered within the folding sandwich sections.

The six main folding panels are hinged to a cantilevered support ring attached to the periphery of the center section. Between the six main panels on the cantilevered ring are six pairs of intermediate panels. Two or more hinges along adjacent edges connect each pair of intermediate panels to the main panels and to each other. The hinges have adjustable stops which locate the panel surfaces accurately in the deployed configuration. Springs in the hinges drive the panels to the deployed position. To ensure synchronization of all panels during deployment, a compound universal coupling interconnects adjacent inboard hinges of the main panels. Either a damping device or a geared motor controls the deployment rate. On ordnance-actuated pin puller supported on one of the tie-down fittings restrains the furled antenna. The number of panels hinged from the fixed center section can be varied as required to optimize the diameter and height of the stowed antenna.

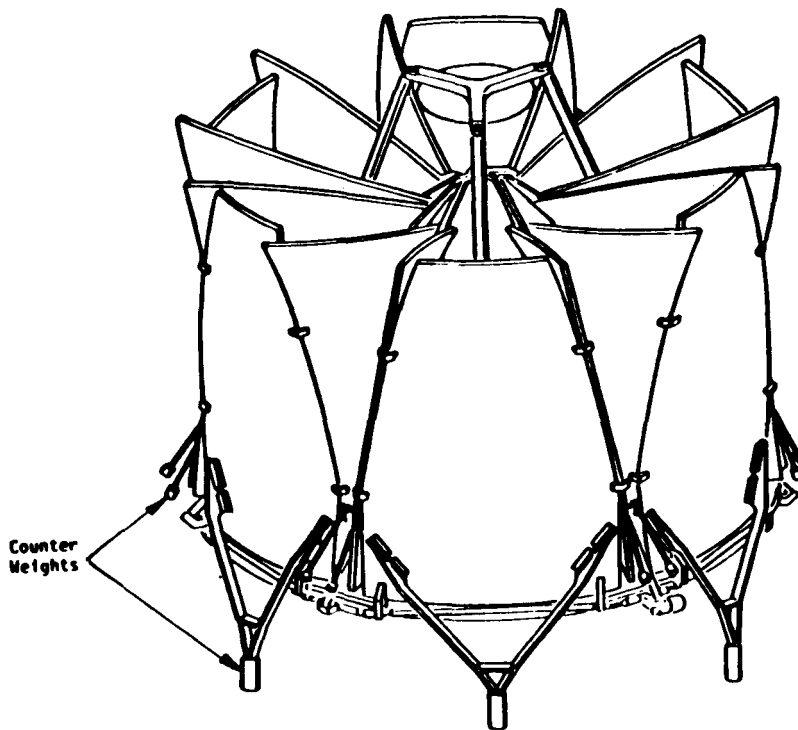


Figure 3. 27.5-foot-diameter deployable solid reflector (stowed).

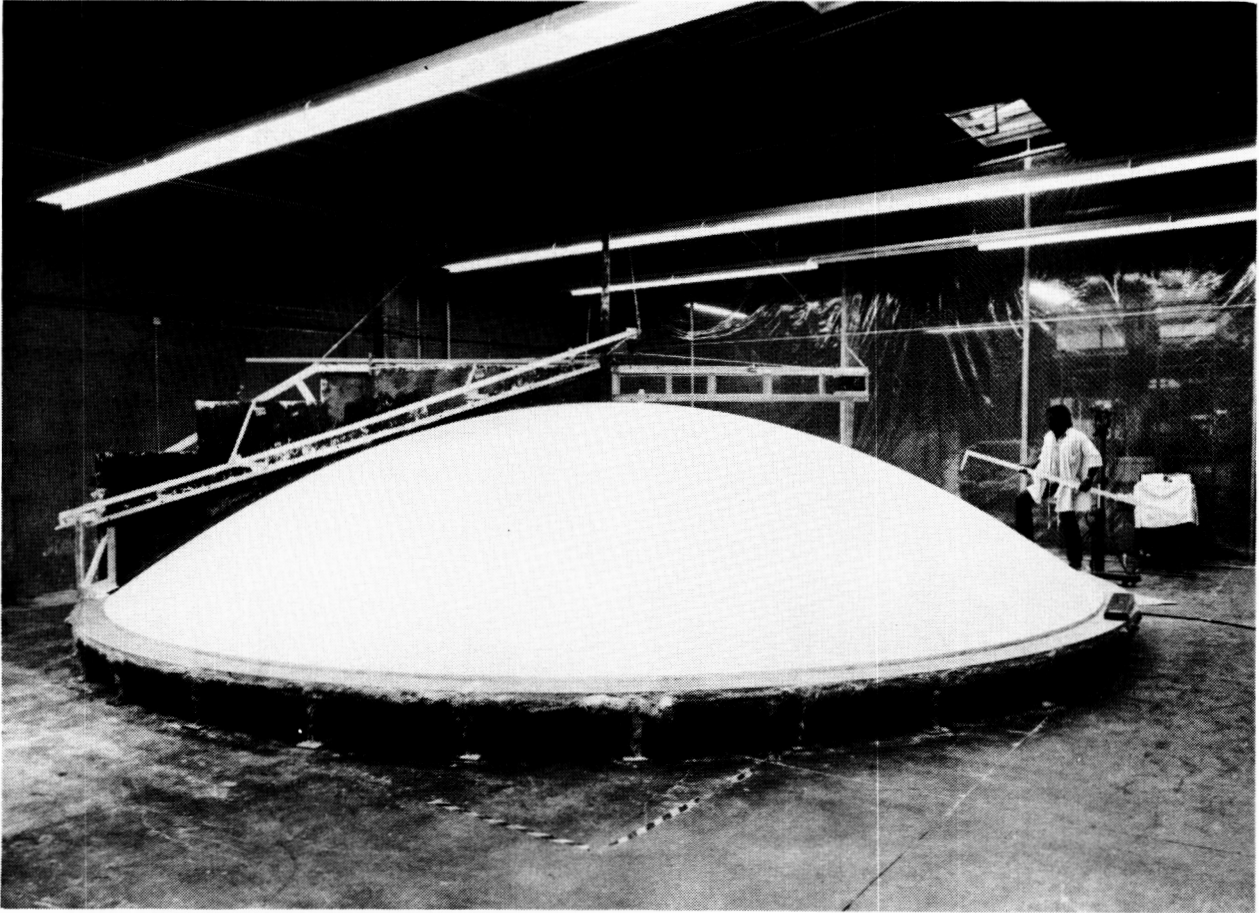


Figure 4. Master layup mold.

## QUASAT REQUIREMENTS

The following specific mechanical requirements constrained the TRW QUASAT study:

- (1) The antenna shall be a deployable reflector configuration.
- (2) The antenna shall be stowable within the Shuttle Orbiter bay.
- (3) The antenna characteristics shall be assessed for a range of apertures from 10 (33) to 20 (66) meters (feet).
- (4) The antenna surface error shall not exceed 0.8 millimeter (0.031 inch).
- (5) The mechanical parameters to be assessed shall include antenna weight, mass properties, stowed envelope, structural interface details, manufactured surface contour, thermal distortion, and materials of construction.
- (6) Cost and schedule parametric data shall be provided.



## QUASAT HYBRID ANTENNA CONFIGURATION

Technical parametric data are provided for antenna diameters of 10 (33), 15 (49), and 20 (66) meters (feet). For each antenna diameter (D), we selected a focal length (F) to maintain a constant F/D ratio of 0.4. In selecting the antenna configurations for each diameter, we designed the stowed envelope dimensions to fit within the Shuttle launch vehicle envelope. This constraint limits the maximum allowable precision Sunflower aperture to 33 feet. A 33-foot-diameter aperture stows in a cylindrical envelope 14.5 feet in diameter by 12.2 feet long. Any larger diameter would exceed the available Shuttle envelope diameter. The hybrid approach, which we discuss below, uses the precision deployable reflector as the core of a larger aperture. The hybrid concept was selected because it offers a practical means of effectively extending the deployable concept with its precision contour advantage to diameters larger than 33 feet while remaining within a stowed envelope of 14.5-foot maximum diameter.

The configurations selected are based upon a common, rigid-panel, precision deployable reflector with an aperture diameter of 33 feet, a size which remains constant for all antenna diameters. Such a central deployable reflector is illustrated in figures 5 to 7. The reflector has the inherent capability of being manufactured with a very low contour root mean square (rms), in the range of 0.005 to 0.015 inch. For the purpose of this study, a value of 0.014 inch was chosen as sufficient to satisfy the system requirements.

As the aperture diameter increases over 33 feet, the diameter of the precision deployable portion holds constant at 33 feet. The increase in total aperture diameter beyond 33 feet is attained by cantilevering an annular disk structure from the 33-foot-diameter precision deployable structure. The nature of the annular disk structure and its attachment to the 33-foot reflector is such that both the annular disk and the supporting central structure deploy simultaneously, as a single structural system.

The behavior of the annular disk structure is that of a flexible membrane. The advantages of this construction over a central rigid-panel structure are lighter weight and flexibility, allowing for storage within the Shuttle envelope, as seen in figure 7. The disadvantage is higher contour rms tolerances compared to the central 33-foot portion.

A 49-foot antenna of hybrid concept consists of a 33-foot-diameter center structure surrounded by an annular disk of 33 feet inside diameter (i.d.) and 49 feet outside diameter (o.d.), the 33-foot center structure being a precision deployable reflector. The 33/49-foot disk with a flexible membrane surface structurally cantilevers from the central precision deployable reflector. Similarly, a 66-foot antenna of this hybrid concept consists of a 33-foot center structure surrounded by an annular disk of 33 feet i.d. and 66 feet o.d. Again, the 33-foot center structure is a precision deployable reflector, and the 33/66-foot disk structure is a flexible membrane surface structurally cantilevered from the central precision deployable reflector.

## QUASAT HYBRID ANTENNA CONFIGURATION ( CONCLUDED)

### Constraint and Release

The stowed configuration for the 33-foot aperture is illustrated in figure 5. Extension arms from the intermediate petals are locked together in the stowed case to provide a rigid integrated structure for reacting the launch loads. For the 49- and 66-foot apertures with the cantilevered annular disk structures, an external ring, when stowed, rigidly constrains the central deployable structure, as illustrated in figure 6. The outer edges of the annular disk are constrained at a point above the feed support structure. The release mechanism is shown in View A-A. In both cases, release is effected by pyrotechnic pin pullers, and deployment is actuated by passive springs and controlled by hydraulic dampers.

### Support Interface

The support interface attachment to the spacecraft is illustrated in figures 5 and 6, and the fitting locations are identified in figure 7. This interface is identical for all apertures.

### Materials

The antenna is fabricated of graphite-epoxy materials. The central deployable reflector is constructed of sandwich panels made of graphite fiber reinforced plastic (GFRP) facesheets over an aluminum honeycomb core. Deep ribs of the same materials reinforce the panels. These materials provide a rigid, thermally stable structure of relatively light weight. The antenna surface is coated with vacuum-deposited aluminum to provide high RF reflectivity. The final coating is of a 0.003- to 0.004-inch-thick thermal control paint which minimizes specularly and reduces the equilibrium temperature of the reflector structure in the orbital solar environment.

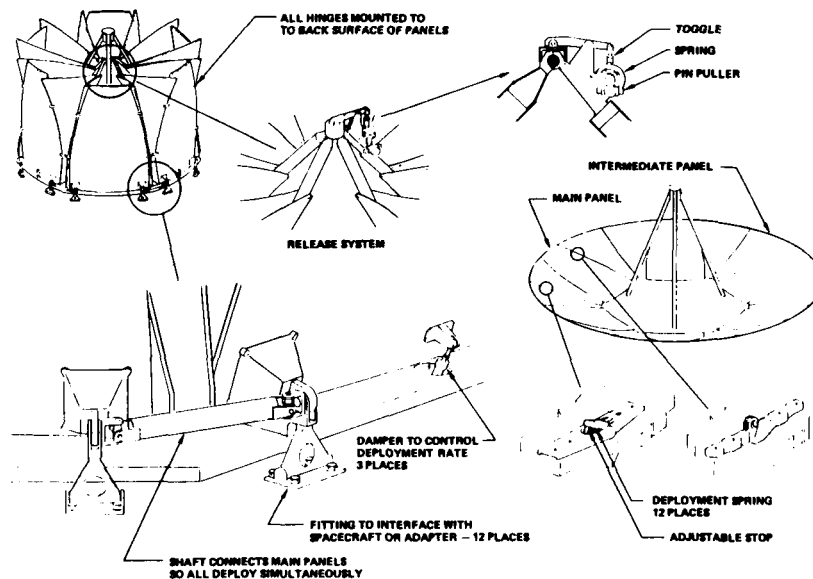


Figure 5. 33-foot-diameter antenna.

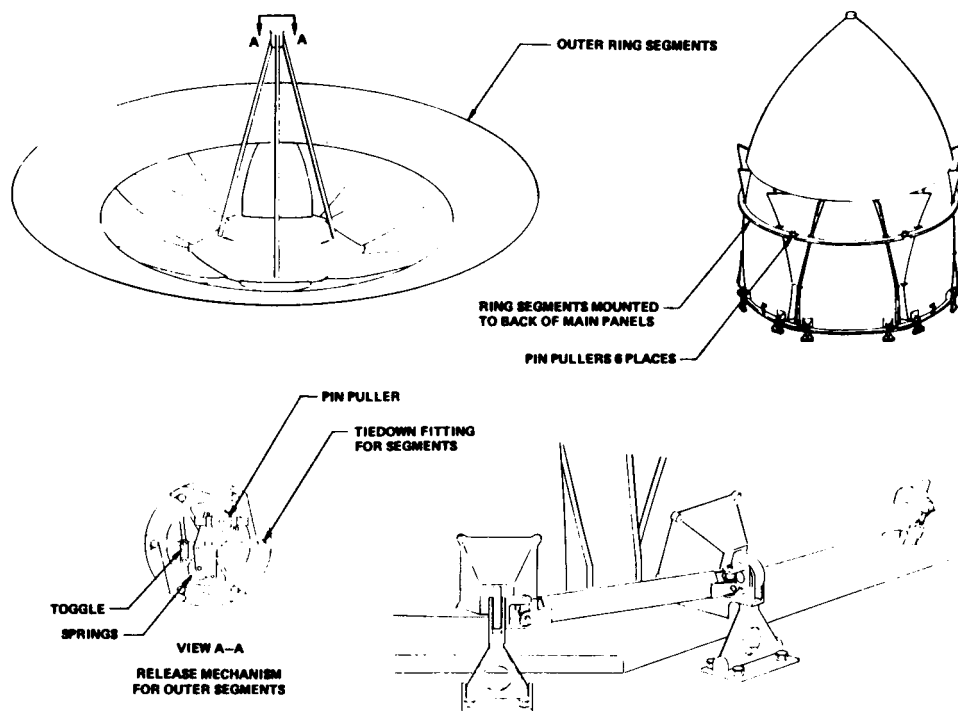


Figure 6. Configuration of 49- and 66-foot-diameter antennas.

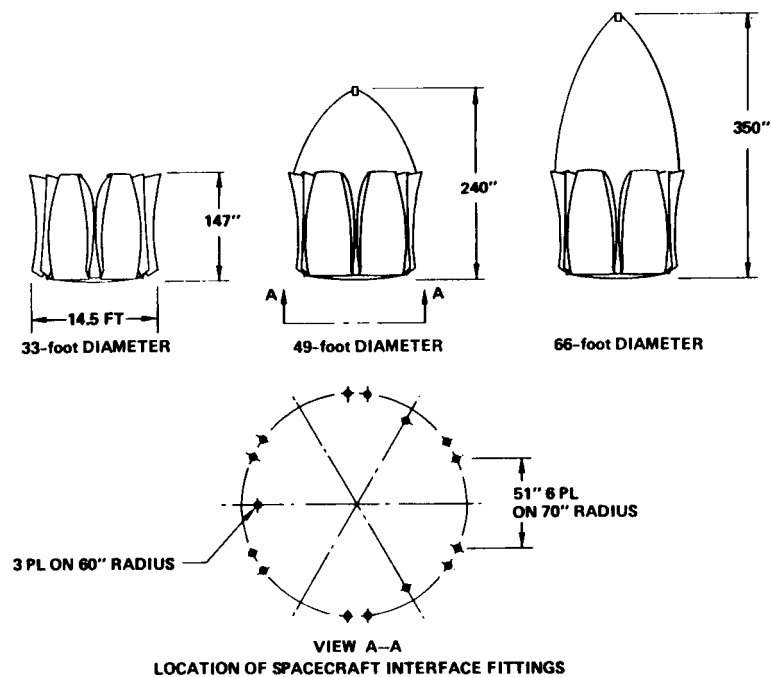


Figure 7. Stowed envelopes ( $F/D = 0.4$ ).

## QUASAT FLIGHT CONFIGURATION

The QUASAT flight configuration using the hybrid antenna configuration is illustrated in figure 8. The furled configuration stowed in the Space Transportation System (STS) bay is illustrated in figure 9.

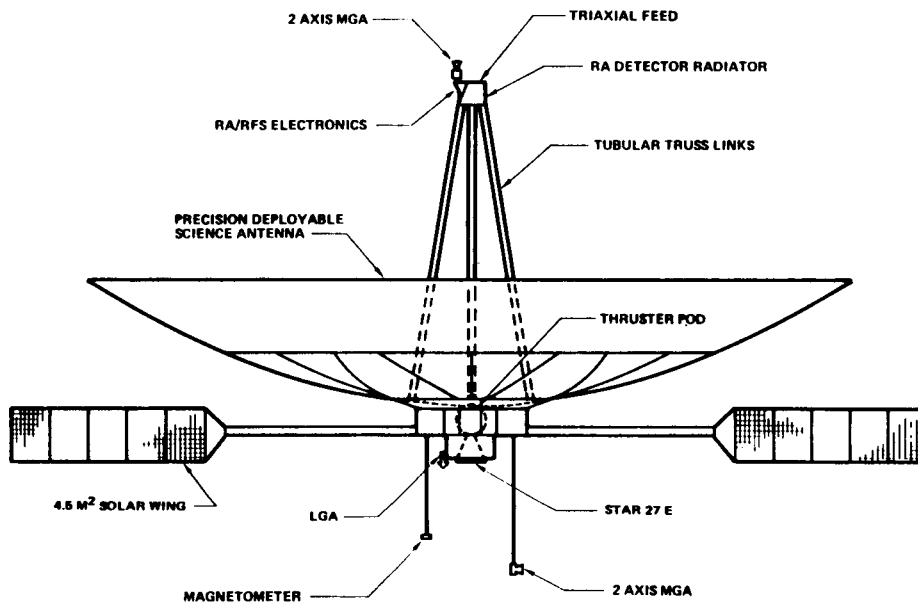


Figure 8. QUASAT flight configuration for advanced sunflower reflector.

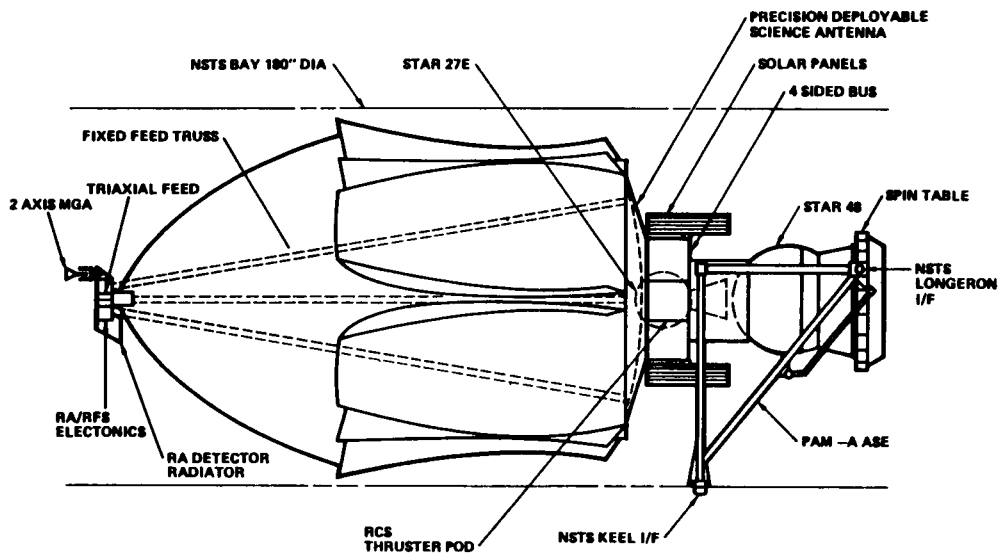


Figure 9. QUASAT advanced sunflower antenna stowed for launch in STS bay.

## HYBRID ANTENNA WEIGHT

TRW's experience with solid reflector construction of many types has shown that antenna weights vary from 0.4 to 1.0 psf of the projected aperture. The highest value is from a very conservative design, which is about 15 years old, whereas the lowest value is indicative of current lightweight large reflector experience. To represent the center portion of the antenna, we have used an average value of 0.6 to 0.7 psf including the weight of the feed support tower and launch constraint mechanisms.

The weight of the annular disk structure is estimated at 0.1 psf. The total reflector weight and the breakdown in weight between the center deployable structure and the outer disk are tabulated in figure 10 and plotted in figure 11 for apertures of 33, 49, and 66 feet.

D (feet)	WEIGHT (lb)		
	CENTER DEPLOYABLE STRUCTURE	ANNULAR DISK STRUCTURE	TOTAL
33	500	0	500
49	550	110	660
66	600	255	855

Figure 10. Weight distribution in antenna structure.

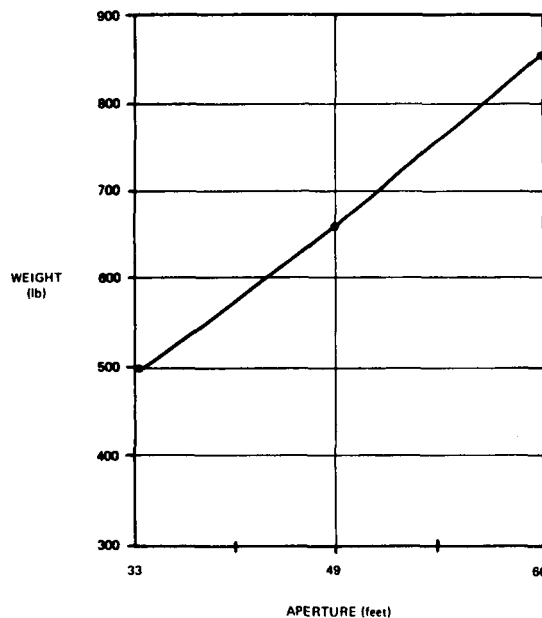


Figure 11. Antenna weight versus aperture.

## HYBRID ANTENNA MASS PROPERTIES

The center of gravity (cg) and the moments of inertia have been based on the stowed and deployed geometric envelopes illustrated previously. The antenna focal-length-to-diameter ratio is constant at 0.4 for all apertures from 33 to 66 feet. Furthermore, the antenna mass is largely concentrated in the central portion of the structure. This results in a relatively constant value of the longitudinal position of the cg for the deployed antenna, except for the effect of the feed support tower.

In the stowed configuration, the cg position estimate is based on the stowed envelope geometry and the mass distribution whereas the estimate of the cg position in the deployed case is based on the deployed envelope geometry and the mass distribution. Figure 12 provides the calculated cg data.

The roll moments of inertia when stowed and deployed are provided in figures 13 and 14.

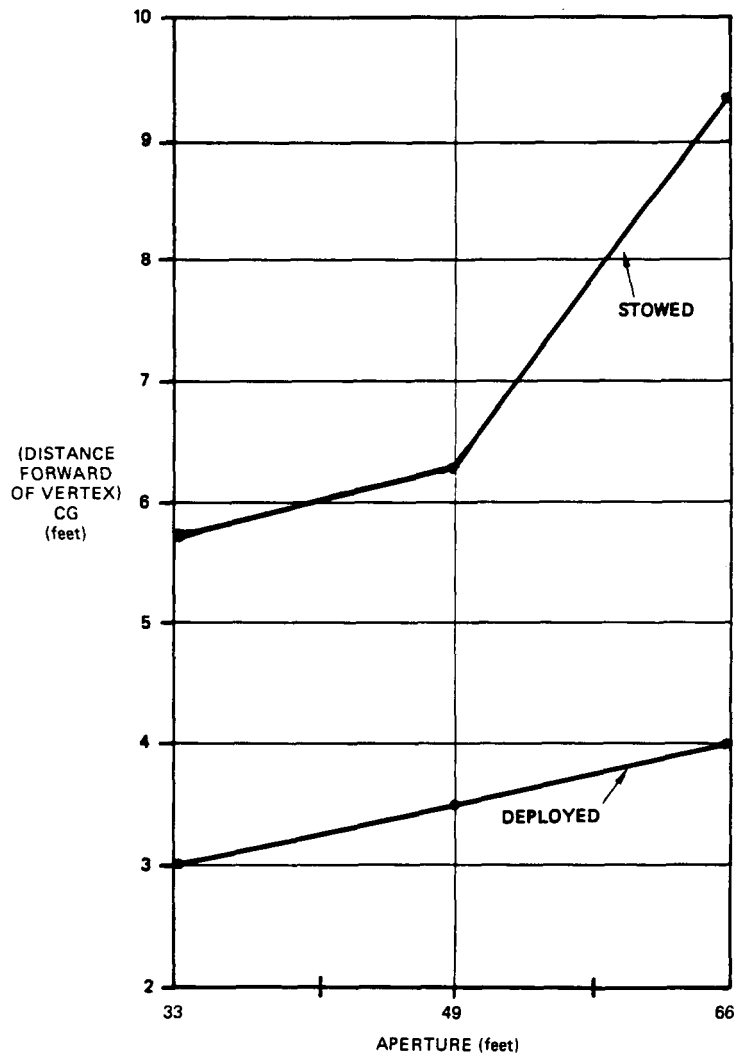


Figure 12. Center of gravity versus aperture.

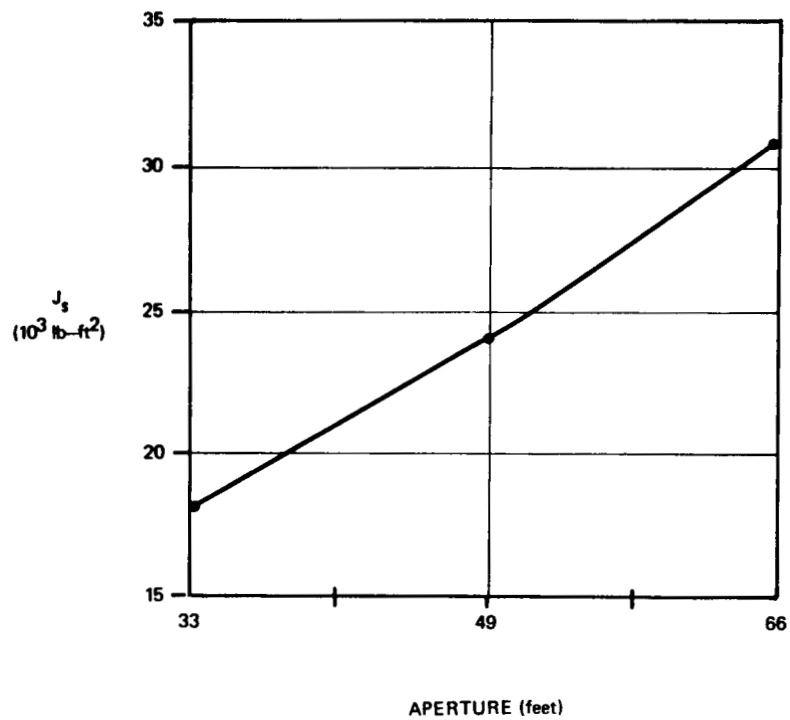


Figure 13. Roll moment of inertia versus aperture (stowed).

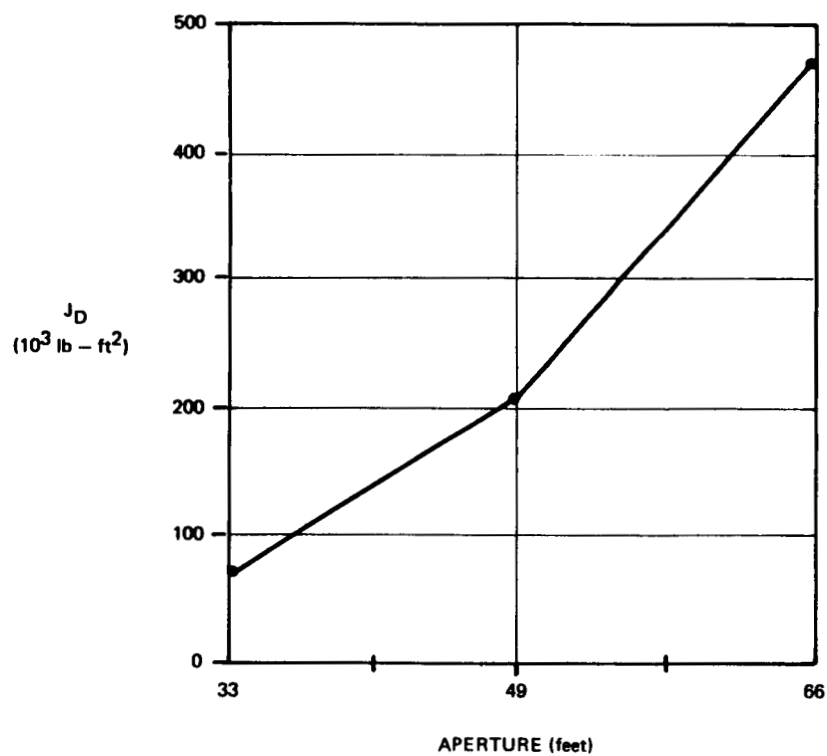


Figure 14. Roll moment of inertia versus aperture (deployed).

## HYBRID ANTENNA FREQUENCY

The fundamental frequency of the proposed concept at the various apertures of 33, 49, and 66 feet is based on extrapolation from a known configuration. A detailed vibration analysis was performed on a 20-foot-diameter precision deployable reflector aperture. The fundamental frequency in the stowed configuration was 12 Hz and in the deployed configuration, 5 Hz. These data have been extrapolated to the apertures being studied by using a single-degree-of-freedom model and accounting for mass and size changes. Figure 15 depicts the results of our analysis.

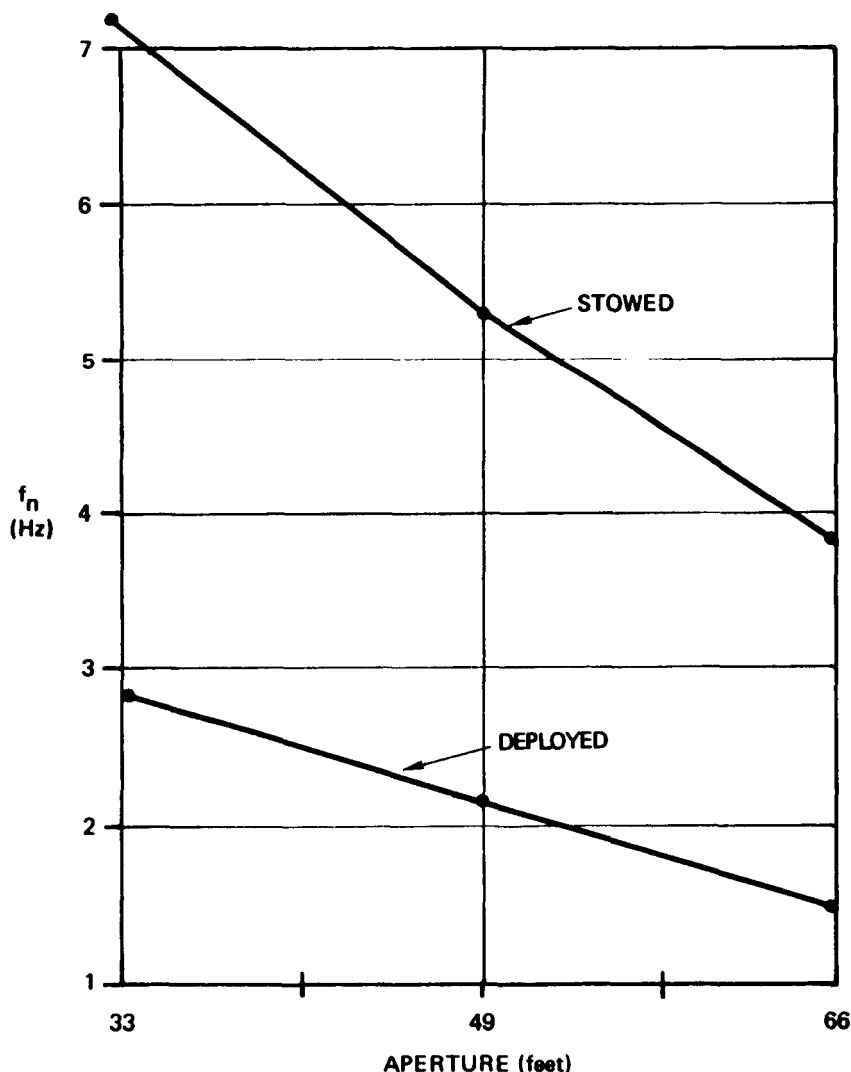


Figure 15. Fundamental frequency versus aperture.



## HYBRID ANTENNA CONTOUR TOLERANCE

The hybrid antenna contour distortion is defined as rms deviation from a perfect parabola. The two principal sources of contour error are manufacturing tolerances and thermal distortion on orbit. The total manufacturing error occurs in three areas - fabrication, assembly, and deployment repeatability.

The basic fabrication error is incurred when making the individual panels of the central deployable structure of the antenna. This error, based on experience with different materials and designs, is shown in figure 16. The proposed construction of graphite-epoxy, rib-supported shells will provide a contour rms-to-diameter ratio of 0.00003. The largest panel of the central reflector has a maximum dimension of 12 feet. We may, therefore, expect the panels to individually have an rms of 0.004 inch under ideal conditions. To be conservative, we allowed a 100-percent safety factor and, in addition, assumed that assembly and repeatability errors have the same order of magnitude. The net result is a total rms, including all effects, of 1.732 times 2 times 0.004 = 0.014 inch for the central 33-foot portion of the antenna.

The rms of the annular disk portion of the antenna is related to the method of support of the flexible membrane. The support structure is selected to maintain a fabricated rms of 0.033 inch for the 66-foot disk. The assembly and deployment repeatability errors are assumed to equal those for the central deployable structure.

The net results for the center and annular segments and for the complete 33-, 49-, and 66-foot antennas are tabulated in figure 17. The total combined rms is determined by root-sum-squares using area weighting for the components.

We estimated the thermal distortion by extrapolation from existing analyses on smaller apertures. A conservative value for graphite-epoxy construction is 0.001-inch rms for a 5-foot-diameter aperture. Linear extrapolation gives rms values of 0.007 inch for 33 feet, 0.010 inch for 49 feet, and 0.013 inch for 66 feet. These values, found in figure 17, when combined with the net manufactured rms give the total on-orbit rms values for each case.

The total on-orbit rms performance satisfies the system requirements for all aperture sizes.

MATERIAL	CONFIGURATION	NORMALIZED CONTOUR RMS ( $\delta/D$ )
FIBERGLASS	SANDWICH SHELL	$> 5 \times 10^{-4}$
	ADJUSTED SHELL	$0.7 \times 10^{-4}$
KEVLAR	RIB-SUPPORTED SHELL	$0.6 \times 10^{-4}$
ALUMINUM	SANDWICH SHELL	$0.5 \times 10^{-4}$
GRAPHITE	SANDWICH SHELL	$0.9 \times 10^{-4}$
	RIB-SUPPORTED SHELL	$0.3 \times 10^{-4}$
	ADJUSTED SHELL	$0.14 \times 10^{-4}$

Figure 16. Nondeployable reflector performance correlation.

(INCHES)

ERROR SOURCE	APERTURE	33 ft	33-49 ft	49 ft	49-66 ft	66 ft
	WT'D AREA	(1)	(1.25)	(2.25)	(1.75)	(4)
FABRICATION		0.008	0.025		0.033	
ASSEMBLY		0.008	0.008		0.008	
DEPLOYMENT		0.008	0.008		0.008	
NET MANUFACTURED RMS		0.014	0.028	0.023	0.035	0.029
THERMAL DISTRIBUTION		0.007		0.010		0.013
TOTAL ON-ORBIT RMS		0.016		0.025		0.032

Figure 17. Contour RMS versus aperture.

## MODIFIED 49-FOOT STOWED CONFIGURATION

STS launch costs are strongly dependent upon the length of bay occupied by the payload to be carried into orbit. The principal problem with the hybrid configuration is the length of the stowed antenna envelope.

The stowed envelope can be shortened by almost 8 feet for the 49-foot antenna by folding the outer-rib mesh annular disk onto the surface of the solid segmented panels of the inner 33-foot-diameter precision deployable antenna. This is accomplished by changing the hinge mechanism on the outer ribs and revising the stowage sequence. The solid panels of the precision deployable antenna are subsequently stowed while supporting the folded ribs of the outer annular portion. This stowage technique is illustrated in figures 18 to 20. It cannot be used for the 66-foot antenna because the ribs in the annular disk are too long to be folded onto the folding panels of the 33-foot central antenna structure.

In order to take full advantage of the reduced length of the STS bay required for launch, the feed support structure must also be made stowable, as shown in figure 21, which illustrates the revised stowage envelope in the STS bay.

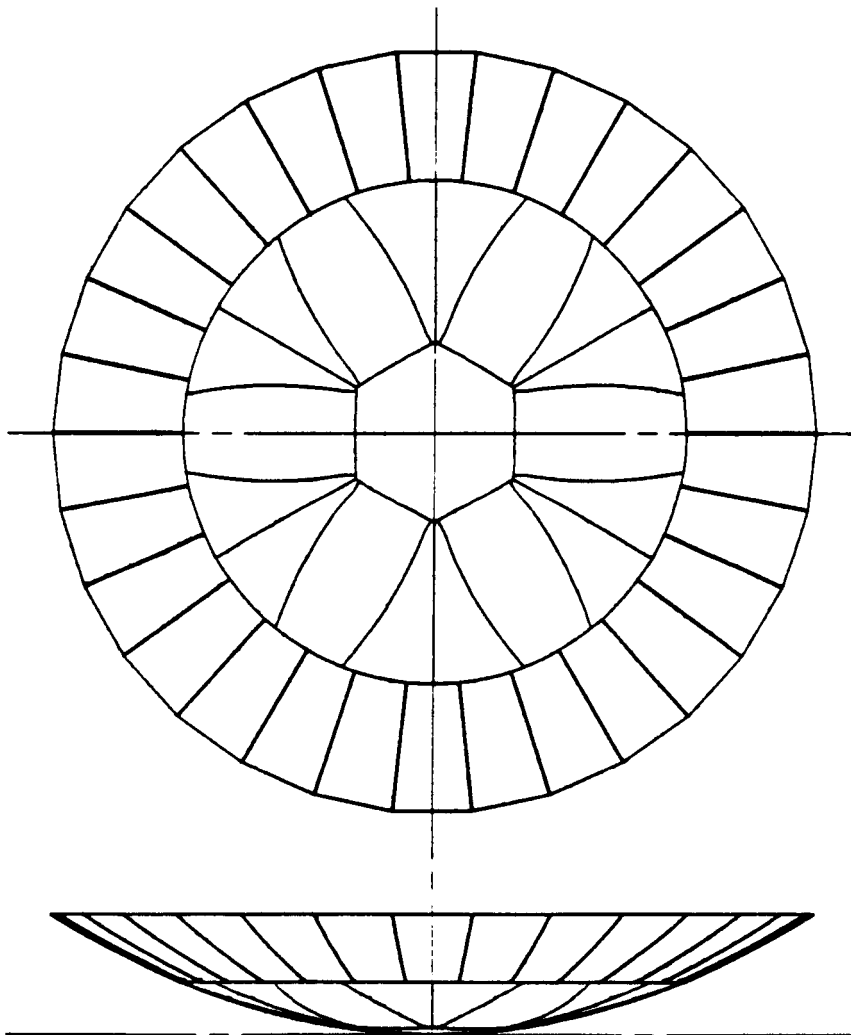


Figure 18. Deployed 49-foot hybrid antenna with modified stowage technique.

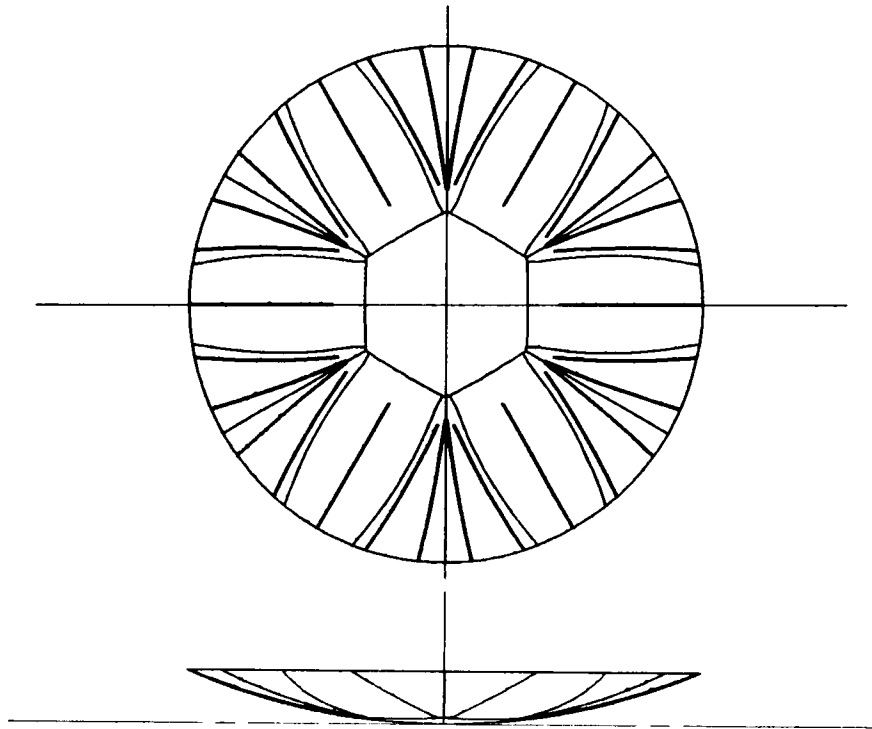


Figure 19. Partially furled 49-foot hybrid antenna with modified stowage technique.

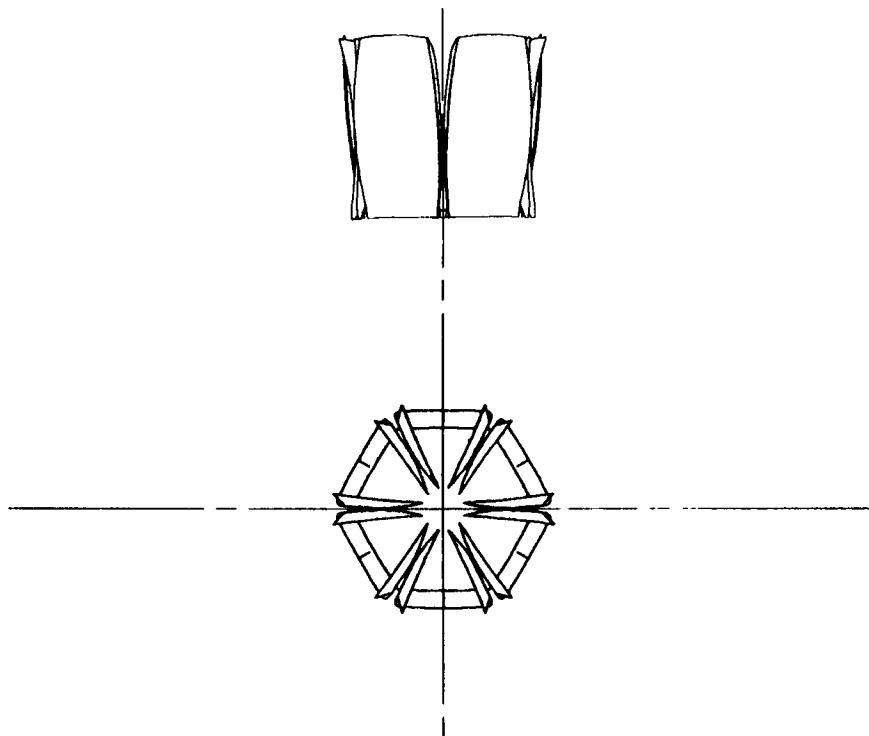


Figure 20. Completely furled 49-foot hybrid antenna with modified stowage technique.

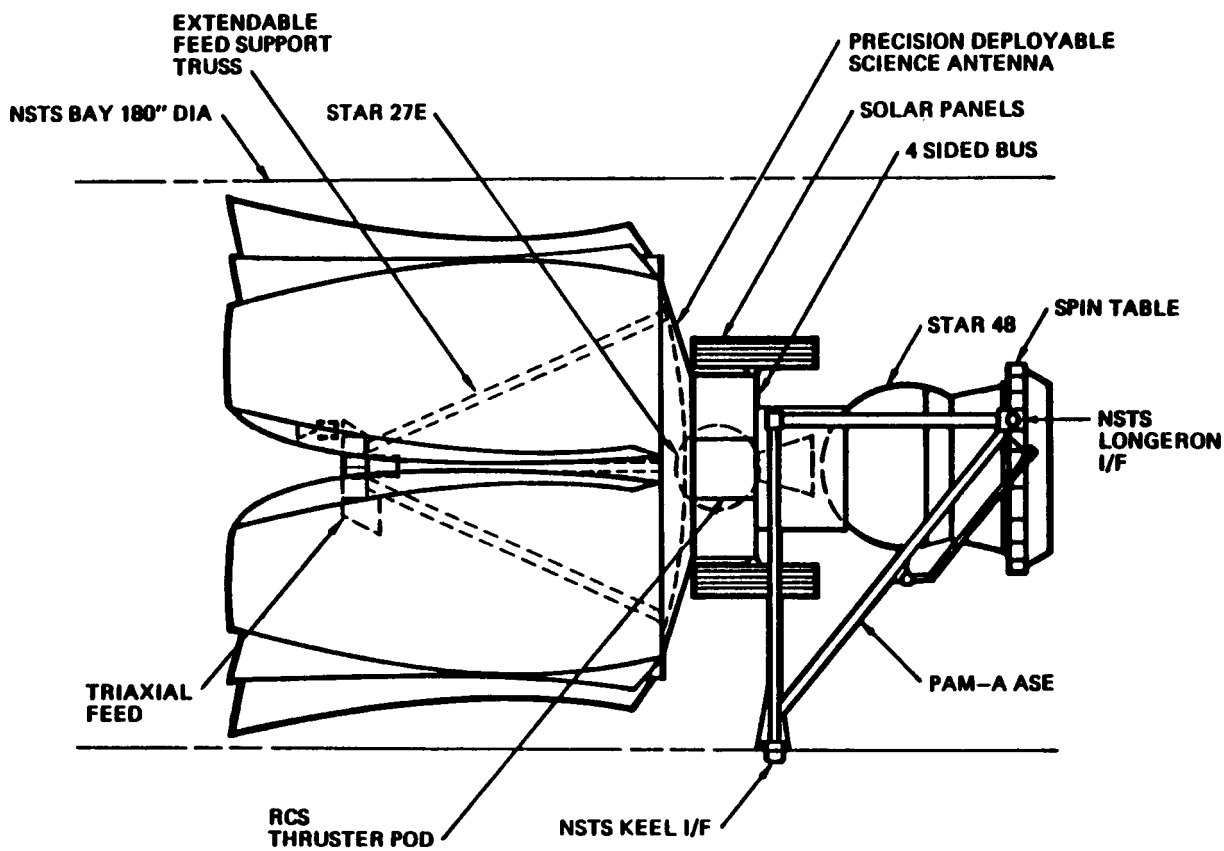


Figure 21. QUASAT 49-foot hybrid antenna stowed in STS bay for launch with modified stowage envelope.

## CONCLUSION

For the QUASAT antenna, the hybrid concept discussed here is a promising alternative to an all-mesh contour. The greater efficiency of the solid antenna surface, the tighter tolerances possible with the solid folding panels, and the potential for using the center 33-foot portion for higher RF frequencies than possible with mesh surfaces open up interesting prospects for future accomplishments. The possibility of storing a 49-foot antenna within a short envelope in the Shuttle's bay contributes immensely to the feasibility of the concept.

CABLE-CATENARY LARGE ANTENNA CONCEPT

W. AKLE  
TRW  
SPACE AND TECHNOLOGY GROUP  
REDONDO BEACH, CA

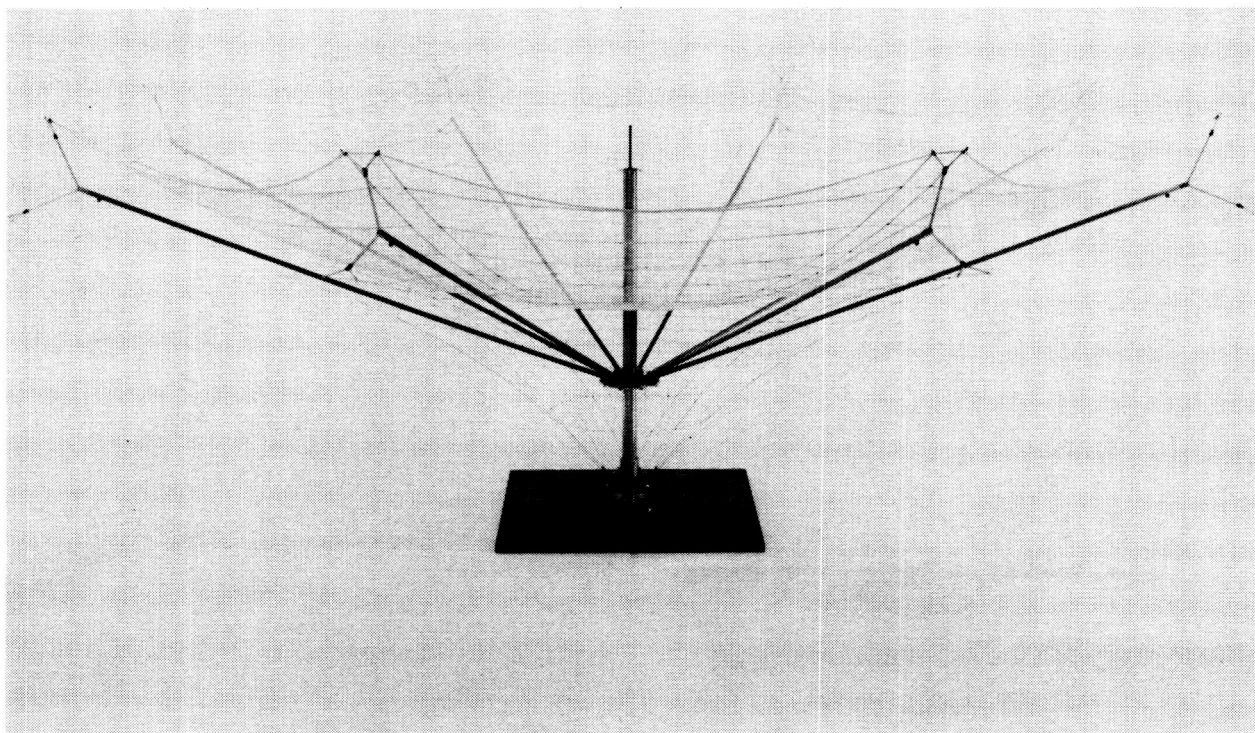
LARGE SPACE ANTENNA SYSTEMS TECHNOLOGY  
DECEMBER 4-6, 1984

## THE CABLE-CATENARY ANTENNA

The cable-catenary antenna (CCA) has been under study by TRW since the late 60's. It is deployable to very large diameters (over 1000 ft), while still remaining compatible with a complete satellite system launch by the STS.

The figure shows a 10 ft. working model of the CCA. Its main elements are:

- 8 radial, deployable boom masts
- A deployable hub and feed support center mast
- Balanced front and back, radial and circumferential catenary cabling for highly accurate (mm) surface control
- No interfering cabling in the antenna field
- An RF reflecting mesh supported on the front catenaries



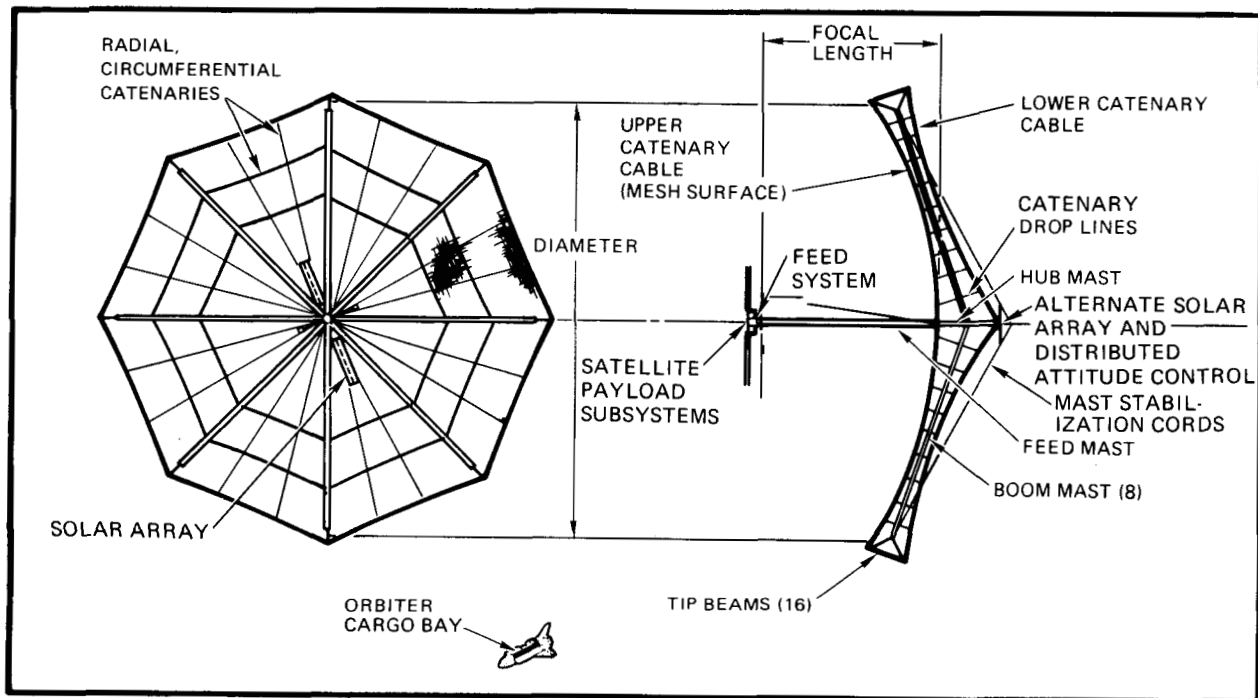


# CABLE-CATENARY ANTENNA - SATELLITE SYSTEM DEPLOYED CONFIGURATION

The CCA is shown deployed in a typical large communication satellite configuration.

The satellite main bus is located behind the focal plane (feeds). To preclude antenna aperture shadowing, the solar array wings can be extended further. Attitude control authority can be enhanced by locating control thrusters far apart at the ends of the center mast.

The number of catenaries to form the reflector plane is dependent on the required operating frequency and sidelobe control.



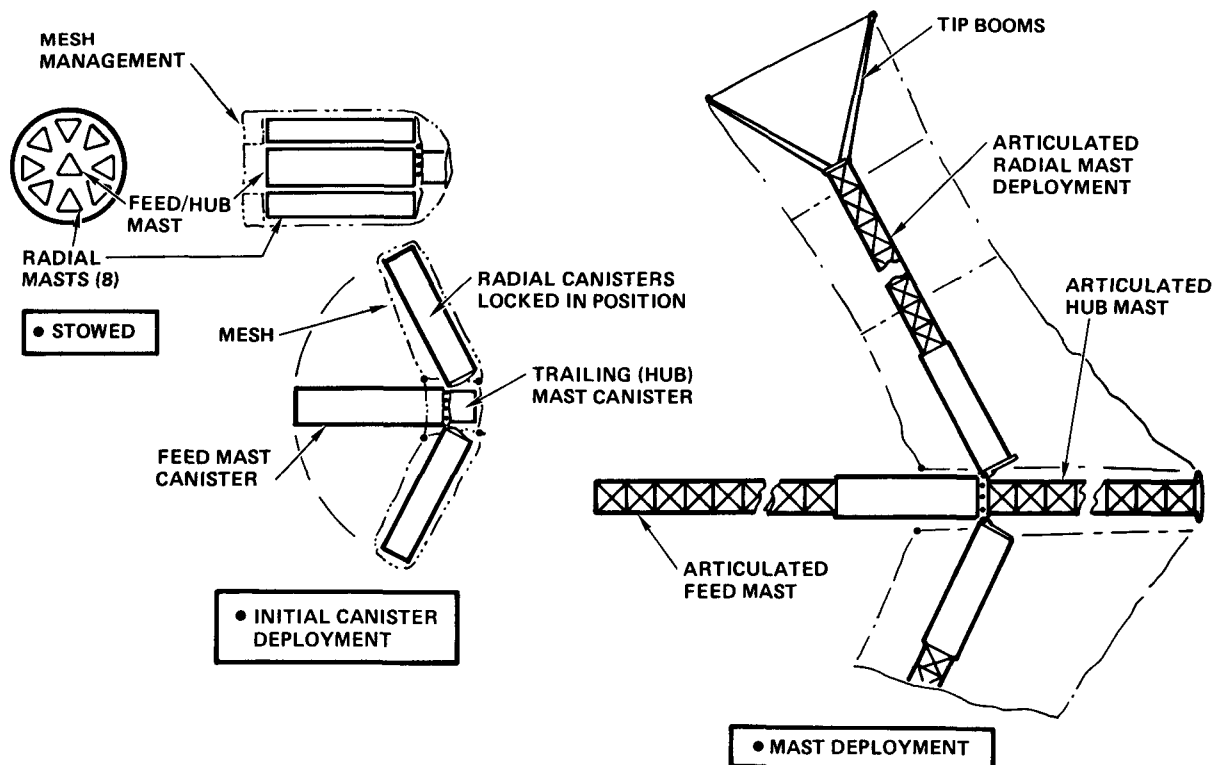
## CABLE-CATENARY ANTENNA - DEPLOYMENT SEQUENCE

In the stowed condition, the CCA radial mast canisters are rotated against and clustered around the center mast canister. The mesh management system is stowed in between and around the mast canisters.

Deployment starts by rotation of the radial mast canisters into position, with the mesh system following this motion. The tip booms are then extended radially from their stowed position in the canisters.

The feed mast is then deployed. All masts are triangular, articulated truss structures. Following this, the radial masts are deployed, with the mesh payout controlled by the mesh management system.

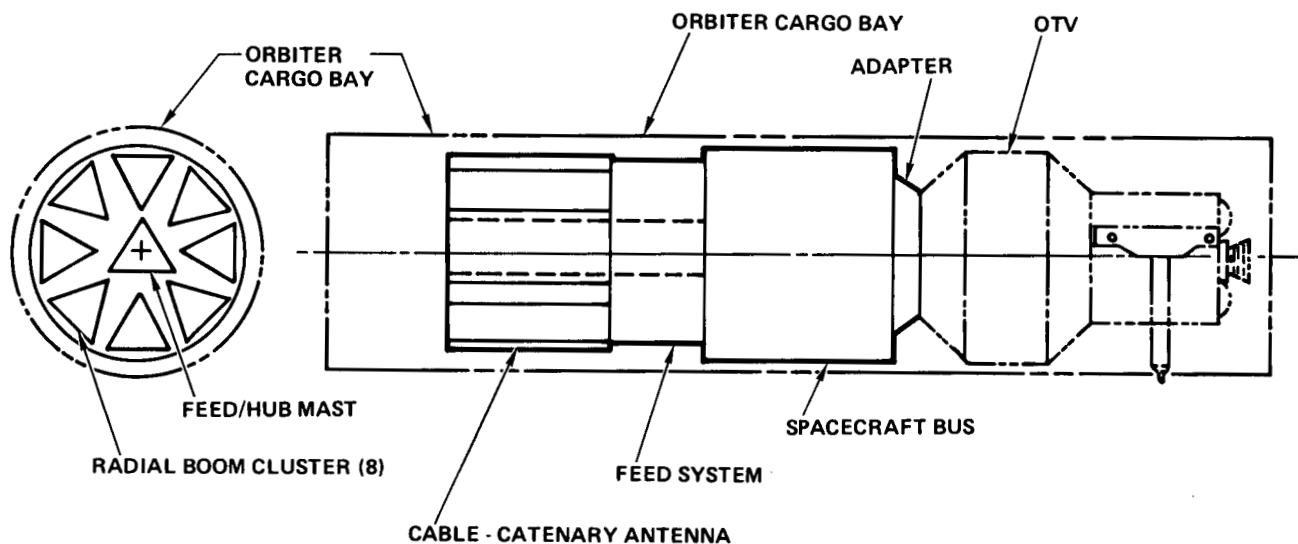
The mesh management also lends itself to surface accuracy adjustments after the CCA is deployed.



## CABLE-CATENARY ANTENNA SATELLITE SYSTEM - STOWED CONFIGURATION

The CCA stows very compactly; less than 10 ft. length for a 300-m aperture. This feature, coupled with a sturdy canister cluster, allows for efficient integration in the Orbiter cargo bay of the complete spacecraft and its Orbital Transfer Vehicle (OTV).

The OTV illustrated is in the Centaur G class; a length allowance of 22 ft is assumed. This leaves approximately 25 ft of effective length for the spacecraft bus and payload. On this basis, the system may be weight limited rather than length/volume limited in the Orbiter cargo bay.

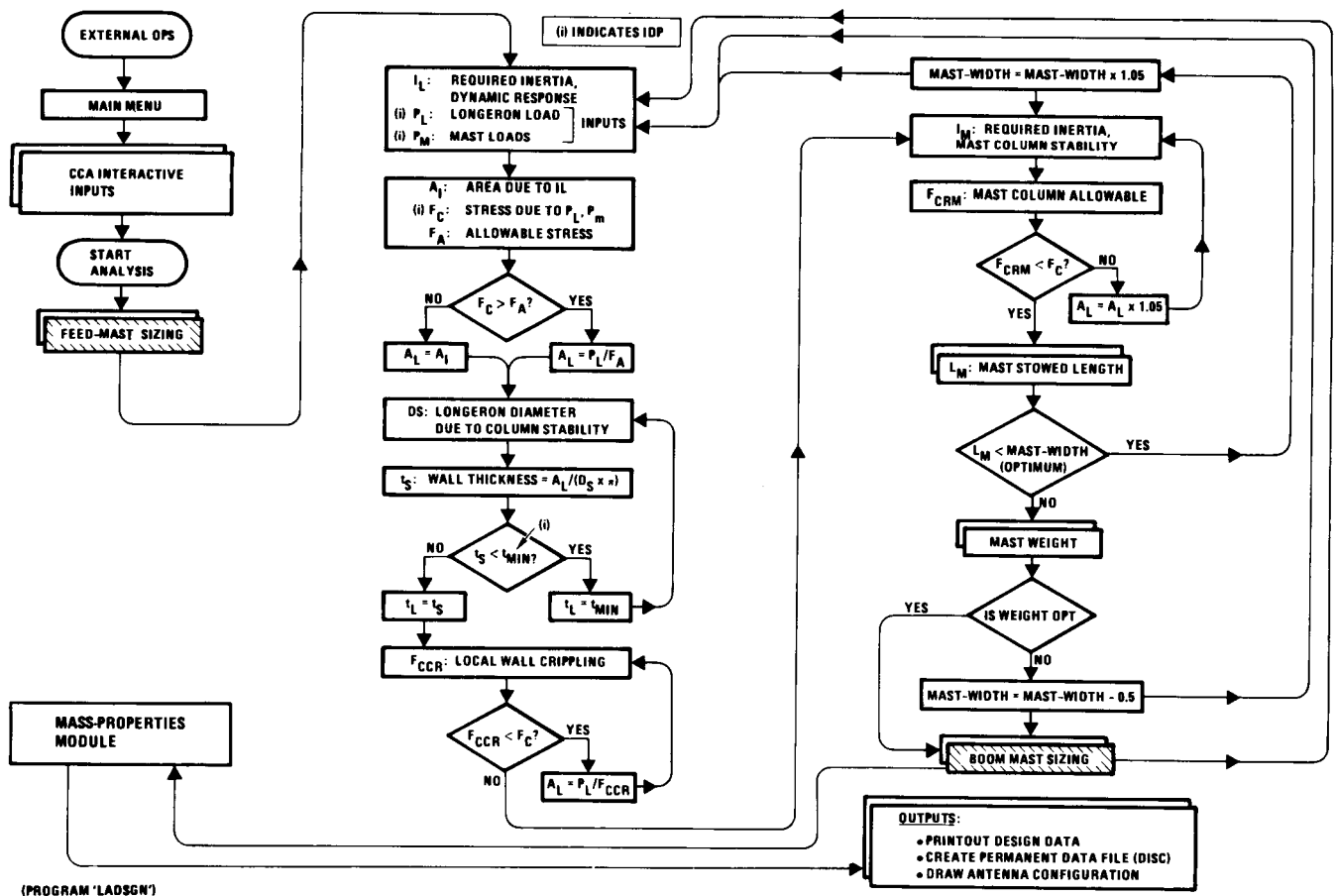


# CABLE-CATENARY ANTENNA - DESIGN ANALYSIS LOGIC

The CCA design and sizing analysis is based on dimensional constraints, payload RF requirements, spacecraft mass distribution, and control bandwidth. The process is automated using an internally developed optimization program called LADSGN. Its logic is shown in the figure.

Inputs are of two types: 1) screen interactive (run time), and 2) internal program parameters that are variable for further parametric analysis.

The analysis then considers static loads, dynamic response lower limits, and material properties. Iterative convergence loops are used to satisfy all the system requirements, including stowed dimensional limits imposed by the Orbiter.



# CABLE-CATENARY ANTENNA - SIZING ANALYSIS OUTPUT

The analysis results in the figure consist of the input system parameters and the output dimensional and weight data for all the critical CCA elements. Detailed mass properties are generated for use by other program modules, such as attitude control.

09:31:58 20 Oct 1983

'LADSGN' PROGRAM ,Wade AKLE , VERSION 1.1

## \*\*\*\*\* CABLE-CATENARY ANTENNA SIZING ANALYSIS \*\*\*\*\*

ANTENNA DIAMETER (Ft)= 100  
 FOCAL LENGTH/DIAMETER (F/D) = .6  
 OPERATING RF FREQUENCY (GHz)= 2  
 SURFACE ACCURACY (WAVELENGTH/MAX ERROR)= 16  
 MAIN ELEMENT STRUCTURAL RESPONSE (Hz)= .1  
 OPERATING RF WAVELENGTH (Ft)= .5  
 NUMBER OF CORES = 14  
 OFF-POINTING ANGLE FROM NADIR (Deg)= 8

\*\*\*\*\*  
 MASTS SIZED TO OPTIMIZE WEIGHT, WITHIN MAX ALLOWED WIDTH

### ===== FEED\_MAST DESIGN DATA OUTPUT:

MAST DESIGNED BY LONGERON BUCKLING DUE TO GENERAL  
 COMPRESSIVE MAST LOADS (Lb)= 1700  
 MATERIAL ALLOWABLE STRESS IS CRITICAL

MAST DEPLOYED LENGTH (Ft)= 67  
 MAST STOWED LENGTH (Ft)= 2.6  
 MAST BAY WIDTH=BAY HEIGHT (Ft)= 1  
 NUMBER OF BAYS = 67

LONGERON DIAMETER (Ft)= .0289  
 LONGERON THICKNESS(Ft)= .00140

CANISTER WEIGHT (Lb)= 19.0  
 LONGERON WEIGHT (Lb)= 15.4  
 BATTENS WEIGHT (Lb)= 7.7  
 DIAGONALS WEIGHT (Lb)= 4.4  
 JOINTS WEIGHT (Lb)= 22.1  
 MECHANISM WEIGHT (Lb)= 12.0

===== TOTAL MAST WEIGHT (Lb)= 80

### ===== CATENARY BOOM-MAST DESIGN DATA OUTPUT:

MAST DESIGNED BY LONGERON BUCKLING DUE TO GENERAL  
 COMPRESSIVE MAST LOADS (Lb)= 1269  
 MATERIAL ALLOWABLE STRESS IS CRITICAL

MAST DEPLOYED LENGTH (Ft)= 50  
 MAST STOWED LENGTH (Ft)= 1.9  
 MAST BAY WIDTH=BAY HEIGHT (Ft)= 1  
 NUMBER OF BAYS = 50

LONGERON DIAMETER (Ft)= .0251  
 LONGERON THICKNESS(Ft)= .00239

CANISTER WEIGHT (Lb)= 19.0  
 LONGERON WEIGHT (Lb)= 4.8  
 BATTENS WEIGHT (Lb)= 2.4  
 DIAGONALS WEIGHT (Lb)= 2.5  
 JOINTS WEIGHT (Lb)= 16.5  
 MECHANISM WEIGHT (Lb)= 12.0

===== TOTAL MAST WEIGHT (Lb)= 57

## \*\*\*\*\* CABLE-CATENARY ANTENNA MASS PROPERTIES \*\*\*\*\*

ANTENNA MESH MESH WEIGHT (Lb)= 19  
 RADIAL CATENARIES WEIGHT = 12  
 CIRCUMFERENTIAL CATENARIES= 2  
 TIP MASTS WEIGHT = 81  
 MECHANISMS WEIGHT = 7

-----  
 TOTAL ANTENNA WEIGHT (Lb) = 664.  
 ANTENNA CG FROM PARABOLA APEX (Ft)= +7.0

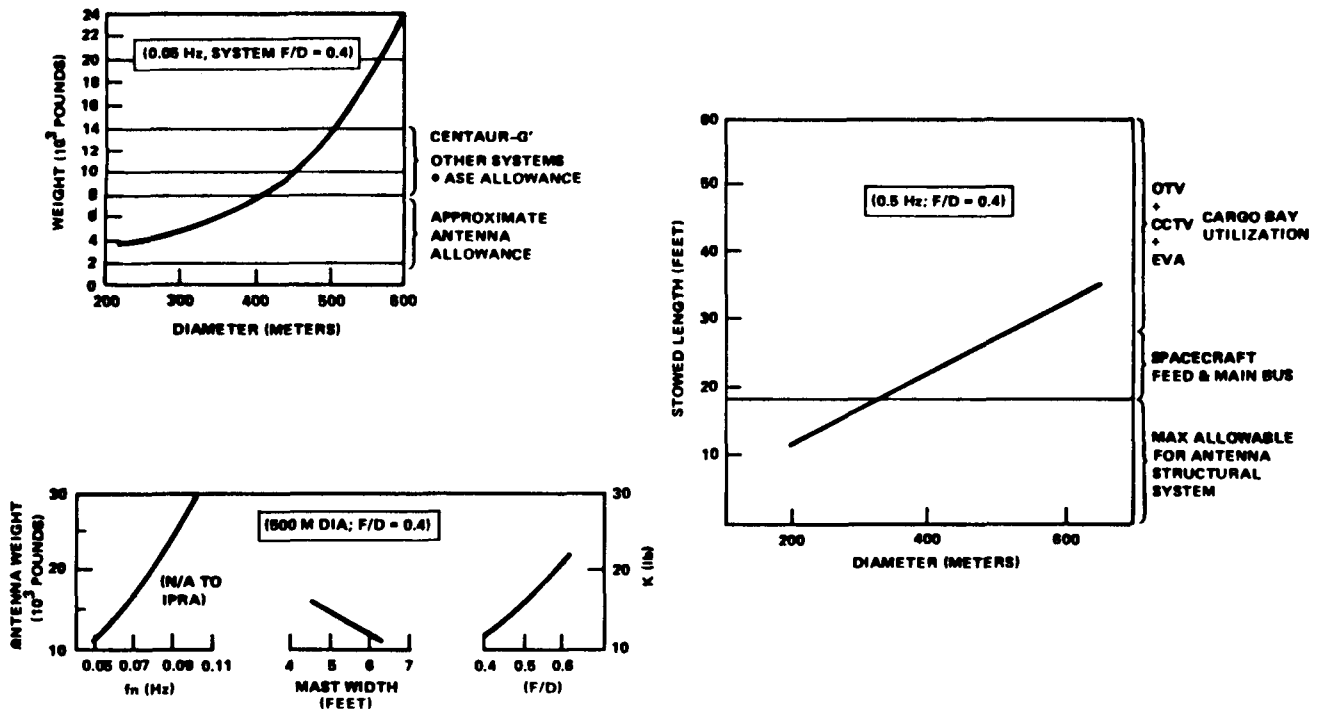
ANTENNA INERTIA (PERPENDICULAR TO AXIS) (Lb-Ft<sup>2</sup>)=+6.01E+05  
 ANTENNA INERTIA (PARALLEL TO AXIS) (Lb-Ft<sup>2</sup>)=+7.27E+05  
 ANTENNA CROSS INERTIA (Lb-Ft<sup>2</sup>)=+0.00E+00  
 OFF-POINTING ANGLE FROM NADIR (Deg)= 8.0

## CABLE-CATENARY ANTENNA - TYPICAL PARAMETRIC DESIGN DATA

Program LADSGN is used to generate a variety of CCA parametric design data. Weight and stowed dimensions, sensitivity to focal length, aperture, dynamic response lower limit frequency, and other parameters are illustrated in the figure for low RF frequency (MHz) systems.

The CCA is a highly adaptable design. It is applicable to many of the proposed spacecraft requiring large aperture. The preliminary tools required to support system trades and studies are available including cost analysis.

TRW believes that this concept is competitive and should be considered in system studies considering large antennas.



# EXTREME PRECISION ANTENNA REFLECTOR STUDY RESULTS

G. R. Sharp  
NASA Lewis Research Center  
Cleveland, Ohio

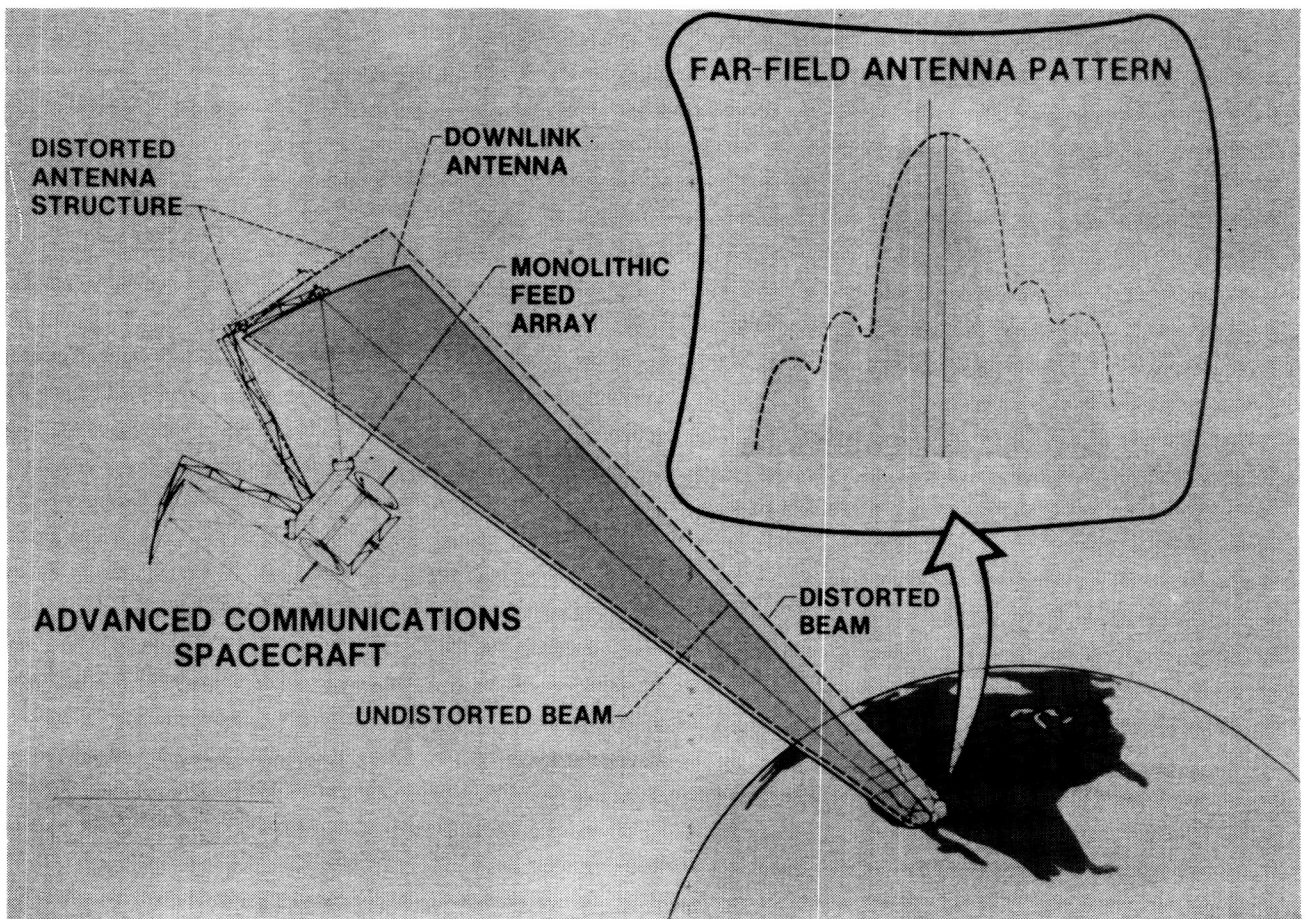
and

L. D. Gilger and K. E. Ard  
Harris Corporation  
Melbourne, Florida

Large Space Antenna Systems Technology - 1984  
December 4-6, 1984

## INTRODUCTION

The changing thermal environment at geosynchronous orbit can cause antenna structures to warp and distort over the twenty-four-hour orbit period. The distortion pattern and amplitude also vary seasonally. The mechanical distortion of the antenna reflector and structures in turn can cause deleterious effects in the far-field antenna pattern; the main antenna lobe may broaden, its amplitude decrease, its aiming point shift, and the antenna sidelobes increase in amplitude. The resulting degradation in RF performance can be a serious problem in large complex systems.





## COMMUNICATIONS ANTENNA DESIGN TRENDS

Communications antennas are now being designed to operate at higher frequencies since the lower frequency bands are becoming crowded. They are also being designed to conserve the frequency spectrum by featuring various frequency reuse concepts. Multiple narrow spot beams are used for trunking and for scanning or beam hopping. If these beams are at the same frequency, they must be isolated by polarization.

Thus, future communications antennas will be more complex than those at present and will require accurate dimensionally stable antenna reflectors and structures built from new materials.

- HIGHER OPERATING FREQUENCIES
- LARGE APERTURE DIAMETERS
- COMPLEX ANTENNAS (MULTIPLE FIXED AND SCANNING BEAMS)

## EXTREME PRECISION ANTENNA REFLECTOR AND STRUCTURE DESIGN STUDY OBJECTIVE

The design study objective is shown in the figure below.

SELECT AND ANALYZE THE BEST MECHANICAL /  
THERMAL DESIGN FOR EXTREME PRECISION SPACE-  
BASED ANTENNAS FROM 2M TO 15M-APERTURE  
DIAMETER AND UP TO 90 GHZ

## TASK DESCRIPTION AND STATUS

In early 1982, the Harris Corporation was awarded a contract for an "Antenna Design Study for Extreme Precision Antenna Reflectors and Systems Using Advanced Materials and Structural Techniques," NAS 3-23249 (Research in progress, G. R. Sharp, NASA Ames, L. D. Gilger and K. E. Ard, Harris Corporation). That study is nearing completion. Reports have been published on the materials assessment, thermal control system assessment and thermal distortion analysis techniques tasks. The report on the antenna system design task is nearly complete and materials properties verification testing of the selected materials is in progress.

The combination of computer programs and interconnecting programs used in the thermal distortion analysis task has consequently been refined at NASA LeRC to provide a very accurate tool for calculating the on-orbit variations in antenna patterns.

o TASKS	STATUS
- MATERIALS ASSESSMENT	- COMPLETE
- THERMAL CONTROL ASSESSMENT	- COMPLETE
- THERMAL DISTORTION ANALYSIS TECH.	- COMPLETE
- ANTENNA SYSTEM DESIGN	- COMPLETE
- MATERIALS PROPERTIES VERIFICATION	- IN PROGRESS

## CURRENT ANTENNA REFLECTOR AND STRUCTURE FABRICATION TECHNOLOGY

Currently, antenna reflectors are constructed using carbon fibers in an epoxy matrix in order to minimize weight and the coefficient of thermal expansion and hence antenna thermal distortion. The reflector structures typically are of two types: unidirectional plies of carbon/epoxy arranged to give planarly isotropic near-zero coefficient of thermal expansion in a solid reflector or thin honeycomb sandwich panel reflectors with very thin planarly isotropic carbon/epoxy face sheets. After construction, these reflectors are fastened to a lightweight strongback structure that is used to adjust the reflector to as nearly a true parabolic shape as possible.

Other antenna structures such as the antenna feed support towers are constructed using carbon/epoxy or carbon /polyimide tubes and structural shapes.

A 2.7M-aperture-diameter state-of-the-art offset fed parabolic reflector was recently constructed by TRW as a part of an advanced 30-GHz proof-of-concept antenna system. The 0.25-in.-thick reflector was made from honeycomb sandwich panel with carbon/epoxy face sheets and a Nomex core. The reflector was mounted to a strongback also constructed from carbon/epoxy honeycomb sandwich panel. The strongback was used both to support and for final adjustment of the reflector surface. The maximum zero-to-peak deviation from a true parabola was 0.020 inches. The RMS deviation from a true parabola was 0.0055 inches RMS. When this reflector was manufactured, problems were encountered with excess adhesion to the molding surface. Therefore, accuracy for state-of-the-art manufacturing of a flight-type reflector should be perhaps 0.003 inches RMS.

### o DESIGN

- REFLECTOR - HONEYCOMB SANDWICH PANEL
  - CARBON/GLASS FACE SHEET (PLANAR QUASI-ISOTROPIC LAYUP) (+60<sup>0</sup>, 0<sup>0</sup>, -60<sup>0</sup>)
  - CARBON/GLASS EGGCRATE CORE
  - ASSEMBLY BY SLUMP FORMING AND FRIT BONDING
- ANTENNA STRUCTURE - CARBON/MAGNESIUM OR CARBON/ALUMINUM TUBES AND STRUCTURAL SHAPES

### o ACCURACY (FOR A 4-METER REFLECTOR) (TDAS)

- REFLECTOR - MAXIMUM ZERO-TO-PEAK DEVIATION FROM TRUE PARABOLA
  - .004 INCHES
  - SURFACE ROOT MEAN SQUARE (RMS) DEVIATION FROM TRUE PARABOLA - .001 INCHES RMS

## CURRENT ANTENNA REFLECTOR AND STRUCTURE FABRICATION TECHNOLOGY (CONTINUED)

The advantages of carbon/epoxy construction for antenna reflectors are that the uni-directional plies can be tailored and assembled in such a way as to yield a near-zero coefficient of thermal expansion (CTE) in the plane of the reflector and that the construction technology is well developed.

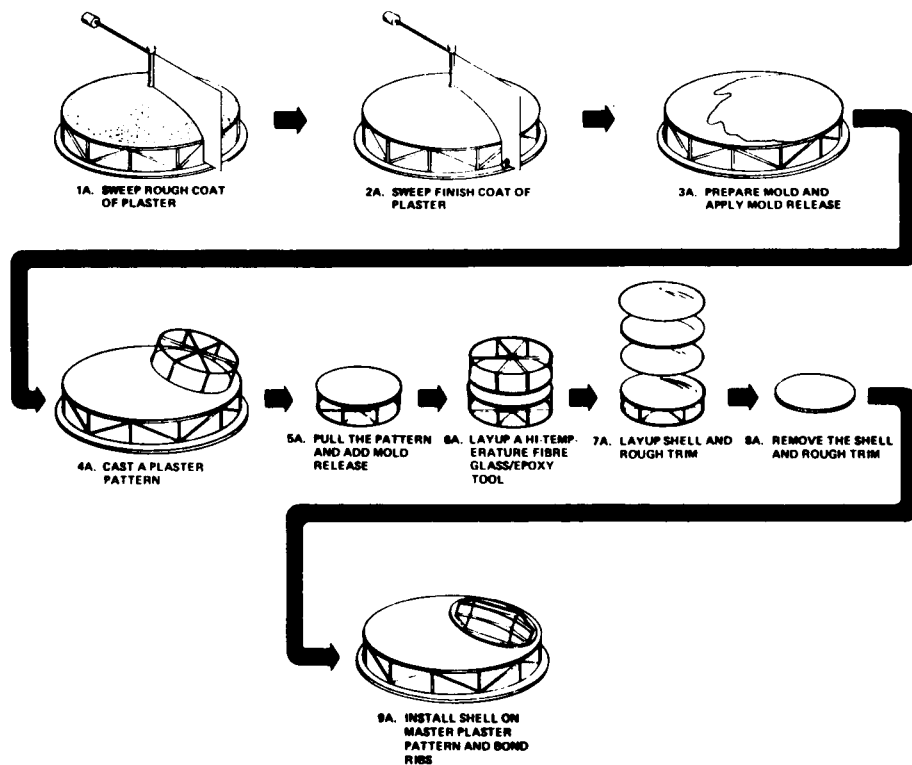
The drawbacks of carbon/epoxy construction are listed below. The most serious of these are the non-linear coefficient of thermal expansion (reflector operational temperatures at geosynchronous orbit range from -260°F to +175°F) and permanent creep that occurs as construction stresses are relieved.

- o ADVANTAGES OF CARBON/EPOXY CONSTRUCTION
  - NEAR-ZERO COEFFICIENT OF THERMAL EXPANSION (CTE)
  - DEVELOPED TECHNOLOGY
  
- o DISADVANTAGES OF CARBON/EPOXY CONSTRUCTION
  - NON-LINEAR COEFFICIENT OF THERMAL EXPANSION WITH RESPECT TO TEMPERATURE
  - EFFECT OF ABSORBED MOISTURE AND SUBSEQUENT DRY-OUT IN SPACE ON FINAL REFLECTOR SHAPE AND FINAL COEFFICIENT OF THERMAL EXPANSION
  - MICRO-CRACKING - ALLOWS DIMENSIONAL CHANGES FROM FORMED SHAPE TO NEW SHAPE
  - CREEP - IF UNDER CONSTANT STRESS WILL TEND TO RELIEVE STRESS AND MOVE TO NEW POSITION

## CURRENT SPACE ANTENNA REFLECTOR FABRICATION TECHNOLOGY

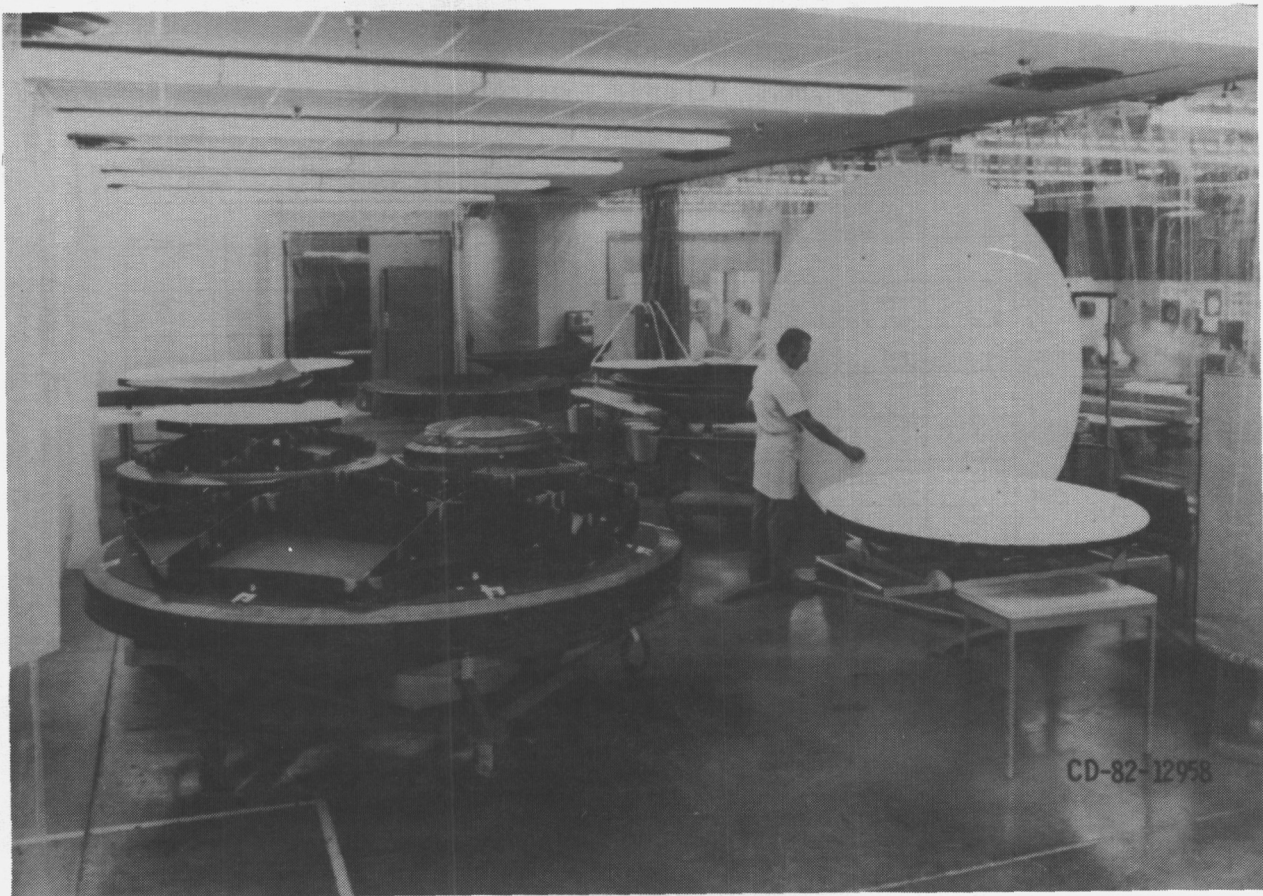
The method of fabrication for present-day carbon/epoxy antenna reflectors is illustrated. First, a convex plaster mold is prepared of the desired surface contour. Subsequently, a plaster concave and then a high-temperature convex mold are prepared. The antenna shell is cured then on a high-temperature convex mold. It is then fitted to the plaster mold whereon final adjustment of the reflector surface takes place.

### 30-GHZ 9-FT DIA. MBA OFFSET REFLECTOR FABRICATION-FLOW DIAGRAM



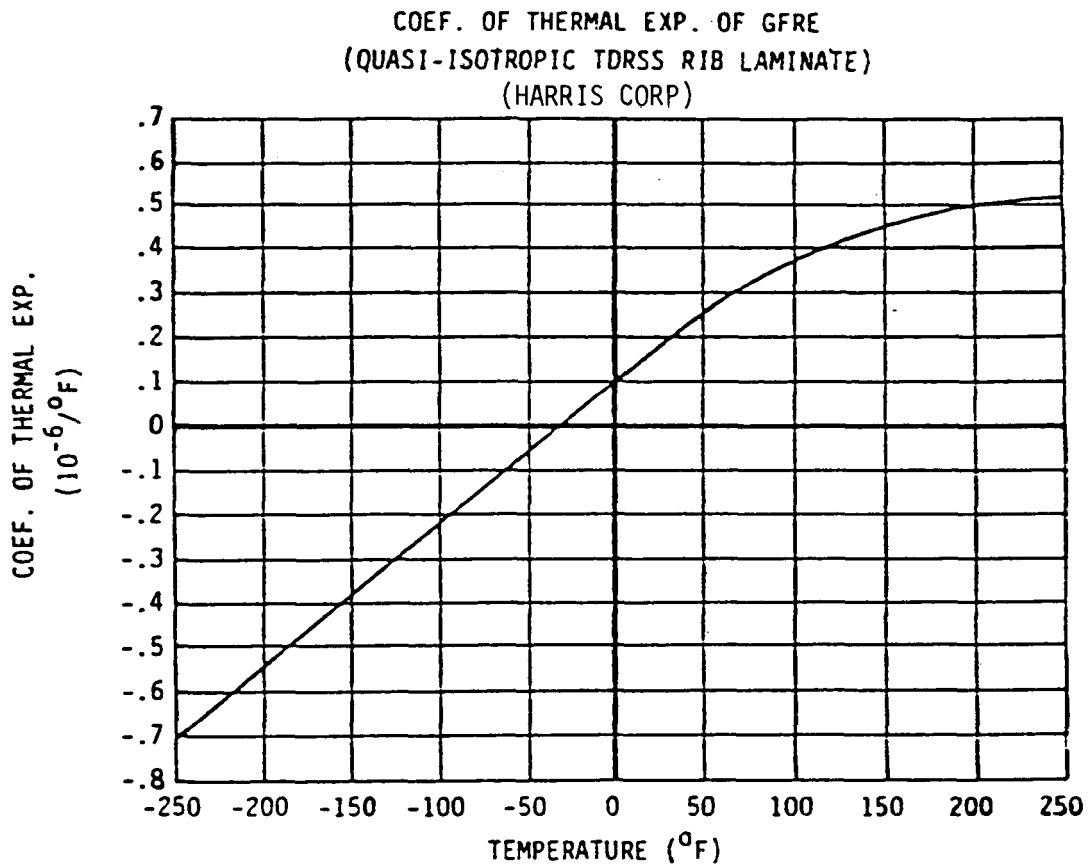
## REFLECTOR FINAL ADJUSTMENT

The reflector is shown after final adjustment to the master mold. This was accomplished by permanently deforming the reflector surface by moving it with respect to a strongback frame and then locking the reflective surface in place.



# COEFFICIENT OF THERMAL EXPANSION OF CARBON/EPOXY (HARRIS CORPORATION)

Note that while at room temperature, the coefficient of thermal expansion (CTE) is +0.3, at the typical lower expected operating temperature of -260°F the CTE drops to -0.7. In a situation wherein the unprotected reflector face is coming out of shadow and into sunlight, reflector temperatures can typically simultaneously vary from -20°F to -190°F. Over the range, the CTE could instantaneously vary from -0.5 to +0.05 over the reflector. Thus, the reflector thermal distortion and hence the antenna pattern can be affected by the non-linear CTE properties of the carbon/epoxy composite.





## REQUIRED ANTENNA REFLECTOR AND STRUCTURE FABRICATION TECHNOLOGY

When more accurate reflectors are needed and if the dimensional stability problems of carbon/epoxy construction are to be overcome, new matrices and fabrication technology will be required. Both glass and polyimide matrices were considered for carbon-filament-reinforced composite reflectors.

### o DESIGN

- REFLECTOR - HONEYCOMB SANDWICH PANEL
  - CARBON/EPOXY OR CARBON/POLYIMIDE FACE SHEETS (PLANAR QUASI-ISOTROPIC (+60°, 0°, -60° PLIES))
  - NOMEX OR ALUMINUM HONEYCOMB CORE
- ANTENNA STRUCTURE - CARBON/EPOXY OR CARBON/POLYIMIDE TUBES AND STRUCTURAL SHAPES

### o ACCURACY (FOR A 3-METER REFLECTOR)

- REFLECTOR - MAXIMUM ZERO-TO-PEAK DEVIATION FROM TRUE PARABOLA .020 INCHES
  - SURFACE ROOT MEAN SQUARE (RMS) DEVIATION FROM TRUE PARABOLA - 0.0055 INCHES RMS

## REQUIRED ANTENNA REFLECTOR AND STRUCTURE FABRICATION TECHNOLOGY (CONTINUED)

Glass was chosen as the favored matrix because carbon/glass composites can be constructed with near-zero coefficients of linear expansion (CTE) and they are impervious to moisture and dryout distortion. Near optical-type stability can be obtained since creep values are low in comparison to carbon/epoxy. Also, extreme precision surfaces can be ground or lapped on the hard stable surface if required. The carbon/glass also has good resistance to particle and ultra-violet radiation and a wider operating temperature range.

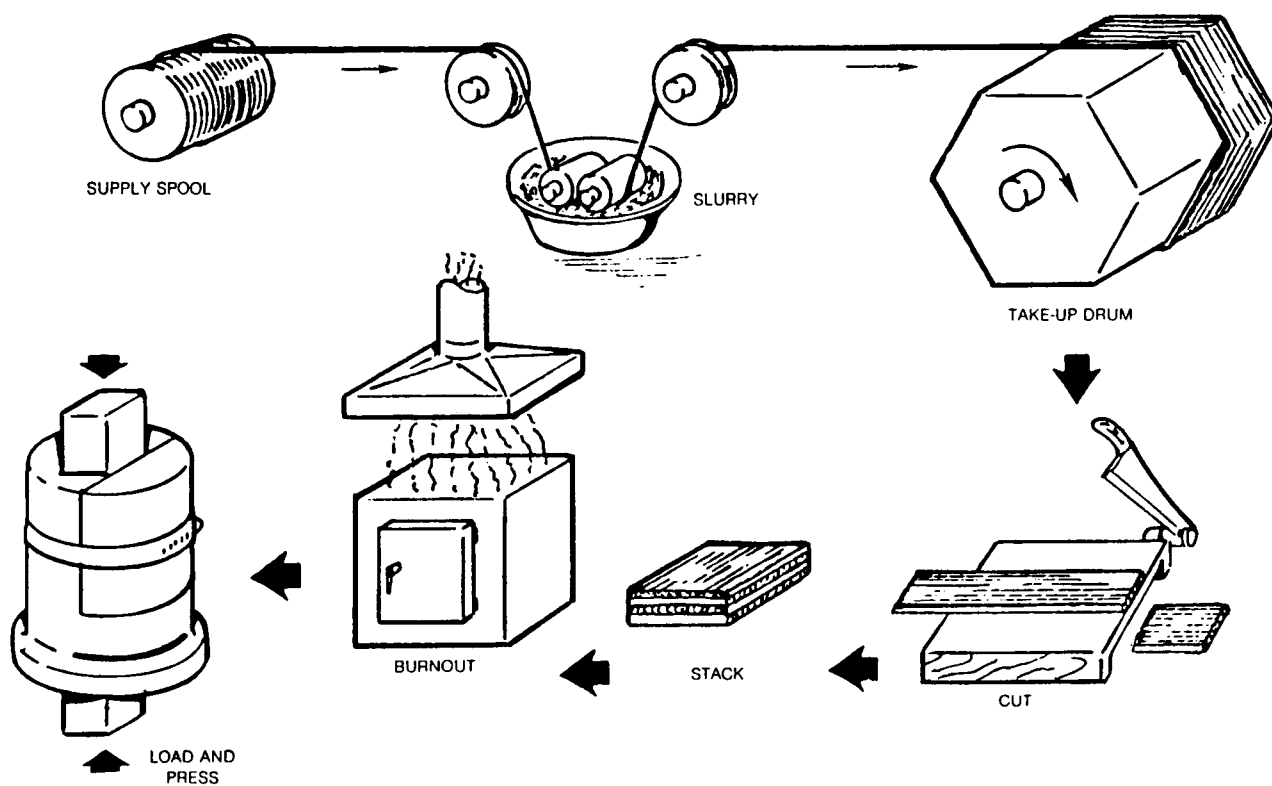
However, the carbon/glass used to construct a reflector is processed at high (2,000°F) temperatures. Also, additional development is needed on the processes for manufacturing and assembling the materials.

- o ADVANTAGES OF CARBON/GLASS CONSTRUCTION
  - NEAR-ZERO COEFFICIENT OF THERMAL EXPANSION
  - IMPERVIOUS TO MOISTURE AND DRYOUT DISTORTION
- o DISADVANTAGES OF CARBON/GLASS CONSTRUCTION
  - HIGH (2,000°F) GLASS TILE SUB-ASSEMBLY FORMING TEMPERATURE
  - MATERIALS PROCESSING AND ASSEMBLY NEED DEVELOPMENT AND TESTING

## CARBON/GLASS MANUFACTURING SEQUENCE

In a fashion very similar to that for carbon/epoxy, the raw fiber is infiltrated and coated with the matrix (in this case powdered glass). After drying, it is cut just like carbon/epoxy prepreg (carbon fibers or cloth that have been infiltrated with epoxy but not cured). The plies are then stacked in the desired configuration and the volatiles removed. The final step is high-temperature pressing into the finished form (ref. 1).

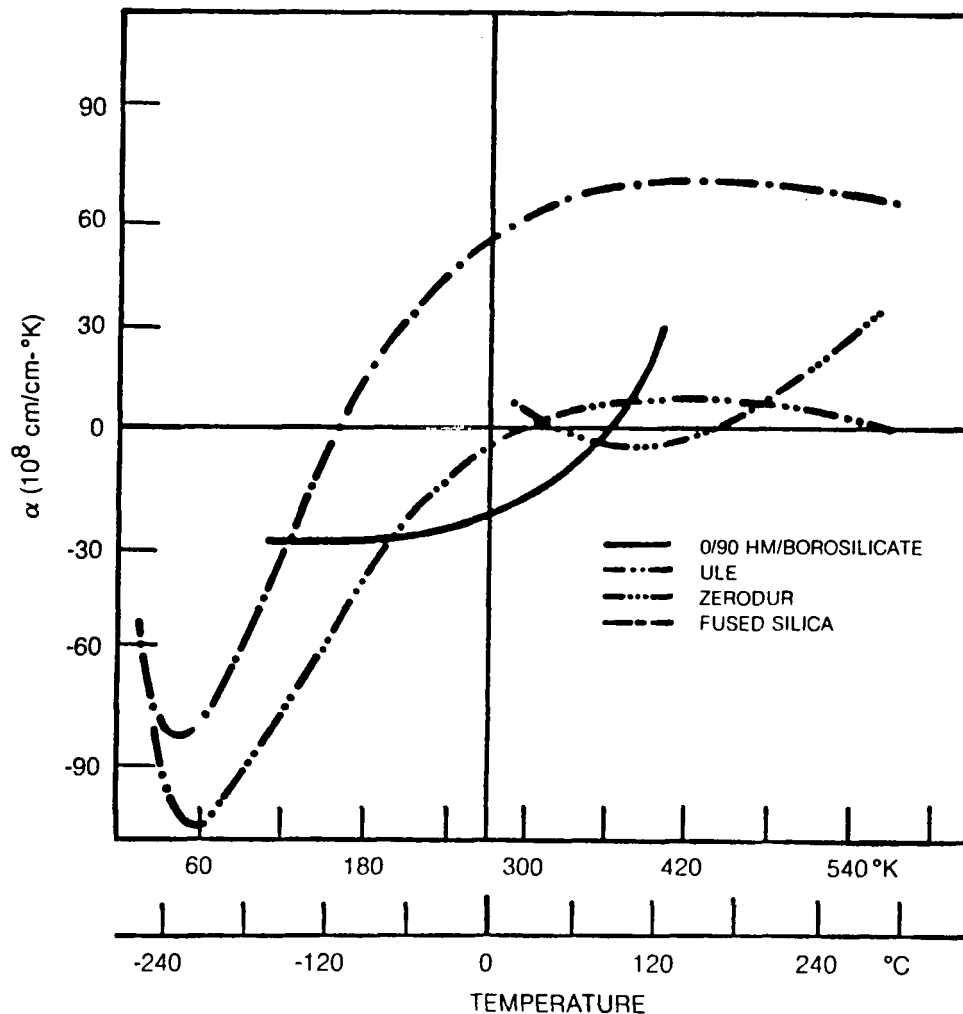
### TAPE LAYUP PROCESSING



## COEFFICIENT OF THERMAL EXPANSION (CTE) OF CARBON/GLASS

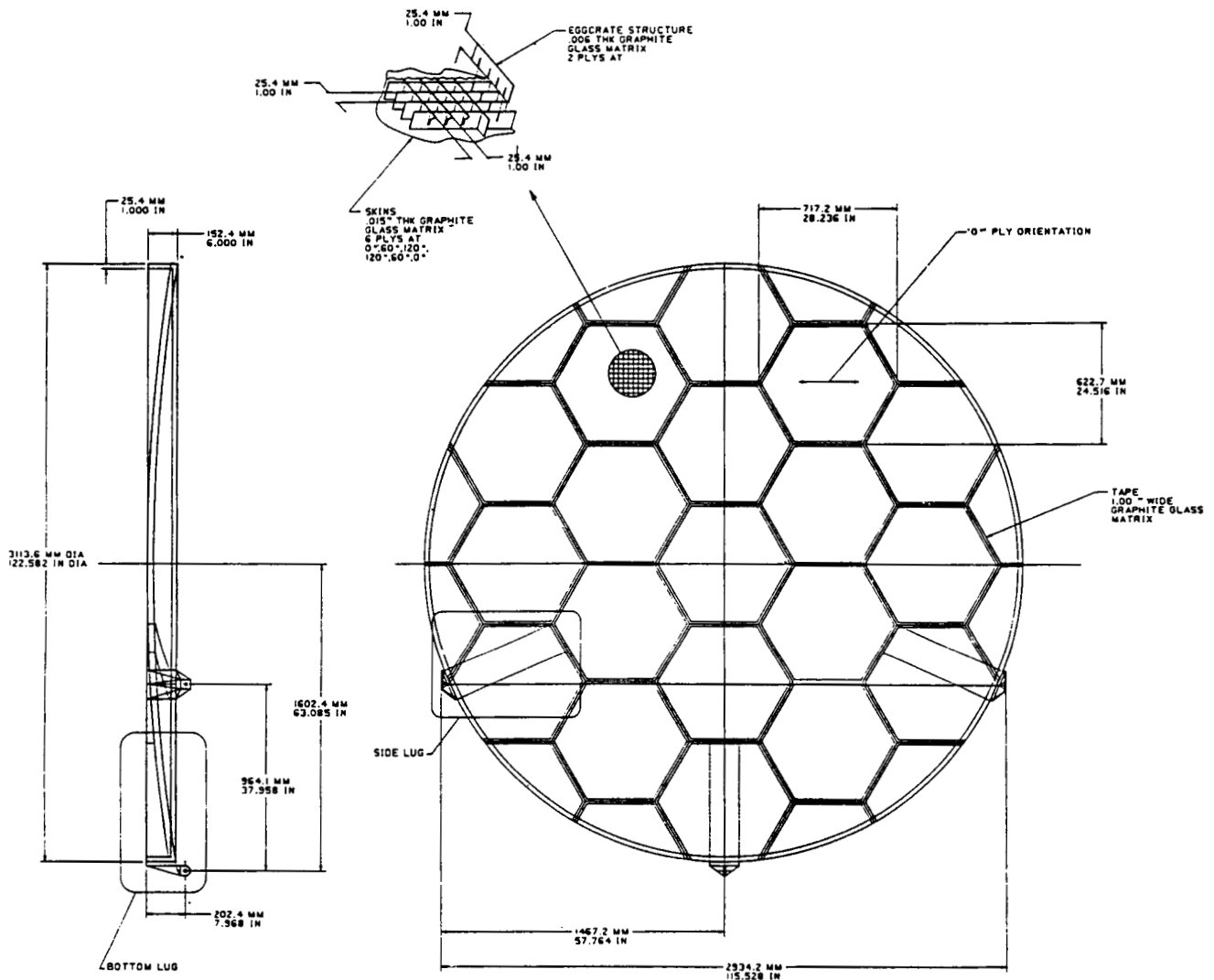
The 0/90-ply orientation HM carbon fiber/borosilicate glass matrix composite CTE changes very little as a function of temperature below 0°C as compared to carbon/epoxy (see figure for coefficient of thermal expansion of carbon/epoxy - Harris Corporation) and even compared to other pure glasses (ULE, Zerodur and fused silica).

### THERMAL EXPANSION OF CONTINUOUS FIBER COMPOSITES RELATIVE TO CURRENT MATERIALS



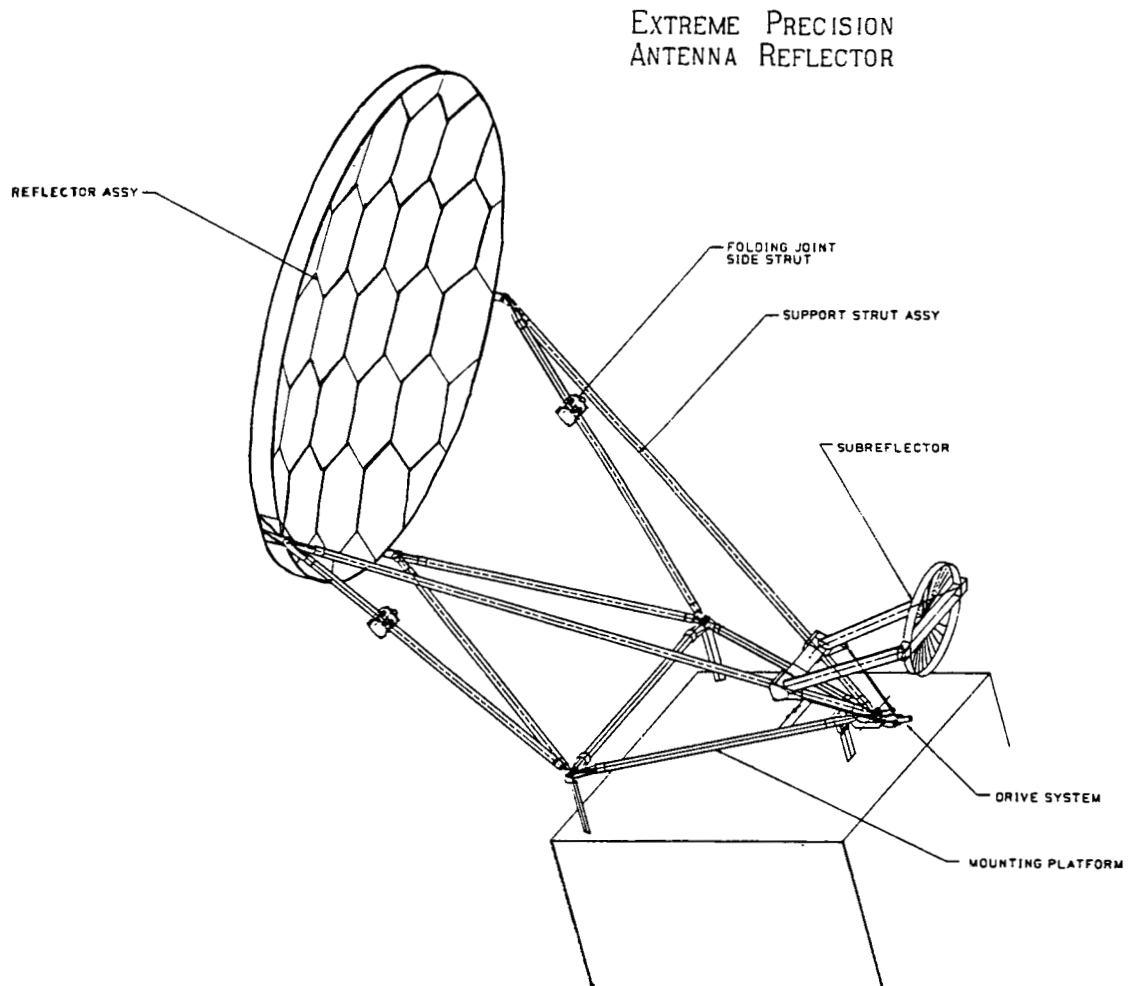
## CARBON/GLASS REFLECTOR ASSEMBLY

A parabolic reflector of carbon/glass would be constructed of honeycomb sandwich panel. The face sheets would be made of tiles laid up in a planarly isotropic pattern (+60°, 0°, -60°). The reflective surface would be of random-oriented fibers. The core would be carbon/glass eggcrate construction. The reflector would be assembled using the tiles and eggcrate core and then heated to slump-form and frit-bond (lower temperature melting ground glass particles) the parts together. Final contour machining of the random fiber surface should assure accuracies of 0.004 in zero-to-peak deviation from a true parabola and RMS deviation of less than 0.001 inches.



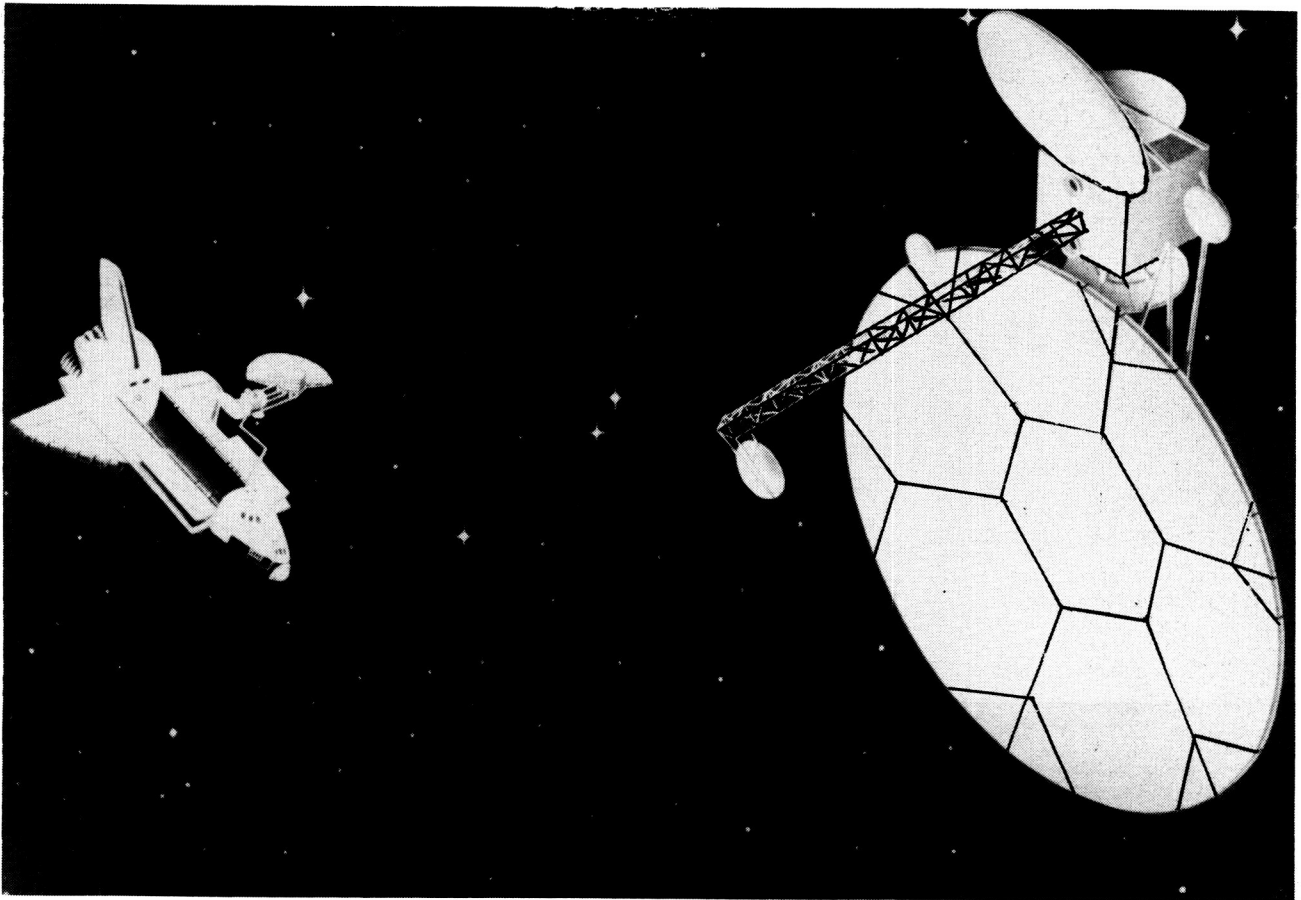
## CARBON/GLASS ANTENNA ASSEMBLY

The carbon/glass antenna reflector is shown here in an offset configuration typical of space communications applications.



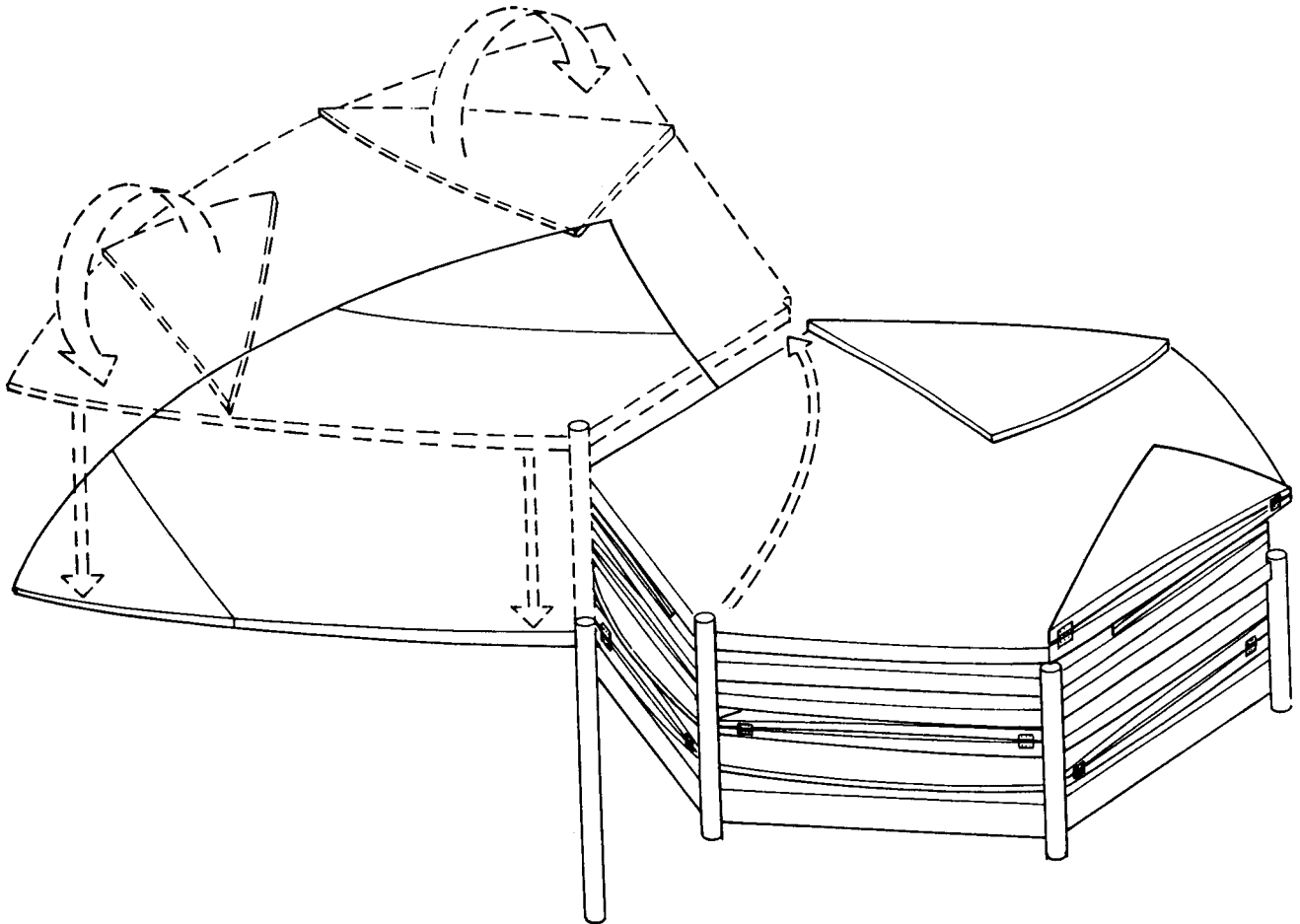
## EXTREME PRECISION DEPLOYABLE REFLECTOR CONCEPT

The 3M-aperture-diameter carbon/glass reflector can be used as a sub-assembly for larger reflectors. Preliminary design studies resulted in this concept for a 10.5-meter offset-fed precision antenna. Because carbon/glass has such a low CTE in combination with excellent dimensional stability, it was determined that a deployable antenna back-up truss or structure would not be necessary for this concept.



## DEPLOYABLE REFLECTOR DEPLOYMENT SEQUENCE

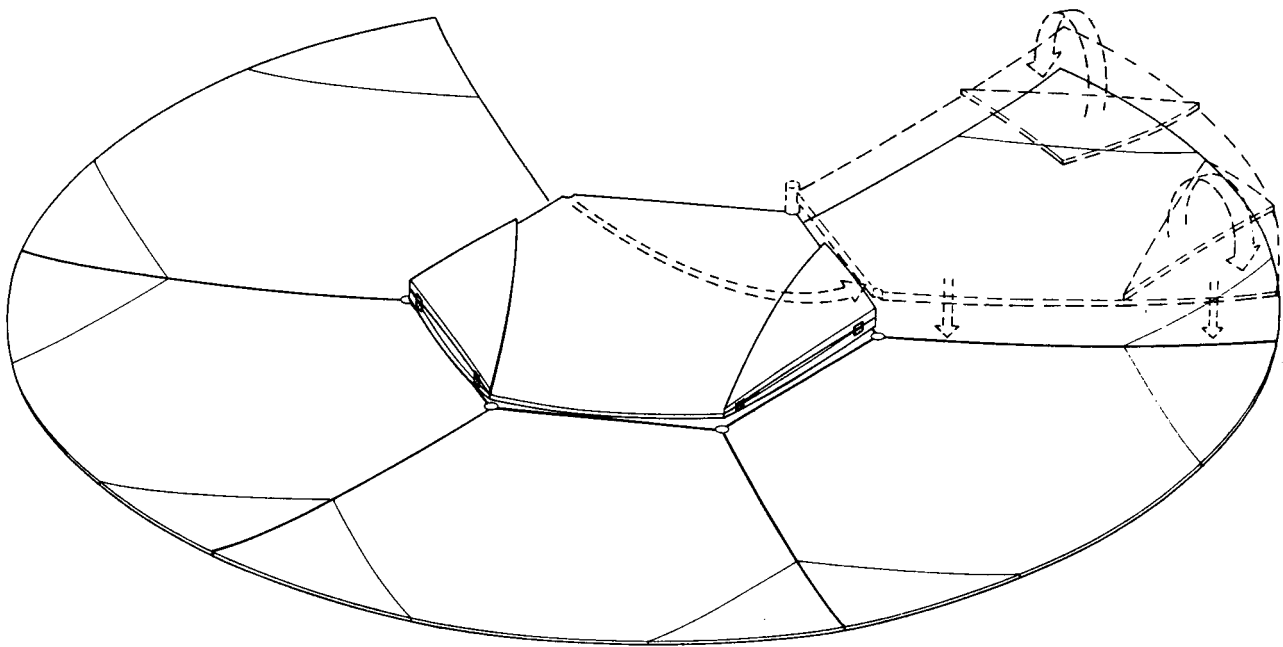
The deployment sequence for the 10.5M-aperture-diameter antenna is shown here. The upper panel is first lifted clear of the central stack. It is then rotated into position. A jackscrew is then used to lower the panel into place where locking mechanisms will be used to lock it to the central panel. Each subsequent panel is deployed in a similar sequence.





## DEPLOYABLE REFLECTOR DEPLOYMENT SEQUENCE

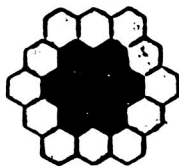
When all panels have been deployed and locked in place, micro-jacks at the panel edges can be used for final reflector adjustment. This can be done on either a one-time or continual basis.



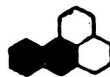
## DEPLOYMENT SEQUENCE FOR LARGER REFLECTORS

Panels can be assembled as sub-stacks in the central stack rather than as single panels. Then, from the initial central stack, a single panel can be used to swing out two more panels (a three-pedal sequence) in addition to itself. A sequence of such deployments could result in a 16-meter deployable reflector. A six-pedal sequence is also shown. Here, a single central panel would deploy a stack of six panels from which the sequences of two and three panels could be deployed.

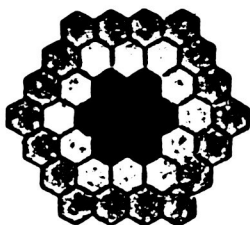
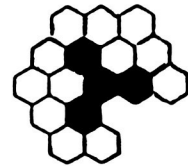
The design study demonstrated that the great advantage of this method of solid reflector panel deployment was that the packing density in the launch vehicle could be many times that of other deployment methods such as radial or pie-shaped panel deployments which require long narrow stacks for larger diameter reflectors.



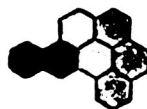
**DOUBLE RING  
16-METER DIAMETER**



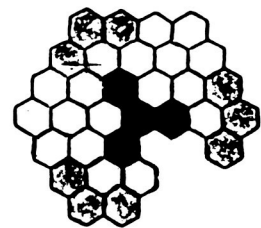
**THREE-PEDAL  
SEQUENCE**



**TRI-RING  
22-METER DIAMETER**



**SIX-PEDAL  
SEQUENCE**



## EXTREME PRECISION ANTENNA FUTURE PLANS

It is planned to design and build an engineering model of a small extremely precise antenna (such as might be suitable for a model of a 60-GHz intersatellite link antenna) in FY '86-'87. The antenna would use standard lightweight materials for the reflector support structure. However, the reflector would be constructed from carbon/glass subpanels and thus would act as a pathfinder for lightweight carbon/glass reflector technology.

- o PROGRAM - ENGINEERING MODEL DEVELOPMENT
- o DESCRIPTION - 1 1/2 TO 3-M APERTURE DIAMETER
  - 57 GHz
  - DIRECT FED (SINGLE HORN)
  - FLIGHT-TYPE REFLECTOR, ENGINEERING MODEL STRUCTURE
- o SCHEDULE - FY '86 TO '88
- o ESTIMATED RESOURCES - 1 TO 2 M
- o MAJOR TECHNICAL CHALLENGE - PRECISION REFLECTOR CONSTRUCTION

## REFERENCE

1. K. M. Prewo and E. J. Minford: Graphite Fiber Reinforced Thermoplastic Glass Matrix Composites for Use at 1,000°F, Proceedings of the 16th National SAMPE Conference, Anaheim, CA, April 21-23, 1981.

NASA SPACE MATERIALS RESEARCH

Darrel R. Tenney, Stephen S. Tompkins, and George F. Sykes  
NASA Langley Research Center  
Hampton, Virginia

Large Space Antenna Systems Technology - 1984  
December 4-6, 1984

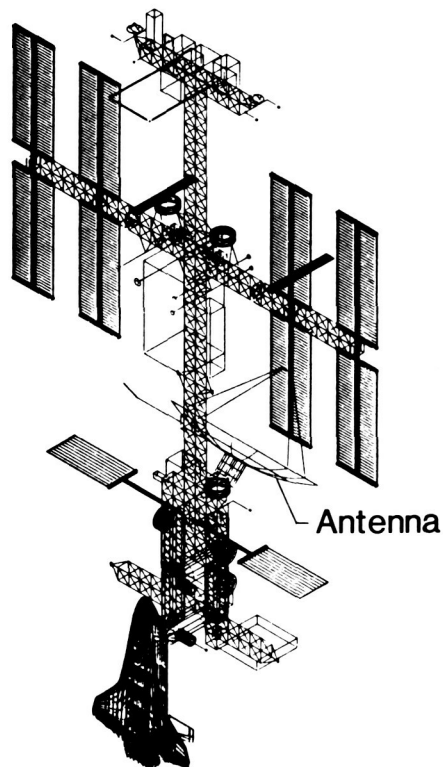
## INTRODUCTION

Long-term stability within the space environment is a major materials concern for a variety of spacecraft components found on large space antenna systems. For low Earth orbit (LEO) applications, the key environmental variables are atomic oxygen, UV, high vacuum, and thermal cycling. For geosynchronous Earth orbit (GEO) applications, the key variables are high-energy electron and proton radiation, UV, high vacuum, and thermal cycling. For long-life (10 to 20 years) space missions (fig. 1), the durability of thin films, thermal control coatings, and structural composites in the space environment must be established for confident design of economical systems.

This paper will review some of the more recent work on the effect of the space environment on (1) thermal control coatings and thin polymer films, (2) radiation stability of 250°F and 350°F cured graphite/epoxy composites, and (3) the thermal mechanical stability of graphite/epoxy, graphite/aluminum, and graphite/glass composites. Degradation in mechanical properties due to combined radiation and thermal cycling will be highlighted. Damage mechanisms will be presented and suggested chemistry modifications to improve stability will be discussed. The dimensional instabilities in graphite/epoxy composites associated with microcracking during thermal cycling will be examined. Finally, thermal strain hysteresis found in metal-matrix composites will be discussed.

## FOCAL MISSIONS FOR TECHNOLOGY DEVELOPMENT

Space Station - LEO



Antenna - GEO

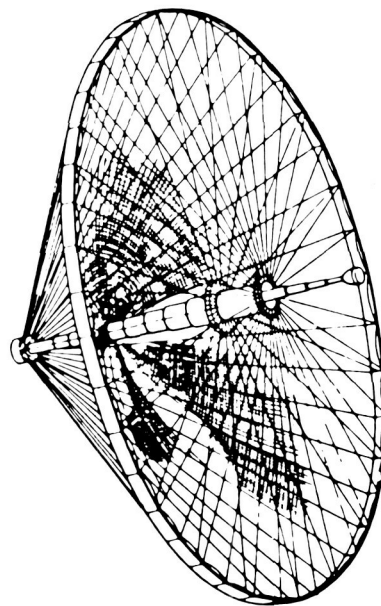


Figure 1

## SILOXANE-MODIFIED POLYIMIDE FOR SPACE APPLICATIONS

Early Shuttle flights (STS-3 and STS-5) have demonstrated that the LEO environment could be a significant threat to certain classes of polymeric films and coatings. Polymer films exposed on these early short flights, for example, showed serious surface erosion and corresponding weight losses (ref. 1). Surface and chemical analyses following exposure have attributed the erosion to interaction of atomic oxygen with the material surface. Efforts are now under way to identify new stable materials and/or protection schemes for existing materials that would provide for the materials needs of long-life LEO missions.

A siloxane-modified polyimide copolymer being investigated at Langley (ref. 2) has been found to be less reactive to atomic oxygen than other commonly used spacecraft polymer films (fig. 2). The copolymer incorporates stable siloxane segments into the basic polyimide backbone to provide a unique material that retains general polyimide properties. Characterization of cast films of this material has shown that the siloxane segments of the copolymer migrate to the surface and provide a siloxane "molecular coating" on a basic polyimide substrate. The atomic oxygen stability of this material has been evaluated in ground-based facilities and a recent Shuttle flight (STS-8). In the Shuttle flight, polymer film strips were mounted on a temperature-controlled plate in the cargo bay and received a high flux of atomic oxygen. Following the exposure flight, weight loss analysis showed that the copolymer had about an order-of-magnitude lower reaction rate than the normally used polyimide Kapton (manufactured by E. I. du Pont de Nemours & Co., Inc.). Some erosion of the surface was observed, however, and research on this novel class of copolymers is continuing in an attempt to obtain additional improvements and an understanding of the mechanisms of atomic oxygen interaction with these materials.

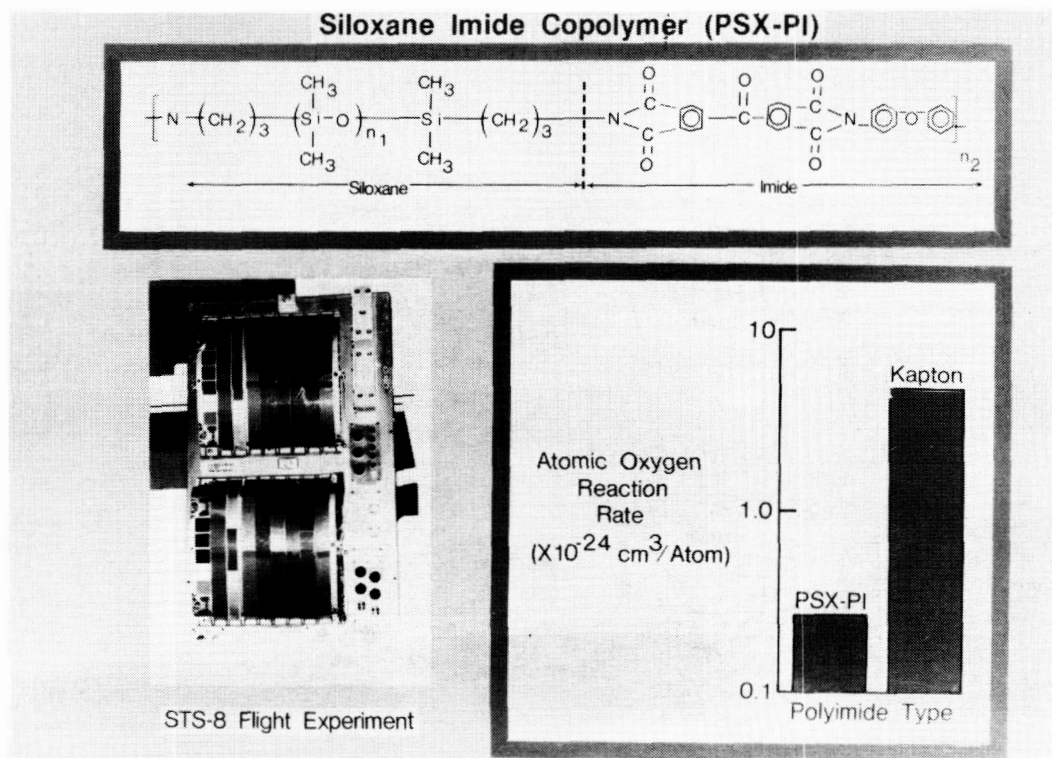


Figure 2

# DR-FTIR SPECTRA OF T300/5208 COMPOSITE

The effect of atomic oxygen on the erosion of neat polymer films is well documented, as noted in the previous figure. However, other materials such as composites have important potential uses in low Earth orbit and, therefore, their response to atomic oxygen has also been considered. Figure 3 shows results from characterization (ref. 2) of one material, T300/5208 graphite/epoxy system (manufactured by Narmco Materials, a subsidiary of Celanese Corporation), following exposure to atomic oxygen. This sample was flown on the STS-8 flight experiment (225-km orbit) where it was exposed for 41 hours (oxygen impingement normal to surface) and received a total oxygen fluence of  $3.5 \times 10^{20}$  atoms/cm<sup>2</sup>. The figure shows diffuse reflectance infrared spectra of the control sample (covered during the flight) and spectra of both front and rear surfaces of the exposed specimen. The rear surface of the exposed specimen was shielded and not directly exposed during the flight. The data show that major chemical degradation does not occur during atomic oxygen exposure; that is, the exposed sample has generally identical major absorption bands as the control specimen. Several of the major bands are identified in the figure. However, the spectra do show, as evidenced by the appearance of the  $>C=O$  absorption band near  $1700\text{ cm}^{-1}$ , that oxidation is the primary mechanism of atomic oxygen interaction with the composite matrix. This oxidation is accompanied by an erosion very similar to that observed in the neat polymer films. The IR spectrum of the back surface of the composite also indicated oxidation of the polymer. The composites were mounted on an aluminum plate but were not sealed. The mechanism of oxidation of the back surface is not known. These data therefore indicate that use of current advanced composite systems, such as the T300/5208 system for LEO applications, will require development of stable atomic oxygen resistant coatings.

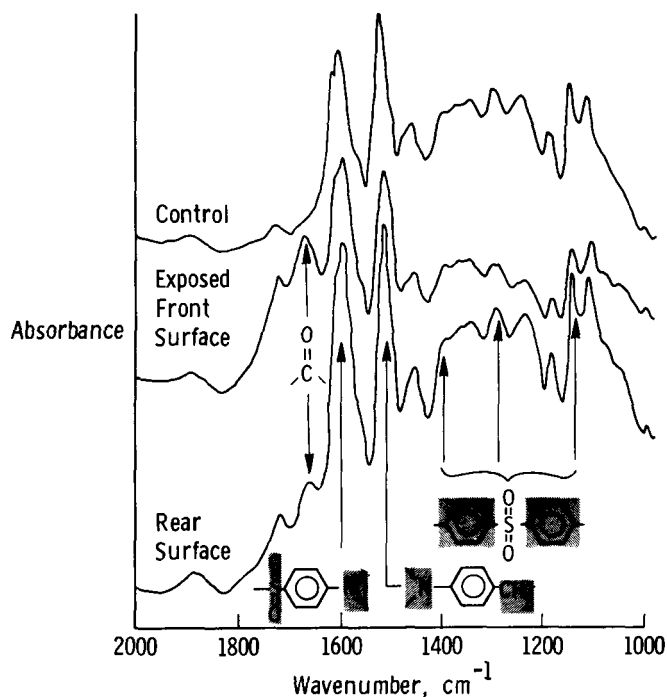


Figure 3



## COMPOSITE COATING DEVELOPMENT

Graphite/epoxy composite tubes are being considered for use in space antenna structures because of their high specific strength and stiffness and good dimensional stability. Composites used in space need to be coated to protect the resin from UV degradation, atomic oxygen erosion (LEO applications), and low-energy electron and proton degradation for GEO applications. Coatings are also needed to minimize the temperature range over which composites will cycle in space. The upper left portion of figure 4 shows the range of temperatures that composite tubes will cycle over with (1) no coating, (2) white paint, and (3) aluminum coating. Also shown is the temperature range that a composite tube would cycle over if the coating had a solar absorptance ( $\alpha$ ) of 0.20 to 0.35 and emittance ( $\epsilon$ ) of 0.15 to 0.25.

Several experimental coatings have been developed (by W. S. Slemp, NASA Langley) which give optical properties in the desired range. Three of these are shown at the bottom of figure 4. These coatings were all produced by vapor depositing thin layers of metals and metal oxides to form multilayer coatings with the required combination of low  $\alpha$  (0.20 to 0.35) and low  $\epsilon$  (0.15 to 0.25). The thicknesses of the individual layers are a few thousand angstroms and were selected to achieve the optical properties shown. Aluminum,  $\text{SiO}_2$ , and  $\text{Al}_2\text{O}_3$  have excellent resistance to atomic oxygen and should protect the composite substrate for LEO applications. These materials also have good stability to electron, proton, and UV radiation. Space qualification testing of these coatings is under way and, if they prove to have sufficient durability, alternate application techniques will be investigated to economically coat full-size structural subelements.

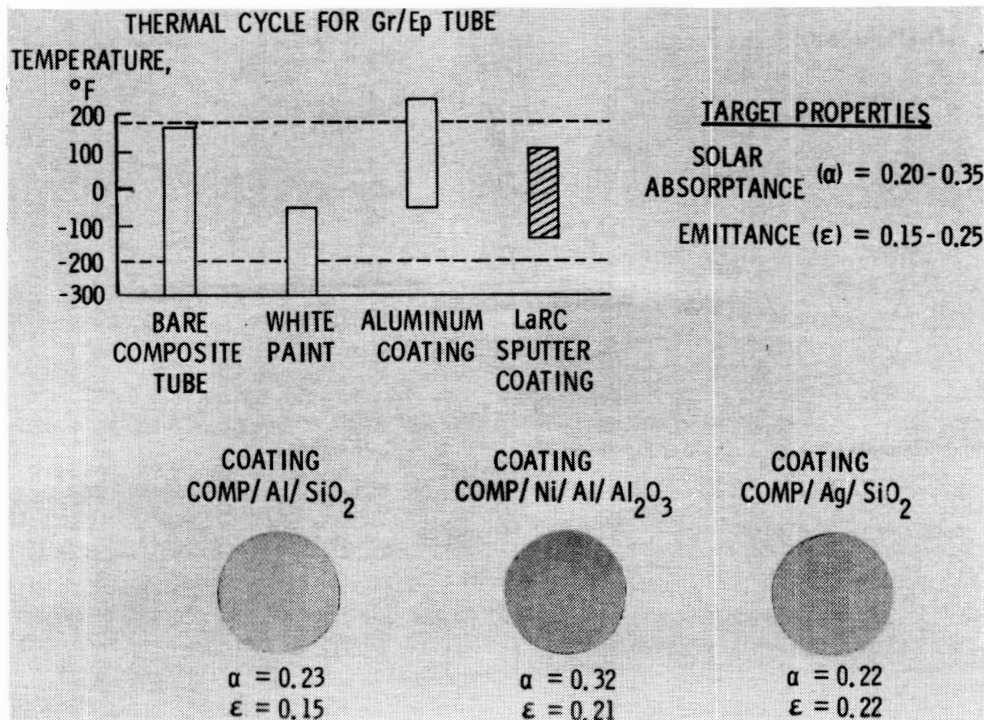
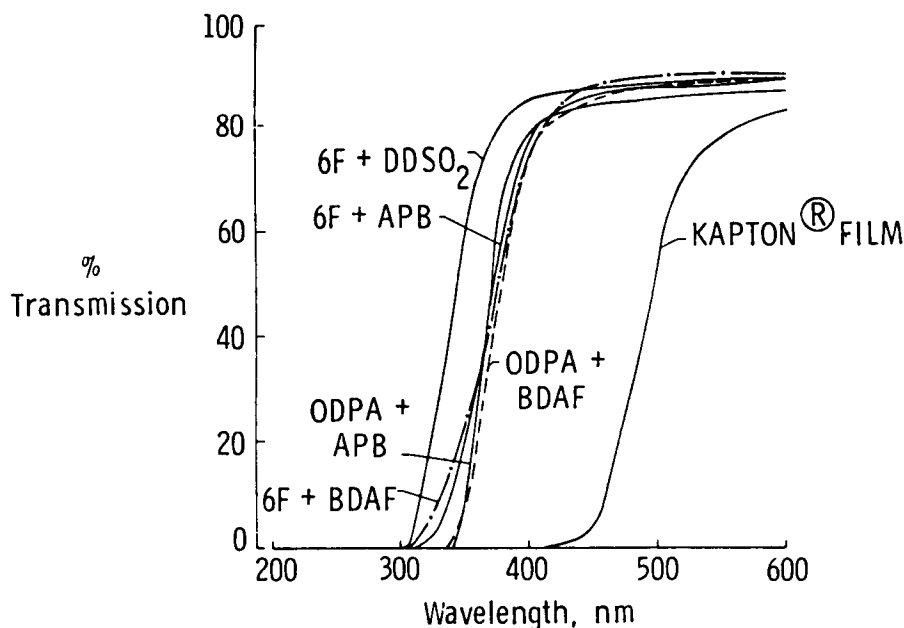


Figure 4

## UV-VIS SPECTRA OF COLORLESS FILMS VERSUS KAPTON

A series of novel, optically transparent aromatic polyimides were synthesized to obtain films with maximum optical transparency for use in space as second surface mirror coatings (ref. 3). Color in the films was lowered by reducing the electronic interaction between chromophoric centers in the polymer chemical structure and by monomer purification procedures. The percent transmission of these films compared to Kapton in the UV-visible wavelength range is shown in figure 5. At the solar wavelength (500 nm), for space application on solar cells and thermal control systems, Kapton is approximately 40 percent transparent (depending on thickness) and the linear aromatic films are approximately 85 to 90 percent transparent. Also, some of these polyimides have potential for spray coating applications because they are soluble in low-temperature boiling solvents. Both UV and electron irradiation exposures will be conducted to evaluate the stability of these films to the space radiation environment.



(TAKEN FROM REF. 3)

Figure 5

## RADIATION STABILITY OF POLYMERS AND COMPOSITES

Spacecraft placed at GEO will be subjected to high doses of electron and proton radiation. For long-term exposures (20 to 25 years), the total absorbed radiation dose in resin-matrix composites will exceed  $10^9$  rads and changes in matrix-dominated properties are likely.

NASA has been conducting research to determine the magnitude of property changes in composites when subjected to high doses of electron and proton radiation. This work has been conducted at Langley Research Center, at Jet Propulsion Laboratory, and at Marshall Space Flight Center. Emphasis has been placed on (1) determining the bounds on changes in mechanical properties, (2) measuring the matrix embrittlement of 250°F and 350°F cure epoxies resulting from radiation exposure, (3) studying the microcracking behavior during thermal cycling, and (4) establishing a fundamental understanding of damage mechanisms to guide future new materials development. Some of the recent results obtained in the areas shown in figure 6 are presented in figures 7 through 15.

- Mechanical property changes
- Matrix embrittlement
- Damage mechanisms

Figure 6

# TRANSVERSE STRENGTH AND STIFFNESS FOR BASELINE AND IRRADIATED T300/934 GRAPHITE/EPOXY COMPOSITES

Several state-of-the-art advanced graphite/epoxy composite systems have been evaluated in the NASA programs to determine their response to the GEO environment. Figure 7 shows typical mechanical property data from a recent investigation (ref. 4). The transverse strength and modulus of T300/934 graphite/epoxy (manufactured by Fiberite Corporation) before and after radiation are shown for three different test temperatures. The irradiated samples received an electron dose of  $1 \times 10^{10}$  rads at a dose rate of  $5 \times 10^7$  rads per hour in the Langley radiation exposure facility. The total radiation dose simulates a worst case, 20- to 25-year GEO radiation exposure.

The data suggest that electron irradiation tends to embrittle this 350°F cured composite system. The stiffness of the irradiated specimens was greater than that of the baseline system in the room temperature and lower temperature tests. Transverse strength was also lower through this temperature range. Above room temperature, the stiffness of the irradiated material was slightly lower than that of the baseline material. Little or no change was found in the fiber-dominated tensile properties.

Other research on the chemistry of electron interaction with this epoxy resin has shown that some degradation products are produced and these products effectively plasticize the matrix in the elevated temperature test, thus giving lower stiffness. A corresponding lower glass transition temperature was also found for the irradiated matrix material.

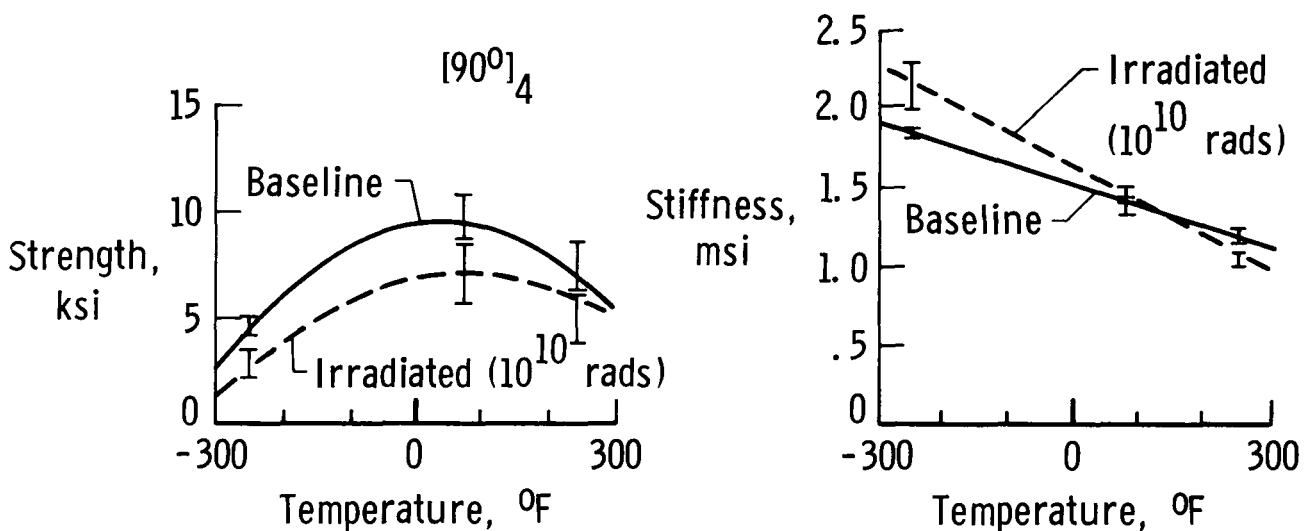


Figure 7

# EFFECTS OF ELECTRON RADIATION ON CRITICAL STRAIN-ENERGY-RELEASE RATES OF T300/934 GRAPHITE/EPOXY

As noted previously, evaluation of the fiber-dominated tensile properties following electron irradiation ( $1 \times 10^{10}$  rads) generally did not show differences between the irradiated and baseline material. However, because the matrix-dominated behavior [90]<sub>4</sub> indicated epoxy embrittlement, a series of tests were conducted (by J. Funk, NASA Langley) on the effect of radiation on the interlaminar fracture toughness of the T300/934 graphite/epoxy system. The results of these tests are given in ure 8. Two experimental test specimens were evaluated. Miniature specimens for both a double-cantilever-beam (DCB) test and an edge-delamination test (EDT) were used to determine the change in critical strain-energy-release rate ( $G_C$ ) with radiation exposure. The DCB test used a unidirectional specimen 3 in. by 0.2 in. and the EDT used a 5 in. by 0.5 in. specimen. The irradiated specimens received  $1 \times 10^{10}$  rads in the Langley radiation exposure facility. In the DCB test the specimen is subjected to peel stresses (mode I) and in the EDT the specimen is subjected to a mixed-mode state of stresses, peel (mode I) and shear (mode II). In both experiments (DCB and EDT), the strain-energy-release rate for the irradiated specimens was equal to or slightly greater than that of the baseline material, indicating that radiation did not degrade the toughness of the exposed composites. However, radiation does cause matrix embrittlement which leads to a much higher density of microcracks in the composite after thermal cycling (see fig. 12). Therefore, additional fracture toughness testing has been initiated to evaluate samples after combined radiation and thermal cycling.

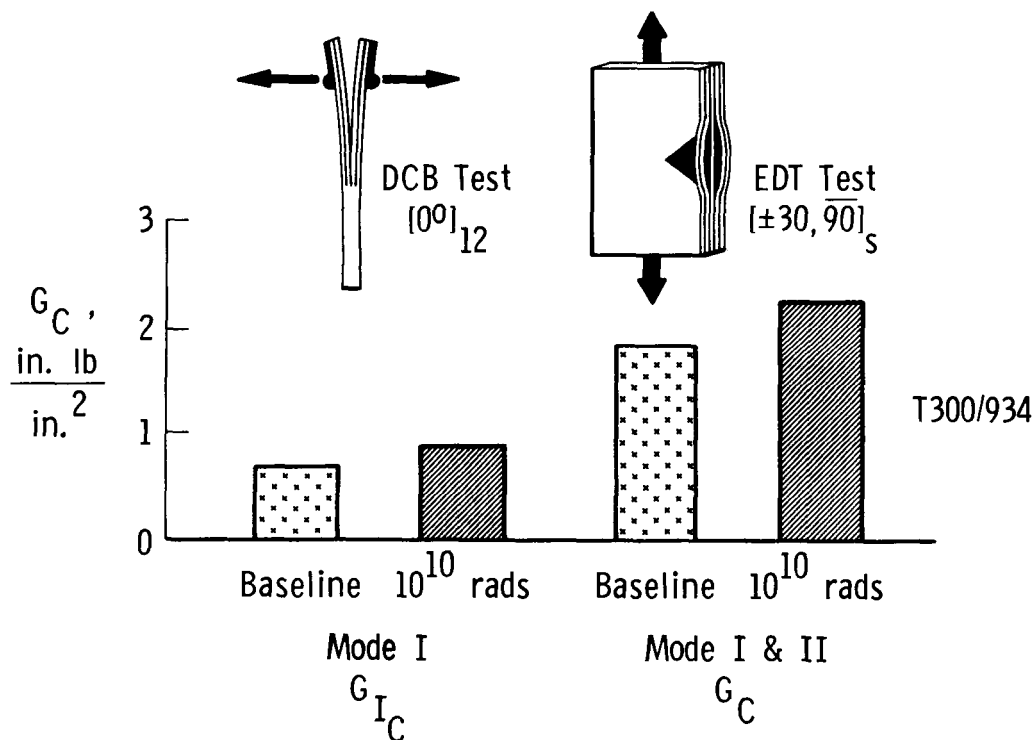


Figure 8

## EFFECTS OF RADIATION ON THERMAL EXPANSION

A primary requirement of composite materials for precision space structural applications is that they be dimensionally stable and maintain this stability during their use life. For GEO applications, radiation and repeated thermal cycles are parts of the exposure environment that may affect the stability of composite materials. Figure 9 shows the effect of penetrating electron irradiation and a single thermal cycle on the expansion characteristics of the T300/5208 graphite/epoxy system. The thermal expansion of the baseline and irradiated ( $6 \times 10^9$  rads) laminates  $[0_2/90_2]_s$  is shown through the temperature range from  $-250^\circ\text{F}$  to  $250^\circ\text{F}$ . The thermal cycle involved heating from room temperature to  $250^\circ\text{F}$  and then cooling to  $-250^\circ\text{F}$  followed by heating to room temperature. Although only one cycle is shown, the baseline laminate could be cycled repeatedly through this cycle without deviation from the expansion curve shown. The irradiated samples, however, upon reaching about  $200^\circ\text{F}$  on the first cycle, displayed a significant change in CTE that continued to the upper temperature of the test ( $250^\circ\text{F}$ ). During cooling to the lower test temperature, the sample took on a permanent set of about 100 microstrain, but displayed no change in CTE. Further cycling did not produce any further changes. These data indicate that the elevated temperature properties of the composite were probably modified by the electron irradiation (see fig. 10). A more complete analysis of the effects of radiation on dimensional stability of this  $350^\circ\text{F}$  system is provided in reference 5.

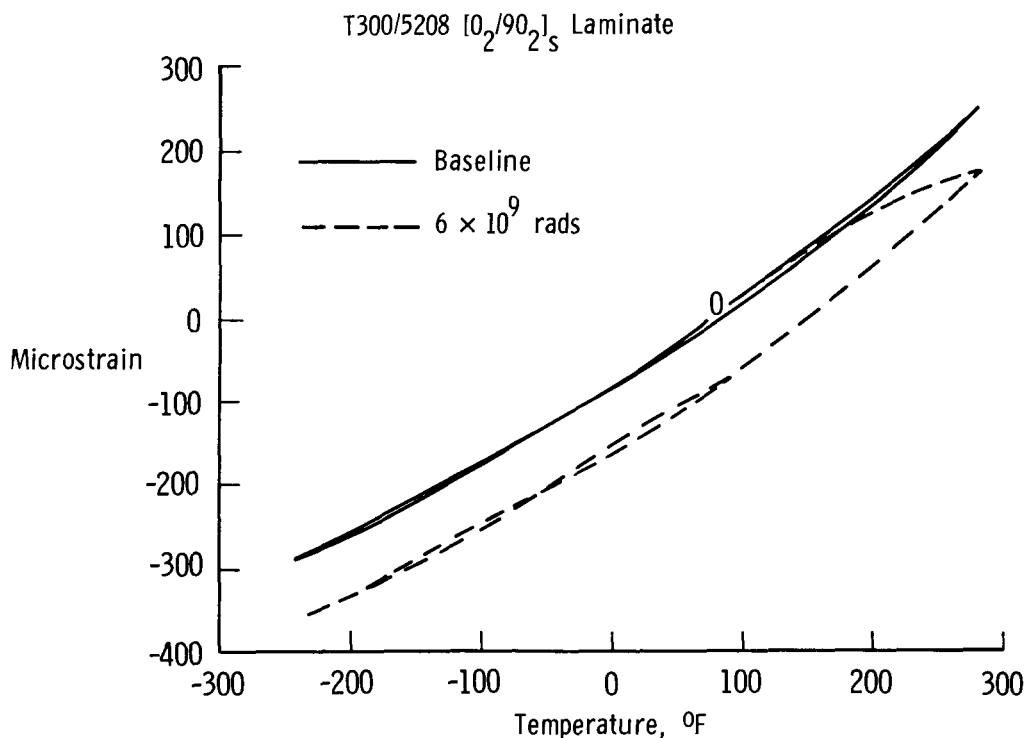


Figure 9

# DYNAMIC MECHANICAL ANALYSIS OF T300/5208 GRAPHITE/EPOXY

Figure 10 shows the dynamic mechanical analysis of the T300/5208 baseline and irradiated laminates discussed in figure 9. The upper part of this figure shows the change in dynamic modulus with temperature and the lower part shows the loss modulus as a function of test temperature for both laminates. Electron irradiation lowers the glass transition temperature ( $T_g$ ) of the epoxy about 50°F. Also, the "rubbery range" associated with the  $T_g$  is lowered in temperature and broadened so that it extends into the test range of the thermal expansion test. The dynamic modulus also shows the lower temperature of softening following irradiation. These data indicate that the change in slope of the expansion curve (fig. 9) for the irradiated material reflects a softening of the matrix and the expansion characteristics of the laminate take on the expansion behavior of the fibers. The lowered glass transition temperature and related rubbery range indicate that radiation has an effect upon the chemistry of the 5208 epoxy matrix. Because major changes in tensile properties and toughness have not been observed, the basic epoxy structure is assumed to remain essentially intact following radiation exposure.

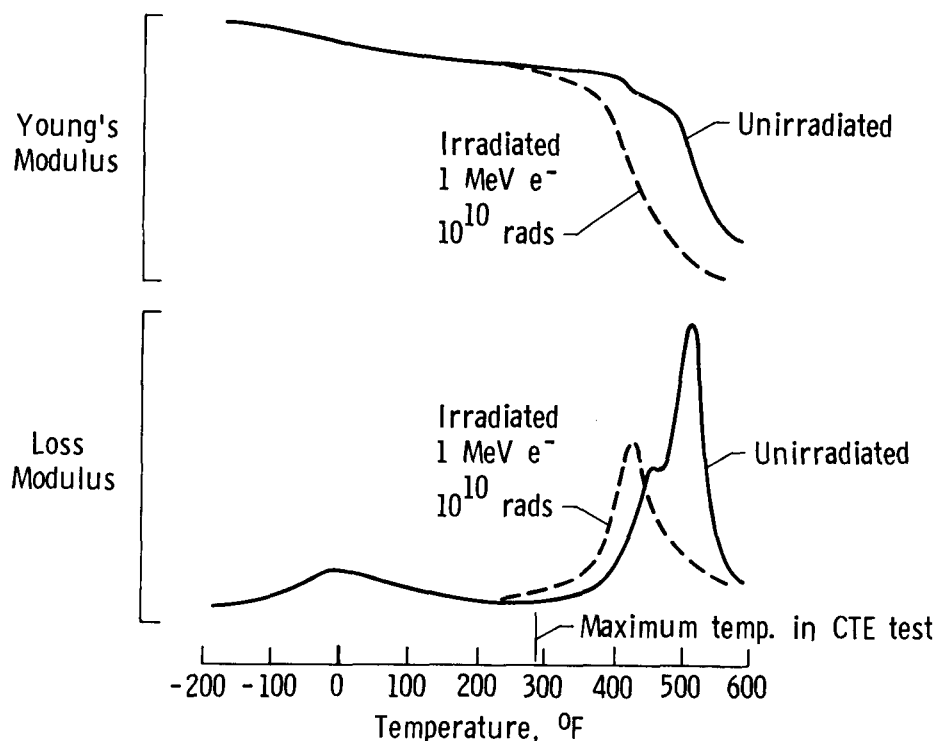


Figure 10

EFFECT OF RADIATION AND THERMAL CYCLING ON MICROCRACK FORMATION  
IN T300/934 LAMINATES [0/90/90/0]

Composite materials that are used in GEO applications will be exposed to a combined environment consisting of radiation, vacuum, and thermal cycles that will repeatedly raise and lower the material temperature during exposure. The effect of these temperature excursions during irradiation has not been determined, but a series of sequential (radiation followed by thermal cycles) exposures on the T300/934 graphite/epoxy system have been performed in an effort to obtain an initial assessment of the combined effects on this material. The results of this study are shown in figures 11 and 12. Figure 11 shows X-ray photographs of 4-ply [0/90/90/0] laminates before exposure, after 500 thermal cycles, after 500 cycles and irradiation ( $10^{10}$  rads), and after irradiation followed by 500 thermal cycles. In each case the thermal cycles consisted of cycling the specimen between  $-250^{\circ}\text{F}$  and  $250^{\circ}\text{F}$  using a 20-minute cycle period. As shown in these photographs, the baseline and thermal-cycled-only specimens showed only a few microcracks in the [0] direction. The specimen that was thermal cycled and then irradiated also exhibited no increase in microcrack density and the cracks that were present extended in the [0] direction. However, the laminate that received radiation followed by 500 thermal cycles microcracked extensively. Cracks were noted in both the  $90^{\circ}$  and  $0^{\circ}$  plies for this latter exposure sequence. No  $90^{\circ}$  cracks were found near the end of the specimen where the clamp covered the specimen during the radiation exposure.

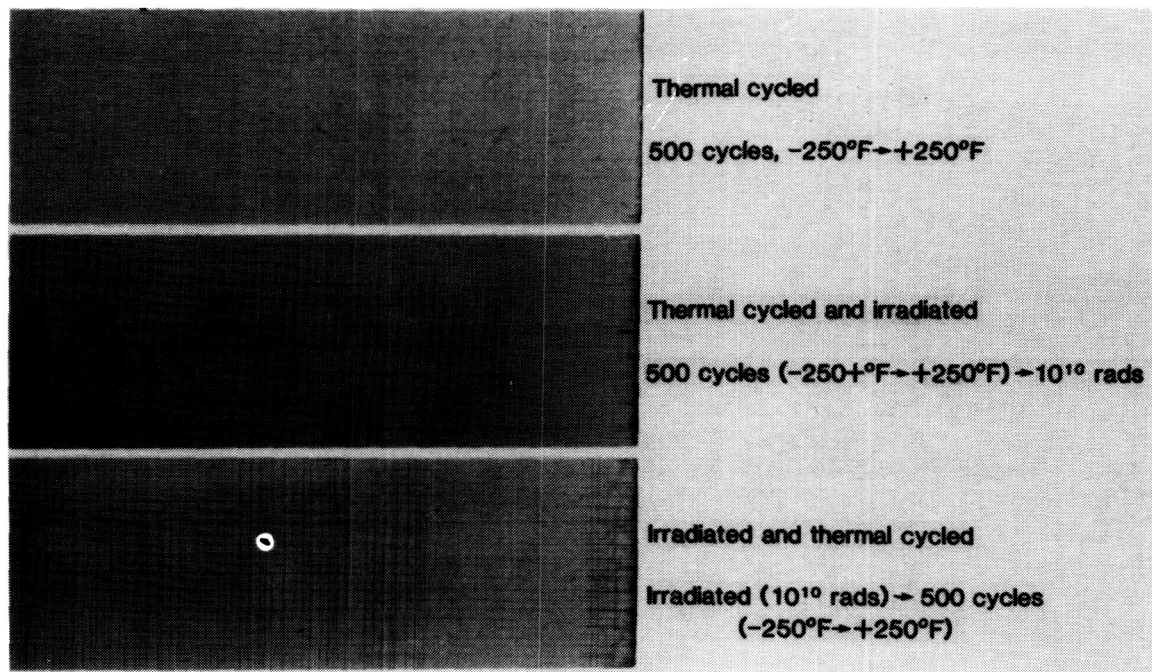


Figure 11



EFFECT OF RADIATION ON MICROCRACK FORMATION IN A  
350°F CURED EPOXY COMPOSITE

Figure 12 presents, in bar graph form, the crack densities observed in the micrographs of the samples presented in figure 11. For the thermal-cycled-only specimen, the crack density was about 25 cracks/inch. For the specimen that was thermal cycled after receiving the radiation, the crack density was about 75 cracks/inch. The high density of microcracks suggests that the radiation exposure caused significant embrittlement of the matrix. The effect of crack densities of this magnitude on the thermal expansion characteristics of this epoxy system will be discussed in conjunction with the results presented in the section entitled "Effect of Thermal Cycling on Microcrack Density."

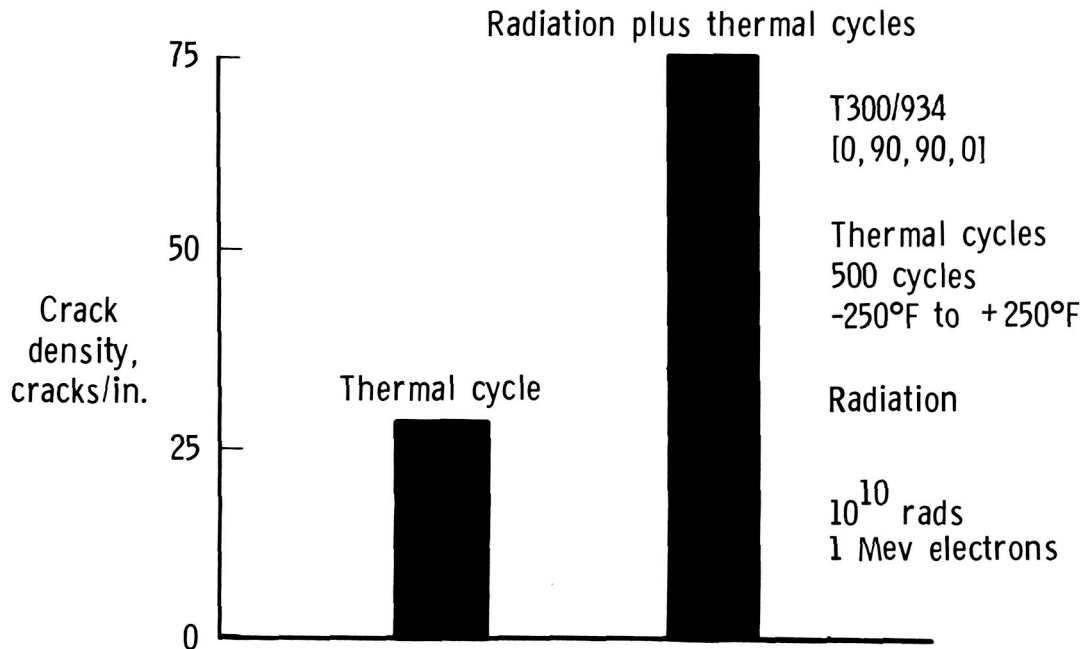


Figure 12

RADIATION EFFECTS ON THE TENSILE PROPERTIES OF T300/CE339 [0]<sub>4</sub>  
(1 MeV ELECTRONS AT  $5 \times 10^7$  RADS/HR)

Radiation effects studies of advanced state-of-the-art aerospace 350°F cured graphite/epoxy composites show that this class of materials is generally embrittled by radiation doses equivalent to 20 to 25 years in GEO. This embrittlement results in extensive microcracking during thermal cycling (fig. 12). Because microcracking can significantly limit the usefulness of composites in precision space structures, toughened matrix material systems with lower initial crosslink density are being considered. Figure 13 shows results from an evaluation of the radiation effects on a system of this type (ref. 6). The material evaluated was the space-qualified T300/CE339 system, manufactured by Ferro Corporation, which has a 250°F cured elastomer-toughened epoxy matrix. The elastomer is assumed to be of the CTBN family frequently used to toughen epoxy resins. The figure shows the ultimate tensile strength of a unidirectional [0]<sub>4</sub> baseline and irradiated specimen tested at room temperature. The irradiated specimen received  $1 \times 10^{10}$  rads at  $5 \times 10^7$  rads/hour using 1 MeV electrons. The ultimate tensile strength of the irradiated fiber-dominated specimen was about 50 percent of that observed for the baseline composite. The fractured specimen for each material, baseline and irradiated, was also significantly different. The baseline sample fractured, leaving relatively large broken fiber/matrix bundles. The irradiated sample left a single "fluffy" bundle of individual graphite fibers, indicating that the brittle matrix shattered at failure. Examination of individual fibers in the "fluffy" bundle of the irradiated specimen showed that little, if any, resin remained on the fiber surface after fracture. These data indicate that this 250°F elastomer-toughened system is more sensitive to radiation than the comparable 350°F cured epoxy systems and thus could not be considered for long-life use in a GEO environment.

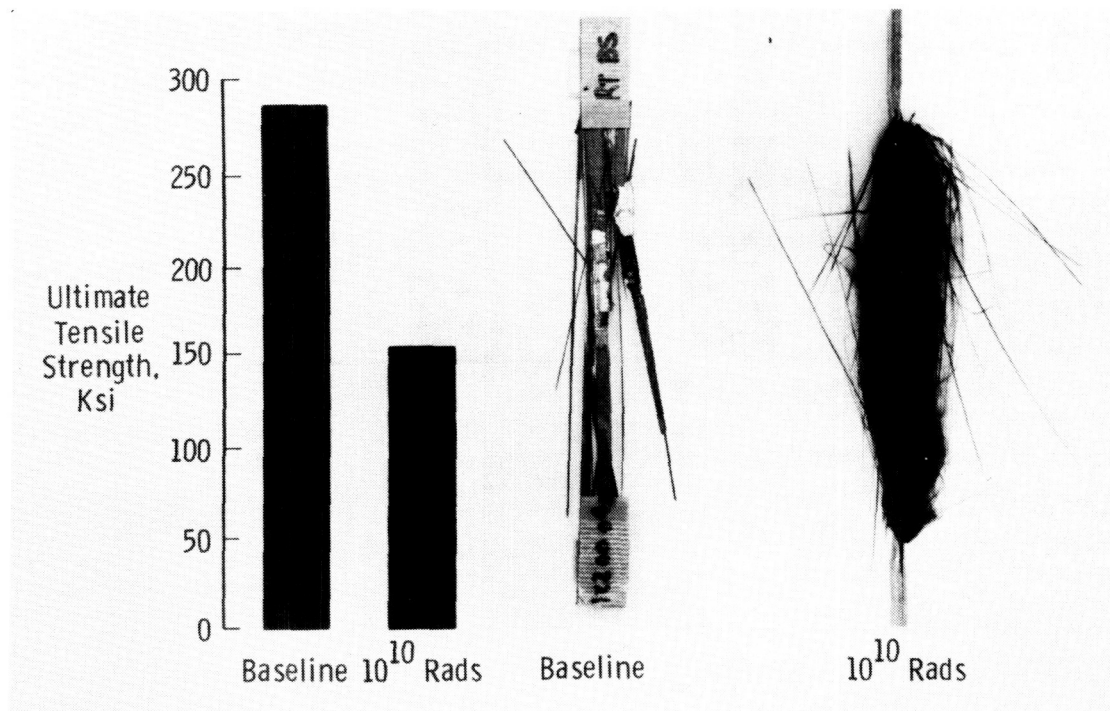


Figure 13

EFFECT OF RADIATION TOTAL DOSE ON MICROCRACK FORMATION IN  
THERMAL-CYCLED T300/CE339 COMPOSITES

Although it has been shown in the previous figure that the T300/CE339 elastomer-toughened graphite/epoxy composite system is sensitive to high doses of radiation ( $10^{10}$  rads), there are spacecraft materials applications that require high dimensional stability for relatively low-radiation-intensity orbits. A toughened epoxy system such as the CE339 matrix could be considered for these applications. Figure 14 shows the effect of total radiation dose and thermal cycling on microcrack formation in this epoxy system (ref. 6). The crack density is given for the base-line material and specimens that received electron doses between  $1 \times 10^7$  and  $1 \times 10^{10}$  rads and then thermal cycled 1, 10, and 100 times between  $-200^\circ\text{F}$  and  $175^\circ\text{F}$ . As shown, no microcracks were found in the baseline material after thermal cycling, indicating that this epoxy system is more resistant to microcracking than similar  $350^\circ\text{F}$  cured epoxy systems. However, after irradiation all samples microcracked, even those that received the lowest total dose of  $1 \times 10^7$  rads. This shows that matrix crosslinking and embrittlement began at a low radiation total dose. At total doses greater than  $1 \times 10^8$  rads, microcracking was extensive, and at  $1 \times 10^{10}$  rads the crack density was equivalent to that observed in irradiated and thermal-cycled  $350^\circ\text{F}$  cured epoxy systems. Chemical characterization of this CE339 system (ref. 6) indicates that the low-radiation-dose embrittlement is related to crosslinking of the CTBN type elastomers. This suggests that the radiation stability of the system might be improved by substituting a more radiation stable elastomer for the CTBN.

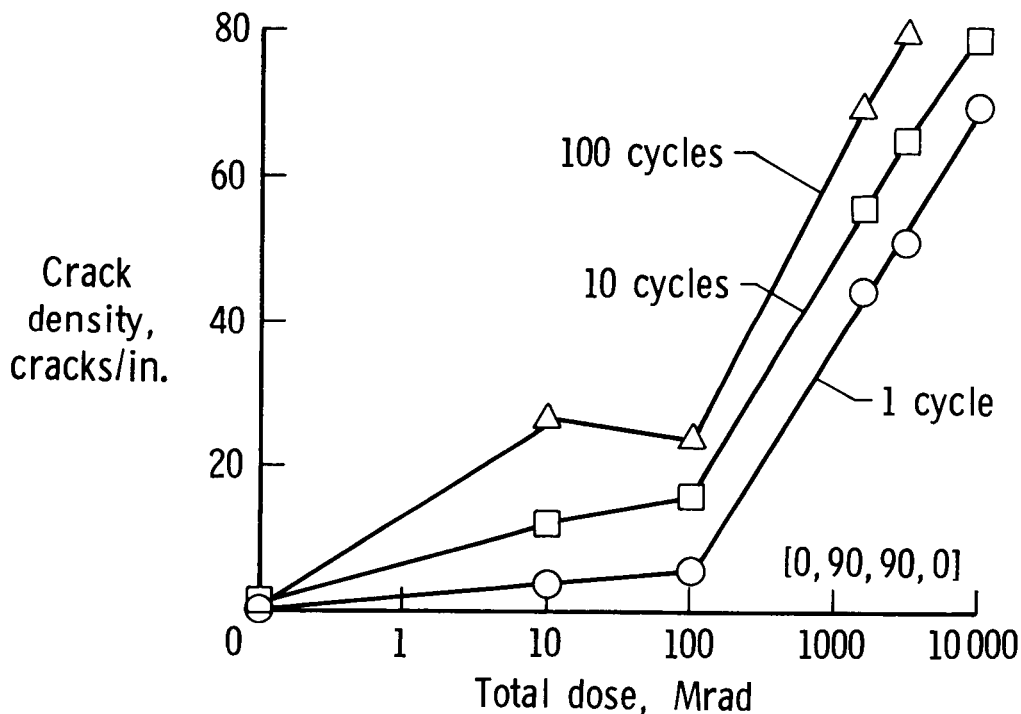


Figure 14

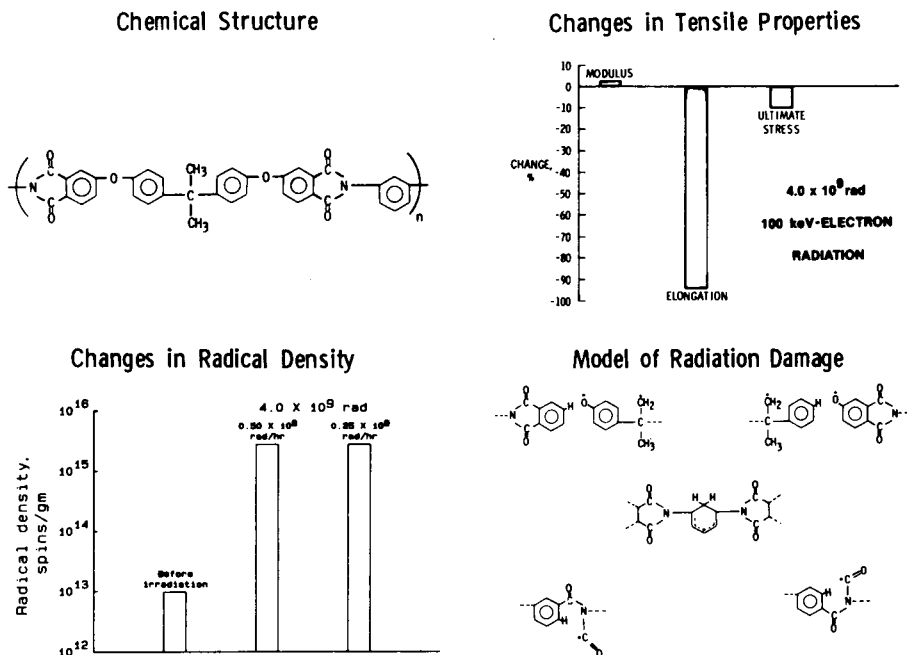
## RADIATION DAMAGE MECHANISMS IN A THERMOPLASTIC MATERIAL

Ultem polyetherimide is a relatively new thermoplastic polyimide manufactured by the General Electric Company. This polymer is one of several recently developed advanced thermoplastic systems that has potential for space applications. To assess the durability of Ultem for possible long-term (20 to 25 years) use in the space environment (GEO), an experimental study of its radiation stability was conducted (ref. 7). Film samples (0.003 in. thick) were irradiated with 100 keV electrons in vacuum and given radiation doses of 1.6, 4.0, and 6.0  $\times 10^9$  rads. Following the radiation exposure, changes in mechanical properties (tensile), radical concentration (EPR), and molecular structure (IR) were determined. Figure 15 provides a summary of this characterization.

Only small changes in tensile stress and modulus were observed following the radiation exposure. Elongation, however, was significantly reduced. Solubility of the baseline and irradiated films indicated that radiation-induced crosslinking was extensive.

Electron paramagnetic resonance (EPR) spectroscopy and infrared (IR) spectroscopy were performed to determine changes in the chemical structure of the polymer. The density of organic radicals (spins/gm) increased by over two orders of magnitude at 4  $\times 10^9$  rads. Four distinct radical species were identified: phenoxyls, gem-dimethyls, ketones, and cyclohexadienyls. Analyses of the EPR and IR spectra indicated that radiation caused dehydrogenation of methyl groups and rupture of ether linkages. At the highest dose the imide ring was opened. At least three of the four radical species observed led to crosslinking between the linear chains.

### Polyetherimide (Ultem)



(TAKEN FROM REF. 7)

© IEEE, 1984)

Figure 15

## THERMAL MECHANICAL STABILITY OF COMPOSITES

Graphite-reinforced composite materials are leading candidates for construction of precision space structures because of their high specific stiffness and low coefficient of thermal expansion (CTE). In addition to low CTE, good dimensional stability is required for precision antenna structures where maintaining a preset surface contour is critical to antenna performance. Small dimensional changes in the antenna structure can cause defocusing of the antenna or an increase in the surface roughness of the reflector surface. Dimensional changes in resin-matrix composites can be caused by thermal expansion, loss of moisture, microcracking of the resin, applied stress, and radiation damage to the resin matrix. For metal- and ceramic-matrix composites, thermal cycling and mechanical loading can cause dimensional changes.

A research program is under way at NASA Langley to characterize and model the dimensional stability of low expansion composites of interest for precision antenna structures. Emphasis has been placed on development of laser interferometry measurement techniques and characterization of thermal cycling damage to both resin- and metal-matrix composites. Some of the recent results obtained in the areas listed in figure 16 will be presented in the following figures.

- Laser interferometer technique
- Thermal cycling damage development
- Thermal strain hysteresis in Gr/metals and Gr/glass

Figure 16

## SCHEMATIC DIAGRAM OF LASER INTERFEROMETER DILATOMETER SYSTEM

A Fizeau-type, laser interferometer dilatometer system has been developed to characterize the thermal expansion of low expansion composite materials (fig. 17). This system, described in reference 8, consists of (1) a Fizeau interferometer, (2) an environmental chamber, (3) an optical train, (4) a He-Ne laser, and (5) a camera. A photodiode array, a waveform analyzer, and a microcomputer have also been incorporated to automate the testing and data reduction process. The entire system is automated with the computer controlling the temperature in the environmental chamber, triggering the camera, recording data from the waveform analyzer, and then incrementing the temperature to cover a preselected temperature range. The thermal expansion of the specimen is measured relative to the thermal expansion of a known reference material. The current reference material is fused silica, calibrated by the National Bureau of Standards. The strain resolution with this system is less than 1 microstrain.

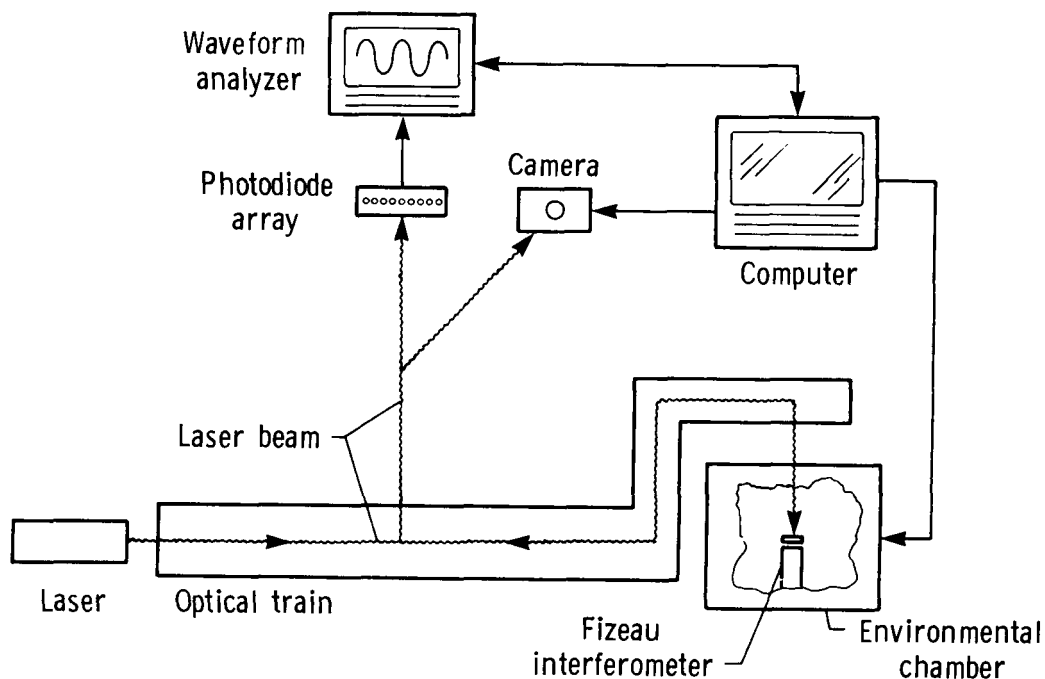


Figure 17

## EXPANSION OF INVAR 36

The laser interferometer system described in figure 17 is used for precision measurement of small dimensional changes in composites. The change in length of a test specimen is directly proportional to the change in the light interference pattern, the fringe density. Two methods are used for recording and analyzing fringe data. In the first method, individual fringe patterns are recorded on 35-mm film. At the conclusion of a test, the 35-mm negatives are enlarged in a microfiche reader and the fringes are visually counted over a defined gauge length. The fringe density is the number of fringes divided by the gauge length. The second method allows fringe patterns to be analyzed in real time. The fringe pattern is imaged onto a light-sensitive linear photodiode array. The photodiode array is electrically scanned and the fringe pattern is digitized. The digitized signal, which has a sinusoidal form, is then transmitted to a waveform analyzer. The waveform analyzer performs a fast Fourier transform on the signal to determine the frequency content. The predominant frequency in the signal is the sine wave frequency, from which the fringe density can be directly computed.

A comparison of thermal expansion data computed from 35-mm film and from the fast Fourier transform analysis is shown in figure 18. The data shown are for one test of an Invar 36 specimen (ref. 8). The two sets of data are in good agreement, with a maximum difference of 4.7 microstrain. The majority of this difference is caused by a misalignment of the fringe pattern image on the photodiode array. A method to more accurately align the fringe pattern on the photodiode array is currently under development.

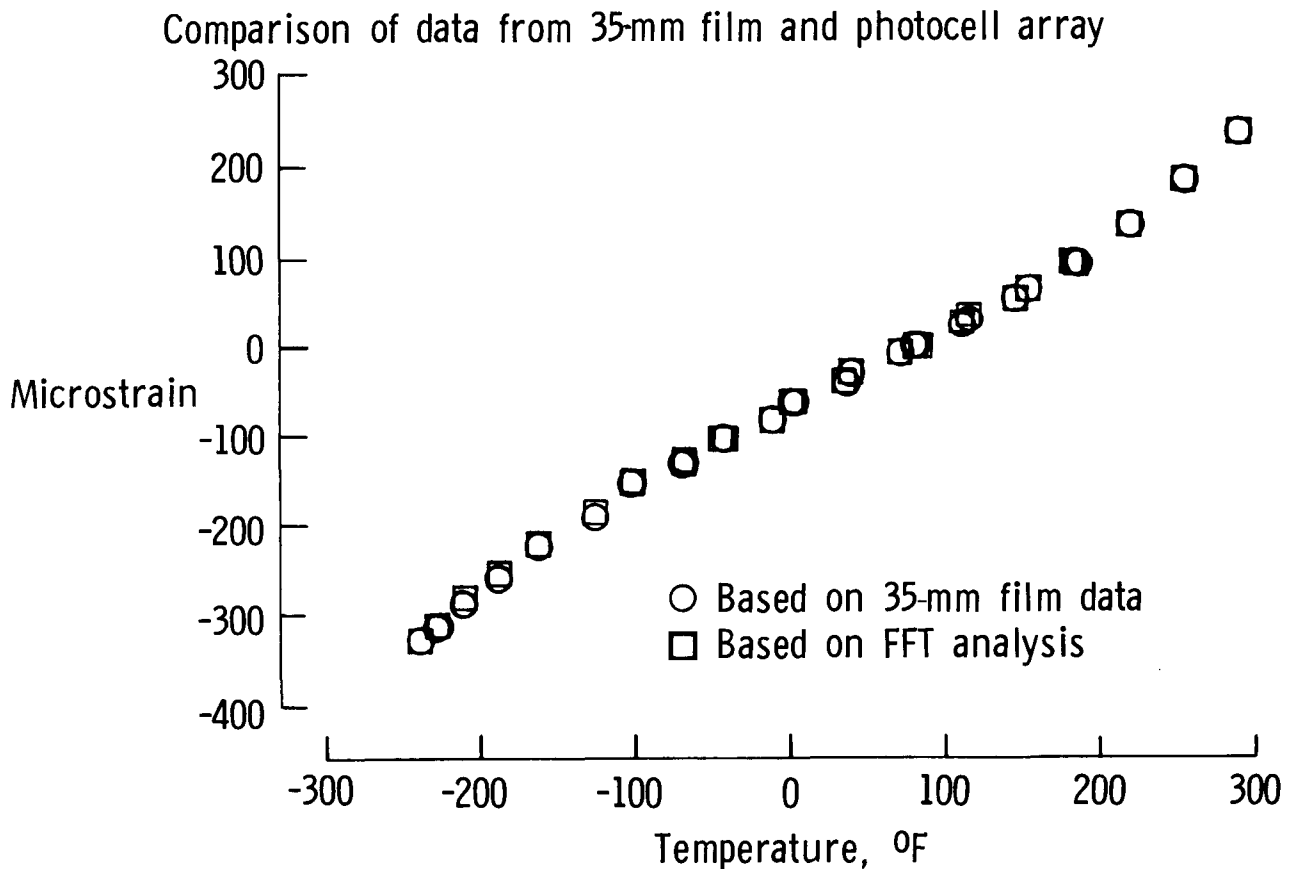


Figure 18

# THERMAL EXPANSION OF GRAPHITE/POLYIMIDE COMPOSITE LAMINATES (C6000/PMR-15)

The laser dilatometer system previously described has a strain resolution of less than 1 microstrain and thus can be used to measure the expansion behavior of low expansion unidirectional composite laminates. However, higher expansion laminates such as quasi-isotropic layups where the total strain range may be several hundred microstrain can also be examined. The versatility of this dilatometer is illustrated by the data presented in figure 19. Expansion data are presented for an 8-ply unidirectional laminate and a quasi-isotropic laminate of graphite/polyimide composite, C6000/PMR-15, composed of Celion 6000 graphite fibers (Celanese Corporation) and PMR-15 polyimide resin. The total expansion of the unidirectional laminate was relatively small, about 80 microstrain, over the temperature range -250°F to 250°F. The total expansion of the quasi-isotropic laminate was about 475 microstrain over the same temperature range.

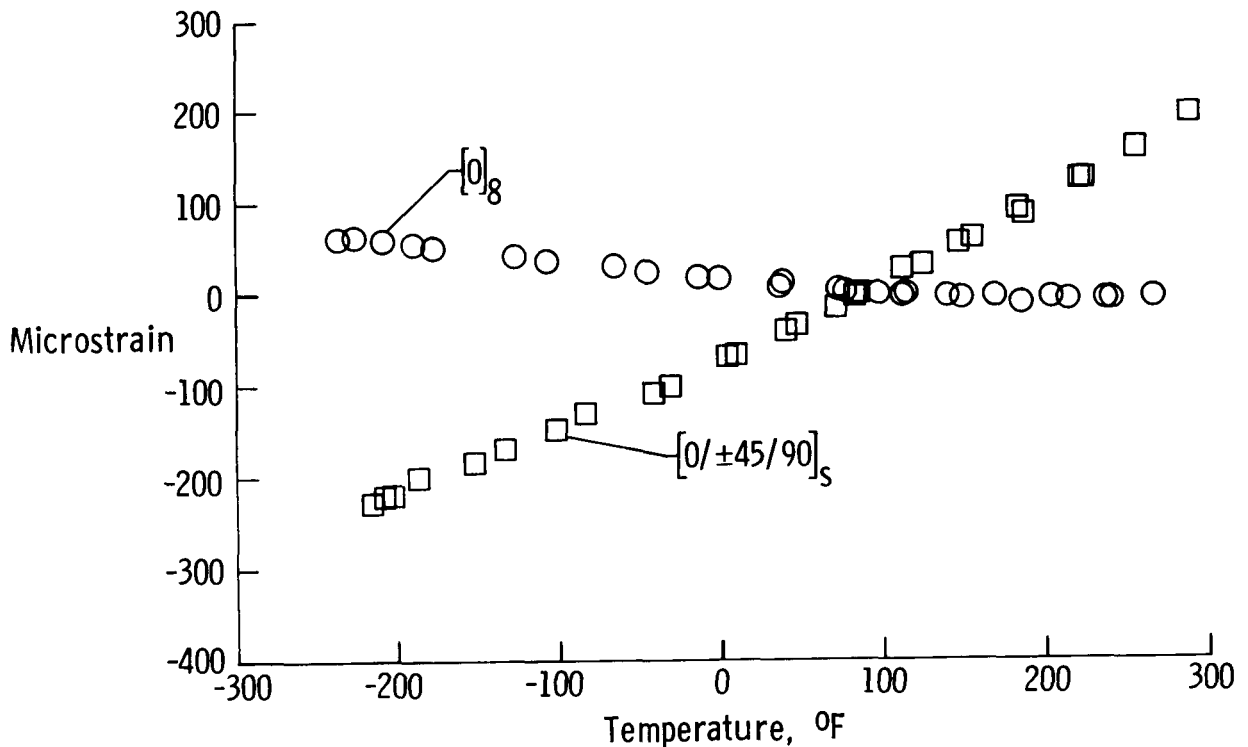


Figure 19



## EFFECT OF THERMAL CYCLING ON MICROCRACK DENSITY

The room-temperature coefficient of thermal expansion (CTE) of T300 graphite fibers along the axis of the fibers is approximately  $-0.3 \times 10^{-6}$  in/in/°F while 5208 epoxy resin has a CTE of approximately  $30$  to  $32 \times 10^{-6}$  in/in/°F at room temperature. This large difference in expansion behavior gives rise to high residual stresses being developed in graphite/epoxy composites when they are cooled from the processing temperature ( $350^{\circ}\text{F}$  for T300/5208) or during any subsequent thermal cycling. The state of stress can be particularly high in cross-ply laminates, such as  $[0_2/90_2]_s$ , where a very low expansion  $[0]$  ply is bonded to a high expansion  $[90]$  ply. Stresses can reach sufficient magnitude to cause microcracking of the brittle epoxy resin.

Data presented in figure 20 show that for a  $[0_2/90_2]_s$  laminate of T300/5208 cycled between  $-250^{\circ}\text{F}$  and  $250^{\circ}\text{F}$  the number of cracks per inch increases with the number of thermal cycles. The crack density was 15 cracks/inch after 500 cycles and is expected to reach an equilibrium value between 20 and 22 cracks/inch after several hundred more cycles.

The equilibrium density estimated from a finite-element analysis (ref. 9) of microcracking in this composite system is shown by the dashed line on the figure (about 22 cracks/inch). This analysis appears to reasonably predict an upper bound on crack density due to thermal cycling.

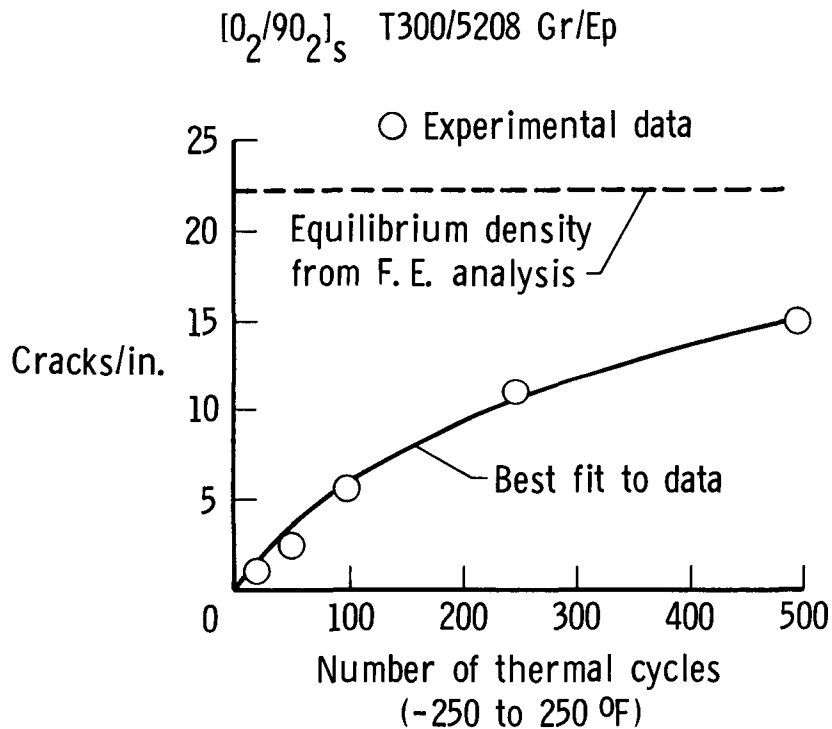


Figure 20

# EFFECTS OF MICROCRACKS ON COEFFICIENT OF THERMAL EXPANSION OF $[0_2/90_2]_S$ T300/5208 GRAPHITE/EPOXY

Results from an analytical study of the effects of microcracks on the coefficient of thermal expansion (CTE) of  $[0_2/90_2]_S$  T300/5208 graphite/epoxy (ref. 9) are shown in figure 21. The analytical results were obtained by using a finite-element analysis in conjunction with classical lamination theory (CLT) to model the effects of microcracks on the CTE of the laminate. The analysis shows, for a crack density of 75 cracks/inch in the  $90^\circ$  plies of a  $[0_2/90_2]_S$  laminate, the CTE in the  $[0]$  fiber direction is reduced to 30 percent of its original value. For cracks in both the  $0^\circ$  and  $90^\circ$  plies at this same crack density, the CTE is reduced to 13 percent of its original value. Therefore, the addition of cracks in the  $0^\circ$  plies does affect CTE, but to a much lesser extent than cracks in the  $90^\circ$  plies.

Also shown in figure 21 are the values of CTE determined from CLT assuming a 100-percent reduction in the transverse stiffness ( $E_2$ ) of the crack plies. The value of  $\alpha_y$ , predicted by CLT for cracks in the  $90^\circ$  plies only, is nearly equal to  $\alpha_y$  predicted for cracks in both the  $0^\circ$  and  $90^\circ$  plies. Therefore, the effect of microcracks on  $\alpha_y$  is overpredicted by CLT even at large crack densities (75 cracks/inch).

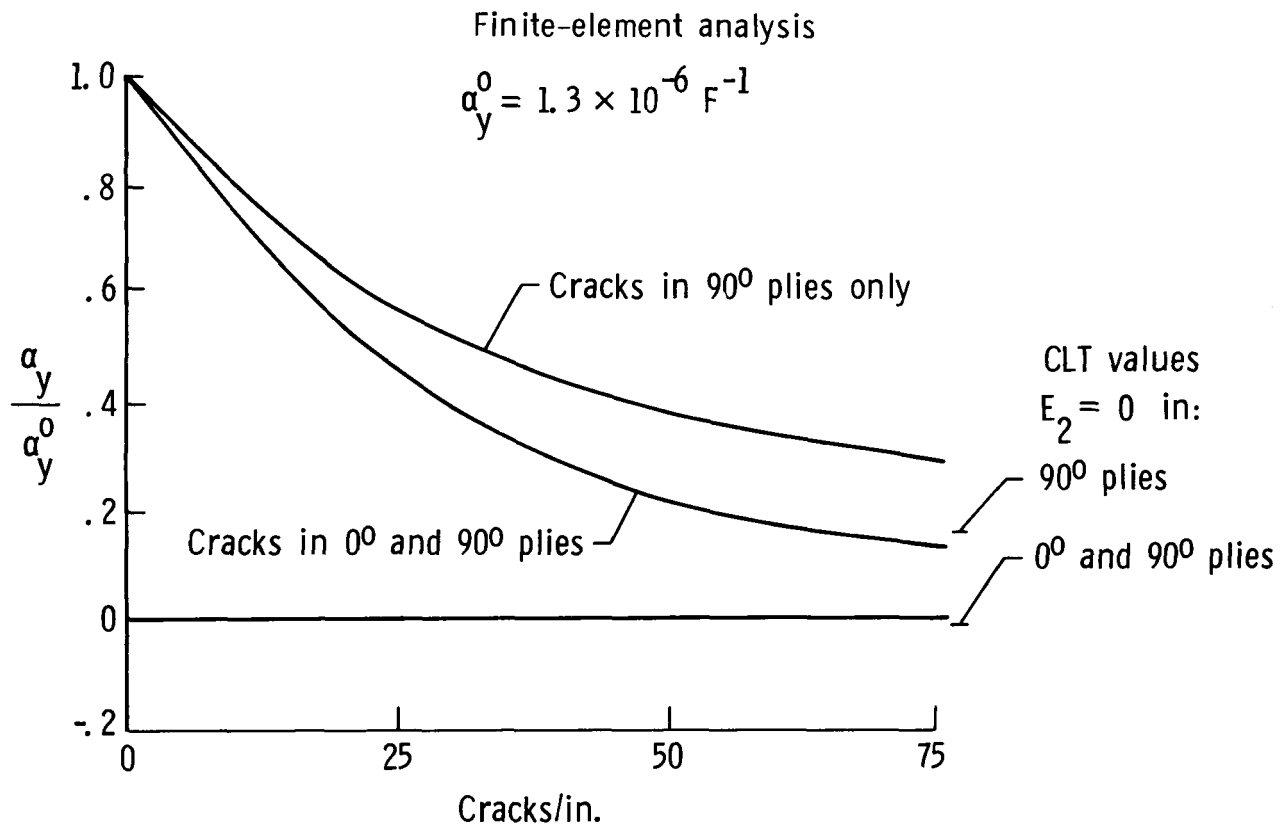


Figure 21

MICRODAMAGE IN GRAPHITE/EPOXY TUBES AFTER 500 THERMAL  
CYCLES BETWEEN  $-250^{\circ}\text{F}$  AND  $200^{\circ}\text{F}$

Graphite/epoxy tubes are being considered for construction of high stiffness truss structures for a number of different space systems. The durability of composite tubes subjected to the types of thermal cycles expected in space is a current research focus within NASA. A preliminary study of the effects of thermal cycling on the integrity has recently been completed (ref. 10). In this study, one-half-inch-diameter composite tubes with a  $[90/0_6/90]$  wall were cycled between  $-250^{\circ}\text{F}$  and  $200^{\circ}\text{F}$  up to 500 times. Different material systems were used in each of three tubes. Each tube had T300 fibers in the  $90^{\circ}$  plies. The same resin system was used throughout each tube. The  $0^{\circ}$  plies in each of the three tubes were T300/934, P75S/934, and P75S/CE339, respectively. Microdamage induced in the T300-P75S/934 tube by 500 thermal cycles is shown in figure 22. This is typical of the damage induced in each material.

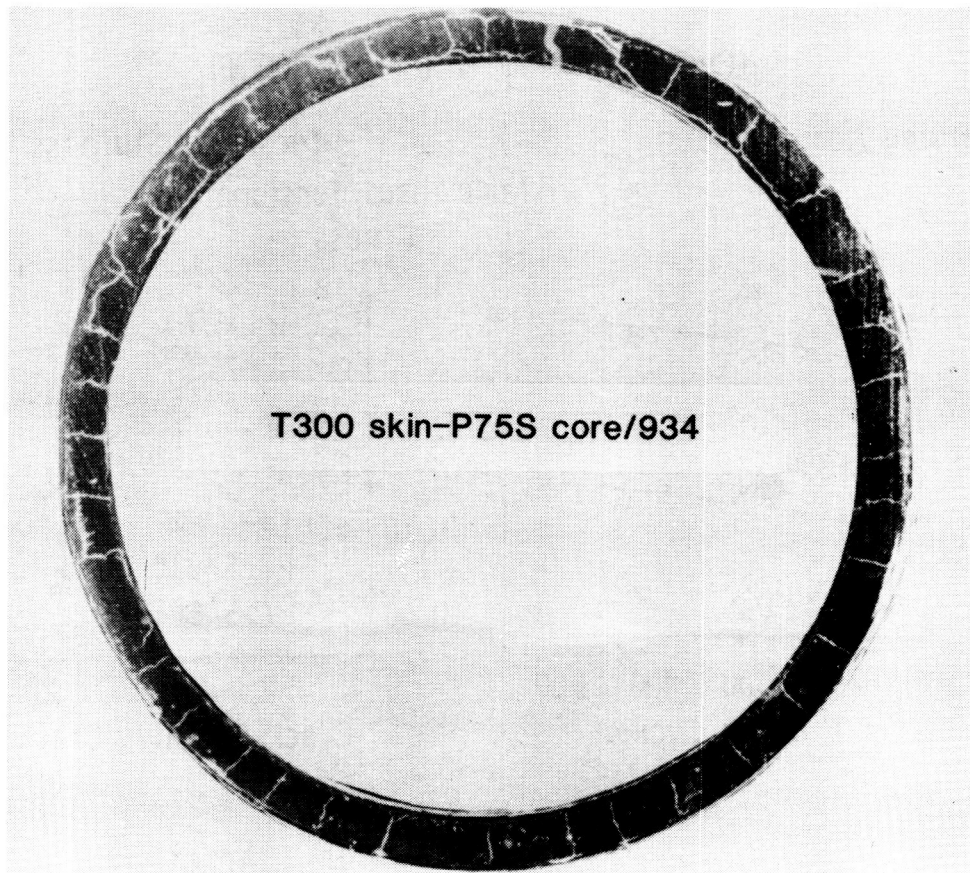


Figure 22

## EFFECTS OF THERMAL CYCLING ON COMPOSITE TUBES

The changes in microcrack densities in each of three [90/0<sub>6</sub>/90] graphite/epoxy 0.5-inch-diameter tubes due to thermal cycling are shown in figure 23. The crack density in each tube has not reached equilibrium even after 500 cycles. The data show a significant difference between the crack densities in the three materials. These differences are attributed to the differences in the expansion of fibers used and differences in the stiffness of the matrix resins used.

The effects of microcracks on the torsional stiffness of each tube (ref. 10) are also shown in figure 23. The data show a significant and rapid reduction in stiffness due to microcracks. The stiffness of all three materials appears to have the same sensitivity to microcracks. The data show about a 35-percent reduction in torsional stiffness at a crack density of about 25 cracks/inch or after 500 cycles between -250°F and 200°F.

(Cycled Between -250°F and 200°F)

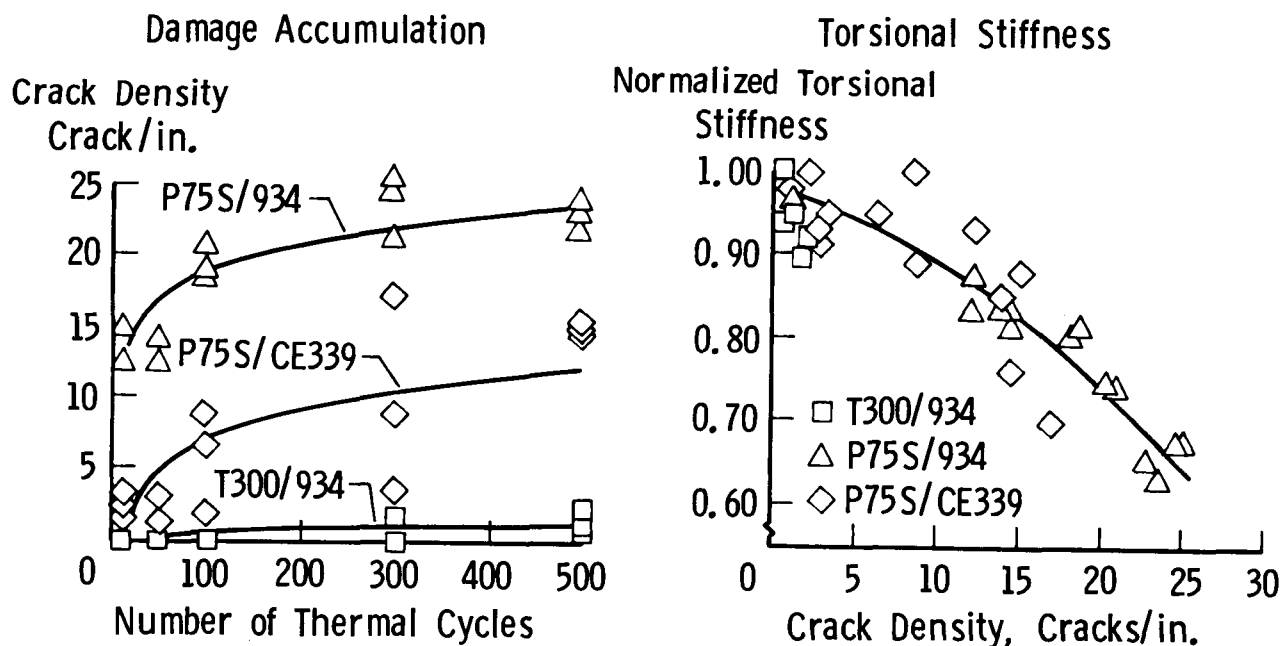


Figure 23

# EFFECTS OF THERMAL CYCLING ON EXTENSIONAL AND FLEXURAL STIFFNESSES OF GRAPHITE/EPOXY TUBES

The extensional and flexural stiffnesses of each of three 0.5-inch-diameter  $[90/0_6/90]$  tubes before and after 500 thermal cycles between  $-250^{\circ}\text{F}$  and  $200^{\circ}\text{F}$  (ref. 10) are shown in figure 24. The data show no significant effects of thermal cycling on the extensional and flexural stiffnesses of these tubes. Therefore, the radial microcracks induced by thermal cycling (fig. 22), which have a large effect on the torsional stiffness of these tubes (fig. 23), are not expected to be a major concern for truss structures designed with nonrigid joints where no appreciable torsional loadings are expected to be introduced in the tubes.

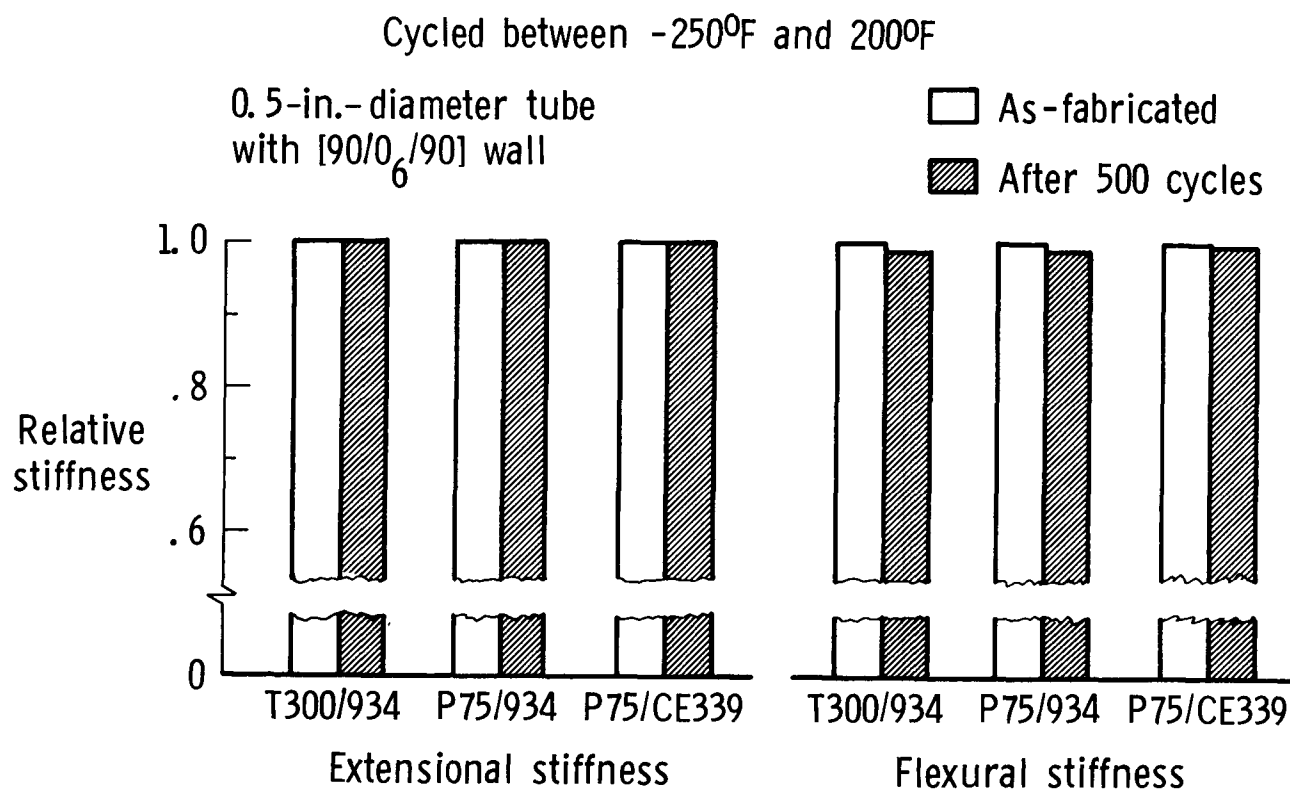


Figure 24

# THERMAL EXPANSION OF P100/6061 BEFORE AND AFTER THERMAL PROCESSING TO MINIMIZE THERMAL STRAIN HYSTERESIS

Graphite-reinforced metal-matrix composites (MMC) represent a new class of high stiffness, low thermal expansion materials for structural applications on dimensionally critical spacecraft. These materials have higher electrical and thermal conductivity than resin-matrix composites, are more radiation resistant, and have no outgassing. Currently, the 6061 aluminum alloy is one of the primary metals being considered as the matrix for MMC. However, composites made with this alloy exhibit large hysteresis during thermal cycling and residual dimension changes induced by thermal cycling. This behavior is unacceptable for the reliable performance of dimensionally critical spacecraft.

The thermal expansion of a graphite/aluminum, P100/6061, as-fabricated, is shown in figure 25. The expansion is characterized by a large hysteresis loop and residual strain. Samples fabricated by both diffusion bonding (fabricated by DWA Inc.) and hot isothermal roll bonding (fabricated by MCI) exhibit essentially the same expansion behavior. A postfabrication process has been developed which significantly reduces the hysteresis loop and eliminates the residual strain. Thermal expansion after processing is also shown in figure 25. The postfabrication processes consist of standard heat treatments, followed by cryogenic prestraining, i.e., cryogenic soak. A different heat treatment was required for samples fabricated by each of the two methods. Different treatments were required because the fabrication techniques caused different microstructures and different amounts of magnesium depletion within the aluminum matrix (ref. 11). This change in chemistry alters the heat treatment required to strengthen the matrix alloy.

Fabricated by: Diffusion Bonding

Hot Isothermal Rolling

Microstrain

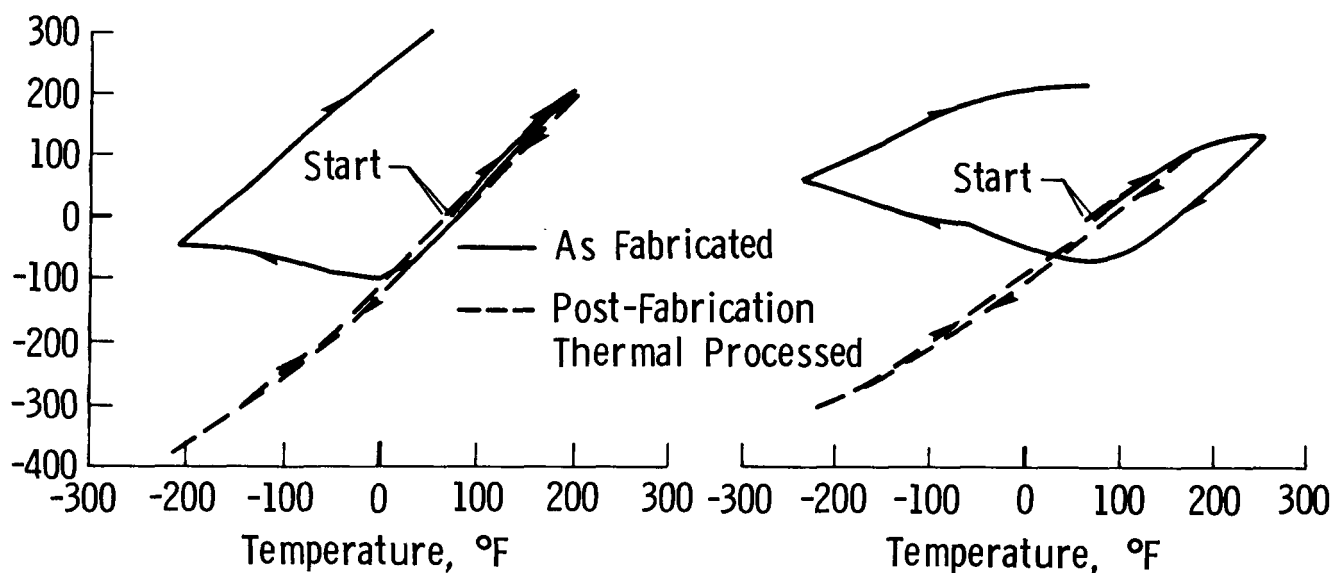


Figure 25

# THERMAL EXPANSION OF $[0/\pm 60]_S$ GRAPHITE/GLASS COMPOSITE

Graphite/glass is a relatively new material being considered for space structures. The thermal expansion of a quasi-isotropic graphite/glass (HMS/borosilicate) is shown in figure 26. The fiber volume fraction of this sample was 44 percent and the laminate orientation was  $[0/\pm 60]_S$ . The expansion of this laminate is characterized by a hysteresis loop. However, there was no residual strain after one thermal cycle. The coefficient of thermal expansion for this laminate, based on the end-points, is about  $0.02 \mu\epsilon/^\circ\text{F}$ . Additional tests on other graphite/glass samples are under way to determine the cause of the observed hysteresis and the thermal mechanical stability of this class of composite.

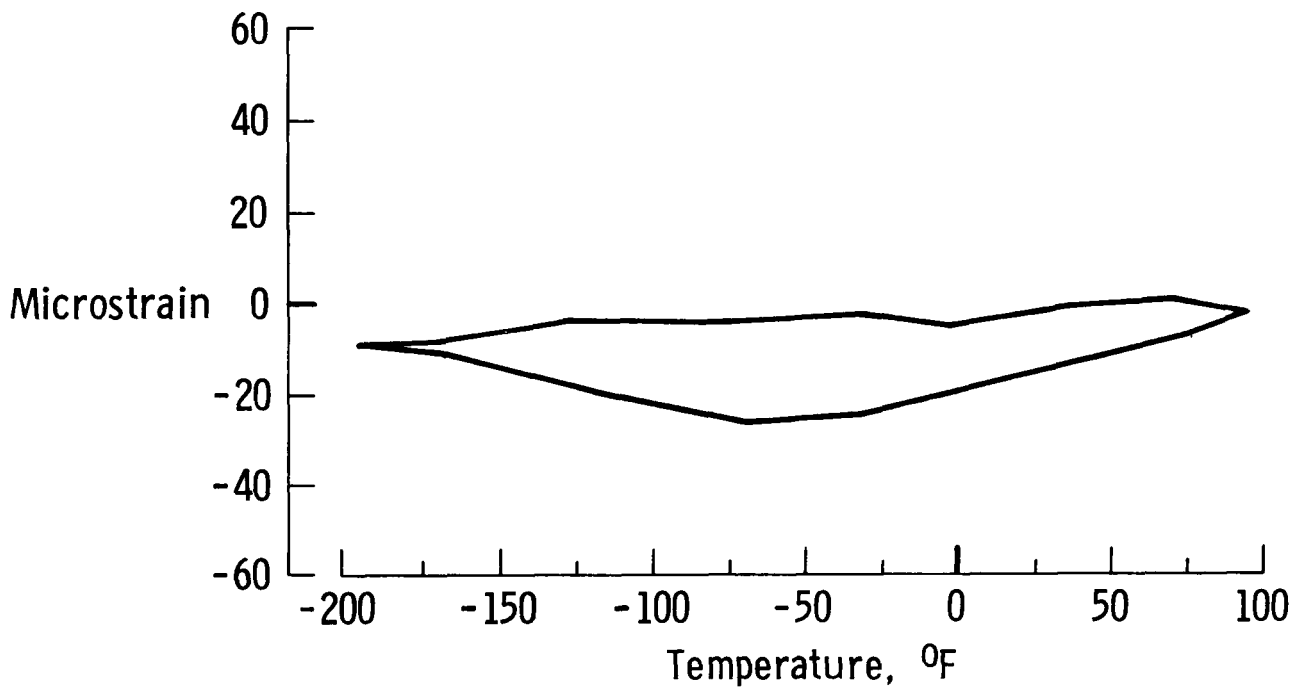


Figure 26

## SUMMARY

Spacecraft materials research is a continuing research activity within NASA. The thrust of this research is to gain a fundamental understanding of the performance of advanced composites, coatings, and polymer films in the space environment. Emphasis has been placed on identification of damage mechanisms to guide new materials development. Some of the recent results of this activity are summarized in figure 27 below.

- Metallic coatings provide atomic oxygen stability and low solar absorptance and emittance
- Weight loss of siloxane-modified polyimides 1/10th that of Kapton in LEO exposures
- High doses of electron radiation cause embrittlement of Gr/Ep composites
- Radiation damage mechanisms identified in CE339 and Ultem resins
- Thermal cycling causes strain hysteresis in Gr/metal and Gr/glass composites
- Radial microcracks cause large (35%) reduction in torsional stiffness of composite tubes

Figure 27



# REFERENCES

1. Leger, Lubert: Oxygen Atom Reactions with Shuttle Materials at Orbital Altitudes. NASA TM-58246, May 1982.
2. Slemp, Wayne S.; Santos-Mason, Beatrice; and Sykes, George F.: Effects of STS-8 Atomic Oxygen Exposure on Composites, Polymeric Films, and Coatings. Presented at the AIAA 23rd Aerospace Sciences Meeting, Reno, NV, January 14-17, 1985. (AIAA Paper No. 85-0421).
3. St. Clair, Anne K.; St. Clair, Terry L.; and Shevket, Keziban I.: Synthesis and Characterization of Essentially Colorless Polyimide Films. Proceedings of the 188th Meeting of the American Chemical Society, vol. 51, August 1984, p. 62.
4. Milkovich, Scott M.; Herakovich, Carl T.; and Sykes, George F.: Space Radiation Effects on Graphite-Epoxy Composite Materials. VPI-E-84-20, Virginia Polytechnic Institute and State University, June 1984.
5. Bowles, David E.; Tompkins, Stephen S.; and Sykes, George F.: Electron Radiation Effects on the Thermal Expansion of Graphite/Resin Composites. Presented at the AIAA 19th Thermophysics Conference, Snowmass, CO, June 25-28, 1984. (AIAA Paper No. 84-1704).
6. Sykes, George F.; and Slemp, Wayne S.: Space Radiation Effects on an Elastomer Toughened Epoxy/Graphite Composite. Presented at the 30th National SAMPE Symposium/Exhibition, Anaheim, CA, March 19-21, 1985.
7. Long, Sheila A. T.; and Long, Edward R., Jr.: Effects of Intermediate-Energy Electrons on Mechanical and Molecular Properties of a Polyetherimide. IEEE Transactions on Nuclear Science, December 1984.
8. Tompkins, S. S.; Bowles, D. E.; and Kennedy, W. R.: A Laser Interferometer Dilatometer for Thermal Expansion Measurements of Composites. Proceedings of V SESA International Congress on Experimental Mechanics, June 1984, pp. 367-377.
9. Bowles, D. E.: Effect of Microcracks on the Thermal Expansion of Composite Laminates. Journal of Composite Materials, vol. 18, March 1984, pp. 173-189.
10. Cohen, D.; Hyer, M. W.; and Tompkins, S. S.: The Effects of Thermal Cycling on Matrix Cracking and Stiffness Changes in Composite Tubes. Hi-Tech Review 1984, National SAMPE Technical Conference Series, vol. 16, 1984, pp. 577-588.
11. Dries, Gregory A.; and Tompkins, Stephen S.: Thermal Processing of Graphite Reinforced Aluminum to Minimize Thermal Strain Hysteresis. NASA TP-2402, 1985.

**Page intentionally left blank**

NEW CONCEPTS IN DEPLOYABLE BEAM STRUCTURES

Marvin D. Rhodes  
NASA Langley Research Center  
Hampton, VA 23665

Large Space Antenna Systems Technology - 1984  
December 4-6, 1984

## NEW CONCEPTS IN DEPLOYABLE BEAM STRUCTURES

During the past twenty years a number of concepts have been proposed for deployable beam structures which can be used in space applications. Two years ago a number of these concepts were surveyed by independent studies and the results of those surveys are reported in references 1-3. An evaluation of these references indicates that the design of deployable structures involves a complicated tradeoff of packaging efficiency, the overall mechanisms associated with deploying and latching beam joints, and the requirements and complexity of the beam deployer/repacker.

Recently the LaRC Structures and Dynamics Division has had an in-house effort supplemented by limited contract support to reexamine deployable structures and propose some new concepts which can improve some of the basic features of those evaluated in references 1 and 2. The beams evaluated in the current paper involve new deployable beam concepts in the general areas of three longeron deployable beams, controllable geometry beams and deployable/erectable beams. These new concepts have, in most cases, been developed to the point of fabricating operational demonstration models. The concepts are discussed in the order presented in figure 1.

- Three longeron deployable beams
- Controllable geometry beams
- Deployable/erectable beams

Figure 1

## JOINTS DOMINATE BEAM STRUCTURAL RESPONSE

All deployable beams have some type of hinge joint incorporated in each deploying bay. The response of these joints can significantly influence the structural behavior of the beam. A clevis joint that is considered to be representative of one of the simplest joints that can be used in deployable structures was tested to evaluate load/deflection response and the results are shown in figure 2. At very low values of load the joint has a dead band region due to free play between the pin and its load bearing members. The cumulative effect of this free play in a deployed beam could be significant due to the large number of joints involved. This effect would be manifest in the beam by the inability to accurately position the beam tip as shown by the sketch on the right. On either side of the joint free play region is a nonlinear region which is associated with seating of the pivot pin. This effect could be manifest as nonlinear response of the deployed beam structure.

At loads above the pin seating region the response of the joint is nearly linear; however, the joint is approximately 50% stiffer in compression than it is in tension. The difference in stiffness is inherent in the joint due to the load path through the joint. The clevis joint tested was a very simple joint and the characteristics noted are likely to be evident to an even greater extent in complex multimember joints.

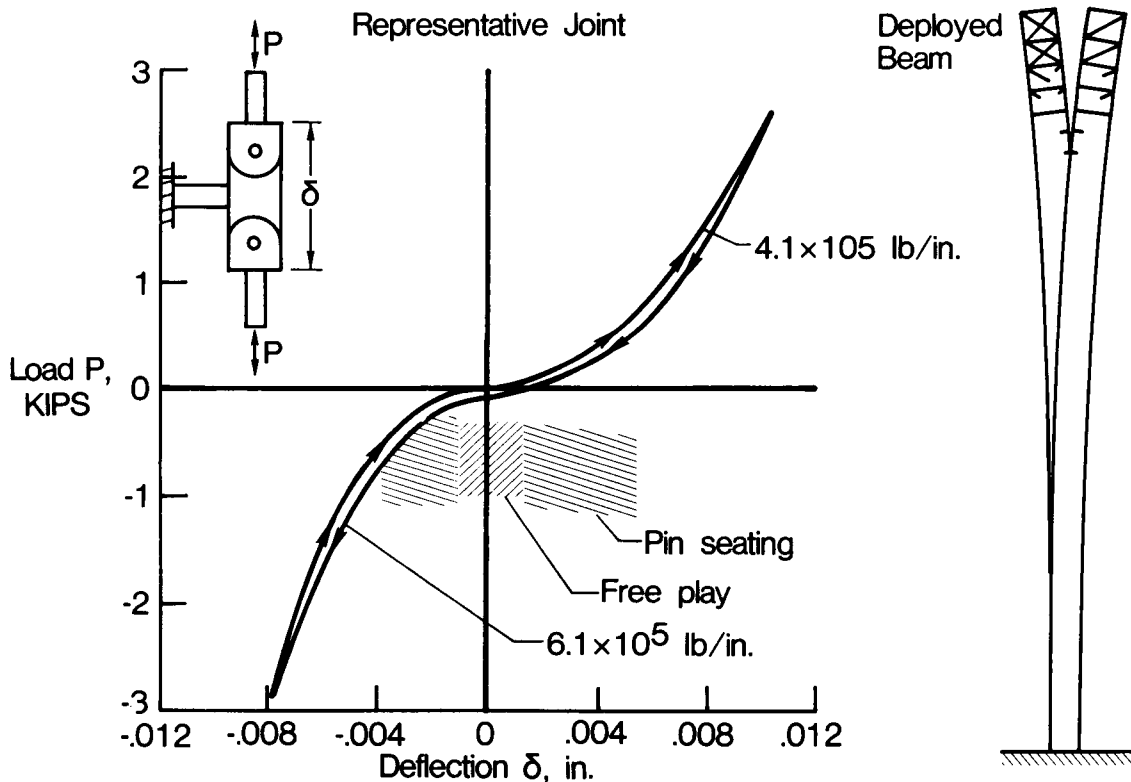


Figure 2

### BATTEN AUGMENTED TRIANGULAR (BAT) BEAM

Since a large number of joints are generally required in deployable beams it would be desirable to incorporate features in the beam design that would eliminate or reduce undesirable joint effects such as free play and pin seating. A three longeron batten augmented triangular (BAT) beam has been designed for this purpose. The important aspects of the beam are illustrated in the sketches of figure 3. The beam is a single fold deployable configuration which has each longeron connected by cross laced diagonals and a batten. Each bay of the beam is internally preloaded by buckling the batten and the three battens that constitute a batten frame are connected together at the batten ends so as to buckle simultaneously. To retract the beam the longerons hinge at the bay mid-length and at the batten/diagonal connector to fold into the center of the bay. The diagonals telescope and hinge at the batten diagonal connector to nest between the battens which are H shaped members.

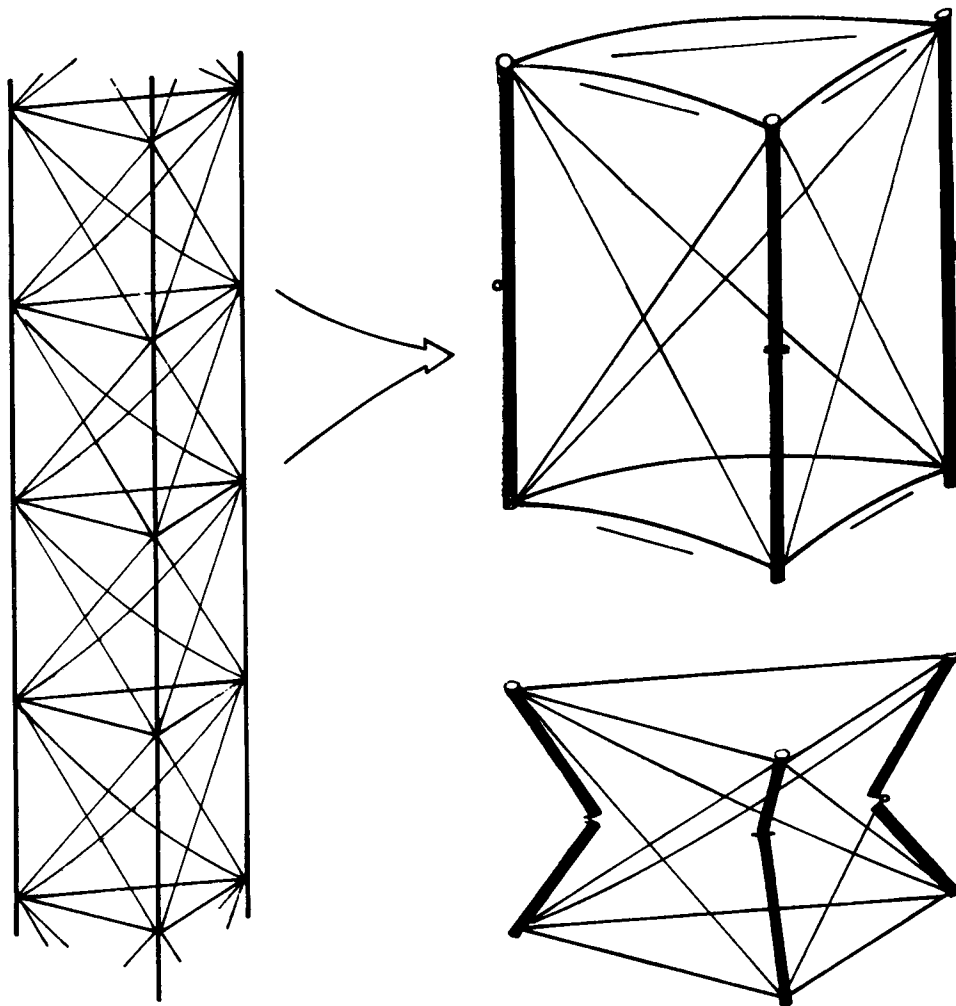


Figure 3

## DEPLOYABLE BAT BEAM MODEL

A demonstration model of the deployable bat beam was designed and fabricated for concept evaluation. Photos of the model are shown in figure 4. The photo on the left is of the model in the stowed (retracted) position attached to a plywood base. The center photo illustrates the deployment sequence with the top bay being deployed. The model fully deployed is shown on the right of figure 4. The model has a longeron length of 2 meters per bay and a deployed to packaged height ratio of about 80:1. All longeron and diagonal members were fabricated from continuous filament graphite tubes and rods. The longeron diameter is about 1.3 cm (.5 in) and the ratio of the axial stiffness of the longeron to the axial stiffness of the diagonal is approximately 4:1. The longeron members have a simply supported Euler buckling load of approximately 50 lbs and the longeron preload induced by the buckled fiberglass batten is 11 lbs. The midlength longeron joints have a self deploying mechanism incorporated in the joint to maintain the hinge in the deployed position.

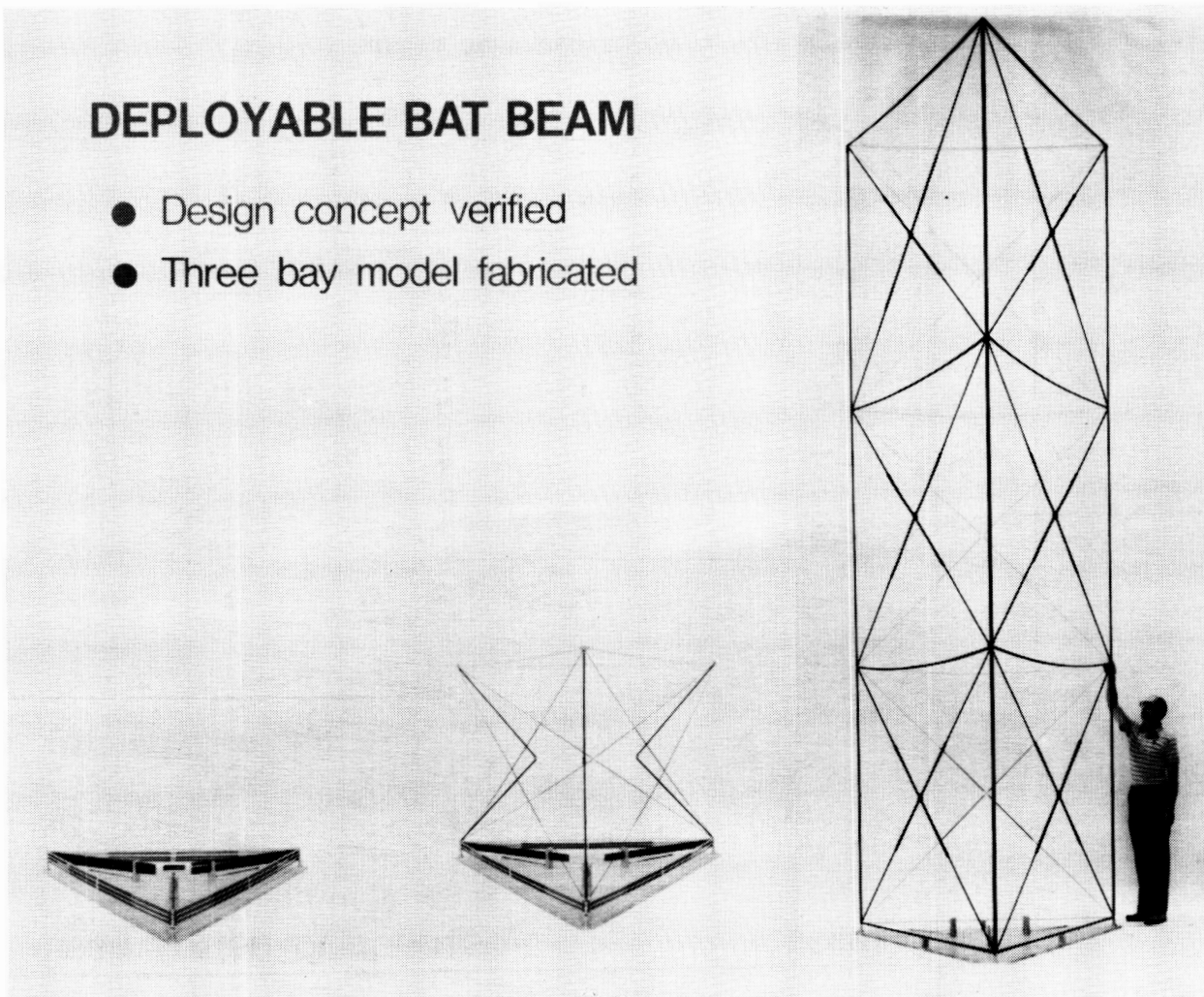


Figure 4

## BAT BEAM DEPLOYER

A concept was developed for a BAT beam deployer and sketches are shown in figure 5 to depict the operation of the deployer. This work was supported by contract and detailed information can be obtained in reference 4. The packaged configuration of the beam is shown on the left of figure 5. For this configuration the beam corner longeron joints are stacked on each other and supported by guide rails at the three corner locations. Beam deployment is accomplished by moving the nodes away from the deployer using the acme threaded lead screws shown in the left insert. In the stowed configuration, the lead screws are threaded into all the nodes to support the nodes for launch and to provide a storage location for the screw. To initiate deployment the lead screws are turned so that they back out of the stacked nodes until the guide rails deploy and latch in the deployed position as shown in the sketch on the right of figure 5. When the guide rails latch the lead screws remain threaded in the nodes of the top batten frame. The lead screw rotation is then reversed and the beam begins to deploy. The beam deployment from this point is continuous; however, it can be stopped within one bay at any partially deployed location. Additional information can be found in a subsequent figure.

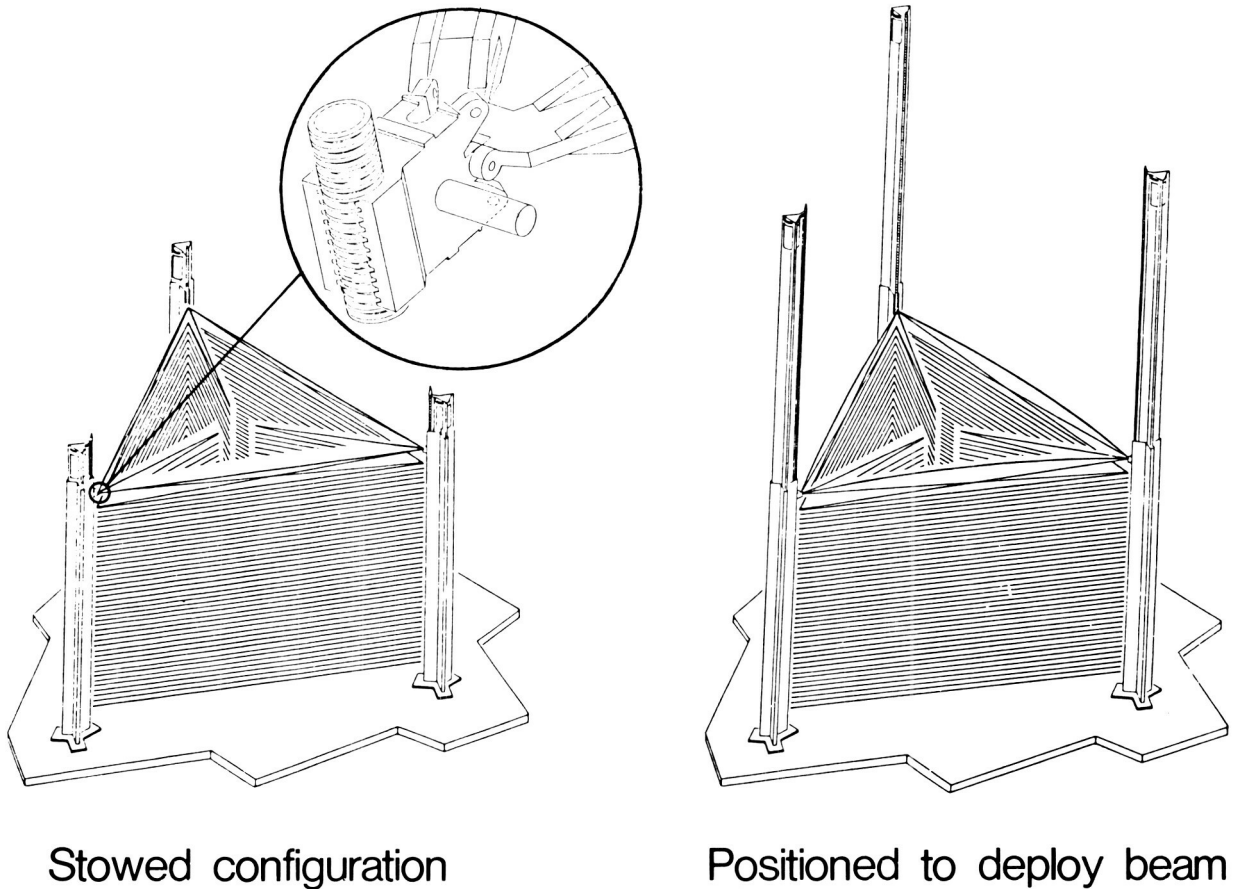


Figure 5



## BAT BEAM DEPLOYER

The sequence for continuous deployment of the BAT beam is illustrated in figure 6. As each node deploys it causes the longeron to unfold and the diagonals to telescope outward. The deploying bay base node is prevented from premature engagement by the escapement mechanism shown adjacent to the guide rail in the sketch on the left. When the longeron and other members of the deploying bay are fully deployed the base node is pulled through the escapement wheel which is friction loaded and onto the lead screw. As it is pulled to the lead screw the node moves laterally to buckle the batten. The bay top node exists from the top of the lead screw and the sequence repeats until the beam is fully deployed. To retract the beam the entire process is reversed.

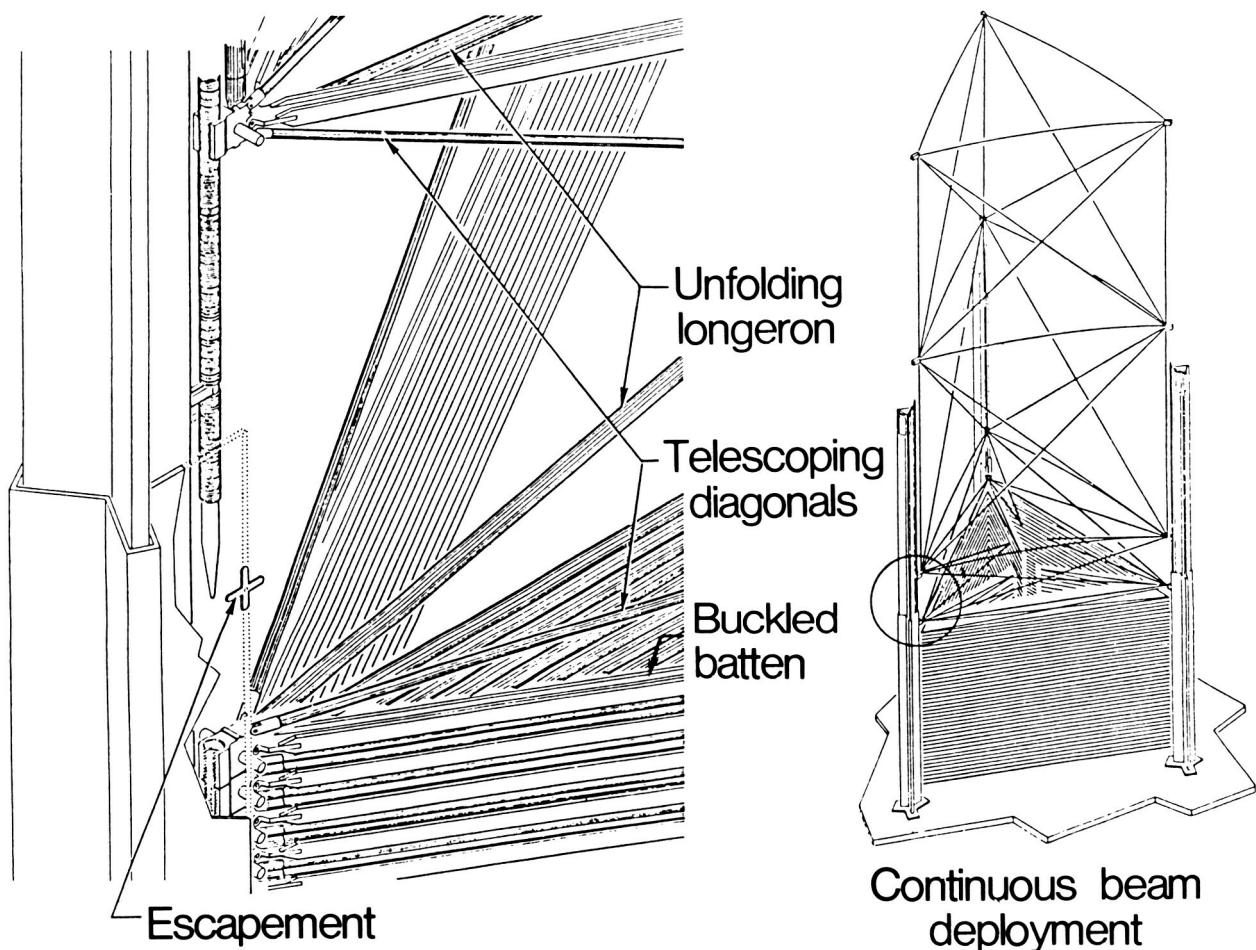


Figure 6

## DEPLOYABLE TETRAHEDRAL BEAM DOUBLE FOLD CONCEPT

A concept for a deployable beam whose basic repeating element is an irregular tetrahedron has been investigated. The beam geometry and folding technique are illustrated in the photographs of a simple working model shown in figure 7. This work was performed under NASA Contract NAS1-17536-2. The objective of the contract was to define the folding sequence and hinge axis orientation to package the tetrahedral beam into a compact unit. To illustrate the process the sequence required to retract the deployed model is described below. The retraction sequence is initiated by hinging the diagonal in the foreground of figure 7 (a and b) into a plane formed by the longerons in the foreground. The next retraction step is shown in figure 7c where the hinge in the diagonal identified by the dot is rotated so the joint nodes fold in the manner indicated by the arrow in figure 7c to the folded position shown in figure 7d. The diagonal indicated by the dot in figure 7d is then hinged to move the joint node to the new position indicated by the arrow. The new folded position is shown in figure 7e. The three step folding process initiated in figure 7b is then repeated as many times as required to fold the beam into a compact package such as the double fold arrangement shown in figure 7f.

This beam has a number of very desirable structural features: (1) it has no joints in the longerons except those near the nodes, (2) all joints are simple single axis hinge pivots, (3) each joint body is fixed to the end of one member which serves to stabilize the body and reduce any rocking motion that may occur due to misalignment, and (4) it can be folded into a very compact package without requiring simultaneous folding of all bays or any extra joints in the members over those that would be required for a single fold configuration.

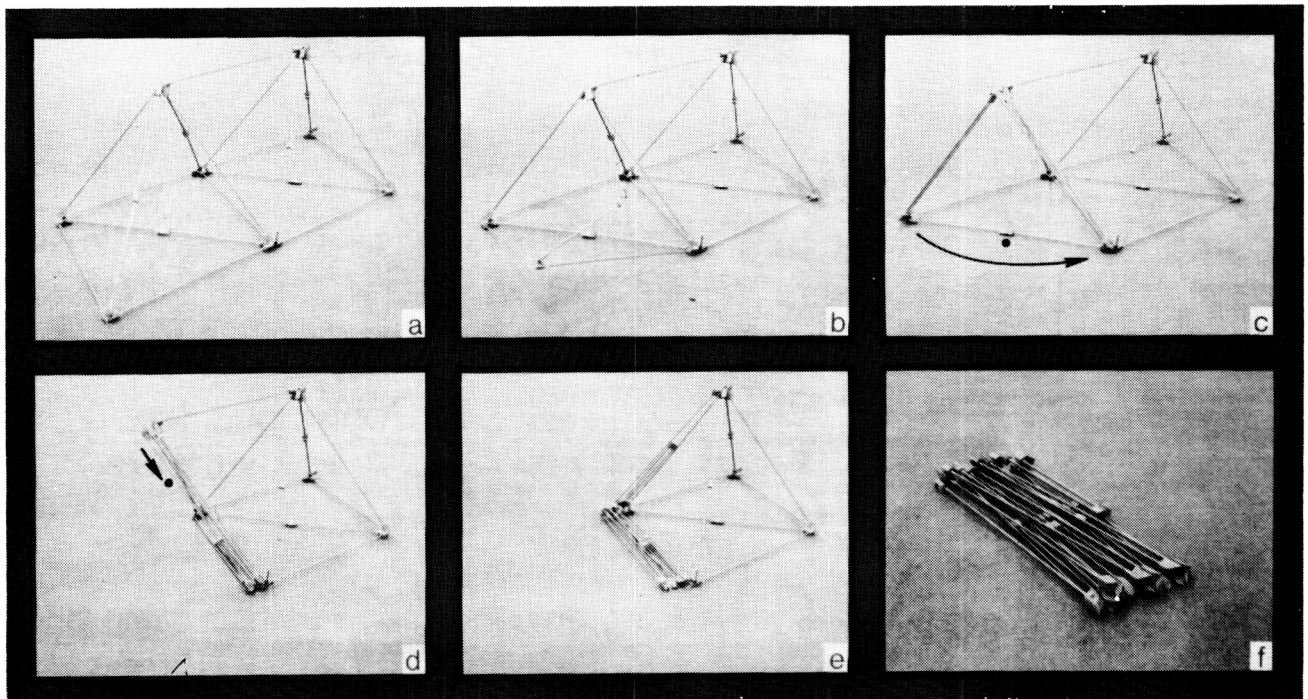


Figure 7

## TWO BAY CONTROLLABLE GEOMETRY GEODESIC TRUSS MODEL

Most deployable beams such as those discussed in references 1 and 2 as well as the BAT beam discussed previously require a special purpose deployer mechanism to unfold and support the beam and the deployer then serves no useful purpose. These beams must also be deployed straight along the final beam axis. A new concept in deployable beam technology known as controllable geometry beams has been investigated. A controllable geometry beam has a number of members which are extensible link actuators and can serve to deploy the beam as well as cause it to deform in a predictable manner. The two bay beam model shown in figure 8 is one such controllable geometry beam concept. It is called a geodesic truss model because it is formed by connecting a series of flat sided triangular frames. The three photos of the model shown in figure 8 are the model deployed straight along the beam axis, the beam deployed in a serpentine manner with the beam tip canted and the beam fully retracted to the stowed position. The beam can serve structural functions in any deployed configuration which permits its use as an articulating serpentine structure to move masses into areas that would be otherwise difficult to reach; to correct for alignment errors in applications that require precision structural control; or to serve as a moveable joint in a space crane or manipulator arm. Details of the configuration are shown on figure 9.

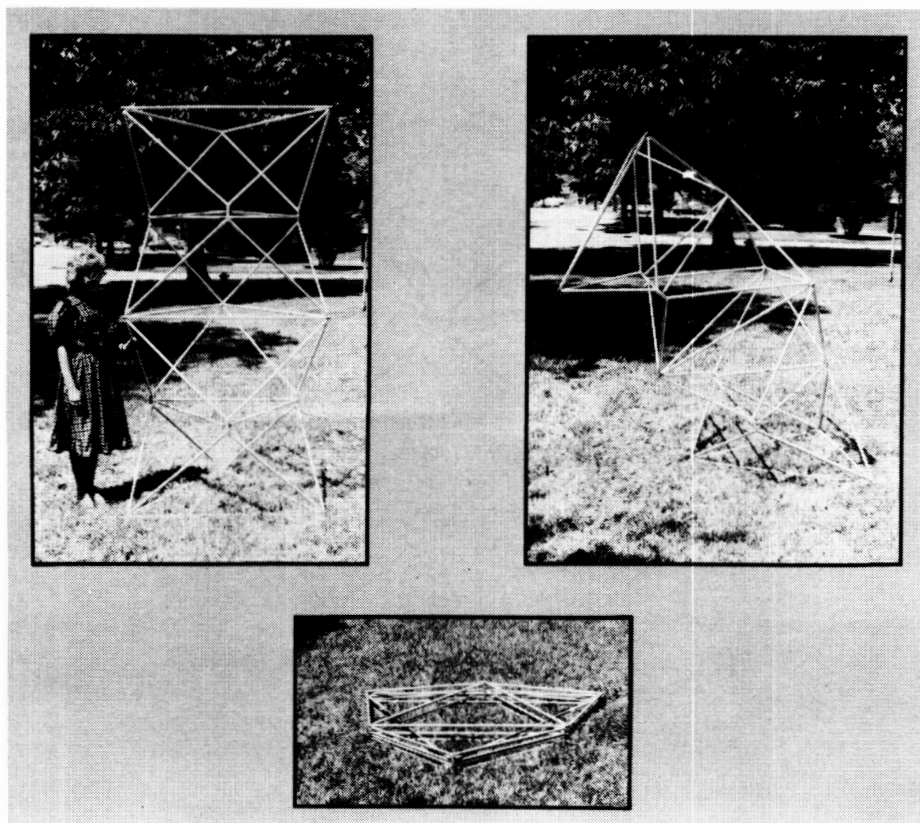


Figure 8

## TWO BAY CONTROLLABLE GEOMETRY GEODESIC TRUSS MODEL (CONCLUDED)

Some details of the geodesic beam are illustrated using the sketch of the two bay model shown in figure 9. At the center of each bay are three actuator members which connect to form the triangular actuator frame noted in the figure. Each actuator can move independently to permit the beam to achieve the required range of motion. At the end of each bay is a batten frame which is composed of three fixed length members. Connecting the actuator and batten frames are a series of longitudinal crossed members which are primary load carrying members for both longitudinal and torsional beam loads. The beam has two joint types noted in the figure as A and B. All joints in the batten frame (joint A) are alike and all joints in the actuator frame (joint B) are alike.

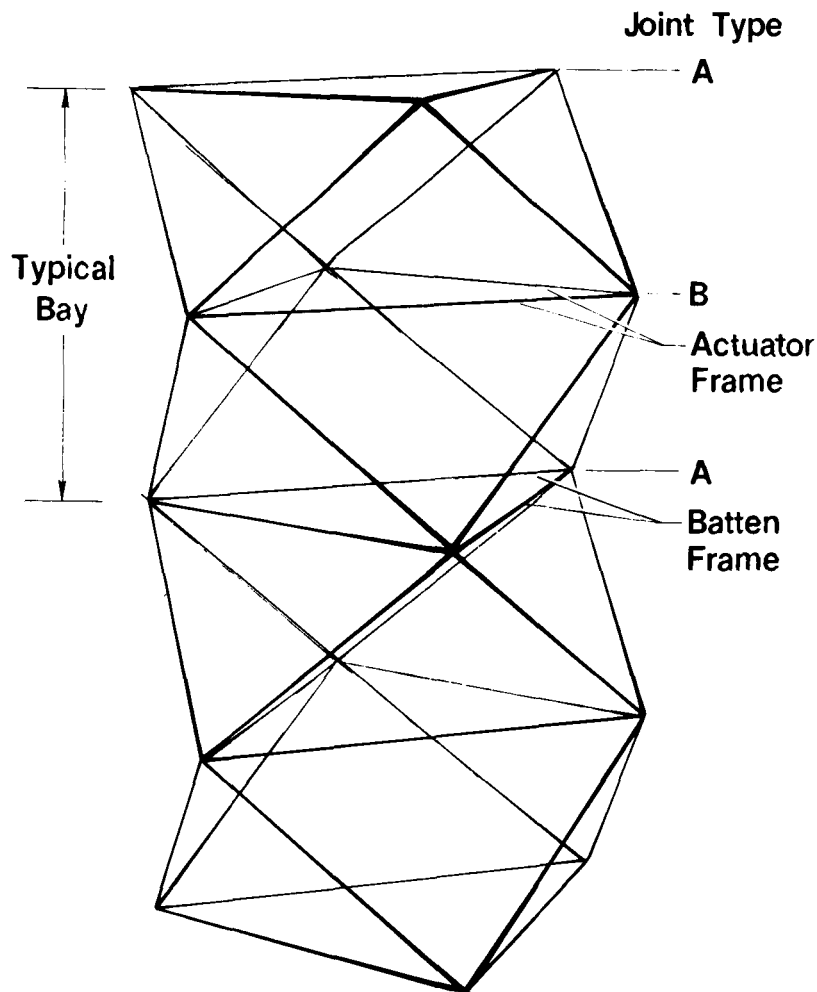


Figure 9

## GEODESIC BEAM TEST SETUP

The demonstration model of the geodesic beam which is shown in figure 8 was tested over a range of potential operating positions. The test setup is shown in figure 10 with the model fully deployed. The model was loaded axially in both tension and compression. The load was applied at the end joints using displacement screw jacks and the platens of the test machine shown in the figure were used as stationary backstops to react the load. The axial displacement of each node was measured as well as the strain in each member of one bay of the beam. Some typical test results are shown in a subsequent figure.

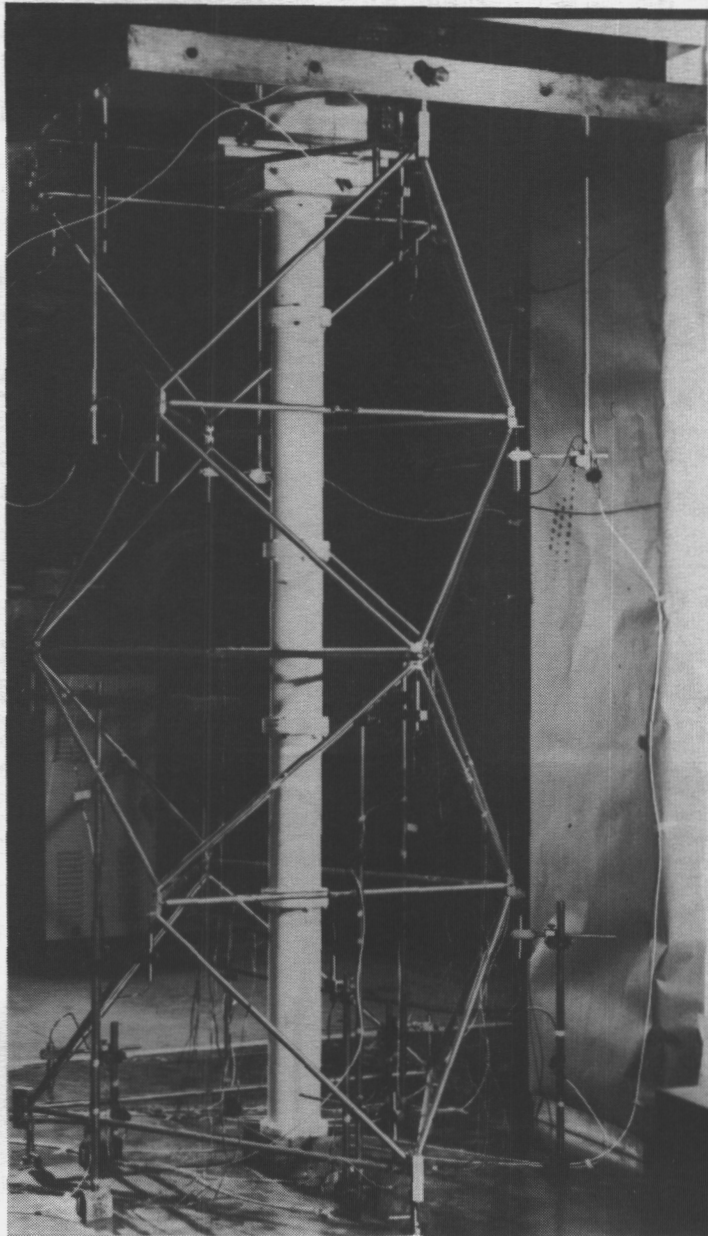


Figure 10

## GEODESIC BEAM TEST RESULTS

Load displacement results from tests conducted on the geodesic beam model in the fully deployed position are shown in figure 11. The results in the figure are averages of displacement gages located at the three joints at four axial stations along the beam as noted on the sketch. At low loads the test results are nonlinear at each of the four stations along the beam. For applied loads above approximately 30 lbs, however, all load displacement curves are linear. The test results for this beam which had 15 moderately complicated joints are similar to the results for the simple clevis joint shown on figure 2. Both demonstrate nonlinear load displacement results for low ranges of test load and linear results for loads in the high range of the test values. Although not shown on figure 11 the geodesic beam also had a different axial stiffness when it was loaded in tension than it did when it was loaded in compression.

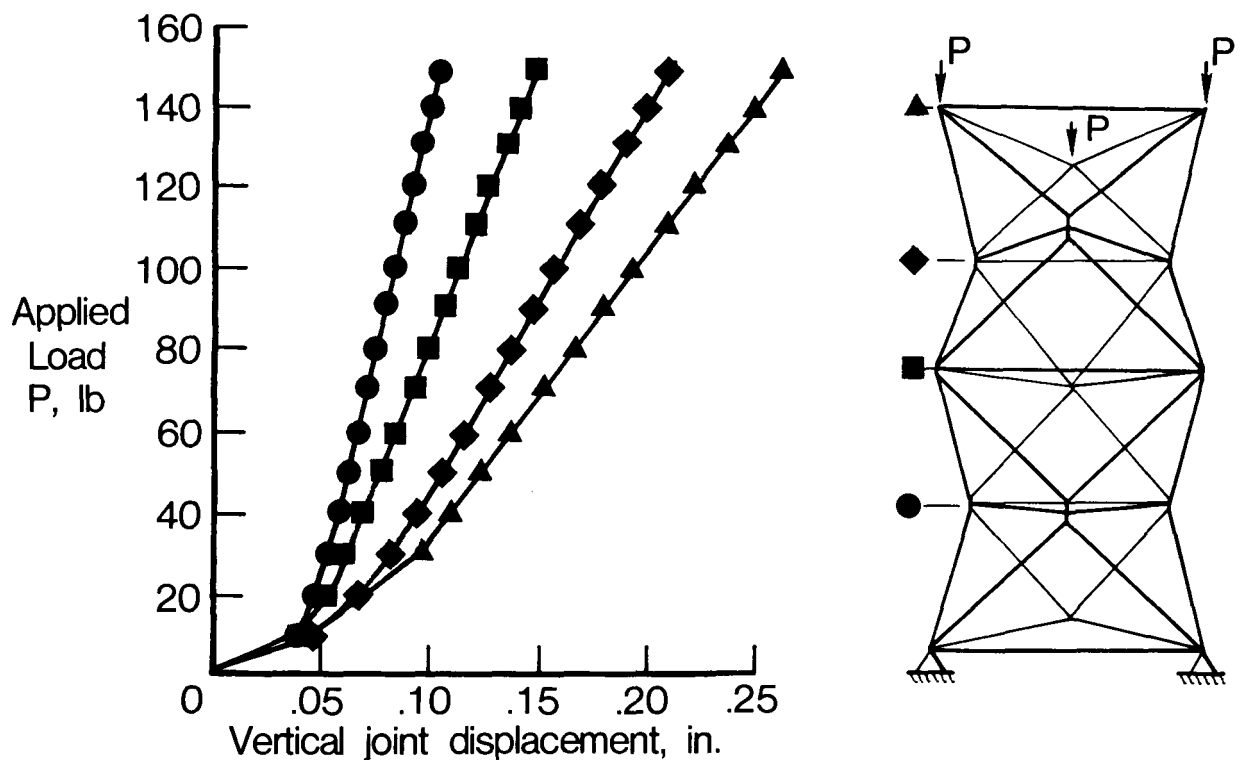


Figure 11

## SPACE CRANE APPLICATION FOR CONTROLLABLE GEOMETRY STRUCTURES

One potential application for the geodesic beam concept involves the use of one or more bays attached to a truss with fixed joints which could then be used as a space crane. A sketch of this configuration is shown in figure 12. The bays of the geodesic beam would provide the required longitudinal and meridional maneuverability found only in massive pin joints normally used in crane applications. By using only a few bays of the geodesic beam the number of actuators would be limited which would reduce the mechanical complexity without sacrificing performance.

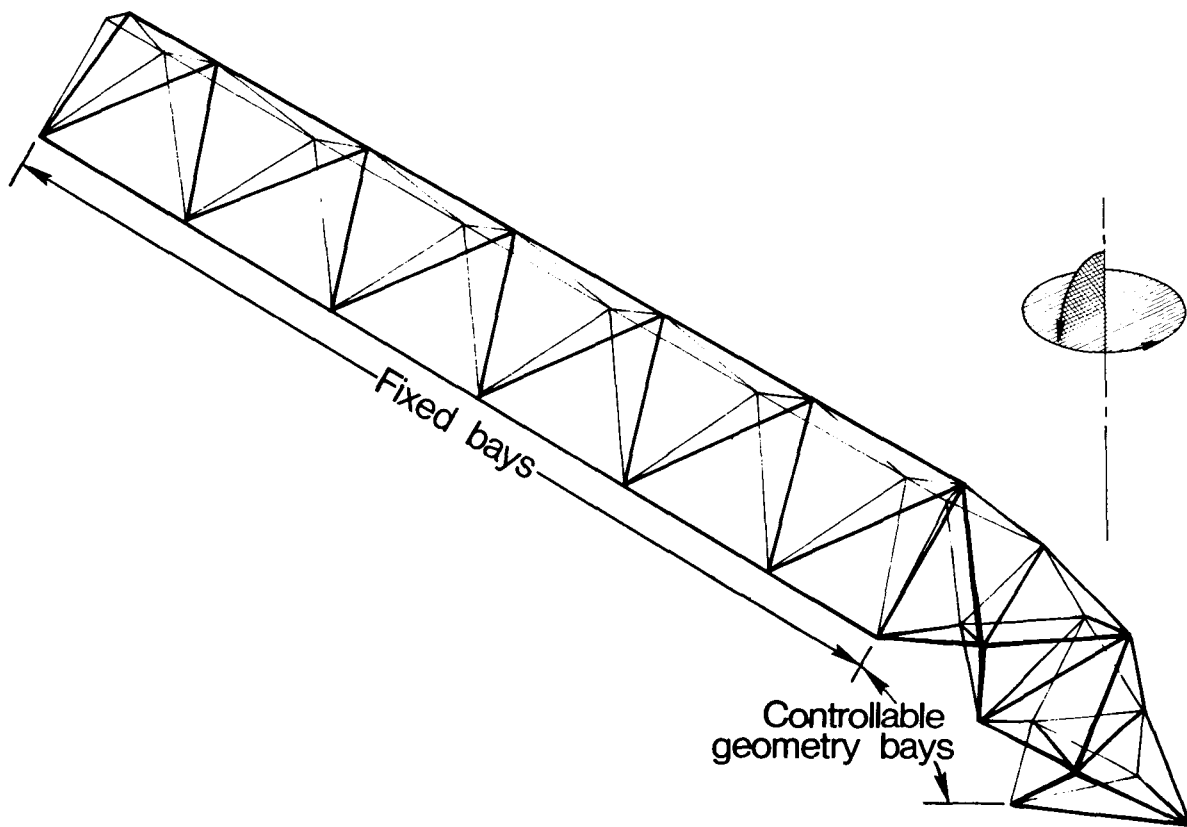


Figure 12



# ANALYSIS OF CONTROLLABLE GEOMETRY BEAM STIFFNESS DURING DEPLOYMENT AND RETRACTION

To support the model development work on controllable geometry beams analytical studies have been performed to evaluate the stiffness changes a beam may encounter as articulation occurs. One analytical study was performed and the results are reported in reference 5. The study used a simple two dimensional finite element model of a warren truss and some results from the study are shown in figure 13. The deployed truss beam had identical member component stiffnesses (EA) and was configured to have a tip deflection to deployed length ratio of 0.01 when subjected to a lateral tip load of about .72 lbs. The beam model did not include any effect of joint mass nor were any effects of joints discussed in figure 2 included in the analysis.

For cantilever beam structures the ratio of the bending stiffness is proportional to the square of the frequency ratio; therefore, a determination of the natural frequency was chosen as the method to evaluate trends in stiffness. Shown in figure 13 are curves which illustrate the square of the frequency ratio as a function of deployed length for two methods of beam retraction. The curve for uniform retraction indicates that a significant loss in stiffness occurs during beam retraction. It was observed that during uniform retraction the fundamental mode changes from pure bending to a mode that is principally bending with some axial coupling. At low deployment ratios (approximately 0.15) the mode shifts to one with only axial motion. The curve for selective retraction indicates that the operational stiffness of the beam can increase significantly as the beam is retracted. This is due in part to the fact that the most heavily loaded bays at the beam root are fully deployed. In addition to the results shown in figure 13 the reference 5 study has examined the stiffness ranges that can occur in a beam during serpentine operation.

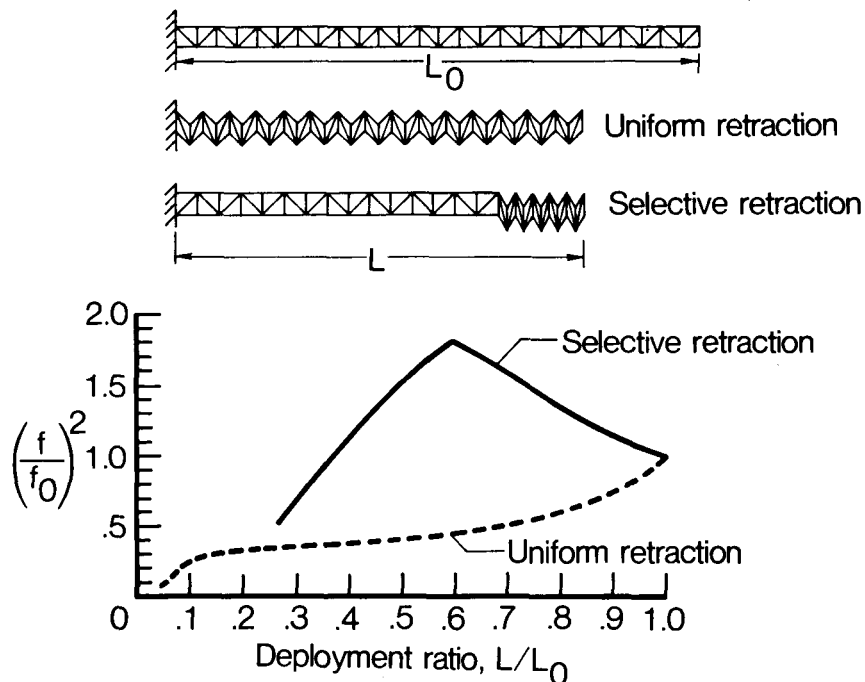


Figure 13



DEPLOYABLE/ERECTABLE BEAMS  
POTENTIAL ADVANTAGES OF HYBRID APPROACH

The development of space structures technology has been primarily focused on concepts that are totally deployable or totally astronaut erected. A considerable technology base has been established in both deployable and erectable structures as evidenced by information reported in references 1, 2, 6, 7, 8. Many advantages and disadvantages exist to support or refute each approach. However, little work has apparently been done to incorporate the advantageous features of both systems into a single hybrid approach. The type of system one might consider could involve the automatic deployment of a single bay (or part thereof) using a simple stored energy system and once deployed an astronaut would connect the bays together to form a beam or planar truss. Several potential advantages of such a hybrid system are shown in figure 14.

- Good packaging and structural efficiencies
- Kinematically simple
- Fewer deployable joints required
- Reduce astronaut requirements
- Simple deployer/assembly aids

Figure 14

## DEPLOYABLE/ERECTABLE HYBRID BEAM CONCEPT

An example of a deployable/erectable hybrid beam is shown in figure 15. The beam would be packaged as individual bays and could be double folded for efficient packaging. Each beam would incorporate simple deployable joints in the battens and diagonals with erectable type joints being used to connect the longerons. The four erectable joints at the corners of the bay would snap together simultaneously as the bay is slid into position.

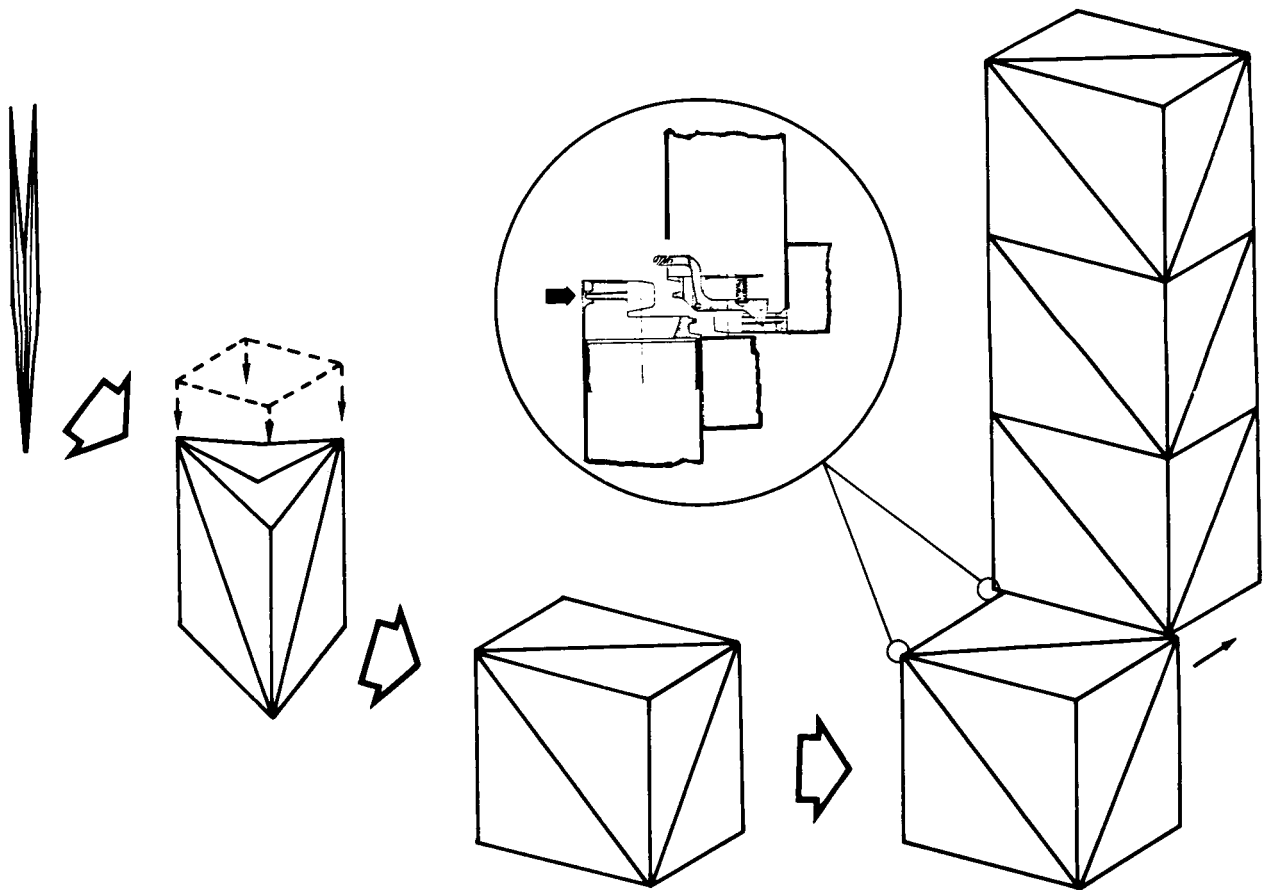


Figure 15

## SUMMARY

A number of new concepts for deployable beam structures have been investigated. The status of this concept development is shown in figure 16. Although much additional work needs to be done in this area advances are being made in LaRC's Structures and Dynamics Division using an integrated approach of fabricating demonstration models and performing generic analytical studies.

### Three longeron deployable beams

- Single fold bat beam design eliminates joint free play-predictable tip position
- Packaging scheme and hinge axes defined for double fold tetrahedral beam

### Controllable geometry beams

- Beam concept defined and demonstration model fabricated
- Analysis of generic beam provides insight on operation to obtain high structural efficiency

### Deployable/erectable hybrid beams

- New concepts examined to exploit benefits of both erectable and deployable beams

Figure 16

## REFERENCES

1. Greenberg, H. S.: Development of Deployable Structures for Large Space Platforms. NASA CR-170689, December 1982.
2. Cox, R. L.; and Nelson, R. A.: Development of Deployable Structures for Large Space Platforms. NASA CR-17090, December 1982.
3. Mikulas, Martin M., Jr.; and Bush, Harold G.: Advances in Structural Concepts. Large Space Antenna Systems Technology-1982, NASA CP-2269, Part 1, 1983, pp. 257-283.
4. Adams, Louis R.; and Hedgepeth, John M.: Batten Augmented Triangular Beam. NASA CR-172461, January 1985.
5. Dorsey, John T.: Vibration Characteristics of a Deployable Controllable-Geometry Truss Beam. NASA TP-2160, June 1983.
6. Heard, Walter L., Jr.; Bush, Harold G.; Wallson, Richard E.; and Jensen, J. Kermit: A Mobile Work Station Concept for Mechanically Aided Astronaut Assembly of Large Space Trusses. NASA TP-2108, March 1983.
7. Watson, Judith J., Heard, Walter, L. , Jr. and Jensen, J. Kermit: Swing-Arm Beam Erector (SABER) Concept for Single Astronaut Assembly of Space Structures. NASA TP-2379, January 1985.
8. Akin, David; Broden, Mary; and Mar, James: Manned Assembly of Space Structures. Large Space Antenna Systems Technology - 1982, NASA CP-2269, Part 1, 1983, pp. 285-300.

PRECISION SPACE STRUCTURES

Keto Soosaar  
Cambridge Research Associates  
Cambridge, Massachusetts

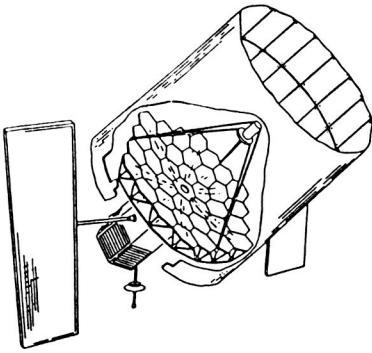
Large Space Antenna Systems Technology - 1984  
December 4-6, 1984

## ISSUES

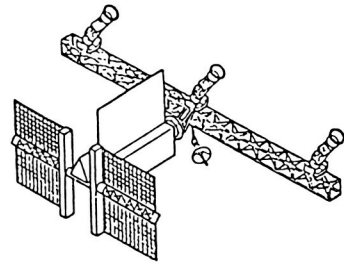
- NASA LARGE SPACE STRUCTURES EFFORTS TO DATE AIMED TOWARDS
  - LARGE, FLEXIBLE ANTENNA-LIKE STRUCTURES (30-100M)
  - RELATIVELY LONG WAVELENGTHS (1-30cm)
  - MODERATE DISTURBANCES LEADING TO SOME STRUCTURE-CONTROL INTERACTION
- NASA ALSO HAS POTENTIAL MISSIONS IN "OPTICS" REGIME
  - SMALLER REFLECTORS/MIRRORS
  - SHORT WAVELENGTHS (VISIBLE TO 100 $\mu$ )
  - VERY TIGHT TOLERANCES IN SURFACE, ALIGNMENT, POINTING STABILITY
  - POTENTIAL OF CONSIDERABLE ON-BOARD DISTURBANCES
- NEED TO EXAMINE TRANSFERABILITY OF TECHNOLOGY, NEW PROBLEMS

## REVIEW OF REQUIREMENTS

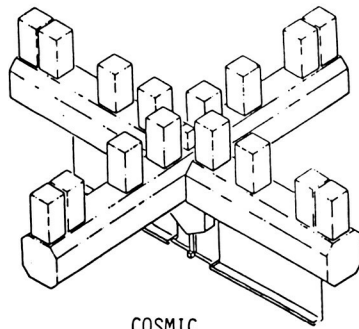
- BASED ON NASA SPACE SYSTEMS TECHNOLOGY MODEL (JAN. 84)
- REVIEW INCLUDED BOTH
  - "MISSION SYSTEMS AND PROGRAMS"
    - APPROVED, PLANNED AND CANDIDATE CONCEPTS
  - "OPPORTUNITY SYSTEMS AND PROGRAMS"
    - GENERALLY POST-1995 SYSTEMS
- "PRECISION SYSTEMS" < 100 $\mu$  OPERATIONAL WAVELENGTH
- REVIEW TO IDENTIFY STRUCTURE-CONTROL INTERACTION POTENTIAL
  - FIGURE (SURFACE) CONTROL
  - VIBRATION (ALIGNMENT) CONTROL
  - ATTITUDE CONTROL



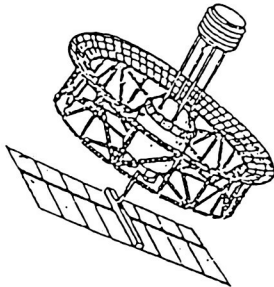
LARGE DEPLOYABLE REFLECTOR



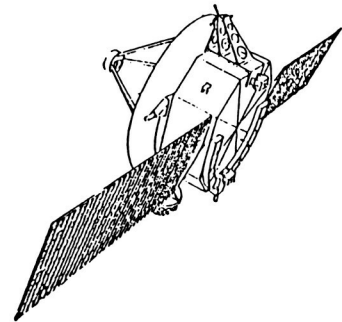
INFRARED INTERFEROMETER



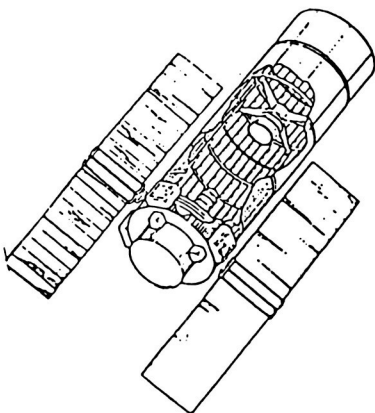
COSMIC



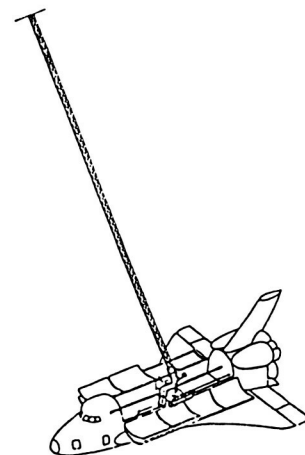
100M THINNED APERTURE



MOLECULAR LINE SURVEY



VERY LARGE SPACE TELESCOPE



PINHOLE OCCULTER FACILITY

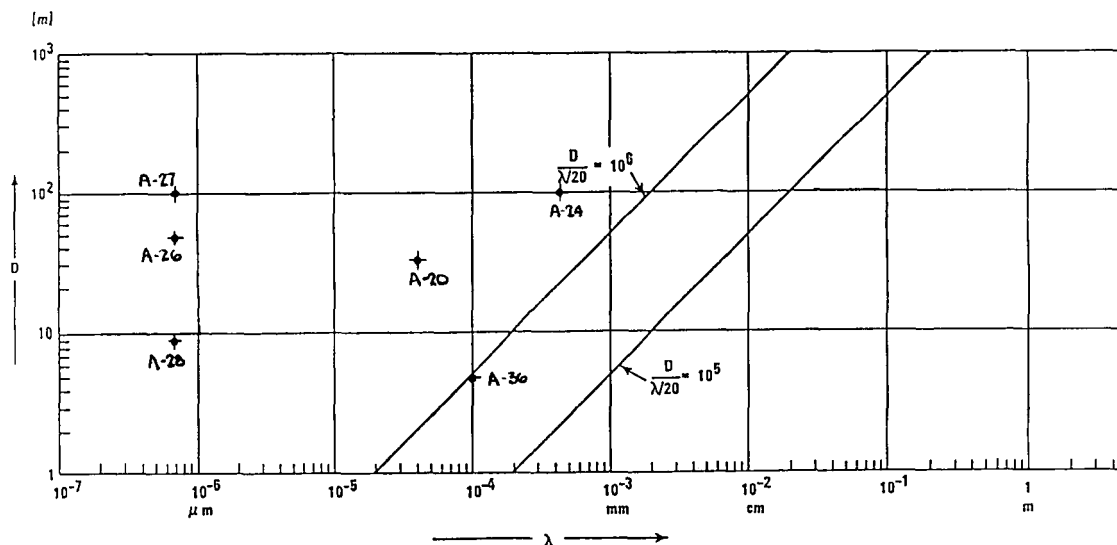
# NASA-PLANNED PRECISION SPACE STRUCTURES

<u>NASA NO.</u>	<u>NAME</u>	<u>SIZE</u>	<u>WAVELENGTH</u>	<u>POINTING STABILITY</u>
A-20	LARGE DEPLOYABLE REFLECTOR	20M	30μ+	.15μr
A-24	INFRARED INTERFEROMETER	3M X 100M	300μ+	(5μr)
A-26	COSMIC	1.8M X 34M	VIS	2nr
A-27	100M THINNED APERTURE	100M	VIS	.5nr
A-28	VERY LARGE SPACE TELESCOPE	8M	VIS	10nr
A-36	MOLECULAR LINE SURVEY	3.5M	100μ	(8μr)
A-18	PINHOLE OCCULTER FACILITY	50M	XRAY, UV, VIS	1μr

# NASA-PLANNED PRECISION SPACE STRUCTURES

<u>NASA NO.</u>	<u>D/RMS</u>	<u>f<sub>n</sub>(EST.)</u>	<u>D/f<sub>n</sub>λ</u>	<u>POSSIBLE DISTURBANCES</u>	<u>CONTROL NEEDS</u>		
					<u>FIGURE</u>	<u>STRUCTURE</u>	<u>ATTITUDE</u>
A-20	10 <sup>7</sup>	5	10 <sup>5</sup>	CHOP, SLEW, CMG, CRYO	X	X	X
A-24	6 X 10 <sup>6</sup>	2	10 <sup>5</sup>	CMG, APPEND	X	X	X
A-26	10 <sup>8</sup>	10	10 <sup>6</sup>	CMG, APPEND	X	X	X
A-27	1.6 X 10 <sup>9</sup>	1	10 <sup>8</sup>	CHOP, CMG, APPEND	X	X	X
A-28	2.5 X 10 <sup>8</sup>	5	2 X 10 <sup>5</sup>	CMG, APPEND	X	X	X
A-36	7 X 10 <sup>5</sup>	10	3.5 X 10 <sup>3</sup>	CHOP, CMG	X	NO	X
A-18	NA	NA	NA	SHUTTLE		(X)	X
<u>THRESHOLD</u>	<u>10<sup>5</sup></u>	<u>THRESHOLD</u>	<u>10<sup>4</sup></u>				

# DIAMETER AND WAVELENGTH ESTIMATION





## VIBRATION CONTROL

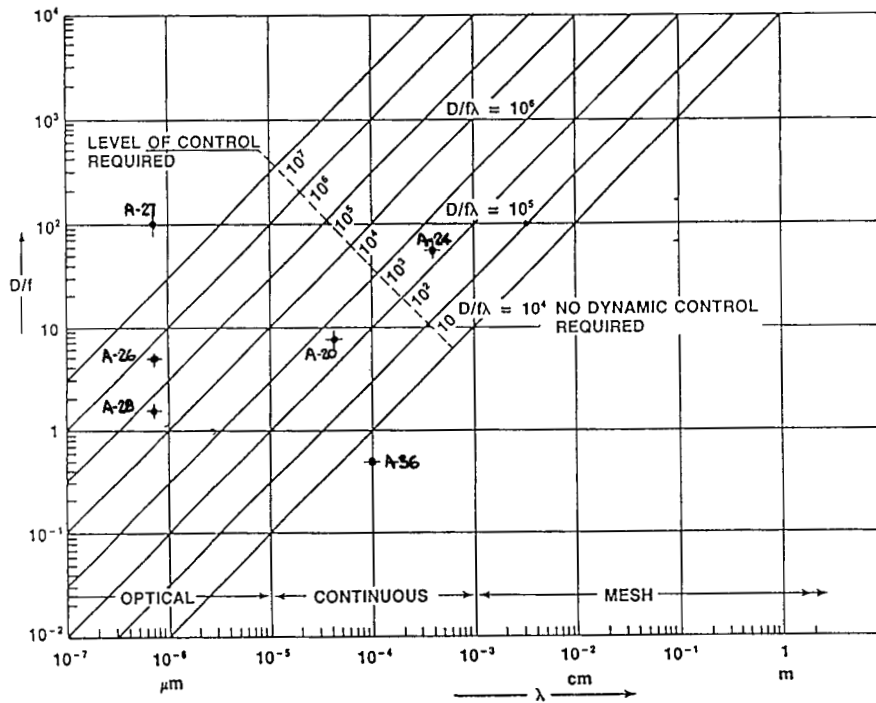
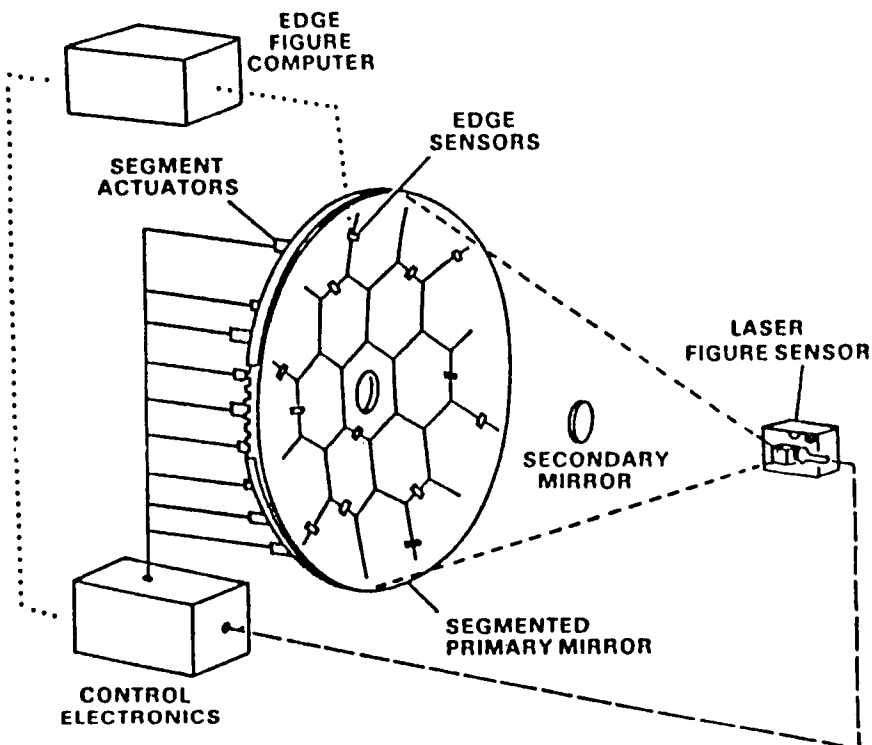


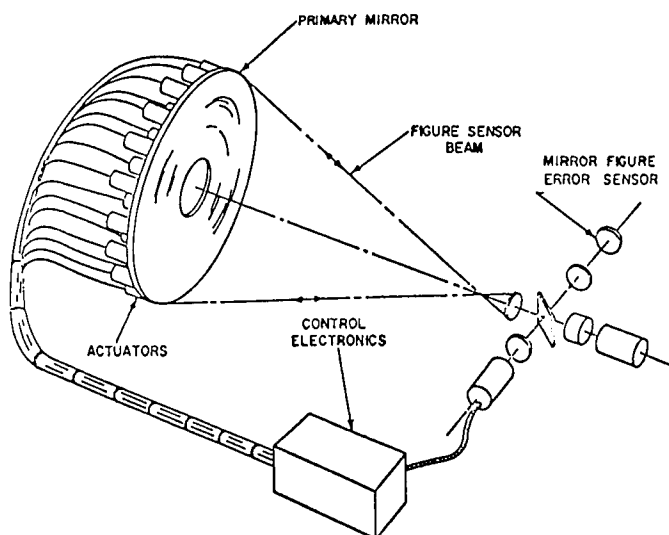
FIGURE CONTROL

- EARLIEST RECOGNIZED INSTANCE OF STRUCTURE-CONTROL INTERACTION
- GENERALLY A QUASI-STATIC CONTROLS APPROACH - THERMAL DRIVERS
  - RIGID SEGMENT ALIGNMENT TO DESIRED FIGURE
    - BACK-UP STRUCTURE MAY NEED TO BE CONTROLLED AS WELL
    - DISPLACEMENT ACTUATORS
  - CONTINUOUS MIRROR - ACTUATORS ELASTICALLY COUPLED
    - FORCE ACTUATORS - HIGH DEGREE OF COUPLING
    - DISPLACEMENT ACTUATORS - EFFECT MORE LOCALIZED
    - REAL ACTUATORS - INTERMEDIATE EFFECT - MUST MODEL
  - HYBRID VERSIONS OF SEGMENTED/CONTINUOUS BEING CONSIDERED
- NOT DIFFICULT TO DO STRUCTURE ANALYSIS OR CONTROLS DESIGN
  - UNLESS MIRRORS EXHIBIT STRUCTURAL DYNAMICS RESPONSE
    - MAY BE POSSIBLE TO STIFFEN MIRRORS SOMEWHAT  $> 30$  HZ
    - OTHERWISE - CONTROLS APPROACHES FROM ANTENNAS - HIGH BW
- SENSORS/ACTUATORS - RESOLUTION TO  $.01\lambda$  OPERATING WAVELENGTH
  - TRANSFER FROM ANTENNAS LESS LIKELY



- THE LASER FIGURE SENSOR MONITORS EACH SEGMENT SURFACE
- THE EDGE SENSOR TESTS ALIGNMENT BETWEEN PAIRS OF SEGMENTS

### FIGURE/SURFACE CONTROL

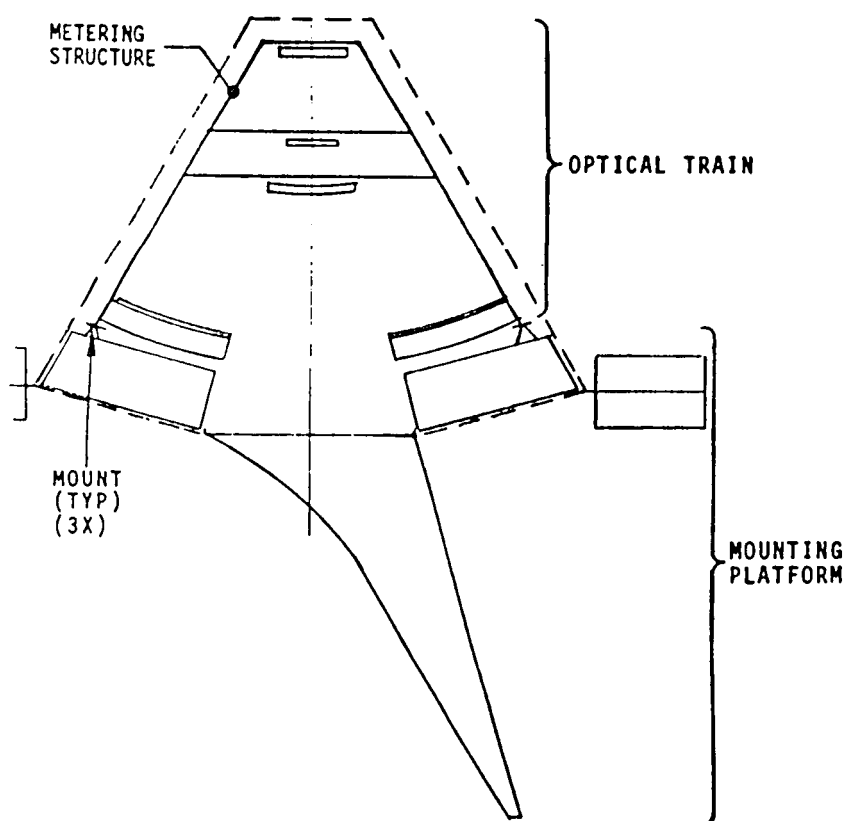


- DISTRIBUTED PARAMETER CONTROL FLEXIBLY COUPLED
- TECHNOLOGY DEVELOPED IN EARLY 1970'S FOR STATIC CORRECTION - NASA/DOD
- HIGH-BANDWIDTH OPTICS DEVELOPED
- CORRECTION FOR MIRROR DYNAMICS LARGELY UNEXPLORED

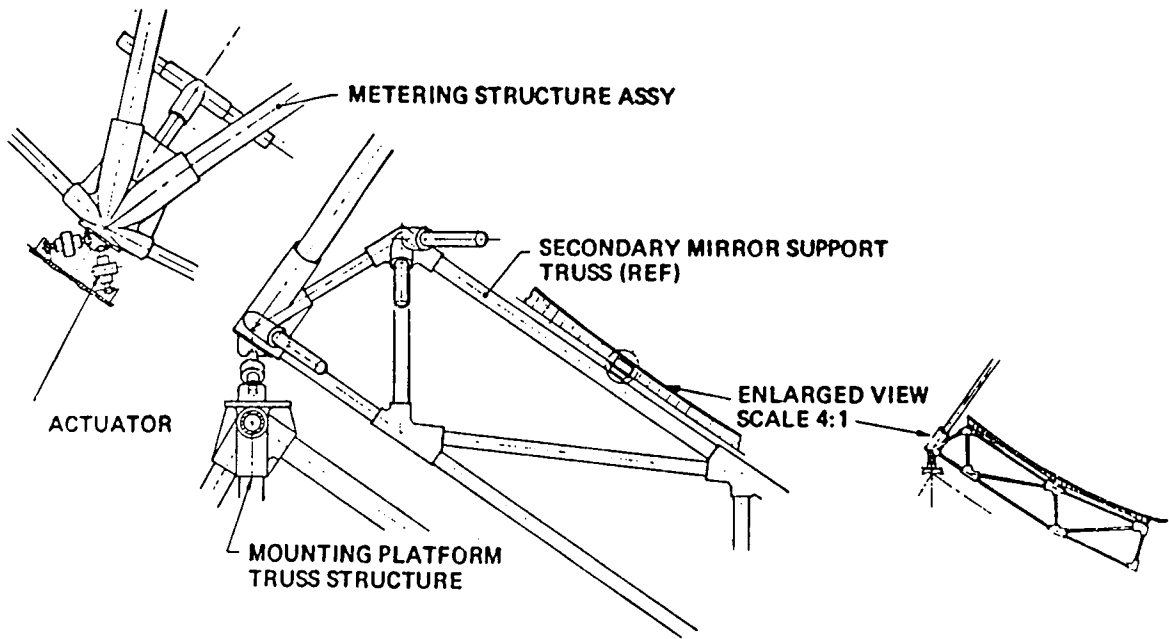
## VIBRATION (ALIGNMENT) CONTROL (1)

- SOME BUT NOT MUCH SIMILARITY TO ANTENNA CONTROL PROBLEM
- CONTROL BW  $\sim 50$  HZ; 100 MODES IN BW; 30 MODES CONTROLLED
- RESPONSE REDUCTION GOALS NEAR  $10^4$
- SPACECRAFT DESIGN OPTIONS PERMIT SOME ATTENUATION
  - ISOLATION (ACTIVE OR PASSIVE) OF OPTICAL TRAIN
  - DISTURBANCE LEAKAGE STILL CAN OCCUR
  - INERTIALLY DISTRIBUTED FORCES NOT AFFECTED BY ISOLATION (SLEW, CHOP)
  - SENSOR-ACTUATOR DYNAMICS AND NOISE CAN BE TROUBLESOME
  - HENCE REDUCTION OF VIBRATIONS IS NEEDED

## OVERALL SPACECRAFT DESIGN APPROACH



- TWO MAJOR COMPONENTS
  - 1) OPTICAL TRAIN
  - 2) MOUNTING PLATFORM
- OPTICAL TRAIN: "ISOLATED" FROM MAJOR DISTURBANCES
- MOUNTING PLATFORM: A NON-PRECISION STRUCTURE CONTAINING MOST OF THE SOURCES OF DISTURBANCES AND APPENDAGES SUCH AS SOLAR PANEL AND SUN-SHADE
- OPTICAL TRAIN AND PLATFORM ARE ATTACHED THROUGH KINEMATIC MOUNTS. MOUNT DESIGN IS SUCH THAT IT FILTERS UNDESIRABLE LOW FREQUENCIES



#### VIBRATION (ALIGNMENT) CONTROL (2)

- OPTIONS:

- NATURAL DAMPING - CLOSER TO .1% OF CRITICAL
- DAMPING MATERIALS - MAY BE LIMITED BY
  - BROAD BANDWIDTH OF RESPONSE
  - CRYO TEMPERATURES OF SYSTEMS
  - BROAD TEMPERATURE SWINGS OF SYSTEM
  - OUTGASSING AND CONDENSATION ON COLD OPTICS
- MULTI-INPUT MULTI-OUTPUT CONTROL
  - THEORETICAL BASIS SAME AS IN ANTENNA PROBLEMS
  - MORE DETAILED STRUCTURAL MODELS NEEDED - MORE MODES IN BW
  - STRUCTURAL LINEARITY AT MICRO-STRAINS QUESTIONABLE
  - DEPLOYMENT HINGES AND LATCHES MUST FULLY FREEZE
  - SENSOR-ACTUATOR DYNAMICS CLOSER IN BW TO EXCITED MODES
  - ACTUATOR NOISE CAN BE LARGE DISTURBANCE SOURCE
  - ACTUATOR AND SENSOR RESOLUTION
    - $.01\lambda/D$  ANGULAR
    - $.01\lambda$  LINEAR
    - TRANSFER FROM ANTENNAS UNLIKELY
  - SYSTEM ID MAY BE CONFUSED BY ISOLATORS
  - AVIONICS - MAY NEED TO PROCESS MUCH LARGER SYSTEM

## ATTITUDE CONTROL

- ISOLATORS MAY MAKE LOW BW SYSTEM POSSIBLE
  - COARSE POINTING AND SLEW BY MOUNTING PLATFORM
  - FINE POINTING BY OPTICAL TRAIN USING ISOLATORS
- COARSE SENSORS AND ACTUATORS - TRANSFERABLE FROM ANTENNAS
- FINE SENSORS AND ACTUATORS - UNIQUE TO PRECISION MISSIONS

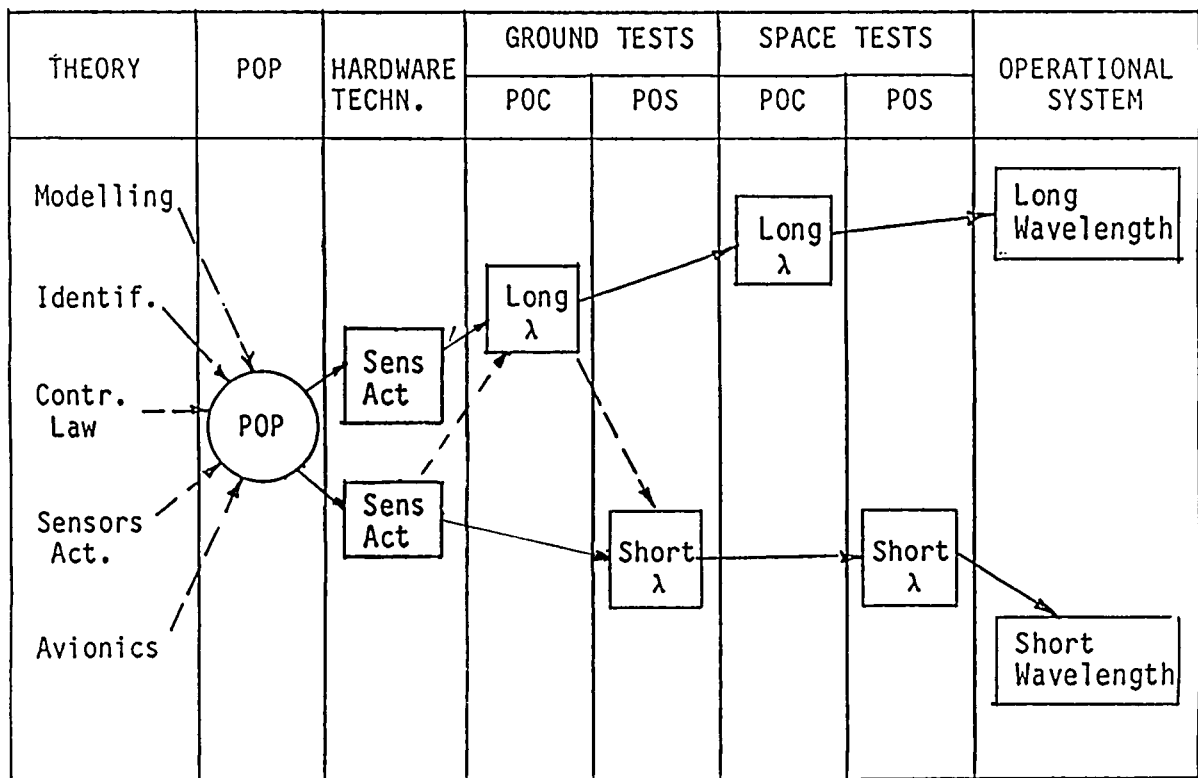
## NET NASA MISSIONS - ACTIVE STRUCTURES GOALS

	<u>SHORT <math>\lambda</math> - OPTICAL</u>	<u>LONG <math>\lambda</math> - RADAR</u>
D	15	100
$\lambda$	1 $\mu$	3 cm
TOLERANCES		
SURFACE	0.03 $\mu$	0.4 mm
DEFOCUS	0.2 $\lambda$	0.2 $\lambda$
POINTING	10 nrad	10 mrad
DISTURBANCES	PERIODIC, RANDOM, SLEW	SCAN, SLEW, PERIODIC
CONTROLS GOALS		
LOS	10 <sup>2</sup> - 10 <sup>4</sup>	10 - 10 <sup>2</sup>
WAVEFRONT	0 - 10	10 - 10 <sup>2</sup>
MODES IN BW	100	50
CONTROLLED MODES	30	30
CONTROL BW	50	5

## TEST AND VERIFICATION - PRECISION SYSTEMS

- SMALLER, STIFFER THAN ANTENNAS
  - LESS OF 1G EFFECTS ON GROUND - LINEARITY MAINTAINED
  - ATMOSPHERIC MASS DURING TEST INSIGNIFICANT
  - ATMOSPHERIC DAMPING MAY BE IMPORTANT SINCE NATURAL DAMPING LOW
  - TESTING IN VACUUM FOR OPTICAL PATH INTEGRITY
- UNLIKE ANTENNAS SIGNIFICANT LEVELS OF SYSTEM INTEGRATION CAN BE TESTED IN A VACUUM TANK

### "CRITICAL PATH" CHART



## SUMMARY

- A NUMBER OF NASA PRECISION SPACE STRUCTURES ARE IDENTIFIABLE
- NEARLY ALL EXHIBIT SOME POTENTIAL FOR STRUCTURE-CONTROL INTERACTION
- DIFFERENCES FROM ANTENNA SYSTEMS CAN BE NOTED
  - FIGURE/SURFACE CONTROL CAN BE QUASI-STATIC
  - ACTIVE/PASSIVE ISOLATION SCHEMES ARE POSSIBLE
  - VIBRATION CONTROL IS NECESSARY
    - THEORETICAL FOUNDATION TRANSFERABLE
    - STRUCTURAL LINEARITY AT SMALL STRAINS OF CONCERN
    - ON-BOARD DISTURBANCES CAN BE SIGNIFICANT
    - HIGHER BW, LARGER NUMBER OF MODES
    - ACTUATOR/SENSOR RESOLUTION MUCH HIGHER
  - ATTITUDE CONTROL SYSTEM CAN BE LOW BW
  - GROUND TESTING MORE FEASIBLE THAN WITH ANTENNAS

**Page intentionally left blank**



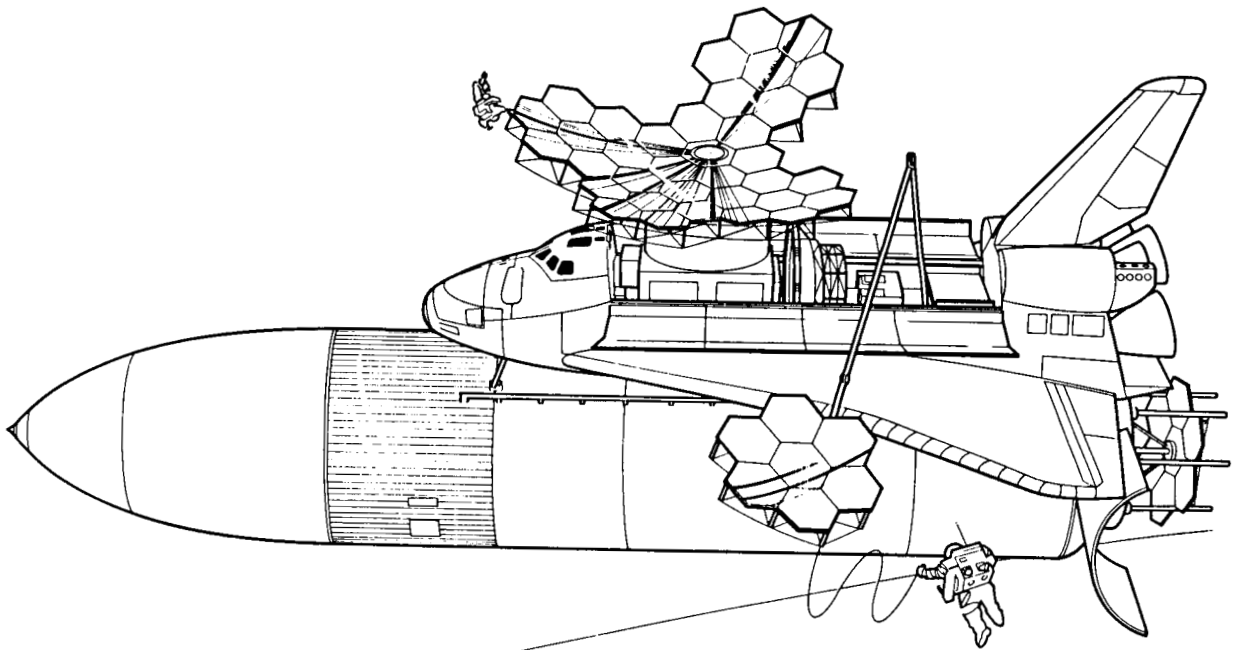
**PRECISION ANTENNA REFLECTOR STRUCTURES**

**John M. Hedgepeth  
Astro Research Corporation  
Carpinteria, California**

**Large Space Antenna Systems Technology - 1984  
December 4-6, 1984**

## ASSEMBLY OF THE LARGE PRECISE REFLECTOR INFRARED TELESCOPE

The advancing capabilities of the Shuttle and systems designed for use with the Shuttle should have a beneficial impact on the way in which large space structures are established in space. In particular, the probable availability of a large-volume launch compartment built on the aft end of the main propellant tank could allow the preconstruction of large modules which can be assembled in space in order to create the desired aperture. This so-called Aft Cargo Carrier has a large enough diameter to allow a large aperture to be assembled from a small enough number of separate modules to make the assembly practical. The assembly approach is illustrated in Figure 1, which is taken from Reference 1.



(From Reference 1)

Figure 1

## GENERAL SCIENTIFIC REQUIREMENTS

An example future mission is that of space-based astronomy at infrared and submillimeter wavelengths. Previous studies (see Reference 2, for example) indicate that a telescope 20 to 30 m in diameter is a highly desirable instrument. This telescope is often called the Large Deployable Reflector (LDR), but is herein called the Large Precise Reflector (LPR). The general telescope requirements were developed in a workshop (ref. 2) held in June 1982 and are included in Table 1.

DIAMETER	$\geq 20$ m
SHORTEST WAVELENGTH OF DIFFRACTION-LIMITED PERFORMANCE ( $\lambda_c$ )	30-50 $\mu\text{m}$
LIGHT BUCKET BLUR CIRCLE	$\leq 2$ ARCSEC AT 1-4 $\mu\text{m}$
TEMPERATURE AND EMISSIVITY	PRIMARY $\leq 200$ K, $\epsilon = 0.01$ AT $\lambda = 1$ mm, $\epsilon = 0.05$ FOR $\lambda \leq 1$ mm
CHOPPING	2 Hz, 1 ARCMIN (REACTIONLESS)
SIDELOBES	LOW NEAR SIDELOBES
SCAN	1° BY 1° - LINEAR SCAN AT 1°/MIN
SLEW	$\geq 50^\circ/\text{MIN}$
FIELD OF VIEW	$\geq 3$ ARCMIN
ABSOLUTE POINTING, JITTER	0.05 ARCSEC, 0.02 ARCSEC

Table 1

## THE AFT CARGO CARRIER

The Aft Cargo Carrier (ACC), shown in Figure 2, is a structural enclosure that attaches to the aft end of the STS external tank. (See Reference 3 for a full description.) It provides additional cargo volume and will accommodate payloads which are incompatible with the 4.6-m diameter of the orbiter bay. The ACC can handle circular payloads up to 7.6 m in diameter.

The external tank, the ACC skirt, and the payload support structure are carried into orbit. After the payload is removed, the remaining structure is then deorbited and reenters the atmosphere for safe ocean disposal.

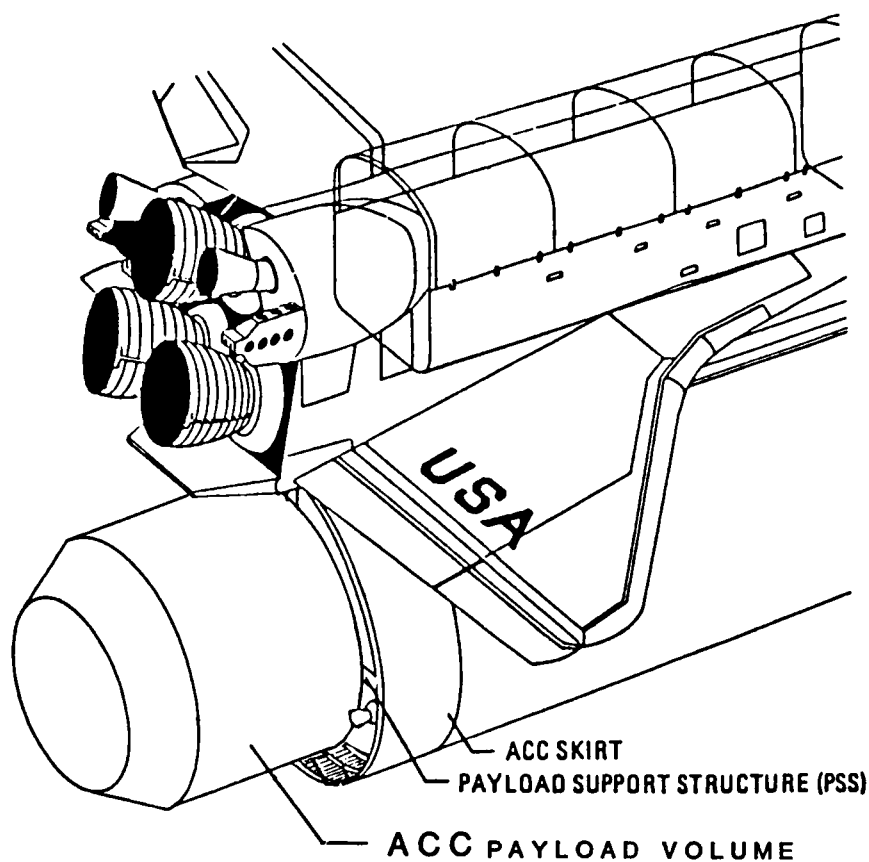


Figure 2

## LARGE PRECISION REFLECTOR STRUCTURE

The most likely structural configuration for the LPR will include a segmented primary reflector composed of highly precise and polished panels which are mounted to a very stable support truss by means of adjustable actuators. One version is shown in Figure 3. A feedback control system will be used to command the actuators to adjust the positions of the segments.

The analyses of Reference 4 deal with a tetrahedral truss structure with surface struts of length  $L$  and a truss depth of  $H$ . The numerical results obtained for the 20-m aperture reflector and values of  $L$  and  $H$  of 2 m showed that hollow struts 2 cm in diameter composed of graphite/epoxy were stiff enough to resist the operational accelerations without allowing deleterious deflections. For the present study, the same tetrahedral-truss geometry is used with appropriate values chosen for  $L$  and  $H$ . The formulas derived in Reference 4 can therefore be used to predict the structural characteristics of the new concepts.

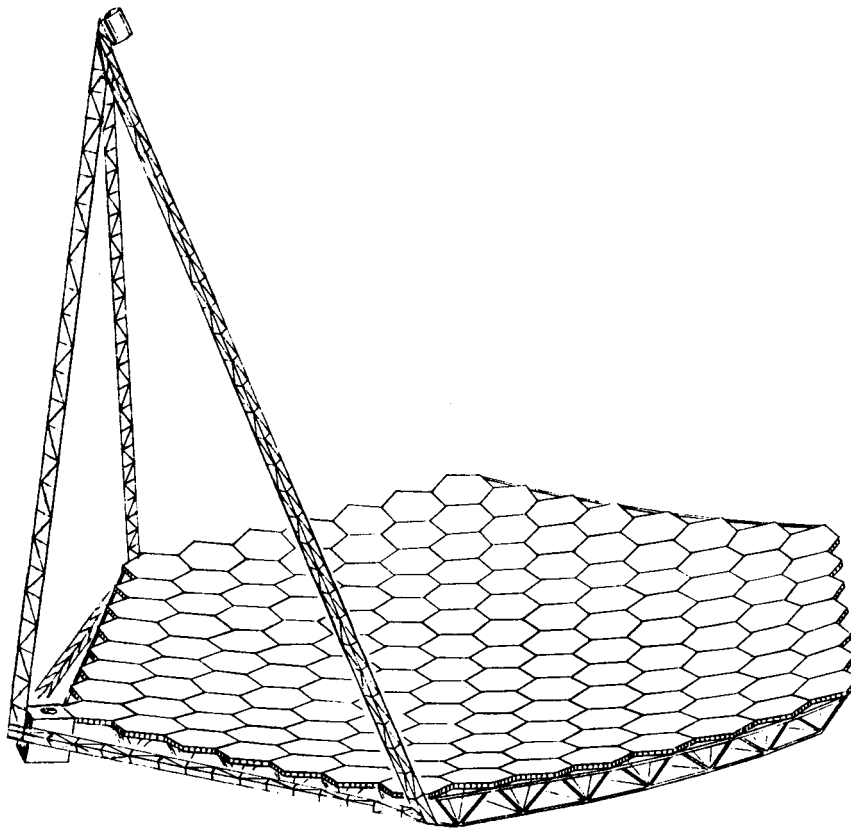


Figure 3

## PACKAGING OPTIONS

A study was performed of the areal packaging efficiency of various geometries of panels. Results were obtained for logical arrangements of hexagonal and square panels. Also included was the possibility of using partial panels to fill out the notches at the boundary. In addition, geometrical arrangements with petals surrounding a central polygon might be useful. Some examples are shown in Figure 4.

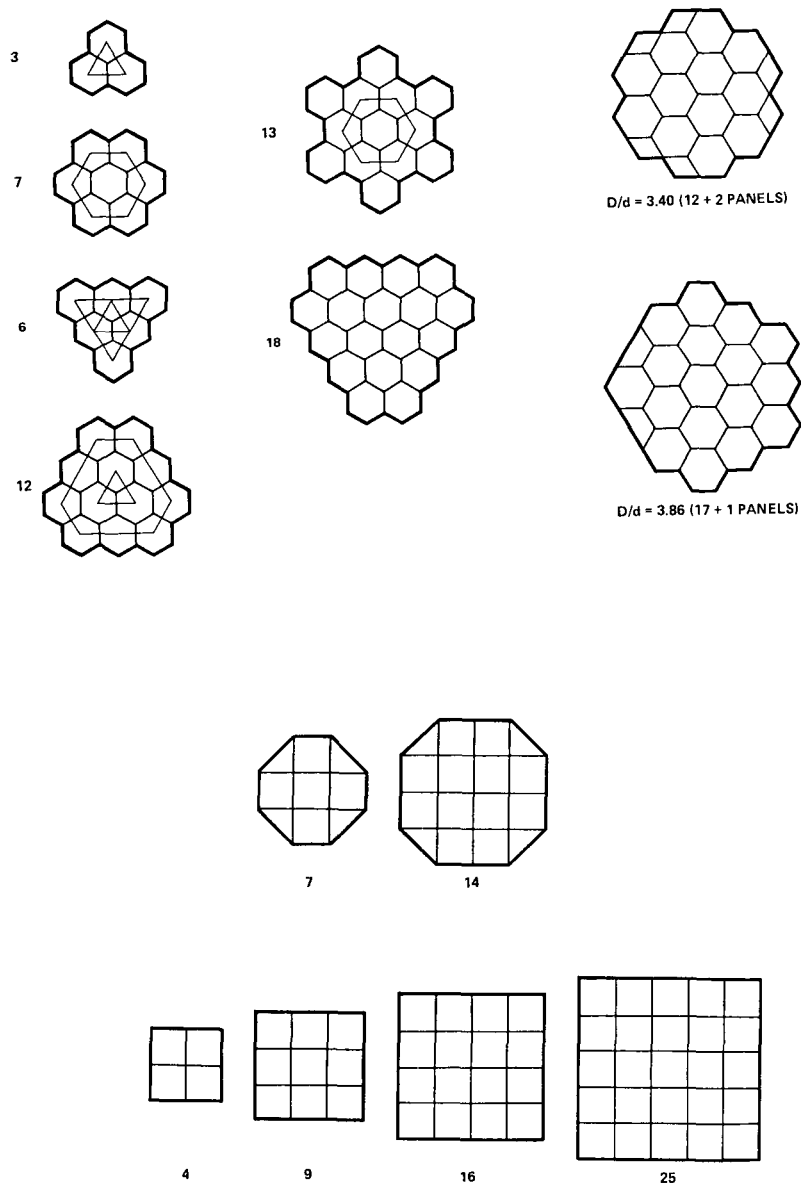


Figure 4

# VARIATION OF THE RATIO BETWEEN EFFECTIVE DIAMETER AND MODULE SIZE FOR VARIOUS PANEL GEOMETRIES

A measure of efficiency is the number of panels, each of which is stowable in a diameter  $d$  to produce an assembled aperture of area equal to that of a circle of diameter  $D$ . The results are summarized in Figure 5 in which  $D/d$  is plotted against the number of panels in the packaged stack. Shown on the plot are horizontal lines at  $D/d = 2.53$  and  $3.80$  which are the necessary values for an aperture of 20 m and 30 m if the package diameter is 7.9 m. Also shown is a horizontal line pertaining to the achievement of a 20-m aperture with panels stowed in the Shuttle cargo bay  $d = 4.5$  m. The open symbols represent cases in which the number of separate pieces is equal to the number of panels in the stack. In those cases where partial panels are used to round out the boundary, the number of pieces exceeds the number of panels and is indicated by the solid symbols.

In general, the hexagonal panel gives superior results. Square panels have no advantages. The petaled configurations could be interesting, particularly the seven-sided one, which is a candidate for meeting the 20-m requirement. The packaged depth is the same as that for the hexagonal panels, but the number of pieces (eight) is less than that for the rounded hexagonal case (13). In a similar way, the folded-petal configuration is attractive for the 30-m objective. This can be met with 18 or 19 hexagonal panels. A possible competitor with smoother outer edges would be the 11-sided petaled arrangement.

It should be noted that the serrated hexagon arrangement shown in Figure 1 is equivalent in efficiency to the hexagonal panel. This arrangement is attractive because each separate facet is a hexagon and therefore approaches the circular shape which is intuitively desirable for fabrication.

Another case in which each modular panel is made up of hexagonal tiles is the 12-tile module. The efficiency is 4 percent lower but would be tolerable if the smaller tiles would be significantly easier to fabricate. This arrangement is discussed more fully in the following pages.

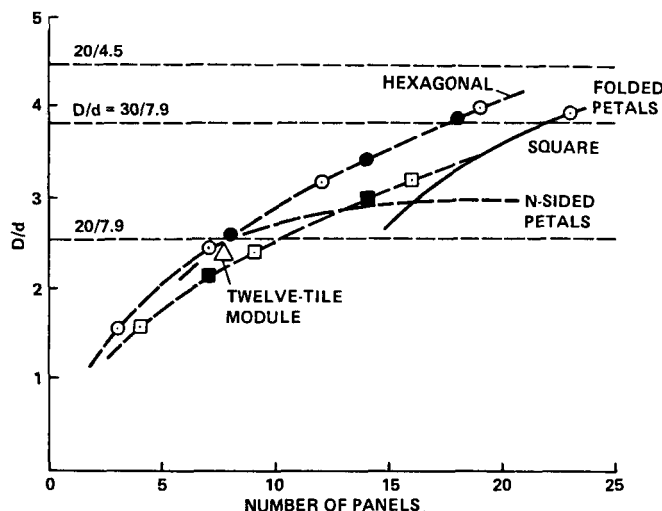


Figure 5

## PACKAGING CONCEPTS

In order to reduce the thickness of the stowed modules, the deep support truss must be packaged. The approach chosen to package the tetrahedral support truss is to shear one of the surfaces against the other as is illustrated in the sketches in Figure 6. One set of intersurface members has knee joints at their centers that allow them to bend and permit the shearing motion. The other intersurface members hinge at their intersection with the surface in order to allow free shearing. Note that the hinges are indicated by the black circles and that the assembly joints to the adjacent modules are indicated by the triangles. Note also that an intersurface member is seemingly missing at the left-hand end. This absence is purposeful in that doubling up of members in the assembly is thereby avoided. Of course, if the module were an edge module, extra members would be added to close out the structure.

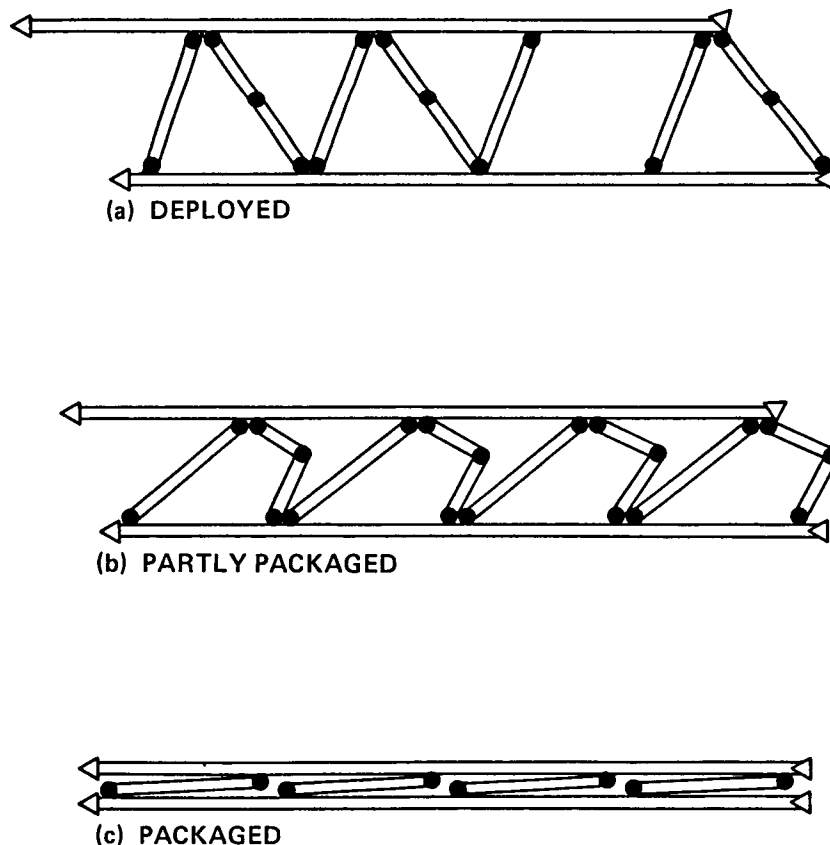


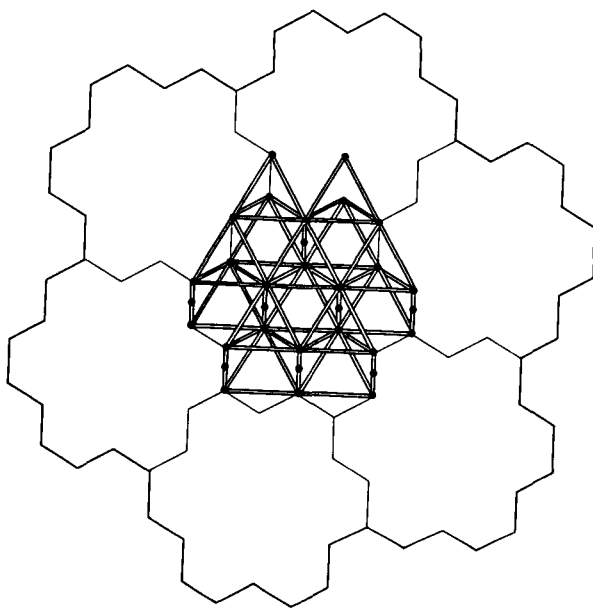
Figure 6



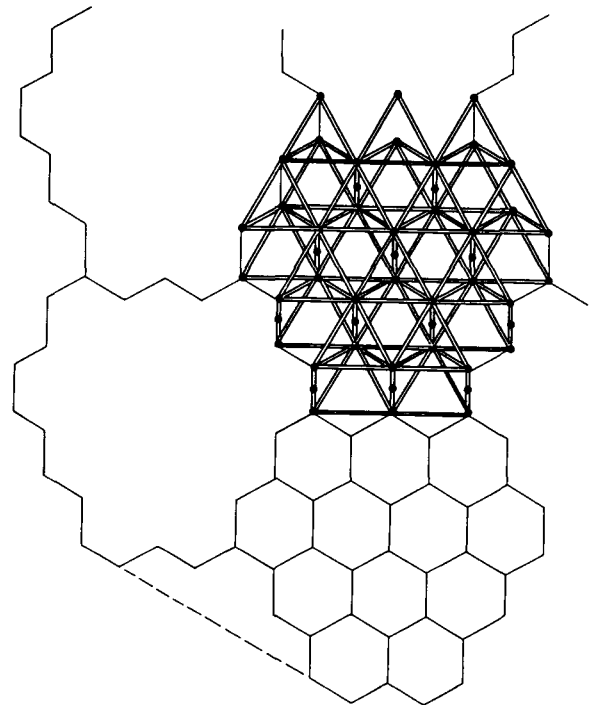
## SUPPORT TRUSS GEOMETRY

The arrangement of present and missing members is shown in Figure 7a for the seven-tile module and Figure 7b for the 12-tile module. In both figures, the support truss for a module is shown as it appears when viewed looking through the truss to the rear of the reflector tiles.

Note that two choices can be made as to which of the intersurface members will act as knees. The choice shown involves a minimum of joints. The other pivoting set, however, along with the surface members, comprises a statically determinate "rib" which will package by rotation only if the truss is flat. Thus, the modules cannot be stacked together snugly. The alternative would be to put knee joints in the other set; then the pivoting set would not constitute a structure and would therefore tolerate a curved truss.



(a)



(b)

Figure 7

## STOWAGE DEPTH

Since it is possible to have the packaged truss occupy the same area as do the reflector panels, the measure of packaging efficiency is the depth of the package. Assume that the reflector tiles are 0.1-m thick. Assume that the structural truss can be packaged in a 0.1-m depth (this seems reasonable for truss members about 2.5 cm in diameter). Then the total local thickness would only be 0.2 m if the modules could be efficiently nested. Thus 23 panels could be stacked in the cylindrical length of the ACC payload compartment.

As mentioned above, a significant simplification results if the truss can be made flat. The cost is greater package depth. The depth of curvature of a single module is

$$\delta = \frac{(7.9)^2}{8 \times 20}$$
$$\approx 0.4 \text{ m}$$

Therefore, the package depth with a flat truss would be 0.6 m. For a seven-module truss, the total depth would be 4.2 m, which is well within the length available in the ACC. The greater simplicity of the flat truss could therefore be used. If more modules were desired, then the factor of three improvement of the curved truss would be needed.

### EXAMPLE CONSTRUCTION SCENARIO

The entire spacecraft would consist of the primary reflector, a secondary reflector, a science package, a spacecraft bus, and a thermal shield. The order of assembly might be as follows for an on-axis, seven-module design (see Figure 8).

1. Assemble central reflector module to bus (the LEASECRAFT is an example of a possible bus). The interface between the bus and the module would be three struts packaged with the central module that connects three corners of the module to three hard points on the bus.
2. Assemble the science package adapter to the central module. The adapter would be mounted to a portion of the structure prior to launch with appropriate care for thermal aspects. The portion of the structure would be assembled in flight to close out the truss.
3. Assemble the secondary mirror unit to the central module. The interface would be through six struts, packaged with the secondary reflector, joining three points on the secondary reflector with the same three corners of the central module to which the bus is attached.
4. Deploy and assemble the outer modules to the central module. Each module can carry its own thermal insulating blanket.
5. Install remaining rear insulation
6. Install thermal shield
7. Mount science modules
8. Separate from Shuttle, deploy solar array, and check out
9. Boost into operational orbit

This scenario can be varied readily for other example configurations.

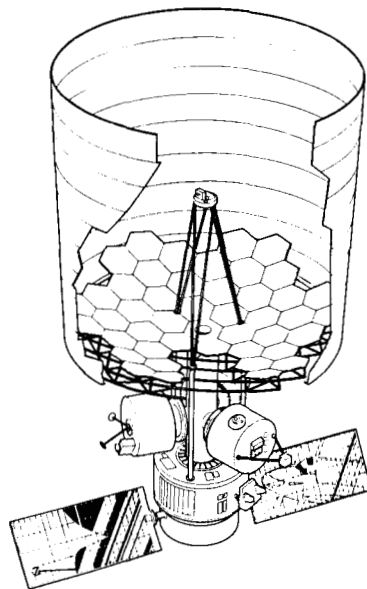


Figure 8

#### REFERENCES

1. Pittman, R.; Leidich, C.; Masey, F.; and Swenson, B.: A Modular Approach to Developing a Large Deployable Reflector. Proceedings of SPIE, vol. 430, Infrared Technology IX, 23-25 August 1983, pp. 115-128.
2. Leidich, C.; and Pittman, R., eds.: Large Deployable Reflector Science and Technology Workshop, vol. 1, Executive Summary. NASA Conference Publication 2275, June 1984.
3. Williams, F.L., et al: Aft Cargo Carrier (ACC) and Shuttle Derived Cargo Vehicle (SDCV) Definition Study, Final Report. Martin Marietta Corporation, Report No. MMC-SDV-DR-6-3, NASA Contract NAS8-34183, February 1983.
4. Hedgepeth, John M.: Support Structures for Large Infrared Telescopes. NASA CR-3800, June 1983.

#### ACKNOWLEDGEMENT

The author wishes to acknowledge the contributions of R. Pittman of NASA Ames to the packaging arrangements discussed herein and of Messrs. T.B. Mobley of Martin Marietta (Michoud) and T.C. Taylor of Taylor & Associates to the ACC description.

INTELSAT ACTIVITIES ON LARGE ANTENNA STRUCTURES\*

J. Agrawal  
INTELSAT  
Washington, DC

Large Space Antenna Systems Technology - 1984  
December 4-6, 1984

\* Paper unavailable at time of publication.

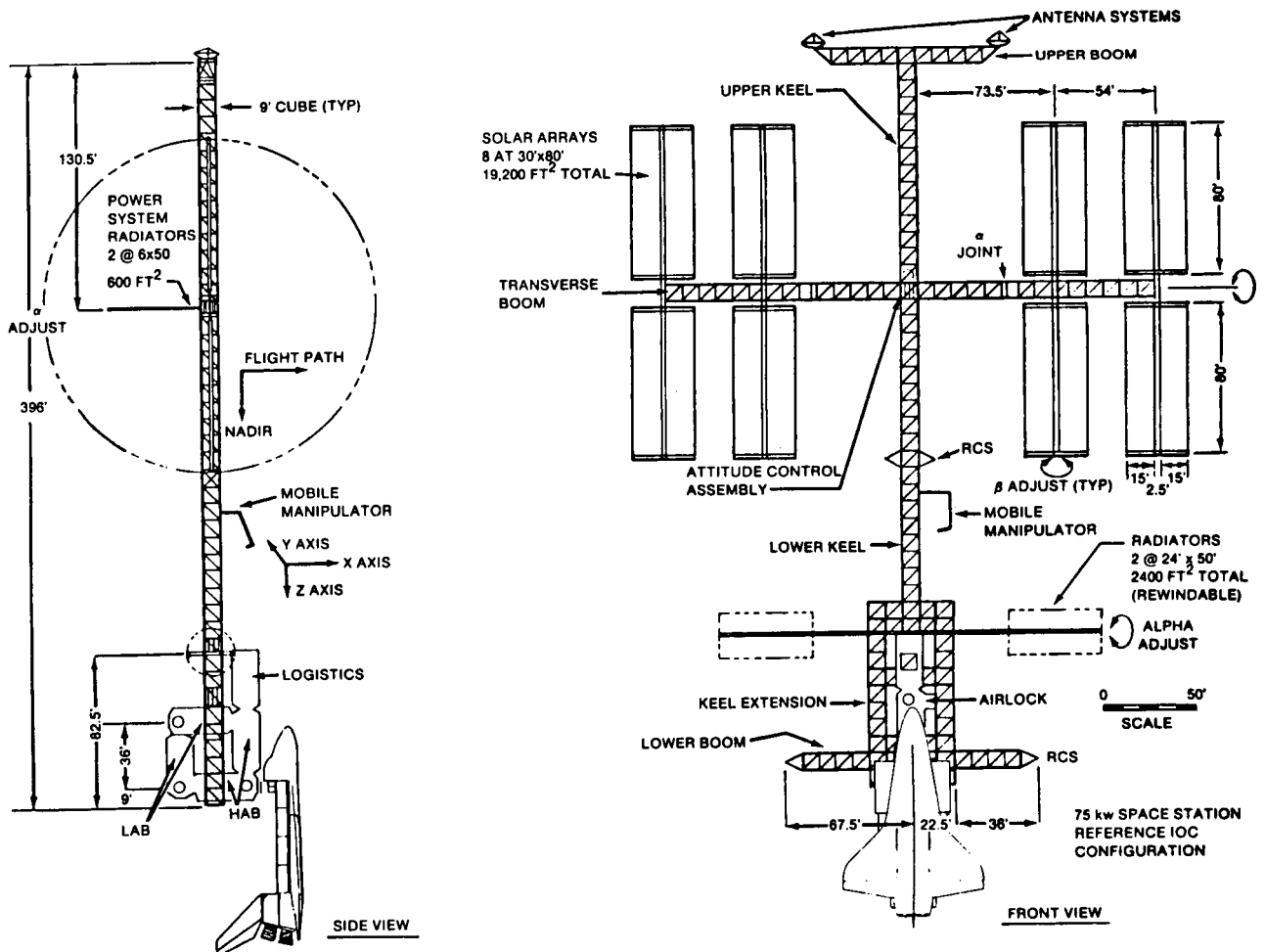
**Page intentionally left blank**

## SPACE STATION STRUCTURES

W. Schneider  
NASA Johnson Space Center  
Houston, Texas

Large Space Antenna Systems Technology - 1984  
December 4-6, 1984

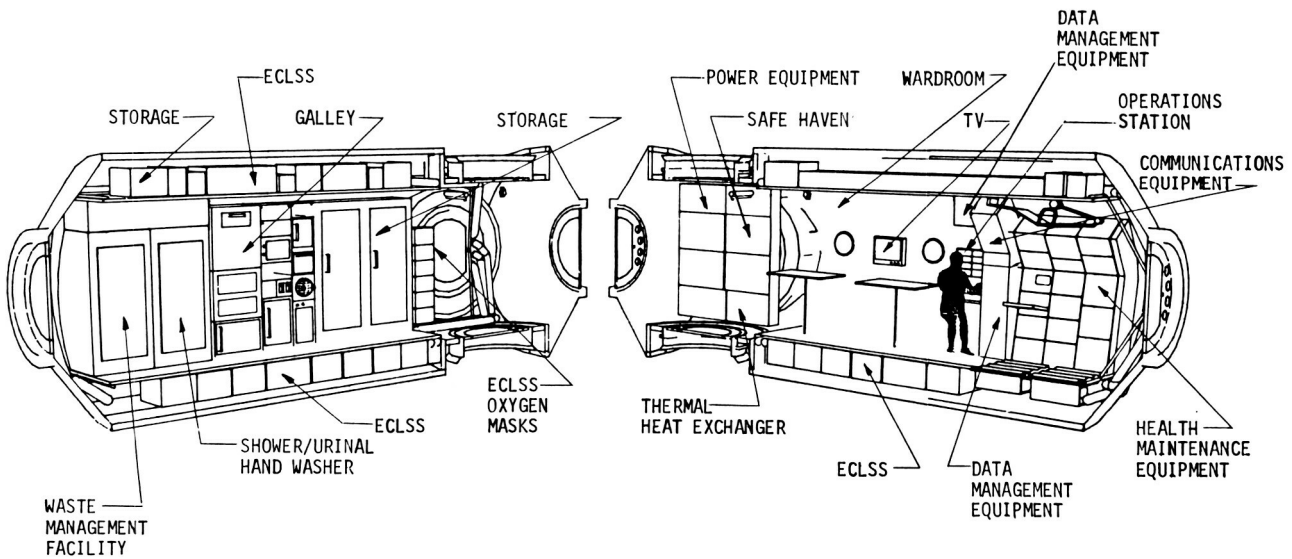
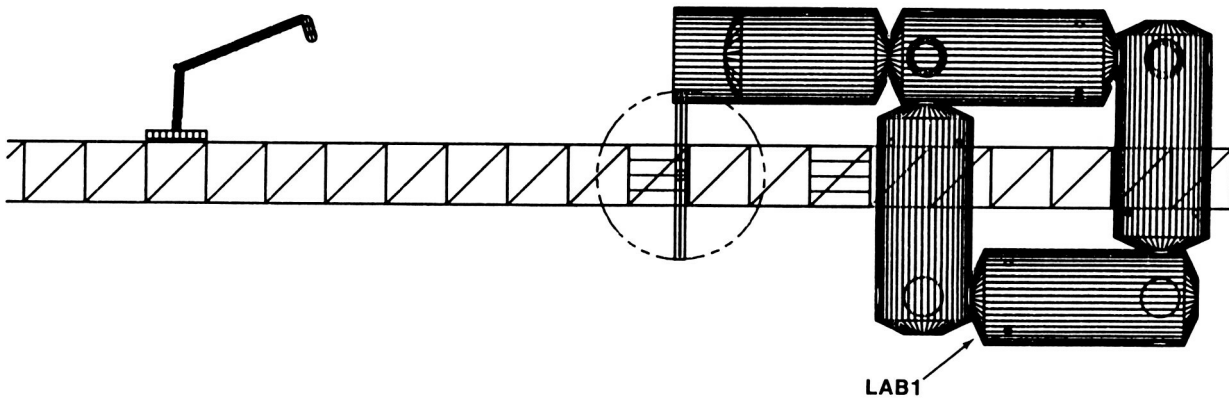
- 0 WILL PRESENT BRIEF OVERVIEW OF SOME STRUCTURAL RESULTS THAT CAME FROM SPACE STATION
- "SKUNK WORKS"
- 0 PRESSURIZED MODULES
- 0 PRIMARY TRUSS STRUCTURE
  - 0 DEPLOYABLE SINGLE FOLD BEAM
  - 0 ERECTABLE BEAM
  - 0 DEPLOYABLE DOUBLE FOLD
- 0 TYPICAL TRUSS ATTACHMENT DEVICES
- 0 DEPLOYMENT BACKUP PROCEDURES
- 0 CONCLUDING REMARKS



REFERENCE CONFIGURATION



# I. PRESSURIZED MODULES



**HAB MODULE**

THE PRIMARY STRUCTURE OF THE MODULES USES TYPICAL AIRCRAFT CONSTRUCTION

- 0 I.E. 0 SKIN-STRINGER
- 0 HONEYCOMB

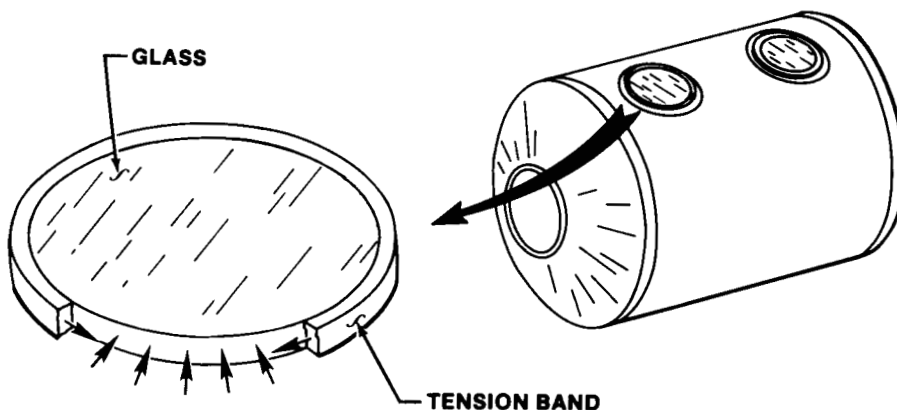
0 IT IS DESIGNED PREDOMINANTLY BY ORBITER LAUNCH LOADS.

SOME UNIQUE ITEMS THAT ARE BEING STUDIED FOR POSSIBLE USE ON THE MODULES ARE:

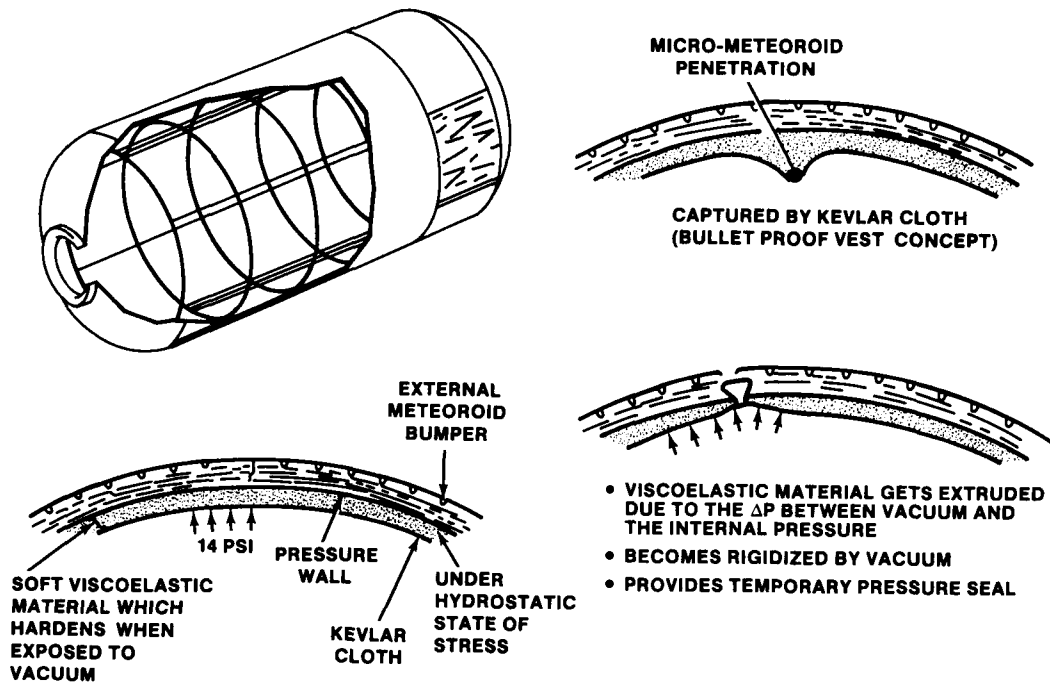
- 0 MECHANICALLY PRESTRESSED CIRCULAR WINDOWS
- 0 PENETRATION TOLERANT STRUCTURE

## **MECHANICALLY PRESTRESSED CIRCULAR WINDOWS**

- GLASS FLAW GROWTH RELATED TO TENSILE STRESS
- WINDOWS SENSITIVE TO SURFACE DAMAGE
- TEMPERED WINDOWS FAIL WHEN SURFACE COMPRESSION PENETRATED
- MECHANICAL PRESTRESS MINIMIZES TENSION IN GLASS
- MECHANICAL PRESTRESSED WINDOW DEVELOPMENT SUPPORTS  
LONG TERM SPACE PROGRAMS

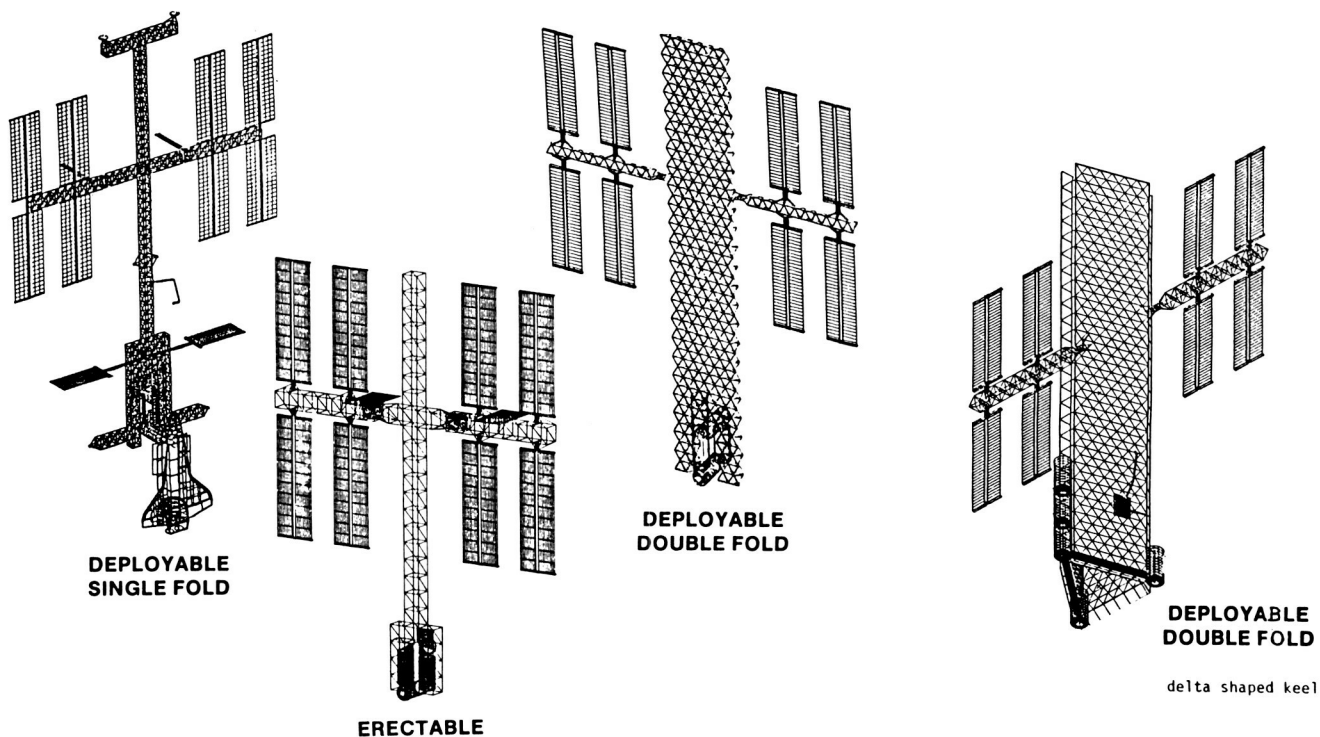


## PENETRATION TOLERANT STRUCTURE

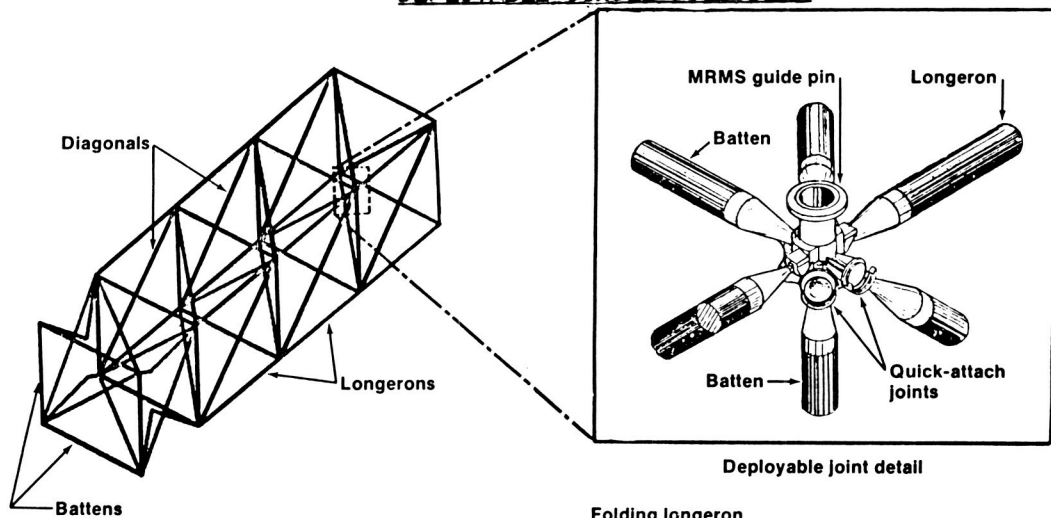


## II. SPACE STATION PRIMARY TRUSS STRUCTURE

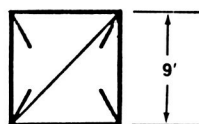
- O NUMEROUS SPACE STATION CONFIGURATIONS WERE CONSIDERED BUT A GRAVITY GRADIENT STABILIZED STATION WAS SELECTED AS A REFERENCE
- O SUCH A CONFIGURATION USES A LONG TRUSS ( 400 FT) BEAM AS ITS BACKBONE TO WHICH ARE ATTACHED SUCH COMPONENTS AS THE PRESSURIZED MODULES, SOLAR COLLECTOR STRUCTURE, VARIOUS PAYLOADS, ETC.
- O ALL COMPONENTS MUST BE BROUGHT TO ORBIT BY THE SPACE SHUTTLE AND ASSEMBLED IN SPACE
- O VARIOUS DEPLOYABLE AND ERECTABLE STRUCTURES ARE BEING CONSIDERED FOR THE PRIMARY TRUSS



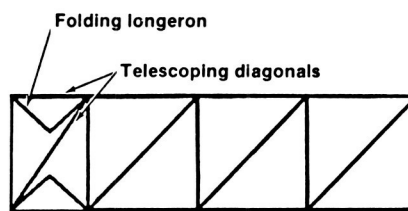
### DEPLOYABLE SINGLE FOLD BEAM



0 UTILITIES CAN BE  
PREINTEGRATED

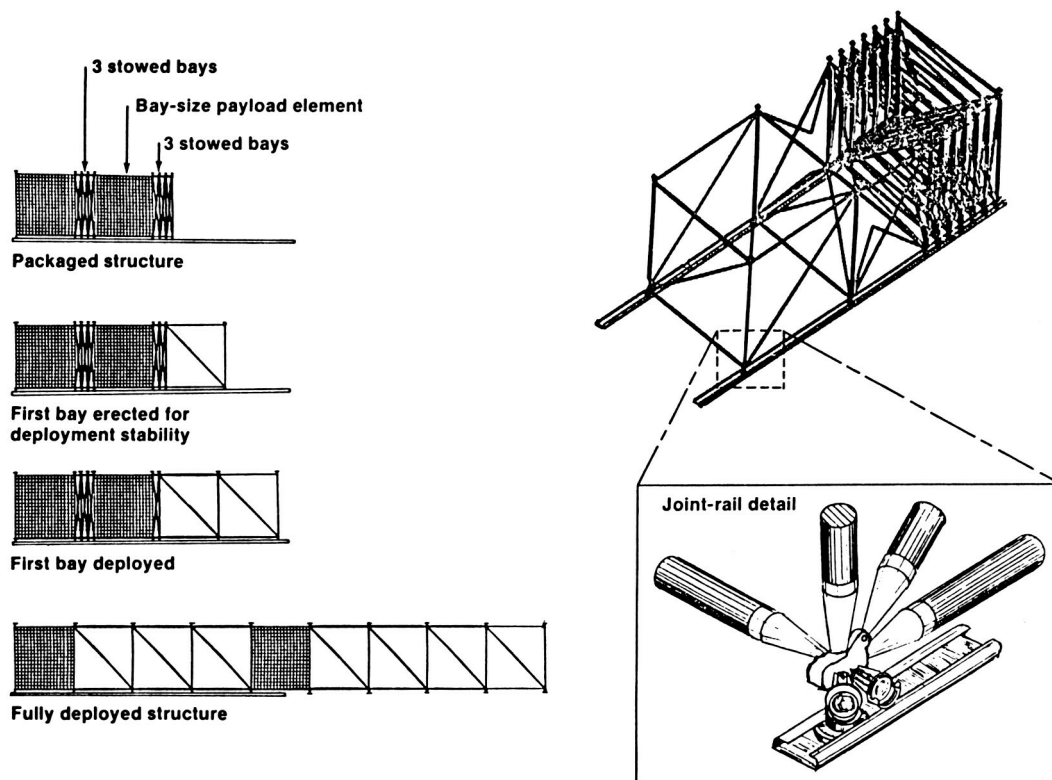


End view

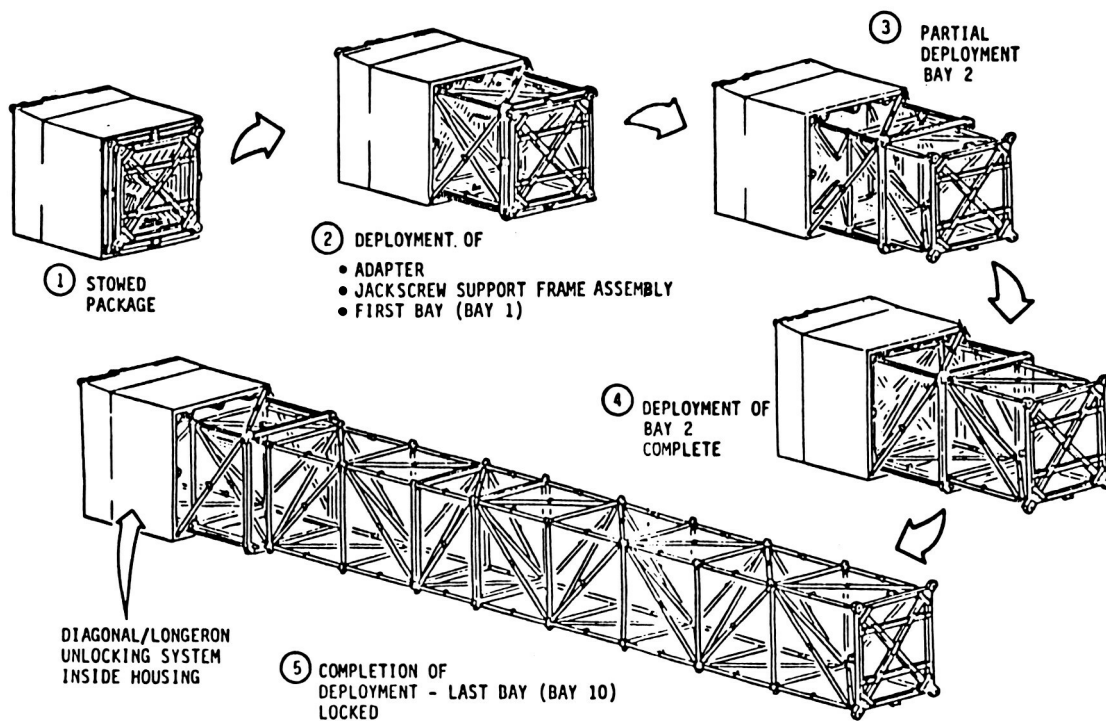


Side view

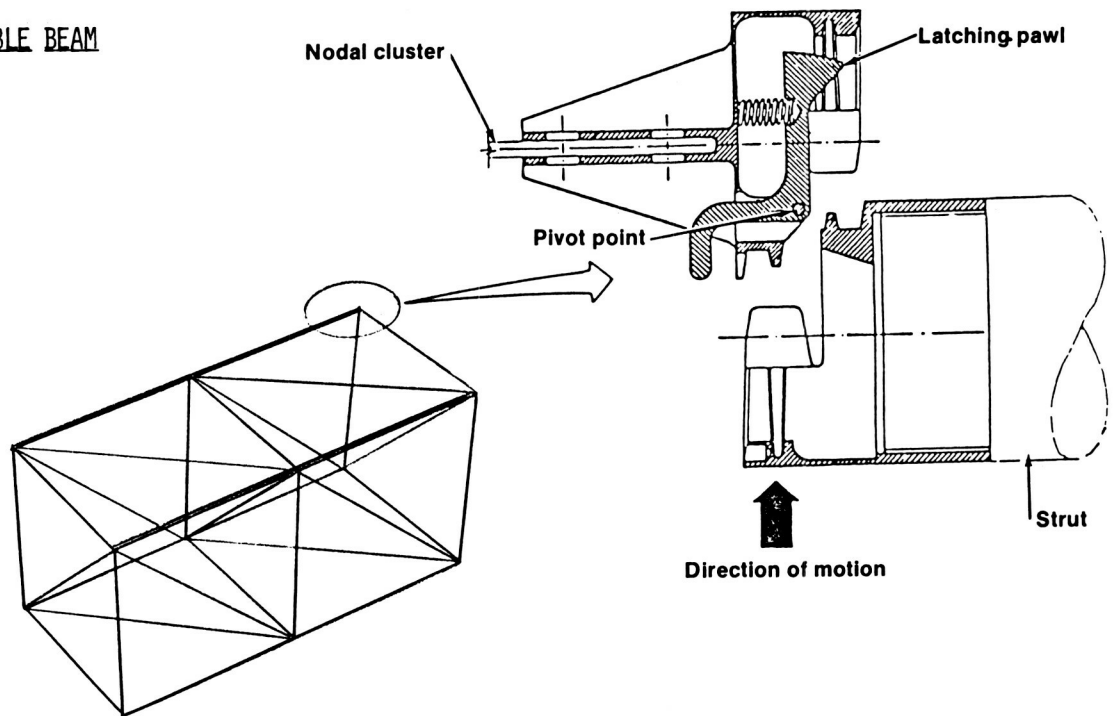
Schematic of deployable beam showing one bay being deployed and detail of joint.



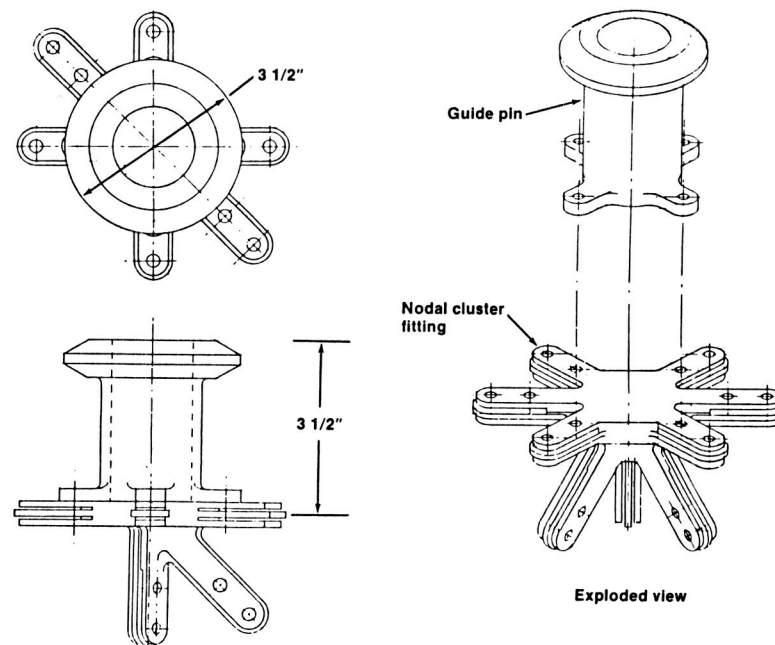
Truss deployment sequence and rail detail.



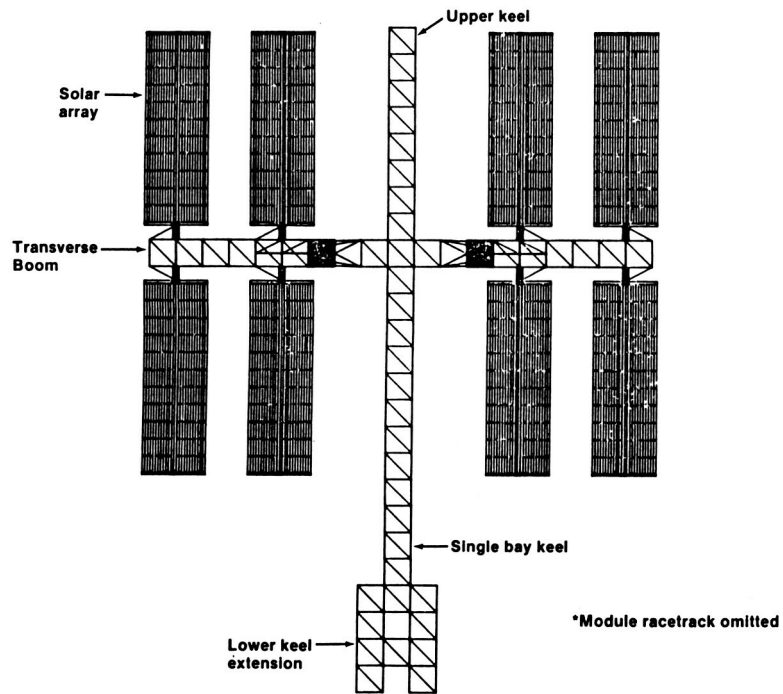
## ERECTABLE BEAM



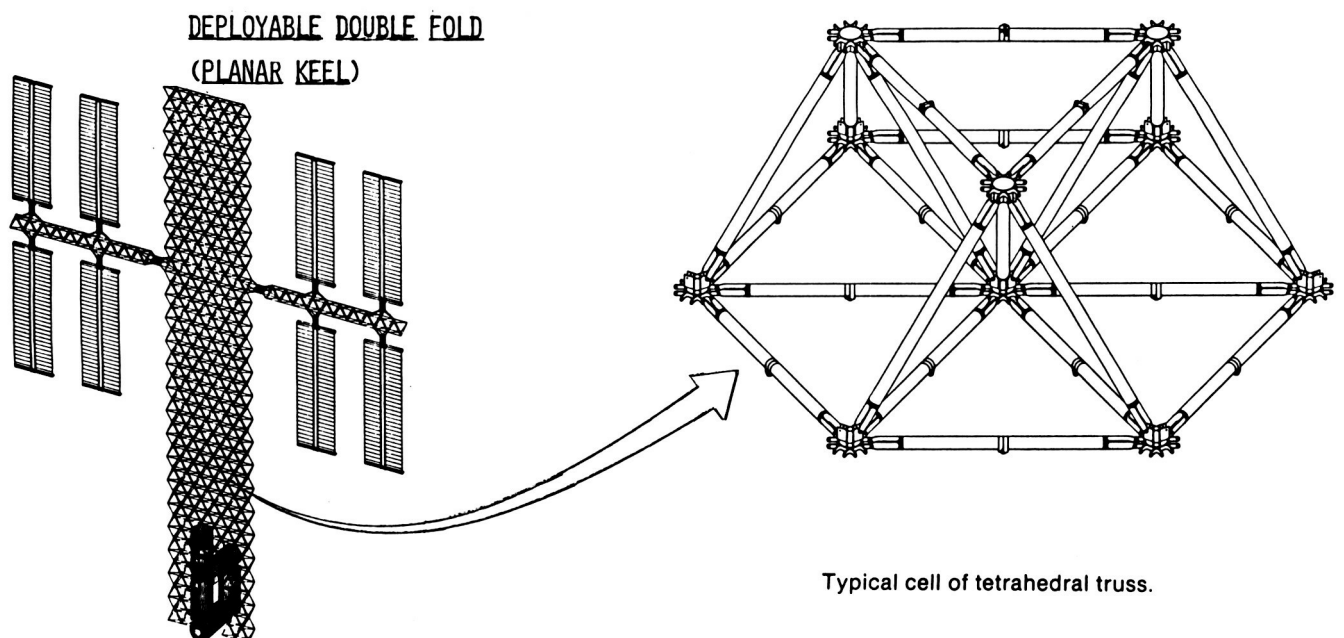
Erectable strut quick attachment joint.



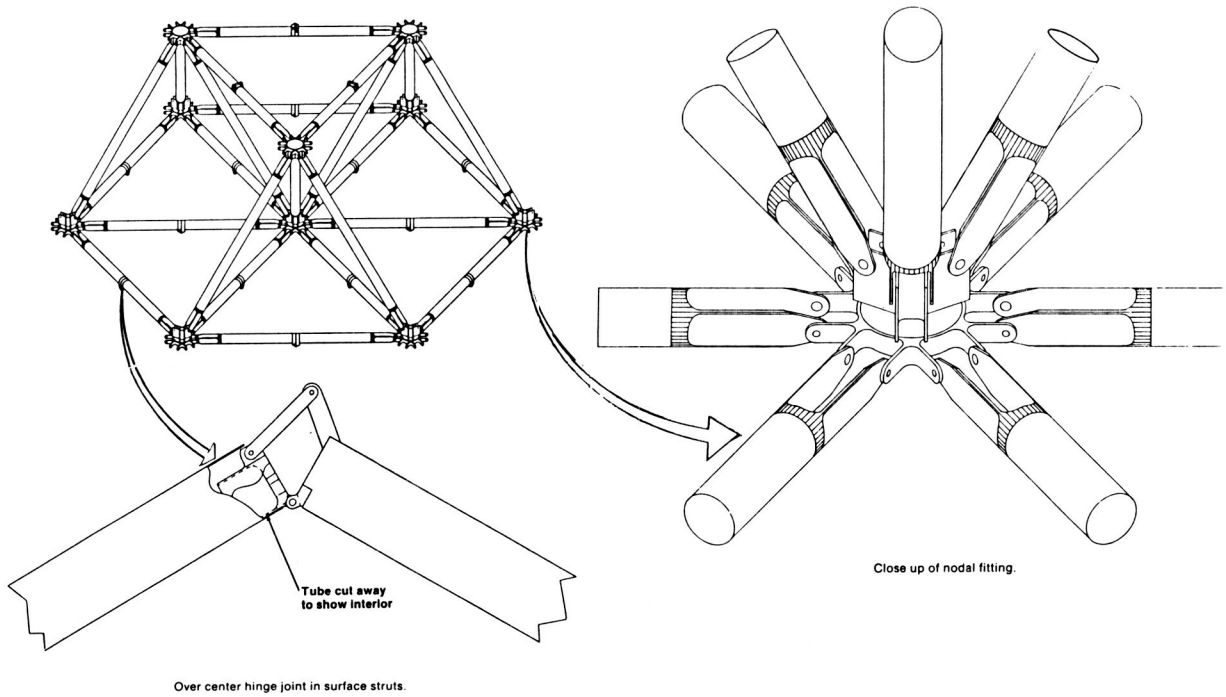
Nodal cluster fitting and MRMS guide pin.



Space station 15-foot beam structure.

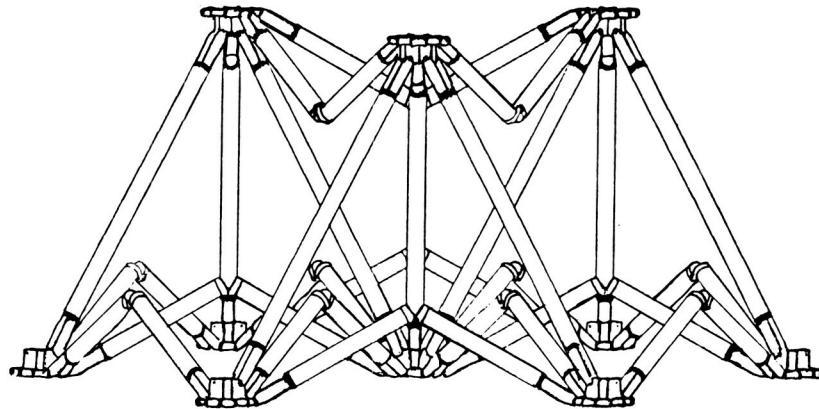


Typical cell of tetrahedral truss.

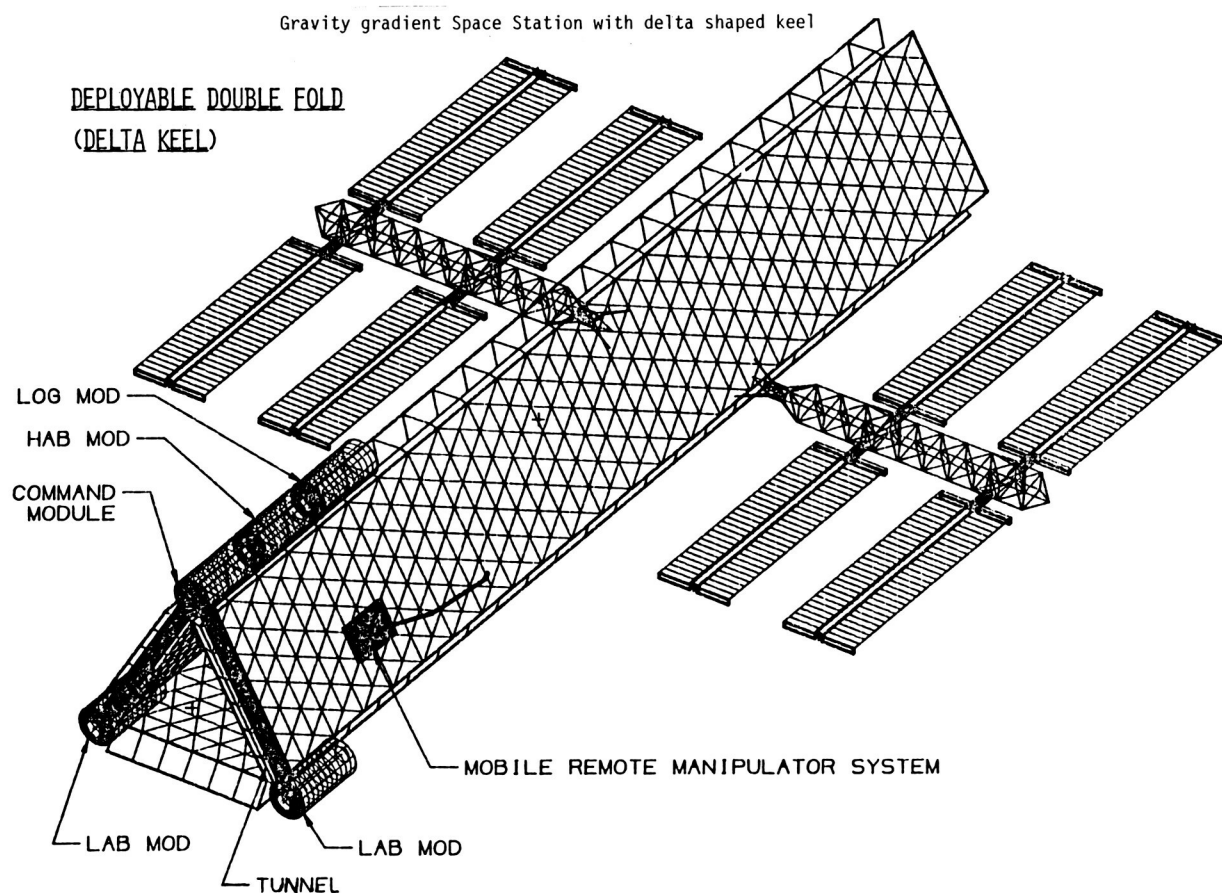


## DEPLOYABLE TETRAHEDRAL TRUSS

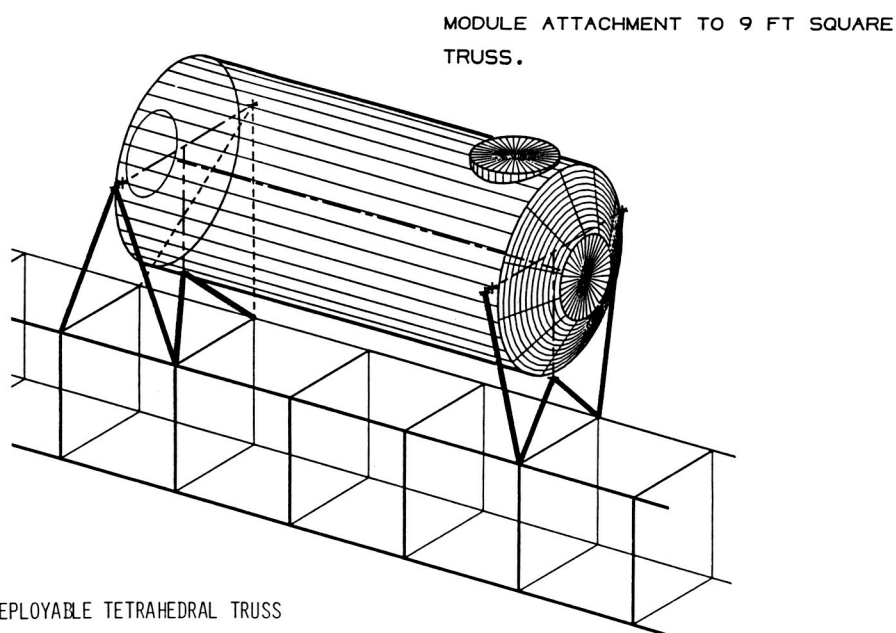
- o THE TORSIONAL AND BENDING STIFFNESSES OF THE DIAGONAL AND THE FOLDABLE STRUTS (IGNORING JOINT TOLERANCES) FORCE NODES TO REMAIN PARALLEL AND RESTRICT JOINTS TO DEPLOY TOGETHER



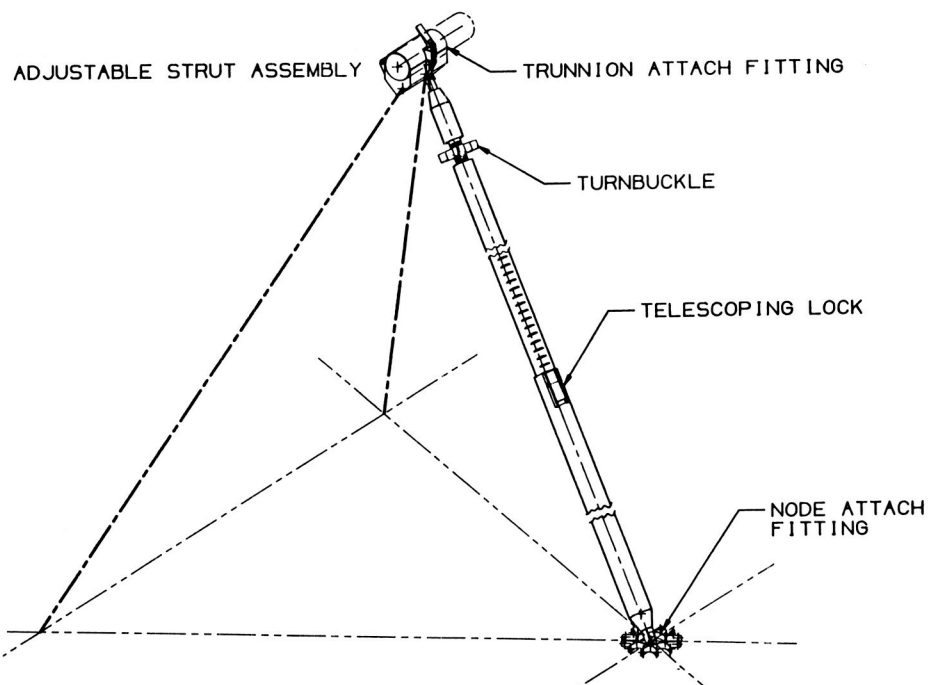
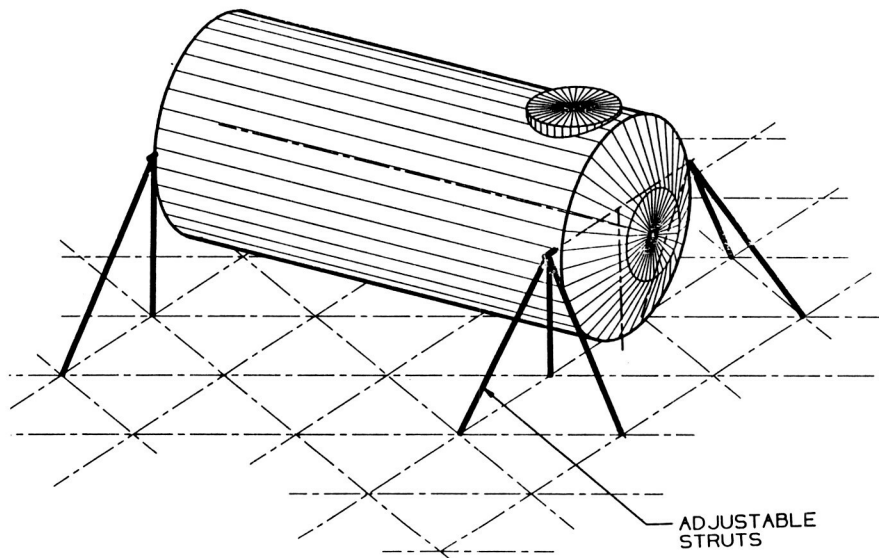


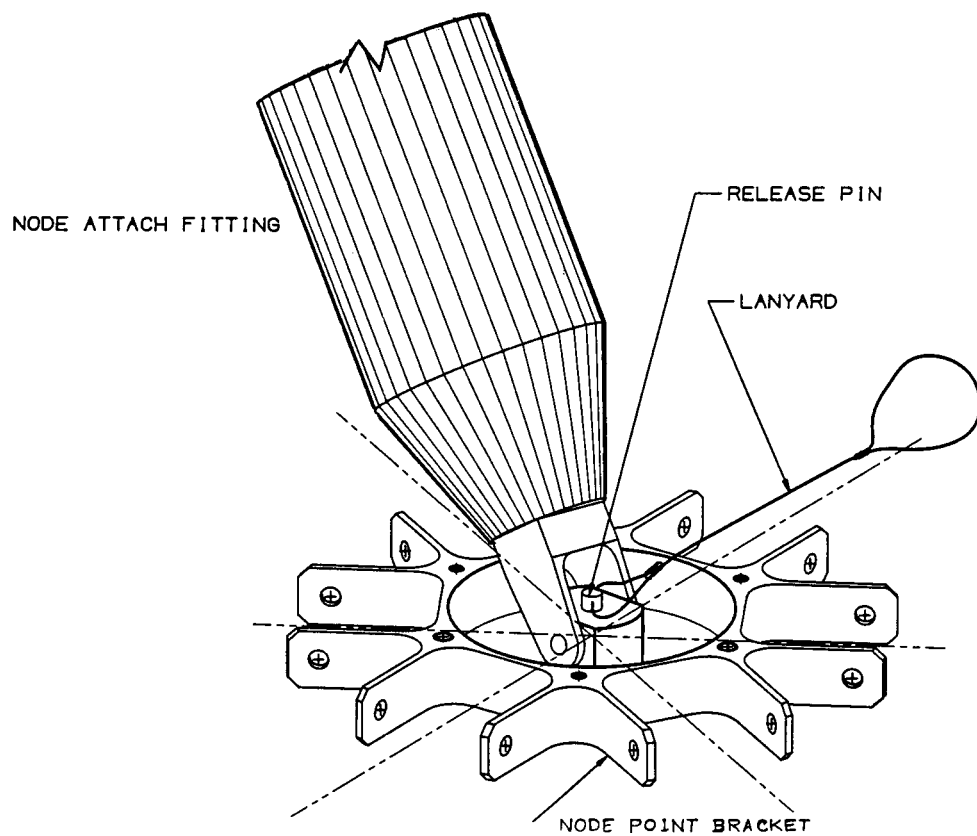


### III. TYPICAL TRUSS ATTACHMENT DEVICES

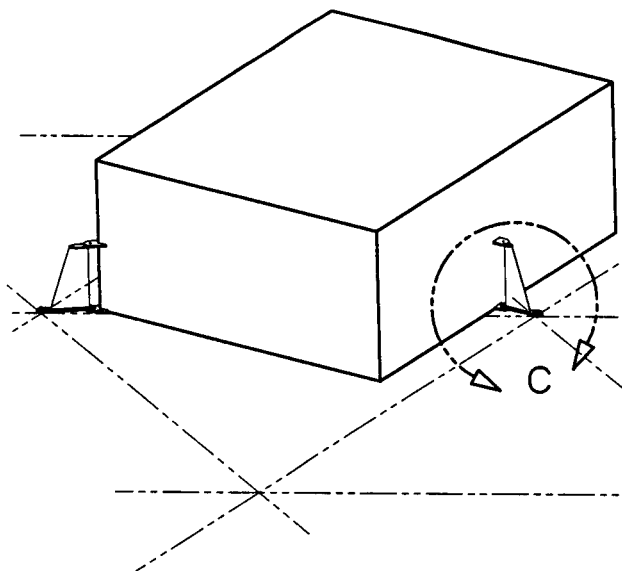


MODULE ATTACHED TO FLAT SIDE OF TRUSS.

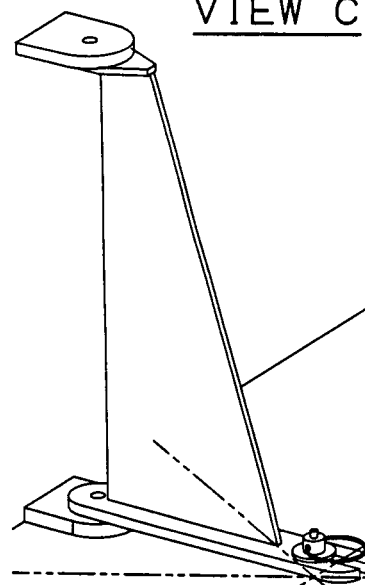


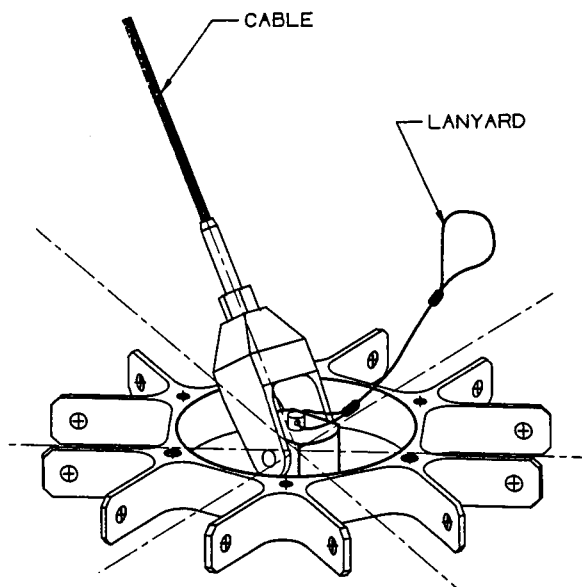
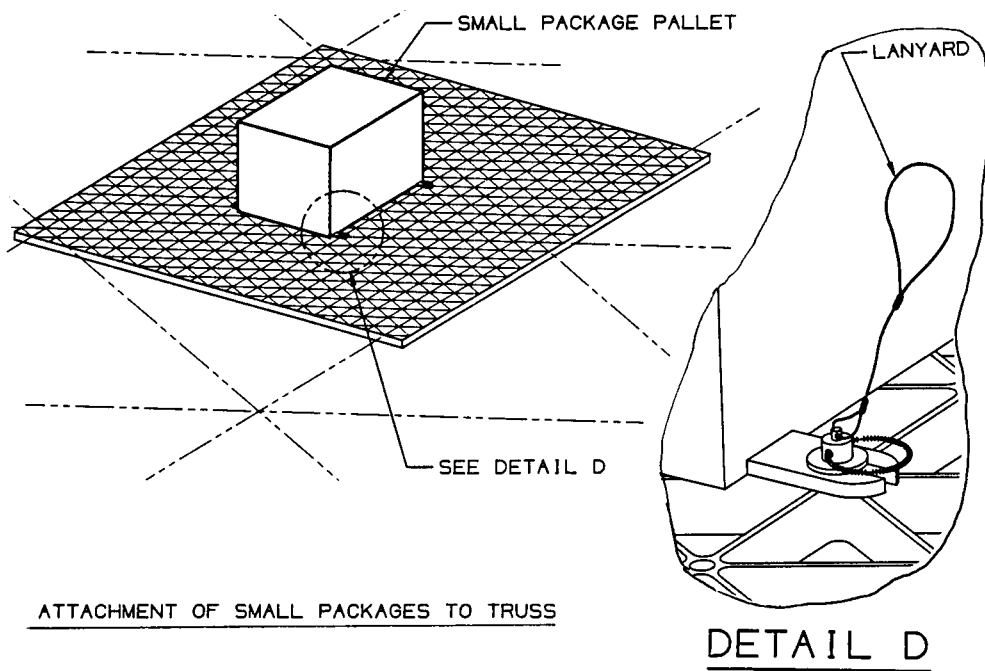


ATTACHMENT OF LARGE PACKAGES TO TRUSS.



VIEW C

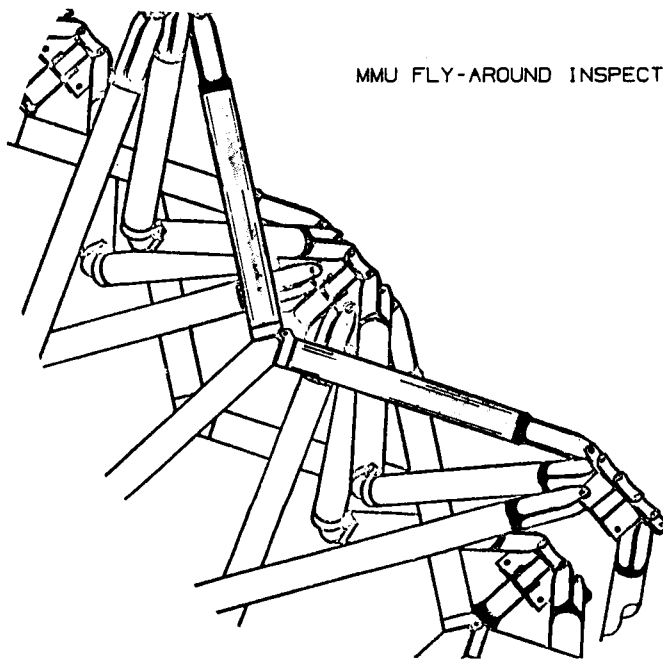




DEPLOYMENT

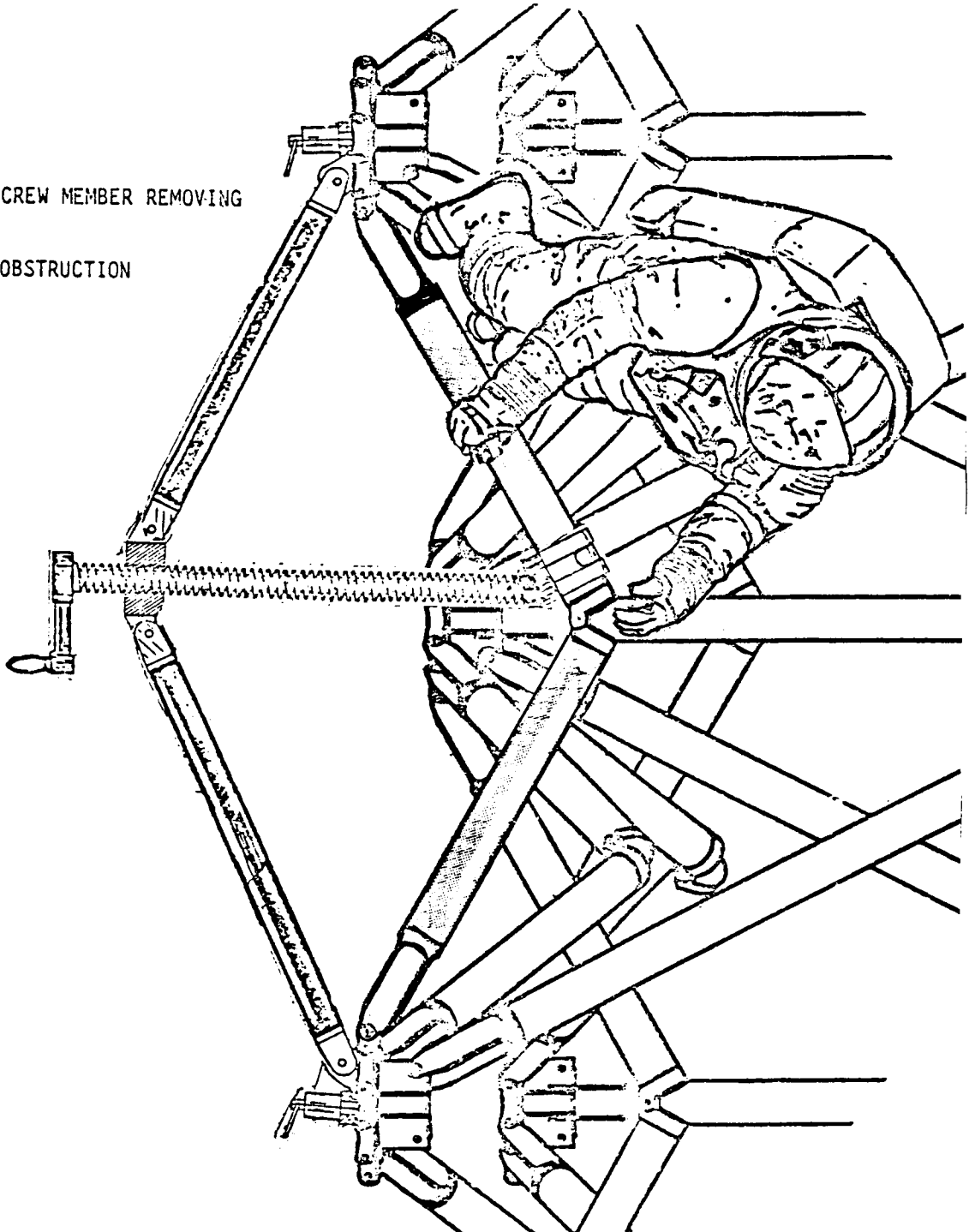
IV. BACKUP PROCEDURES

MMU FLY-AROUND INSPECTION



## ON ORBIT USE OF JACK

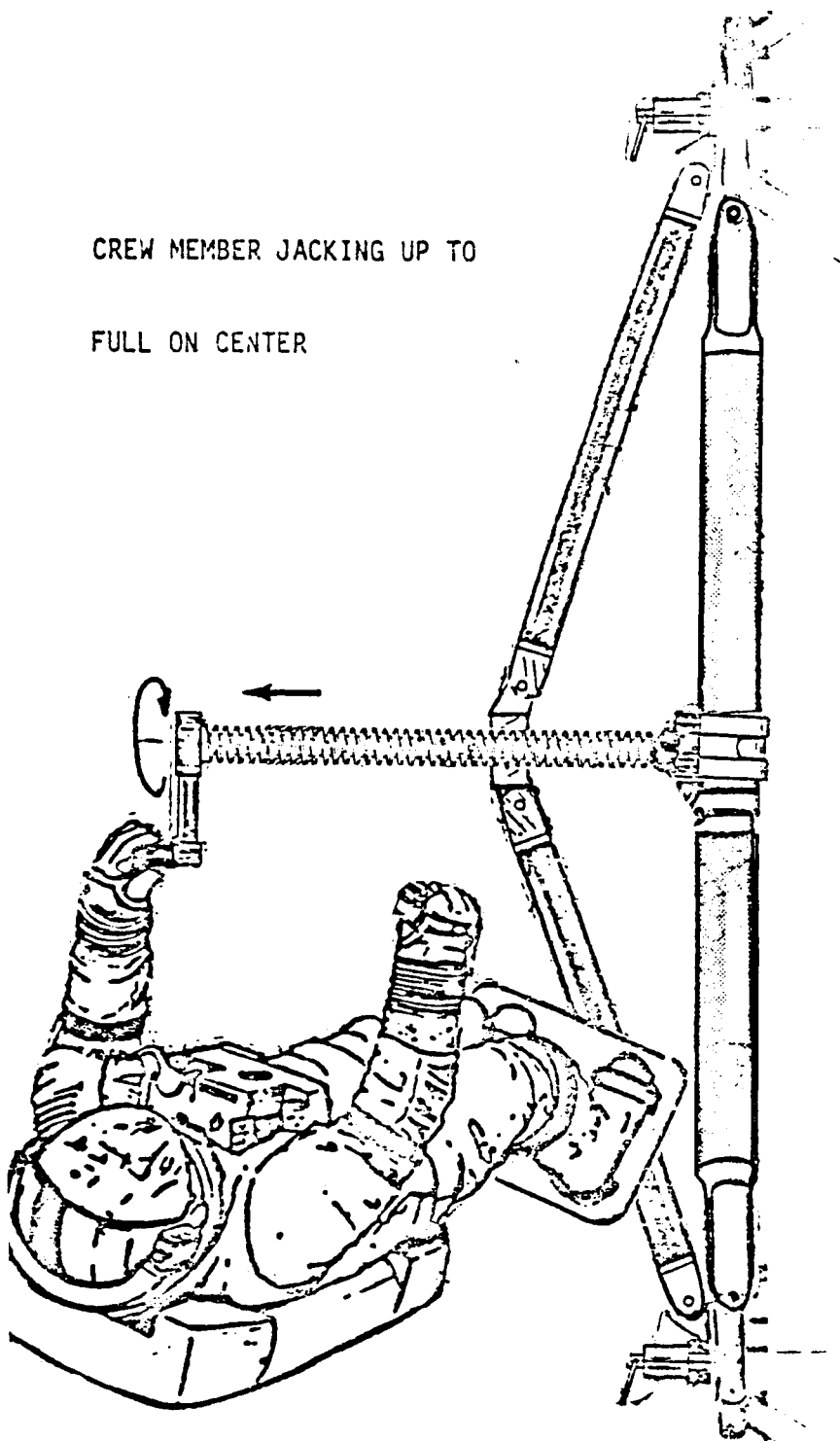
CREW MEMBER REMOVING  
OBSTRUCTION



## ON ORBIT USE OF JACK

CREW MEMBER JACKING UP TO

FULL ON CENTER



#### CONCLUDING REMARKS

- O NEXT YEARS WILL BE HEAVILY OCCUPIED WITH CHALLENGING STRUCTURES WORK.
- O THE SPACE STATION IS MORE SPACE FACILITY THAN THE SPACE VEHICLE.
- O LAUNCH VOLUME IS MORE CRITICAL THAN LAUNCH WEIGHT.
- O ONE OF THE GREATEST CHALLENGES PRESENTED WILL BE THAT OF SPACE STATION ASSEMBLY
  - O CONSTRAINTS IMPOSED BY SHUTTLE SIZE AND CENTER OF GRAVITY
  - O BEHAVIOR AT EACH STEP OF CONSTRUCTION
- O WE ARE ON A THRESHOLD OF SPACE WHERE THE CREW MEMBER WILL SHARE WITH THE HARDWARE IN PROVIDING FULL SYSTEM RELIABILITY AND MAINTENANCE.



VERIFICATION FOR LARGE SPACE STRUCTURES

J. Chen and J. Garba  
Applied Mechanics Technology Section  
Jet Propulsion Laboratory  
California Institute of Technology  
Pasadena, California

Large Space Antenna Systems Technology - 1984  
December 4-6, 1984

Traditionally, most aerospace structural systems must be subjected to some form of verification prior to flight. The verification procedure often includes the experimental identification of structural characteristics such as the natural frequencies and normal modes using modal tests. It may also include a direct structural integrity verification under simulated dynamic environments. In the past the design criteria for the structural systems were required to survive only the launch loads, hence these verification procedures were performed under a 1-g environment and posed no particular concern.

#### **FOR CONVENTIONAL AEROSPACE STRUCTURES**

- STRUCTURAL VERIFICATION PRIOR TO FLIGHT
- EXPERIMENTAL IDENTIFICATION OF STRUCTURAL DYNAMIC CHARACTERISTICS -  
LOADS MODEL VERIFICATION
- SIMULATED DYNAMIC ENVIRONMENTS FOR STRUCTURAL INTEGRITY
- DESIGN CRITERIA - LAUNCH LOADS IN 1.0 G

For true space structures erected/fabricated/deployed in orbit, the environment in space is quite benign, the applied loads are apt to be small, and the strength of the structure is not a pacing factor. On the other hand, the demands placed on antenna structures and solar reflectors for accurate positioning and the requirements of adequate stiffness to avoid undesirable structural distortions are often serious and thereby dictate the design.

For large space structures, the design criteria are different. The operational environments such as maneuver, deployment, docking, etc., are the events that are expected to generate the critical loads.

#### **FOR LARGE SPACE STRUCTURES**

- DESIGN CRITERIA - MANEUVER, DEPLOYMENT, DOCKING, ETC.
- STIFFNESS FOR ACCURATE POSITIONING AND SHAPE REQUIREMENTS
- ACCURATE DYNAMIC CHARACTERISTICS FOR ACTIVE CONTROL
- ZERO GRAVITY REQUIREMENT
- GROUND TEST VERIFICATION

The dynamic characteristics of the space structure related to the control and sensor/actuator location become the primary concerns for the verification. Therefore, instead of verifying the load carrying capability of the structure, properties such as modal density, range of natural frequencies, and modal displacements at the potential sensor/actuator location are important and must be simulated for the verification of the structure/control closed-loop system.

#### **GROUND TEST CONSIDERATION**

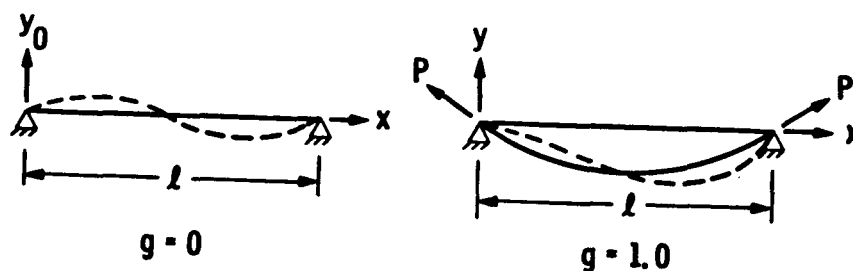
- GRAVITY EFFECTS ON DYNAMIC CHARACTERISTICS
- VERIFICATION OF LOAD CARRYING CAPABILITY NOT REQUIRED
- DYNAMIC CHARACTERISTICS RELATED TO CONTROL REQUIRED
- MODAL DENSITY, FREQUENCY RANGES, MODAL DISPLACEMENTS AT SENSOR/ACTUATOR LOCATIONS, ETC.

The generic structural element chosen for the study is a space beam which is a beam with a large slenderness ratio. For simplicity, the conditions of simple beam theory will be assumed. The figure shows the vibrating beam in a zero gravity environment and a 1-g gravity environment.

In what follows, the governing equation for the vibrating beam in a 1-g environment will be examined. The zero gravity condition will be treated as a special case in which the effects of the gravity will be eliminated.

#### A SPACE BEAM

- BEAM WITH LARGE SLENDERNESS RATIO
- GRAVITY EFFECTS ON DYNAMIC CHARACTERISTICS AS FUNCTION OF NON-DIMENSIONAL PARAMETERS



It is postulated that the response can be divided into two parts, namely, the static deflection due to gravity and the vibrational response. However, the induced axial force  $P$  remains unknown and the solution is a function of  $P$ . The fact that  $P$  is not zero indicates that both end supports are not movable and the beam must be stretched to accommodate the lateral deformation. This elongation along the axial direction should be a function of the reaction force  $P$ . It is obvious that the length increment can be related to the curvature due to lateral deflection.

### GOVERNING EQUATIONS

$$EI \frac{\partial^4 y}{\partial x^4} - p \frac{\partial^2 y}{\partial x^2} + \rho \frac{\partial^2 y}{\partial t^2} = -\rho g$$

$$y(x,t) = y_s(x) + \bar{y}(x,t)$$

$$EI \frac{d^4 y_s}{dx^4} - p \frac{d^2 y_s}{dx^2} = -\rho g$$

$$EI \frac{\partial^4 \bar{y}}{\partial x^4} - p \frac{\partial^2 \bar{y}}{\partial x^2} + \rho \frac{\partial^2 \bar{y}}{\partial t^2} = 0$$

The static deflection due to gravity satisfies the simply supported end conditions and was obtained by the Galerkin's approximation method. For simplicity, the magnitude of the first derivative is limited to be small.

### ASSUMPTIONS

$$y_s = \left( \frac{-1}{76.5 + 7.75(p\ell^2/EI)} \right) \frac{\rho g \ell^4}{EI} \sin\left(\frac{\pi x}{\ell}\right)$$

$$\left| \frac{dy_s}{dx} \right| \leq \frac{1}{10}$$

### • NON-DIMENSIONAL PARAMETERS

NON-DIMENSIONAL WEIGHT  $\alpha = \frac{\rho g \ell}{AE}$

SLENDerness RATIO  $\beta = \frac{\ell}{r}, r^2 = \frac{I}{A}$

NON-DIMENSIONAL AXIAL FORCE  $\eta = \frac{P}{AE}$

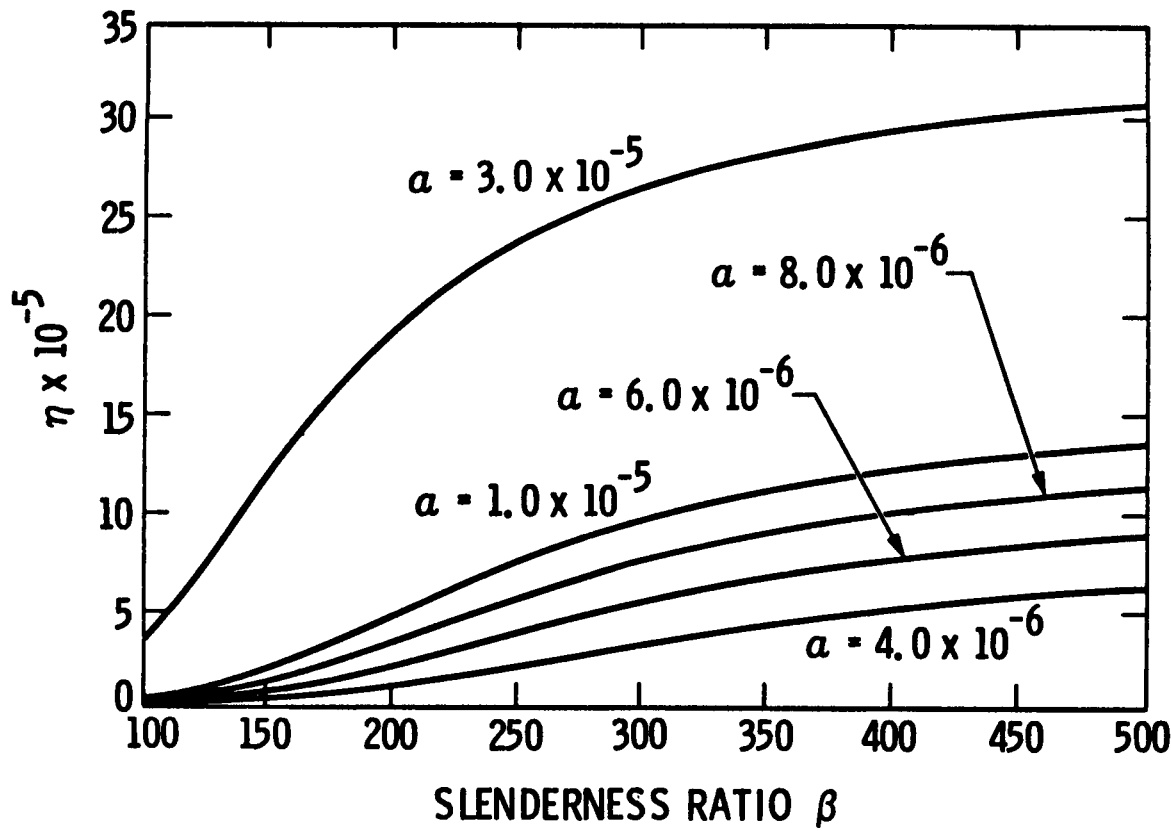
WEIGHT-LENGTH PARAMETER  $\gamma = \frac{1}{2}\eta \cdot \beta^2$

NON-DIMENSIONAL FREQUENCY  $\lambda_n^2 = \frac{\rho \ell^4 \omega_n^2}{EI}$

FREQUENCY RATIO  $\Omega_n = \frac{\lambda_n}{\lambda_{n+1}}$

From the axial elongation condition, the axial force can be related to the gravity loading and slenderness ratio of the beam.

NON-DIMENSIONAL AXIAL FORCE





The eigenvalue and eigenvector are functions of a single non-dimensional parameter. For a simply supported case, the eigenvector is an invariant, independent of the beam geometry.

## EIGENVALUES AND EIGENVECTORS

### SIMPLY SUPPORTED CASE:

$$\lambda_{\eta} = \eta^2 \pi^2 \left( 1 + \frac{2}{\eta^2 \pi^2} \gamma \right)^{\frac{1}{2}}$$

$$\phi_{\eta} = a \sin \left( \eta \pi \frac{x}{\ell} \right)$$

### BUILT-IN CASE:

$$\lambda_{\eta} = (1 - \cos \sigma_{\eta} \cosh \mu_{\eta}) + \gamma \sin \sigma_{\eta} \sinh \mu_{\eta} = 0$$

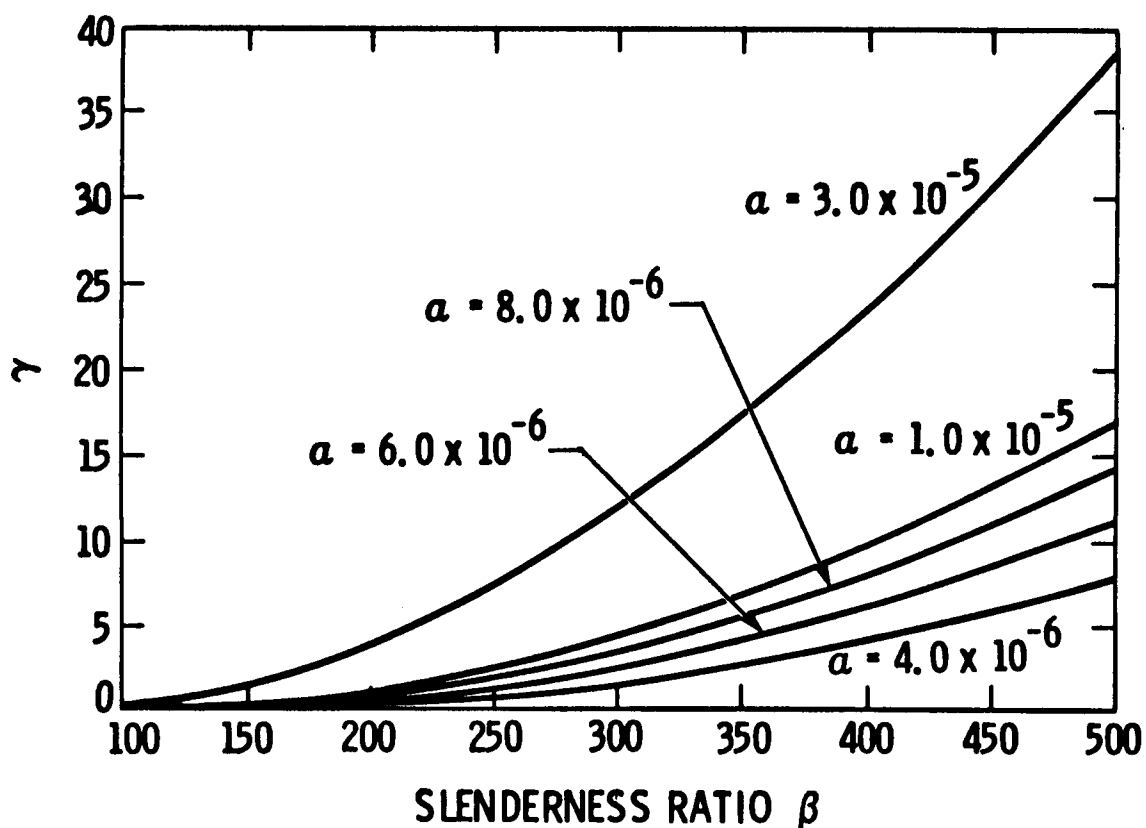
$$\sigma_{\eta} = (-\gamma + \sqrt{\ell^2 + \lambda_{\eta}})^{\frac{1}{2}}, \mu_{\eta} = (\gamma + \sqrt{\ell^2 + \lambda_{\eta}})^{\frac{1}{2}}$$

$$\phi_{\eta} = \sin \left( \sigma_{\eta} \frac{x}{\ell} \right) - \frac{\sigma_{\eta}}{\mu_{\eta}} \sinh \left( \mu_{\eta} \frac{x}{\ell} \right)$$

$$+ \frac{\sigma_{\eta} (\cos \sigma_{\eta} - \cosh \mu_{\eta})}{\sigma_{\eta} \sin \sigma_{\eta} + \mu_{\eta} \sinh \mu_{\eta}} \times [\cos \left( \mu_{\eta} \frac{x}{\ell} \right) - \cosh \left( \mu_{\eta} \frac{x}{\ell} \right)]$$

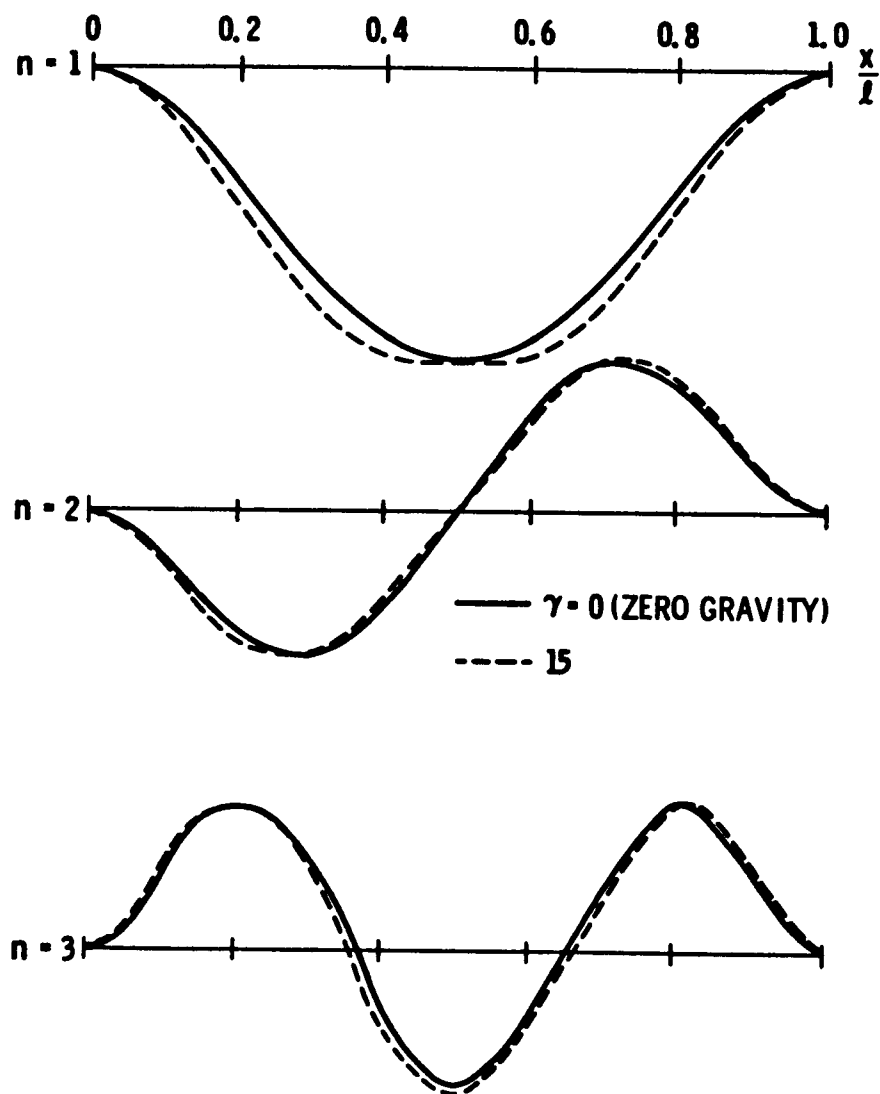
Once the geometry and the material properties of the beam are given, the weight-length parameter can be determined. On the other hand, for a given weight-length parameter, one may find a variety of beams with different geometric and material properties that will have the same parameter value.

### WEIGHT LENGTH PARAMETER

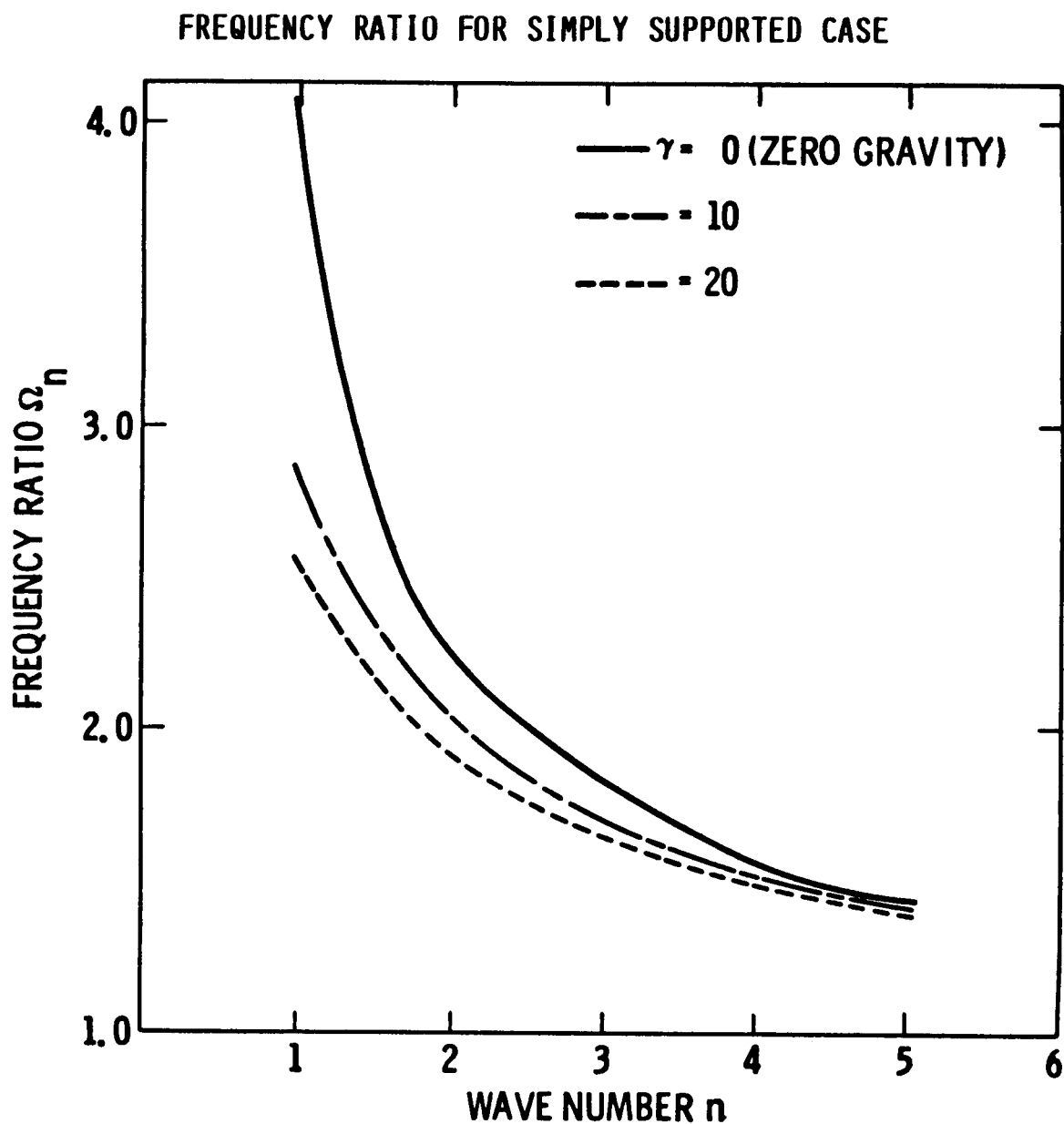


Unlike the case of simply supported boundary conditions, the mode shapes for the beams with built-in ends are a function of the weight-length parameters. However, the mode shapes for 0-g and 1-g are very similar.

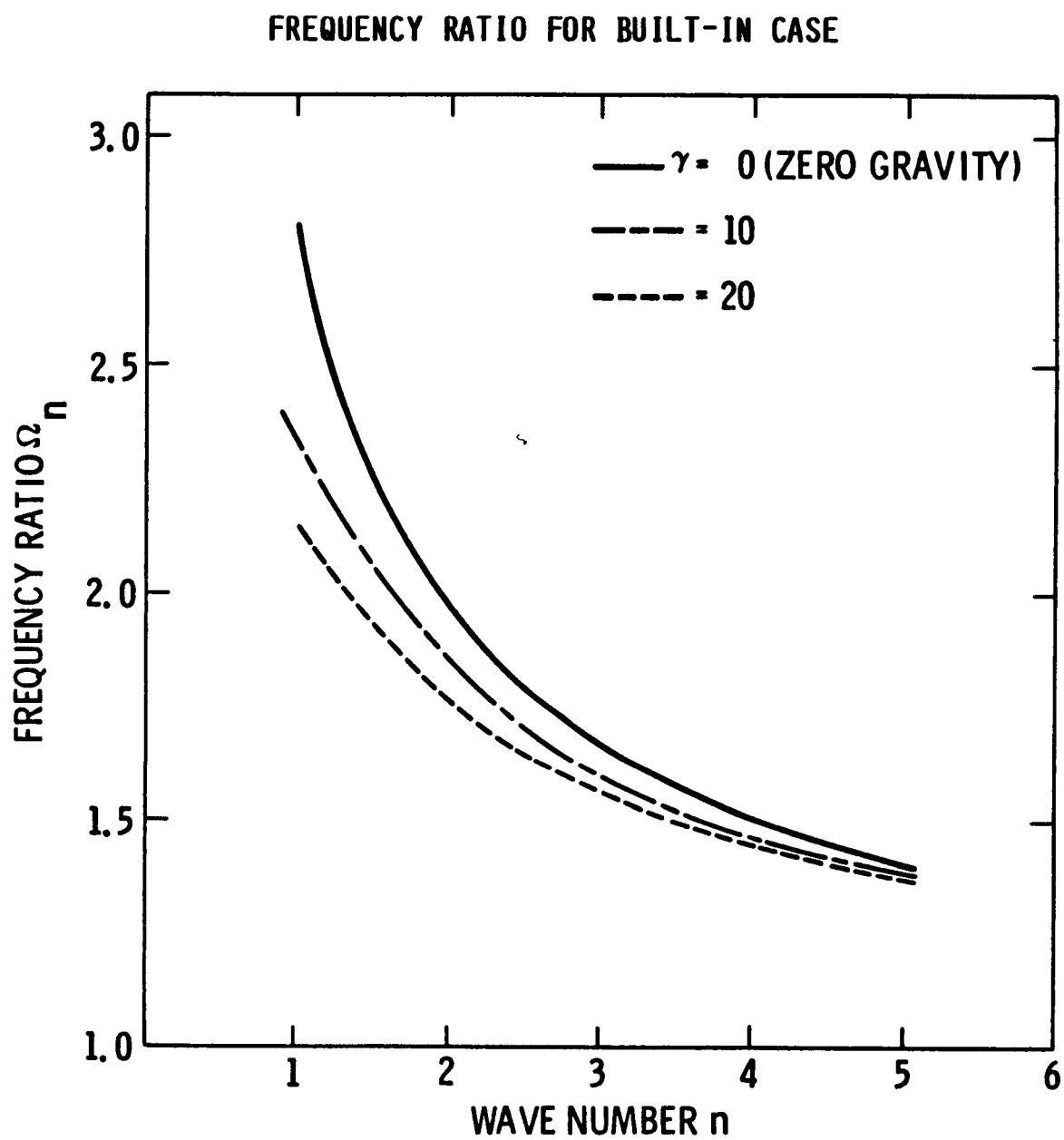
### MODE SHAPE COMPARISON



For a simply supported case, it is found that for lower modes with larger weight-length parameters the frequency ratio is quite different from that of the 0-g case. In other words, the higher frequency modes are easier to simulate by a scale model test than the lower frequency modes. Unfortunately, it is the latter that are in general, more important.



For the case of built-in boundary conditions, similar results are found for the frequency ratio.



For ground testing verification of large space structures the feasibility of using a scale model is dependent not only on the structure itself, but also on the control systems. Accurate modal displacements and modal density distributions are the important parameters to be considered. For large complex space structures the ground test may be very expensive and time consuming, such that the test consideration may become part of the design requirement. However, since very little experience is available in this respect, a more systematic study in realistic large space structural systems should be performed.

#### CONCLUDING REMARKS

- FOR A GIVEN SPACE BEAM WITH ITS WAVE-LENGTH PARAMETER, THE FREQUENCY DENSITY DEVIATION DUE TO 1 G CAN BE READILY FOUND.
- FOR A GIVEN ERROR TOLERANCE IN MODAL DENSITY, THE FEASIBILITY OF PERFORMING GROUND TESTING FOR VERIFICATION CAN BE DETERMINED.
- OTHER CHARACTERISTICS WILL BE INVESTIGATED.
- STUDIES ARE EXTENDED TO OTHER LARGE SPACE STRUCTURES.
- VERIFICATION OF STRUCTURES/CONTROL CLOSED LOOP SYSTEM WILL BE INVESTIGATED.

AN OPTIMIZATION STUDY TO MINIMIZE SURFACE  
DISTORTIONS OF A HOOP/COLUMN ANTENNA

G. A. Wrenn  
Kentron International, Inc.  
Hampton, Virginia

Large Space Antenna Systems Technology - 1984  
December 4-6, 1984

## INTRODUCTION

The objective of this study was to develop a computer-based procedure to minimize the surface distortions in a hoop/column antenna. The approach uses mathematical optimization techniques to select a set of control cable tensions which minimize the distortions. The motivation for this study was a need for an automated procedure to lessen the tedium of the manual approach currently used to solve this problem. The overall method uses three fundamental elements. The Engineering Analysis Language (EAL) finite element analysis program (ref. 1) is used to calculate the antenna surface distortions due to externally applied loads and the derivatives of surface distortions with respect to the control cable tensions. The CONMIN general purpose optimization program (ref. 2) is used to determine the set of control cable tensions which minimize the antenna surface distortions. A program based on ref. 3 is used to calculate the best fit parabola passing through a distorted antenna shape and to calculate the RMS distortion error. This paper discusses the interim results of a feasibility study in which the procedure is demonstrated by correcting antenna distortions due to externally applied loads. These loads are useful for check purposes, but do not necessarily represent realistic loads found in orbit. (See fig. 1.)

- Problem - Develop a procedure to optimize control cable tensions in a hoop/column antenna to minimize surface distortions
- Motivation - Need for a systematic approach
- Overall method
  - Use EAL finite element analysis
  - Use CONMIN optimizer
  - Use RMS surface distortion algorithm
- Feasibility study in progress
- Loads cases - simulated to test method

Figure 1



## ARTIST'S CONCEPT OF HOOP/COLUMN ANTENNA

Figure 2 shows an earth orbiting hoop/column antenna which requires a parabolic surface to reflect radio frequency energy properly. Once in orbit, externally applied loads, such as nonuniform thermal loads, distort the reflector surface from its desired shape. The surface control cables and hoop support cables can be pulled in a particular arrangement such that the antenna surface distortions will be minimized for that particular external load.

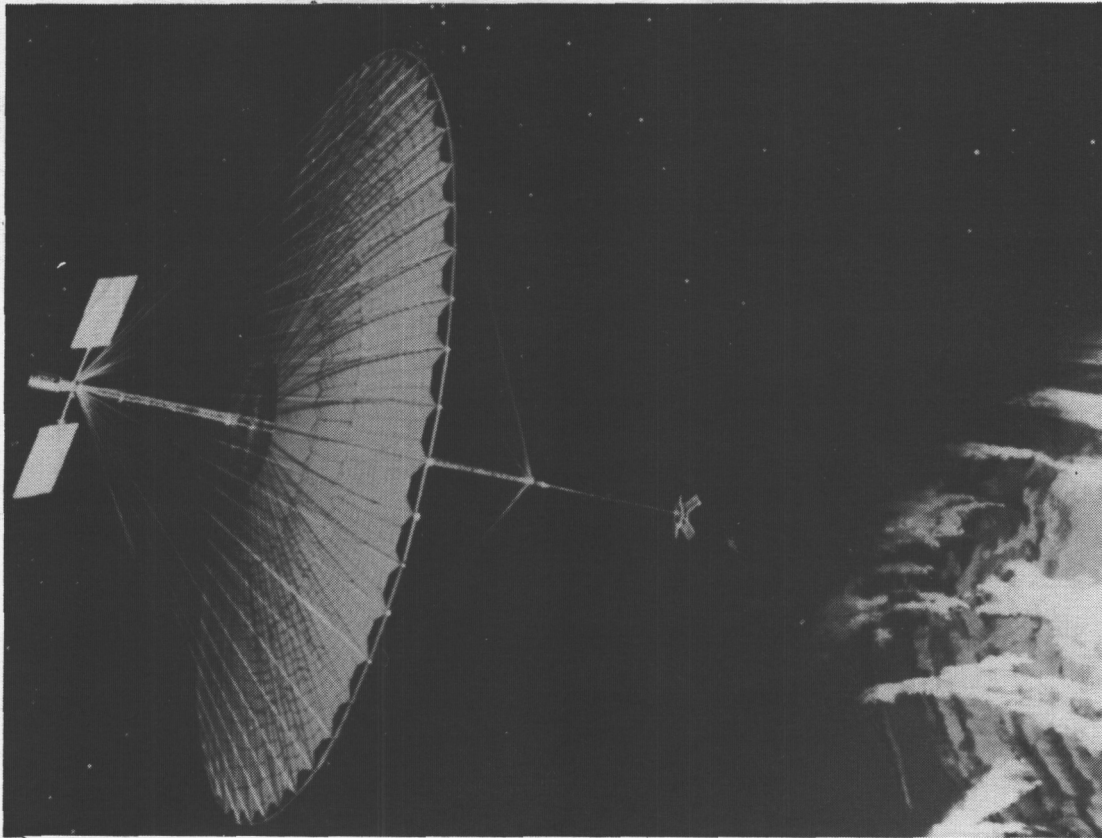


Figure 2

### 122 METER HOOP/COLUMN ANTENNA CONFIGURATION

The cross-section view of figure 3 shows the major components of a 122 meter hoop/column antenna. It is based on an antenna studied by the Harris Corporation and NASA Langley Research Center (ref. 4). The reflector surface must be kept as nearly parabolic as possible. The surface control cables are connected to the cable truss network located just below the reflector surface. The hoop support cables are connected to the rigid hoop, which is connected to the outer edge of the reflector surface. The shape of the reflector surface is highly dependent on the tensions in these cables.

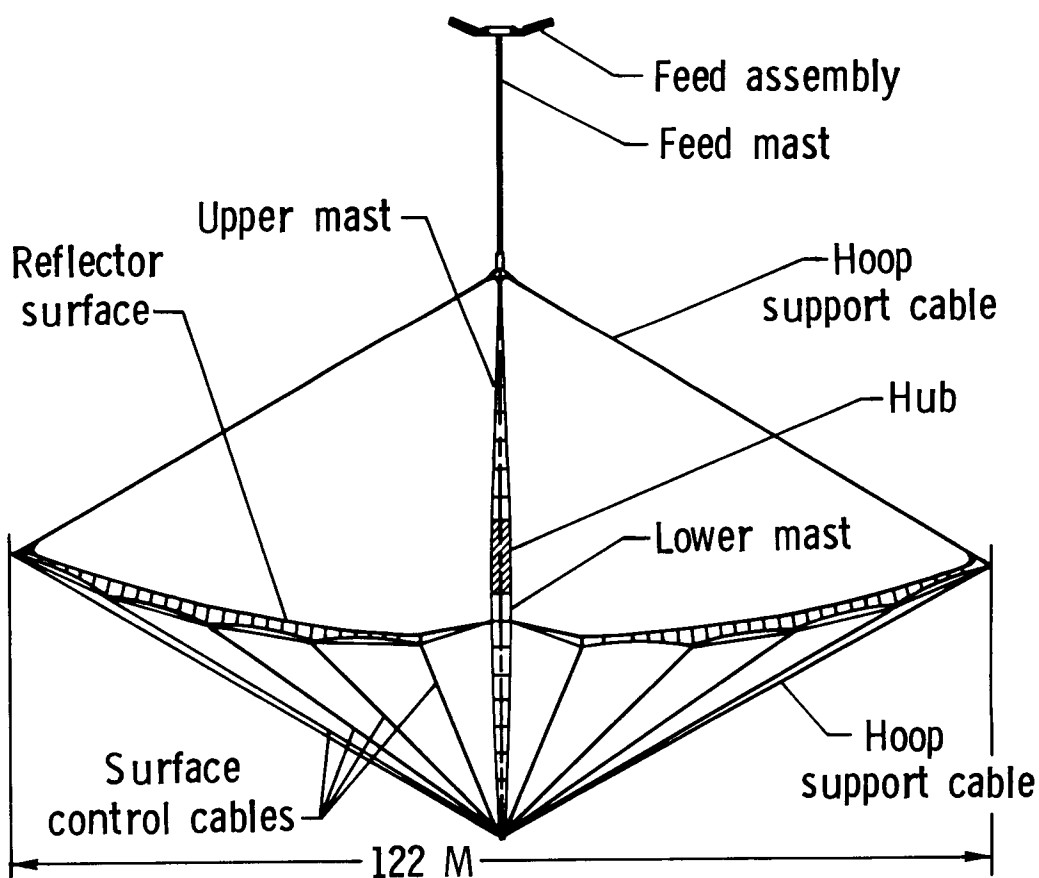


Figure 3

## ELEMENTS OF OPTIMIZATION PROCEDURES

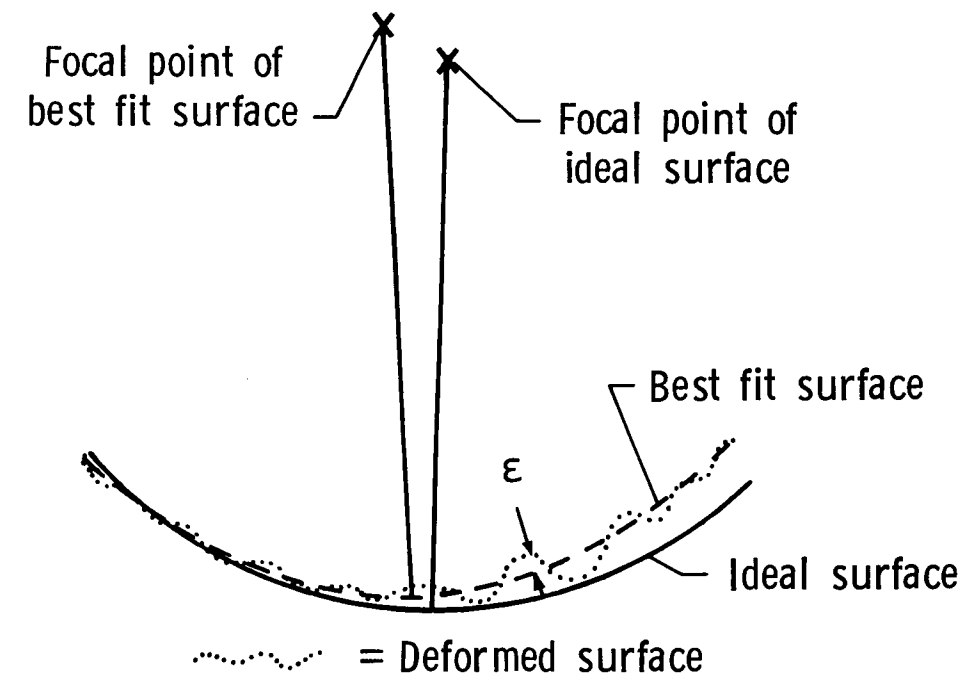
The primary elements of any optimization procedure are shown in figure 4. The objective function is a measure of how good the design is. Its value will either be minimized or maximized for an optimum design. The design variables are the quantities which vary during the optimization process. Their values are the final product of the optimization and represent the quantities which make the objective function optimum. Constraints appear in two forms and are used to place restrictions on the design. Behavior constraints are limits on the response of the system being optimized. A typical example in solid mechanics is a stress constraint limiting the maximum stress allowable in some component of a structure. Side constraints are upper and/or lower limits on the values of individual design variables. An example, also from solid mechanics, is a minimum or maximum gage for a structural component such as a plate or truss element, that is allowed to vary in size.

- Objective function
- Design variables
- Constraints
  - Behavior
  - Side

Figure 4

## DEFINITION OF OBJECTIVE FUNCTION

The ideal surface shown in figure 5 represents the parabolic shape of the undeformed antenna. When external loads are applied, the ideal surface deforms to the shape indicated by the dotted line. The dashed line is the best fit parabola that can be passed through the deformed shape. Epsilon is the normal distance between the deformed and best fit surfaces. The epsilons are measured at 66 points over the antenna surface in this study. The objective function is the RMS error measure for the epsilons. Minimizing the objective function forces the deformed surface toward the best fit parabolic shape, which is not necessarily the same parabola as the ideal surface. The best fit parabola's focal point can be different from that of the ideal surface, and restrictions can be put on focal point movement. One restriction could be to force the best fit and ideal focal points to be the same, which means that the best fit surface is the ideal surface. Another restriction could be to require the focal length to be the same for the best fit and ideal surfaces, but to allow the point to move giving boresight errors and translation of the origin of the parabola. A third option might be to impose no restrictions on the focal point. In this study, the focal length was held constant.



$\epsilon$  = Normal distance from deformed surface to the best fit surface

$$\text{Objective function} = \left[ \frac{1}{n} \sum \epsilon^2 \right]^{1/2} = \text{RMS error}$$

Figure 5

## MODEL OF HOOP/COLUMN ANTENNA SURFACE

Figure 6 shows a plan view of a hoop/column antenna. It is constructed of 48 gores with 4 surfaces of illumination indicated by the dashed circles. The shaded region is the one gore used as the analytical model for this study. Since each of these 48 gores is very much alike, any one of them would be adequately represented by this choice of analytical model. Because of this symmetry, boundary conditions imposed on the analytical model are vertical planes of symmetry along the gore edges. This means that only displacements normal to the antenna surface will be allowed on those two edges.

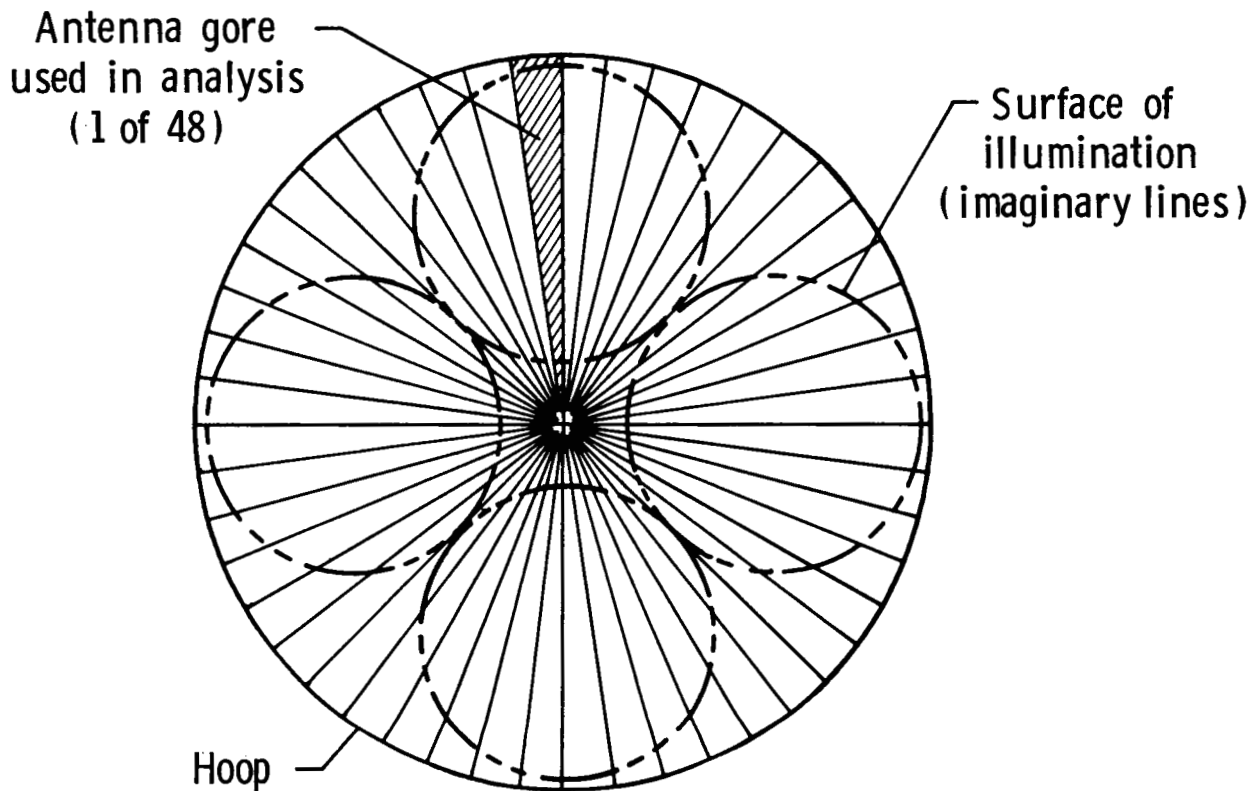


Figure 6

## DEFINITION OF DESIGN VARIABLES

An exploded view of the one gore analytical model is shown in figure 7. Simplified representations of the cable trusses connect the surface control cables to the reflector surface. The hoop bar is connected to the reflector surface at the corner points. The design variables used in this study are the tensions in the 12 numbered cables. Cables 1-8 are surface control cables and cables 9-12 are hoop support cables. The only constraints used in this study are side constraints which prevent the control cables from being in compression. The EAL finite element model of this gore is comprised of 166 joints, 234 rod elements, 92 surface membrane elements, and 498 degrees of freedom. The model is initially pre-tensioned, which is represented by a geometric stiffness matrix. The geometric stiffnesses would ordinarily change when tensions are changed in the model, leading to a nonlinear analysis problem. These changes have been neglected for this study, which means the tensions in the control cables are applied as external forces in the equilibrium equation. In addition, the values of the design variables are tension increases above that of the pre-tensioned state, not the total tensions in the control cables.

Design variables are tensions in numbered cables

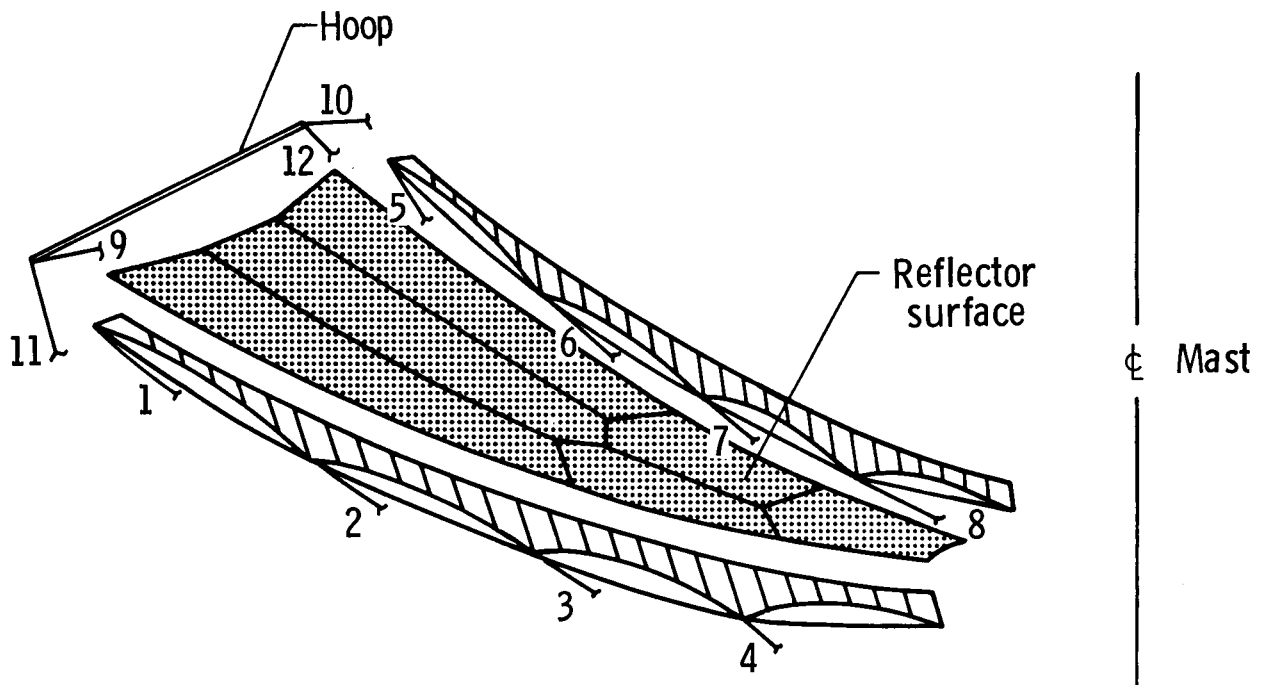


Figure 7

## SUMMARY OF OPTIMIZATION PROCEDURE

Figure 8 summarizes the optimization procedure. The procedure finds the set of control cable tensions which results in the best parabolic antenna surface subjected to externally applied loads. The objective function is the RMS error of the surface distortions. The design variables are the values of tensions applied to the control cables. The constraints are side constraints which prevent the control cables from being in compression. The minimization is performed using CONMIN, a widely used general purpose optimization program which employs usable/feasible directions methods and nonlinear programming techniques. The EAL finite element analysis program is used to calculate the surface distortions caused by externally applied loads and derivatives of surface distortions with respect to control cable tensions.

- Find design variables which minimize objective function subject to constraints
  - Objective function is RMS surface distortion
  - Design variables are tensions in control cables
  - Constraints are requirement for positive control cable tensions
- Minimization carried out using CONMIN
  - Usable/feasible directions
  - Non-linear programming techniques
- Method requires derivatives of displacements with respect to control cable tensions
  - Performed in EAL

Figure 8

## DISTRIBUTIONS OF TEMPERATURE AND PRESSURE USED TO VALIDATE PROCEDURE

The three shapes in figure 9 show the load distributions used in test cases to validate the procedure. Shape 1 is a uniform distribution of load over the antenna surface. Shape 2 is a linearly varying distribution across the width of the gore. Shape 3 is a linearly varying distribution along the length of the gore. These are the three most logical initial choices for testing purposes and do not necessarily represent load distributions found in orbit. Pressure distributions are used to cause more severe displacements normal to the antenna surface to better test the procedure.

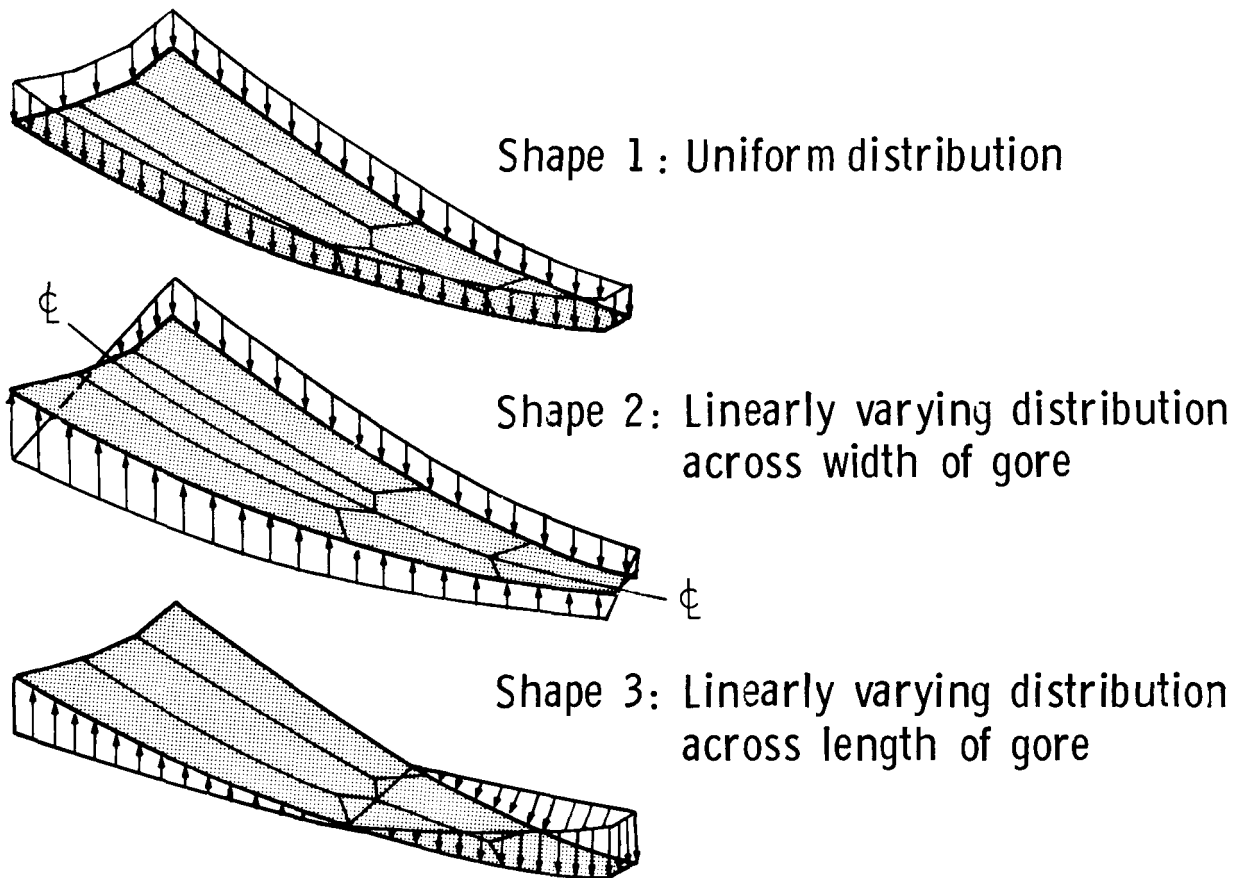


Figure 9



## FLOW DIAGRAM FOR OPTIMIZATION PROCEDURE

The flow diagram shown in figure 10 outlines the implementation of the optimization procedure. First, EAL calculates the displacements of the antenna surface due to externally applied loads. EAL then calculates the analytical derivatives of surface displacements with respect to control cable tensions. Since changes in geometric stiffnesses are neglected, these derivatives are constant and need be calculated only once. Next, EAL evaluates the surface displacements due to the current set of control cable tensions with a first order Taylor series approximation using the previously calculated derivatives and the current values of the design variables. The net displacements are the differences between the initial displacements and the displacements due to control cable tensions. A best fit parabola is passed through the net displacements, and the normal distances from the net displacements to the best fit surface are found. The RMS distortion error is computed as the objective function. CONMIN checks whether or not the RMS error is a minimum. If it is not, then CONMIN updates the tensions and the procedure reevaluates the surface displacements. The process continues until CONMIN verifies that the RMS error is a minimum. At this point, the procedure terminates and the result is a set of control cable tensions that produce the best antenna surface. The procedure exhibits slow convergence and typically requires about 40 iterations and 80 cp seconds on a CYBER 175 computer.

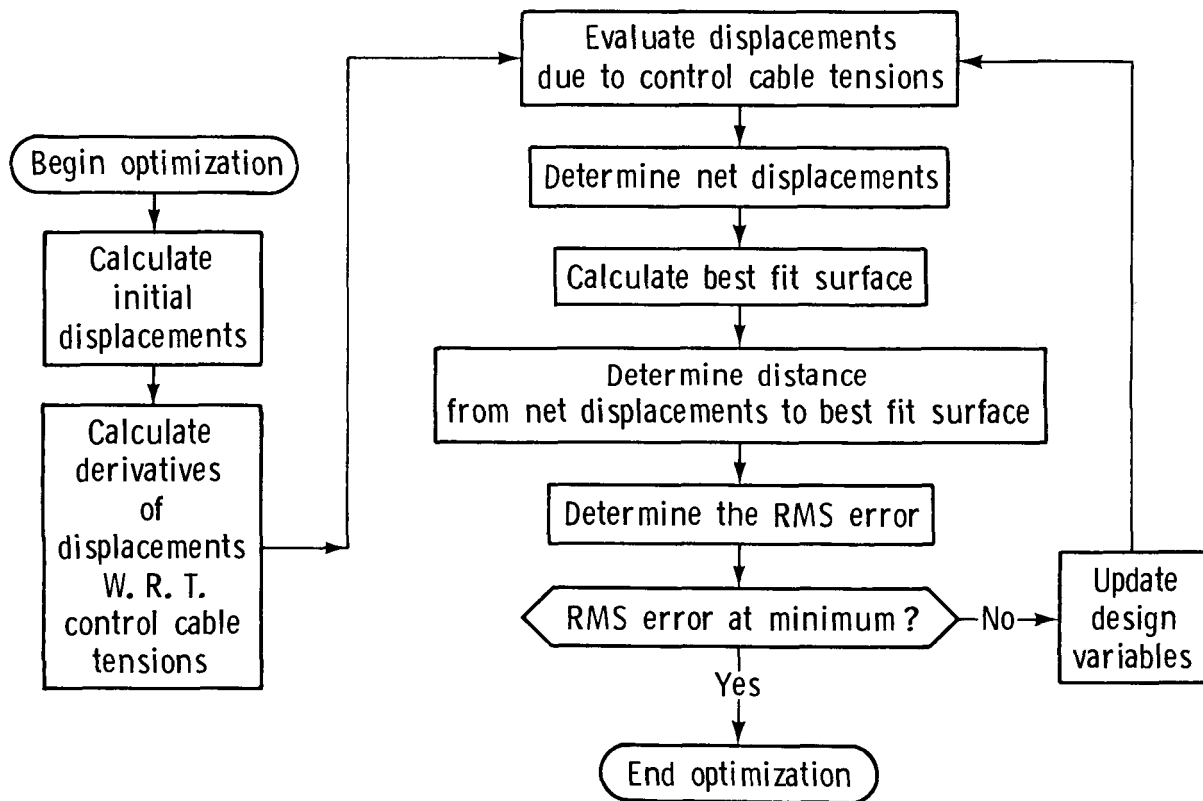


Figure 10

# SHAPE CORRECTION FOR ANTENNA-TEMPERATURE LOADING

Representative results are presented in figure 11 to indicate the level of distortion correction attainable by optimally assigning tensions in 12 control cables of a 122 meter hoop/column antenna. The figure shows the results of five test cases using temperature distributions which cause initial surface distortions. Each of the cases had a maximum temperature magnitude of 100° F. The column labeled "Uncorrected RMS distortion" is the initial RMS error of the antenna surface with the indicated temperature load applied. After the optimization procedure is used, the RMS error is changed to that listed in the column labeled "Corrected RMS distortion". The resulting reductions in the RMS error of the surface distortions ranged between 22 and 58 percent.

Load shape	Maximum temperature (°C)	Uncorrected RMS distortion (cm)	Corrected RMS distortion (cm)	Percent reduction
1	38	0.0207	0.0156	25
1	-38	0.0207	0.0161	22
2	38	0.0266	0.0152	43
3	38	0.0511	0.0244	52
3	-38	0.0511	0.0215	58

Figure 11

# SHAPE CORRECTIONS FOR ANTENNA-PRESSURE LOADING

Figure 12 shows representative results of five test cases using pressure distributions to cause initial surface distortions. Each of the cases had a maximum pressure magnitude of  $10^{-5}$  pounds per square inch. The sign of the maximum pressure indicates to which side of the antenna surface the load is being applied. The column labeled "Uncorrected RMS distortion" is the initial RMS error of the antenna surface with the indicated pressure load applied. After the optimization procedure is used, the RMS error is changed to that listed in the column labeled "Corrected RMS distortion". The resulting reductions in the RMS error of the surface distortions ranged between 16 and 45 percent.

Load shape	Maximum pressure (N/sq. m $\times 10^6$ )	Uncorrected RMS distortion (cm)	Corrected RMS distortion (cm)	Percent reduction
1	.34875	2.1996	1.8501	16
1	-.34875	2.1996	1.6812	24
2	.34875	.5535	.3023	45
3	.34875	1.0055	.8161	19
3	-.34875	1.0055	.7950	21

Figure 12

### UNCORRECTED AND CORRECTED DISTORTIONS ALONG GORE CENTERLINE

As a typical result, figure 13 shows the uncorrected and corrected distortions along the gore centerline for a  $100^{\circ}\text{ F}$  temperature distribution which varies linearly along the length of the gore. The vertical axis indicates the normal displacements from the best fit surface (previously defined as epsilon) and the horizontal axis is the nondimensional length of the antenna gore. The horizontal reference line is the best fit parabola. The solid curve is the uncorrected distortion of the antenna surface along the gore centerline. The dashed curve is the corrected distortion of the antenna surface after the optimization procedure determines a set of control cable tensions which minimize the RMS error. It can be seen that the corrected curve closely follows the horizontal reference line and therefore is nearly parabolic, which is the objective of the optimization procedure.

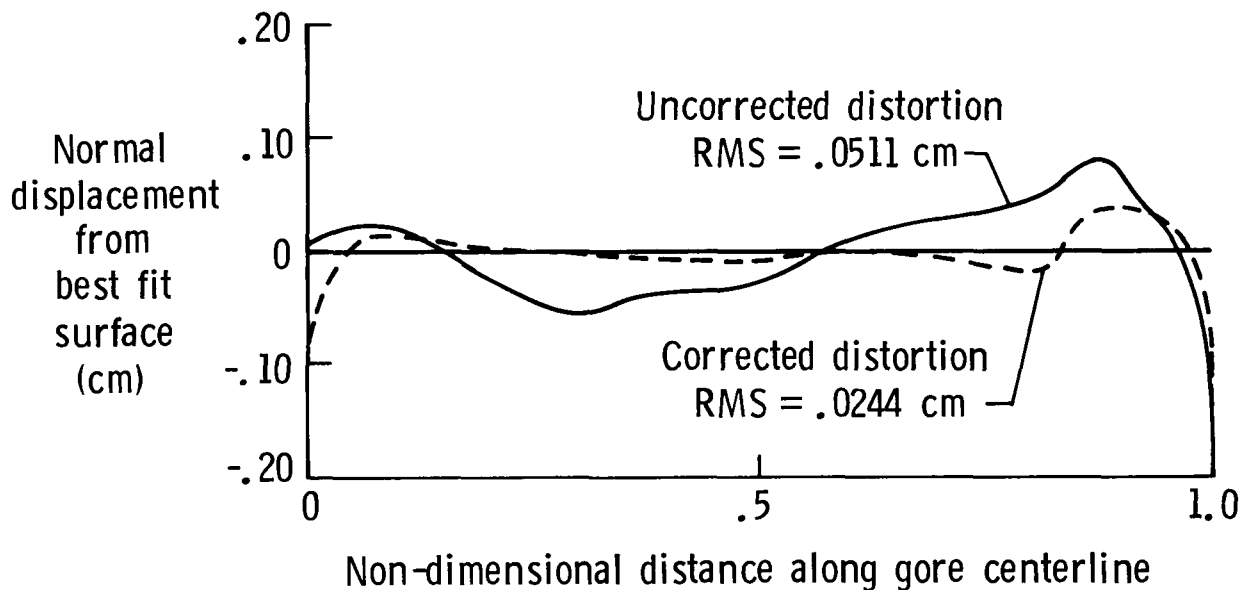


Figure 13

## CONCLUDING REMARKS

A systematic, computer-based procedure using mathematical optimization has been developed to minimize the surface distortions of a hoop/column antenna caused by externally applied loads. The procedure is built around the EAL finite element analysis program and the CONMIN general purpose optimization program, both of which are widely used and available. Improvements in RMS error were obtained for every test case attempted during the validation of the procedure. Future plans call for testing the procedure using a finite element model of a complete 48 gore hoop/column antenna, and use of more realistic load conditions that would be encountered in orbit. Also, the inclusion of other parameters in the optimization procedure will be studied. These may initially consist of boresight and focus errors in the objective function or constraints. (See fig. 14.)

- Developed procedure based on mathematical optimization to control antenna distortions
- Used EAL, CONMIN, RMS algorithm
- Successfully tested procedure on hoop/column antenna
- Future work
  - Test procedure on full antenna model
  - Use more realistic loading conditions
  - Include boresight and focus errors in objective function

Figure 14

## REFERENCES

1. Whetstone, W. D.: EISI-EAL Engineering Analysis Language Reference Manual. Engineering Information Systems, Inc., July 1983.
2. Vanderplaats, Garret N.: CONMIN - A Fortran Program for Constrained Function Minimization - User's Manual. NASA TM-X 62282, August 1973 and May 1978.
3. Katow, M. S.; and Schmele, L.: Utku/Schmele Paraboloid RMS Best-Fit Program. In Computer Programs for Antenna Feed System Design and Analysis, Volume 1: Programs and Sample Cases. (Edited by A. Ludwig) Jet Propulsion Laboratory. JPL Technical Report No. 32-979, April 1967.
4. Sullivan, Marvin R.: LSST (Hoop/Column) Maypole Antenna Development Program. NASA CR 3558, Part 1 and 2, June 1982.

## STRUCTURAL DYNAMICS ANALYSIS

J. Housner, M. Anderson, W. Belvin and G. Horner  
NASA Langley Research Center  
Hampton, Virginia

Large Space Antenna Systems Technology - 1984  
December 4 - 6, 1984

## DYNAMIC ANALYSIS CONSIDERATIONS

Dynamic analysis of large space antenna systems must treat the deployment as well as vibration and control of the deployed antenna. Candidate computer programs for deployment dynamics, and issues and needs for future program developments are reviewed in subsequent charts. Some results for mast and hoop deployment are also presented.

Modeling of complex antenna geometry with conventional finite element methods and with repetitive "exact elements" is considered. Analytical comparisons with experimental results for a 15 meter hoop/column antenna revealed the importance of accurate structural properties including nonlinear joints. Slackening of cables in this antenna is also a consideration. In addition, the maturing technology of designing actively damped structures through analytical optimization is discussed and results are presented.

### ● ANTENNA DEPLOYMENT DYNAMICS

- Candidate Programs
- Issues and Needs
- Mast and Hoop Deployment

### ● ANTENNA VIBRATION AND CONTROL

- Finite Element and Repetitive Models
- Important Effects
  - Nonlinear joints
  - Cable slackening
- Design of Actively Damped System



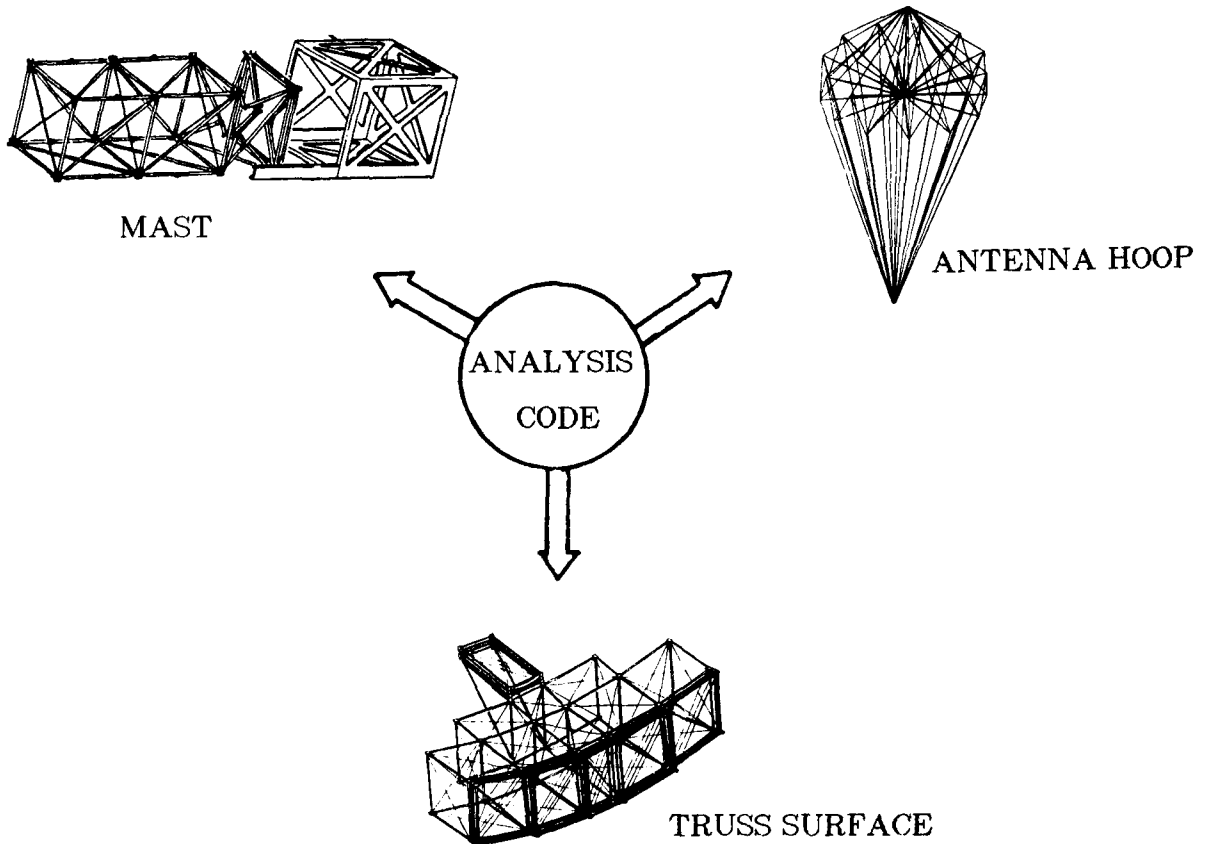
## POTENTIAL BENEFITS FROM DEPLOYMENT DYNAMICS ANALYSIS

Deployment is a candidate mode for construction of structural antenna components. By its very nature, deployment is a dynamic event, possibly involving large angle unfolding of flexible beam members. Validation of proposed designs and conceptual deployment mechanisms is enhanced through analysis. Analysis may be used to determine member loads thus helping to establish deployment rates and deployment control requirements for a given concept. Furthermore, member flexibility, joint free-play, manufacturing tolerances and imperfections can affect the reliability of deployment. Analyses which include these effects can aid in reducing risks associated with a particular concept. Ground tests which can play a similar role to that of analysis are difficult and expensive to perform. Suspension systems just for vibration ground tests of large space structures in a 1 g environment present many challenges. Suspension of a structure which spatially expands is even more challenging. Analysis validation through experimental confirmation on relatively small simple models would permit analytical extrapolation to deployment of larger more complex space structures.

- **Deployment A Potential Candidate For Antenna System Construction**
- **Deployment Is a Dynamic Event**
- **Design And Concept Validation**
  - **Determination of Member Loads**
    - Deployment Rate**
    - Deployment Control**
  - **Reliability of Deployment Mechanism**
    - Flexible Members**
    - Joint Free-Play**
    - Tolerances and Imperfections**
  - **Ground Tests Difficult and Expensive**
    - Suspension System In 1 g Environment**
    - Size Limitations**

## APPLICATIONS OF DEPLOYMENT ANALYSIS PROGRAMS

Deployment analysis programs find application in masts, truss type antenna surfaces and entire antenna structures. Deployment programs belong to a larger class of multi-body programs and as such are also applicable to mechanisms and robotics.



## CANDIDATE MULTI-BODY PROGRAMS FOR DEPLOYMENT

Shown in this chart is a list of some of the existing U.S. computer multi-body programs which are candidates for performing deployment analyses. Some of these programs were originally designed for mechanisms, while others were designed for satellites with appendages. Most of these programs are in a constant state of improvement and most have or will soon have capability for treating flexible members and perhaps sophisticated joint behavior. However, efficient simulation of a deploying structure with a large number of components will require considerable further development. The next chart addresses some of the issues and developmental needs in this area.

**ADAMS ----- Mechanical Dynamics**

**ALLFLEX ----- Lockheed Missiles and Space**

**CAPPS ----- TRW**

**DADS ----- U. of Iowa**

**DISCOS/NBOD - Martin Marietta**

**IMP ----- U. of Wisconsin**

**LATDYN ----- NASA (pilot code)**

**SNAP ----- General Dynamics**

**TREETOPS ----- Honeywell**

## ISSUES AND NEEDS IN DEVELOPMENT OF DEPLOYMENT PROGRAMS

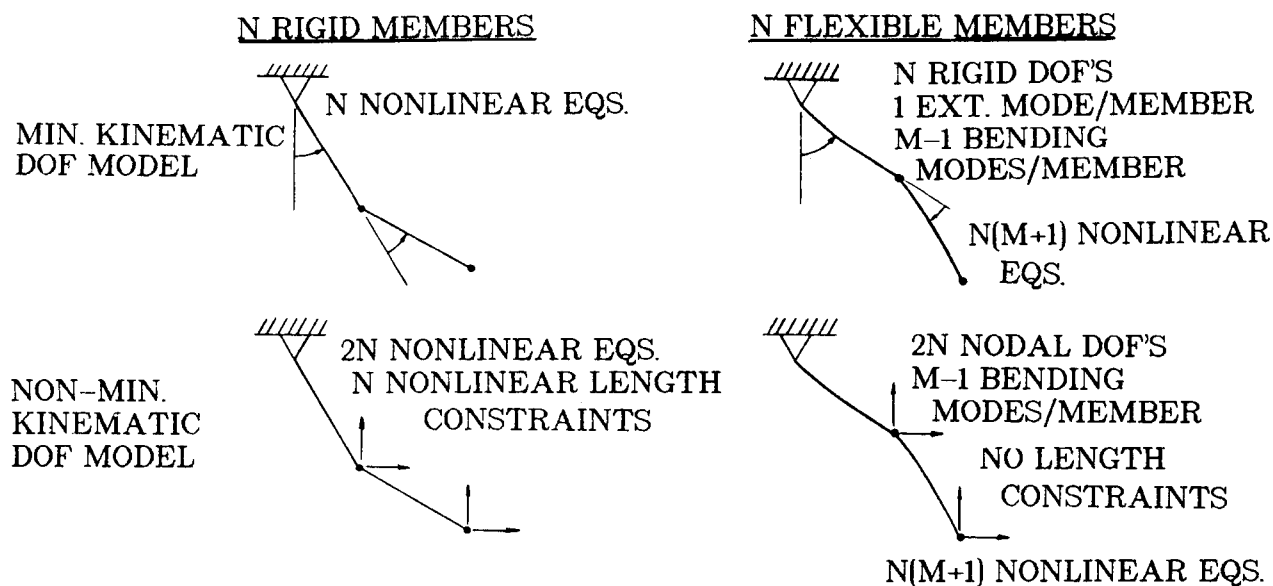
One outstanding developmental need is in structural modeling. Member flexibility, joint free-play, joint lock-up and closed loop topologies are needed for proper deployment simulation. Recently progress has been made in adding these capabilities to those programs which were originally oriented or designed for rigid mechanisms. Usually member flexibility is accounted for by adding deformation modes of the members to their rigid body motion. Unfortunately, this addition greatly increases the size of the problem and consequently only those deployables with a small number of members can be treated in a reasonably efficient manner. In addition, as shown in the next chart, the problem formulation and modeling which had obvious advantages with rigid members no longer retains those advantages when member flexibility is added. It is then questionable as to whether an efficient program for flexible structures can be obtained by extending rigid member programs. One critical issue which stands as an obstacle to an efficient deployment simulation is one of integrating the nonlinear equations of motion in time subject to constraints. Concurrent processing which makes use of multiple processors is very promising in this area. The ground work in this area for multi-body problems is to be found in the CAPPS program listed in the previous chart. Use of concurrent processing and/or new time integration algorithms may require new formulations of the problem.

- **Modeling**
  - **Member Flexibility**
  - **Joints**
  - **Lock-up Constraints**
  - **Closed Loop Topologies**
- **Time Integration**
- **Concurrent Processing**

## EFFECT OF FLEXIBILITY ON STRUCTURAL MODELING FOR DEPLOYMENT

In order to demonstrate the consequences of flexibility on the size of a multi-body problem, a planar N body pendulum is considered. For a pendulum composed of all rigid members, there are N independent degrees of freedom. Thus a minimum size kinematic model involves the solution of N equations of motion which are nonlinear when large angular excursions are permitted. An alternate modeling of the rigid member pendulum leads to  $2N$  nonlinear equations plus N nonlinear length constraints when generalized orthogonal coordinates are selected at the pendulum pinned joints. Clearly the minimum kinematic modeling is preferable when the members are rigid. If the members are flexible and the minimum kinematic modeling is extended to account for flexibility, the usual approach is to add flexible modes to the set of kinematic or rigid body ones. In this example one extensional mode and M-1 flexible modes per member are added. The resulting problem is M+1 times bigger than in the rigid member case. If on the other hand the non-minimal modeling of the rigid member pendulum is similarly extended, an extensional mode does not need to be added since it is already accounted for by the superfluous generalized coordinates of the model and the length constraints are no longer appropriate. Consequently, the resulting number of equations is precisely the same and the modeling approach which is clearly preferable for rigid members has no clear advantage for flexible members. Since the resulting problem size is considerably larger with flexible members, extension of programs for rigid members may not lead to efficient programs.

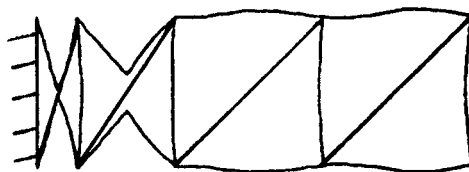
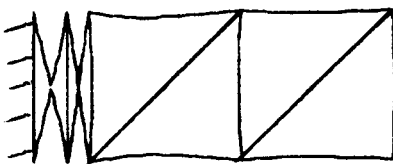
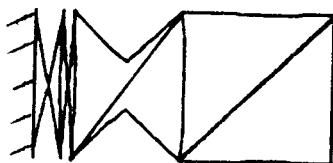
### PLANAR MULTI-BODY PENDULUM



**CONCLUSION: WHAT WAS IMPORTANT IN RIGID MEMBER SYSTEM MAY NOT BE IMPORTANT IN FLEXIBLE MEMBER SYSTEM**

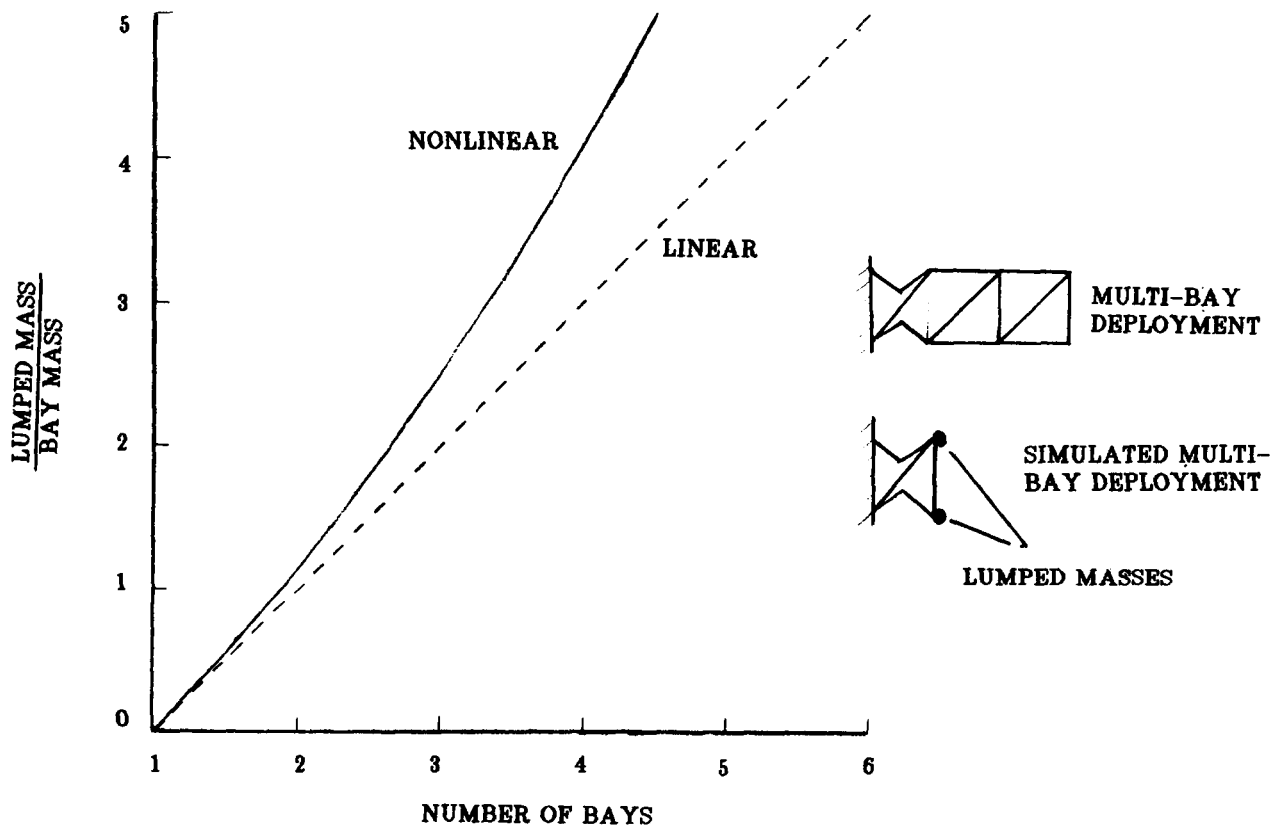
## UNCONTROLLED DEPLOYMENT SEQUENCE OF FOUR BAY MAST

In this chart, the analytically simulated deployment of an uncontrolled four bay mast composed of flexible members is shown. (The analysis was performed using the NASA LATDYN computer program and involved 64 degrees of freedom.) The deployment involves unfolding of the longerons of each bay which have lockable joints mid way along their length. The diagonals are assumed to telescope out during the deployment and the deployment is driven by precompressed rotational springs at each lockable joint. Typically such masts are controlled to deploy sequentially, that is, one bay is permitted to deploy at a time. Nevertheless, an uncontrolled deployment sheds light on the natural deployment character of the design. Moreover, insight is gained into the simultaneous deployment which can occur in other deployables such as a tetrahedral trusses. The chart shows that the mast has a natural tendency to deploy nearly sequentially even in the absence of control. This appears to be due to the larger inertial mass which must be pushed by the inner bays and to the choice of the spring constants driving the deployment. Thus sequential deployment for a mast is a natural selection.



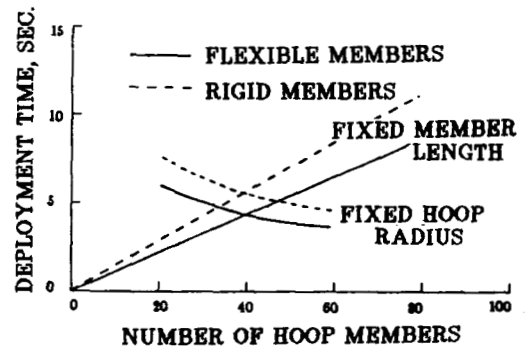
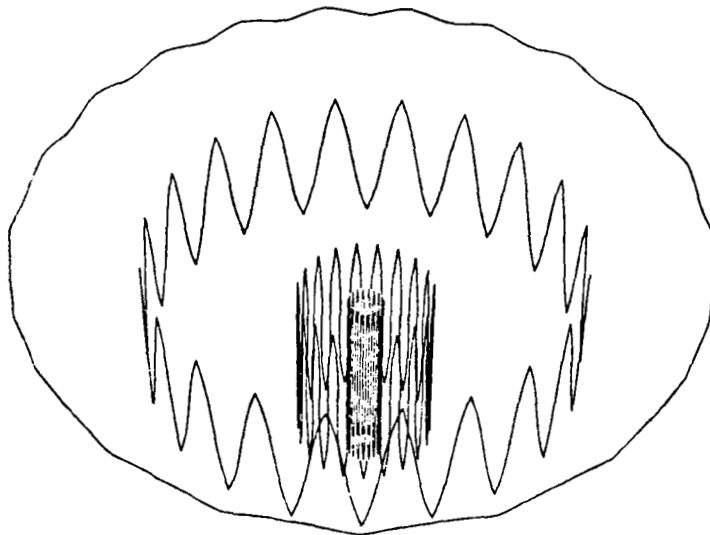
# LUMPED MASS NECESSARY TO SIMULATE UNCONTROLLED MULTI-BAY DEPLOYMENT

Due to the large computational time requirements of the mast deployment in the previous chart, it becomes desirable to simulate the multi-bay deployment using only one bay with lumped masses representing the inertial effect of the remaining bays. The nonlinear curve indicates the amount of lumped mass which must be added to a single bay in order to simulate the deployment time of the multi-bay analysis. The linear curve indicates the consequences of assuming that the added mass is equal to that of the simulated bays. The linear representation becomes increasingly inaccurate as the number of bays to be simulated increases. The reason for this is probably traceable to the vibrations and some unfolding of the simulated bays during deployment.



## UNCONTROLLED DEPLOYMENT OF FLEXIBLE MEMBER HOOP

Deployment of hoops composed of a various number of flexible hinged members is considered in this chart. The left hand figures depict the deployment sequence of a 40 member hoop. Bending of the hoop members is observable during deployment and after lock-up. The right hand portion of the chart indicates the variation of hoop deployment time with number of hoop members. Two sets of curves are shown. In one set of curves, the length of the hoop members is fixed so that as the number of members increases, the hoop radius also increases. In the second case, the hoop radius is fixed so that as the number of members increases, the member length decreases. Effectively, in the second set of curves, the total weight of the hoop remains fixed. Deployment time is measured from the time the packaged hoop is released to the time all the joints lock up. The figure indicates that hoops composed of flexible members reach lock-up sooner.





## ANALYSIS OF REPETITIVE LATTICE STRUCTURES

A structure that has a nodal geometry that repeats in one or more coordinate directions may be analyzed for buckling or vibration by considering only one repeating element of the structure. If cylindrical coordinates are used, configurations such as the hoop-column antenna structure shown on the next figure may be treated. For lattice structures composed of beams and tensioned cables, it is possible to use "exact" member theory in developing member stiffnesses. This theory is based on the solution of the beam column or string equations to develop an exact relation between forces and displacements as a function of frequency and member axial load. There are no further approximations in the analysis and exact results for all frequencies are obtained with nodes located only at joints. A typical finite element equilibrium equation relates the displacement vector of the basic repeating element,  $D_0$ , with the displacement vector of other repeating elements,  $D_j$ , to which it is connected. The key step is the assumption of a periodic mode shape which is exact for structures having rotational periodicity as do many antenna structures. For many structures that are repetitive in rectangular coordinates, such as booms or platforms, this assumption is exact for simple support boundary conditions for a wavelength twice the actual length of the structure. The  $D_j$  may be eliminated from the equilibrium equation by

$$D_j = D_0 \exp i\phi$$

where  $\phi$  is a function of wavelength and harmonic of the mode and the connectivity of the structure. The equilibrium equation then can be written in terms of  $D_0$  only and buckling or vibration is determined from the eigenvalues of a  $6N \times 6N$  complex, Hermitian matrix where  $N$  is the number of nodes in one repeating element.

### STIFFNESS FROM "EXACT" MEMBER THEORY

$$\text{EQUILIBRIUM EQUATION } K_0 D_0 + \sum K_j D_j = 0$$

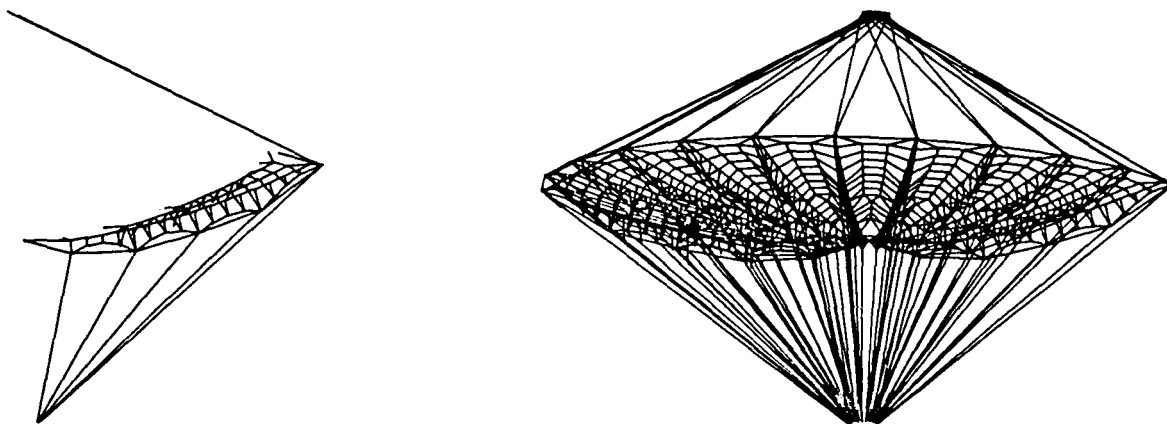
$$\text{PERIODIC MODE SHAPE } D_j = D_0 \exp i\phi$$

### SOLUTION OF $6N \times 6N$ MATRIX

## STRUCTURAL MODEL OF HOOP-COLUMN ANTENNA

The computer program incorporating the theory for repetitive lattice structures is quite general in its capability. Such things as eccentric connections at joints, spring connected members (including the limiting cases of pinned or sliding connections) and the ability to determine vibration of structures that are free in space make it especially useful for many antenna configurations.

The 15m hoop-column antenna being fabricated by the Harris corporation is shown in the figure. The variation in geometry necessary to produce the four side feed antennas is ignored so that only one gore is modeled for the vibration analysis of the complete antenna. It is believed the results for this simple model will be close to those for the actual geometry and can be used to study variations in the many structural parameters. There are 57 structural nodes in the repeating element which is the size of the model input to the computer program. If the repeating element is indexed in the circumferential direction 24 times, the complete model is obtained. For clarity, only one half the total model is shown in the figure. All the members except the hoop are tensioned cables so that most of the nodes have just three degrees of freedom. This model was generated for harmonic responses having two or more circumferential waves. The central compression mast does not participate in these modes and is not shown in the model. The final values of member stiffness and pretension are not known at present so that frequency results are not available.



REPEATING ELEMENT

## 15 M HOOP COLUMN ANTENNA DYNAMIC CHARACTERIZATION WITHOUT SURFACE

The dynamic characterization of an antenna must be performed on both an experimental and analytical basis. Experimental data is invaluable in verifying analysis assumptions and in determining effective material properties when using composite structures. On the other hand, analysis can identify closely spaced modes that may otherwise be overlooked in a test program. Shown below is the 15 M hoop column antenna prior to surface installation. Also shown are the steps taken to characterize its vibration behavior. Prior to surface installation only the upper and lower hoop support cables are present. A tripod of six inch aluminum tubes was attached to the column to support the antenna. The flexibility of the tripod support was included in the analysis models. Since the BUNVIS analysis computer program may be unfamiliar to the reader, it is described briefly on the figure and the BUNVIS repeating element for the 15 M antenna is shown.

- PERFORMED IMPACT TEST FOR SYSTEM IDENTIFICATION

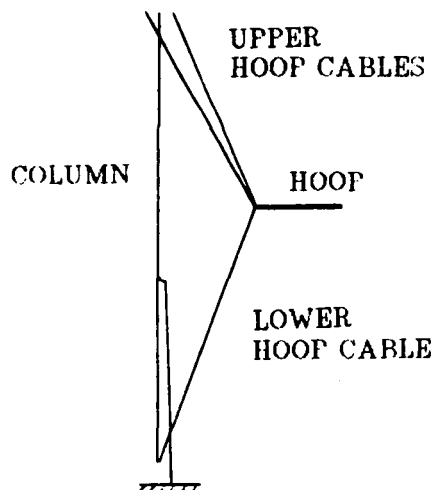
- 48 MEASUREMENTS ON HOOP
  - 4 MEASUREMENTS ON COLUMN

- ANALYZED ANTENNA WITH TEST BOUNDARY CONDITIONS VIA

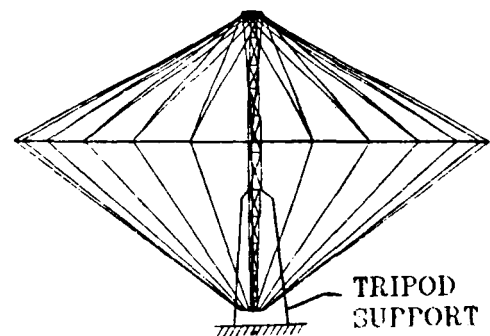
- NASTRAN (525 DEGREES OF FREEDOM)
  - BUNVIS (84 DEGREES OF FREEDOM)

- BUNVIS USES REPEATING ELEMENTS TO MODEL THE ANTENNA

REPEATING ELEMENT



15 M ANTENNA



# COMPARISON OF TEST AND ANALYSIS FREQUENCIES

Test data has been reduced and compared to both analytical models in the table shown below. Analysis consistently predicted higher frequencies than test data for the first three modes. Analysis predicts the fourth and fifth modes to occur at lower frequencies than test data indicates. Some possible reasons for the test and analysis discrepancies are discussed on the next chart. Note the damping data obtained from the test program is considerably higher than the one-half to one percent critical damping usually assumed for large space structures.

MODE SHAPE	FREQUENCY (HZ)			DAMPING (C/C CRITICAL)
	NASTRAN	BUNVIS	TEST	
HOOP TORSION	0.078	0.084	0.067	0.035
HOOP ROCKING/ COLUMN BENDING	0.969	1.39	0.785	0.12
HOOP INPLANE MOTION/ COLUMN BENDING	1.61	2.05	1.36	0.041
HOOP OUT-OF-PLANE TRANSLATION	7.24	7.10	7.50	UNKNOWN

## POSSIBLE SOURCES OF ERROR BETWEEN ANALYSIS AND TEST

Three major sources of error are possible in dynamic models of structures such as the 15 M Hoop Column antenna. Composite material properties are sometimes difficult to model at low strain levels because the fibers are not stressed uniformly. This results in nonlinear EA properties as verified by tests of the hoop support cables. Another source of error involves modeling of inertial properties. Total mass is often available to the analyst, however mass moments of inertia of individual parts are rarely measured. This is believed to account for the error between test and analysis for the fourth mode. The last source of error described herein is the modeling of joints. Traditionally joints are modeled as rigid links in the analysis which accounts for the test frequencies usually being lower than analysis predictions. The following chart shows a new approach for modeling of joints to account for their stiffness and damping.

- MATERIAL PROPERTIES

- EA, EI, GJ (LAMINATE ANALYSIS PERFORMED)
  - NONLINEARITIES (CABLE AE MEASURED)

- MASS AND ROTATIONAL INERTIAS

- ACCURATE MODELING OF JOINT MASSES REQUIRED

- JOINT FLEXIBILITIES AND NONLINEARITIES

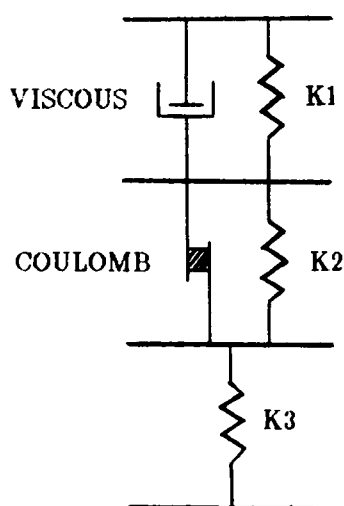
- NEED JOINT MODELS TO CHARACTERIZE JOINT STIFFNESS AND DAMPING CONTRIBUTIONS

## ANALYSIS OF JOINT STIFFNESS AND DAMPING

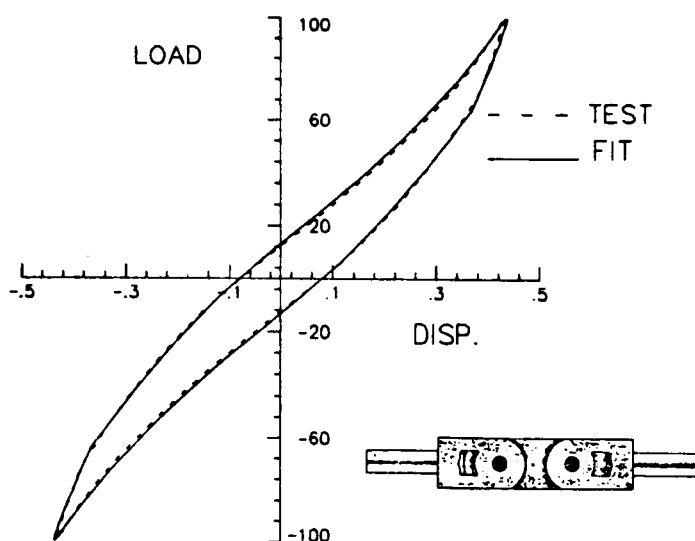
An approach for developing joint models is to measure the load deflection curves of a statistical sample of joints used in a structure. Then using the measured data an empirical model is developed such as the one shown below. The coefficients of the empirical model are determined such that the squared error is minimized over the operating load deflection range of the joint. This results in an empirical joint model which may be incorporated in the overall structure model for the prediction of stiffness and damping characteristics. Shown below is a load deflection curve obtained by identifying the coefficients of the model shown to minimize the squared error from simulated joint data.

### EMPIRICAL MODELS DEVELOPED TO ACCOUNT FOR NONLINEAR STIFFNESS, COULOMB FRICTION AND VISCOUS DAMPING

COEFFICIENTS DETERMINED BY A LEAST SQUARES ERROR MINIMIZATION METHOD WITH MEASURED LOAD-DEFLECTION CURVES



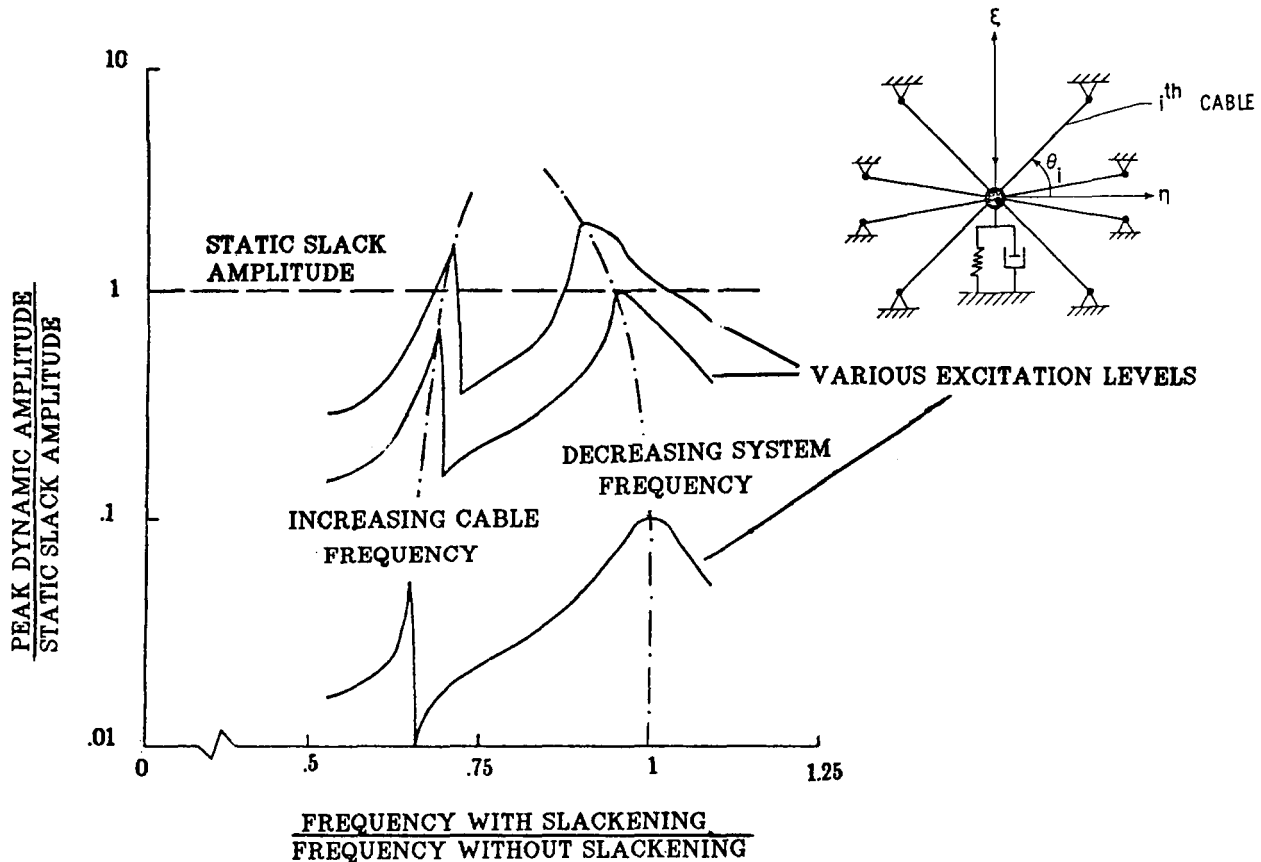
EMPIRICAL MODEL



COMPARISON OF SIMULATED JOINT LOAD DEFLECTION WITH EMPIRICAL ANALYSIS MODEL

## EFFECT OF CABLE SLACKENING ON SYSTEM FREQUENCY

Systems which depend on cables to provide stiffness can suffer stiffness and hence frequency reduction when the primary structure moves in such a fashion so as to allow a cable to go slack. Since cables are usually lightly loaded, slackening of cables is possible. This chart examines a simple spring/mass/damper system stiffened by a set of pretensioned cables. Frequency depends on the system response amplitude. The dash-dot curve indicates the decreasing system frequency as peak amplitude of motion increases. When the peak motion exceeds an amplitude at which the cable would slacken in a static environment, the system frequency starts to decrease even more rapidly. Also depicted on the figure is a second dash-dot curve which increases in frequency with increasing amplitude of dynamic motion. This frequency is associated with cable lateral motion and stiffens as the amplitude of the lateral motion increases.



## DISTRIBUTED ACTIVE DAMPING FOR FLEXIBLE STRUCTURES

A design technique for the distribution of damping on flexible structure will be formulated which includes the force/torque limitation of the actuators which will be used as active dampers. It is assumed that a large finite element model exists which describes the structure.

The design technique will first reduce the order of the finite element model. Next, active damping gains will be determined for a given disturbance while not allowing the actuators to saturate. The design problem is cast as an optimization problem to be solved by a nonlinear mathematical programming algorithm. Finally, the design results are put in the original finite element model and the performance requirements which are stated as part of the optimization problem are verified.

**OBJECTIVE: TO DETERMINE ACTIVE DAMPING GAINS FOR  
FLEXIBLE STRUCTURES WHILE CONSIDERING  
DISTURBANCE MODELS, ACTUATOR LIMITS, AND  
STRUCTURAL PERFORMANCE CRITERIA**

**GIVEN: A LARGE FINITE ELEMENT MODEL OF A FLEXIBLE  
STRUCTURE, A DISTURBANCE MODEL, AND  
PERFORMANCE REQUIREMENTS**

**DEVELOP: REDUCED ORDER MODEL TO BE USED IN DAMPER  
DESIGN**

**ACTIVE DAMPING GAINS SUCH THAT ACTUATORS  
DO NOT SATURATE**

**OPTIMIZATION FORMULATION**

**VERIFIED DYNAMIC RESPONSES THAT SATISFY  
PERFORMANCE REQUIREMENTS**



## OPTIMIZATION FORMULATION

The goal of the design process is to determine the gains of the diagonal damping matrix,  $C$ . It is assumed that the mass and stiffness matrices of the structure are known via some finite element formulation. Also, it is assumed that the disturbance is known and that spacecraft performance requirements (i.e. line-of-sight error or minimum vibration amplitude) exist which mathematically define the conditions which must be achieved to ensure acceptable mission performance. At the same time it is recognized that actuators which will be used to damp the structure are limited in their force/torque output.

Starting with the undamped structure, the modes and frequencies are calculated and some smaller set of modes is used to then reduce the damped equations of motion to a small set of first order equations. The objective function used in the optimization algorithm minimizes the energy dissipated during the control cycle. Finally, the mission performance requirements which might be response limits are defined as inequality constraints in the optimization algorithm.

**GIVEN: MASS AND STIFFNESS MATRICES, DISTURBANCE  
FORCE, AND PERFORMANCE REQUIREMENTS**

**DETERMINE: DIAGONAL DAMPING MATRIX,  $C$**

METHOD:  $M \ddot{x} + Kx = 0$

$$\Downarrow$$

$$\lambda, \phi$$

$$x = \phi q$$

$$\Downarrow$$

$$\frac{d}{dt} \begin{pmatrix} \dot{q} \\ q \end{pmatrix} = \begin{bmatrix} 0 & I \\ -\Lambda & -\Phi^T C \Phi \end{bmatrix} \begin{pmatrix} \dot{q} \\ q \end{pmatrix} + \begin{pmatrix} 0 \\ \Phi^T F \end{pmatrix}$$

REDUCED MODEL

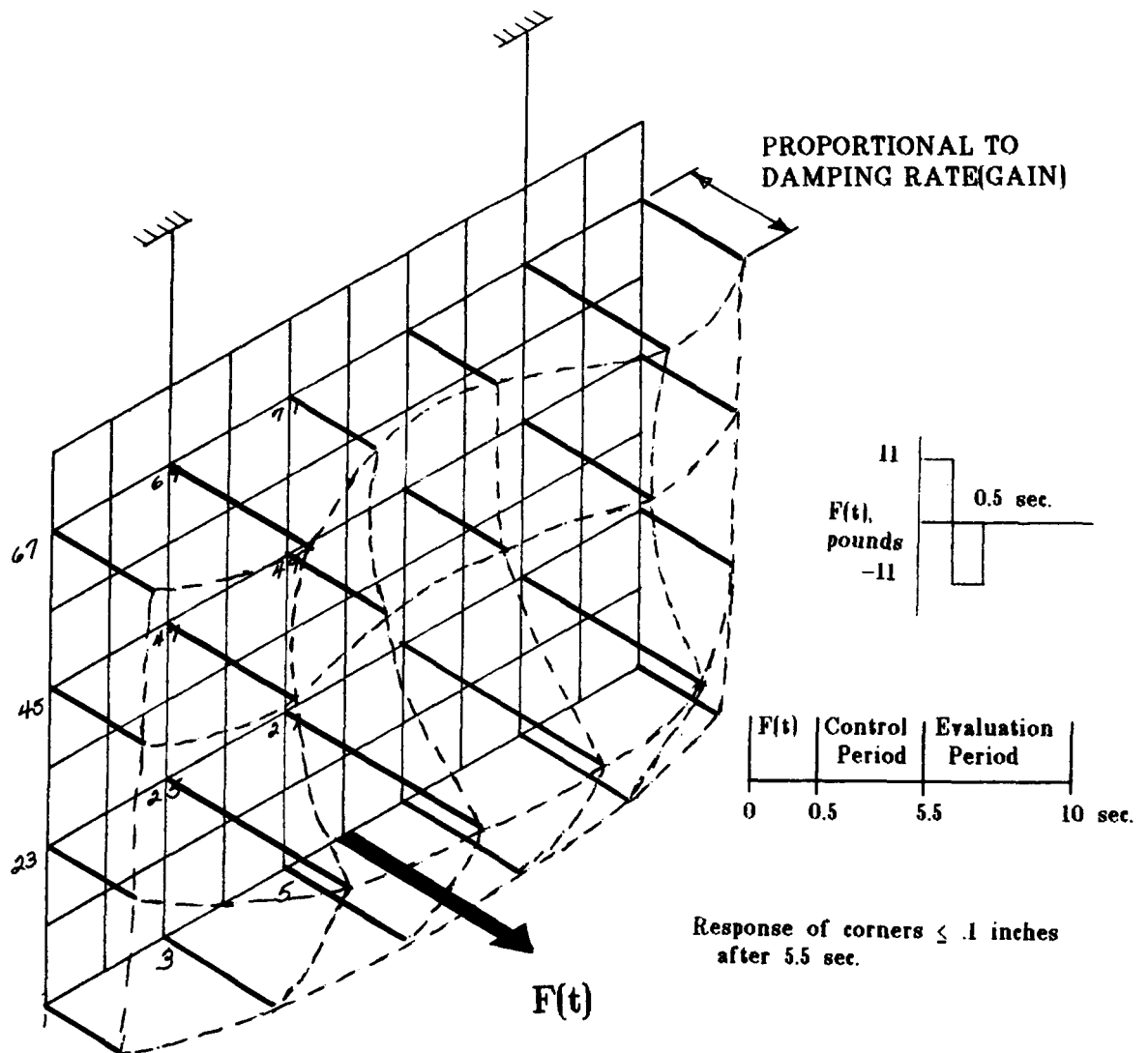
**OBJECTIVE FUNCTION: MINIMIZE DISSIPATION  
ENERGY**

**CONSTRAINTS: RESPONSE LIMITS**

# OPTIMIZATION RESULTS USING A GRILLAGE EXAMPLE

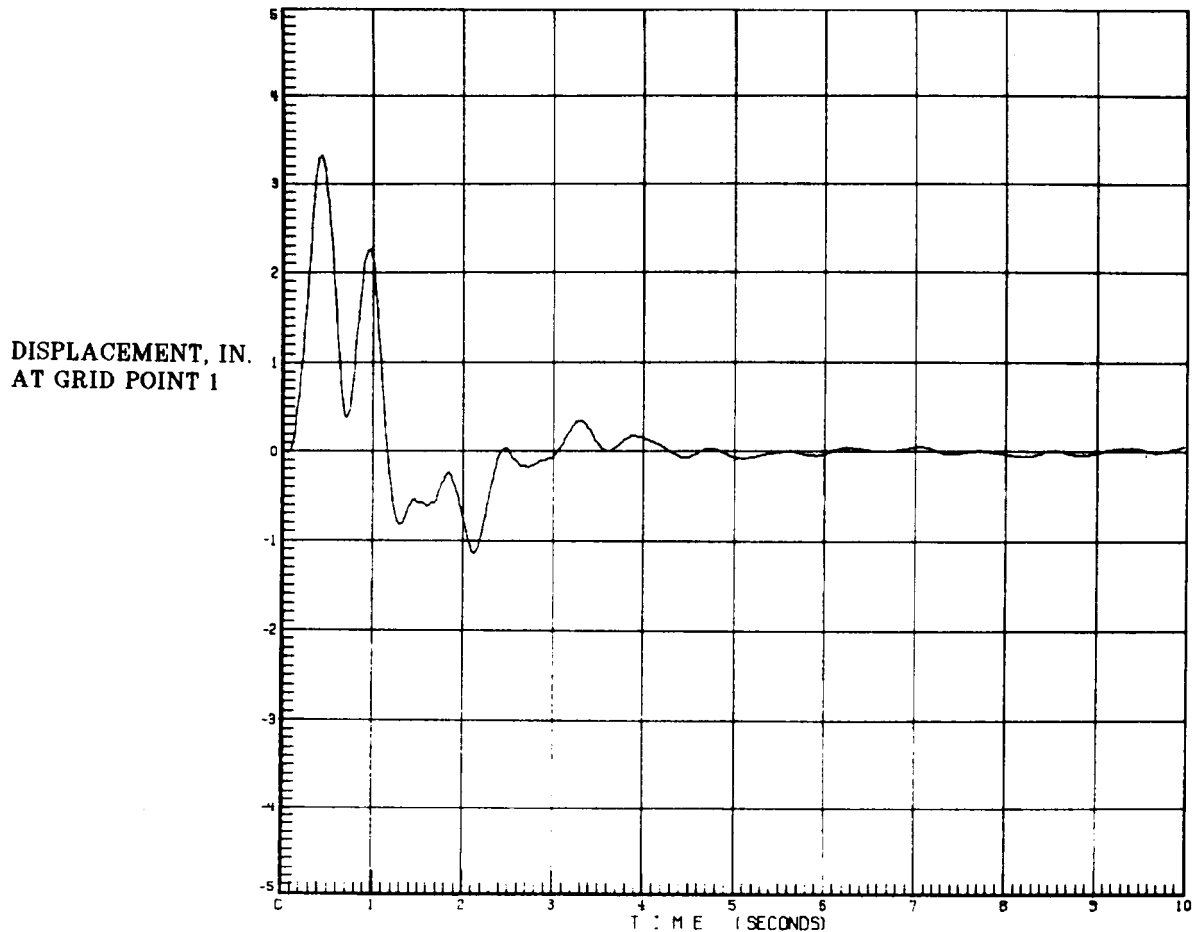
Results are obtained using a grillage as an example in the design process. A disturbance is applied to the center of the lower edge of the grillage. This disturbance is applied in the time interval from 0 to 0.5 seconds and is shown on the right of the slide. From 0.5 to 5.5 seconds the actuators are turned on and it is required that the response amplitude of the four corners of the grillage be less than 0.1 inches at the end of the control period. From 5.5 to 10 seconds there is no control but the response is monitored to ensure that no peak exists in this time period which exceeds the performance requirements.

The bars drawn normal to the surface of the grillage indicate the location of the actuators and the length of the bar is proportional to the gain at the particular location. Only force actuators are considered in this grillage example model.



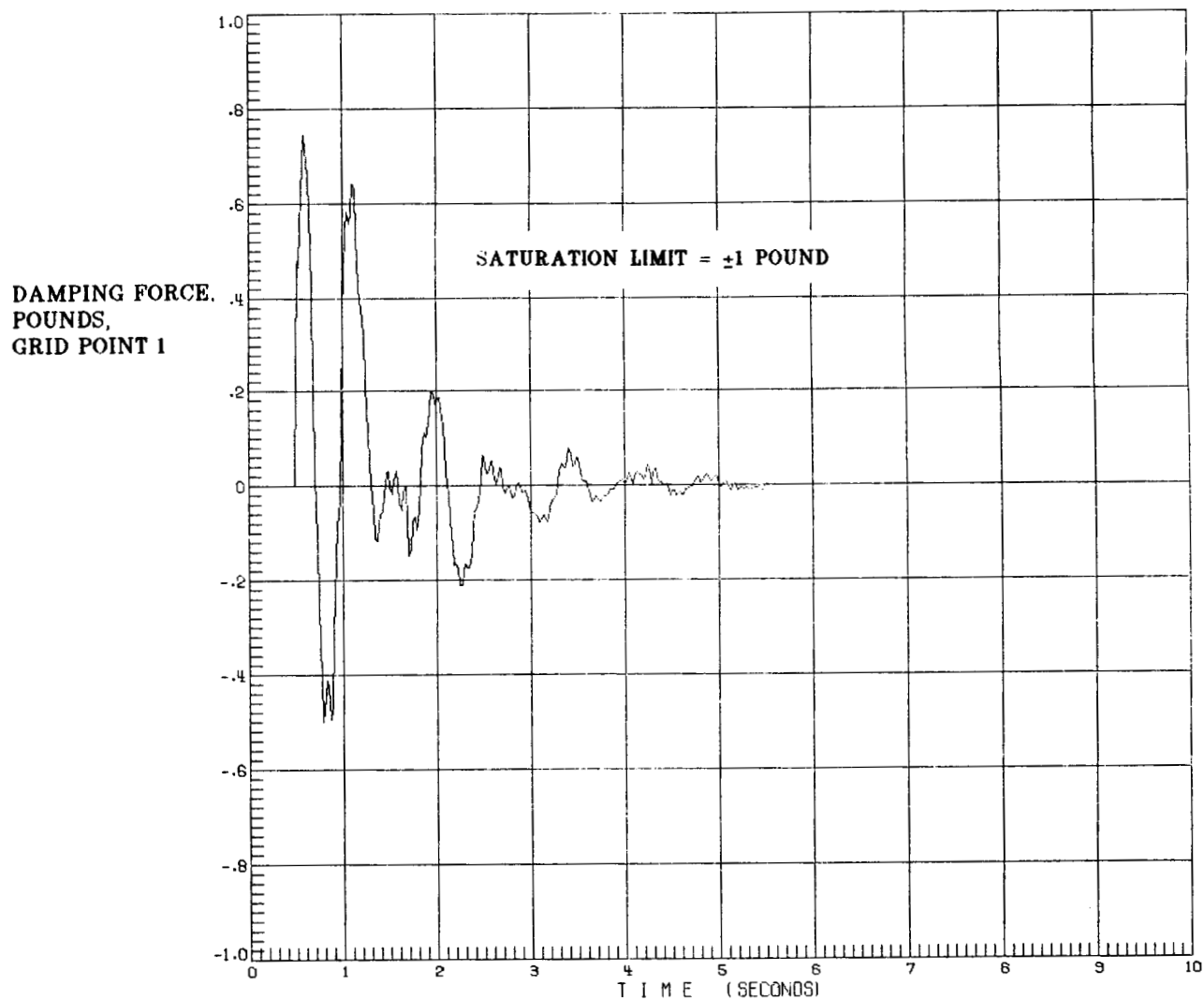
## CLOSED-LOOP SIMULATION USING ORIGINAL FINITE ELEMENT MODEL

The displacement at grid point 1 (lower left corner) of the grillage model is shown below. These results were obtained using NASTRAN with the original finite element model, the damping forces simulated as a follower force calculated from the rate at the corresponding grid point location, and the disturbance applied to the model as shown in the previous slide. Note that the peak displacement from 5.5 to 10 seconds does not exceed the specified value of .1 inches.



# CLOSED-LOOP SIMULATION USING ORIGINAL FINITE ELEMENT MODEL

Saturation of the actuators is considered in the design algorithm and the damping force applied at grid point 1 is shown in the slide below. The saturation limit is assumed to be  $\pm 1$  pound force. From the plot it is seen that the saturation limit is not exceeded. Again, these results were obtained from NASTRAN with the closed loop model.



## SUMMARY

Candidate computer programs for analytical deployment simulation exist, but until progress is made on improving the time integration of the equations for deployment simulation, problem size will be effectively limited by solution cost. Simulation costs can be reduced by either development of better time integration algorithms or use of concurrent processing computer hardware. For the deployed or erected antenna, repetitive analysis is a viable approach to reducing analysis effort in computing vibration modes and frequencies, but accurate properties of antenna components must be measured and used in the analysis if good correlation with test is to be accomplished. This includes improved modeling of joints especially in their nonlinear behavior. For cable stiffened antennas, it is imperative to also have the structure in equilibrium to a fine order of precision under the cable pretension loads used in the analysis. Vibration control studies need to include realistic constraints of actuator capability and such realism is now being added to such studies.

- **CANDIDATE COMPUTER PROGRAMS EXIST FOR DEPLOYMENT, BUT ARE LIMITED TO SMALL PROBLEMS ESPECIALLY IF MEMBERS ARE FLEXIBLE**
  - **NEW TIME INTEGRATION ALGORITHM AND PERHAPS ASSOCIATED FORMULATION**
  - **CONCURRENT PROCESSING MUST BE EXPLOITED**
- **REPETITIVE ANALYSIS GREATLY REDUCES COMPUTATIONAL EFFORT IN ANTENNA VIBRATIONS**
- **ACCURATE PROPERTIES OF ANTENNA COMPONENTS NEEDED TO ACHIEVE GOOD TEST/ANALYSIS CORRELATION**
- **NONLINEAR JOINT BEHAVIOR IMPORTANT TO FREQUENCY AND DAMPING PREDICTIONS**
- **ANALYTICAL STUDIES IN VIBRATION CONTROL NOW ACCOUNTING FOR SOME REALISTIC LIMITATIONS**

**Page intentionally left blank**

AFWAL SPACE CONTROL TECHNOLOGY PROGRAM

V. O. Hoehne  
Flight Control Division  
Flight Dynamics Laboratory  
Air Force Wright Aeronautical Laboratories  
Wright-Patterson Air Force Base, Ohio

Large Space Antenna Systems Technology - 1984  
December 4-6, 1984

## ABSTRACT

The space-oriented control technology programs under way in the Air Force Wright Aeronautical Laboratories (AFWAL) predominantly are being done in the Flight Control and Structures and Dynamics Division of the Flight Dynamics Laboratory. The nature of these programs extends from basic research performed in-house to exploratory development and advanced development programs done under contract. The objective of this paper is to overview only those programs that are applicable to flexible large space structures. Sufficient information about each program will be provided for the reader to understand the objective of the program, the approach used to perform the study, and the final payoff expected. The names of the people involved in the program are provided along with their organizational symbols and telephone numbers. Through contacting these people, information to any level of detail desired can be acquired.

In general, the spacecraft control activity in the Flight Dynamics Laboratory is interdisciplinary, bringing together activities in structures, structural dynamics and control. This is very important since the large flexible structures to be controlled have many physical factors that influence the final controllability of the vehicle. Factors such as rigidity of both structural elements and joints, damping inherent in both the material as well as discrete dampers located throughout the structure, and the bandwidth of both sensors and actuators used to sense motion and control it are several examples of those physical factors that are interdisciplinary and influence control.

The Flight Dynamics Laboratory spacecraft control program is not complete within itself, rather, it augments work already under way and planned at NASA, the Air Force Space Technology Center, and other organizations by addressing issues needed by those missions that have a military goal. The work being done relies heavily on the expertise of the Laboratory gained through activities associated with developing technology for advanced aircraft. This is possible because the closer technology is to basic research, the more generic it becomes, having application to both aircraft and spacecraft with relatively minor changes in the given conditions.

## INTRODUCTION

Traditionally, the AFWAL Flight Dynamics Laboratory has been involved in advancing technology for controlling military aircraft and tactical missiles since its formation. Considerable experience has been gained in areas of technology that not only include control but also the structural and dynamic characteristics that impact the control of the vehicle. Some of this experience is generic and with minimal modifications can be applied to the development of technology for space vehicles. Hence, when it became obvious that the military use of space would require technological advancements in some technology in areas where experience existed, programs were initiated first in the Structures and Dynamics Division of the Laboratory and later in the Flight Control Division. Our approach to the technology efforts is interdisciplinary in nature. In it we bring together the structures technology that deals with the strength and elasticity of the structure with the structural dynamics technology that defines the dynamic response of the structure to both operational and environmental loads and then combine these with the controls technology that defines both the algorithms and the system for controlling this dynamic structure. We feel this interdisciplinary approach is essential in successfully controlling space structures because in these structures strength,



flexibility, and control are inseparable. We also recognize that as the structure becomes larger, it becomes more flexible since rigidity is related to weight and weight must be kept within practical bounds. This flexibility places greater demands on the control system since many of the missions planned for spacecraft require very precise aiming, shaping, and vibration or jitter limiting. Additional considerations that require the interdisciplinary approach to the design for military operations include the need for autonomous operation and high reliability.

Many spacecraft to date have been designed and built as "one-of-a-kind" research or operational vehicles. If space is to be used as an effective support for the military, the devices that are used will need to be produced in "more-than-one" quantity with standards established to increase reliability and limit cost. This requires that design techniques be shared and standards developed. Using the experience base on which to build and the somewhat unique qualities of the military need as the drivers, the AFWAL Flight Dynamics Laboratory has programs both under way and planned that are directed toward providing a technology base to meet future military needs. Care is being taken not to duplicate work done by NASA or other governmental agencies in DoD. Our work is what we call "full spectrum" - it includes basic research in-house efforts as well exploratory development and advanced development contracted efforts.

The purpose of this paper is to overview the work under way in the AFWAL community that is applicable to the control of flexible antenna systems. The information here does not cover work being done in other laboratories of the Air Force nor does it cover work being done in AFWAL that is applicable to spacecraft such as the Advanced Military Spaceflight Capability (AMSC) and/or the Transatmospheric Vehicle (TAV). Work applicable to such vehicles falls outside the scope of this conference.

In the following descriptions of programs, an attempt is made to provide sufficient information to the reader to gain an understanding of what is being done, how it is being approached, and what the payoff is if successful. In addition, and most important, the people working the area and responsible for contracts in AFWAL are listed with their telephone numbers to simplify contacting them. Discussions are important to us; differences of opinion and reinforcement of opinion need to be brought forth.

The following descriptions start with programs that are in-house basic research in both the Flight Control and Structures and Dynamics Divisions followed by contracted exploratory development programs in both Divisions. Only on-going work is described.

#### IN-HOUSE SPACE-ORIENTED CONTROL ACTIVITIES

All of the in-house control activities to be reviewed are oriented toward application in space. They are fundamental basic research studies and, as such, are actually generic in nature and can apply to many control problems. Orienting them toward space only means that the test problems used and the application jargon applied are spacecraft oriented with weights, frequencies, bandwidths, etc. being those common to flexible space structures and their control systems rather than to aircraft. All of the work overviewed is supported by the Air Force Office of Scientific Research.

#### Reduced-Order Control Theory

In general, the high-frequency dynamics of large, flexible space structures are not well known with the order of the dynamics too large to

design an effective controlling system. Methods are needed to control the low-frequency modes without exciting the high-frequency dynamics inherent in the structure. This is the objective of this study; it has been under way since 1982.

For study purposes, a reduced-order model is used as a "design model" while a full-order model is used as an "evaluation model." The approach used is a frequency-shaped linear quadratic Gaussian (LQG) methodology that makes it possible to apply less control energy to the high-frequency modes and more to the low-frequency modes to better regulate or control all modes. This is done by choosing the quadratic state and control weighting in the LQG methodology as functions of frequency. If the standard LQG methodology is used, it can apply equally to the whole dynamic spectrum possibly causing the control gains to spill over into the high-frequency modes causing instabilities. Weighting prevents this.

The study approach that has been used is to examine the step-by-step application of this frequency-shaped LQG methodology to better understand the reduced-order control design theory. As work progresses, the payoffs and costs of the methodology are documented so that guidelines can be developed for choosing the frequency dependent quadratic state and control weightings. To aid in understanding the meanings of these weightings, they are being interpreted in terms of classical control concepts. For example: it has been shown that shaping the state weighting is the same as using a dynamic compensator in the feedback loop; also, shaping the control weighting is the same as using a roll-off filter in the feed forward loop. The major cost of using this method is the additional states required in the design model. For simple systems, this is no problem because the additional hardware needed for implementation is simple and increases in computational burdens are minimal. For realistic space structures, however, the addition of states could require that some design states must be discarded for a realistic control design thus leading to losses in model information.

The researchers working this area are Dr. Siva Banda and Capt. Brett Ridgely of AFWAL/FIGC. Their telephone numbers are Area Code 513, 255-8677, and 255-8678 respectively. Their past publications are noted in References 1, 2, and 3.

### Vibration Control of Flexible Space Structures

The objective of this basic research program is to design the structure and its control system of a large space satellite to either eliminate structural vibration or reduce it to a desired level within a reasonable time span. Both active and passive means for vibrational control are being considered. The computation issues being addressed include the accurate dynamics modelling of the structure, modelling disturbances, the optimization of the structure for vibration resistance, and the development of control algorithms for large-order systems. A matter of prime importance is the integration of a large-order structural optimization with the algorithms for a closed-loop control system so that both can be used to effectively control the large-order system. Arrangements have been made to use the CRAY computer to support this work.

The payoff of this work will be the analysis techniques for synthesizing the algorithms for large-order systems. An example of a system that will benefit from this work is space-based lasers where significant vibration or jitter reductions is required as well as precise pointing, slewing, and focusing.

The optimization of such a system using both active and passive means not only improves system effectiveness but also reduces the control input required. The ability to solve linear optimal regulator problems of 100 state variables with between 50 to 100 actuators now exists in this program. This structural dynamics capability generates the state and control weighting matrices to solve either infinite time control problems, finite time control problems or control saturation problems.

The AFWAL researchers working this area are Drs. V. B. Venkayya and N. S. Khot, and Ms. V. A. Tischler, AFWAL/FIBR. Their telephone number is (513) 255-6992. Their publications are noted as References 4, 5 and 6.

### Robustness of Multivariable Control Systems

In large space structures, there are a number of uncertainties that can impact the control system because they can't be anticipated and modelled during the control system design process. These uncertainties can be either in the spacecraft or plant that is being modelled or the environment in which the plant operates. Examples of these include plant parameter variations due to manufacturing, assembling and deploying in space; spacecraft dynamics either not modelled at all or not modelled well; on-board disturbances from power sources; structural deformations from unmodelled solar radiation gradients; space dust impact; sensor errors, etc. Robustness of the control system refers to the property of the closed-loop control system that allows it to tolerate these uncertainties without losing stability of the plant or allowing a degradation in plant performance. The objective of our program is to develop the technological fundamentals that will support the design of a robust multivariable control system. This includes the development of the tools to analyze and synthesize the control system and the techniques for applying these tools to the design process. The primary military need for robustness of the control system is the ability to operate autonomously, i.e., without continual monitoring by and adjusting through a network of satellite ground stations.

The robustness concept is not new. Classical controls engineers have been concerned with it since the beginning of control theory. Rather than calling it robustness, they called it feedback and used it to reduce the sensitivity of the system to both plant and operational variations. There are both stability robustness and performance robustness of a system - the AFWAL work has concentrated on stability robustness. This work uses singular values to analyze and test the robustness of the system. Several singular value robustness tests can be used; they are not equivalent and they do not imply that the resulting system is a practical system. These robustness tests are very conservative, which is related to the structure of the uncertainty. To reduce the conservatism of the test, norm-bounded test procedures are now being used to account for the structure of the uncertainty. This work is continuing; upon completion it will be applied to a practical structural space system.

The researchers working this area in AFWAL are the same ones noted above in the Reduced-Order Control Theory section plus Lt Tim McQuade, telephone number, Area Code 513, 255-8675. Past publications in this area are listed as References 7-10.

### CONTRACTED SPACE-ORIENTED CONTROL ACTIVITIES

The work overviewed in this section is contract supported by both Small Business Innovation Research (SBIR) and exploratory development. Even though many of the technical details of the work discussed are generic in

nature and can apply to a variety of systems, the emphasis here will be on the application to large space structures. One program overviewed, Vibrational Control of Space Structures (VCOSS I), has been completed; but since it forms the foundation for a follow-on program, VCOSS II, it is included for completeness. The financial support for the programs is through AFWAL.

### Robustness Technology

Since robustness technology for large space structures is not as yet well understood, there is no consensus on the best way to achieve robustness as well as on how to apply it. Hence, it is best to examine a number of researchers' ideas on robustness so that no high-payoff idea is overlooked. With this in mind, three Small Business Innovation Research (SBIR) contracts have been let with the objective to examine and compare various methods of achieving robust control to evaluate the benefits, drawbacks and applications of each method. The SBIR contract is a vehicle by which a researcher is provided a small amount of seed money to pursue a concept to the first stage of proving its feasibility. If feasibility is shown, then the next stage can be contracted, thus developing the concept. This second stage can have a much larger contract amount. Using the experience and knowledge gained by the AFWAL personnel working in the robust control areas that were noted above, these SBIR contracts are being monitored closely and their results carefully judged on the basis of their worth.

The three contracts, the organizations working them and the contract durations are as follows:

- a. Stevens Institute of Technology  
Time Domain Design of LQG Regulators  
1 June 1984 to 1 June 1985
- b. Alphatech Inc.  
Robust Decentralized Control-Singular Value Theory  
16 August 1984 to 15 February 1985
- c. Scientific Systems, Inc.  
Robust Decentralized Control-Algebraic Theory  
15 August 1984 to 15 February 1985

The robust technology developed under each of these contracts will be applied to a space structure chosen by the researcher. Because of the size of the contracts, these structures will be rather simple in nature.

The AFWAL contract monitor for these efforts is Dr Siva Banda, Area Code 513, 255-8677.

### Large Space Structures Pointing and Shape Control

The Department of Defense has sponsored considerable work directed at developing the analytical tools and techniques for understanding the dynamics and control of large flexible space structures. These efforts have resulted in a number of uncoordinated reports from a number of studies that include the DARPA-funded ACOSS and AFWAL-funded VCOSS I programs. Coupling this to the extensive NASA technology activities in this same area indicates that a rather large body of technical results exists that deals with the control of flexible space structures. This program is directed toward bringing together this state of knowledge in an orderly controls study to establish procedures and tools for the preliminary design of control systems for flexible space structures that

have stringent slewing, pointing, shaping, and vibrational controlling specifications.

The thrust of the program is to develop control algorithms for a large space antenna of a type that could be used for surveillance or reconnaissance. The structural design of the antenna was left to the contractor with the requirements that it be realistic and that it meet the operational and accuracy requirements established by AFWAL. These requirements are rather arbitrary, being established primarily to test the control design so that (a) useable results for a range of spacecraft configurations would result and (b) the maturity and completeness of the state of the art of technology developments in areas of dynamics and control could be determined. In the program, the contractor is required to mathematically model the structure and structural dynamics of the antenna resulting from both the vehicle motions and the environmental disturbances, model these motions and disturbances, and develop algorithms for simultaneously slewing, pointing, shaping and vibrationally damping the structure. Using the noted foundation information, trade-off studies will be made to evaluate actuators and sensors to accomplish the control actions. These studies may lead to the establishment of performance specifications that exceed existing hardware capabilities for control system hardware that are needed to control military large flexible structures in space. Other trade-off studies to be done will examine the trade-offs between active control and passive damping for the control of the vibration of space structures. Application of robustness concepts will be included as well as an attempt to define an optimal control scheme for the antenna structure being studied.

The resulting program, which started in September 1983, is 31 months long. General Dynamics, Convair Division, is the prime contractor with H. R. Textron subcontracting to them. Figure 1 diagrammatically illustrates the objective of the program. Figure 2 is a 3-section view of the antenna that has been modelled. In general, it is a 100-meter offset antenna made up of a truss structure. A complete NASTRAN model of the structure has been established with the model characteristics defined up to 100 modes. Only 45 modes are being considered to develop the control algorithms. Figure 3 describes the program. There are four tasks: model definition, control algorithms, trade-off studies and documentation. The first task is completed now: it prepares the structural definition of the antenna, its dynamic characteristics, and the mathematical models of the disturbances that result from the mission and environment. The second task will define the control system componentry and element placement and develop the candidate operational algorithms to meet the needs of the mission. It is roughly one-half complete. The third task examines the influence of structural and control system variables on performance, seeking an optimal mix of passive and active control. The final task documents the results of the study. Figure 4 diagrammatically shows the interaction of the four elements of control being studied. This figure emphasized the significant interaction between pointing and vibrational control in a large flexible antenna structure such as this. For example, when the structure line of sight is changed, stopping this slewing motion - or using pointing control - causes the structure to vibrate due to the change in momentum of its members.

The AFWAL Project Engineer of this program is Capt. Brett Ridgely, Area Code 513, 255-8678. The Task I report is currently being reviewed and will be available in the near future (ref. 11).

## The Application of Robust Control Technology to Large Space Antennas

This program is a new Exploratory Development program under contract to the Honeywell Systems Research Center. The objective of the program is to apply robust control technology to the large RF antenna being studied under the Large Space Structures Pointing and Shape Control program described. The contractor will use the structural dynamics characteristics of the antenna model, the disturbance characteristics, and the control requirements for slewing, pointing, shaping, and vibrationally controlling the model that General Dynamics has developed under Task 1 of that program (see Figure 2). This robust control program will provide practical analysis and design techniques for applying robust control techniques to a large space antenna. It will address critical issues of model reduction for robust control design for achieving performance and stability robustness, and for making control law simplification for design implementation.

The start of the program is keyed to the completion of Task 1 of the previously described program. The program period is 14 months in length so that the study results can fold back into the large space structures program before Task 3 of that program is complete.

The Project Engineer for this program is Dr. S. S. Banda, AFWAL/FIGC, (513) 255-8677.

### Vibrational Control of Space Structures (VCOSS)

The VCOSS program consists of two efforts: VCOSS I and VCOSS II. Although VCOSS I was completed in mid-1983, its results form the foundation for VCOSS II requiring that it be summarized to form the foundation for VCOSS II.

VCOSS I used the Draper Model 2 as a study configuration. Two contractors performed parallel studies: Lockheed Missiles and Space Company, Inc. and the Space and Technology Group of TRW. The objective of these studies was to apply modern control techniques and state-of-the-art sensor and actuator hardware concepts to actively control the vibration of the Draper Model 2 and compare the line-of-sight error and cost to a passive, stiffness-oriented design. Inherent in this objective is the assessment of the characteristics of sensors and actuators, the placing of them on the structure to gain their greatest benefit, and the evaluation of the resulting mass loading on the structure.

As expected, the study results from each contractor differed somewhat in specifics because they used different sensor/actuator sites, but they agreed in general. Both showed significant reductions in line-of-sight error through a closed-loop active control system. Both also showed that the power required and weight added by the active control system were a cost factor to be considered during preliminary design.

Both contractors differed in the number and type of sensors and actuators used and their location on the study structure. The VCOSS A by LMSC used HAC/LAC hardware implementation<sup>(12)</sup> and VCOSS B by TRW used momentum exchange and truss damping control hardware<sup>(13)</sup>. Both selected hardware as well as sensor and processor hardware that was compatible with their control implementation. Actually these differences added value to this Exploratory Development program in that they illustrated that different implementation techniques and analysis philosophies can be used to control a flexible structure. The overriding conclusion common to both was that much larger reductions in LOS error can be achieved through rather simple active control systems than can be achieved by

structural stiffening. The AFWAL Project Engineer on the VCOSS I study was Mr. Jerome Pearson, AFWAL/FIBG, (513) 255-5236.

To test the conclusions achieved during VCOSS I, a program was planned that would compare the predicted to the measured influence of active control on a realistic space structure. This program is now under contract to the TRW Spacecraft Engineering Division and is called Large Space Structure Vibration Control - VCOSS II. The test model to be used is the Astromast suspended arrangement located at the NASA Marshall Space Flight Center. It includes the mast and an offset feed parabolic antenna (Figure 5). The Astromast has the same design as the masts flown on Voyager and Mariner Satellites. The objectives of VCOSS II are twofold: 1) to develop and optimize the sensor and actuator combinations for application to a test structure, and 2) to assess the adequacy of the analytical models for control system design by comparing experimental results to analytical predictions.

The issues to be addressed during this program are those that are common to the design of either a spacecraft or a test arrangement. These include the technique to be used for the test, sensor sensitivity and saturation, actuator, nonlinearities such as friction, etc. (Figure 6). The payoff of this type of test program is that it should verify the analysis and modelling techniques used, showing ways to improve our ability to model the structure and develop control algorithms. In the long run, this should yield greater control accuracy for flexible large space structures contributing to the design of lower weight structures. The AFWAL Project Engineer for the VCOSS II program is Maj. Hugh Briggs, (513) 255-5236.

#### COMPONENTRY DEVELOPMENT

Included within the AFWAL Laboratories is a Flight Control Actuator Laboratory that has a significant history of developments for the actuation of aerodynamic surfaces for aircraft and missiles. This laboratory has done pioneering work in both hydraulic and electromechanical linear actuators. Based on this experience and the military interest in space, work is under way to develop two actuation concepts that have a possible use in large space structures. These are overviewed in the following.

#### Hydraulic Linear Actuator

The positioning of one element of a large space structure with relation to another element without a residual force or torque can be useful in the shaping of such structures. The residual force and torque of a rocket controller and a control moment gyro have to be counteracted to stop the motion and can be costly in energy. An actuator that requires low power, is responsive and low in weight is an ideal solution but it must also be able to operate over a large temperature range and with steep temperature gradients typical of the space environment. The objective of this activity is to develop such an actuator based on the use of a hydraulic fluid (Figure 7).

The actuator design conceived and built (Figure 8) is an enclosed system using a high flash point silicon fluid as a working fluid. The silicon fluid has the property of having a minimal expansion with temperature change allowing the fluid to be contained within bellows in the actuator (Figure 9). Although the pump in the laboratory model (Figure 10) is an electrically operated displacement device, it is possible to make this pump work by the piezoelectric principle and, thereby, reduce the power required.

The laboratory test model has been fabricated (see Figure 10) and will shortly start undergoing testing. The project manager of the effort is Mr. Greg

Cecere, Area Code 513, 255-2831. The work is performed by Dynamic Control, Inc., an on-site contractor.

### Piezoelectric Technology

Piezoelectric devices are currently used industrially and are being studied by aerospace companies for use in space. Another program just starting in the AFWAL actuator laboratory has as its objective to apply this technology in conjunction with the hydraulic linear actuator just described both as actuator and as a high-pressure fluid transfer pump. Figure 8 illustrates a piezoelectric actuator element as integral with the actuator rod of the hydraulic actuator. This combination can provide large motion at high force levels along with extreme positioning accuracy and up to 1000-Hz frequency response for small strokes. Primary development problems that must be addressed are hysteresis in the discs and the control circuitry required to achieve desired positioning accuracy as well as high frequencies. Figure 11 illustrates a disc stack that has potential for this application along with expected actuator characteristics.

The project manager for this activity, which is starting this fiscal year, is also Mr. Greg Cecere and the work performed by the on-site contractor as noted above.

### SUMMARY

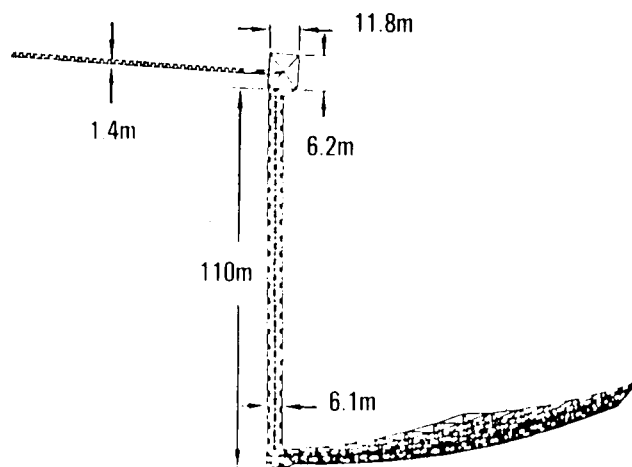
The foregoing is an overview of the AFWAL activities that are currently under way and are relevant to the control of large flexible space structures. The method of carrying out this work is interdisciplinary with the Flight Control and Structures and Dynamics Divisions working closely together on the various technology efforts. The work is supported or funded by the Air Force Office of Scientific Research in the basic research area and AFWAL in the exploratory development area. Hence, the work covers the spectrum from the very fundamental analytic research level to the fabrication and testing of large structural components. No attempt has been made to present details of the work being done; rather, only sufficient information is provided to tell the reader the who, what and why of each program. In all cases, the people performing and/or managing the work are cited along with their AFWAL symbol and telephone number. Contacting them will provide details to whatever depth the reader desires.

Not all the space-oriented dynamics and control work in AFWAL has been overviewed. Work is either in planning or under way on technologies applicable to the control of vehicles categorized under the Advanced Military Spaceflight Capability (AMSC) activity and the Transatmospheric Vehicle (TAV). This work differs from that overviewed because the structures are more rigid and some of the vehicles are planned to be manned. Air data sensor work has been supported in the past and is planned for future support to measure real gas densities in the region near the outer reaches of the atmosphere for use in control system gain computations for maneuvering of an AMSC/TAV. Linear actuator development for application to either large space structures or AMSC-type spacecraft is also under way. If information is desired on any of the work not overviewed, contact the author at AFWAL/FIGC, (513) 476-1075.



## REFERENCES

1. D. B. Ridgely, S. S. Banda and D. V. Palmer, "Reduced Order Control Design Benefits and Costs of Frequency-Shaped LQG Methodology" AIAA Guidance and Control Conference, Gatlinburg, TN, 15-17 August 1983.
2. S. S. Banda, D. B. Ridgely and H. H. Yeh, "Robustness of Reduced Order Control ", Fourth VPI and SU/AIAA Symposium on Dynamics and Control of Large Structures", Blacksburg, VA, 6-8 June 1983.
3. S. S. Banda, D. B. Ridgely, H. H. Yeh, and D. V. Palmer, "Design and Robustness Analysis of Reduced Order Controllers for Large Flexible Space Vehicles", AGARD Symposium on Guidance and Control Techniques for Advanced Space Vehicles", Florence, Italy, 27-30 September 1983.
4. D. F. Miller, B. R. Todd, W. R. Wells and V. B. Venkayya, "Structural Vibration Suppression: A Problem in Combined Structural and Control Optimization", SECTAM-XII Conference, Calaway Gardens, GA, 10-11 May, 1984.
5. V. B. Venkayya and V. A. Tischler, "Frequency Control and the Effect on the Dynamics Response of Flexible Structures" AIAA/ASME/ASCE/AHS Structures, Structural Dynamics and Materials Conference, Palm Springs CA, 14-18 May 84.
6. N. S. Khot and V. B. Venkayya, "Structural Modifications to Reduce LOS Error in Space Structures" AIAA/ASME/ASCE/AHS Structures, Structural Dynamics and Materials Conference, Palm Springs, CA, 14-18 May, 1984.
7. H. H. Yeh, D. B. Ridgely and S. S. Banda, "Nonconservative Evaluation of Uniform Stability Margins of Multivariable Systems", AIAA Guidance and Control Conference, Seattle, WA, 20-22 August 1984.
8. R. K. Yedaralli, S. S. Banda and D. B. Ridgely, "Time Domain Analysis of Stability Robustness of Large Scale LQG Regulators", AIAA Guidance and Control Conference, Gatlinburg, TN, 15-17 August 1983.
9. H. H. Yeh, S. S. Banda and D. B. Ridgely, "Stability Robustness Measures Utilizing Structural Information", American Control Conference, San Diego, CA, 6-8 June 1984.
10. H. H. Yeh, S. S. Banda, and D. B. Ridgely, "Regions of Stability for Gain or Phase Variations in Multivariable Systems," Presented to 23rd Control Design Conference, Las Vegas, NV, 12-14 Dec 84.
11. Large Spacecraft Pointing and Shape Control - Phase I, Model Development, GDC-AFS-84-002, General Dynamics Corporation, October 1984.
12. Vibration Control of Space Structures - VCOSS A: High and Low-Authority Hardware Implementations, AFWAL-TR-83-3074, Lockheed Missiles and Space Company, Inc., July 1983.
13. Vibration Control of Space Structures - VCOSS B: Momentum Exchange and Truss Damping, AFWAL-TR-83-3075, TRW Space and Technology Group, July 1983.



### OBJECTIVE:

DEVELOP ONE CONTROL ANALYSIS / DESIGN METHODOLOGY FOR  
REALISTIC LARGE SPACE ANTENNA FOR:

SLEWING  
POINTING  
SHAPING  
VIBRATION CONTROLLING

### APPROACH:

- MODEL REALISTIC ANTENNA AND ACTUATOR / SENSORS
- DEFINE MISSION DRIVERS AND ENVIRONMENTAL FACTORS
- DEVELOP CONTROL ALGORITHMS
- PERFORM CONTROL TRADE-OFF STUDIES
- REPORT OPTIMAL ALGORITHMS AND HARDWARE SHORT FALLS

### CONTRACTOR:

- GENERAL DYNAMICS CONVAIR DIVISION
- SUB: HR TEXTRON

### PAYOFF:

- FOCUS CONTROL TECHNOLOGY ON REALISTIC CONFIG.
- TEST TECHNOLOGY MATURITY / COMPLETENESS

Figure 1. Large Spacecraft Pointing and Shape Control Program Objective.

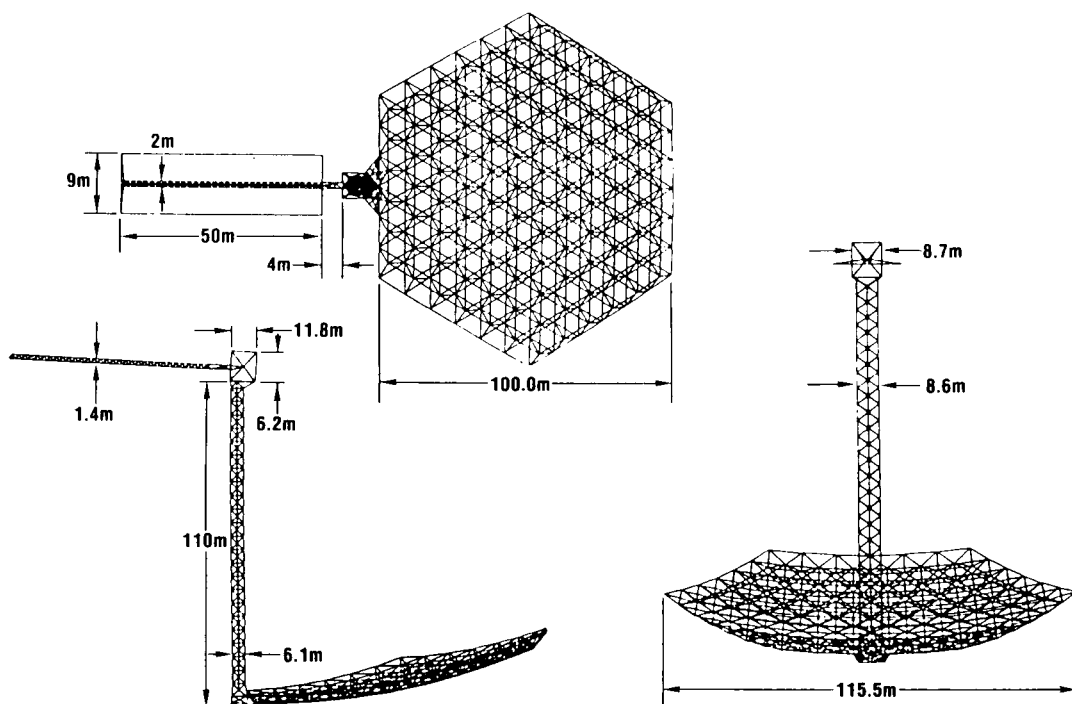


Figure 2. Program Spacecraft Geometry.

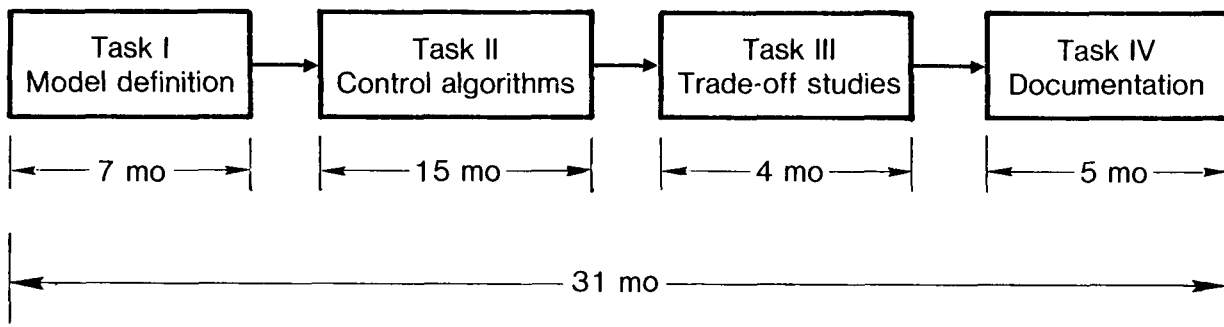


Figure 3. Program Contract Tasks and Timing.

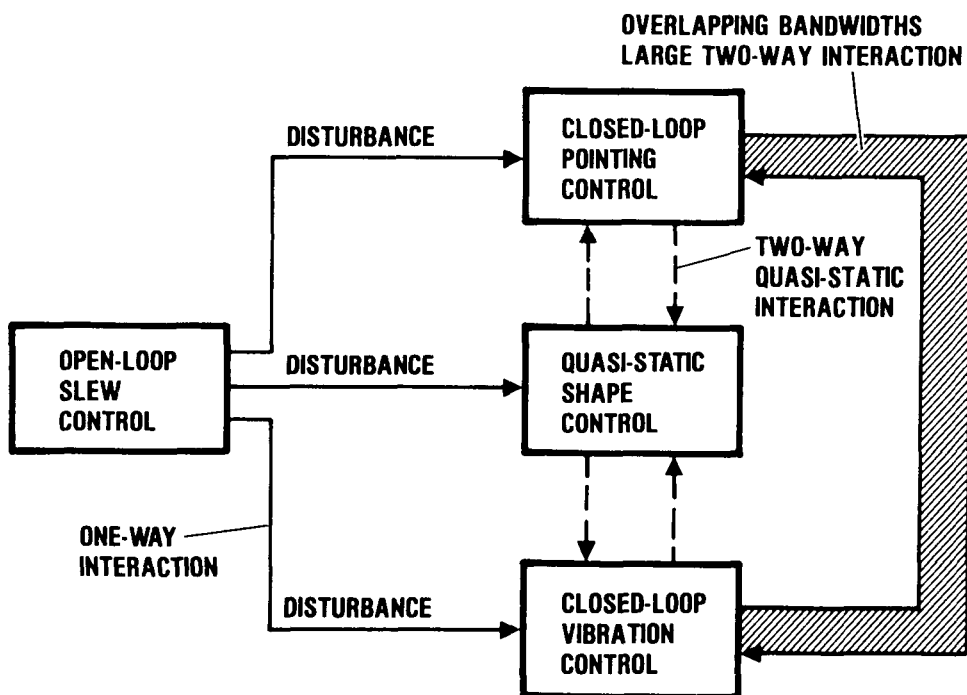
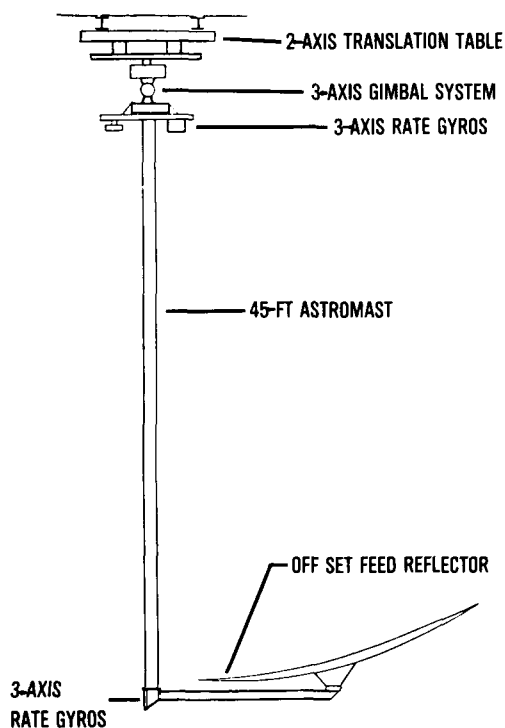


Figure 4. Control Subsystem Interaction.



## OBJECTIVES

- DEVELOP AND OPTIMIZE SENSOR / ACTUATOR COMBINATIONS
- COMPARE EXPERIMENTAL RESULTS TO ANALYTICAL PREDICTIONS TO ASSESS ADEQUACY OF ANALYTICAL MODEL

## TEST MODEL

- LOCATED AT MARSHALL SPACE FLIGHT CENTER
- SUSPENDED ASTROMAST SAME AS FLOWN ON VOYAGER/MARINER
- SUSPENDED THRU GIMBAL SYSTEM

## CONTRACT

- TRW-SPACECRAFT ENGINEERING DIVISION APR 84 - SEP 86

Figure 5. VCOSS II Program Test Arrangement.

### \* TECHNICAL ISSUES

- \* Lab Testing Techniques
- \* Sensor Sensitivity and Saturation
- \* Actuator Stiction
- \* Sensor/Actuator/Structure Interactions
- \* Control Algorithms

### \* PAYOFFS

- \* Lab Confirmation of Analytic Studies
- \* Improved Dynamic Modeling
- \* Improved Control Algorithms
- \* Lighter Space Structures
- \* Greater Alignment Accuracy

### \* GROWTH POTENTIAL

- \* Space Shuttle Test
- \* Distributed Control of Reflecting Surfaces
- \* Improved Adaptive Control Algorithms

Figure 6. VCOSS II - Program Specifics.

### OBJECTIVE:

- DEVELOP HYDRAULIC LINEAR ACTUATOR CAPABILITY THAT CAN WITHSTAND TEMPERATURE RANGE / GRADIENT IN SPACE

### MILITARY NEEDS:

- ABILITY TO POSITION SPACECRAFT COMPONENTS WITHOUT RESIDUAL FORCE / MOMENT ACTING ON TOTAL SPACECRAFT
- LOW WEIGHT, RESPONSIVE, LOW POWER, LINEAR ACTUATOR FOR SBL, AMSC, ETC.

### APPROACH:

- ELECTRO-HYDRAULIC USING SILICON BASED FLUID-FLASH POINT  $> 500^{\circ}\text{F}$
- ENCLOSED SYSTEM WITH POTENTIAL FOR MTBF  $\geq 10$  YRS
- LABORATORY TEST MODEL:
  - POWER =  $\sim 25$  WATTS
  - FORCE = 40 LBS
  - FREQUENCY  $\sim 1$  Hz MAX
  - TEMP. RANGE:  $-200 \leq T \leq +300^{\circ}\text{F}$
  - STROKE:  $\pm 1$  INCH, 0.1 IN / SEC

### SCHEDULE:

- CONCEPTUAL DESIGN-COMplete
- TEST MODEL DESIGNED / FABRICATED - SEP 84
- BENCH TEST (VACUUM, TEMPERATURE) - SEP 85
- DEVELOP DESIGN GUIDE SPEC - JAN 86

Figure 7. Hydraulic Linear Actuator Program.

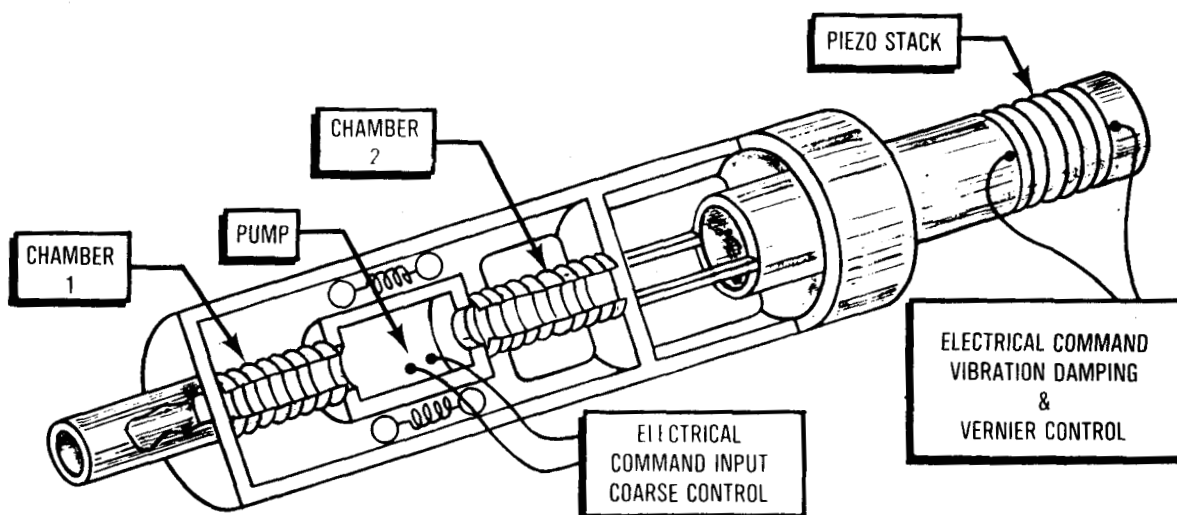


Figure 8. Hydraulic Linear Actuator Schematic.

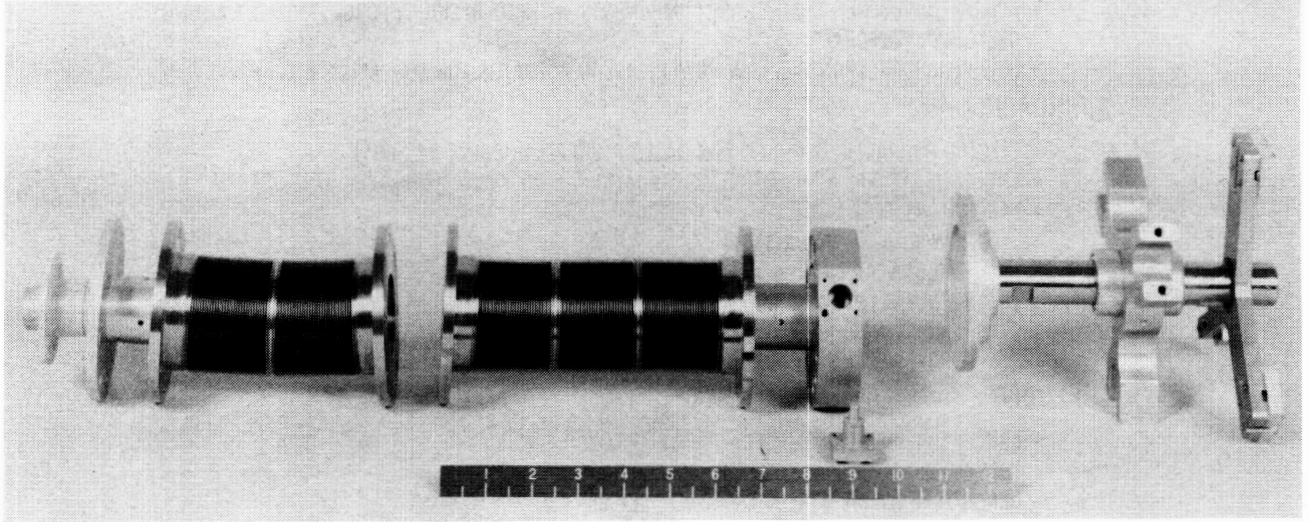


Figure 9. Linear Actuator Componentry.

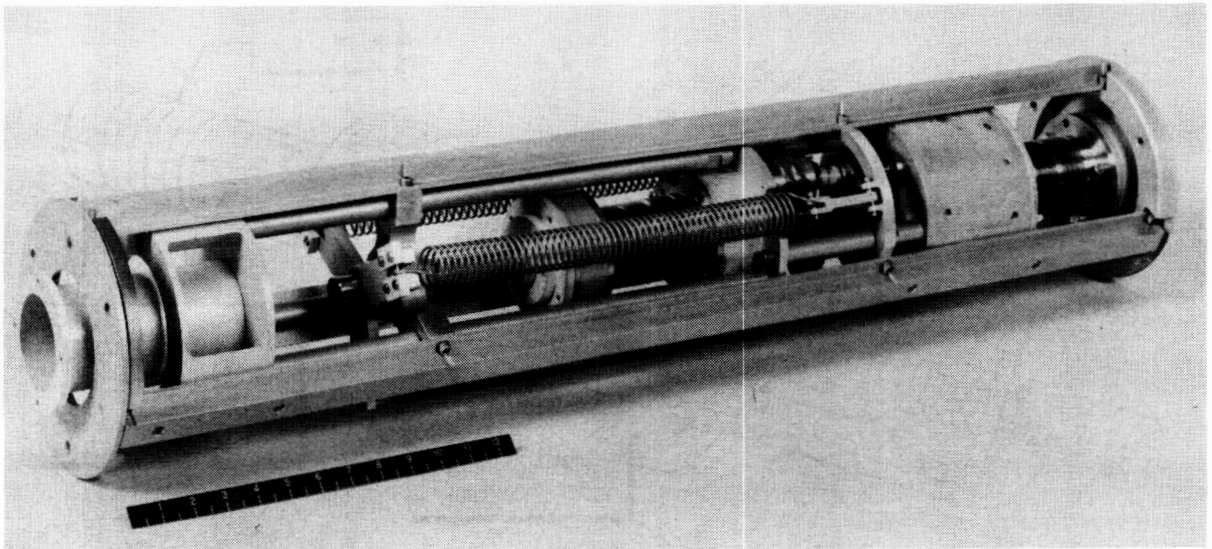
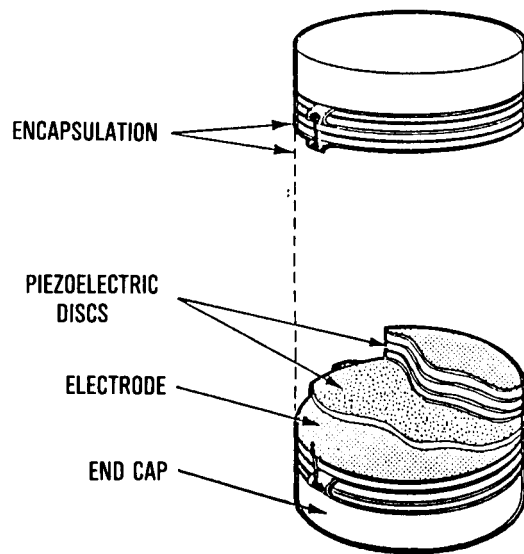


Figure 10. Bench Test Configuration of Linear Actuator.



#### **SCHEDULE:**

- DEV. PROG. START - FY85

#### **OBJECTIVE:**

- TO DEVELOP ABILITY TO APPLY INDUSTRIALLY AVAILABLE PIEZOELECTRIC TECHNOLOGY TO SPACECRAFT

#### **APPLICABILITY:**

- LARGE FORCE, WIDE BANDWIDTH, PRECISION LINEAR ACTUATOR
- HIGH-PRESSURE FLUID TRANSFER PUMP FOR HYDRAULIC ACTUATOR

#### **MILITARY NEED:**

- MIRROR CONTROL IN SBL

#### **POTENTIAL PERFORMANCE CAPABILITY:**

- POWER - 10 WATTS MAX.  
(DEPENDS ON NO. OF DISCS)
- FORCE - 200 - 300 LBS
- FREQUENCY -  $\leq 1000$  Hz
- TEMPERATURE -  $-270^{\circ} \leq T \leq 300^{\circ}\text{C}$
- STROKE - 0.0015 IN. / .001 IN. DISC THICK

Figure 11. Piezoelectric Actuator Program.

1. Report No. NASA CP-2368, Part 1		2. Government Accession No.		3. Recipient's Catalog No.	
4. Title and Subtitle  LARGE SPACE ANTENNA SYSTEMS TECHNOLOGY - 1984				5. Report Date April 1985	
				6. Performing Organization Code 506-62-23-01	
7. Author(s) William J. Boyer, Compiler				8. Performing Organization Report No. L-15950	
9. Performing Organization Name and Address  NASA Langley Research Center Hampton, Virginia 23665				10. Work Unit No.	
				11. Contract or Grant No.	
12. Sponsoring Agency Name and Address National Aeronautics and Space Administration Washington, DC 20546				13. Type of Report and Period Covered Conference Publication	
				14. Sponsoring Agency Code	
15. Supplementary Notes					
16. Abstract <p>This publication is a compilation of the papers presented at the NASA Conference on Large Space Antenna Systems Technology held at the NASA Langley Research Center, Hampton, Virginia, December 4-6, 1984. The conference, which was sponsored jointly by the NASA Office of Aeronautics and Space Technology (OAST) and the NASA Langley Research Center, was organized into seven sessions: Mission Applications for Large Space Antenna Systems, Large Space Antenna Structural Systems, Materials and Structures Technology, Structural Dynamics and Control Technology, Electromagnetics Technology, Large Space Antenna Systems and the Space Station, and Flight Test and Evaluation. All speakers and topics were selected by the session co-chairmen and included representation from industry, universities, and government. The program was organized to provide a comprehensive review of space missions requiring large antenna systems and of the status of key technologies required to enable these missions.</p>					
17. Key Words (Suggested by Author(s)) Large space antenna systems Structures, materials, and analyses Flight technology experiments Structural dynamics and control			18. Distribution Statement  Unclassified - Unlimited  Subject Category 15		
19. Security Classif. (of this report) Unclassified	20. Security Classif. (of this page) Unclassified	21. No. of Pages 479	22. Price A21		